Context Awareness for Enhancing Heterogeneous Access Management and Self-Optimizing Networks

Verbesserung von heterogenem Funkzugangsmanagement
und Selbst-Optimierender Netzwerke
mittels kontextsensitiver Verfahren

von

Dipl.-Ing. Andreas Klein

geboren in Traben-Trarbach

Vom Fachbereich Elektrotechnik und Informationstechnik
der Technischen Universität Kaiserslautern
zur Verleihung des akademischen Grades
Doktor der Ingenieurwissenschaften (Dr.-Ing.)
genehmigte Dissertation

D 386

Datum der mündlichen Prüfung: 1. Dezember 2014

Dekan des Fachbereichs:	Prof. Dr.-Ing. Hans D. Schotten
Prüfungsvorsitzender:	Prof. Dr.-Ing. Ralph Urbansky
1. Berichterstatter:	Prof. Dr.-Ing. Hans D. Schotten
2. Berichterstatter:	Prof. Dr.-Ing. Andreas König

To my family

Abstract

The heterogeneity of today's access possibilities to wireless networks imposes challenges for efficient mobility support and resource management across different Radio Access Technologies (RATs). The current situation is characterized by the coexistence of various wireless communication systems, such as GSM, HSPA, LTE, WiMAX, and WLAN. These RATs greatly differ with respect to coverage, spectrum, data rates, Quality of Service (QoS), and mobility support.

The performance of wireless networks is typically assessed by "snapshot" based simulations and system-level metrics, such as spectral efficiency or cell throughput. However, these system metrics are based on aggregated statistics that do not adequately reflect the situation of specific environments or individual users. For example, network coverage depends on terrain, building development, as well as network deployment. Further, snapshot based simulations lack the possibility of analyzing the impact of parameter evolutions over time, e.g., receive level variations due to user movements, or effects on End-To-End (E2E) performance caused by signaling delay. In real systems, mobility-related events, such as Handover (HO) procedures, directly affect resource efficiency and E2E performance, in particular with respect to signaling efforts and users' QoS. In order to lay a basis for realistic multi-radio network evaluation, a novel evaluation methodology is introduced in this thesis. This novel evaluation methodology extends existing single RAT methodologies by incorporating realistic modeling of user mobility as well as HO processes and allows for jointly evaluating heterogeneous RATs.

A central hypothesis of this thesis is that the consideration and exploitation of additional information characterizing user, network, and environment context, is beneficial for enhancing heterogeneous access management and Self-Optimizing Networks (SONs). For example, it has been shown that improved network selection and HO decisions can be taken by considering user movement estimates. Further, Mobile Network Operator (MNO) revenues are maximized by tightly integrating bandwidth adaptation and admission control mechanisms as well as simultaneously accounting for user profiles and service characteristics. In addition, mobility robustness is optimized by enabling network nodes to tune HO parameters according to locally observed conditions.

For establishing all these facets of context awareness, various schemes and algorithms are developed and evaluated in this thesis. System-level simulation results demonstrate the potential of context information exploitation for

enhancing resource utilization, mobility support, self-tuning network operations, and users' E2E performance.

Many proposals have been made in literature for implementing concepts, such as *always best connected* or *seamless mobility*, and improving network selection, intra- and inter-RAT mobility, as well as common Radio Resource Management (RRM). However, none of these approaches considered the integration of wireless network functionalities with context management systems for establishing context awareness, e.g., at network-sided decision making entities. Therefore, a concept for Intelligent Radio Network Access (IRNA) is developed that is able to leverage user, network, and environment context information for enhancing network selection and mobility support across heterogeneous networks. In particular, the IRNA concept has shown to significantly reduce the overall number of intra- and inter-RAT HOs of high-speed users by approximately 40% or even 70%, respectively.

Further, a novel approach for combined Dynamic Bandwidth Adaptation (DBA) and Joint Call Admission Control (JCAC) is introduced that enables maximizing MNO's revenue while simultaneously accounting for user profiles and service-specific QoS requirements. The core JCAC task is mapped to a *generalized assignment problem*, which is well-suited for revenue maximization and known to be NP-hard. Moreover, a generic utility measure is presented that is used for assessing the impact of JCAC and RRM strategy on resource utilization and MNO's revenue. System-level performance results show an improvement in overall gained utility of approximately 6% in contrast to a state-of-the-art JCAC approach, while system Key Performance Indicators (KPIs), such as blocking and dropping rates, are kept at an acceptable level.

In further investigations, the fact that mobility of commuters is not purely random is exploited for predicting user cell transitions. In particular, the prediction of movement trajectories of users moving jointly in the same vehicle (e.g., bus, train, etc.) has shown to significantly improve system KPIs, such as connection dropping, HO and call blocking ratios. Given this knowledge on user trajectories, the arrival of users or user groups in a certain cell can be anticipated and used to pro-actively trigger a load balancing mechanism in order to prevent imminent congestion. Regarding evaluated KPIs, such as blocked access attempts, blocked HO attempts, and connections drops, improvements of 10%, 26%, and 32%, respectively, have been obtained.

Further, maximum achievable gains of context information exploitation, such as user movement or Signal-to-Interference-plus-Noise Ratio (SINR) estimates, are evaluated using realistic 3D environment and radio propaga-

tion models. System-level results indicate that system throughput can be increased by approximately 60%, if user movements can be predicted with sufficient accuracy, or even by 100%, if SINR estimates are available.

Moreover, a Fuzzy Q-Learning (FQL) based approach for Mobility Robustness Optimization (MRO) in SONs is developed that aims at establishing context awareness at network nodes in order to reduce Operational Expenditures (OPEX). Due to the self-learning nature of the employed algorithm manual tuning and optimization of system parameters can be avoided. This novel MRO scheme has shown that multiple KPIs, such as connection dropping, HO failure, and ping-pong HO ratios, can be simultaneously improved in an autonomous manner as soon as the learning phase of the respective network node is finished. In particular, it has been shown that one variant of the FQL based MRO schemes that is able to incorporate knowledge on cell-pair related performance issues in parameter adaptation decisions improves the Overall Performance Indicator (OPI) by 36%. Regarding specific KPIs, such as the number of connection drops, HO failures, and ping-pong HOs, this context-aware MRO scheme yields reductions of 20%, 80%, and 87.5%, respectively.

In order to evaluate the performance of the developed concepts, a multi-radio network simulation tool was implemented and embedded into a newly created simulation framework. Further, this tool allows for integrating and exploiting context information on users, networks, and environment. Moreover, the developed concepts for context information exploitation and the multi-RAT evaluation methodology represent important contributions of the author to the European FP7 project METIS. The METIS project already proposed scenarios [MET13a] and simulation guidelines [MET13c] for evaluating the performance of future wireless technologies and the fifth generation of wireless communication systems (5G). In particular regarding the evaluation of developed concepts, the METIS project also aimed at more realistic modeling of network deployment, radio propagation, and user mobility.

In essence, the conducted research activities and presented results motivate and substantiate the consideration of context awareness as key enabler for cognitive and autonomous network management. Further, the performed investigations and aspects evaluated in the scope of this thesis are highly relevant for future 5G wireless systems and current discussions in the 5G infrastructure Public Private Partnership (PPP) [5G-14].

Keywords – context awareness, context management, wireless networks, heterogeneous access management, self-optimizing networks, mobility robust-

ness optimization, fuzzy logic, reinforcement learning, fuzzy Q-learning, handover optimization

Zusammenfassung

Die Mobilkommunikation hat sich zu einem wesentlichen Bestandteil unseres immer stärker durch Mobilität geprägten Alltags entwickelt. Sie erleichtert Menschen nicht nur im Privatleben die unmittelbare Erfüllung sozialer Bedürfnisse, wie Informationsaustausch oder Organisation, sondern hat vor allem auch im wirtschaftlichen Bereich zu effizienteren Prozessen geführt.

Mit der Einführung neuer Mobilfunk-Technologien, die dem Nutzer hocheffiziente, zuverlässige und unmittelbare Kommunikation ermöglichen, steigt der Bedarf nach höheren Datenraten, flächendeckender Verfügbarkeit und effizienten Verfahren für nahtlosen Funknetzwechsel insbesondere für mobile Dienste weiter an. Darüber hinaus ist das *Internet der Dinge* nicht länger nur eine Zukunftsvision, sondern laut der *Organization for Economic Cooperation and Development* (OECD) [OEC12] auf dem besten Wege, Wirklichkeit zu werden. Vorhersagen der *Global System for Mobile Communications Association* (GSMA) [Glo11] zufolge wird es bis zum Jahr 2020 Milliarden von Geräten geben, beispielsweise im Bereich *Maschine-zu-Maschine-Kommunikation* (M2M), die sowohl eine Funkanbindung an das Internet benötigen als auch bidirektionale *Peer-to-Peer* (P2P) Verbindungen nutzen werden und somit lokal zu einer potentiellen Erhöhung der Funk-Interferenz beitragen werden.

Auf Grund der Heterogenität heutiger Zugangsmöglichkeiten zu Funknetzwerken stehen technologieübergreifende Lösungen für effiziente Mobilitätsunterstützung und Funk-Ressourcen-Management (*Radio Resource Management* (RRM)) vor enormen Herausforderungen. Die gegenwärtige Situation ist gekennzeichnet durch die Koexistenz heterogener Funkkommunikationssysteme, wie zum Beispiel GSM, HSPA, LTE, WiMAX und WLAN, die sich bezüglich Netzabdeckung, Spektrum, Datenraten, Dienstgüte und Mobilitätsunterstützung stark unterscheiden.

Typischerweise wird die Leistungsfähigkeit von Funksystemen mittels Schnappschuss-basierter Simulationsverfahren und System-Metriken, wie spektrale Effizienz und Datendurchsatz der Funkzellen, bewertet. Allerdings beruhen diese System-Metriken auf aggregierten Statistiken, die Situationen in bestimmten Umgebungen oder einzelner Nutzer nicht oder nur unzureichend widerspiegeln. Die Netzabdeckung hängt unter anderem von Gelände, Bebauung und Netzaufbau ab. Des Weiteren mangelt es Schnappschuss-basierten Simulationsverfahren an Möglichkeiten, den Einfluss zeitlicher Parameter-Entwicklungen zu untersuchen. Hierzu zählen beispielsweise Variationen der

Empfangsstärke auf Grund von Nutzerbewegungen oder durch Signalisierungsverzögerung verursachte Auswirkungen auf die Ende-zu-Ende-Leistungsfähigkeit. In realen Systemen beeinträchtigen mobilitätsbedingte Ereignisse, wie Handover-Vorgänge, direkt die Ressourcen-Effizienz und Ende-zu-Ende-Leistungsfähigkeit. Diese Einflüsse zeigen sich besonders im Hinblick auf Signalisierungsaufwände und Nutzer-Dienstgüte.

Daher wurde im Rahmen dieser Arbeit eine neue Evaluierungsmethodik entwickelt, die die Grundlage für eine realistischere Evaluierung von Szenarien mit heterogenen Funknetzwerken legen soll. Diese neue Evaluierungsmethodik erweitert existierende Einzel-Funknetzwerk-Methodiken, indem Nutzer-Mobilität und Handover-Prozesse realistischer modelliert und heterogene Funktechnologien gemeinsam evaluiert werden können.

Eine zentrale Hypothese dieser Arbeit ist, dass die Berücksichtigung und Ausnutzung zusätzlicher Informationen, die Nutzer-, Netzwerk- und Umgebungskontext charakterisieren, gewinnbringend zur Steigerung der Leistungsfähigkeit von heterogenem Funkzugangsmanagement und selbst-optimierenden Netzwerken verwandt werden kann. Es konnte beispielsweise gezeigt werden, dass Entscheidungen über Netzauswahl und Handover verbessert werden können, indem Nutzerbewegungsschätzungen berücksichtigt werden. Des Weiteren wurde nachgewiesen, dass sich durch die Integration von Mechanismen zur Bandbreiten-Adaptation und Funkzugangskontrolle sowie die gleichzeitige Einbeziehung von Nutzer-Profilen und Dienst-Charakteristika Netzbetreibererlöse maximieren lassen. Zudem konnte die Netzrobustheit gegenüber Nutzermobilität durch das von Netzwerkknoten selbstständig erlernte Anpassen von Handover-Parametern entsprechend lokal beobachteter Bedingungen optimiert werden.

Zur Realisierung all dieser positiven Aspekte von Kontextbewusstsein wurden im Rahmen dieser Arbeit verschiedene Modelle und Algorithmen entwickelt und evaluiert. Auf Systemebene generierte Simulationsergebnisse zeigen das Potenzial, das in der Ausnutzung von Kontextinformationen zur Optimierung der Ressourceneffizienz, der Mobilitätsunterstützung, des selbst-adaptierenden Netzbetriebs und der den Nutzern zu Gute kommenden Ende-zu-Ende-Leistungsfähigkeit liegt.

In der Literatur finden sich viele Vorschläge, Konzepte, wie *always best connected* (immer die beste Verbindung) oder *seamless mobility* (nahtlose Mobilität), zu implementieren und Netzauswahl, Intra- und Inter-Funktechnologie-Mobilität sowie gemeinsames Ressourcen-Management zu verbessern. Allerdings sieht keiner dieser Ansätze die Integration von Funktionalitäten der Funkzugangsnetzwerke mit Kontext-Management-Systemen zur Realisierung

von Kontextbewusstsein, beispielsweise in netzwerkseitigen Entscheidungseinheiten, vor. Aus diesem Grund wurde ein Konzept für intelligenten Funknetzzugang (*Intelligent Radio Network Access* (IRNA)) entwickelt, das in der Lage ist, Nutzer-, Netzwerk- und Umgebungskontext wirksam zur Optimierung von Netzauswahl und Mobilitätsunterstützung über heterogene Netzwerke hinweg einzusetzen. Dieses IRNA-Konzept bildete in weiteren Untersuchungen die Grundlage zur Optimierung von Netzauswahl und heterogenem Funkzugangsmanagement (*Heterogeneous Access Management* (HAM)). Die Umsetzung des IRNA-Konzepts hat gezeigt, dass die Gesamtanzahl der Intra- und Inter-Funktechnologie-Handover von Nutzern mit hoher Geschwindigkeit um ca. 40% beziehungsweise sogar ca. 70% reduziert werden können.

Ferner wurde ein neuartiger Ansatz für gemeinsame Funkzugangskontrolle (*Joint Call Admission Control* (JCAC)) und dynamische Bandbreitenanpassung (*Dynamic Bandwidth Adaptation* (DBA)) eingeführt, der unter gleichzeitiger Berücksichtigung von Nutzer-Profilen und Dienst-Charakteristika die Maximierung der Netzbetreibererlöse ermöglicht. Dabei wird das Kern-Problem der gemeinsamen Funkzugangskontrolle (JCAC) auf ein sogenanntes "Verallgemeinertes Zuweisungsproblem" (*Generalized Assignment Problem* (GAP)) abgebildet, das sich sehr gut zur Maximierung von Erlösen eignet.

Weiterhin wird ein allgemeines Nutzen-Maß präsentiert, das zur Bewertung des Einflusses von JCAC- und RRM-Strategie auf den Netzbetreibererlös verwendet wird. Auf Systemebene gewonnene Simulationsergebnisse zeigen eine Verbesserung im Gesamtnutzen bzw. -erlös von ca. 6% gegenüber einem vergleichbaren, dem Stand der Technik entsprechenden JCAC-Verfahren, während Indikatoren zur System-Leistungsfähigkeit, wie Verbindungsblockier- und Verbindungsabbruch-Raten auf akzeptablen Niveaus verbleiben.

In weiteren Untersuchungen wurde die Tatsache, dass die Mobilität von Pendlern nicht zufallsbedingt ist, ausgenutzt, um Funkzellen-Übergänge der Nutzer vorherzusagen. Besonders die Vorhersage der Bewegungsrichtungen von Nutzern, die sich gemeinsam in einem Fortbewegungsmittel (z.B. Bus, Zug, etc.) befinden, hat enorme Verbesserungen hinsichtlich System-Leistungsfähigkeitsindikatoren, wie Verbindungsabbruch-, Handover- und Verbindungsblockier-Raten, erzielt. Unter Berücksichtigung des Wissens um Nutzerbewegungsrichtungen kann die Ankunft von Nutzern oder Nutzergruppen in einer bestimmten Funkzelle vorausgesagt und pro-aktiv Lastverteilungsmechanismen aktiviert werden, um andernfalls bevorstehende Überlastsituationen zu vermeiden. In Bezug auf die untersuchten System-Metriken, wie blockierte Verbindungsversuche, blockierte Handover-Versuche und Verbindungsabbrüche, konnten Verbesserungen um 10%, 26% beziehungsweise 32% realisiert

werden.

Des Weiteren wurden maximal erzielbare Gewinne bei der Ausnutzung von Kontextinformationen, wie Nutzerbewegungs- oder Signal-zu-Interferenz-plus-Rauschabstands-Schätzungen, unter Verwendung realitätsnaher Modelle der Funkausbreitung und Nutzerumgebungen in 3D evaluiert. Auf Systemebene ermittelte Simulationsergebnisse zeigen, dass der Gesamt-System-Durchsatz um bis zu 60% erhöht werden kann, falls Nutzer-Bewegungen hinreichend genau vorhergesagt werden können. Falls Signal-zu-Interferenz-plus-Rauschabstands-Schätzwerte vorliegen, sind sogar Steigerungen um 100% möglich.

Darüber hinaus wurde ein auf *Fuzzy* Logik (unscharfe Logik) und *Q-Learning* basierender Ansatz für die Optimierung der Funknetzrobustheit gegenüber Nutzermobilität in selbst-optimierenden Funknetzwerken entwickelt. Dieses Verfahren zielt auf die Realisierung von Kontextbewusstsein an Netzwerkknoten ab, um die operativen Ausgaben für Netzbetrieb und -management zu verringern. Durch den selbstlernenden Algorithmus kann ein manuelles Anpassen und Optimieren von Systemparametern vermieden werden.

Des Weiteren hat dieser neuartige Ansatz zur Optimierung der Funknetzrobustheit gegenüber Nutzermobilität gezeigt, dass mehrere Indikatoren für die System-Leistungsfähigkeit, wie Verbindungsabbruch-, Handover-Fehler- und Ping-Pong-Handover-Raten, gleichzeitig und in autonomer Art und Weise verbessert werden können, sobald die Lernphase des jeweiligen Netzwerkknotens abgeschlossen ist. Insbesondere konnte gezeigt werden, dass diejenige Variante der *Fuzzy Q-Learning*-basierten Optimierungsverfahren, die in der Lage ist, Kenntnisse um Zell-Paar-bezogene Netzwerk-Probleme bei der Entscheidungsfindung zu Parameteranpassungen zu berücksichtigen, die Gesamt-Performance-Metrik um 36% verbessert.

Im Hinblick auf einzelne System-Metriken, wie die Anzahl der Verbindungsabbrüche, Handover-Fehler und Ping-Pong-Handover, konnten diese durch das kontextsensitive Optimierungsverfahren um 20%, 80% beziehungsweise 87.5% reduziert werden. Dazu werden insbesondere vom Netzwerkknoten gesammelte Kontext-Informationen über Art und Richtung aufgetretener Netzwerkprobleme unter den jeweiligen Nachbarzellen ausgetauscht. Darunter fallen Daten wie Ausgangs- und Zielzelle von Handover-Vorgängen, deren Häufigkeit und eventuell aufgetretene Probleme. Diese Informationen ermöglichen es, Rückschlüsse über Fehlerort und -art zu ziehen, so dass beispielsweise häufig beobachtete Verbindungsabbrüche während Handover-Vorgängen oder Ping-Pong-Handover mittels selbstlernender Verfahren reduziert werden

können.

Zur Evaluierung der Leistungsfähigkeit der entwickelten Konzepte wurde ein Multi-Funknetzwerk-Simulator implementiert und in eine neu entwickelte Simulationsumgebung eingebettet. Diese verfügt über effiziente Schnittstellen zu Datenbanken und Visualisierungssoftware, die Möglichkeiten zur Offline-Datenauswertung und -Analyse sowie der Visualisierung von zu untersuchenden Funknetzwerkproblemen bieten. Ferner erlaubt dieser Funknetz-Simulator die Einbeziehung und Ausnutzung von Kontextinformationen über Nutzer, Funknetzwerke und Umgebungen.

Darüber hinaus stellen die vom Autor entwickelten Konzepte zur Ausnutzung von Kontextinformation und die Multi-Radio-Evaluierungsmethodik wichtige Beiträge zum Europäischen FP7-Projekt METIS dar. Das Projekt METIS hat bereits Szenarien [MET13a] und Simulationsrichtlinien [MET13c] zur Evaluierung zukünftiger Funktechnologien und der 5. Generation der Mobilfunksysteme (5G) vorgeschlagen. Insbesondere hinsichtlich der Evaluierung der entwickelten Konzepte zielt METIS dabei ebenfalls auf eine realistischere Modellierung von Ausbau der Netzkomponenten, Funkausbreitung und Nutzermobilität ab.

Zusammenfassend lässt sich feststellen, dass die geleisteten Forschungsarbeiten und vorliegenden Ergebnisse die Berücksichtigung von Kontextinformationen als Voraussetzung für kognitives und autonomes Netzwerkmanagement motivieren und untermauern. Ferner sind die im Rahmen dieser Arbeit durchgeführten Untersuchungen und evaluierten Aspekte von hoher Relevanz für zukünftige 5G Funk-Systeme und aktuelle Diskussionen im Rahmen des 5G-Infrastruktur *Public Private Partnership* (PPP) [5G-14].

Schlagwörter – Context Awareness, Context Management, Wireless Networks, Heterogeneous Access Management, Self-Optimizing Networks, Mobility Robustness Optimization, Fuzzy Logic, Reinforcement Learning, Fuzzy Q-Learning, Handover Optimization

Contents

List of Figures

List of Tables

List of Acronyms

2D	Two Dimensional
3D	Three Dimensional
3G	Third Generation
3GPP	3rd Generation Partnership Project
3GPP2	3rd Generation Partnership Project 2
4G	Fourth Generation
5G	Fifth Generation
AAA	Authentication, Authorization, Accounting
AJCAC	Adaptive Joint Call Admission Control
AMC	Adaptive Modulation and Coding
AMPS	Advanced Mobile Phone System
AMR	Adaptive Multi Rate
ANR	Automatic Neighbor Relation
ANSI	American National Standards Institute
AP	Access Point
ARPU	Average Revenue Per Unit
AWGN	Additive White Gaussian Noise
BMBF	Bundesministerium für Bildung und Forschung (Federal Ministry of Education and Research)
BLER	Block Error Rate
BS	Base Station
BSC	Base Station Switching Center
BTSs	Base Transceiver Stations
CAC	Call Admission Control
CAPEX	Capital Expenditures
CBR	Constant Bit Rate
C-CAST	Context Casting
CCCH	Common Control Channel
CDF	Cumulative Distribution Function
CDMA	Code Division Multiple Access

CDR	Connection Dropping Ratio
CIO	Cell Individual Offset
CM	Configuration Management
CMS	Context Management System
CN	Correspondent Node
CoA	Care-of Address
COG	Center of Gravity
CORAS	Context Aware Radio Network Simulator
CPICH	Common Pilot Channel
CQE	Context Quality Enabler
CQI	Channel Quality Indicator
CRRM	Common Radio Resource Management
CxB	Context Broker
CxC	Context Consumer
CxP	Context Provider
D2D	Device-To-Device
DBA	Dynamic Bandwidth Adaptation
DHCP	Dynamic Host Control Protocol
DHT	Distributed Hash Table
DL	Downlink
DP	Dynamic Programming
DSM	Dynamic Spectrum Management
E2E	End-To-End
EEP	Exploration/Exploitation Policy
EGPRS	Enhanced General Packet Radio Service
EKF	Extended Kalman Filter
EMA	Exponential Moving Average
eNB	Evolved Node B
eNBs	Evolved Node Bs
ETSI	European Telecommunications Standards Institute
EU	European Union
E-UTRAN	Evolved Universal Mobile Telecommunications System Terrestrial Radio Access Network
FA	Foreign Agent
FCC	Federal Communications Commission
FDD	Frequency Division Duplex
FIS	Fuzzy Inference System
FP	Framework Programme
FQL	Fuzzy Q-Learning

FTP	File Transfer Protocol
GAP	Generalized Assignment Problem
GBR	Guaranteed Bit Rate
GGSN	Gateway General Packet Radio Service Support Node
GPRS	General Packet Radio Service
GPS	Global Positioning System
GSM	Global System for Mobile Communications
GSMA	Global System for Mobile Communications Association
GW	Gateway
HA	Home Agent
HAM	Heterogeneous Access Management
HARQ	Hybrid Automatic-Repeat-Request
HD	High Definition
HLR	Home Location Register
HO	Handover
HFR	Handover Failure Ratio
HOM	Handover Margin
HOP	Handover Operating Point
HPI	Handover Performance Indicator
HSDPA	High Speed Downlink Packet Access
HS-PDSCH	High Speed-Physical Downlink Shared Channel
HSPA	High Speed Packet Access
HTTP	HyperText Transfer Protocol
HYS	Hysteresis
ICT	Information and Communications Technologies
IEEE	Institute of Electrical and Electronics Engineers
IETF	Internet Engineering Task Force
IMS	Internet Protocol Multimedia Subsystem
IoT	Internet of Things
IP	Internet Protocol
IRNA	Intelligent Radio Network Access
IS	Interim Standard
ISD	Inter-Site Distance
ISP	Internet Service Provider
Itf-N	Northbound Interface
ITU-T	International Telecommunication Union Telecommunication Standardization Sector
JCAC	Joint Call Admission Control
JMM	Joint Mobility Management

JRRM	Joint Radio Resource Management
KPI	Key Performance Indicator
LB	Load Balancing
LTE	Long Term Evolution
LUT	Look-Up Table
M2M	Machine-To-Machine
MAC	Medium Access Control
Mbps	Megabits Per Second
MCS	Modulation and Coding Scheme
MDP	Markov Decision Process
MICS	Media Independent Command Service
MIES	Media Independent Event Service
MIH	Media Independent Handover
MIIS	Media Independent Information Service
MIMO	Multiple Input Multiple Output
MIP	Mobile Internet Protocol
MLB	Mobility Load Balancing
MME	Mobility Management Entity
MN	Mobile Node
MNO	Mobile Network Operator
MRO	Mobility Robustness Optimization
MTS	Mobile Telephone Service
MTU	Maximum Transmit Unit
NB	Node B
NBs	Node Bs
NE	Network Element
NGMN	Next Generation Mobile Networks
NGN	Next Generation Network(s)
NMT	Nordic Mobile Telephone
NP	Non-deterministic Polynomial-time
NTT	Nippon Telegraph and Telephone
O&M	Operation & Maintenance
OECD	Organization for Economic Cooperation and Development
OFDM	Orthogonal Frequency Division Multiplexing
OFDMA	Orthogonal Frequency Division Multiple Access
OPEX	Operational Expenditures
OPI	Overall Performance Indicator
OWL	Web Ontology Language
P2P	Peer-to-Peer

PBCH	Physical Broadcast Channel
PDF	Probability Density Function
PDP	Packet Data Protocol
PDSCH	Physical Downlink Shared Channel
PER	Packet Error Rate
PF	Proportional Fair
PHY	Physical
PHR	Ping-Pong Handover Ratio
PM	Performance Management
PPP	Public Private Partnership
PRB	Physical Resource Block
PSTN	Public Switched Telephone Network
QAM	Quadrature Amplitude Modulation
QoE	Quality of Experience
QoS	Quality of Service
RAN	Radio Access Network
RANs	Radio Access Networks
RAT	Radio Access Technology
RATs	Radio Access Technologies
REST	Representational State Transfer
RDFS	Resource Description Framework Schema
RL	Reinforcement Learning
RLC	Radio Link Control
RLF	Radio Link Failure
RNC	Radio Network Controller
RRC	Radio Resource Control
RRM	Radio Resource Management
RSRP	Reference Signal Received Power
RTP	Real-Time Transport Protocol
RTT	Round Trip Time
SAE	System Architecture Evolution
SBHOA	Sum Based Handover Optimization Algorithm
SCTP	Stream Control Transmission Protocol
SDF	Shadowing Factor
SDR	Software Defined Radio
SDU	Service Data Unit
SF	Spreading Factor
SGSN	Serving General Packet Radio Service Support Node
SID	Silence Insertion Descriptor

SINR	Signal-to-Interference-plus-Noise Ratio
SIP	Session Initiation Protocol
SISO	Single Input Single Output
SLA	Service Level Agreement
SMS	Short Message Service
SON	Self-Organizing/Optimizing Network
SONs	Self-Organizing/Optimizing Networks
TBHOA	Trend Based Handover Optimization Algorithm
TBS	Transport Block Size
TCP	Transmission Control Protocol
TD	Temporal Difference
TDD	Time Division Duplex
TTI	Transmission Time Interval
TTT	Time-To-Trigger
Tx	Transmission
UE	User Equipment
UL	Uplink
UML	Unified Modeling Language
UMTS	Universal Mobile Telecommunications System
UTRAN	Universal Mobile Telecommunications System Terrestrial Radio Access Network
VHO	Vertical Handover
VoIP	Voice over IP
WCDMA	Wideband Code Division Multiple Access
WiFi	Wireless Fidelity
WiMAX	Worldwide Interoperability for Microwave Access
WLAN	Wireless Local Area Network
WWW	World Wide Web
XML	Extensible Markup Language

1 Introduction

Radio transmission for the first time achieved worldwide attention with the commercialization of practical radio systems by Guglielmo Marconi at the beginning of the 20th century. Marconi benefited from fundamental works of several famous scientists, e.g., James Clerk Maxwell (1865), Heinrich Hertz (1888), or Nikola Tesla (1891). From that time on, radio transmission influenced mankind's evolution, particularly in World War I and II where massive military use was made of radio communication. Broadcast and reception of information over the air became an inherent part of our everyday life, while available receivers were still bulky. The rapid evolution in microelectronics, boosted by the success of John Bardeen, Walter Houser Brattain, and William Bradford Shockley in inventing a point-contact transistor in 1947 [Ame00], laid the foundation for handheld devices. It was not until 1973 though, before first handheld mobile phones were produced by Motorola [CDL+73].

After successful installation of the first mobile communication system in St. Louis in 1946 [Mol11], AT&T, an American telecommunications provider, started introducing the Mobile Telephone Service (MTS) to hundreds of towns and highway corridors. However, the MTS was not automated and calls to the Public Switched Telephone Network (PSTN) had to be switched by human telephone operators. Moreover, each local system soon met its limitations due to a total amount of only six radio channels for a whole city [Mol11]. This issue motivated engineers at Bell Laboratories[1] to start thinking about the question of how the number of supportable users could be increased while the amount of spectrum remained the same. Their innovative solution was the so-called *cellular principle*. According to this concept, the service area to be covered is split into smaller geographical areas, referred to as *cells*. Radio frequencies are reused among those cells in such a way that maximum distance between cells operating at the same frequency is ensured. The joint work of Bell Labs engineers Richard H. Frenkiel, Joel S. Engel, and Philip T. Porter, and their technical report on "High Capacity Mobile

[1] "also known as Bell Labs and formerly known as AT&T Bell Laboratories and Bell Telephone Laboratories" [Wik14a]

Telephone System Feasibility Studies and System Plan", filed with Federal Communications Commission (FCC) in 1971 [Fre10], led to a much better understanding of system planning issues. Mobile Network Operators (MNOs) still apply this principle for system frequency planning today. Although one major issue of spectral resource reuse seemed to be solved, another was still ahead for realizing a real mobile communication system: how to transfer an ongoing connection from one cell to another. This procedure is usually referred to as *handover* or *handoff*[2].

Early mobile communication systems were pure telecommunication systems and part of the PSTN. Mobile telephones were awkwardly shaped and usually mounted in cars or trucks. Further, mobile phone users had to stay within the coverage area of a radio transmitter or Base Station (BS) throughout the phone call, otherwise the call would have been "dropped". There was no handover procedure, i.e., a concept for service continuity and roaming across cells, yet. In 1970 [Joe70], Amos E. Joel Jr. filed a patent on a "three-sided trunk circuit" that should support call handover from one cell to another. In particular, he provided a dual access switching apparatus "wherein communication paths established over communication links to certain cell areas may be switched onto communication links to other cell areas while maintaining continuity of communications between roaming mobile stations" [Joe70]. However, his concept was never implemented, since evolution of digital switching technology was faster. In 1979, Nippon Telegraph and Telephone (NTT) launched the first commercially automated cellular network in Tokyo. In 1981, the Nordic Mobile Telephone (NMT) system was put into operation in Sweden, Finland, Denmark, and Norway. It was the first fully automatic cellular phone system in Europe that implemented a standardized handover procedure and that allowed for combining different cells in a large area into a single network [Mol11].

While the first generation (1G) of mobile communication systems, for example, Nordic Mobile Telephone (NMT) in Sweden or Advanced Mobile Phone System (AMPS) in North America, was based on analog transmission, the second generation (2G) uses digital signaling, therewith, for the first time, enabling system operators and service providers to offer more than telephone services. One example is the Short Message Service (SMS), which

[2]"The term *handover* is more common in British English. It is used within international and European organizations such as ITU-T, IETF, ETSI, and 3GPP, and standardized within European originated standards such as GSM and UMTS. The term handover is more common than *handoff* in academic research publications and literature, while handoff is slightly more common within the IEEE and ANSI organizations. The term handoff is most commonly used within some American organizations such as 3GPP2 and in American originated technologies such as CDMA2000." [Wik12]

was originally thought of as means for notifying the user, e.g., of a deposited voice mail, rather than for user to user communication. Nevertheless, SMS became one of the greatest success stories in 2G networks and still is till today, especially in developing countries [Wor12].

2G systems, such as the European Global System for Mobile Communications (GSM) or the competing Code Division Multiple Access (CDMA) based Interim Standard (IS)-95 developed in U.S., entirely rely on digital transmission schemes between User Equipment (UE) and BS. Further, they efficiently support handovers among cells as well as roaming between networks of different operators or countries. In general, there are different kinds of handover and handover control approaches in Wireless Local Area Networks (WLANs) and cellular networks. In WLANs, triggering of a handover process is solely terminal controlled. Typically, *hard* handovers that follow the *break-before-make* principle are performed, i.e., radio resources in the source cell are released, before new resources are assigned by the target Access Point (AP). In contrast to WLANs, handover decision making in cellular networks is supported by terminal measurements, but finally a network entity that is in charge of managing radio link resources controls handover process initiation and execution. In case a handover process is triggered, the decision making entity ensures that radio resources are reserved at the respective target BS, issues a handover command toward the terminal, and upon completion of link establishment to the target cell, formerly used radio resources are released at the source cell. Furthermore, *soft* handover is typical for CDMA based systems. In soft handover, the UE is simultaneously connected to source and target BS and can receive transmissions from both BSs during handover. If in a CDMA based system a handover occurs between cell sectors of the same BS, this is referred to as *softer* handover.

The third generation of mobile communication systems, 3G, is based on Wideband Code Division Multiple Access (WCDMA) and provides superior data rates compared to 2G systems, and thus a wider range of advanced services, e.g., web browsing or broadband data services. Nowadays, the most convenient and common way of communication is facilitated by using modern handheld devices, such as smartphones.

As our everyday life is more and more dependent on having latest news, guiding information, or various communication services available, mobile radio access to networks providing these services is essential. The current generation of mobile communications, 4G, allows for access to these services, e.g., web services, navigation services, or video telephony. However, the future generation of mobile communications, 5G, will be more than only Internet

anywhere, anytime. Mobile services will be used not only for communication, but also for education, entertainment, healthcare, and commerce. All these desirable capabilities and dimensions concerning various facets of our everyday life imply that the coming generation of mobile communication systems, 5G, will be necessarily a global and versatile communications system or more clearly: wireless and wired networks will inter-operate to provide all forms of communication, information, and entertainment.

Moreover, the development of the next generation of mobile communications, 5G, is envisioned to be driven by demands of the future information society and to exhibit characteristics, such as "amazingly fast", "great service in a crowd", "ubiquitous things communicating", "best experience follows you", and "super real-time and reliable connections" [MET13a].

Human beings utilize wireless communication for satisfying social needs and for achieving practical objectives, e.g., information exchange and organization. With the advent of new mobile communication technologies that facilitate people's need for highly efficient, reliable, and instantaneous communication, the demand for supporting high data rates and seamless connectivity, in particular for mobile services, keeps on growing. Further, the Internet of Things (IoT) is no longer a vision but is becoming reality, as for example, stated by the Organization for Economic Cooperation and Development (OECD) [OEC12]. Forecasts of the Global System for Mobile Communications Association (GSMA) [Glo11] indicate that by 2020 there will be billions of devices, for example, in the Machine-To-Machine (M2M) communication domain, that require wireless connectivity to the Internet and that will also exploit bidirectional Peer-to-Peer (P2P) links, thus locally contributing to and potentially increasing interference in the air. Already today, the heterogeneity of wireless access possibilities imposes challenges for efficient mobility support and resource management across different Radio Access Technologies (RATs). The current situation is characterized by the coexistence of various mobile communication systems, such as GSM, HSPA, LTE, WiMAX, and WLAN, which differ greatly with respect to coverage, spectrum, data rates, Quality of Service (QoS), and mobility support. For example, Figure 1.1 depicts different levels of mobility that are supported by various RATs versus supported data rates that can be provided by each RAT.

Moreover, upcoming 5G technologies, emerging mobile cloud and edge computing, as well as concepts such as "fixed mobile convergence", "always best connected", and "seamless mobility" are driving the evolution toward comprehensive network management approaches, where the Internet Protocol (IP) is regarded as basic control protocol for enabling integrated telecommunication

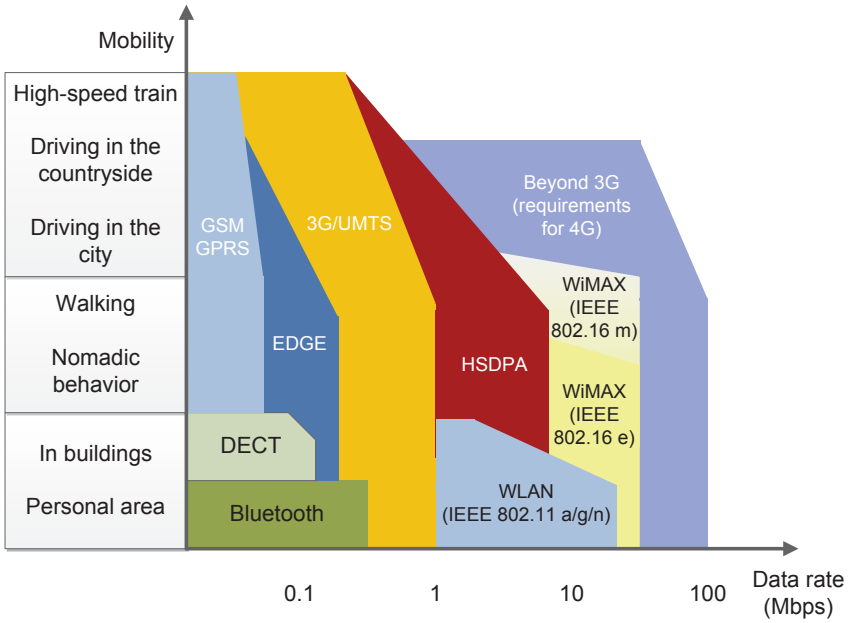

Figure 1.1: Performance of various RATs with respect to mobility and data rates [Asc04]

and multimedia services as well as network convergence [BBM+09]. Further, new topological elements, such as home base stations, femto or phantom cells [KBNI13], and the vision of a more flexible, cognitive shared spectrum usage will result in an even more complex wireless access landscape. The major question arising from these observations is: How can we keep up with this evolution, enable seamless mobility, and enhance user experience?

Hence, this thesis addresses some major challenges in mobile communication systems that are directly related to the afore mentioned issues:

- Development of a multi-Radio Access Network (multi-RAN) evaluation methodology and simulation tool that allows for modeling real-world user mobility, network deployments, handover processes, traffic, and environment, and analyzing the impact of context information on system performance,
- Network selection and Heterogeneous Access Management (HAM) approaches that efficiently realize *seamless mobility* in a heterogeneous network environment using context information,
- Joint Call Admission Control (CAC) and Radio Resource Management (RRM) in multi-RAN scenarios that aims at improving overall resource utilization and service provisioning,
- User movement estimation for enhancing network selection and handover decisions enabling pro-active Radio Resource Management (RRM),

- Development of self-learning and -optimizing capabilities for Mobility Robustness Optimization (MRO) in future RANs.

User mobility and the nature of the wireless links between users and base stations, which are usually modeled as wide sense stationary, random processes, make it extremely difficult to derive a complete analytical model of handover processes in wireless networks. Further, imperfections with respect to measurement accuracies or hardware tolerances require the need for incorporating "noise"-like error terms in every modeling attempt. Hence, any approach for modeling user mobility and related system processes, such as handover parameter adaptations, has to take a number of uncertainties into account. Furthermore, the success and future-proofness of strategies that aim at optimizing network performance, and in particular providing efficient means for robust mobility support, load balancing, and self-optimization, are heavily depending on the availability of context information. Within the scope of this thesis, solutions are proposed to tackle these issues by exploiting context information on technologies, environment, networks, spectrum, terminals, and users provided by Context Management Systems (CMSs) to anticipate future user and network situations. Thus, besides enhanced network selection, handover and resource management decisions, also sophisticated algorithms for MRO, and approaches enabling self-optimization capabilities were developed that yield improved system performance.

In detail, the following contributions with respect to the afore mentioned challenges are provided by the author:

- Architectural concepts and protocols for enabling efficient context management and dissemination in distributed systems [SMKS12b], [SMKS12a], [SLK+11], [SKMS11], [SWM+11], [MKSS11b], [SMKS10a], [MRS+10], [MAS+10], [SMKS10b], [SKMS10], [SKMS09] have been developed. For example, widely deployed wireless sensor and actuator networks that are controlled by computational entities are used to "perceive" physical quantities and act on their environment are envisioned to be integrated with the Future Internet for realizing cyber-physical systems.
- Context information, e.g., user location and movement estimates, are used to improve network selection and handover decisions in a heterogeneous network environment. In several works, the benefit of employing context information, such as user movement estimation based on location and velocity information, for facilitating optimum RAT selection [KMS09], [MKSS09b], [MKSS09a], [MKS11b], efficient multicasting [JSA+09], [CMK+10], [MKSS11a], [MSKS11], intelligent access

for mobile cloud computing [KMSS10], for enhancing Radio Resource Management (RRM) and handover performance [MKSS10], [SWP+10], [KMS+10], [SMK+11], [KRSS14], dynamic spectrum management [KMSS11], [QKS13], autonomous wireless mesh networks [MLKS12], [MLS+12], [MCKS13], [MSC+13] and Device-To-Device (D2D) communications [JKK+14], [JKKS14] was demonstrated.

- Concept for combined Call Admission Control (CAC) and RRM across various RATs that has shown to enhance service provisioning and overall resource utilization in multi-Radio Access Network (RAN) scenarios [KLM+11a], [KLM+11b], [LKMS12],
- Cell transition prediction scheme that exploit knowledge on recurring user movement patterns for pro-actively triggering Load Balancing (LB) actions [KKSS13b], thus improving system performance,
- Fuzzy Q-Learning (FQL) based approach for self-optimizing Handover (HO) parameter adaptations [KKSS13a] whose characteristics highlight its extensibility toward future Self-Organizing/Optimizing Network (SON) use cases. This scheme enables each network node (e.g., BS) to learn the effectiveness of applied, state-dependent actions and to perform optimum HO parameter adaptations according to locally observed conditions, thus establishing context awareness.

Further, with his research work the author contributed to numerous European (FP7: C-CAST, METIS), national (BMBF: ScaleNet, G-Lab, SolarMesh, CoMoRa, PROPHYLAXE), and bilateral industry projects.

The remainder of this thesis is organized as follows: Chapter 2 presents the developed and applied evaluation methodology, including considered RAT characteristics, environment, mobility, and user traffic models as well as the created simulation framework. In Chapter 3, issues and solutions with respect to network selection, Heterogeneous Access Management (HAM), Common Radio Resource Management (CRRM), and intra- and inter-RAT mobility are described. Chapter 4 gives an overview on context awareness, its history, and definitions. Further, it provides an introduction to CMSs and motivates their integration with HAM and SON solutions. Chapter 5 illustrates the incorporation of context management and HAM into an Intelligent Radio Network Access (IRNA) solution and presents first contributions for improving network selection, handover performance, and service provisioning in heterogeneous networks. In Chapter 6, approaches that laid the foundation for developing self-learning and self-optimizing network adaptation schemes are introduced. Chapter 7 provides an overview on recent SON approaches and

describes in detail developed contributions for MRO, including FQL based self-tuning mechanisms. Chapter 8 illustrates and evaluates scenario-specific performance results. Finally, Chapter 9 concludes this thesis, summarizing major findings and providing an outlook on potential future applications and research directions.

2 Multi-Radio Evaluation Methodology and Network Simulation Framework

The performance of mobile communication technologies evolved continuously in the past decade. Enhancements of hardware components and chipsets, efficient link adaptation and scheduling algorithms, as well as the use of novel, cooperative multi-antenna operation modes provided rapid increase with respect to data throughput along with higher system capacity. With the advent of 4G technologies, such as 3GPP's LTE Advanced and IEEE's Mobile WiMAX, the limit of achievable data rates will be pushed even further in regions of hundreds of megabits or even gigabits per second. While the landscape of existing Radio Access Technologies (RATs) becomes more and more diverse, performance comparisons across various RATs become eminent. These multi-radio network evaluations strongly require common baseline assumptions of operating conditions and the use of common metrics for performance assessments. Since the results of system-level simulations considerably vary with the use of different propagation models and interference conditions as well as with the number, distribution, and degree of mobility of users within the considered service area, it is important to carefully report underlying assumptions and parameters used for performance evaluation.

In analytical evaluation approaches [YK07], [SNMRW08], [GPRSA08], [HF08], user arrival times are modeled equivalent to session initiation times, and connection or session durations as realizations of Poisson and exponentially distributed random processes, respectively. However, these models do not account for possible signal level degradations that occur due to user mobility or connection timeouts during Handover (HO) processes due to induced delays.

Typically, system-level performance is evaluated by averaging over a large number of scenario "snapshots". For each "snapshot", users are randomly

dropped into the considered service area. Statistics on individual user link performance are aggregated and cell- or system-level Key Performance Indicators (KPIs) are determined, e.g., spectral efficiency in bit/s/Hz. In this thesis, user movements and thereby triggered HO processes are explicitly modeled and evaluated for the sake of more realistic system performance evaluations. Individual user movements and the physical environment users pass through have a direct impact on user link quality and thus throughput. Further, direction-oriented user mobility inevitably leads to HO processes that are triggered for handing over ongoing sessions from one Base Station (BS) to another. However, these HO processes do not occur instantaneously but induce some delay and thus potentially affect user-specific End-To-End (E2E) performance. The detailed modeling of user mobility and HO processes is particularly relevant for delay-sensitive services that are prone to performance degradation due to delays in data packet delivery. Hence, user mobility may severely affect E2E performance and needs to be considered for realistic system performance evaluation.

Moreover, a multi-RAT evaluation methodology is developed that incorporates realistic modeling of user mobility and allows for jointly evaluating various RATs that differ greatly with respect to cell sizes, transmission schemes, and Radio Resource Management (RRM) aspects. In particular, various cell sizes pose a major problem for multi-RAT deployment modeling, since standard "wrap-around" techniques [ZKAQ01] cannot be applied. In case multiple RAT deployments are to be modeled, the number of BSs and RAT-specific Inter-site Distances (ISDs) or site-to-site (s2s) distances determine the size of the cell layout. For example, if an equal number of cells for all RATs shall be considered, the RAT with the largest ISD defines the size of the cell layout. Further, at least one additional ring of cells of the RAT with the largest ISD and a corresponding number of cells of the RATs with smaller ISDs have to be added in such a way, that the cell layouts of the latter ones are extended up to the borders of the RAT with largest cell sizes. These cells that surround the considered evaluation area are additionally simulated in a multi-cell, multi-RAT evaluation in order to avoid edge effects. In particular, interference from outer cell rings on inner cells is modeled and taken into account. Furthermore, rules for user mobility at the border of evaluation area are to be defined in order to prevent undesired effects or events. For instance, if users are reflected back into reverse direction toward the inner part of the evaluation area as soon as they cross the border of the evaluation area, an increased number of mobility-related events, such as ping-pong HOs, may be observed. Further, this would yield an accidentally high number of

ping-pong HOs at BSs located at the evaluation area border. In essence, this novel multi-cell, multi-RAT evaluation approach extends the framework of "snapshot" based evaluation methodologies that do not account for realistic user mobility or induced delays, e.g., due to HO procedures, and aligns simulation time scales of heterogeneous RATs. Figure 2.1 schematically illustrates the conceptual design approach.

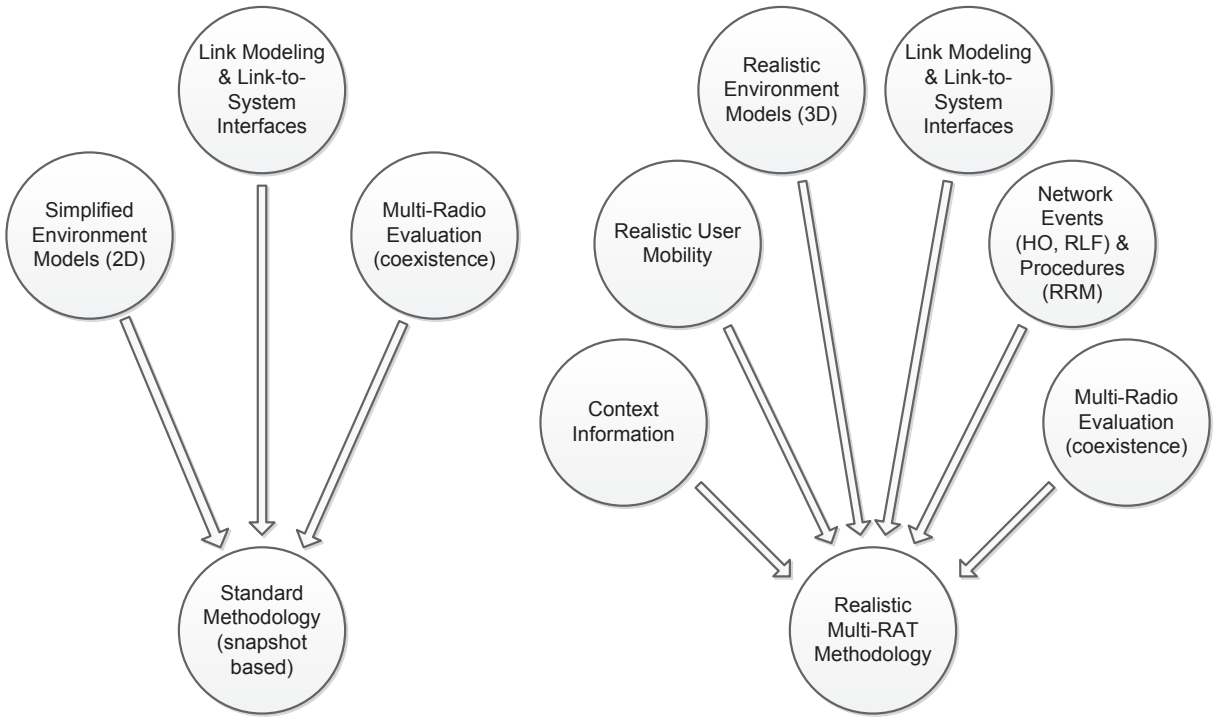

Figure 2.1: New multi-RAT evaluation methodology

Typically, "snapshot" based methodologies employ simplified environment models, such as 2D shadowing maps, and do not consider continuous user movements as well as related network events, such as HO or Radio Link Failure (RLF). In contrast, the developed multi-radio evaluation methodology takes specified user mobility, thereby caused network events and related procedures, realistic 3D environment models, and additional context information into account.

In the following, a review of the state-of-the-art modeling approaches that are used by major standardization bodies and described in various system evaluation methodologies, including [ITU97], [Nex07b], [3GP06], [3GP10a], [IEE08], [IEE05], and [3GP04], is presented. The essence of these modeling approaches lays the basis for the novel multi-RAT evaluation methodology, thus consistency and compatibility with state-of-the art modeling approaches is ensured.

2.1 Radio Access Technologies

For evaluating the performance of the developed solutions presented in Chapter 5 and Chapter 7, the Downlink (DL) characteristics of two major, packet switched RATs, HSDPA [HT07] and LTE [HT09], are considered and modeled in detail in the developed multi-radio network simulation framework (cf. Section 2.8). This includes modeling access and resource management as well as packet transmission emulation on a frame level. Table 2.1 lists typical baseline parameters for RAT-specific performance evaluation. Both RATs exhibit fundamental differences with respect to system architecture, Physical (PHY) and Medium Access Control (MAC) layers, and RRM mechanisms. Their most important DL aspects are briefly summarized in the following subsections.

Table 2.1. RAT-specific DL parameters [3GP06], [IEE08], [HT09], [3GP10a]

Parameters	HSDPA	LTE
Carrier Frequency	2.0 GHz	
Bandwidth	5 MHz	10 MHz
Cell layout	Hexagonal grid, 19 cell sites, 3 sectors per site	
Site-to-site distances	500, 1732 m	
Antenna patterns (horizontal)	$A_H(\varphi) = -\min\left[12\left(\frac{\varphi}{\varphi_{3\text{dB}}}\right)^2, A_m\right]$, $\varphi_{3\text{dB}} = 70°$, $A_m = 20$ dB	$A_H(\varphi) = -\min\left[12\left(\frac{\varphi}{\varphi_{3\text{dB}}}\right)^2, A_m\right]$, $\varphi_{3\text{dB}} = 70°$, $A_m = 25$ dB
Antenna patterns (vertical)		$A_V(\theta) = -\min\left[12\left(\frac{\theta-\theta_{\text{etilt}}}{\theta_{3\text{dB}}}\right)^2, SLA_V\right]$, $\theta_{3\text{dB}} = 10°$, $SLA_V = 20$ dB, θ_{etilt} is the electrical downtilt (case 1: 15°, case 3: 6°)
Combining method for 3D antenna pattern	$A(\varphi,\theta) = -\min\left\{-\left[A_H(\varphi)+A_V(\theta)\right], A_m\right\}$	
Antenna main lobe gain (horizontal)	17 dBi	
BS noise figure	5 dB	
BS cable loss	2 dB	
UE noise figure	7 dB	
Thermal noise power	-174 dBm/Hz + 10 $\log_{10}(B$ (Hz))	
BS Tx power	43 dBm for 5 MHz	46 dBm for 10 MHz

2.1.1 High Speed Downlink Packet Access (HSDPA)

The PHY layer of HSDPA (3GPP Release 5) is based on Wideband Code Division Multiple Access (WCDMA), where a fix Spreading Factor (SF) of 16, denoted by ψ, is used for High Speed-Physical Downlink Shared Channel (HS-PDSCH) transmissions. For one user transmission up to 15 orthogonal spreading codes can be allocated. Further, fast PHY layer retransmissions, a lower scheduling or Transmission Time Interval (TTI) of 2 ms, and 16-QAM modulation yield a resulting gross data rate of 14 Mbps (peak bit rate = max{TBS}/TTI, UE cat. 10: 27952/2 ms [3GP12d]) or even 28 Mbps when exploiting macro diversity. Often, HSDPA peak bit rates are approximated using the following formula:

$$\begin{aligned} R &= \frac{N_c}{\psi} W \log_2 M \\ &= \frac{15}{16} 3.84 \text{ Mcps } 4 \frac{\text{bit}}{\text{chip}} \\ &= 14.4 \text{ Mbps}, \end{aligned} \tag{2.1}$$

where N_c denotes the number of allocated spreading codes, ψ the corresponding spreading factor, W the WCDMA chip rate, and M the size of the modulation alphabet. The WCDMA PHY layer frame structure is depicted in Figure 2.2.

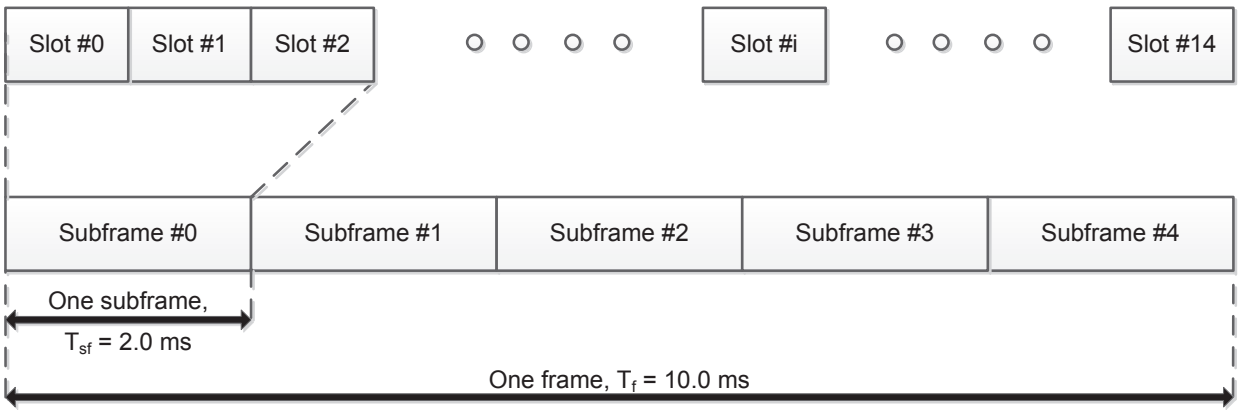

Figure 2.2: HSDPA frame structure [3GP10b]

The basic resources in WCDMA systems are transmit power and spreading codes. RRM entities in HSDPA networks, such as Radio Network Controller (RNC), have to assess whether enough resources are available for serving a terminal at a specific location by a certain BS, also referred to as Node B (NB). Therefore, it is necessary to calculate required transmit power for providing a certain Quality of Service (QoS) given UE's receive conditions

and service requirements. According to [SHLSW00], the required transmit power for a considered UE i can be determined as follows:

$$p_i = \frac{\xi_i \; R_i}{W} \left((1-\alpha_i) \; P + P \sum_{n=1, n\neq m}^{N} \frac{L_{m,i}}{L_{n,i}} + P_N \; L_{m,i} \right), \tag{2.2}$$

where ξ_i is the E_b/N_0 requirement of the requested service of UE i, R_i denotes its required bit rate, W is the chip rate, P is the total transmit power of the BS, N is the number of relevant neighboring BSs, α_i is the *orthogonality* factor modeling the impact of multipath propagation conditions, $L_{m,i}$ is the path loss from the serving BS m, $L_{n,i}$ is the path loss from another, neighboring BS n to UE i, and P_N is the thermal noise power. Further, in order to assess current BS load situation, DL load can be calculated using the following equation [SHLSW00]:

$$\chi_{DL} = \sum_{i=1}^{N_{UE}} \left[\frac{\xi_i \; R_i \; a_i}{W} \left((1-\alpha_i) + \sum_{n=1, n\neq m}^{N} \frac{L_{m,i}}{L_{n,i}} \right) \right], \tag{2.3}$$

where N_{UE} is the total number of served UEs and a_i is the channel activity factor for each considered UE i. In order to account for realistic operation conditions, a 20% overhead is considered. The overhead incorporates an efficiency loss of 10% due to Common Pilot Channel (CPICH) and usage of 10% of transmission power for other common channel operations [EMN00].

In order to determine achievable data rates on system level given current Signal-to-Interference-plus-Noise Ratio (SINR) conditions, a generic link-to-system level interface is required. This interface greatly reduces additional processing overhead for system level simulations, since starting a separate link level simulation per active link during system level evaluation would significantly increase overall simulation time. For determining user receive conditions, the so-called *geometry* or *G-factor* is used for system level evaluation and is defined as the average own cell power I_{or} to the other-cell power plus noise ratio I_{oc} [HT07]. With WCDMA and OFDMA in a wide system bandwidth this corresponds to the average wideband signal to interference plus noise power ratio (SINR) [MNK+07]:

$$G = \frac{I_{or}}{I_{oc}} = \frac{RSRP_m}{\sum_{n=1, n\neq m}^{N} RSRP_n + P_N}, \tag{2.4}$$

where $RSRP_m$ and $RSRP_n$ denote the Reference Signal Received Power (RSRP) values of the connected and neighboring BSs, respectively, and $P_N = k \; T_0 \; B$

represents the thermal noise power determined by the Boltzmann constant $k = 1.3806504 \cdot 10^{-23}$, ambient temperature $T_0 = 290$ K, and system bandwidth B (cf. Table 2.1).

2.1.2 Long Term Evolution (LTE)

In contrast to HSDPA, LTE (3GPP Release 8) utilizes a completely different transmission scheme that is based on Orthogonal Frequency Division Multiplexing (OFDM). Medium access is organized by assigning two-dimensional resources, so-called Physical Resource Blocks (PRBs) each of 180 kHz bandwidth, to DL data transmissions. Further, scheduling is performed on a TTI basis (TTI = 1 ms) that supports the beneficial utilization of fast link adaptation techniques, such as AMC and HARQ retransmission protocols. Assuming 20 MHz transmission bandwidth, 64-QAM modulation, no MIMO antenna operation, a gross data rate of approximately 75 Mbps (peak bit rate = 75376/1 ms [3GP12c]) can be achieved. Typically, the DL peak bit rate is advertised as approximately 100 Mbps, which results from the following equation [Kle08]:

$$\begin{aligned} R &= \Delta f \; N_{sc} \; \frac{\log_2 M}{1 + G_{CP}} \\ &= 15 \text{ kHz } 1200 \; \frac{6 \text{ bit}}{1 + 1/14} \\ &\approx 100 \text{ Mbps}, \end{aligned} \tag{2.5}$$

where Δf denotes the subcarrier spacing of 15 kHz, N_{sc} the overall number of subcarriers for the given bandwidth, M the size of the modulation alphabet, and G_{CP} the ratio of cyclic prefix time to effective symbol time. However, the number of subcarriers or two-dimensional resource elements that are used for user data transmissions on PDSCH is usually smaller, thus resulting in a smaller transport block size. The LTE frame structure is depicted in Figure 2.3.

The DL load in a LTE system is determined based on the number of currently assigned N_{PRB}^{use} and totally available PRBs N_{PRB}^{tot} as follows:

$$\chi_{DL} = \frac{N_{PRB}^{use}}{N_{PRB}^{tot}}, \tag{2.6}$$

Further, overhead due to control signaling (e.g., PBCH and CCCH), synchronization signals, and pilot symbol based channel estimation could be taken into account by reducing the N_{PRB}^{tot} accordingly. In this thesis, a constant

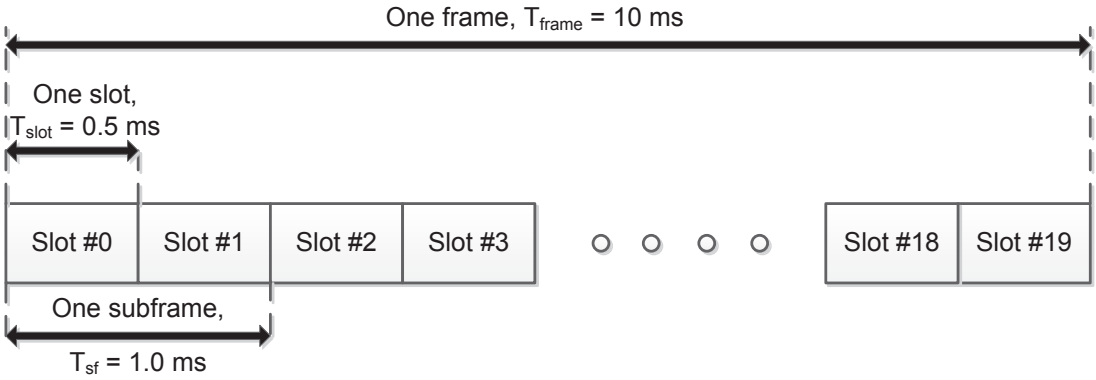

Figure 2.3: LTE frame structure (FDD) [3GP12b]

overhead of 6 PRBs per TTI is considered, which corresponds to 12% or 1.08 MHz, resulting in $N_{PRB}^{tot} = 44$ given 10 MHz system bandwidth.

2.1.3 Link-To-System Interfaces and Modeling of Packet Error Rates

The link-to-system approaches described in the following are based on SISO system operation, i.e., only a single transmit and receive antenna are used for user data transmission and reception, respectively. The link-to-system interface used for HSDPA system-level evaluations accounts for the fact that 15 of the 16 SF spreading codes ($\psi = 16$) can be assigned for user data transmissions, resulting in the following G-factor dependent approximation for effective SINR values ξ [HT07]:

$$\xi = \frac{W}{R} \frac{P_i}{P_{tot,m}} \frac{1}{(1-\alpha_i)+G^{-1}} = \psi \frac{P_i}{P_{tot,m}} \frac{1}{(1-\alpha_i)+G^{-1}}, \tag{2.7}$$

where the fraction $\frac{W}{R}$ is quantized taking into account the discrete set of SFs ψ, P_i is the transmit power assigned to HSDPA transmission of UE i, and $P_{tot,m}$ is the total transmit power of BS m. Further, Shannon's link capacity formula given AWGN channel conditions is used for approximating link-level data rates of HSDPA transmissions as follows [Sha48]:

$$R = W \log_2(1+\xi) = \frac{3.84\ N_c}{\psi} \log_2\left(1+\frac{\xi\ \psi}{N_c}\right) \text{ Mbps}, \tag{2.8}$$

where N_c represents the number of spreading codes assigned to the respective transmission.

Similarly as in the case of HSDPA system level evaluations, the G-factor is used for describing user receive conditions in LTE system-level simulations.

Moreover, a link-to-system interface is utilized that incorporates technology-specific features, such as frequency domain packet scheduling (FDPS), as well as efficiency losses, e.g., due to control signaling overhead, and yields a mapping of G-factor values onto spectral efficiency [MNK+07]. In particular, efficiency losses due to bandwidth efficiency (50 PRBs with 180 kHz each only yield 9 MHz bandwidth), cyclic prefix (normal cyclic prefix length results in $G_{CP} = 1/14$), and overhead due to pilot symbol assisted channel estimation and dedicated as well as common control channels are taken into account. Thus, the resulting effective user data rates are determined as follows [MNK+07]:

$$R = B_{eff} \; B \; \log_2\left(1 + \xi/\xi_{eff}\right), \tag{2.9}$$

where B_{eff} and ξ_{eff} are set to 0.6 and 1, respectively. Equation (2.9) approximates transport format switching behavior and AMC operation, respectively. Additionally, in order to model the impact of packet transmission errors on E2E system-level performance, the following procedure is applied:

- Based on channel state information as well as the RAT-specific RLC SDU size and link-to-system mapping (e.g., cf. Equation (2.9)), the number of packets for PHY layer transmissions is derived. First, the number of packets that can be transmitted $N_{\mathrm{pks}_{\mathrm{pre}}}$ are determined as the minimum of the packets in the scheduler queue and the estimated number of transmittable packets based on channel quality feedback, i.e., the channel state information of the previous time instance. Then, the number of packets that could be transmitted $N_{\mathrm{pks}_{\mathrm{inst}}}$ is calculated based on the current channel state information. In real systems, the current channel state information is not instantaneously available for scheduling decisions and is not known until channel measurements have been signaled by the UE in the UL, resulting in delayed feedback. However, in the simulation tool, the instantaneous channel state information can be immediately used for determining $N_{\mathrm{pks}_{\mathrm{inst}}}$.
- For each scheduled transmission, the number of packets that can be transmitted $N_{\mathrm{pks}_{\mathrm{pre}}}$ based on channel quality feedback is compared with the number of packets that could be transmitted $N_{\mathrm{pks}_{\mathrm{inst}}}$ given instantaneous channel state information. Therefore, the ratio of the number of packets ϱ is calculated as follows:

$$\varrho = \begin{cases} \dfrac{N_{\mathrm{pks}_{\mathrm{pre}}}}{N_{\mathrm{pks}_{\mathrm{inst}}}} & \text{if } N_{\mathrm{pks}_{\mathrm{inst}}} > 1, \\ N_{\mathrm{pks}_{\mathrm{pre}}} & \text{otherwise,} \end{cases} \tag{2.10}$$

where $N_{\mathrm{pks}_{\mathrm{pre}}}$ and $N_{\mathrm{pks}_{\mathrm{inst}}}$ are the number of packets that can be transmitted considering previous and instantaneous channel state information, respectively.

- Further, a simplified modeling approach that aims at accounting for the impact of link transmission errors and imitating the behavior of link adaptation techniques without the need for conducting separate link level simulations in parallel was developed. Typically, link level performance is represented by Block Error Rate (BLER) curves, sometimes also referred to as *waterfall* curves [Fit92] due to their characteristic shapes, as shown in Figure 2.4(a). The behavior of link adaptation techniques, such as Modulation and Coding Scheme (MCS) adaptation, can be imitated by approximating the transport format switching behavior depicted in Figure 2.4(b).

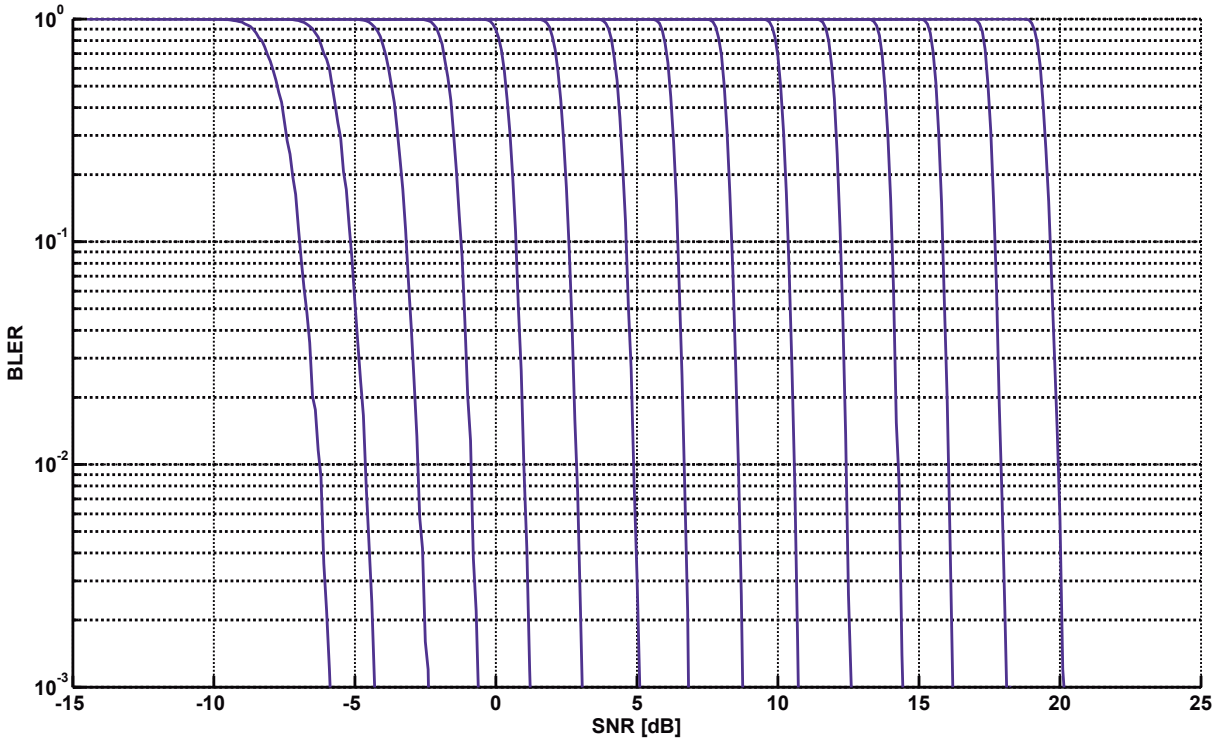

(a) BLER curves obtained from SISO AWGN simulations for all 15 CQI values (from CQI 1 (leftmost) to CQI 15 (rightmost))

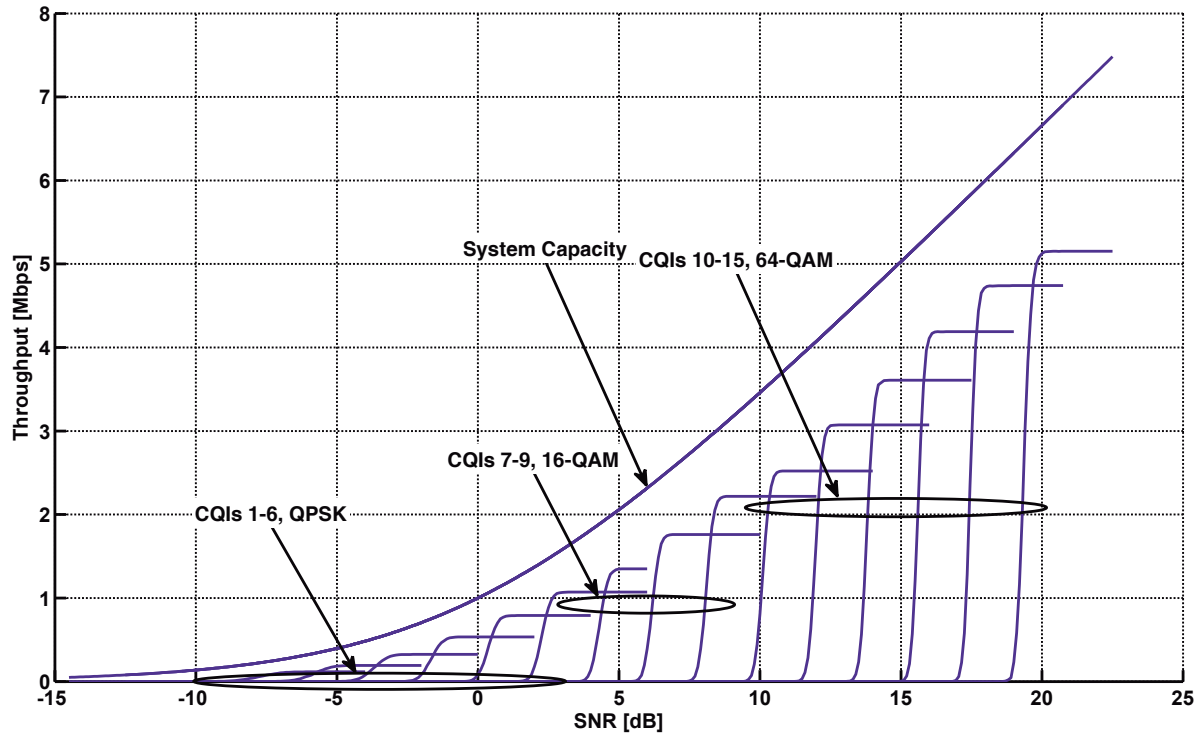

(b) Throughput performance over an AWGN channel for individual CQIs without HARQ

Figure 2.4: BLER curves and throughput performance over an AWGN channel for LTE (cf. [MWI+09])

- Further, two E2E performance schemes have been defined: 90%/90% and 95%/95%. For instance, the 95%/95% scheme guarantees that 95% of the scheduled users receive 95% of their RLC packets error-free. Moreover, for a delay-sensitive service, such as VoIP, it is ensured that 95% of packets are delivered within a pre-defined amount of time depending on a service-specific timeout value. In this thesis, two E2E performance schemes have been considered and two functions were calibrated to meet the respective E2E performance criteria. The packet ratio ϱ is used as input for these functions that map ϱ on the respective Packet Error Rate (PER). They are illustrated in Figure 2.5 and defined as follows:

$$\Omega_{90/90}(\varrho) = \arctan(50\ (\varrho - 0.95))/\pi + 0.5, \tag{2.11}$$

$$\Omega_{95/95}(\varrho) = \arctan(50\ (\varrho - 0.5))/\pi + 0.5, \tag{2.12}$$

In order to model the impact of transmission errors and imitate transport format switching upon transmission errors, a random experiment is carried out for each packet transmission. For this purpose, a uniformly distributed random variable is drawn and compared with the output value of the function that tries to emulate the E2E performance policy, e.g., Equation (2.11). If the random variable is less than $\Omega(\varrho)$, the packet transmissions is considered error-free. Otherwise, a retransmission may be triggered.

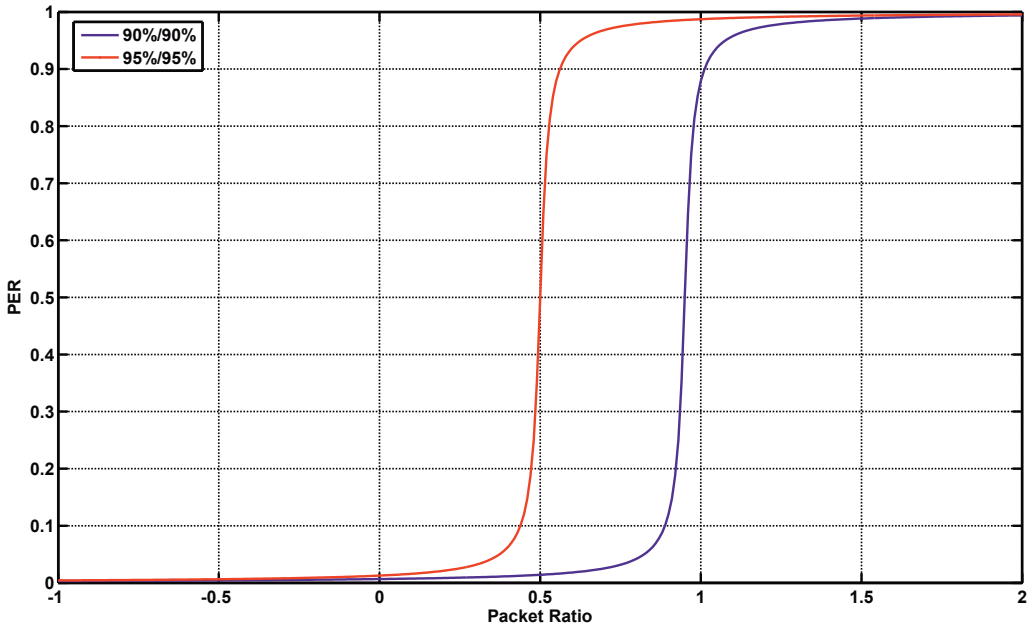

Figure 2.5: Packet error emulation functions

2.2 Deployment Models

In the following subsections, details on modeling the radio propagation environment, typical processes affecting radio propagation, and baseline parameters for evaluating macro-cell deployments, which emanate from evaluation methodologies of NGMN [Nex07b], 3GPP [3GP06], IEEE [IEE08], [IEE05], and 3GPP2 [3GP04], are stated.

2.2.1 Cell Layout and Radio Propagation

All organizations, such as NGMN, 3GPP, IEEE, and 3GPP2, agreed on a common site layout, where a hexagonal grid with 19 cells, three sector antennas per site, and evaluation area wrap around is considered, i.e., terminals leaving the service area will enter the cell layout again at the corresponding position of the opposite border. However, the standard wrap around approach exhibits limitations when trying to evaluate multi-radio network scenarios. As soon as site-to-site distances are chosen that are not multiples of each other or where the centers of the cell layouts are shifted by an arbitrarily chosen offset, a sophisticated process for aligning these overlapping layouts would be required. In order to avoid this burden, the developed multi-radio network simulation framework offers the possibility of creating several overlapping cell layouts with varying numbers and locations of BSs (e.g., at the intersection of 3 sectors or at cell center) and with different site-to-site distances. Further, a so-called evaluation area border is defined as a circle around the center BS of the RAT with the largest site-to-site distances. Users reaching the limits of the evaluation area bounce back with a randomly chosen direction as illustrated in Figure 2.6 for the single RAT case, where a group of users "hits" the evaluation area border.

The typical propagation law, where path loss depends on separation between transmitter and receiver as well as on the transmission's carrier frequency, is applicable for scenarios in urban and suburban areas outside the high rise core where the buildings are of nearly uniform height [ITU97]:

$$L = 40\ (1 - 4 \cdot 10^{-3}\ \Delta h_b)\ \log_{10} R - 18\ \log_{10} \Delta h_b + 21\ \log_{10} f + 80, \quad (2.13)$$

where R denotes the separation between BS and UE in km, f is the carrier frequency in MHz, and Δh_b denotes the BS height in m, measured from the average rooftop level. Typically, the BS antenna height is fixed at 15 m above the average rooftop, i.e., $\Delta h_b = 15$ m. Further, applying a carrier frequency

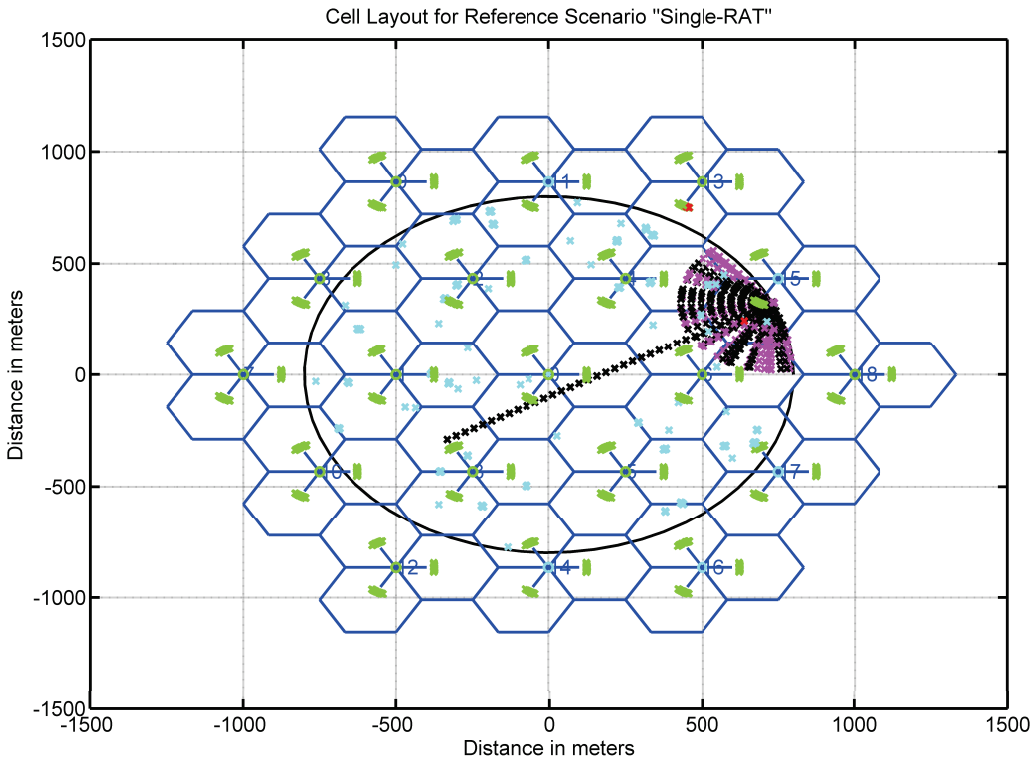

Figure 2.6: Evaluation area

of 2 GHz results in a simplified radio propagation law:

$$L = 128.1 + 37.6 \log_{10} R, \tag{2.14}$$

that is used in 3GPP's evaluation methodologies [3GP06], [3GP10a]. However, the derived path loss, which indicates loss of transmitted signal power depending on distance and carrier frequency, shall in no circumstances be less than the free space loss (between isotropic antennas) [ITU97]:

$$\begin{aligned} L &= -10 \log_{10} \left(\frac{\lambda}{4 \pi R} \right)^2 \\ &= 20 \log_{10} \left(\frac{4 \pi R}{\lambda} \right) \\ &= 20 \log_{10} \left(\frac{4 \pi R f}{c_0} \right) \\ &= 20 \left[\log_{10} \left(\frac{4 \pi}{c_0 / 10^9} \right) + \log_{10} (R/1000) + \log_{10} \left(f/10^6 \right) \right] \\ &= 20 \log_{10} \left(\frac{4 \pi}{c_0 / 10^9} \right) + 20 \log_{10} R' + 20 \log_{10} f' \\ &\approx 32.45 + 20 \log_{10} R' + 20 \log_{10} f', \end{aligned} \tag{2.15}$$

where c_0 denotes the speed of light, R' states the distance between transmitter and receiver in km, and f' denotes the carrier frequency in MHz.

2.2.2 Shadowing and Fast Fading

The performance of wireless communication is naturally limited by the mobile radio channel and the environment of transmitters and receivers. The transmission path between the transmitter and the receiver can vary from line-of-sight to one that is severely obstructed by buildings, mountains, and foliage. Further, physical effects inherent to electromagnetic radio wave propagation, such as reflection, refraction, diffraction, and scattering, induce performance losses as well. Since most cellular radio systems operate in urban areas, the presence of high-rise buildings causes severe diffraction losses and usually, there is no line-of-sight transmission path between the transmitter and the receiver. Due to multiple reflections of the electromagnetic wave from various, in particular metal, objects, multiple, usually weaker signal copies arise and travel along different paths of varying length and may superpose at the receiver's location in a constructive or destructive manner. Additionally, the speed of motion influences how rapidly the signal power level fades as a mobile terminal moves [TV05] and the direction of the relative movement of transmitter and receiver affects the received signal frequency. This physical effect is also referred to as *Doppler* shift. Characteristics of the mobile radio channel are the random variations over frequency and time. These variations can be roughly divided into two types:

- *Large-scale fading*:
  - The strength of the transmitted signal decreases as the distance between the transmitter and the receiver increases (*propagation loss*). If the signal is greatly attenuated, it vanishes.
  - Large objects, such as buildings and hills, prevent the user's terminal from signal reception (*shadowing*) and due to the user's motion, signal paths may appear or disappear at the receiver.

  Large-scale fading occurs as the mobile moves through a distance of the order of a cell size and is typically frequency independent. It is also referred to as *slow fading*.
- *Small-scale fading*:
  - Multiple signal paths superpose at the receiver in a constructive and/or destructive manner.

  Small-scale fading occurs at the spatial scale of the order of the carrier wavelength and is frequency dependent. It is also referred to as *fast*

fading.

The standard shadow fading model, as recommended by [3GP06], [Nex07b], [IEE08], and [3GP10a], is the so-called *Gudmundson* model [Gud91] that models shadowing as log-normally distributed random variables with zero mean and a standard deviation of 8 dB, where good fitting results are achieved in suburban areas. In case of macro cell deployments, a typical correlation distance is 50 m [3GP06] and shadowing correlation between cells and sectors is assumed to be 0.5 and 1.0 [EMN00], [3GP06], respectively. The realizations of the slow fading process vary with distance Δx, thus shadowing values of spatially adjacent locations are correlated. The term correlation distance refers to the fact that there exists a location- and environment-specific correlation between spatial shadowing realizations. For example, if a user moves away from its original position by a linear distance larger than the correlation distance, the shadowing realizations experienced by the user at previous and current locations can be considered as uncorrelated. The normalized autocorrelation function $R(\Delta x)$ of the slow fading process can be described with sufficient accuracy by an exponential function [Gud91]:

$$R(\Delta x) = \sigma^2 \, \varepsilon_D^{\frac{|\Delta x|}{D}} = \sigma^2 \, \varepsilon_D^{\frac{\nu \, T}{D}}, \tag{2.16}$$

where ε_D is the correlation between two random variable realizations separated by distance D, ν the UE velocity, and T the sampling interval. In order to accelerate simulation runs a two-dimensional shadowing grid is precomputed with a resolution of 50 meters, which corresponds to the correlation distance. Shadowing factors (SDFs) ς for a specific location $g_{k,l}$ are derived by linear interpolation according to [IEE08]:

$$\begin{aligned} \varsigma(g_{k,l}) \;=\; & \sqrt{1-\frac{x_{\text{pos}}}{d_{\text{corr}}}} \left[S_{0,l} \sqrt{\frac{y_{\text{pos}}}{d_{\text{corr}}}} + S_{3,l} \sqrt{1-\frac{y_{\text{pos}}}{d_{\text{corr}}}} \right] \\ & + \sqrt{\frac{x_{\text{pos}}}{d_{\text{corr}}}} \left[S_{1,l} \sqrt{\frac{y_{\text{pos}}}{d_{\text{corr}}}} + S_{2,l} \sqrt{1-\frac{y_{\text{pos}}}{d_{\text{corr}}}} \right], \end{aligned} \tag{2.17}$$

where the shadowing grid values $\{S_{0,l}, S_{1,l}, S_{2,l}, S_{3,l}\}$ of the respective squares, in which the currently considered BS or UE are located, are determined first. d_{corr} denotes the pre-defined correlation distance and x_{pos} and y_{pos} the corresponding offsets within the considered shadowing grid square with respect to the x- and y-axis, respectively. Figure 2.7 exemplarily illustrates the afore mentioned parameters.

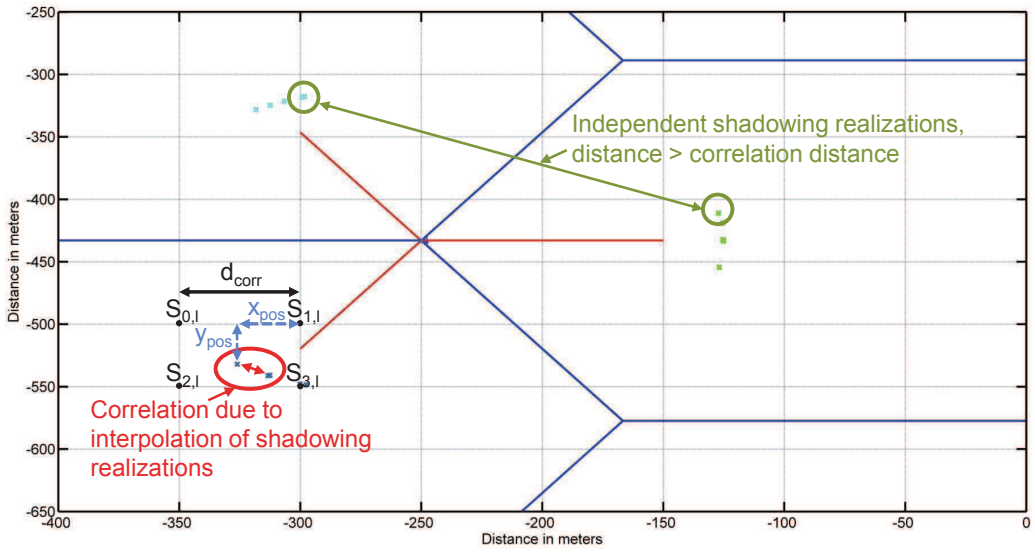

Figure 2.7: Exemplary shadowing factor grid and shadowing realizations obtained via interpolation

Finally, the effective shadowing factor ς_{eff} is calculated as follows [IEE08]:

$$\varsigma_{\text{eff}} = a\ \varsigma_{\text{UE}} + b\ \varsigma_{\text{BS}}, \tag{2.18}$$

where $a^2 = b^2 = 1/2$. Figure 2.8 depicts resulting shadowing factors of the considered evaluation area.

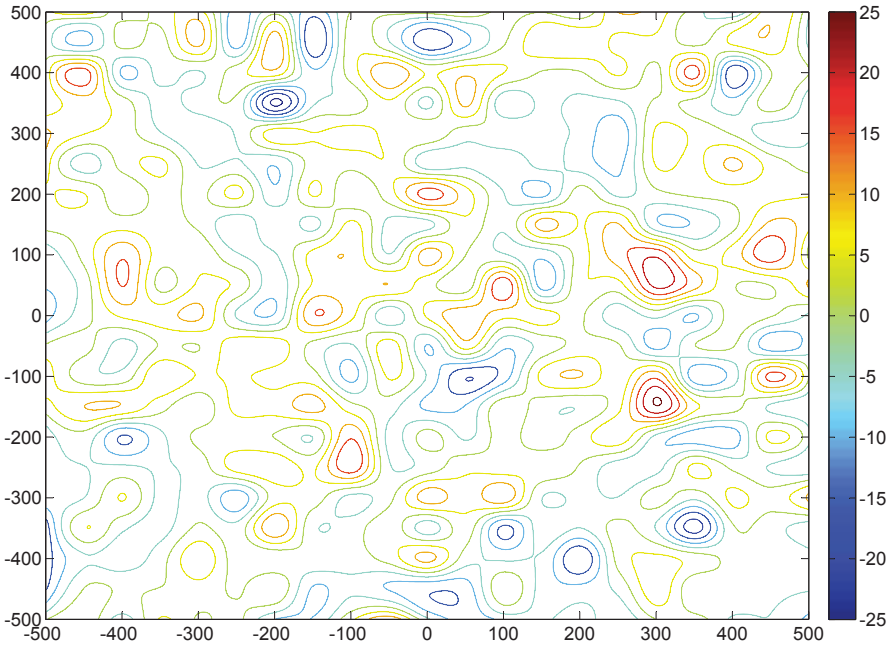

Figure 2.8: Interpolated shadowing map (in dB)

Further, path loss and geometry intensity maps that account for effective BS antenna patterns (cf. Table 2.1) are illustrated in Figure 2.9(a) and Fig-

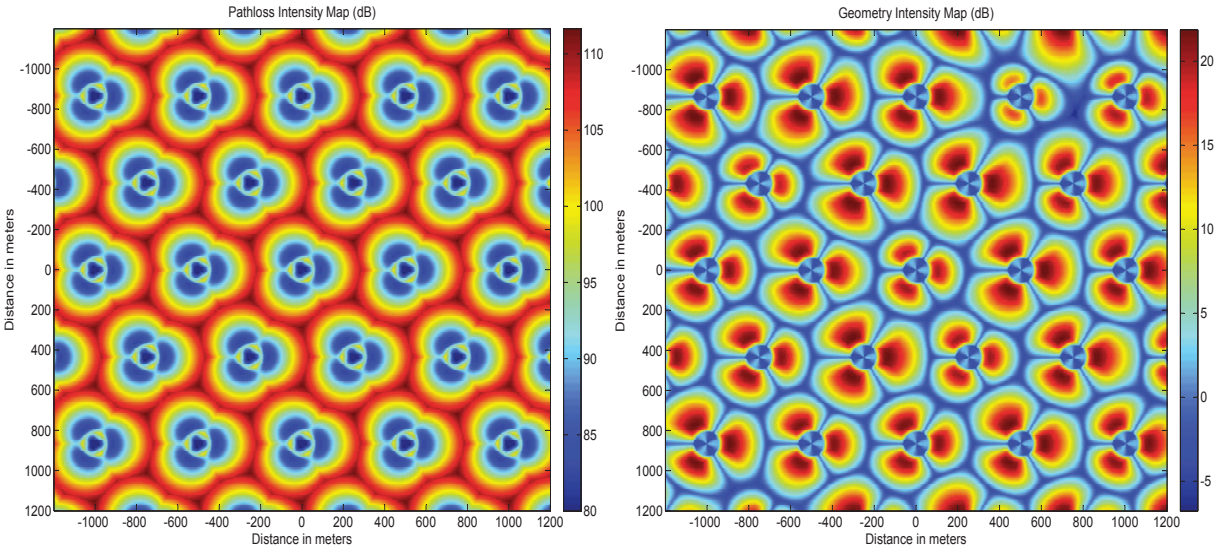

(a) Path loss intensity map

(b) Geometry intensity map

Figure 2.9: Path loss and geometry intensity map in dB

ure 2.9(b), respectively. In order to account for the impact of frequency- and velocity-dependent fading on received signal strength values, a pre-calculated fast fading trace [YB00] is sampled during simulation and used for link-level evaluation of instantaneous SINR values. However, for modeling more realistic scenarios, new three dimensional models are required that reflect the heterogeneity of today's living spaces and that incorporate typical building development dependent effects, such as street corner effects, or ray tracing results for environments that bear high probabilities for reflection, refraction, and diffraction. An example for system level network performance evaluation incorporating realistic deployment, propagation, and user mobility models is presented in Section 5.2.4.

2.3 User Mobility Models

In order to evaluate mobility-related Radio Access Network (RAN) performance as well as the performance of different HO optimization and Load Balancing (LB) strategies in detail, user mobility needs to be modeled as realistically as possible. In [CBD02], Camp et al. propose to classify mobility models into *entity mobility models*, where entity movements are independent of each other, and *group mobility models*, where entity movements are dependent on each other. Further, mobility models used in simulation tools can be differentiated into two types: traces based and synthetic models [CBD02]. Typically, traces are based on observed and recorded user movement patterns

in real-world environments. Traces based models can be used, if a specific real-world scenario is to be modeled, e.g., for network optimization purposes. However, creating traces based models involves collecting a large amount of user data, e.g., movements, for a reasonably long period of time. Further, for handling large data volumes in a large scale network simulation, adequate computational resources are required. In contrast, synthetic models attempt to realistically represent and imitate real-world behavior, e.g., user movements, without the use of traces. In the following, different synthetic entity mobility models are listed [CBD02] and described in more detail in the following paragraphs:

- Random walk mobility model,
- Random waypoint mobility model,
- Random direction mobility model,
- Boundless simulation area mobility model,
- Gauss-Markov mobility model,
- Probabilistic version of random walk mobility model,
- City section (Manhattan) mobility model.

Random Walk Mobility Model

The random walk mobility model is a widely used mobility model that tries to imitate the behavior of entities in nature that move in extremely unpredictable ways. Sometimes it is also referred to as *Brownian* motion, where movements originate from observations of random particle movements of a gas or liquid that are attributed to thermal molecular movements. Each particle movement is assumed to be independent of the movements of other particles. In the random walk mobility model, an entity, e.g., user, moves from one location to another by randomly selecting a velocity and direction, i.e., angle, in which to travel from pre-defined ranges, $[v_{\min}, v_{\max}]$ and $[0, 2\pi]$, respectively. Typically, each entity movement occurs in either a constant time interval T or a constant distance traveled d, at the end of which a new direction and velocity are determined [CBD02].

Simplified Random Walk Mobility Model

Besides modeling simple user movements on straight lines, such as streets, railway tracks, etc., or circular movements, a simplified user mobility model has been implemented in this thesis, which yields random walk-like user movements.

In this random walk-like mobility model, user velocity v is kept fix according to the value initialized at simulation setup, while the maximum deviation from current UE direction compared to the previous simulation time step may vary by angle θ_{max} that is calculated as follows:

$$\theta_{\max} = \pi \exp(-v/v_m), \tag{2.19}$$

where $v_m = 20$ m/s is a normalization factor used to yield realistic movements. The maximum angle of deviation depends on the UE speed. In case of slow moving users, it is more likely that deviations from the previous course will be larger than in case of fast moving users. The deviation angle θ per UE is updated at each simulation time step by drawing a random number from a uniform distribution of random variables between $-\theta_{max}$ and $+\theta_{max}$. In Figure 2.10, two exemplary user trajectories of users moving at 3 and 120 km/h, respectively, are illustrated.

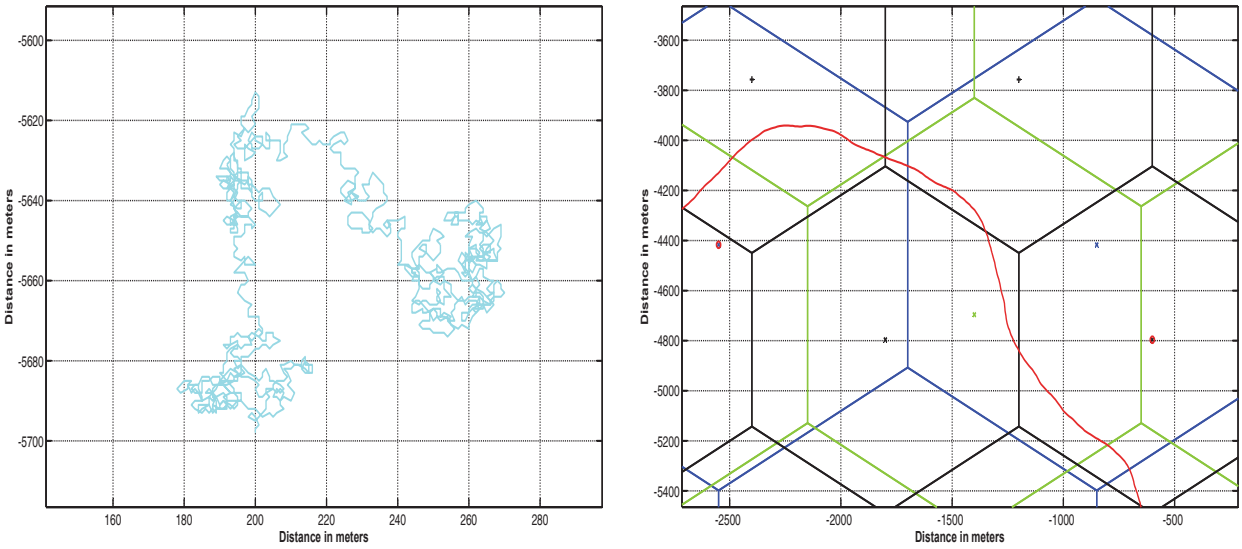

(a) $v = 3$ km/h (b) $v = 120$ km/h

Figure 2.10: Random walk-like movements

Random Waypoint Mobility Model

The random waypoint mobility model is similar to the random walk mobility model and also widely used. In contrast to the random walk mobility model, it includes pre-defined entity pause times between changes in direction and/or velocity. The considered entity stays in one location until the pause time expires. Then, it chooses a random destination in the considered evaluation area and a uniformly distributed velocity from the range of $[v_{\min}, v_{\max}]$, and

travels toward the chosen destination. Upon arrival, the entity remains idle for specified pause time before starting the process again [CBD02].

Random Direction Mobility Model

The random direction mobility model was developed to overcome a limitation of the random waypoint mobility model. In the random waypoint mobility model, there is a high probability that an entity will select a destination located in the center of the evaluation area or a destination that requires traveling through the middle of the evaluation area, which results in a high concentration of entities in a certain part of the evaluation area. In the random direction mobility model, an entity randomly selects a direction in which to travel similar to the random walk mobility model. Then, it moves into the chosen direction until the evaluation area border is reached. Here, it remains idle for a specified amount of time. When the pause time is expired, the entity randomly selects a new direction from an interval of uniformly distributed angles ranging from $[0, \pi]$ and continues the process [CBD02]. There also exists a modification of this model, where moving entities are no longer forced to reach evaluation area boundary before stopping to change direction [CBD02]. Instead, after selecting a random direction, a destination anywhere along that direction of travel can be chosen. Here, the moving entity pauses before randomly selecting a new direction. In essence, movement patterns generated using this modified random direction mobility model could be simulated by the random walk mobility model with pause times [CBD02].

Boundless Simulation Area Mobility Model

The boundless simulation area mobility model exhibits two characteristics that are different from the previously described mobility models. First of all, there is a relationship between previous and current travel direction and velocity of moving entities. Both velocity and position vectors are updated at every time step Δt as follows [CBD02]:

$$\begin{aligned} v(t+\Delta t) &= \min\{\max[v(t)+\Delta v, 0], v_{\max}\}, \\ \theta(t+\Delta t) &= \theta(t)+\Delta\theta, \\ x(t+\Delta t) &= x(t)+v(t)\ \cos(\theta(t)), \\ y(t+\Delta t) &= y(t)+v(t)\ \sin(\theta(t)), \end{aligned} \tag{2.20}$$

where $v_{\max}$ is the maximum defined velocity, Δv is the change in velocity that is uniformly distributed between $[-A_{\max}\Delta t, +A_{\max}\Delta t]$, $A_{\max}$ is the maximum

acceleration of a given entity, $\Delta\theta$ is the change in direction that is uniformly distributed between $[-\alpha,+\alpha]$, and α is the maximum angular change in the direction a moving entity is traveling [CBD02].

Further in the boundless simulation area mobility model, the way how the moving entities behave at the boundary of the evaluation area is different. In contrast to the afore mentioned models, the moving entities are not reflected off the evaluation area boundary or do not pause for a pre-defined amount of time. The moving entities that reach one side of the evaluation area continue traveling and reappear on the opposite side of the evaluation area, thus creating a torus-shaped evaluation area enabling moving entities to travel unhampered [CBD02].

Gauss-Markov Mobility Model

In general, the Gauss-Markov mobility model was designed to adapt to different levels of randomness via one tuning parameter α [CBD02]. In the Gauss-Markov mobility model, each entity is initially assigned a velocity and direction. At fixed time intervals t, the velocity v and direction θ of each moving entity is updated, where velocity and direction to be set at time t depend on the velocity and direction values at the previous time step $t-1$ and a random variable α. The new velocity and direction values are calculated based on the following formulas [CBD02]:

$$\begin{aligned} v(t) &= \alpha v(t-1) + (1-\alpha)\overline{v} + \sqrt{(1-\alpha^2)v_{x_{t-1}}}, \\ \theta(t) &= \alpha\theta(t-1) + (1-\alpha)\overline{\theta} + \sqrt{(1-\alpha^2)\theta_{x_{t-1}}}, \end{aligned} \tag{2.21}$$

where $v(t)$ and $\theta(t)$ are the new velocity and direction values at time t. α, where $0 \leq \alpha \leq 1$, is the tuning parameter used to vary the impact of randomness, $\overline{v}$ and $\overline{\theta}$ are constants representing the mean value of velocity and direction as $t \to \infty$, and $v_{x_{t-1}}$ and $\theta_{x_{t-1}}$ are random variables drawn from a Gaussian distribution [CBD02]. There are two extreme settings for α: $\alpha = 0$ results in totally random values (or *Brownian* motion) and $\alpha = 1$ yields linear motion. The level of randomness can be varied by adapting the value of α. At each time interval, the next location is determined based on current location, velocity, and direction as follows [CBD02]:

$$\begin{aligned} x(t) &= x(t-1) + v(t-1)\cos(\theta(t-1)), \\ y(t) &= y(t-1) + v(t-1)\sin(\theta(t-1)), \end{aligned} \tag{2.22}$$

where $(x(t),y(t))$ and $(x(t-1),y(t-1))$ are the Cartesian coordinates of the moving entity's position at time intervals t and $t-1$, respectively, and $v(t-$

1) and $\theta(t-1)$ are the entity's velocity and direction, respectively, at time interval $t-1$ [CBD02].

Probabilistic Version of Random Walk Mobility Model

In the probabilistic version of the random walk mobility model developed by Chiang [CBD02], a probability matrix is used to determine the future position of a specific moving entity. For each particular entity, there is a probability matrix that comprises three different states for position x and three different states for position y. State 0 represents the entity's current (x or y) position, state 1 represents the entity's previous (x or y) position, and state 2 represents the entity's next position, if the entity continues to move in the same direction. The probability matrix used is stated as follows [CBD02]:

$$P = \begin{pmatrix} P(0,0) & P(0,1) & P(0,2) \\ P(1,0) & P(1,1) & P(1,2) \\ P(2,0) & P(2,1) & P(2,2) \end{pmatrix}, \tag{2.23}$$

where each entry $P(a,b)$ denotes the probability that a moving entity will transit from state a to state b. The values stored in this matrix are used for updating both the entity's x and y coordinates [CBD02]. Further, each entity moves randomly at a preset average velocity.

City Section (Manhattan) Mobility Model

In the city section mobility model, the evaluation area is a street network representing a section of a city, where the streets and speed limits are based on the type of city to be simulated. Each moving entity begins its movements at a defined point in the street layout and chooses a random destination that is also represented by a point on some street. The movement algorithms determines a path corresponding to the shortest travel time between the current location and the chosen destination. Additionally, characteristics such as speed limits and minimum distance allowed between any two moving entities exists. Upon reaching its destination, the moving entity remains idle for a pre-defined pause time before randomly selecting a new destination in the street layout and repeating the process [CBD02].

Further, Camp et al. [CBD02] propose enhancements to the city section mobility model, e.g., including pause times at certain intersections and destinations, incorporating acceleration and deceleration, as well as accounting for higher/lower concentrations of entities depending on the time of day. Some

of these aspects that aim at modeling user mobility in a more realistic way are already considered in today's modeling approaches, e.g., cf. Section 5.2.4 and [MET13c].

Group Mobility Models

In contrast to the afore mentioned entity mobility models that assume that each entity's movement is mutually independent of the movement of another entity, there are several so-called group mobility models. These group mobility models account for the fact that in real-world scenarios, e.g., public transportation, several users move jointly in a correlated manner. A list of widely used group mobility models is provided in [CBD02]:

- Exponential correlated random mobility model: This model generates entity movements based on a motion function, where the rate of the change from the entity's previous to its new location depends on a random Gaussian variable.
- Column mobility model: The column mobility model defines a set of moving entities that move around a given line (or column), which is moving in a forward direction (e.g., a row of soldiers marching together toward their enemy). A slight modification of this model allows the individual entities to follow one another (e.g., a group of young children walking in a single-file line to their classroom).
- Nomadic community mobility model: The nomadic community mobility model represents groups of moving entities that collectively move from one point to another. However, individual entities maintain their own personal spaces within each group, where they randomly move.
- Pursue mobility model: This model defines moving entities that track a particular target, where the movement of a particular entity is used as reference for the others, for example, police officers attempting to catch an escaped criminal.
- Reference Point Group Mobility (RPGM) model: In the RPGM model, the random motion of a group of moving entities as well as the random motion of each individual entity within the group is represented. Group movements are based on the trajectory traveled by a logical center for the group. The logical center for the group is used as reference for calculating group motion using a group motion vector. The motion of the group center completely characterizes the movement of its corresponding group of moving entities, including their direction and

velocity. Individual entities randomly move about their own predefined reference points, whose movements depend on the group movement. As the individual reference points move from time t to $t+1$, their positions are updated according to the group's logical center. Once the updated reference points are determined, they are combined with a random motion vector to represent the random motion of each entity about its individual reference point.

2.4 Traffic Models

A major objective of system-level simulations is to provide system designers and Mobile Network Operators (MNOs) with a view of the maximum number of active users that can be supported for a given service mix under a specified system configuration at a given coverage level. Further, in order to evaluate service-specific E2E performance, several widely used traffic models and their service requirements [OCK+07], [IEE08], [3GP10a] have been implemented in the developed simulation framework, where main differentiating characteristics are the "best effort" or Guaranteed Bit Rate (GBR) and delay-sensitive nature of services.

2.4.1 Full Buffer

One baseline scenario, which is referred to as "full buffer" or "full queue" and which assumes infinitely large and always filled BS transmit buffers, is often used to benchmark service-specific evaluation results. The traffic models, described in the following, should be understood as simplifications for analyzing E2E performance by using random processes to model user activity as well as traffic demands and by averaging over several random process realizations.

2.4.2 Web Browsing (HTTP) and File Transfer Protocol (FTP)

The HyperText Transfer Protocol (HTTP) and File Transfer Protocol (FTP) traffic models are two service examples that exhibit a "best effort" behavior, i.e., the service is not provided with a guaranteed bit rate, but the data rate depends on the available BS resources for this service type. In case only few or no resources are left, best effort services may not be served at all, whereas

in conditions, where the BS scheduler does not need to handle GBR services or disposes of unused capacity, all available resources may be used to serve all best effort services at once.

Typically, users browsing the World Wide Web (WWW) using their mobile terminals result in traffic patterns that reflect the nature of human interaction. This interaction is characterized by ON/OFF periods, as illustrated in Figure 2.11, and causes the HTTP traffic to have a bursty nature.

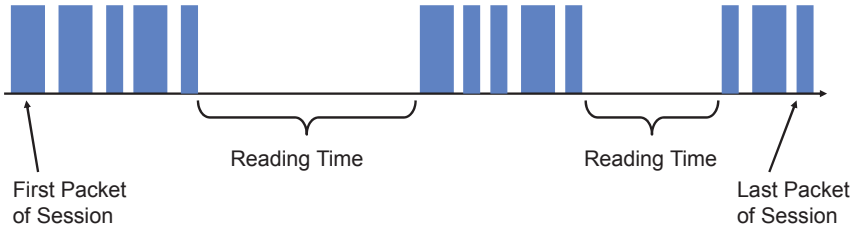

Figure 2.11: HTTP traffic pattern [IEE08]

The ON periods represent the sequence of packets in which the different objects of a web page are transferred from source to destination, while the OFF periods represent the time the user spends reading the web page before transitioning to another page. This time is also known as *reading time* [IEE08]. The overall amount of information passed from source to destination during ON periods heavily depends on the web page structure, since a web page usually consists of a main object and a number of embedded objects. The size of the main object, in addition to the number and size of the embedded objects define the amount of bytes passed from source to destination [IEE08]. The following listing specifies the HTTP traffic model parameters:

- S_M: Size of main object in page
- N_d: Number of embedded objects in a page
- S_E: Size of an embedded object in page
- D_{pc}: Reading time
- T_p: Parsing time for the main page

In general, the HTTP traffic behavior also depends on the used HTTP version. However, for simplification reasons only one active TCP session at once per UE is modeled and implemented in the system-level simulation tool. Further, only a single Maximum Transmit Unit (MTU) size of 1500 bytes (including TCP header) is considered. Table 2.2 provides an overview on the model parameters for HTTP traffic.

Table 2.2. HTTP traffic parameters [IEE08]

Component	Distribution	Parameters	PDF
Main object size S_M	Truncated Lognormal	$\overline{S_M} = 10710$ bytes $\sigma_{S_M} = 25032$ bytes $S_{M\min} = 100$ bytes $S_{M\max} = 2$ Mbytes (before truncation)	$f_X = \frac{1}{\sqrt{2\pi}\sigma x} \exp\left[\frac{-(\ln x - \mu)^2}{2\sigma^2}\right]$, $x \geq 0,\ \sigma = 1.37,\ \mu = 8.37$ if $x > S_{M\max}$ or $x < S_{M\min}$, discard and generate a new value for x
Embedded object size S_E	Truncated Lognormal	$\overline{S_E} = 7758$ bytes $\sigma_{S_E} = 126168$ bytes $S_{E\min} = 50$ bytes $S_{E\max} = 2$ Mbytes (before truncation)	$f_X = \frac{1}{\sqrt{2\pi}\sigma x} \exp\left[\frac{-(\ln x - \mu)^2}{2\sigma^2}\right]$, $x \geq 0,\ \sigma = 2.36,\ \mu = 6.17$ if $x > S_{E\max}$ or $x < S_{E\min}$, discard and generate a new value for x
Number of embedded objects per page N_d	Truncated Pareto	$\overline{N_d} = 5.64$ $N_{d\max} = 53$ (before truncation)	$f_X = \frac{\alpha k^\alpha}{x^{\alpha+1}},\ k \leq x < m$ $f_X = \left(\frac{k}{m}\right)^\alpha,\ x = m$ $\alpha = 1.1,\ k = 2,\ m = 55$ Subtract k from the generated random value to obtain N_d if $x > N_{d\max}$, discard and generate a new value for x
Reading time D_{pc}	Exponential	$\overline{D_{pc}} = 30$ s	$f_X = \lambda \exp(-\lambda x),\ x \geq 0$ $\lambda = 0.033$
Parsing time T_p	Exponential	$\overline{T_p} = 0.13$ s	$f_X = \lambda \exp(-\lambda x),\ x \geq 0$ $\lambda = 7.69$

FTP traffic is characterized by file transfer sequences that are separated by reading times. Reading time is defined as the time between end of transfer of the first file and the transfer request for the next file [IEE08]. Figure 2.12 illustrates a typical FTP session.

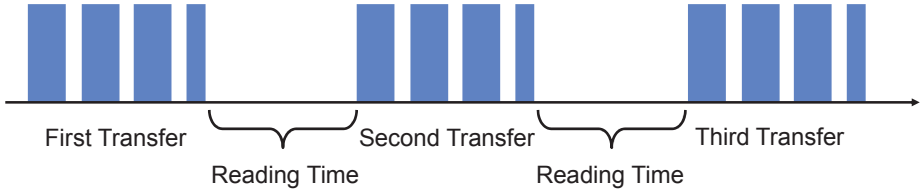

Figure 2.12: FTP traffic pattern [IEE08]

For simplification reasons, the FTP packet transfer only considers MTU sizes of 1500 bytes (including TCP header). Table 2.3 summarizes the FTP traffic model parameters.

Table 2.3. FTP traffic parameters [IEE08]

Component	Distribution	Parameters	PDF
File size S	Truncated Lognormal	$\overline{S} = 2$ Mbytes $\sigma_S = 0.722$ Mbytes ($S_{\min} = 100$ bytes) $S_{\max} = 5$ Mbytes (before truncation)	$f_X = \frac{1}{\sqrt{2\pi}\sigma x} \exp\left[\frac{-(\ln x - \mu)^2}{2\sigma^2}\right]$, $x \geq 0,\ \sigma = 0.35,\ \mu = 14.45$ if $x > S_{\max}$ or $x < S_{\min}$, discard and generate a new value for x
Reading time D_{pc}	Exponential	$\overline{D_{pc}} = 180$ s	$f_X = \lambda \exp(-\lambda x),\ x \geq 0$ $\lambda = 0.006$

2.4.3 Voice over IP (VoIP)

In contrast to the afore mentioned services, VoIP traffic represents a service type for real-time delivery of voice packets across networks using the Internet Protocol (IP) with tight delay constraints. There are a variety of encoding schemes for voice (i.e., G.711, G.722, G.722.1, G.723.1, G.728, G.729, and Adaptive Multi Rate (AMR)) that result in different bandwidth requirements [IEE08]. In this thesis, AMR encoding is considered for VoIP packet generation. Table 2.4 summarizes relevant VoIP traffic parameters that are assumed for simulation purposes.

Table 2.4. VoIP traffic parameters [OCK+07][IEE08]

Parameter	Characterization
Codec	RTP AMR source rate 12.2 kbps
Encoder frame length	20 ms
Voice activity factor	50%
Payload	Active: 33 bytes; inactive: 7 bytes
SID payload	not modeled
Protocol overhead	RTP AMR source rate 12.2 kbps

Typically, a phone conversation is characterized by periods of active talking/talk spurts (ON periods) interleaved by silence/listening periods (OFF periods) as illustrated in Figure 2.13.

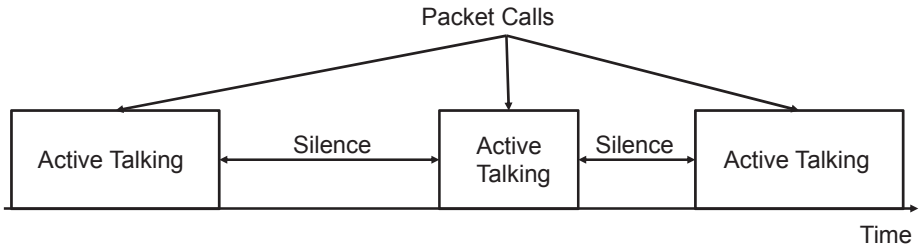

Figure 2.13: Phone conversation profile [IEE08]

In the simple 2-state voice activity model[3], depicted in Figure 2.14, the probability of transitioning from the active speech state (state 1) to the inactive or silent state (state 0) while in active state 1 is equal to a, while the probability of transitioning from state 0 to state 1 while in state 0 is c. The model is assumed to be updated at the speech encoder frame rate $R = 1/T$, where T is the encoder frame duration (typically 20 ms) [OCK+07].

2.4.4 Traffic Model States

User IP packet data transmissions are modeled and virtually transferred from their source (e.g., Internet server) toward corresponding network nodes and finally via the air interface to their sink (requesting UE). A simplified IP packet data life cycle includes the states illustrated in Figure 2.15.

At simulation start-up, each connected UE's traffic state is initialized with a random reading time according to the configured traffic model. The various

[3] "Clearly, a 2-state model is extremely simplistic, and many more complex models are available. However, it is amenable to rapid analysis and initial estimation of talk spurt arrival statistics and hence reservation activity." [OCK+07]

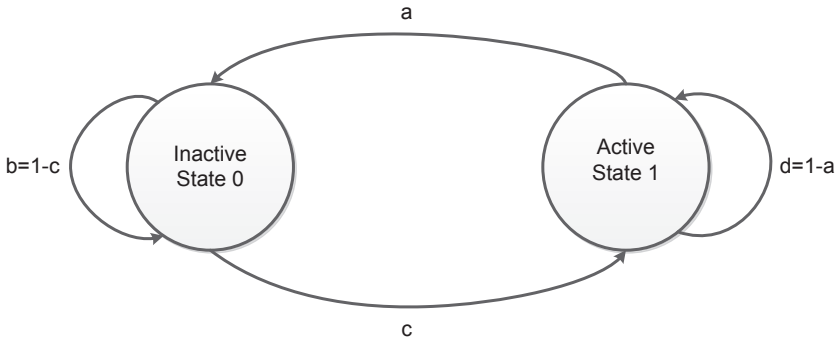

Figure 2.14: 2-state voice activity model [OCK+07], [IEE08]

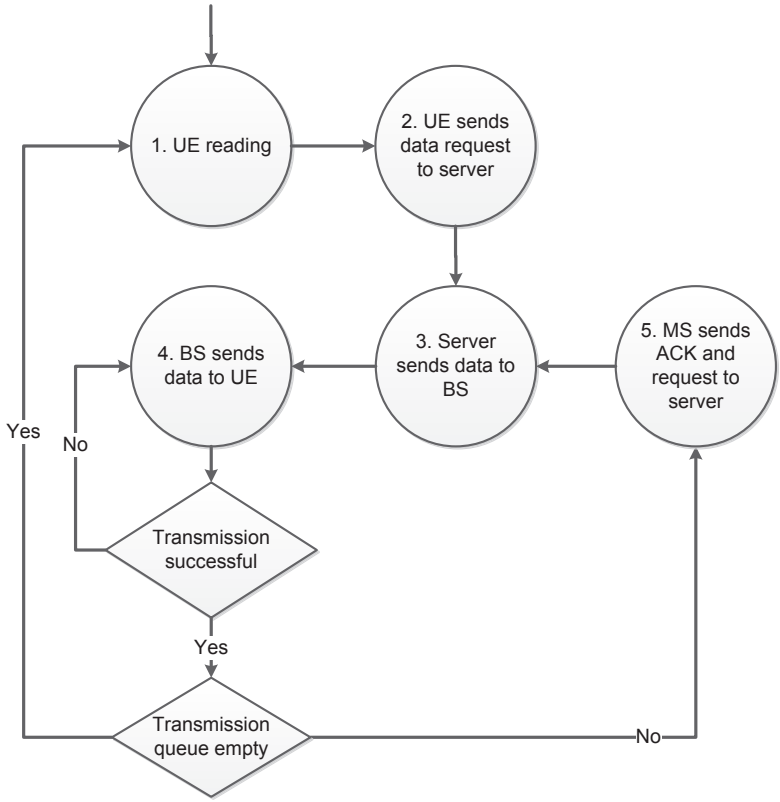

Figure 2.15: Traffic model states

traffic model states allow for incorporating processing and state transition delays, where the minimum delay that can be modeled is limited by the simulation interval. As soon as the reading time is expired, a connected UE requests a number of bytes according to the configured, UE-specific traffic model from a virtual server. This server sends a corresponding number of MTU-sized packets to the serving BS. The serving BS segments the IP packets following RAT-specific protocols and starts transmitting RLC SDUs via the air interface. In case a packet transmission failed, retransmissions are executed until a maximum number of retransmissions is reached or a service-specific retransmission timer expires. After successful reception of requested packets, the UE returns to reading state.

2.5 End-To-End (E2E) Latency

E2E latency is an important aspect for the performance of many services and applications. In particular, delay-sensitive applications, such as voice, real-time gaming, or other interactive applications, in the first place require low latency rather than high data rates. Typically, latency is measured by the time it takes for a small IP packet to travel from the UE through the network to the correspondent server and back [HT09]. This measure is referred to as Round Trip Time (RTT). In Figure 2.16, RTT measurement and relevant components for the case of LTE are depicted. Further, relevant components

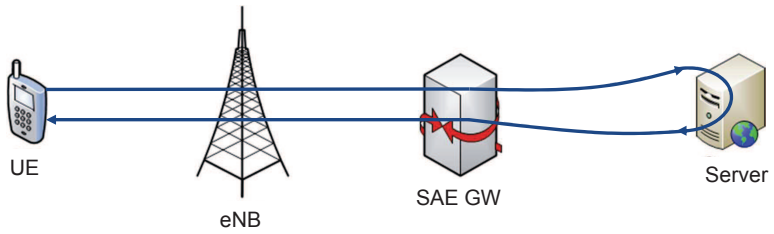

Figure 2.16: Round trip time measurement [HT09]

of the LTE E2E delay budget are exemplarily listed in Table 2.5 [HT09].

Table 2.5. LTE E2E latency components [HT09]

Delay Component	**Delay (ms)**
Transmission time UL + DL	2
Buffering time (0.5× transmission time)	$2 \times 0.5 \times 1 = 1$
Retransmissions 10%	$2 \times 0.1 \times 8 = 1.6$
UL scheduling request	$0.5 \times 5 = 2.5$
UL scheduling grant	4
UE delay estimated	4
eNB delay estimated	4
Core network	1
Total delay with pre-allocated resources	13.6
Total delay with scheduling	20.1

The LTE subframe size of 1 ms allows for a very low transmission time. Further, following assumptions apply [HT09]: on average, the packet needs to wait for 0.5 ms for the start of the next frame. Retransmissions take 8 ms at best. The assumed retransmission probability is 10%. The average delays for sending scheduling request and grant are 2.5 ms and 4 ms, respectively.

Moreover, a UE processing delay of 4 ms, an eNB processing delay of 4 ms, and a core network delay of 1 ms are assumed. The average RTT including retransmission can be well below 15 ms, if resources are pre-allocated. If the scheduling delay is included, the RTT will be approximately 20 ms. These RTT values are low enough even for applications with very strict delay requirements (e.g., real-time gaming). The practical RTT in the field may be higher, if the transport delay is longer, or if the server is far away from the core network. Often, the E2E RTT can be dominated by non-radio delays, e.g., by the distance and by other elements in the Internet. For instance, the propagation time of 5000 km is more than 20 ms [HT09].

2.6 Scheduling Algorithms

The scheduling functionality that is in charge of allocating system resources, such as channels, time slots, PRBs, etc., resides at MAC layer and is part of the Radio Resource Control (RRC). The scheduler assigns resources for PHY layer transmissions of different service types according to a set of predefined scheduling metrics, for instance, reported Channel Quality Indicator (CQI). Further, a typical assumption is that the scheduler calculates available resources after accounting for all control channel and protocol overhead [IEE08]. Moreover, the MNO may enforce the prioritization of certain service types due to their QoS requirements, such as GBR or minimum delay, by implementing a corresponding policy. In the following, some well-known scheduling strategies are listed:

- Round Robin (RR) is based on the idea of sharing resources in the time domain on a round-per-round basis, where the allocation of resources, i.e., time slices per round, may be fixed for the whole service duration or may be influenced by further service requirements or MNO policies.
- Maximum Carrier-to-Interference ($\max C/I$) ratio based approaches preferably serve those users that face the "best" receive conditions in terms of carrier-to-interference ratio compared to other users handled by the same scheduler.
- Proportional Fair (PF) scheduling computes a metric for all active users to be served for a specified scheduling interval. Users are sorted with respect to this scheduling metric, where the users with the highest metrics are allocated the available resources. The metrics for all users are updated before the next scheduling interval and the process repeats [IEE08].

Usually, PF scheduling operates on a fix scheduling or Transmission Time Interval (TTI). However, there may also be some exceptions for certain service types, e.g., VoIP in LTE [HT09], where so-called *semi-persistent* scheduling uses persistently allocated resources for transmission of control information in order to avoid control channel limitations. In case of OFDMA, the definition of scheduling resources must be extended to apply to a two-dimensional OFDMA frame, consisting of PRBs of 12 contiguous subcarriers each [HT09] and OFDM symbols. The number of resources eventually allocated to a user depends on the metric update process, and does not preclude a single user from being assigned multiple or all the resources in a TTI. For system-level simulations assuming a fixed overhead and allowing for up to $N_{\text{partitions}}$ resource partitions, each partition assignment is considered as a separate packet transmission. At scheduling instant t, the scheduling metric $M_i(t)$ for user i is calculated as follows [IEE08]:

$$M_i(t) = \frac{T_i(t)}{(\overline{T}_i(t))^{\alpha}}, \tag{2.24}$$

where $T_i(t)$ is the instantaneous data rate that can be supported at scheduling instant t for user i. $T_i(t)$ is a function of the CQI feedback, and consequently of the modulation and coding scheme that can meet the PER requirement. $\overline{T}_i(t)$ is the average throughput smoothed by a low-pass filter at the scheduling instant t for user i. α is a fairness exponent factor with default value 1. For the scheduled user, $\overline{T}_i(t)$ is computed as follows [IEE08]:

$$\overline{T}_i(t) = \frac{1}{N_{\text{PF}}}\ T_i(t) + \left(1 - \frac{1}{N_{\text{PF}}}\right)\ \overline{T}_i(t-1), \tag{2.25}$$

and for the unscheduled user:

$$\overline{T}_i(t) = \left(1 - \frac{1}{N_{\text{PF}}}\right)\ \overline{T}_i(t-1). \tag{2.26}$$

The latency scale of the PF scheduler N_{PF} is given by [IEE08]:

$$N_{\text{PF}} = T_{\text{PF}}\ N_{\text{partitions}}/T_{\text{frame}}, \tag{2.27}$$

where T_{PF} represents the latency time scale in units of seconds and T_{frame} is the frame duration of the system.

In UTRAN, scheduling decision may be influenced by RNC, for example, due to higher priority of HARQ retransmissions, whereas in E-UTRAN resource allocation decisions are solely taken be the eNB. For system-level performance comparisons and evaluation, it is clear that various scheduling

strategies and their configuration, e.g., subcarrier permutation scheme, will yield different performance and overhead impacts, and thus will have to be aligned.

2.7 Event Definitions

In this section, some of the most important events that are relevant for KPI derivation and performance evaluation are defined, where the following mathematical framework is applied:

- The RAT that a cell or cell sector c belongs to is determined by the function $r = R(c)$, where r is either equal to LTE or HSDPA.
- The cell c serving a UE i at time instant t is given by the connection function $c = x_i(t)$.
- The DL Signal-to-Interference-plus-Noise Ratio (SINR) of a UE i served by cell c at time instant t is denoted by $\xi_{i,c}(t)$. However, in this thesis, the DL geometry G (cf. 2.4), which represents the average wideband SINR, is equivalently used instead of the SINR $\xi_{i,c}(t)$.
- The geometry experienced by UE i connected to cell c at time instant t is expressed by $G_{i,c}(t)$ in dB. Similarly, the geometry of a potential HO target cell c_0 of UE i is expressed by $G_{i,c_0}(t)$.
- A Radio Link Failure (RLF) is detected at time instant t_0, if the geometry $G_{i,c}(t)$ of a UE i connected to cell c falls below a certain threshold Q_{out} for a specified time interval $T_{Q_{out}}$, i.e.,

$$G_{i,c}(t) < Q_{out} \quad \text{for} \quad t_0 - T_{Q_{out}} < t < t_0. \tag{2.28}$$

- For HO decisions during simulation, considered geometry values are averaged over 100 ms.
- The entering condition for HO event A3 [3GP12a] is slightly modified and is fulfilled, if the geometry of the HO target cell $G_{i,c_0}(t)$ is higher than the minimum required geometry level, which is here set to Q_{out}, and a so-called Handover Margin (HOM) M. The HOM consists of a Hysteresis (HYS) value H and Cell Individual Offset (CIO) values of serving O_c and target cell O_{c_0}, respectively (cf. Equation (3.1)). The UE i sends the measurement report at time instant t_0 when the entering condition of the measurement event is fulfilled for a continuous time period of t_{TTT}, which is also referred to as Time-To-Trigger (TTT), i.e.,

$$G_{i,c_0}(t) > Q_{out} \quad \wedge \quad G_{i,c_0}(t) - G_{i,c}(t) > M \quad \text{for} \quad t_0 - t_{TTT} < t < t_0, \tag{2.29}$$

such that $R(c) \neq R(c_0)$, where $M = H + (O_c - O_{c_0})$.

- After a measurement report is sent by UE i, the serving cell c prepares the HO of the UE by sending a HO request to the HO target cell c_0. Then, the serving cell c waits for an acknowledgment from the target cell c_0. This step induces an additional delay T_{HOP}, which is referred to as HO preparation time. Therefore, the HO of a UE i is executed T_{HOP} seconds after the measurement event is triggered as long as the geometry $G_{i,c}(t)$ of the UE is greater than a cell-specific threshold $Q_{fail,c}$. In essence, the HO of a UE i is executed from cell c to target cell c_0 at time instant t_{HO}, if the following conditions hold

$$\begin{aligned} G_{i,c}(t) > Q_{fail,c} &= G_{min,c} + O_c \quad \text{for} \quad t_{HO} - T_{HOP} < t < t_{HO}, \\ R(c) \neq R(c_0) &\wedge G_{i,c_0}(t_{HO}) > Q_{fail,c_0} = G_{min,c_0} + O_{c_0}, \end{aligned} \tag{2.30}$$

where $G_{min,c}$, G_{min,c_0}, O_c, and O_{c_0} denote cell-specific minimum required geometry factors and CIO values of source and target cells, respectively.

2.8 Multi-Radio Network Simulation Framework

Future wireless network infrastructure will consist of a variety of heterogeneous RATs. The selection of the "best" RAT, optimized handover parameters settings, load balancing, and system capacity optimization in current and future multi-RAT scenarios shall be efficiently accomplished, while allowing for the integration of self-organizing and -optimizing network functionalities. These research challenges are addressed in the following chapters. However, specific requirements on the simulation framework emanate from the concepts developed in Chapter 5, where context awareness is seen as key enabler, as well as in Chapters 7 and 8, respectively, where Self-Organizing/Optimizing Network (SON) concepts for Mobility Robustness Optimization (MRO) are developed and evaluated.

In order to meet these requirements, a multi-radio network simulation tool has been developed that provides means for influencing RAT selection, handover, and load balancing decisions based on available context information. This simulation tool is referred to as Context Aware Radio Network Simulator (CORAS).

The proposed CORAS incorporates static as well as dynamic context models for simulating the influence of available context information, e.g., user movement estimates, on HAM and users' E2E performance. For the assessment of HAM network selection decisions and resource utilization, RAT deployment, MNO and user policy models, as well as realistic user mobility models are implemented. Further, occurring HO and packet transmission delays as well as service and signaling costs are taken into account. Thus, all these features allow for quantitatively evaluating the impact of user and network context information on system and E2E performance. In essence, the implemented simulation tool provides:

- a generic solution for evaluating and optimizing mobility support and load balancing in heterogeneous access networks, including self-tuning functionalities for HO optimization, event detection and countermeasures, load estimation mechanism for enhanced load balancing,
- a generic framework for the implementation of RAT selection and admission control concepts depending on QoS, efficiency of network utilization, user Service Level Agreement (SLA) profiles, as well as MNO policies.

In particular, modeled aspects include:

- RAT characteristics (e.g., bandwidth, radio resources, transmit power, carrier frequencies, etc.),
- different deployment scenario and cell layouts (e.g., varying site-to-site distances, one omni-directional vs. three sector antennas, etc.),
- user mobility (e.g., random walk, predefined trajectories of user groups, road-like movements, etc.),
- handover processes (e.g., individual TTT, HYS, and CIO settings per RAT, BS, and cell sector),
- measurement reporting (e.g., accuracy and delay of reporting can be influenced),
- traffic characteristics and delay sensitivity (e.g., best-effort vs. delay-sensitive and GBR services),
- cost metrics in terms of signaling, handovers (HO failure events, ping-pong, or too early/late HOs), user-specific service usage,
- and overall system and E2E performance.

One of the key problems is the simulator timing. Due to the different TTI values of the two considered RATs (HSDPA and LTE), a compromise had to

be found. Table 2.6 summarizes the timing parameters for HSDPA and LTE, respectively.

Table 2.6. RAT-specific timing parameters [3GP10b][3GP12b]

	HSDPA	**LTE**
Frame	10 ms	10 ms
TTI	2 ms = 3 slots	1 ms = 2 slots
Slot/Subframe	2/3 ms	1/2 ms

Since both HSDPA and LTE use a frame length of 10 ms, the simulation time interval was set to 10 ms, i.e., packet transmissions and scheduling decisions are issued and evaluated based on this interval. Further, user locations, user trajectories, and fast fading models cannot be updated faster and changes are also limited to time instances that are multiples of 10 ms. The same applies to events that are detected during simulation time. Changes that occur at a smaller time scale, e.g., rapid link level variations, are left to be modeled by the considered link-to-system interfaces (cf. Section 2.1.3). In principle, the choice for a common simulation timing interval should account for the RAT-specific TTIs or the intervals at which changes in the transmission mode, e.g., change in modulation and coding scheme, may be performed. For example, if several RATs, such as HSDPA, LTE, and WiMAX, which operates in TDD mode with a frame length of $2 \times 5 = 10$ ms, should be jointly evaluated, the least common multiple of 2, 1, and 10 ms yields a common simulation timing interval of 10 ms. Figure 2.17 illustrates the schematic simulation flow.

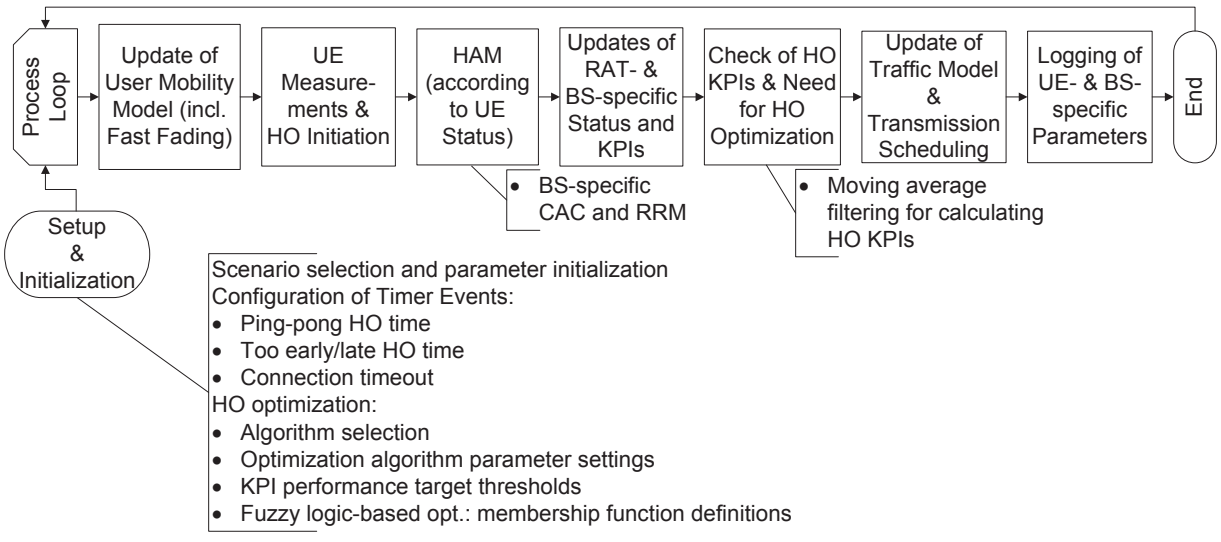

Figure 2.17: Simulation process flow

At simulation setup, scenario specific settings are made and algorithms to be evaluated are selected. Afterward, user locations and the corresponding fast fading models are updated and received signal strength values as well as HO conditions are checked per UE. Then, according to UE status, RRM and CAC are performed and BS-specific parameters as well as KPIs are adjusted. If MRO is activated, the need for HO parameter adaptations is checked and corresponding actions are triggered. Further, UE-specific traffic models are updated and scheduling of DL transmissions is performed. Finally, UE-, BS-, and packet transmission-related parameters are logged.

The simulation framework is implemented in *C* programming language. For tracking UE-, BS-, and packet transmission-related events, specific data structures were created. Further, fast fading as well as user mobility traces can be pre-calculated and accessed during simulation in order to reduce simulation run times. Due to the complexity and dynamics of the considered scenarios (e.g., user mobility, different RAT deployment parameters, etc.), the number of monitored parameters and events can easily grow and slow down the performance of typical desktop computers. Hence, for handling huge amounts of data in parallel, i.e., running multiple instances of the simulation tool, and separating simulation processes from data management and evaluation, the simulation framework is composed of the different components depicted in Figure 2.18.

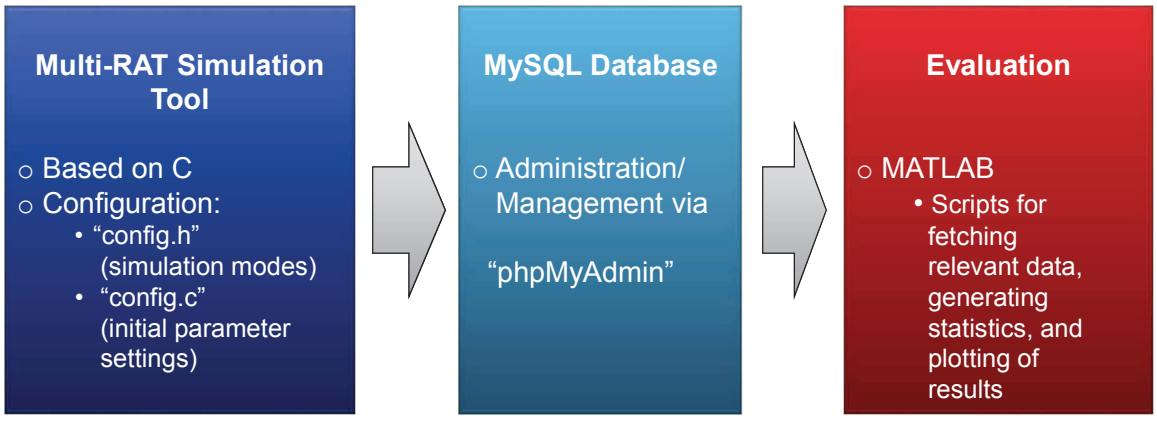

Figure 2.18: Simulation framework

Thus, simulation tasks can be separately handled by powerful computers or remote servers. Simulation data is hosted by *MySQL* based databases, and evaluation of simulation results is performed offline using *MATLAB*® scripts.

2.9 Summary

Since today's situation is characterized by the coexistence of various mobile communication systems with heterogeneous characteristics, approaches for evaluating real-world multi-radio network deployments are important. Previous sections summarize state-of-the-art modeling approaches that are used for "snapshot" based performance evaluations. In addition, realistic mobility, traffic, and latency models as well as an approach for multi-radio network simulations are presented that allow for establishing a multi-radio network evaluation methodology. A similar modeling approach is followed by the European 5G project METIS, where scenarios [MET13a] and simulation guidelines [MET13c] are proposed for evaluating the performance of future wireless technologies and the fifth generation of wireless communication systems 5G using more realistic models, e.g., with respect to deployment, propagation, and user mobility.

Moreover, the author developed a feature-rich simulation tool that provides means for incorporating and quantitatively analyzing the impact of user and network context information on system and E2E performance. This simulation tool lays the basis for evaluating the context aware solutions presented in Chapter 5 and the advanced MRO schemes in Chapters 7 and 8, respectively.

3 Heterogeneous Access Management

In a more and more fragmented and heterogeneous wireless network landscape with an increasing demand for high network availability and capacity, the need for efficient network access, mobility support, and resource management across different Radio Access Technologies (RATs) becomes eminent. The current situation is characterized by the coexistence of various mobile communication systems, such as GSM, HSPA, LTE, WiMAX, and WLAN, that differ greatly with respect to coverage, spectrum, data rates, Quality of Service (QoS), and mobility support. The selection of the "optimum" RAT, the handover between these RATs, admission control, load balancing, and system capacity optimization of these multi-RAT scenarios are referred to as Heterogeneous Access Management (HAM).

Modern communication devices, such as notebooks or smartphones, are nowadays capable of supporting various RATs due to the evolution in integrated circuit design and Software Defined Radio (SDR). Although the concept of SDR is well investigated from a scientific point of view and seen as an enabler for achieving improved spectral efficiency, e.g., via opportunistic spectrum usage [MM99], it is still not clear how and when SDR concepts will be integrated into existing wireless systems. Today, the use of SDR is rather limited to military applications. However, modern smartphone devices that dispose of various RAT interfaces are able to take advantage of sophisticated HAM strategies and realizations.

Further, Mobile Network Operators (MNOs) are interested in protecting their investments in and a continued utilization of already deployed network infrastructure, while aiming at stable revenue evolutions in the long term. With every change in network topology, configuration, or a technology upgrade, they have to perform extensive stability and performance checks. Therefore, network operators prefer a smooth integration of new radio access technologies with existing network infrastructure. In order to realize efficient

HAM across various RATs different approaches may be implemented, where there is a fundamental trade-off with respect to implementation costs and complexity on the one side, and mobility support and resource utilization efficiency on the other side. The latter aspect is particularly addressed in Section 3.3.

Besides improved network selection, which is in the literature often related to the concept of "always best connected" [GJ03], HAM aims at providing the following functionalities: ubiquitous access, seamless mobility, and efficient resource management across various RATs. The following sections present fundamental concepts and state-of-the art approaches for Joint Call Admission Control (JCAC), Joint Mobility Management (JMM), and Common Radio Resource Management (CRRM). The essential characteristics of these approaches are used to develop an integrated HAM concept, which is introduced and evaluated in Chapter 5, in order to achieve objectives, such as efficient network access, mobility support, and resource management across different RATs.

3.1 The Handover Concept and Relevant Parameters

The success of cellular communication as wide area communication technology is based on the so-called *cell concept* that allows for providing global network coverage. MNOs divide the service area into several cells, which ideally are hexagonal, and deploy network nodes for covering certain geographical areas with a number of possibly co-located transmit antennas. Criteria for deciding about the number of cells or transmit antennas that are required to serve a certain region are, for example, population density, expected user traffic demands, topographic data, or existing buildings that could serve as transmission tower locations.

Further, an essential procedure that enables mobile users to seamlessly switch between coverage areas of different cells or Base Stations (BSs) while maintaining a certain Quality of Service (QoS) was standardized [3GP12a] and is referred to as Handover (HO). In this thesis, several concepts are presented that aim at optimizing HO procedures and thus overall network performance.

Figure 3.1 illustrates a HO event and the relation between relevant parameters that determine when a HO process is to be triggered. Important parameters are the Reference Signal Received Power (RSRP) values of target and

serving BSs, respectively, as well as the overall *Handover Margin* (HOM). The HOM consists of a cell-specific *Hysteresis* (HYS) and *Cell Individual Offset* (CIO) parameters, which are to be added to cell-specific measurement quantities [3GP08]. The use of a HYS parameter allows for limiting the amount of occurring HO events, since the HO condition is not entered until the RSRP difference exceeds the HYS value [3GP08]. Further, the HO condition has to be satisfied for a specified amount of successive time instances, referred to as *Time-To-Trigger* (TTT). The application of a BS-specific TTT value creates a certain HO area between neighboring BSs and avoids unnecessary "ping-pong" HOs that would otherwise occur as soon as the HO triggering condition stated in Equation (3.1) becomes true at least once. Moreover, the choice of a too small HYS parameter setting also increases the probability of ping-pong HOs, since minor, but alternating changes in the sign of the RSRP difference would result in permanently switching the mobile connection between serving and target BS. Such a situation typically occurs, if the user moves at the cell edges of neighboring cells while permanently changing its direction either toward target or serving cell, respectively. For example, this applies in case a user is constantly moving from one side of a shopping street to the opposite side and back, where cell edges coincide with the middle of the street.

In cellular networks, Radio Resource Control (RRC) supported by the Mobility Management Entity (MME) is in charge of triggering HO processes as soon as certain conditions become true. For intra-RAT intra-frequency mobility in 3GPP [3GP12a], the following HO condition has to be satisfied for a specified amount of successive time instances, denoted by TTT, until a HO process is initiated:

$$P_{rx,t} + O_t \quad > \quad H_s + O_s + P_{rx,s}, \tag{3.1}$$

where $P_{rx,t}$ and $P_{rx,s}$ denote the RSRP values and O_t and O_s represent the CIO values of the *target* and *serving* BSs t and s, respectively. H_s designates the HYS value set at serving BS s. Solving Equation (3.1) for the term $(P_{rx,t} - P_{rx,s})$ yields a relation between the RSRP difference and the overall HOM, denoted by $M(s,t)$, with respect to serving BS s and target BS t:

$$P_{rx,t} - P_{rx,s} \;>\; H_s + (O_s - O_t), \tag{3.2}$$

$$P_{rx,t} - P_{rx,s} \;>\; M(s,t). \tag{3.3}$$

In [3GP12a], this event is denoted as A3, whereas for inter-RAT mobility the corresponding event is referred to as B2. HO parameter settings and

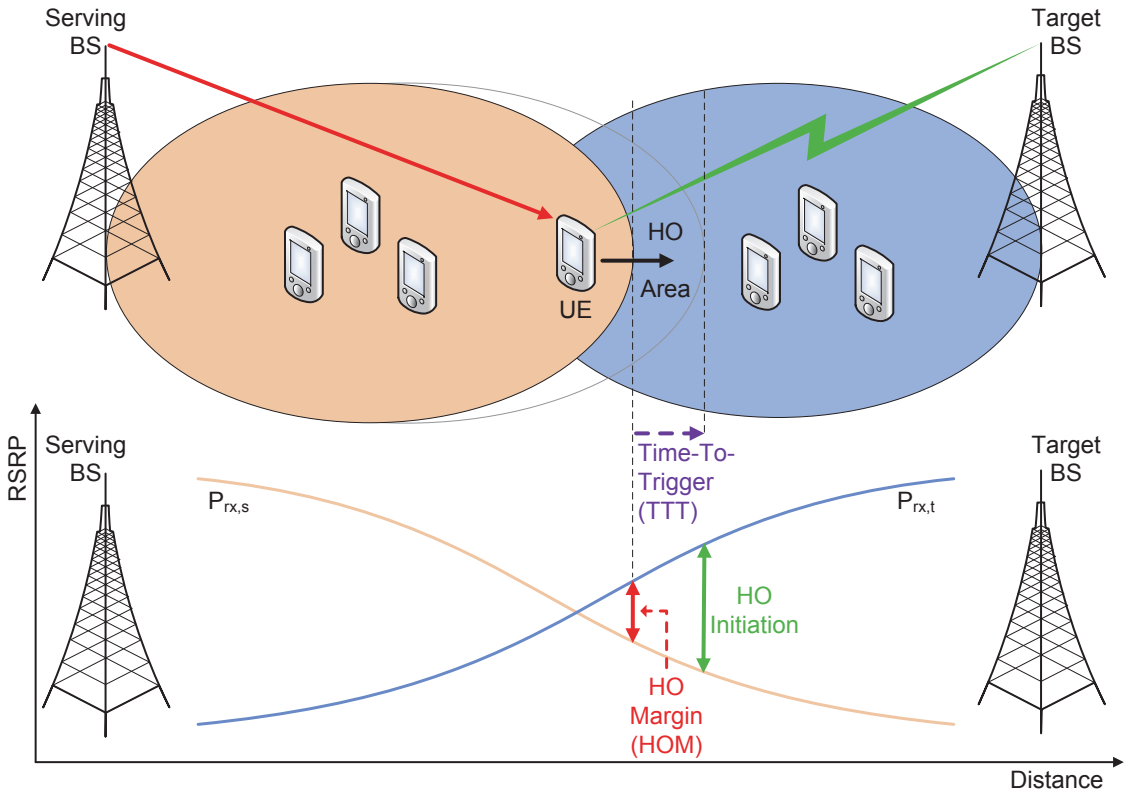

Figure 3.1: Handover event and relevant parameters (adapted from [SOC10b])

changes of the HYS, TTT, and the CIO values have a direct impact on the connection quality during HOs, the success rate of HOs, the occurrence of unwanted ping-pong HOs, and the load distribution between different cells. For example, if a user is moving at a high velocity, a too high TTT setting may delay HO process initiation, while the user's link quality to its serving BS is quickly decreasing due to increasing distance or the environment the user is passing through. Hence, the user's RSRP level may drop below the minimum required level, before the HO procedure is triggered or completed, which results in a Radio Link Failure (RLF).

3.2 Network Selection and Access Management

In a heterogeneous wireless network landscape where many Radio Access Networks (RANs) coexist, attempting to realize the vision of "always best connected" [GJ03] can easily result in continuously solving a complex optimization problem or may simply not be possible due to delay constraints. Further, already specifying the objective function may result in trading-off

user vs. service provider objectives, which is a fundamental issue in network selection. For example, a user may prefer being connected to the RAN providing highest data rates, largest coverage, and lowest service costs. However, these views usually contradict with mobile network operators' or service providers' targets of operating their RANs in the most efficient way. Thus, many factors, such as local RAT deployments, network load, and user distribution, are assigned certain weights and to be incorporated in the decision process from MNO's and service provider's point of view.

In principle, network selection decisions may be taken from network as well as from user perspective. However, in cellular networks, handover processes are typically network controlled and terminal supported, where according to 3GPP the following definition of HO applies [3GP11b]:

> "Handover is the process in which the radio access network changes the radio transmitters or radio access mode or radio system used to provide the bearer services, while maintaining a defined bearer service QoS."

In contrast to cellular systems, such as the Universal Mobile Telecommunications System (UMTS), handover decisions in Wireless Local Area Networks (WLANs) are solely terminal-centric. A typical example is a notebook's WLAN adapter that tries to connect to a WLAN Access Point (AP) from which it receives the strongest beacon signal. However, in the future heterogeneous wireless access landscape, these rather strict paradigms are likely to change due to improvements in inter-working between 3GPP and non-3GPP RATs, in particular with respect to inter-RAT mobility. Here, a so-called *vertical* handover (VHO) from one RAT to another RAT, also referred to as inter-RAT HO, has to be performed in order to yield improved mobility support as well as QoS. Figure 3.2 illustrates typical scenarios where HAM may beneficially exploit velocity information of connected User Equipments (UEs) for improved network selection decisions. For example, in Figure 3.2(a), the low mobility of a pedestrian user allows for switching to a local WiFi AP while strolling through the shopping mall area. Thus, the UE performs a vertical HO from a cellular RAT (e.g., 3G) to a WLAN AP. In contrast, the vehicular user that traverses the service area at moderate to high speed, as depicted in Figure 3.2(b), requires macro cell connectivity in order to ensure QoS. Therefore, a *horizontal* HO between cellular BSs using the same RAT, also referred to as intra-RAT HO, is arranged.

In the literature, many user- or terminal-centric VHO decision approaches have been proposed that, besides signal strength measurements, take addi-

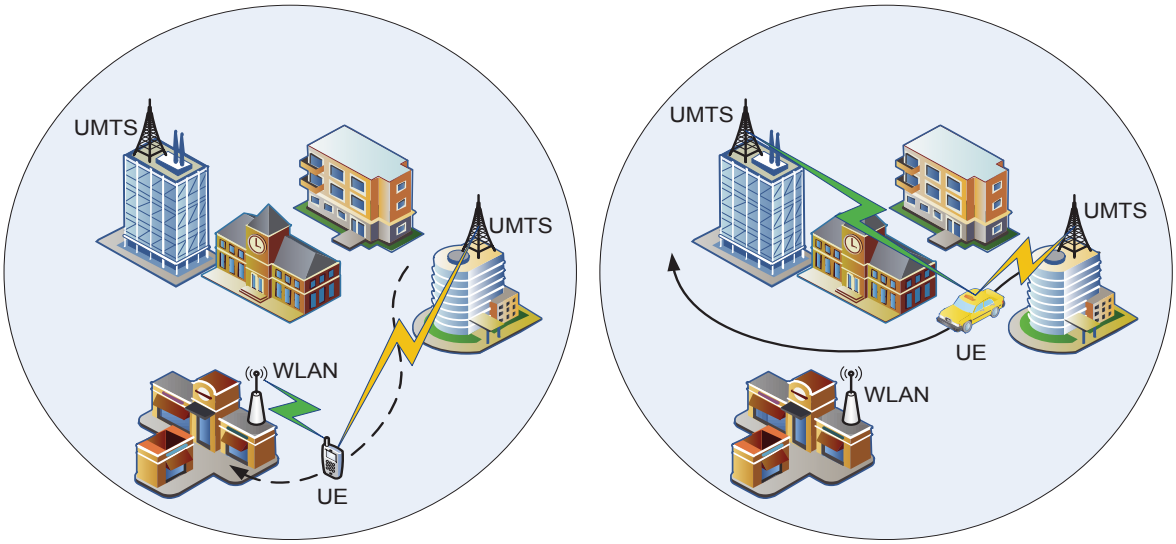

(a) Vertical handover (b) Horizontal handover

Figure 3.2: Different handover types

tional context information, such as service requirements (e.g., in terms of bandwidth and latency), service costs, user velocities and preferences, UE battery power, etc., into account for selecting the currently best access opportunity. Decision making is accomplished, for instance, by maximizing weighted sums [BWKS07], Markov decision processes modeling [SNYW08], or employing fuzzy logic and neural networks [KS11]. A very comprehensive overview on state-of-the art VHO algorithms, decision metrics, protocols, and simulation tools is given in [MBCCM11].

These rather device- and user-driven concepts are complemented by a holistic concept for Intelligent Radio Network Access (IRNA) that has been developed by the author and is presented in Chapter 5, where user, terminal, network and service provider perspectives are taken into account. In Section 5.2.1, a weighted sum approach is introduced that is employed in a context enhanced network selection strategy [MKSS09a], [MKSS10], [KMS+10], for terminal-centric selection of multi-homed connections [CMK+10], as well as for improving mobile access in the area of *Mobile Cloud Computing* [KMSS10]. The developed IRNA concept, on which these approaches are based, is able to incorporate any type of context information, ranging from user, terminal, network, and environment context, and may be easily adapted. Further, it relies on a highly scalable Context Management System (CMS) that is introduced in Section 4.2. Moreover, limits for exploiting context information, such as user movement estimates, in a realistic urban environment are explored in Section 5.2.4.

Since vertical handovers are costly in terms of network resources, the necessary number of VHOs should be kept as small as possible. In particular, an increased amount of control signaling, which possibly includes Authentication, Authorization, Accounting (AAA) processes depending on target network ownership, service interruption during HO execution, if soft handover is not supported, etc., may impose a burden on network capacity, negatively affect service latency, and degrade the user's Quality of Experience (QoE). Context-aware middleware approaches that aim at relieving the application logic from the burden of determining the most suitable interface have been proposed, among others, in [BC04] and [BCG09], where the latter approach achieves accurate estimations of node mobility and consequently performs connection selection and establishment with very limited overhead. In particular, mobile agent based concepts have been found suitable for achieving mobility, autonomy, asynchrony, and location awareness [FPV98]. In [BCMS03], this concept is exploited in such a way that context is determined on the basis of metadata, including declarative management policies and profiles for user preferences, terminal capabilities, and resource characteristics. Additionally, mobile middleware components are implemented that follow the provision-time movement of clients to locally support their customized service access, thus favoring component reusability and automatic service reconfiguration.

In contrast to access management or Call Admission Control (CAC) within a single RAN, JCAC does not only determine whether an incoming call attempt is admitted or not, it is moreover able to decide by which RAN the requested service should be provided. In essence, JCAC has to handle various service requests and to find a mapping of service requirements onto the specific RAT characteristics in order to guarantee a minimum level of QoS. JCAC decisions and actions may be influenced by QoS requirements [FET03], network operator policies [THM04], service level agreements [YBC05], user preferences [OPM05], user location information [PvBW$^+$09], or results of sophisticated resource utilization and cost analysis [GHAM03], [BWKS07]. Further, the integration of a multitude of wireless access networks under a cross-layer context-aware architecture [HNH07] has shown to increase user satisfaction and network throughput. Finally, modeling HAM operations as semi-Markov decision processes and using state aggregation have shown to yield an efficient approximation algorithm for HAM policy optimization [BW10].

3.3 Joint Mobility and Common Radio Resource Management

Joint Mobility Management (JMM) is a concept for handling terminal mobility with respect to intra- as well as inter-RAT handovers, which are also referred to as *horizontal* and *vertical* handovers, respectively. JMM's main purpose is to support *seamless mobility* among RATs, which incorporates tasks such as location area tracking, handover signaling, authentication, security, monitoring terminal activity changes, managing subscription profiles, and service connectivity [HT09]. According to [Gol09] the following functionalities must be present in order to realize seamless mobility across heterogeneous radio access networks:

- Maintaining connectivity for users on the go.
- Choosing among different network types based on need, environment, preferences, and services offered.
- Network monitoring: obtaining timely information and regular updates on the status of the network in order to minimize service disruptions and optimize QoS.
- Network discovery: finding networks available within proximity or within a geographical area.
- Network selection: choosing the target network to which to connect.
- Routing and connection update: updating the routing information so that packets are forwarded to their destination.

JMM is often implicitly considered as a subtask of Common Radio Resource Management (CRRM). CRRM is a concept that facilitates efficient management of a common resource pool by integrating RAT-specific or local RRM functionalities with common (operator-specific) RRM entities, where implementation can be realized in a centralized, a distributed, or a hybrid manner. The main benefits of CRRM are [THH02]:

- Load sharing for efficient resource utilization,
- Interference distribution for achieving higher spectral efficiency,
- Improved QoS management with seamless integration of RATs for ensuring optimum end user performance.

Many sophisticated CRRM concepts that aim at implementing the afore mentioned capabilities have been proposed in the literature. If a proposed

CRRM concept also supports multi-homing[4], it is referred to as Joint Radio Resource Management (JRRM). Devices that support multi-homing are capable of simultaneously maintaining more than one connection, i.e., there may be a different primary path for each application [CMK+10]. Existing solutions for JRRM range from approaches that apply pricing schemes for taking network and user context into account [NSCM05], agent based multi-access RRM schemes that are self-organized and implemented in a distributed manner [FZ06], to fuzzy neural based algorithms that ensure QoS constraints in multi-RAT deployments [GAPRSR08]. Further, an interesting modeling framework for the evaluation of CRRM algorithms based on multi-criteria optimization theory is presented in [Pil10], where the focus is on the evaluation of realistic CRRM scenarios for UMTS and GSM/EGPRS.

In Section 5.2.1, the author introduces a concept for context- and application-aware RRM [SWP+10] that is based on a weighted sum approach. Furthermore, MNOs, managing co-deployed, heterogeneous access technologies, are interested in an optimized utilization of their infrastructure and radio resources while maximizing their revenue. For enhancing service provisioning and optimizing system performance, a utility based approach has been developed and proposed by the author in [KLM+11a], [KLM+11b], [LKMS12]. This approach, described in further detail in Section 5.2.2, is able to handle diverse user service requests, ranging from voice only to bandwidth consuming streaming services, collaboratively by a combined, heuristic JCAC and *Dynamic Bandwidth Adaptation* (DBA) method.

Moreover, cell transition prediction approaches are investigated by the author in Section 5.2.3 that exploit mobile users' movement trajectories and enable network nodes to predict arrival of fast moving users well in advance for pro-actively triggering load balancing mechanisms.

3.4 Inter-Network Cooperation and Mobility Concepts

The degree of coupling or interconnection between RANs may vary from *very tight* coupling to a *very loose* or *open* coupling approach and directly results in a fundamental trade-off between implementation costs and complexity on

[4] "Multihoming refers to a computer or device connected to more than one (computer) network [Wik14b]". In an Internet Protocol (IP)-based system, this means to use a set of IP addresses instead of only one. When having the possibility of maintaining more than one connection, there is the need for deciding with which set of networks to connect and which connection to use as primary connection.

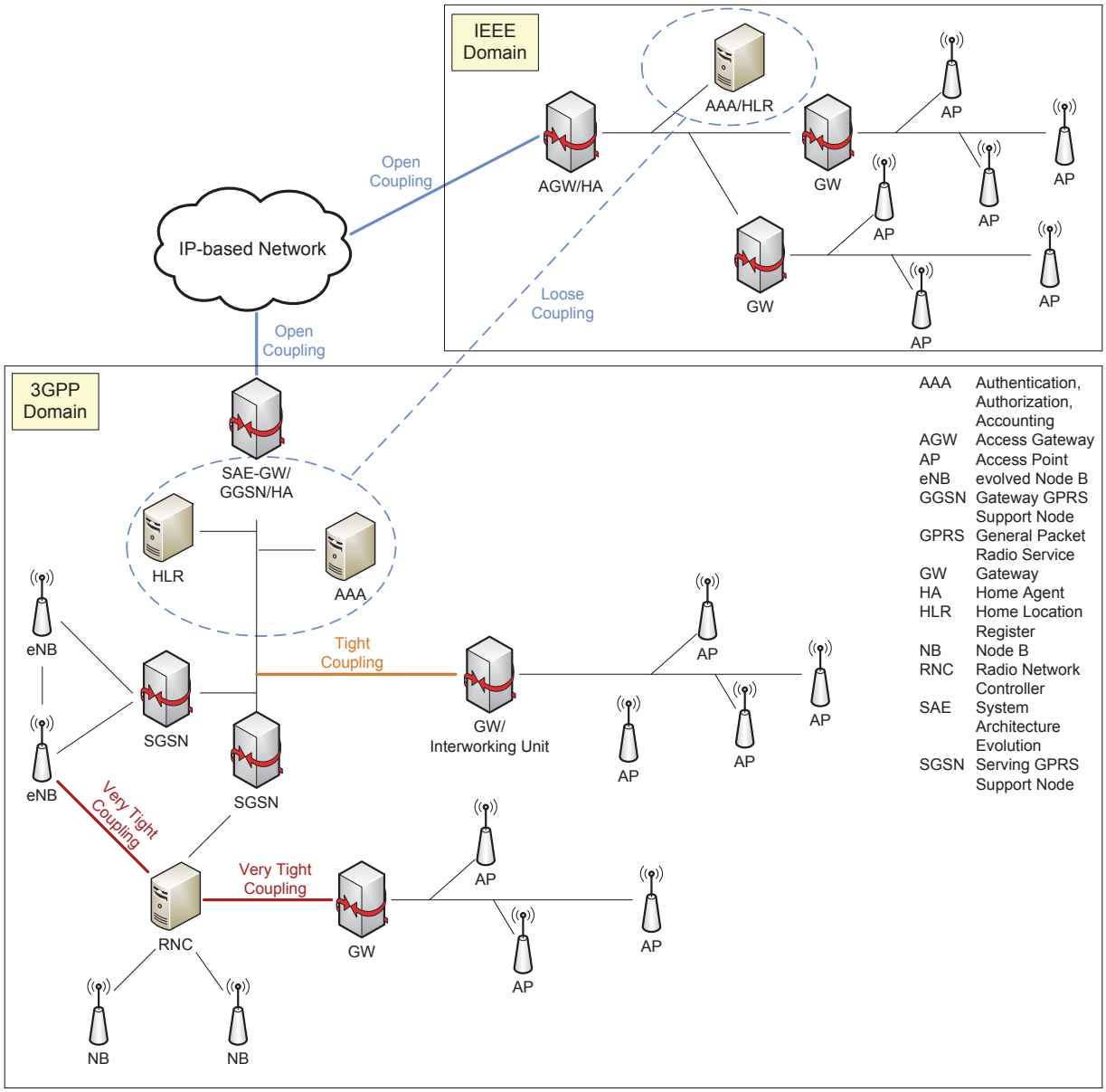

Figure 3.3: Overview of different network coupling concepts

the one hand, and mobility support and resource utilization efficiency on the other hand. For instance, the authors of [SFA03] describe the realization of these levels of network coupling using the example of UMTS and WLAN. In Figure 3.3, an overview of different coupling concepts is depicted.

A very tight coupling or integrated approach allows CRRM entities to influence resource allocation decisions on BS level and requires modifications of RAT-specific RRM functionalities and implementation of proprietary interfaces, e.g., between eNB and RNC. It is thus more complex and costly to realize, but in turn yields more efficient means for enabling seamless mobility. Tightly coupled RANs manage inter-working on a Serving GPRS Support Node (SGSN) and Gateway (GW) level. For example, in case of a tightly

coupled UMTS and WLAN system, the authors of [PSTGG08] found that the connection establishment with the target RAT contributes the most to the overall HO execution delay. Further, they propose protocol enhancements that yield HO delays for VHOs from WLAN to UMTS and from UMTS and WLAN ranging from 630 to 950 ms and from 280 to 600 ms, respectively.

In case of loosely coupled network domains, both RANs provide interfaces for sharing Home Location Register (HLR) and AAA information. For example, in case of a loosely coupled UMTS and WLAN system, overall HO delays may range from 1 to 4 s [PSTGG08]. However, the authors of [MYLR04] developed a sophisticated Stream Control Transmission Protocol (SCTP) based VHO scheme that reduces overall HO delay to 220 ms given association on lower layers is completed.

In contrast, in an open coupling approach the point of integration is implemented beyond the Gateway GPRS Support Node (GGSN), which provides interfaces to external IP based networks. This results in simpler and cost-effective implementation prospects, but larger VHO execution times [SFA03], [PRSA+05], [PSTGG08].

Various protocols have been introduced to cope with the issue of inter-network mobility in *All-IP* networks. MobileIP (MIP) [Per10], [PJA11] and its derivatives, such as Hierarchical Mobile IPv6 (HMIPv6) [SCEB08] or Fast Handovers for Mobile IPv6 [Koo05], laid the basis for IP based vertical handovers. These network layer mobility management concepts can be categorized into *macro-mobility* and *micro-mobility* solutions, respectively [AJM04]. Macro-mobility refers to the case where mobile users or Mobile Nodes (MNs) move between different network domains, while in case of micro-mobility, MN movements only occur between subnets within one domain.

Originally in MIPv4 [Per02], messages and content from the Correspondent Node (CN) were sent to the MN's Home Agent (HA). The HA was in charge of managing the MN's Care-of Address (CoA) and forwarding messages through a tunnel to the Foreign Agent (FA) of the network where the MN was currently attached, raising the issue of triangle routing, as illustrated in red in Figure 3.4 [AMH+98]. In contrast, MIPv6 realizes *route optimization* by introducing a *binding cache* at each CN, where home address and recent CoA information is preserved. The CN will first try to directly send packets to the respective MN, exploiting the IPv6 routing header option as illustrated in green in Figure 3.4. In case no recent CoA information is available in the CN's cache, packets will be sent to the MN's HA that will forward them to the corresponding network. For a realistic "hotspot" deployment scenario, the authors of [PCTMH03] gained interesting insights on the

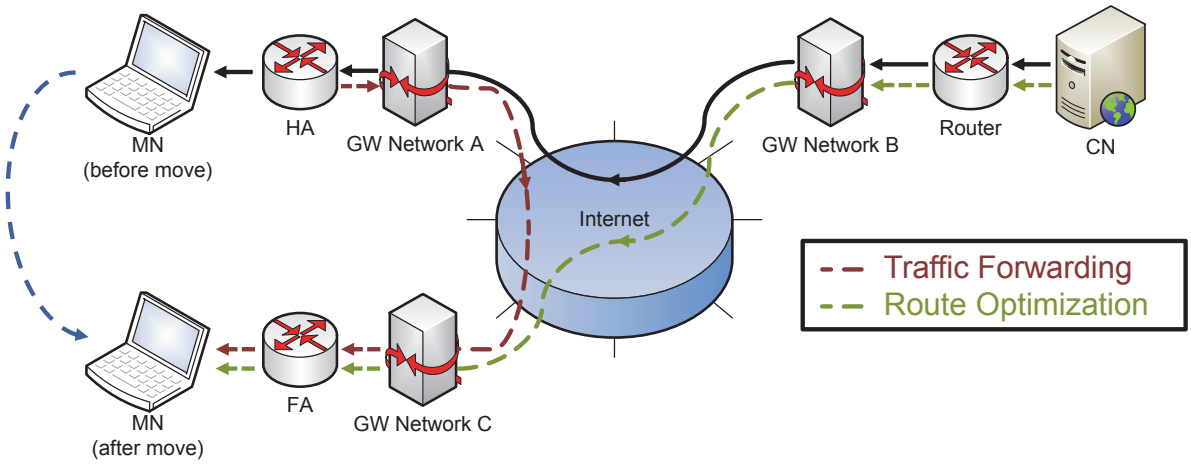

Figure 3.4: Mobile IP concept

performance of MIPv6 and its enhancements. In particular, they were able to show that i) random movements of the observed MN affect the experienced performance but the improvements with respect to the perceived QoS when using one of the various MIPv6 enhancements is still clearly noticeable, ii) in scenarios where the users generate a low rate with small packets, for instance, VoIP sources, the additional overhead introduced by the proposed enhancements can result in a worse performance than the baseline MIPv6 one, and iii) MIPv6 can eventually outperform its proposed enhancements in terms of packet losses in congestion situations due to the higher number of packets discarded directly that lower the load in the wireless channel.

Another approach for enabling mobility between heterogeneous networks was suggested by the IEEE working group 802.21 that published the first standard for Media Independent Handover (MIH) services in 2008 [IEE12] [TOF+09]. Here, a MIH functionality is introduced on each network entity between layer 2 and 3 that supports all specified services, such as Media Independent Event Service (MIES), Media Independent Command Service (MICS), and Media Independent Information Service (MIIS). The main objectives of these services are as follows [IEE09]:

- MIES provides event classification, filtering, and reporting corresponding to dynamic changes in link characteristics, status, and quality.
- MICS enables MIH users to manage and control link behavior relevant to handovers and mobility.
- MIIS provides details on the characteristics and services provided by the serving and neighboring networks. This information enables effective system access and handover decisions.

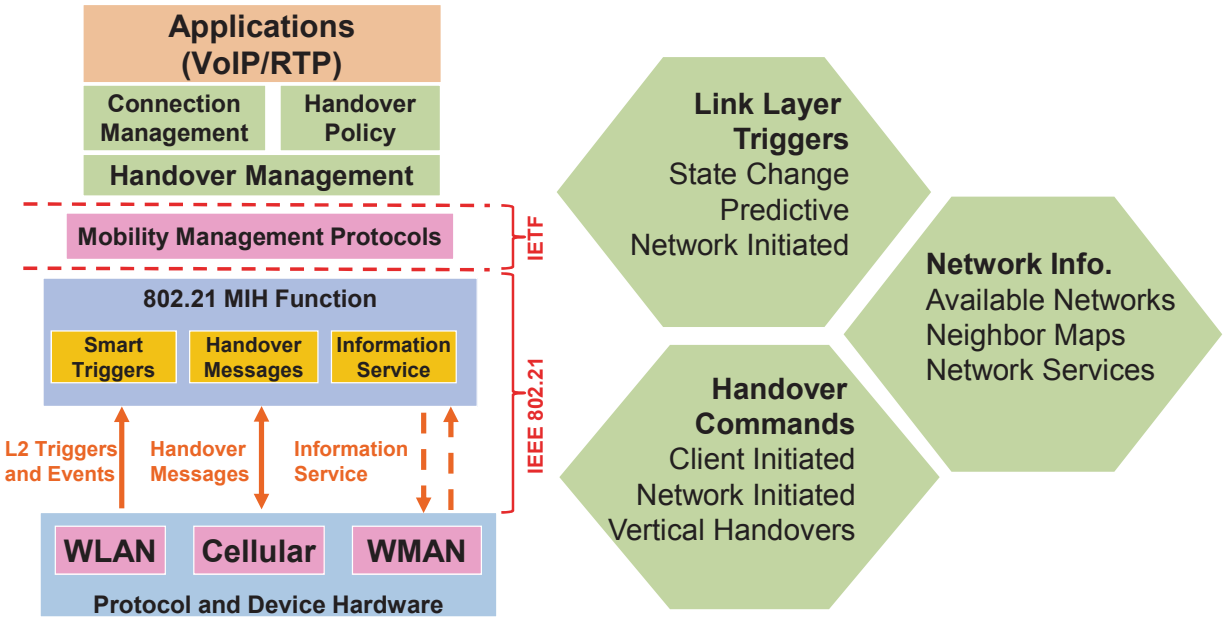

Figure 3.5: IEEE 802.21 key services [Gup06]

Figure 3.5 depicts the MIH concept, involved triggers, network information, and HO commands [Gup06].

In various works, IEEE 802.21's framework has shown to provide suitable means for seamless handover across heterogeneous networks supporting network- and user-triggered handovers [TDYH+09] as well as QoS support in a heterogeneous multi-radio carrier-grade wireless backhaul network [KG10]. However, to the best of the author's knowledge, the IEEE 802.21 standard has not been implemented in a commercial network yet, presumably due to the lack of industry support.

Besides these protocols that aim at supporting network layer mobility, another protocol that is already widely employed by enterprises and IP telephony providers and that handles terminal mobility on application layer has been developed by the Internet Engineering Task Force (IETF). The *Session Initiation Protocol* (SIP) [RSC+02] supports all common forms of mobility, including terminal, personal, session, and service mobility. For terminal mobility, an IPv6 based solution is likely to be preferable, as it applies to all-IP based applications, rather than just Internet telephony and conferencing. In the absence of HAs, however, SIP based mobility can provide mobility services to the most important current mobile application, telephony [SW00].

SIP based mobility is accomplished by updating the ongoing session using "re-INVITE" messages with the same session identification as the current one. The "re-INVITE" message includes the MN's new IP address, that has been provided by the new access network, which allows a CN to adapt the

destination address of the packets associated with the MN accordingly. In essence, there is no need for any intermediate entity, such as HAs, through which packets from the CN pass. This Peer-to-Peer (P2P) based scheme of SIP is its most remarkable advantage over MIP.

However, SIP mobility has a significant drawback: it lacks mobility management for TCP connections [SMZ+07]. Further shortcomings of SIP become evident in case of mid-call mobility, where HO delay, e.g., due to Dynamic Host Control Protocol (DHCP) or Packet Data Protocol (PDP) context activation, can cause considerable packet loss and seriously affect QoS [WBBD05]. One solution to this issue is *soft* handover [BAD06], where a connection to the target BS or AP has already been established before the former connection is terminated. The feasibility of this approach has been demonstrated in [SMK+11].

Furthermore, improved hybrid MIP-SIP concepts that try to combine the strengths of both approaches, e.g., by merging redundant MIP and SIP entities and operations of similar functionality or by integrating them, have been proposed [WDB+03], [QAR06]. However, their deployment is costly, since all components must be installed on both MNs and the core network. In order to avoid these additional costs, the authors of [SMZ+07] propose a SIP based middleware that is in charge of handling session and mobility control exploiting the *local loopback interface* on the MN, in particular with respect to TCP connections, where the implementation still faces issues when transferring TCP connections. In the context of this evolution toward all-IP networks that is driven by ITU-T's vision of *Next Generation Networks* (NGN)[5], 3GPP developed a third generation (3G) networks standard that laid the foundation for providing ubiquitous cellular access to all Internet services: the *IP Multimedia Subsystem* (IMS) [3GP12e]. It aims at merging two of the most successful paradigms in communications, cellular networks and the Internet [CGM08], by constituting an overlay all-IP service architecture for real-time multimedia service provision. Further, it is based on the key signaling and administration protocols developed by the IETF: SIP and *Diameter* [CLG+03]. Nevertheless, although several approaches for VHO based on MIP, SIP, IMS, and IEEE 802.21 have been studied, none of them was fast enough to support real-time applications, as argued in [PSTGG08], where

[5]"A Next Generation Network (NGN) is a packet-based network able to provide services including Telecommunication Services and able to make use of multiple broadband, QoS-enabled transport technologies, in which service-related functions are independent from underlying transport-related technologies. It offers unrestricted access by users to different service providers. It supports generalized mobility which will allow consistent and ubiquitous provision of services to users." [ITU04]

an optimized cross-layer VHO protocol is proposed for improving seamless UMTS/WLAN handovers.

3.5 Summary

The previous sections presented fundamental concepts and state-of-the-art approaches that are relevant for realizing a holistic concept for Intelligent Radio Network Access (IRNA) and developing an integrated HAM solution. Such an integrated HAM concept inherently addresses multiple objectives simultaneously. The solutions developed by the author and described in Chapter 5 aim at jointly enhancing network selection, HO decisions, admission control, load balancing, and optimizing overall system capacity in a multi-RAT environment. However, first, one important key enabler, on which these solutions are based, is introduced in Chapter 4.

4 Context Awareness and Management

Already in 1991, Mark Weiser [Wei91], who is widely considered to be the father of *ubiquitous computing*, envisaged that

> "computers will come to be invisible to common awareness. People will simply use them unconsciously to accomplish everyday tasks."

Today, there are already many application domains and use cases envisioned where any kind of devices, e.g., sensors, or services, e.g., cloud services, communicate for unconsciously supporting people in their every day life tasks. For example, in a *smart* home, the heating system is automatically managed depending on weather conditions, the TV recommends series or movies matching peoples' interests, the refrigerator updates the shopping list on a smartphone, or a call handover is triggered by the mobile phone to a home base station while the home owner is approaching or to its car base station when leaving. All these visions, that could become reality in the not too distant future, rely on one common enabler: *Context Awareness*. If an entity (e.g., service, application, user terminal, network management, actuator) is capable of adapting to a specific context, it is referred to as context-aware. Meanwhile, context awareness is regarded as a key enabler for group management and content selection [C-C08], situation management [HSN+10], group communications [JSA+09], as well as improved system, transport, and service adaptations [BCG07], [APSP10], [LSZ10]. In particular, the capability of a context-aware system of managing large numbers of heterogeneous context sources in large scale highlights its significance for intelligent ICT infrastructures. For instance, enhanced controlling of system behavior and service provisioning are crucial for mobile network operators in order to mitigate Operational Expenditures (OPEX) and to stand out from their competitors. Further, a modular design approach allows for eased integration of modules tailored for specific applications and use cases, such as ambient assisted living scenarios or (network) traffic management.

Moreover, the massive reduction in size and cost of electronic user equipment due to advances in microelectronics and mass market production have further contributed to a reality where the majority of people carries along at least one wireless communication device, for example, a smartphone. Modern user terminals possess a variety of sensors, wireless interfaces, and applications for supporting context-aware services, ranging from everyday life tasks, such as location-related weather forecast, to enhanced mobility support across Radio Access Technologies (RATs). These technological and societal evolutions laid the foundation for researching meaningful opportunities for the exploitation of any kind of context information that is made available. In the scope of this thesis context information is used for improving mobility support and network performance, as illustrated in Chapter 5, as well as for Mobility Robustness Optimization (MRO), as presented in Chapter 7.

In the following, origin and various definitions of context awareness that evolved over time are introduced. Further, in Section 4.2, state-of-the-art approaches and a possible implementation of a context management system are presented, which laid the foundation for developing the holistic Intelligent Radio Network Access (IRNA) concept described in Chapter 5.

4.1 Origin and Definitions

The origin of the term *context-aware* computing is often related to a publication by Schilit and Theimer [ST94], where it is defined as

> "the ability of a mobile user's applications to discover and react to changes in the environment they are situated in."

In their work, they present an active map service that manages location information for objects in a certain region, referred to as "located-objects", and that provides mobile clients with information on those objects and on how they change over time. Similarly, many authors define and enumerate context in detail, e.g., user's location, identities of the people around the user, the time of day, season, temperature, etc. [BBC97], user's location, environment, identity, and time [RPM97], or the user's emotional state, focus of attention, location and orientation, date and time, objects, and people in the user's environment [Dey98]. Further, various authors simply provide synonyms for context, such as environment or situation. For instance, context was defined to be the elements of the user's environment that the user's computer knows about [Bro96b], the situation of the user [FF98], the state of

the application's surroundings [WJH97], the application's setting [RCDD98], or the aspects of the current situation [HNBR97]. In their overview paper, Dey and Abowd [DA00] state that context-aware has meanwhile become synonymous with other terms, such as responsive [EHC+93], reactive [CTB+95], adaptive [Bro96a], environment-directed [FKS97], situated [HNBR97], and context-sensitive [RAH98]. In order to avoid limiting the definition of context to specific types of information provided in the enumerations of one of the many authors, Dey and Abowd [DA00] define context in a general and broader sense. Their definition will further be used in the scope of this thesis and is stated as follows:

> "Context is any information that can be used to characterize the situation of an entity. An entity is a person, place, or object that is considered relevant to the interaction between a user and an application, including the user and applications themselves."

Further, Dey and Abowd [DA00] list location, identity, time, and activity as primary context types for characterizing the situation of a particular entity and consider a system as being context-aware,

> "if it uses context to provide relevant information and/or services to the user, where relevancy depends on the user's task."

Recently, Zimmermann [Zim08] added relation as another primary context category and proposed in his work a conceptual and a software framework that aim at reducing usability problems with respect to designing context-aware applications. Furthermore, a more user-centric view was formulated by Baker et al. [KTB09] to characterize a context-aware system:

> "A system is defined to be context-aware, if it is able to assist its users without their explicit interactivity."

The definition of a context-aware system that will be used in the scope of this thesis is a merger of both afore mentioned statements and is stated as follows:

> "A system is considered as being context-aware, if it uses context to provide relevant information and/or services to the user without explicit interactivity, where relevancy depends on the user's task."

The term *situation* is usually regarded as a part of context and throughout this thesis the following definition provided by Zimmermann [Zim08] will be employed:

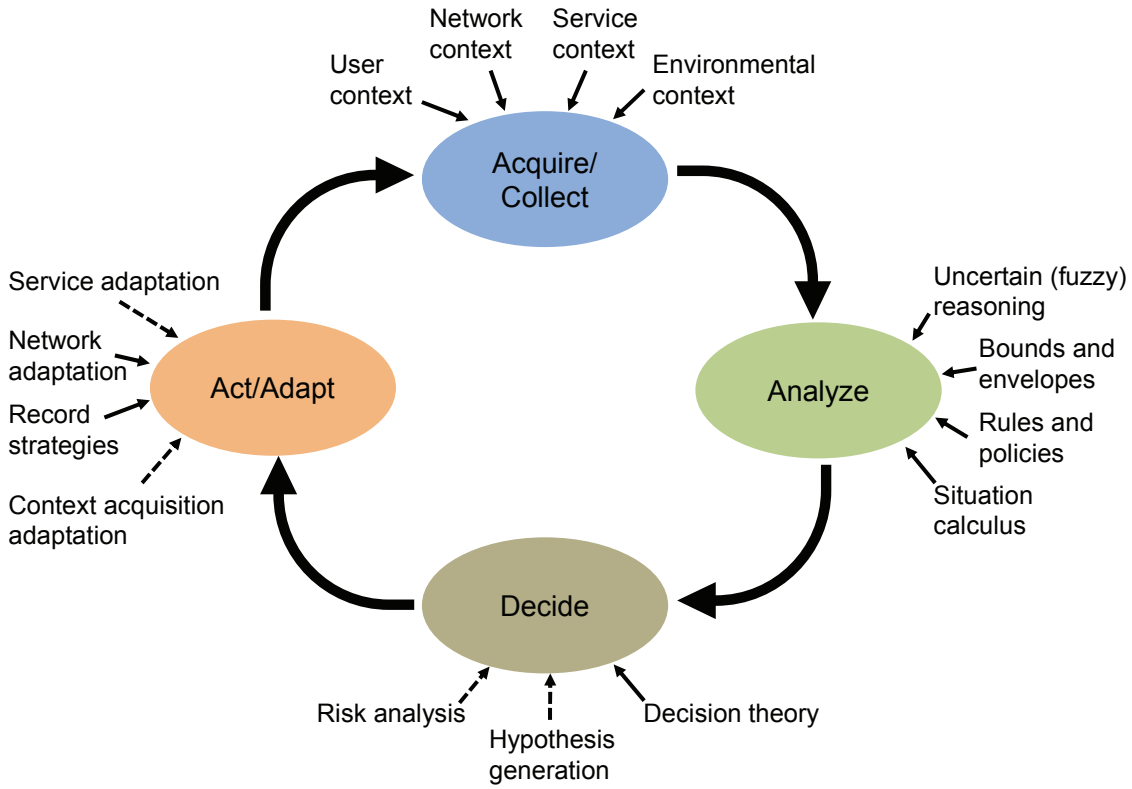

Figure 4.1: Operation cycle of a context-aware system (adapted from [DDF+06])

> "A situation is the state of a context at a certain point (or region) in space at a certain point (or interval) in time, identified by a name."

Relating these views that emanate from the ubiquitous and pervasive computing domain to the area of wireless communications and networks, the author contributed to shaping the following definitions [MET13b]:

> "Context information is the information enabling the perception of states and situations of network entities (e.g., network nodes, terminals, users, etc.) and their interactive relations. A context-aware radio network is a network which utilizes the context information to assist its operation and optimization without explicit interaction with its users."

In 2006, Dobson et al. [DDF+06] describe an autonomic system model that well reflects the operation cycle of a context-aware system. This model has been adapted and a modified version of this model is depicted in Figure 4.1, where dashed arrows refer to functionalities that are out of the scope of this thesis.

Introducing new functionalities that assist in establishing context awareness in wireless and communication networks facilitates entirely autonomous network operation, including self-configuration, -optimization, and -healing. Approaches for enabling self-X capabilities are introduced in Chapter 6. Further, self-tuning mechanisms for optimizing mobility robustness are particularly addressed in Chapter 7.

4.2 Context Management Systems

The importance of context awareness is fostered by the general principle that the more information characterizing a situation, system process, or object is available, the better tailored applications and system control tasks or optimization strategies can be designed. This fundamental relation supports the introduction and application of functionalities and protocols enabling context awareness in various fields, ranging from computer science over communication networks to economics and health care.

A Context Management System (CMS) is usually based on the producer-consumer role model that can frequently be found in the area of context management [PRP+07]. The CMS developed in the scope of the EU FP7 project *Context Casting* (C-CAST) [C-C09a] is shown in Figure 4.2 [6].

A federation of *Context Brokers* (CxBs) provides *Context Consumers* (CxCs), such as applications or a service execution environment, access to context information that originates from *Context Providers* (CxPs). In principle, the nature of context information that is provided by CxPs can range from raw measurement data to processed high-level context. For categorizing access to context sources, Chen [Che04] proposed the following classes:

1. *Direct access to sensors* - Sensors that are available on user terminals or network nodes collect context information such as location or network load.

2. *Middleware infrastructure* - The introduction of middleware infrastructure aims at strictly separating the processes of context acquisition and management, thus improving system extensibility and reusability.

3. *Context server* - A resource-rich context server takes over the task of administering context data that it receives from various context sources.

[6] It should be noted that privacy, security, and Authentication, Authorization, Accounting (AAA) aspects are out of the scope of this thesis and are not reflected in Figure 4.2.

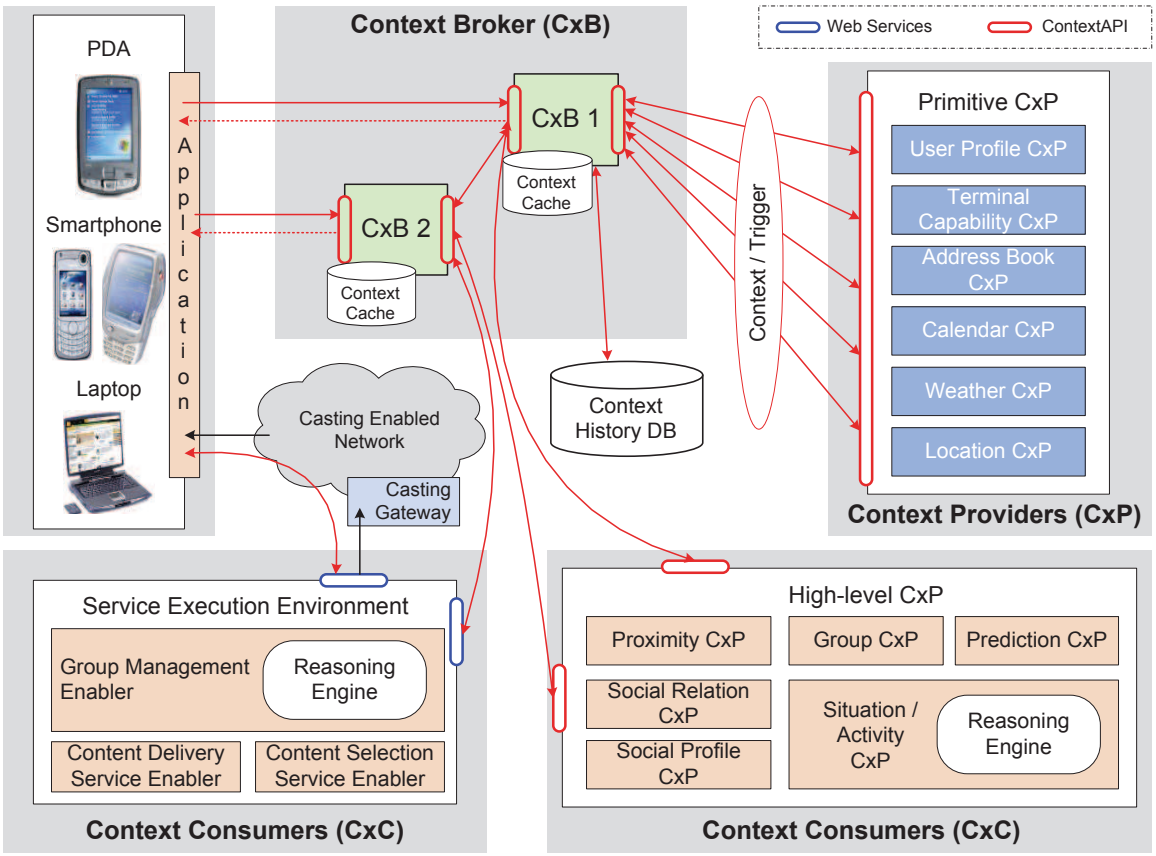

Figure 4.2: Context management architecture [C-C09a]

It relieves terminals and network nodes from managing context requests from other entities.

In summary, CMSs acquire, process, manage, and distribute context information according to the specific needs of applications and services. Figure 4.3 [BZKM09] illustrates the basic context processing flow, where typical steps (with increasing level of abstraction) are: acquisition, representation, reasoning, situation recognition, perception, and adaptation.

Ideally, CMSs should be versatile with respect to application fields and capable of supporting many heterogeneous types of context information that potentially originate from various domains. However, depending on the intended utilization of context information, context management concepts have to comply with different requirements with respect to *modularity*, *reactivity*, *scalability*, and *extensibility*. In order to address these research issues, the author contributed to the design of a CMS that is able to adaptively control and manage context information according to the requirements of different context consumers, such as the Heterogeneous Access Management (HAM) entity that is introduced in Chapter 5.

The CMS concept, which is illustrated in Figure 4.4, was developed and evaluated in the EU FP7 project C-CAST [C-C09a], [C-C09b], [C-C10], and

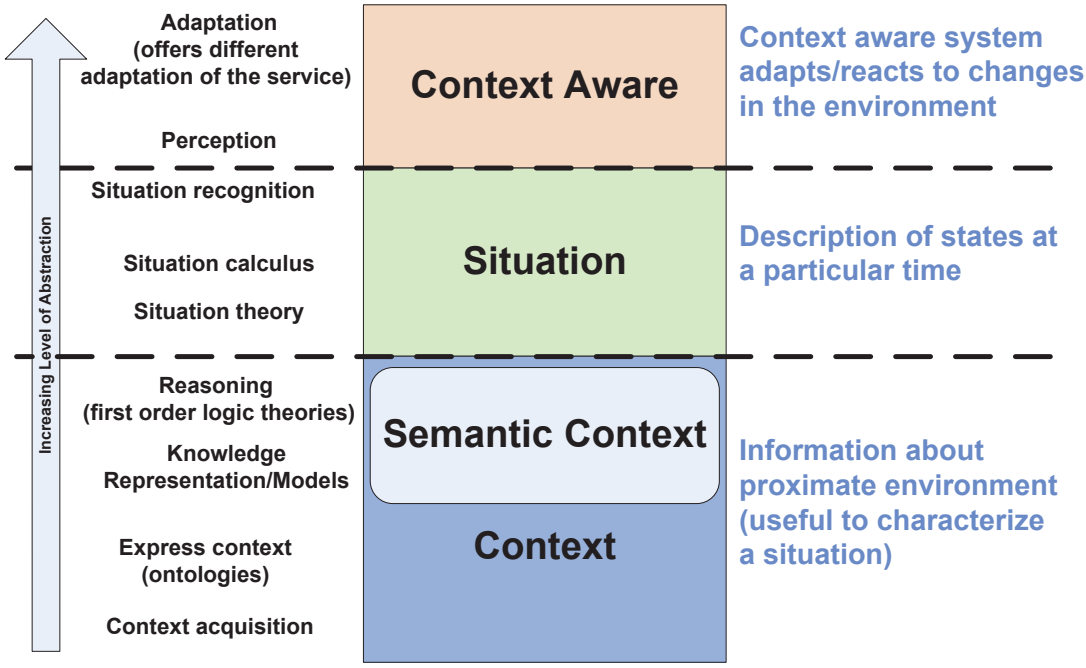

Figure 4.3: Context layers [BZKM09]

also had an impact on the EU FP7 Future Internet Core Platform (FI-WARE) project [FI-13]. As already depicted in Figure 4.3, typical context information processing steps involve sensing and acquisition, aggregation, fusion and reasoning, management and dissemination, and finally application for, e.g., service adaptation or network performance optimization. For the design of the developed CMS concept, the focus was on context acquisition, management, and distribution of context information, while simultaneously controlling context quality, for instance, required for HAM purposes. These functionalities require the following core architectural components: CxPs, CxBs, and CxCs. Two different communication modes are supported by the system. In the asynchronous mode, context is published, if a specified condition or event comes true ("subscribe/publish mode"). In the synchronous mode, a request for context information is instantly answered ("request/provide mode"). The characteristics of the core components are described in the following:

- **Context Providers** (CxPs) gather data from a collection of sensors, network nodes, services (e.g., web services), or other relevant sources (e.g., social networks). A CxP may employ various filtering, aggregation, and reasoning mechanisms to infer high-level context from raw sensor or measurement data. The processed context is then modeled according to a specified representation scheme, such as key-value, mark-up scheme (e.g., XML), graphical (e.g., UML), object oriented, logic based, or ontology based (e.g., RDFS, OWL) models [BSR07]. Each provider

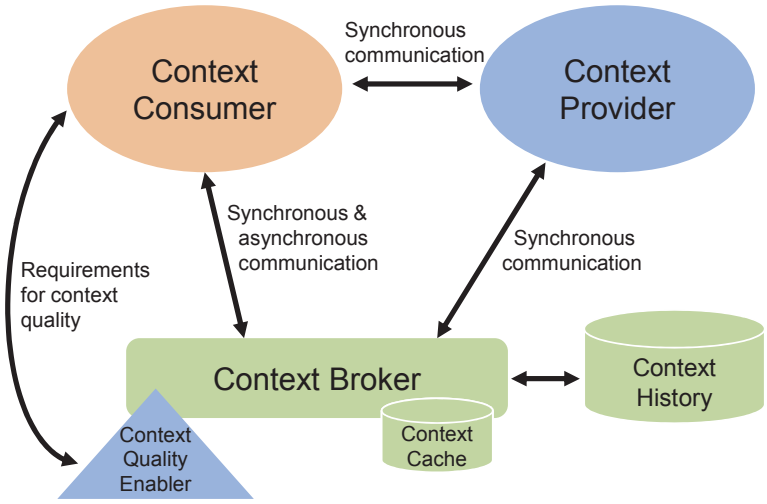

Figure 4.4: CMS component interactions [MKSS09a]

is tailored to provide a particular type of context. For example, a calendar CxP delivers calendar information and a location CxP provides location information of a specified entity, e.g., users or group of users. Every CxP registers its capabilities by sending appropriate announcements to the respective CxB, so-called CxP *advertisements*. Further, it regularly indicates its availability via so-called *context update* messages and provides interfaces to the CMS.

- **Context Brokers** (CxBs) take on the role of intermediaries. Their main functionality is to maintain a distributed registry of available CxPs and their capabilities based on the announcements sent by CxPs. Using this registry, they can provide a CxP look-up service to entities searching for certain context data. CxBs could be organized in a distributed manner forming a federation of CxBs [CFJ03] in order to avoid the bottleneck problem of a centralized implementation. The level of decentralization depends on scalability issues and targeted applications. For instance, in an office environment or a large building with millions of context sources, each floor could be managed by a separate CxB, whereas in a small village with only hundreds of CxPs one CxB might be sufficient for supporting context-aware services.
- **Context Consumers** (CxCs) are architectural components that use context data for their purposes, for instance, a context based application, a network management entity, or a network optimization mechanism. A CxC can retrieve context information by sending a request to the CMS. The CxB either directly provides the respective context that is available in its cache, e.g., via a RESTful [7] interface [Tya06], or pro-

[7] Representational State Transfer (REST) is an architectural style, introduced by Fielding in 2000 [Fie00],

vides the address of a suitable CxP by which the requested context can be delivered. Alternatively, CxCs can subscribe to specific context with the CxB, that will notify the CxCs as soon as the specified notification condition is reached.

- **Context Quality Enablers** (CQEs) ensure that context quality requirements are met. Context management systems supporting CxCs, such as HAM, in a dynamic, multi-RAT, multi-vendor environment have to perform a multitude of tasks to optimize network utilization. In order to facilitate enhanced decisions, e.g., in terms of network selection, link adaptation, prediction of user behavior, and multicasting, HAM entities require context data of high quality. The integration of a CQE into the CMS ensures that only context information that adheres to the stated quality criteria will be used for HAM. Accordingly, only CxPs with the corresponding characteristics are able to deliver the appropriate context data, where main criteria are accuracy, reliability, availability, and provisioning delay of context data. Consequently, the CQE is attached to the CxB, since it is the broker that disposes of information on CxP capabilities and availability. Thus, when requesting context information, CxCs also send minimum requirements with regards to context quality. The CQE uses this information for filtering context information accordingly.

In the work of Mannweiler et al. [MAS+10], the author contributed to the design of a distributed context registry using the concept of *Distributed Hash Tables* (DHTs)[8]. Such a registry needs to be permanently maintained in order to achieve a consistent distribution of information. The concept of the distributed context service registry is illustrated in Figure 4.5 [MAS+10]. In [Ama10], the DHT based system has been successfully tested with 15 to 20 network nodes (including smartphones), each disposing of three to five context services. Thus, it is, for example, possible to access the sensors of a smartphone placed in a remote location. Measurement results showed

for distributed hypermedia systems, such as the World Wide Web. It is a hybrid style derived from several network based architectural styles, e.g., P2P styles, and combined with additional constraints that define a uniform connector interface. Thus, simple HTTP can be used for establishing connections between machines and exchanging context information.

[8] "A distributed hash table (DHT) is a class of a decentralized distributed system that provides a look-up service similar to a hash table; (key, value) pairs are stored in a DHT, and any participating node can efficiently retrieve the value associated with a given key. Responsibility for maintaining the mapping from keys to values is distributed among the nodes, in such a way that a change in the set of participants causes a minimal amount of disruption. This allows a DHT to scale to extremely large numbers of nodes and to handle continual node arrivals, departures, and failures." [Wik13a]

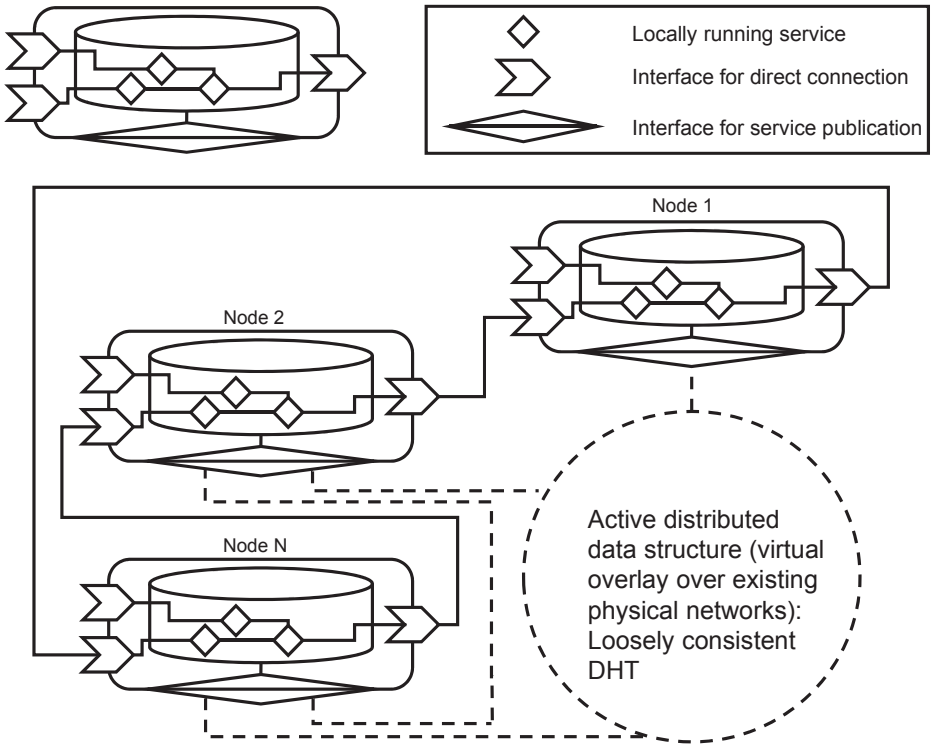

Figure 4.5: DHT based context service registry [MAS+10]

that service look-up requests were answered within less than 160 ms. On the one hand, CxCs, such as context-aware applications and services or network optimization mechanisms, require context information in order to adapt to changes in their environment, for instance, occurring network issues and user-related events. On the other hand, CxPs, such as user terminals and wireless network nodes, are key components for delivering the requested context. Moreover, built-in GPS modules, cameras, gyroscope, temperature, ambient light, and acceleration sensors are becoming widespread with the recent success of smartphones and other mobile devices that are also capable of supporting various RATs. Further, an increased willingness of users to share their interests and parts of their personal profiles can be observed. For example, user information originating from social networks that is complemented with context information acquired from network infrastructure and device sensors facilitates the design and optimization of services and network management strategies, which yield significantly enhanced user experience as well as optimized network performance.

Exploiting the available context information for improving and optimizing network performance is a meaningful application beyond conventional end consumer services, such as location-based services. However, in both cases, a CMS is required in order to properly supply the application or optimization mechanism with appropriate context, thus making it "context-aware". The

majority of early context-aware systems have just been location-aware. Want et al. [WHFG92] created one of the first context-aware applications the so-called *Active Badge Location System*, where the current location of a user was determined using a network of sensors deployed in an office environment. In the late 1990s, location-aware tourist guide systems were developed that replaced or complemented traditional tourist guides [AAH+97], [SEF+98], [CDM+00]. Meanwhile, there have been improvements with respect to both architectural frameworks for context-aware systems, e.g., within the scope of European funded projects, such as *SPICE* [ZZM+06], *MobiLife* [FPN+05], or *C-CAST* [C-C08], and the diversity and quality of available context information (e.g., advanced positioning technology [JLL+07]).

In particular in the framework of the EU FP7 project *C-CAST*, the author contributed to the development of various concepts that aim at realizing intelligent radio network access [KMS09] [MKSS10], context-aware multiparty networking [JSA+09], and improving handover performance [MKSS09a]. Further, in the nationally funded BMBF project *German-Lab* (G-LAB), the idea of context information exploitation was beneficially applied for developing a terminal-centric multihoming approach [CMK+10], for providing scalable and on demand high-quality mobile access in the area of *Mobile Cloud Computing* [KMSS10], for realizing context- and application-aware RRM [SWP+10], context-enhanced HAM [KMS+10] and service provisioning [KLM+11a] [LKMS12], as well as multi-casting [MKSS11a] [MSKS11]. The core ideas of these contributions are described in detail in Chapter 5.

4.3 Summary

In essence, a distributed, scalable, flexible, and open context management approach is of significant importance for adapting system and service behavior as well as infrastructure functionalities according to user needs or operator and service provider objectives by incorporating a multitude of heterogeneous context information. While context awareness is considered as a key enabler for realizing these system features, the implementation and performance of a specific CMS may heavily depend on application requirements, computational capabilities, and available interfaces.

In this thesis, context information albeit related to environment, networks, terminals, or users is acquired, processed, managed, and meaningfully employed for improving radio network performance. The scalable, modular, and open nature of the CMS presented in Section 4.2 allows for integrating

a variety of modules that target specific use cases, for instance, intelligent radio network access and management, which is introduced in Chapter 5. Furthermore, modules performing trend estimation, e.g., for detecting imminent network congestion, can be tailored to location-specific conditions and further enhanced using statistical data for situation recognition. Moreover in the long-term, situation characteristics can be learned and exploited for optimum system adaptations, e.g., for the purpose of Mobility Robustness Optimization (MRO) as described in Chapter 7.

5 Context-Enhanced Heterogeneous Access Management (HAM)

The heterogeneity of today's wireless access possibilities imposes challenges for efficient access and resource management across different Radio Access Technologies (RATs). Moreover, new fields of application, such as the Internet of Things and Machine-to-Machine (M2M) communication, impose challenging requirements regarding wireless access and connectivity. In light of upcoming 5G technologies and emerging mobile cloud computing, concepts, such as *Fixed Mobile Convergence* (FMC) [SC08] and *seamless mobility* [Gol09], are driving the evolution toward comprehensive network management approaches. Further, the increasing availability of both static and dynamic context information has steadily been driving the development of context-aware communication systems. Adapting system behavior according to the current context of the network, the user, and the User Equipment (UE) can yield significant End-To-End (E2E) performance improvements. Incorporating the idea of context awareness into Heterogeneous Access Management (HAM) brings together two areas of research: On the one hand, HAM for enabling improved wireless access has become very relevant in a world that not only increasingly relies on being "online" permanently, but also on guaranteeing Quality of Service (QoS) and on-demand high-speed network connections. On the other hand, context awareness is a key feature of systems that have to decide on how to efficiently manage network resources in order to enhance overall system performance.

5.1 Intelligent Radio Network Access

Today, context information is made available for a broad variety of applications, e.g., context-aware services for mobile terminals, and is still expected to

drive the demand for personalized applications. These services increasingly rely on data gathered by terminal sensors and wireless sensor networks deployed in public places or indoor environments [SKMS09], [SKMS10]. Sensor data is complemented by information stored in databases. Reasoning mechanisms combine numerical data from various sources to infer higher level context information required by actuator networks or for service adaptation, e.g., in smart homes or Ambient Assisted Living (AAL) scenarios. In a similar way, user and network context can be used for optimizing HAM.

In the following, a context-enhanced HAM concept is presented that accounts for network, terminal, and user context while simultaneously trying to accommodate users, facing different environment conditions, with the best possible E2E performance. Therefore, a Context Management System (CMS) (cf. Chapter 4) is utilized that is able to efficiently handle context information as well as the respective providers and consumers. The growing need for wireless Internet access in combination with a more and more diverse landscape of radio access technologies (WLAN, GPRS, UMTS, HSPA, WiMAX, LTE, etc.) increases the demand for efficient HAM. Besides features, such as "always on" and "always best connected" [GJ03], an efficient use of the heterogeneous landscape of RATs shall be achieved. Radio resources are of course limited due to physical, technological, and regulatory constraints. Context, either provided by user terminals, network nodes, or acquired from sensors deployed in the user's environment, may be used to significantly improve the utilization of scarce radio resources and efficiently manage wireless access across heterogeneous RATs. Therefore, HAM entities have to be able to exploit not only radio network parameters but any available context information of the environment, networks, UEs, and users. Further, the availability of both static and dynamic context information has steadily been increasing in recent years, mainly driven by technical advancements with respect to UE capabilities and the users' willingness to share personal information, e.g., via social networks. Accordingly, manifold use cases for these data, especially for consumer services, for instance, location-based services [VMG+01], have been suggested. Since the use of context information enriches the information basis on which HAM decisions are taken, network selection and handover decisions can be significantly improved, given context information, such as network load, user velocities, and estimated user movements, are available. In Figure 5.1, a concept for Intelligent Radio Network Access (IRNA) is presented that the author introduced in [KMS09], [MKSS09a], [MKSS09b] and that relies on a CMS, as depicted in Figure 4.4.

A CMS with its context acquisition and dissemination mechanisms pro-

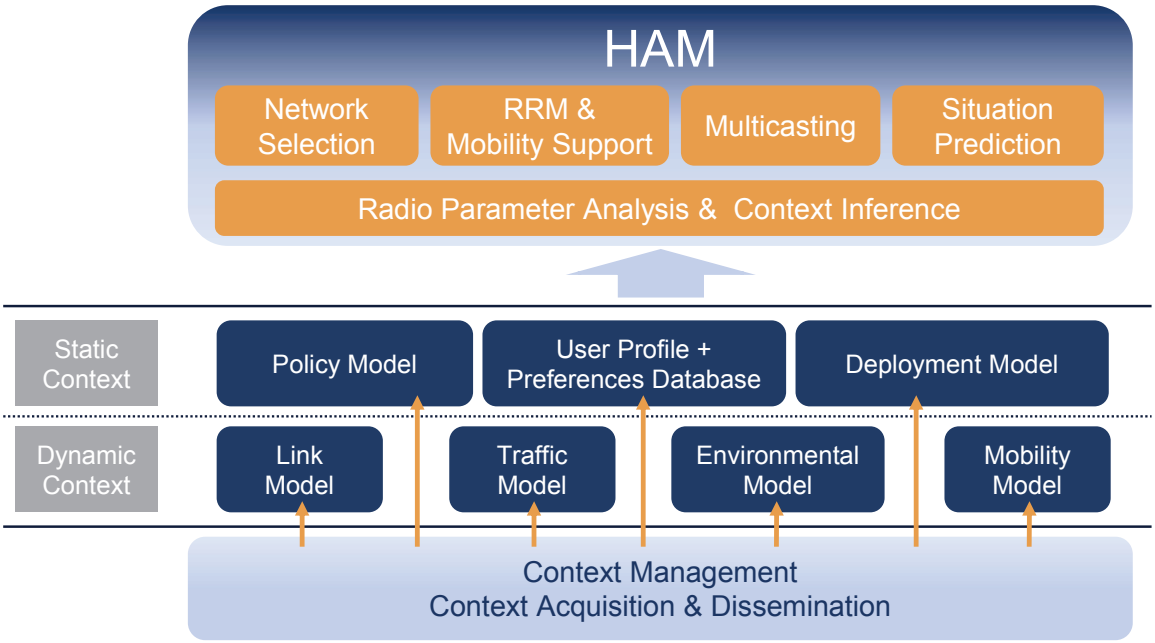

Figure 5.1: Concept for intelligent radio network access [KMS+10]

vides the basis for building several context models, where there is a differentiation between static and dynamic context information. Dynamic context information consists of any information that may quickly vary over time, such as received signal levels, user traffic demands, environments users are passing through, or user mobility. Static context information rather refers to information that may vary over larger time scales or is constant. This includes, for instance, UE hardware capabilities, Mobile Network Operator (MNO) policy for network operation in a specific service area, or RAT deployments. These context models are used for radio parameter analysis and context inference, which form the basis for HAM decisions, e.g., on network selection or Handover (HO). Several examples for context data exploitation are presented in Section 5.2. The IRNA concept was further used for enhancing terminal-centric multihoming approaches [CMK+10], for providing scalable and on demand high-quality mobile access in the area of mobile cloud computing [KMSS10], and for realizing context- and application-aware Radio Resource Management (RRM) [SWP+10].

In a landscape of heterogeneous wireless access technologies, no RAT simultaneously exhibits all desired features, such as wide coverage, high bandwidth, QoS, mobility support, as well as low access and usage costs. The IRNA concept goes beyond by extending the ideas of "always on" and "always best connected" toward a solution that enables optimized HAM performance while accounting for user experience and operator preferences. However, since each wireless access network provides different levels of QoS, capacity, cover-

age, and mobility support, various parameters have to be taken into account for ensuring satisfying E2E performance. Relevant parameters are either static (e.g., system bandwidth) or dynamically change due to users' movements and environment conditions (e.g., received signal strength). While static parameters can be retrieved from databases, dynamic parameters need to be measured, monitored, and assessed. For the purpose of optimizing radio access and in particular HAM, three categories have been identified for classifying context information according to the following criteria [MET13b]:

- Relation to network entities:
  - UE context information: information collected from the UE, for example, position, speed, device capabilities, UE battery status, UE settings, user profiles, buffer status, etc.,
  - Context information of network and lower layers: e.g., radio propagation map, current or historical interference information, network load,
  - Context information of higher layers: for instance, QoS requirements of applications and services.
- Levels of abstraction:
  - Primary context information: information that can be measured or collected from the network directly, e.g., GPS position,
  - Secondary context information: knowledge that needs to be inferred from the primary context information, for example, energy efficiency, UE behavior pattern, traffic pattern.
- Time scale:
  - Static information: e.g., UE capabilities,
  - Quasi-static information: for example, UE settings, handover history,
  - Dynamic information: e.g., UE location, traffic demands.

In order to quantitatively evaluate the benefits of context-enhanced HAM, a COntext-aware multi-RAdio network Simulator (CORAS) has been developed that is based on the modeling approach illustrated in Figure 5.1. Specific features and the applied system level evaluation methodology were introduced in Chapter 2. In addition, this simulator incorporates static as well as dynamic context models to simulate the influence of context quality on HAM and users' E2E performance. For the assessment of HAM decisions,

e.g., on network selection and HO, RAT deployments, MNO policy models, as well as user terminals performing different forms of random walks or directed movements can be simulated. Further, HAM decisions may take signaling costs and occurring handover delays into account. Network selection or HO decisions, based on signal strength measurements and user movement estimations, as well as resource utilization based on context information are evaluated in the following subsections. In particular, location information and movement estimation can be exploited for optimizing terminal HO decisions to be made in a multi-RAT environment, as shown in [KMS+10]. A possible implementation of this system concept is illustrated in Figure 5.2, where the depicted system can also be applied for enhancing multi-homing experience, as presented in [CMK+10].

Another promising application field for the IRNA concept is the area of mobile cloud computing, where envisioned concepts rely on an always-on connectivity and will need to provide a scalable and, when requested, high-quality mobile access. By removing the limitations of mobile devices with respect to storage and computing capabilities and providing a new level of security by a centralized maintenance of security-critical software, e.g., for mobile payment applications, it is expected that such a concept will find broad acceptance on the business as well as consumer side. Research indicates [ABI09] that mobile cloud computing will additionally help to make visions of context-aware services become reality. In [KMSS10], the author presents how a *Mobile Cloud Controller* exploits specific context information for significantly improving user experience when accessing mobile services, thus evolving traditional HAM schemes.

Network, user, terminal, and environment context information are managed by a CMS, which is introduced in Section 4.2, and are used for HAM purposes. For example, user-specific context, such as Service Level Agreement (SLA), UE capabilities, or personal profile data, can be exploited for enhancing mobility support and user experience.

In Figure 5.2, user terminals and Radio Access Networks (RANs) represent those entities where context information is acquired. They are referred to as Context Providers (CxPs). These data are fed to a *context manager* or Context Broker (CxB), which can be implemented in a centralized [C-C10] or decentralized manner [MSC+13], [KSS14]. The CxB disposes of add-on functionalities, such as prediction, reasoning, and caching entities. Moreover, it may have access to user profiles, e.g., provided by the MNO or social networks, where users' approval is assumed. The HAM entity represents the Context Consumer (CxC) that uses context information for its purposes, such

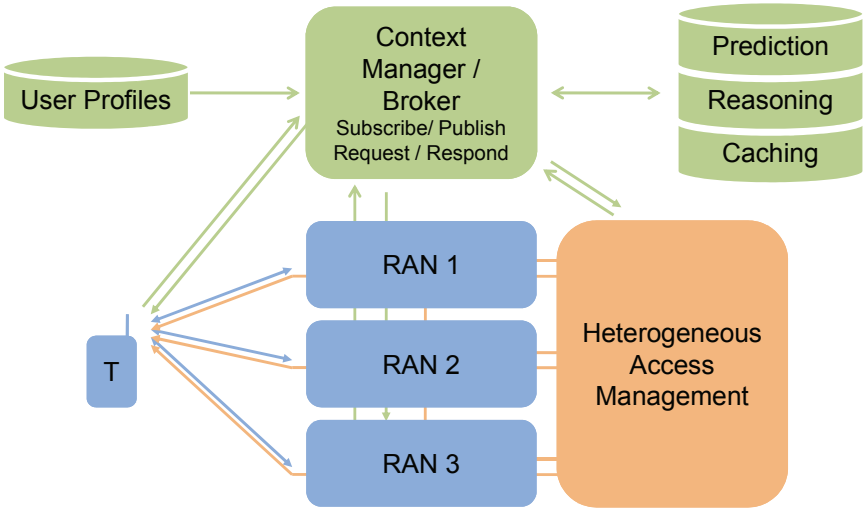

Figure 5.2: Concept for context-enhanced heterogeneous access management

as network selection, HO or RRM decisions.

Due to the heterogeneity of the considered context parameters, such as received signal strength, bandwidth, Base Station (BS) load, intra-/inter-RAT HO costs, etc., a generic approach for HAM decisions was developed and presented in [MKSS09a], [MKSS10], [KMS+10]. Further, this approach was used to realize a terminal-centric multi-homing scheme [CMK+10] that exploits available context information for deciding upon the set of RANs to connect to and the connection to be used as primary connection, given service requirements and user preferences.

In case n real-valued, non-negative context values are available for HAM, their values at time t can be denoted as $x_{1,t}, x_{2,t}, ..., x_{n,t}$, where each of the values lies in the interval $[l_k, u_k]$, $k = 1, 2, ..., n$, that is relevant for HAM decisions. In order to normalize different context values to the interval $[0, 1]$, each $x_{k,t}$ is divided by the respective interval width $u_k - l_k$ taking lower interval limit l_k into account:

$$\tilde{x}_{k,t} = \frac{x_{k,t} - l_k}{u_k - l_k}. \tag{5.1}$$

For HAM, the majority of context parameters have to be considered per user (or UE) and BS, since they describe characteristics of the connection between a certain UE and BS, respectively. One example would be the received signal strengths of various WLAN Access Points (APs) detected by different user terminals. Hence, it is necessary to more specifically denote context values with two additional indexes i and j, where i represents the considered UE and j the respective BS. However, parameter values exist that fulfill $x_{i,j,k,t} = x_{j,k,t}$, i.e., context values being equal for all i, e.g., the current number of users attached to an AP. Moreover, the normalized context values $\tilde{x}_{i,j,k,t}$ can be

weighted according to their relevance $r_{i,j,k} \in [0,1]$ for the evaluation of the potential connection and their confidence level $c_{i,j,k} \in [0,1]$, e.g., in terms of accuracy. In conjunction with Equation (5.1), this yields

$$y_{i,j,k,t} = c_{i,j,k}\ r_{i,j,k}\ \tilde{x}_{i,j,k,t} = c_{i,j,k}\ r_{i,j,k}\ \frac{x_{i,j,k,t} - l_{i,j,k}}{u_{i,j,k} - l_{i,j,k}}. \tag{5.2}$$

For decisions related to HAM, it is crucial to find (based on available context information) the best radio connection for a single UE, while accounting for overall system performance. Hence, for every point in time t, the quality $q_{i,j,t}$ of each possible connection to the available access nodes j, e.g., BSs, APs, etc., is evaluated by calculating

$$q_{i,j,t} = \sum_{k=1}^{n} z_{i,j,k,t}, \tag{5.3}$$

where $z_{i,j,k,t}$ is defined as follows:

$$z_{i,j,k,t} = \begin{cases} y_{i,j,k,t} & \text{if evaluation is positively correlated with } \tilde{x}_{i,j,k,t}, \\ 1 - y_{i,j,k,t} & \text{otherwise.} \end{cases} \tag{5.4}$$

Equation (5.4) reflects the following relation: if $\tilde{x}_{i,j,k,t}$ represents a context parameter, e.g., received signal strength, which is positively correlated with the suitability of a potential connection, this means that the greater $\tilde{x}_{i,j,k,t}$ the larger should be its contribution to the weighted sum that evaluates a connection opportunity. In contrast, if $\tilde{x}_{i,j,k,t}$ models context information, such as connection costs, the relation applies, that the greater $\tilde{x}_{i,j,k,t}$ the smaller should be its rating and contribution to Equation (5.3) that decides on connection selection.

For every UE i, the maximum $q_{i,t,\max}$ of all $q_{i,j,t}$ identifies the best access node to be connected to. However, this does not take into account costs associated with an executed handover (such as terminal battery power, use of network resources, etc.). If $j = j_0$ denotes the access node for the currently active connection of the terminal, a margin $m_{i,j}$ is defined by which $q_{i,t,\max}$ has to exceed $q_{i,j_0,t}$. Thus, the handover is only performed, if the following condition holds for a specified amount of successive time instances, referred to as Time-To-Trigger (TTT):

$$q_{i,t,\max} > q_{i,j_0,t} + m_{i,j}. \tag{5.5}$$

The margin $m_{i,j}$, besides ensuring a better connection quality in absolute terms, allows for trading off handover costs against enhanced connection quality, where handover costs are not limited to signaling costs, but also comprise costs spent for acquiring, processing, and evaluating context information.

In the following section, exemplary approaches for the exploitation of context information are presented that are based on the developed IRNA concept and that rely on integrated context management functionalities.

5.2 Examples for the Exploitation of Context Information

5.2.1 Improving Handover Performance Using Movement Estimation in Multi-RAT Scenarios

In order to exemplarily evaluate the influence of available context information, a movement estimation method is integrated into the context-enhanced multi-radio network simulation tool and movement estimation results are considered for HAM decisions. Simulation settings, in particular with respect to RAT deployment aspects, can be set up flexibly by specifying cell sizes, site-to-site distances, and deployment type. For example, either one centrally positioned BS per cell or one BS serving three cell sectors via directed antennas can be deployed. Further, BSs of different RATs can have a position-related offset with respect to each other and operate on different carrier frequencies using various transmission powers depending on the respective RAT.

The simulated region is divided into an evaluation area and outskirts. Three RATs with overlapping coverage areas are considered, where cell radii vary from 1700, to 1500, to 1200 m, respectively. These three RATs are WCDMA systems that are set to operate at carrier frequencies of 2.0, 2.0, and 2.5 GHz, respectively. Further, 200 user terminals are randomly assigned to these overlapping cell structures. In the considered scenario, the number of users remains constant during simulation time, where simulation is performed in discrete time steps of 10 ms. Figure 5.3 depicts the considered cell layouts including exemplary user traces. Different speed classes are attributed to groups of users and each user performs a simplified form of random walk (cf. Section 2.3), where directional deviation depends on the assigned speed.

Depending on a set of analyzed parameters (distance to BS, free BS capacity, geometry factor [HT07], etc.), the UE is assigned to the best ranked BS. In the current implementation, intra- and inter-RAT HO decisions are controlled by a common HAM entity, assisted by users' context information. As soon as a UE's geometry factor (cf. Equation (2.4)) to available and active BSs in vicinity is, e.g., 3 dB greater with respect to the former location and

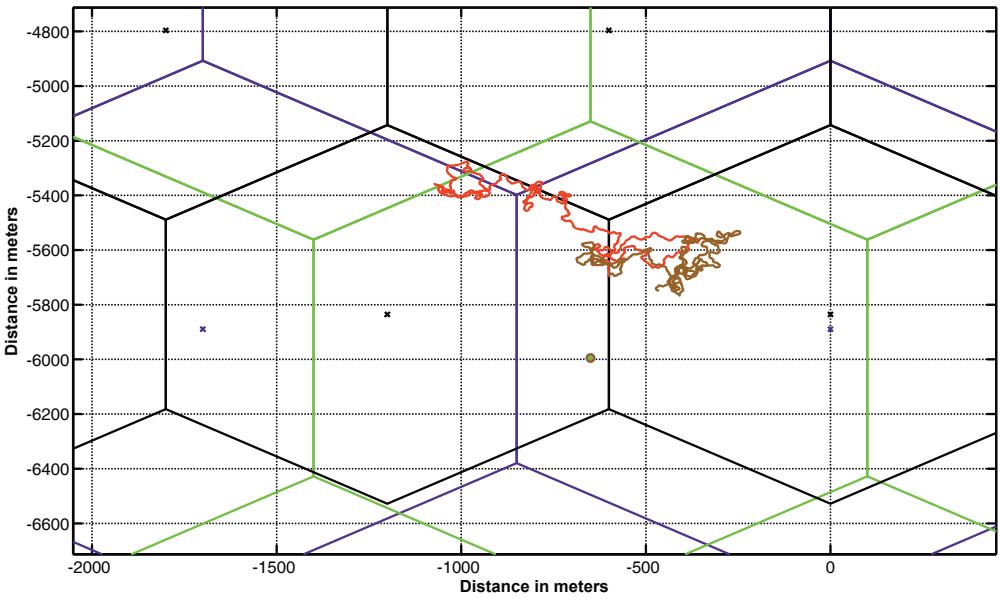

Figure 5.3: Multi-RAT cell layout including exemplary user traces

the user's utility indicates the need for a HO (e.g., utility exceeds a predefined threshold), the HAM controller initiates an intra- or inter-RAT HO, respectively. However, varying context quality, in this case changing accuracy and delay of network and terminal measurements, heavily influences the number of unnecessary HOs. By including a cost function in the decision process, the HO policy allows for trading off HO costs against enhanced connection quality. Moreover, the amount of additional signaling and associated delays heavily depends on the network structure and HAM hierarchy. For obtaining the simulation results depicted in Figures 5.4(a) and 5.4(b), a centralized and quasi-omniscient HAM controller has been implemented, which is in charge of managing the simulated RATs.

The used movement estimation algorithm, which calculates the possible 2D terminal locations three seconds in advance, is based on the "dead reckoning" [KH06] method. Dead reckoning is the process of estimating UE i's future position $\mathbf{x}_{i,t+1}$ based on current position $\mathbf{x}_{i,t}$, and advancing that position based upon known UE speed ν_i, elapsed time Δt, and current course $\varphi_{i,t}$:

$$\mathbf{x}_{i,t+1} = \mathbf{x}_{i,t} + \Delta t \begin{pmatrix} \nu_i \cos\varphi_{i,t} \\ \nu_i \sin\varphi_{i,t} \end{pmatrix}. \tag{5.6}$$

For an initial comparison of HAM performance with and without movement estimation, the number of performed HOs is considered. In general, a lower number is preferable, since a HO is costly in terms of network resources and signaling overhead. Figures 5.4(a) and 5.4(b) illustrate the amount of intra- and inter-RAT HOs for 200 terminals, respectively. The UEs are uniformly

assigned to velocities of 100 and 50 m/s, where the first 100 users are moving at 100 m/s and the following 100 users at 50 m/s.

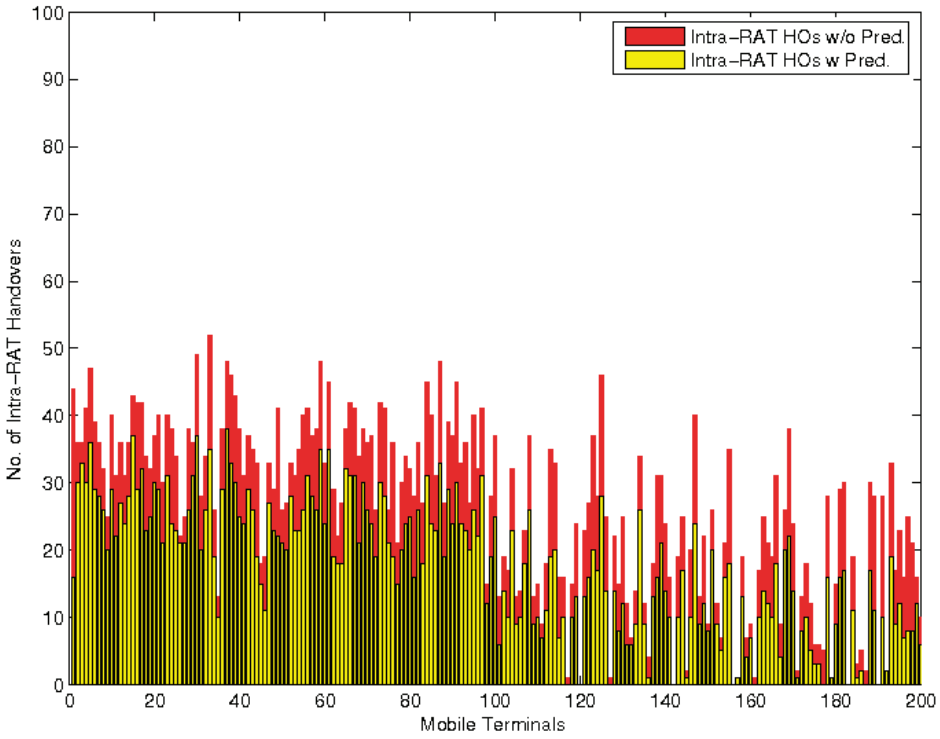

(a) Number of intra-RAT handovers

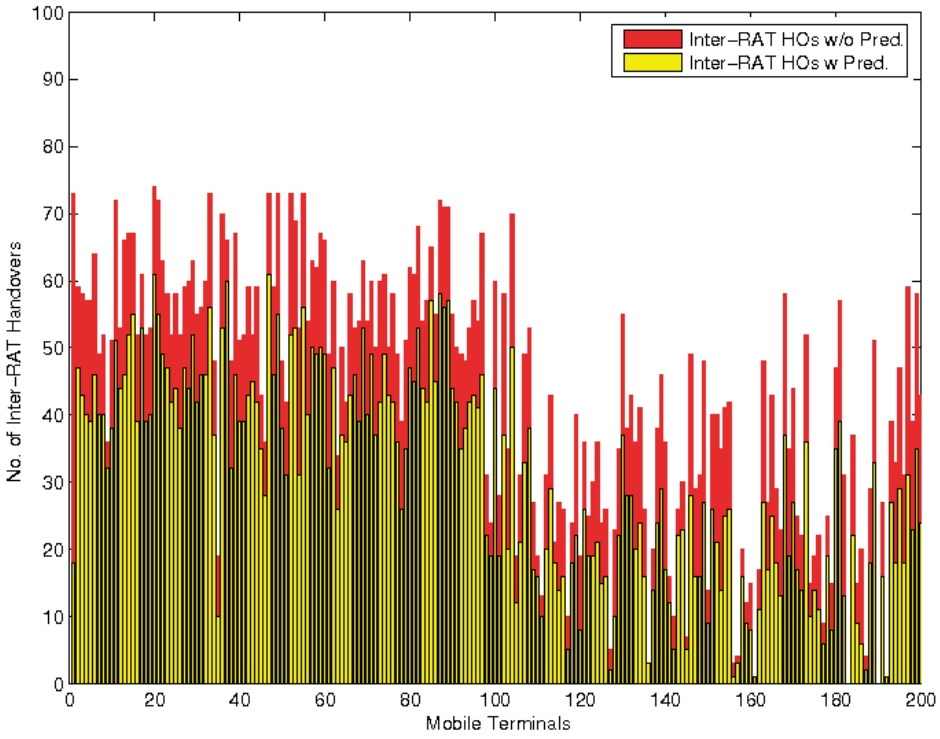

(b) Number of inter-RAT handovers

Figure 5.4: Number of intra- and inter-RAT handovers for users moving at 100 and 50 m/s [KMS+10]

Both figures illustrate a significant higher number of handovers, that would have to be executed per UE, if no movement estimation algorithm was applied and its results were not used for HAM decisions. In order to compare the estimation error for different velocities, the deviation of the estimated position from the actual position is divided by the distance traveled during the considered time interval. The error of movement estimation for high-speed users is approximately 12% for a prediction horizon of 3 s, whereas reducing the time user movements are estimated in advance to 1 s greatly reduces the error of movement estimation to 2%. Further, the average number of intra- and inter-RAT HOs as well as achievable performance gains using movement estimation are listed in Table 5.1.

Table 5.1. Mean number of intra- and inter-RAT HOs as well as achievable performance gains

Velocity	**100 m/s**				**50 m/s**			
Mean	intra-RAT	Gain	inter-RAT	Gain	intra-RAT	Gain	inter-RAT	Gain
w/o pred.	3.48	-	5.58	-	1.68	-	3.00	-
pred. (1 s)	1.97	43%	3.31	41%	0.51	70%	0.87	71%
pred. (3 s)	2.38	32%	4.15	26%	0.81	52%	1.61	46%
pred. (5 s)	2.50	28%	4.23	24%	0.99	41%	1.86	38%

In the considered scenario, a low prediction horizon of 1 s results in most significant performance gains of approximately 70%, in particular for UEs moving at 50 m/s. For the same prediction horizon of 1 s and UEs moving at 100 m/s, the exploitation of user movement estimates reduces the mean number of intra- and inter-RAT HOs by approximately 43% and 41%, respectively. Nevertheless, a prediction horizon of 5 s still yields enhancements in terms of intra- and inter-RAT HOs of approximately 28% and 24%, respectively, for high-speed users moving at 100 m/s. In essence, these results clearly demonstrate the potential of context information exploitation for improving HO decisions.

5.2.2 Optimizing Service Provisioning and Mobile Network Operator Revenue

In order to evaluate the benefits of exploiting context information from Mobile Network Operator (MNO) perspective, a novel approach for combined Joint

Call Admission Control (JCAC) and Dynamic Bandwidth Adaptation (DBA) has been developed by the author and presented in [KLM+11b], [KLM+11a], [LKMS12]. This tightly integrated JCAC and DBA scheme, which is in the following referred to as DBAJCAC, aims at improving network capacity and MNO's revenues while taking user profiles and QoS requirements of requested services into account. Since more users can be served with the same amount of radio resources, these capacity gains may be potentially translated into increased revenues for MNOs. Further, user-specific Service Level Agreements (SLAs) are considered to represent the economic benefits a MNO can achieve by serving a certain user, thus enabling to maximize revenue for service provisioning. In this thesis, the core JCAC task is mapped onto a *Generalized Assignment Problem* (GAP), where an efficient approximation algorithm [CKR06] for solving the GAP is employed.

The radio resources of all RANs are jointly managed by a central HAM entity. Each of the considered RATs employs different schemes for medium access and user data transmissions, such as WCDMA and OFDMA. Further, these RATs allocate different types of radio resources, e.g., orthogonal code sequences, time slots, or OFDM symbols. In order to abstract from these RAT-specific radio resources and to create a basis for common RRM decisions, an *effective bandwidth utilization* measure is introduced. Each BS can provide a maximum effective bandwidth that can be assigned to the requested services. Moreover, spatially co-deployed cells of different RANs form a cluster of co-located cells, which is referred to as *cell area* and exemplarily depicted in Figure 5.5.

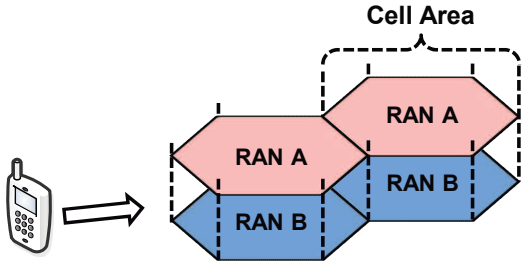

Figure 5.5: Overlapping cell areas of 2 RANs (adapted from [Lot11])

Mobile terminals are characterized by their prioritization class (e.g., based on SLA), a randomly chosen dwell time, which represents the duration the UE is located in one cell, and the number and types of requested services. Further, all mobile terminals are assumed to be multi-mode terminals that support all deployed RATs in the service area. Furthermore, two kinds of services are considered: *elastic* and *non-elastic services*. The QoS characteristics of the former ones are expressed by a range of effective bandwidth

values $b_{\min} \leq b_{\text{desired}} \leq b_{\max}$, among which the effective bandwidth is allowed to vary. The minimum effective bandwidth value $b_{\min}$ is specified by the minimum QoS requirements of the service, while $b_{\max}$ describes the maximum effective bandwidth a service provider grants to a service. The amount of effective bandwidth that is required to provide a certain service at a satisfactory *Quality of Experience* (QoE) level is denoted by b_{desired}. In contrast, non-elastic services are fixed with respect to their QoS requirements and, thus, with respect to the required effective bandwidth, i.e., $b_{\text{non-elastic}} = b_{\min}$. Further, each service class is characterized by its service duration (or active time) and its pause time that describes the time between two service requests of the same service class.

Originally, the concept of *utility* emanates from the field of economics [Mar66]. A utility function is used to represent preferences, for example, of customers favoring one good over another. Here, it represents a generic measure of the gained revenue of the MNO that operates the respective RAN. The MNO's overall utility is assembled by utility functions that account for several factors, which are defined by the SLA between the user and the MNO, the MNO's policies, and QoS requirements of the requested service. The utility $u_{i,j}(b)$ for service j served by RAN i consuming bandwidth b can be stated as follows:

$$u_{i,j}(b) = u(s_j(b), \pi_j, \rho_i), \tag{5.7}$$

where

- $s_j(b)$ describes the service utility function that depends on the QoS requirements of the requested service j and the current effective bandwidth usage b,
- π_j denotes the so-called priority factor that represents the priority of the terminal requesting the respective service as defined by the SLA,
- ρ_i is the RAN factor that emanates from the MNO policy. The higher its value the higher is the utility for the session in the considered RAN.

In the considered scenario, the achievable utility for a MNO that serves a certain service j by BS i using bandwidth b is defined as

$$u_{i,j}(b) = s_j(b)\ \pi_j\ \rho_i, \tag{5.8}$$

where elastic services follow an exponential utility function

$$s_{\text{elastic}}(b) = 1 - e^{-\frac{k\ b}{b_{\max}}} \tag{5.9}$$

and non-elastic services are characterized by a step function

$$s_{\text{non-elastic}}(b) = \begin{cases} 1, & b \geq b_{\min} \\ 0, & b < b_{\min} \end{cases}. \tag{5.10}$$

The factor k is used in Equation (5.9) for scaling the exponential utility function $s_{\text{elastic}}(b)$. Here, k is set to satisfy $s_{\text{elastic}}(b_{\text{desired}}) = 0.5$. The handling of all incoming and handover service requests are performed in a bundled manner, i.e., the handover and new incoming service requests are queued and the DBA and JCAC algorithms are performed each $TTI_{\text{semi-persistent}}$ [HT09] for all cell areas in a central HAM entity. The sequence of algorithm steps is as follows:

1. DBA (*bandwidth adaptation arrival*): Check if sufficient resources are available for all incoming service requests (new services and handover services).

2. JCAC (*handover services*): Serve the handover services first by performing the main JCAC algorithm (reason: dropping a handover service is considered worse than blocking a new service).

3. JCAC (*new services*): Execute the main JCAC algorithm for new incoming service requests.

4. DBA (*bandwidth adaptation departure*): Assign the remaining capacity, i.e., effective bandwidth, to the served elastic services in order to increase resource utilization.

The task of JCAC is mapped onto a GAP that belongs to the class of bin-packing problems. Finding an optimum solution for a bin-packing problem, which can be described using the terminology of knapsack problems, is known to be NP-hard [MT90]. Here, the according knapsack problem is to assign N items (set of services S) to M bins (set of cell sites C). Each bin i has a certain capacity c_i and each item j has a certain weight $w_{i,j}$ and utility $u_{i,j}$, respectively, depending on the considered bin. The objective is to find a subset of items that can be placed in the bins C in such a way that the overall utility or revenue R is maximized. The mathematical formulation of

the problem is as follows:

$$R = \max \sum_{i=1}^{m} \sum_{j=1}^{n} u_{i,j}\, x_{i,j} \tag{5.11}$$

$$\text{s.t.} \sum_{j=1}^{n} w_{i,j}\, x_{i,j} \leq c_i \quad \forall i \in M = \{1,\ldots,m\} \tag{5.12}$$

$$\sum_{i=1}^{m} x_{i,j} = 1 \qquad \forall j \in N = \{1,\ldots,n\} \tag{5.13}$$

$$x_{i,j} = \{0,1\} \qquad \forall i \in M, j \in N \tag{5.14}$$

Here, each bin i represents a cell site or BS of a specific RAN, where each BS is able to provide a certain capacity c_i or amount of effective bandwidth. Services are considered as items j. The corresponding weight of a service $w_{i,j}$ is modeled by the effective bandwidth usage $b_{i,j}$ of the service, while the revenue a specific item generates when being served by BS i is given by its utility $u_{i,j}$. The developed algorithm is split into two main parts: an *outer* and an *inner* algorithm. The first one (cf. Table 5.2) decomposes the GAP into M 0-1 knapsack problems, for which a variety of efficient approximation algorithms exists. In the scope of this thesis, an approximation algorithm that is described in [CKR06] is employed. The *outer* algorithm requires the capacity information of all cells $\mathbf{c}$ as well as RAN-specific weight and utility information for every service bearer $\mathbf{W}$ and $\mathbf{U}$, respectively, as input. As output, it returns the assignment vector $\mathbf{t}$ that contains the index of the cell, by which the respective service is to be served. The M 0-1 knapsack problems are solved by the *inner* algorithm. The *inner* algorithm requires vectors containing the utilities and weights of the service bearers to be assigned for the considered cell $\mathbf{u}_i$ and $\mathbf{w}_i$, respectively, and the current remaining capacity c_i as input. It returns the updated assignment vector $\mathbf{t}$ and capacity information per cell c_i.

In case the 0-1 knapsack solver algorithm exhibits an approximation ratio of α, the approximation ratio of the overall GAP algorithm is $(1+\alpha)$ [CKR06]. In the developed approach, a simple *Greedy* algorithm[9] is used, since it offers the best run-time performance at an eligible approximation ratio (cf. Table 5.2). In order to avoid overload situations that may occur due to the greedy characteristic of the underlying 0-1 knapsack solver algorithm, an additional *prioritization* factor is introduced. In case the load η_i of one cell

[9] "A greedy algorithm is an algorithm that follows the problem solving heuristic of making the locally optimal choice at each stage with the hope of finding a global optimum. In many problems, a greedy strategy does not in general produce an optimal solution, but nonetheless a greedy heuristic may yield locally optimal solutions that approximate a global optimal solution in a reasonable time." [Wik13b]

Table 5.2. GAP and greedy knapsack solver algorithms [KLM+11a]

Outer GAP Solver	Greedy Knapsack Solver
Input: $\mathbf{c}$, $\mathbf{W}$, $\mathbf{U}$ **Output:** $\mathbf{t}$, $\mathbf{c}$	**Input:** $\mathbf{u}_i$, $\mathbf{w}_i$, c_i **Output:** $\mathbf{t}$, c_i

for $i = 1$ to M **do**
{Create utility vector}
for $j = 1$ to N **do**
if $t_j == -1$ **then**
{Service not yet assigned}
do $\mathbf{u}_i(j) = u(i,j)$
else
{Service already assigned}
do $k = t_j$
do $\mathbf{u}_i(j) =$
$u(i,j) - u(i,k)$
end if
 	
KNAPSACK($\mathbf{u}_i$,$\mathbf{w}_i$,c_i)
end for
end for
	{Sort all items according to their utility-weight ratios in a descending manner, i.e., $\frac{u_{i,1}}{w_{i,1}} > \frac{u_{i,2}}{w_{i,2}} > \ldots > \frac{u_{i,n}}{w_{i,n}}$.}
	SORT($\mathbf{u}_i$, $\mathbf{w}_i$)
	for $j = 1$ to N **do**
	if $w_{i,j} > c_i$ **then**
	$t_j = -1$
	else
	$t_j = i$
	$c_i = c_i - w_{i,j}$
	$r_i = r_i + u_{i,j}$
	end if
	end for

in the cell area exceeds a certain threshold $\eta_{i,\text{overload}}$, i.e., $\eta_i > \eta_{i,\text{overload}}$, an additional load-dependent prioritization factor $l_{i,j}$ is applied on the respective service utility, where

$$l_{i,j} = \begin{cases} 1, & \eta_i < \eta_{i,\text{overload}} \\ 1 - \eta_i, & \eta_i \geq \eta_{i,\text{overload}} \end{cases}. \tag{5.15}$$

The factor $l_{i,j}$ is accounted for in the utility that is used for the underlying 0-1 knapsack algorithm and decreases with an increasing cell load, which in turn leads to a smaller utility value for the knapsack decision. The overall utility stated in Equation (5.8) can now be written as follows:

$$u_{i,j}(b) = l_{i,j}\ s_j(b)\ \pi_j\ \rho_i. \tag{5.16}$$

However, this prioritization factor is disregarded when determining the utility value that is relevant for revenue calculation.

The developed DBA algorithm described in the following is separated into two stages: the *arrival* algorithm is performed before and the *departure* algorithm after the JCAC, respectively. First, the *arrival* algorithm acquires as much resources as required by the queued services, which include HO as well as new services, in the considered cell area. For that purpose, it degrades already served elastic services in order to release sufficient resources. The basic steps of the algorithm are depicted in Figure 5.6(a). At the beginning, the total demand of effective bandwidth of the queued services is calculated per considered cell area and RAN i by $B_{\text{req},i} = \sum_j b_{i,j}$. The already granted elastic services are sorted in ascending order according to their *utility-bandwidth ratios*

$$u'_{i,j} = \frac{u_{i,j}}{b_{i,j}}, \tag{5.17}$$

i.e., $u'_{i,1} < u'_{i,2} < \ldots < u'_{i,n}$. In case not enough resources are available in the considered cell area, the service demands might not be met by the available RANs. Therefore, the already granted services are degraded until all incoming services can be admitted or until all admitted elastic services have been degraded to a minimum. This results only in a minor overall utility reduction, since the elastic services, which suffer the least from utility degradation compared to non-elastic services, are degraded first.

In the *departure* algorithm, elastic services are sorted in descending order according to their utility-bandwidth ratios (cf. Equation (5.17)), i.e., $u'_{i,1} > u'_{i,2} \ldots > u'_{i,n}$. In case there are still radio resources available, since system capacity is not completely utilized in the considered cell area, the already served elastic services are assigned more resources in order to increase the overall system utilization and user satisfaction. The elastic services are upgraded until their desired effective bandwidth b_{desired} is reached, or if the bearer is already served with $b = b_{\text{desired}}$, they will be upgraded until $b = b_{\max}$. This allows for improving the gain of bandwidth adaptation, since services with highest utility-bandwidth ratios will be upgraded first. The upgrade procedure continues until the system reaches its maximum capacity or all elastic services are served with the maximum bandwidth.

For evaluating the proposed algorithms, a typical 3GPP system architecture (cf. [HT09]) and co-deployed HSPA and LTE RANs are assumed. The considered scenario includes the respective core network entities of the System Architecture Evolution (SAE)[10], e.g., Mobility Management Entity (MME),

[10]SAE refers to the evolution of the General Packet Radio Service (GPRS) core network architecture. Key characteristics are: simplified architecture, all-IP network, support for higher throughput and lower latency, mobility between and support for heterogeneous access networks, including 3GPP and non-3GPP systems.

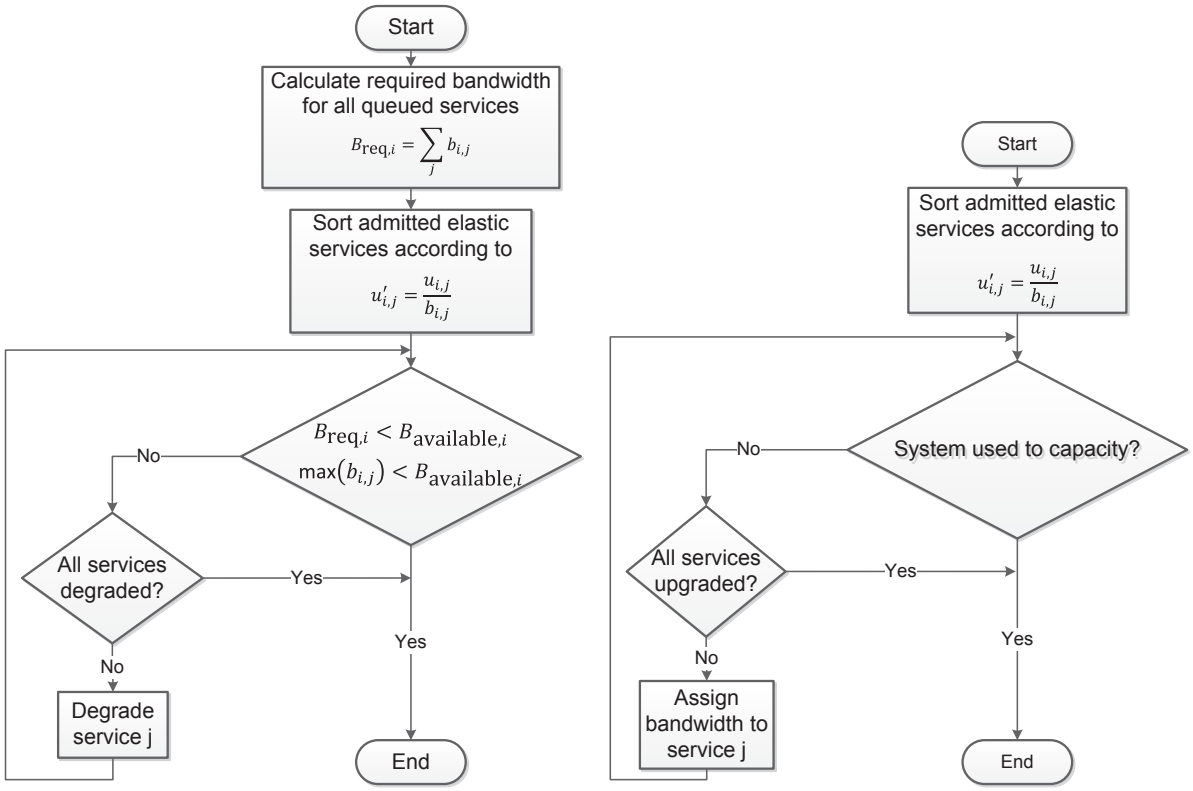

(a) Bandwidth adaptation *arrival* (b) Bandwidth adaptation *departure*

Figure 5.6: Bandwidth adaptation algorithms [KLM+11a]

Serving General Packet Radio Service Support Node (SGSN), etc., as illustrated in Figure 5.7. Relevant entities are modeled and simulated using the *OMNeT++* [Var11] simulation framework. The central decision entity is implemented at the MME, since it is responsible for mobility management and has access to all entities of the SAE that are responsible for service handling via the *control plane* (cf. [HT09]).

In the following, the applied simulation parameters of all relevant components are presented. Mobile terminals, also referred to as User Equipment (UE), are characterized by their UE *class* and their UE *priority factor* π_j. The considered UE classes, service sets, and their distribution are listed in Table 5.3.

Table 5.3. UE parameters [KLM+11a]

UE Class	**A**	**B**	**C**	**D**
Service Set	{1}	{1,3}	{1,3,4}	{2,3,4}
Distribution	0.2	0.5	0.2	0.1

Service sets indicate the service types that are requested by a UE of the respective UE class, whereas the distribution indicates the percentage of

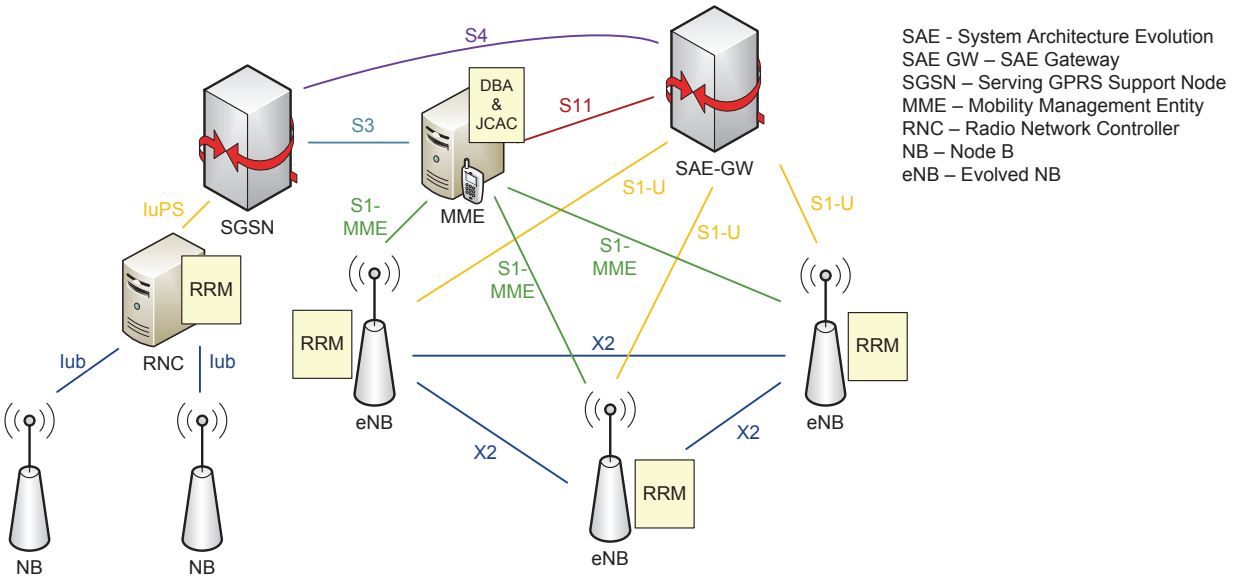

Figure 5.7: System architecture of evaluated scenario

terminals that are assigned to the different UE classes.

Further, several SLA categories are introduced, which model MNO's policy of preferably serving certain user groups that are expected to generate higher revenues. Here, three SLA categories, which are represented by priority factors π_j, are considered and randomly assigned to UEs, where *gold*, *silver*, and *bronze* users are characterized by $\pi_{j,\text{gold}} = 1.0$, $\pi_{j,\text{silver}} = 0.9$, and $\pi_{j,\text{bronze}} = 0.8$, respectively. For example, these prioritization factors may result in lower overall utility values (cf. Equation (5.16)) for *bronze* users, since *gold* users are expected to generate more revenues.

A cell area consists of a HSPA and a LTE cell, as illustrated in Figure 5.5. Each cell is characterized by a defined amount of available bandwidth B_i and a RAN factor ρ_i, which is used in Equation (5.8) to derive overall utility for serving service j by cell i. Table 5.4 lists considered B_i and ρ_i values, respectively, where stated bandwidth values were derived in [Lot11].

Table 5.4. RAN-specific parameters [KLM+11a]

RAN	B_i **(Mbps)**	ρ_i
HSPA	14.4	0.6
LTE	80.23	1.0

Table 5.5 states the characteristics of the services that are supported by the considered RANs. Services 1 and 2 represent non-elastic services that are fixed with respect to their QoS requirements, for instance, VoIP or streaming services. In contrast, services 3 and 4 represent elastic services that are variable with respect to their QoS characteristics. These services are also

referred to as *best effort* services, e.g., web browsing or file transfers (cf. Section 2.4.2).

Table 5.5. Service-specific parameters [KLM+11a]

Service ID	Bandwidth Req. (Mbps)	Active Time (s)	Pause Time (s)
1	$b_{\min} = 0.030$	$\mu_{\text{Duration}} = 90$	$\mu_{\text{Pause}} = 1800$
2	$b_{\min} = 0.256$	$\mu_{\text{Duration}} = 300$	$\mu_{\text{Pause}} = 1800$
3	$b_{\min} = 0.0$ $b_{\text{desired}} = 0.25$ $b_{\max} = 1.00$	$\mu_{\text{Duration}} = 50$	$\mu_{\text{Pause}} = 420$
4	$b_{min} = 0.0$ $b_{\text{desired}} = 1.5$ $b_{\max} = 10$	$\mu_{\text{Duration}} = 120$	$\mu_{\text{Pause}} = 420$

The performance of the combined JCAC and DBA scheme, which is referred to as DBAJCAC, is evaluated with respect to blocking and dropping rates, system load in HSPA and LTE cells, as well as gained overall utility of services. Finally, the level of satisfaction of the granted elastic services is measured by deriving the ratio of satisfied elastic services ($b \geq b_{\text{desired}}$) with respect to all served elastic services. The DBAJCAC approach is compared to a reference scheme, which does not perform JCAC and is referred to as NoJCAC, and a state-of-the-art Adaptive Joint Call Admission Control (AJCAC) scheme presented in [FC07], which has also been implemented for performance benchmarking.

Simulation results demonstrate that blocking ratios of newly arriving and dropping ratios of HO services are on an acceptable low level for both JCAC approaches, even at a high number of initial users per cell. However, in case no JCAC is applied, blocking and dropping ratios significantly increase with larger UE cell populations, as depicted in Figure 5.8(a) and in Figure 5.8(b), respectively.

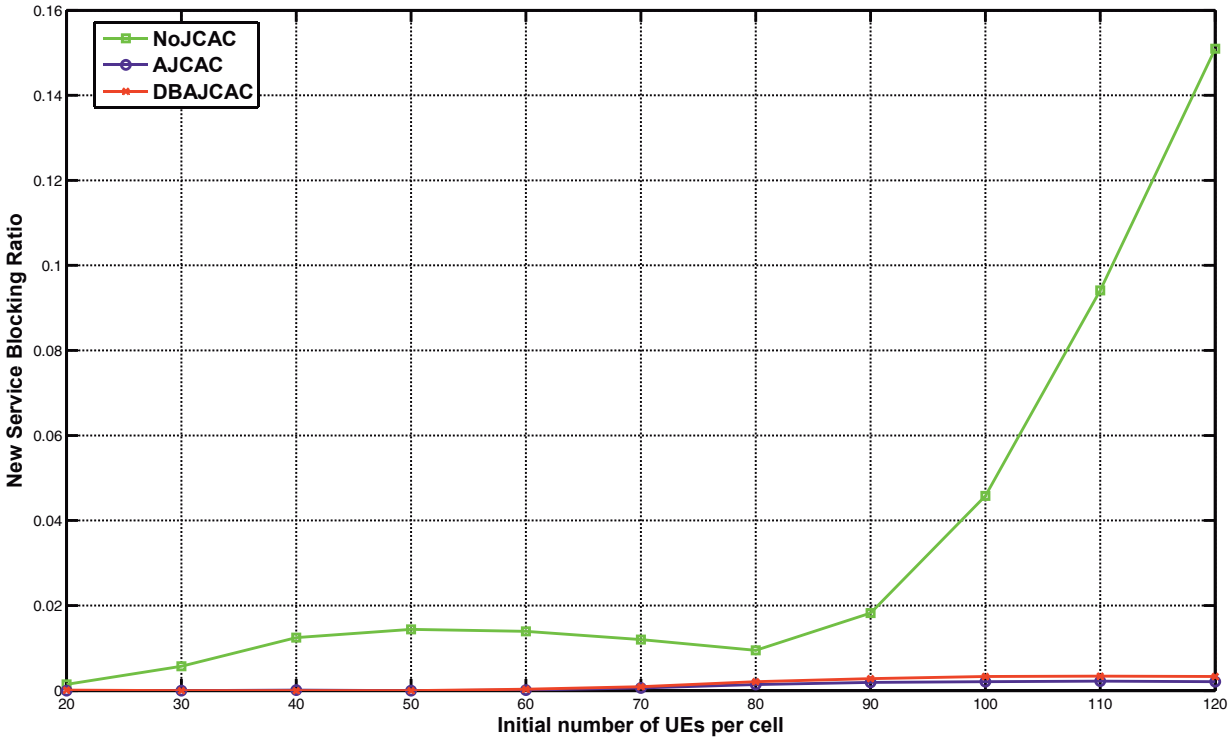

(a) Blocking ratio of newly arriving services (mean)

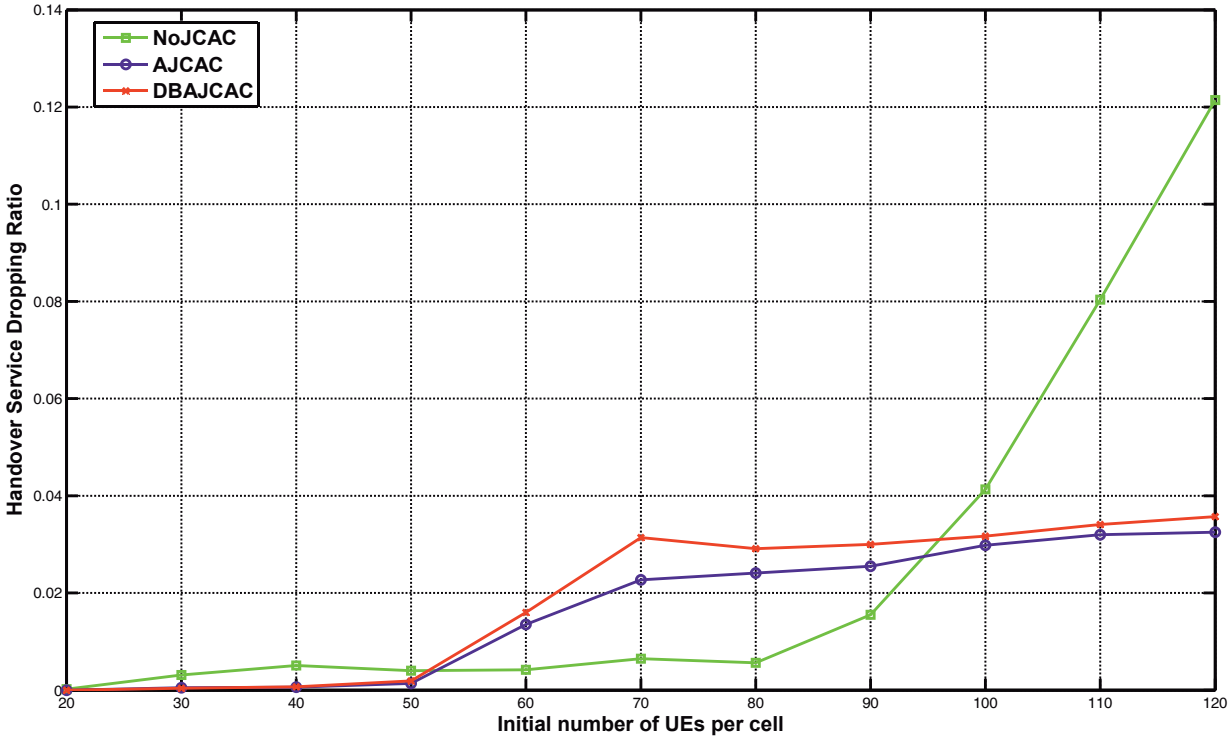

(b) Dropping ratio of arriving HO services (mean)

Figure 5.8: Blocking and dropping ratios of newly arriving services [KLM+11b]

The overall gained utility, illustrated in Figure 5.9(a), is up to 6% higher using the proposed DBAJCAC approach and the difference with respect to the overall utility achievable by the AJCAC scheme increases even further at a high number of initial users per cell. This is due to the greedy characteristic of the underlying GAP solver algorithm, which accounts for the respective utility values of the incoming service requests. Furthermore, DBAJCAC outperforms the reference NoJCAC approach by 35%.

Figure 5.9(b) depicts the relative cell load statistics of each algorithm for both LTE and HSPA cells, respectively. It should be noted that the maximum available effective bandwidth in LTE cells is more than five times higher than in HSPA cells (cf. Table 5.4). Apparently, more UEs are served by LTE cells for both JCAC algorithms up to a number of initial users per cell of $n = 70$. For DBAJCAC, this is due to the utility factor of the RAN ρ_i, which has a higher value for LTE cells (cf. Table 5.4). If the number of initial users per cell increases even further, the cell load of the HSPA cells exceeds LTE cell load. In case of DBAJCAC, this results from the load balancing characteristic of the prioritization factor $l_{i,j}$, where the load threshold $\eta_{i,\text{overload}}$ is set to 0.6 (cf. Equation (5.15) and Equation (5.16)). Furthermore, this leads to a relative increase of the utility used in the underlying 0-1 knapsack algorithm for HSPA cells. In case of the NoJCAC scheme, cell loads of HSPA and LTE cells increase linearly with a growing number of initial UEs. However, even at a high number of UEs, LTE cell load is rather low, whereas HSPA cells are heavily loaded.

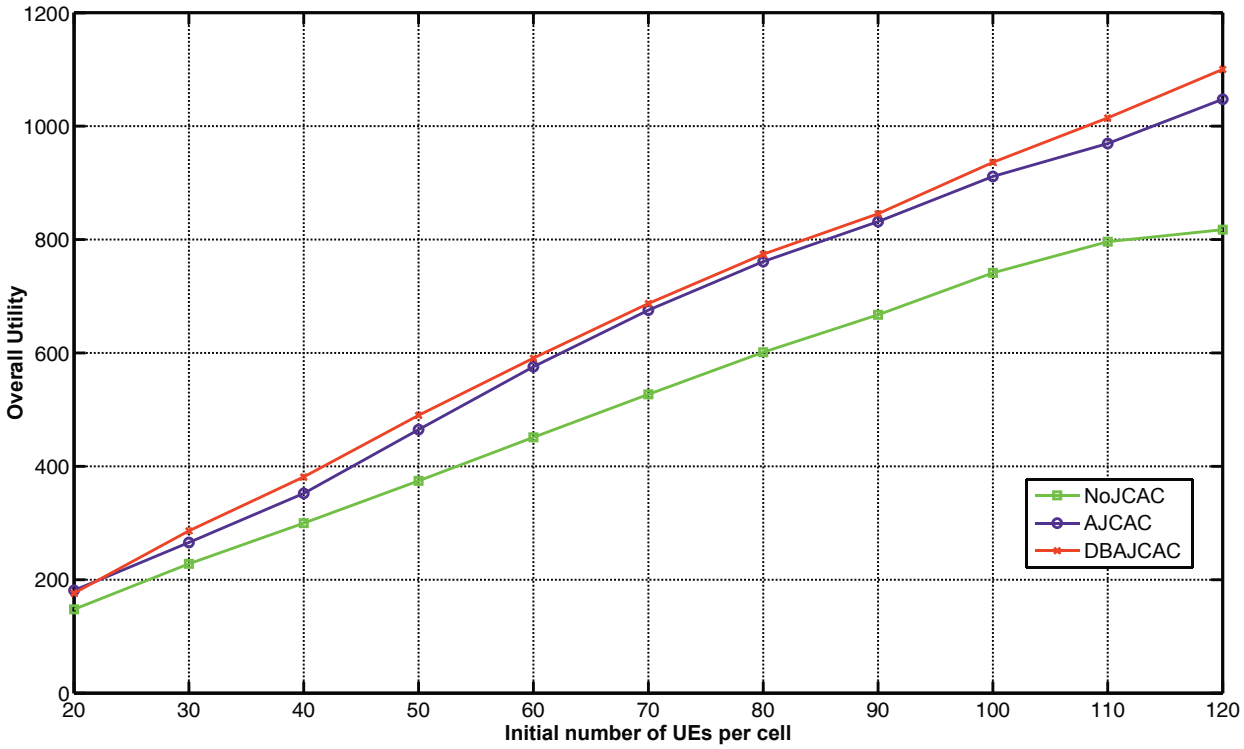

(a) Overall gained utility (mean)

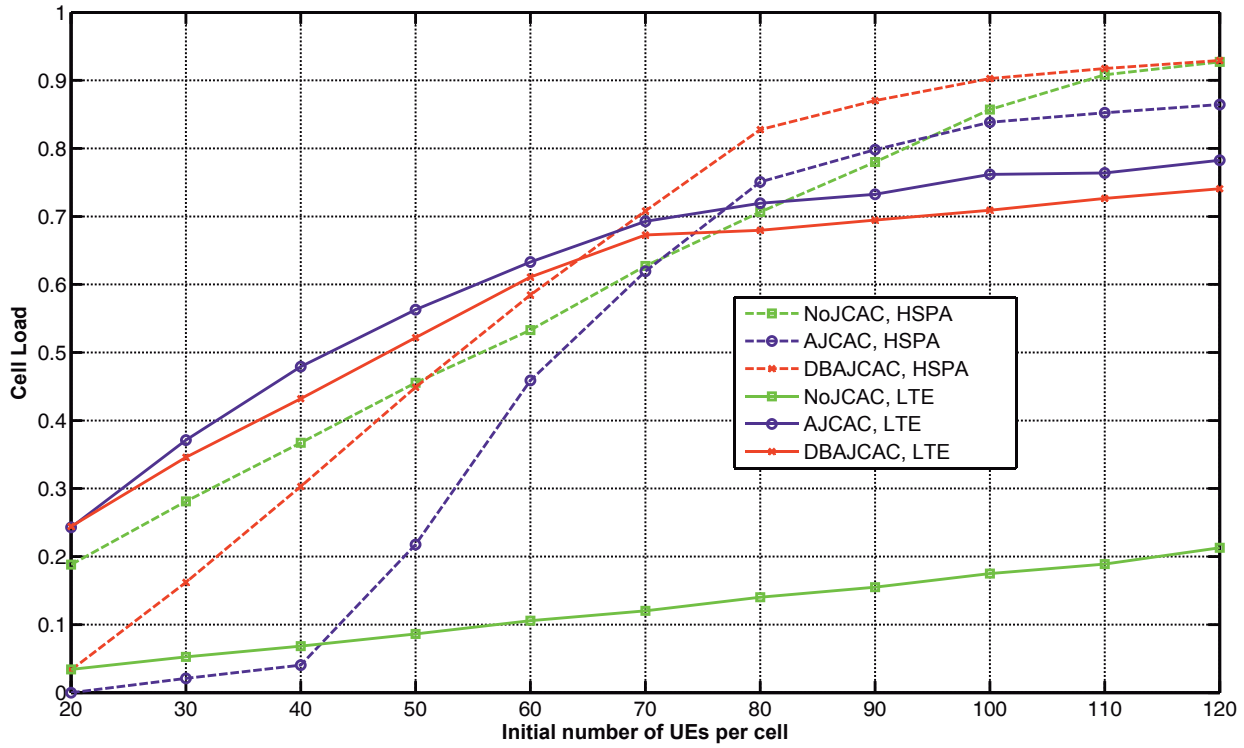

(b) Cell load of LTE and HSPA cells (mean)

Figure 5.9: Overall gained utility and cell load of LTE and HSPA cells [KLM+11b]

The statistics for satisfied elastic services are depicted in Figure 5.10. An elastic service is referred to as satisfied, if a satisfactory level of QoE can be reached, i.e., $b \geq b_{\text{desired}}$. For DBAJCAC, almost all elastic services served by LTE are satisfied independent of the number of initial users per cell. However, in case of HSPA users, the ratio of satisfied elastic services decreases at a high number of initial users per cell. This is due to the load balancing effect of the prioritization factor $l_{i,j}$, which enforces that more services are served by HSPA cells for an increasing number of initial users per cell. As a result, more user services are served by a cell with a comparably small amount of available effective bandwidth. This leads to a massive decrease of assigned effective bandwidth for many elastic services. In the AJCAC approach, elastic services are only admitted to HSPA cells, if LTE cells are already loaded to a certain extent. Hence, satisfaction ratios of HSPA cells for low initial numbers of users per cell are rather low compared to LTE cells. In case of the NoJCAC scheme, all elastic services are satisfied independent of the number of initial users per cell. This is due to the fact that all elastic services are served with $b = b_{\text{desired}}$ and cannot be degraded or upgraded with respect to their effective bandwidth usage. Further, dropped and blocked elastic services (cf. Figure 5.8) are not taken into consideration in the ratio of satisfied elastic services in case of NoJCAC, which leads to a constant satisfaction ratio of 1.

In essence, a novel approach for combined DBA and JCAC has been introduced that aims at maximizing MNO's revenue while accounting for user profiles and service-specific QoS requirements. The core JCAC task is mapped to a general assignment problem, which is well-suited for revenue maximization. Further, a utility based approach has been presented that is used as a generic measurement for the impact of JCAC and RRM strategy on MNO's revenue. The proposed scheme exhibits means for load balancing among RANs and has shown to outperform advanced state-of-the-art approaches.

5.2.3 Cell Transition Prediction for Avoiding Congestion and Enhancing System Performance

Mobility of commuters is not purely random but rather direction oriented and characterized by starting point and destination [SMBS10]. Moreover due to its regularity, it may be learned after monitoring user movements for a couple of business days. Exploiting movement data and context information of daily user movements (public transportation, vehicular users, etc.) allows

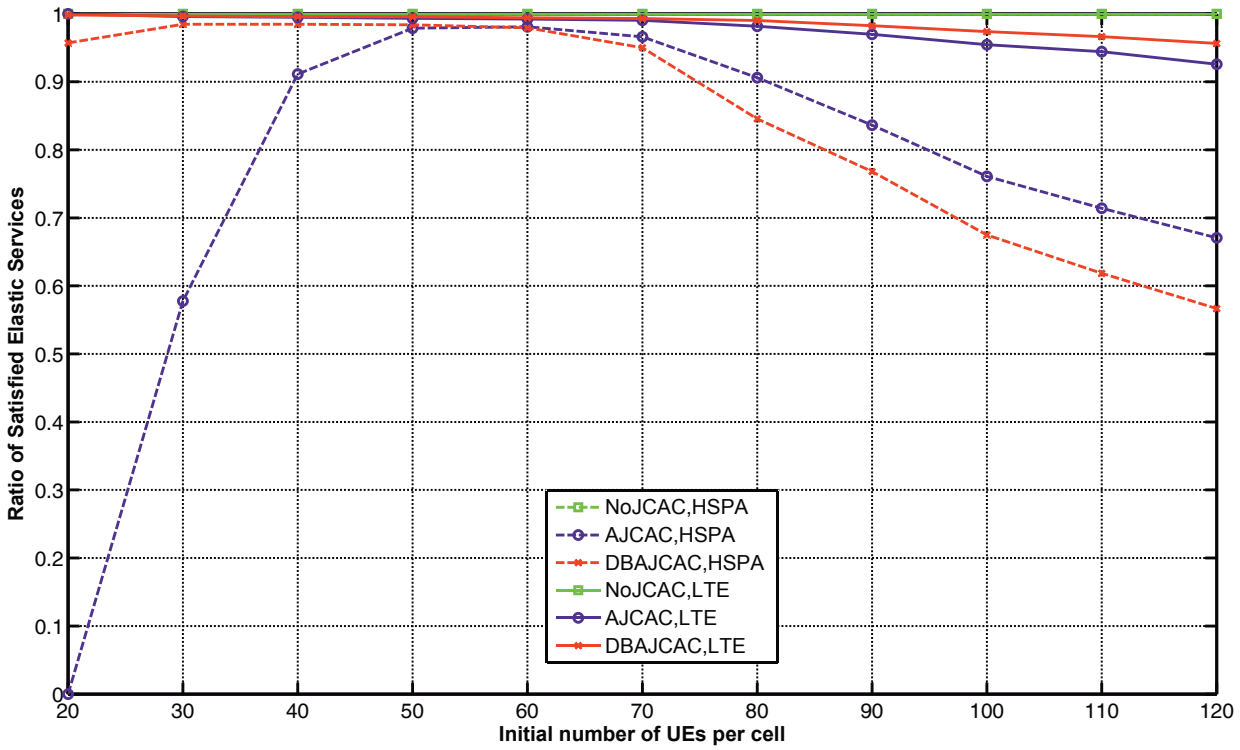

Figure 5.10: Ratio of satisfied elastic services in LTE and HSPA (mean) [Lot11]

for predicting cell transitions and lays the basis for designing efficient resource reservation schemes or smart resource management approaches.

Further, in day to day scenarios, where groups of mobile users travel together in the same vehicle, the data traffic demanded by these users is massive due to growing popularity of mobile multimedia services [Nok11]. In a vehicle with advanced communication and networking capabilities, a mobile router situated within the vehicle could be managing all user connections in the vehicle, in turn limiting required UE transmit powers. This constellation is referred to as *moving network* and may become reality in the not too distant future as stated in [MET13a]. In contrast, a group of users traveling in a conventional vehicle, where connections are individually managed by the serving BS, is referred to as a *moving user cluster*. These variants are expected to occur in service areas of MNOs, leading to dynamically changing and potentially high traffic demands. Given the forecasts in [Nok11], data traffic demands of moving networks/user clusters will keep increasing and will impose challenges on resource and mobility management.

One of the most serious problems caused by data intensive moving user clusters or moving networks is congestion due to a "hotspot" situation in a cell. The congestion caused by such moving entities can be classified as preferential mobility based "hotspot" [JFTK04]. Several techniques, such as channel

borrowing [LNB97], coverage adaptation according to the geographic traffic distribution [DBC03], mobility load balancing [LSJB10], etc., exist to combat such "hotspot" situations. A review and classification of several schemes can be found in [SRG+12], [AB12]. Further, there are several schemes in literature that investigate "hotspot" situation due to network load, blocking or dropping rates [JFTK04], [TMZC04]. The majority of works considers high user arrival rate, low departure rate, or increased bandwidth demand of existing users leading to "hotspot" conditions in a cell [JFTK04]. However, these works do not model realistic "hotspot" scenarios caused by moving networks or moving user clusters.

In the following, prediction schemes are presented that exploit context information, such as location information, for predicting user cell transitions and resulting congestion. These schemes are utilized to anticipate the arrival of data intensive moving user clusters/moving networks in a cell. Thus, user cell transitions are predicted well in advance and this context is beneficially applied for pro-actively triggering Load Balancing (LB) mechanisms as potential countermeasures for combating congestion. Figure 5.11(a) illustrates such a scenario, where the Evolved Node B (eNB) that predicts the potential next cells informs its neighboring eNB about approaching user clusters. These indications are used by the predicted target cell for triggering a LB mechanism and enforcing HOs of cell edge users to neighboring cells in order to free and reserve system capacity. Simulation results, presented at the end of this subsection, demonstrate robust and timely prediction of these events and their applicability for HO optimization and smart resource management even at high velocities.

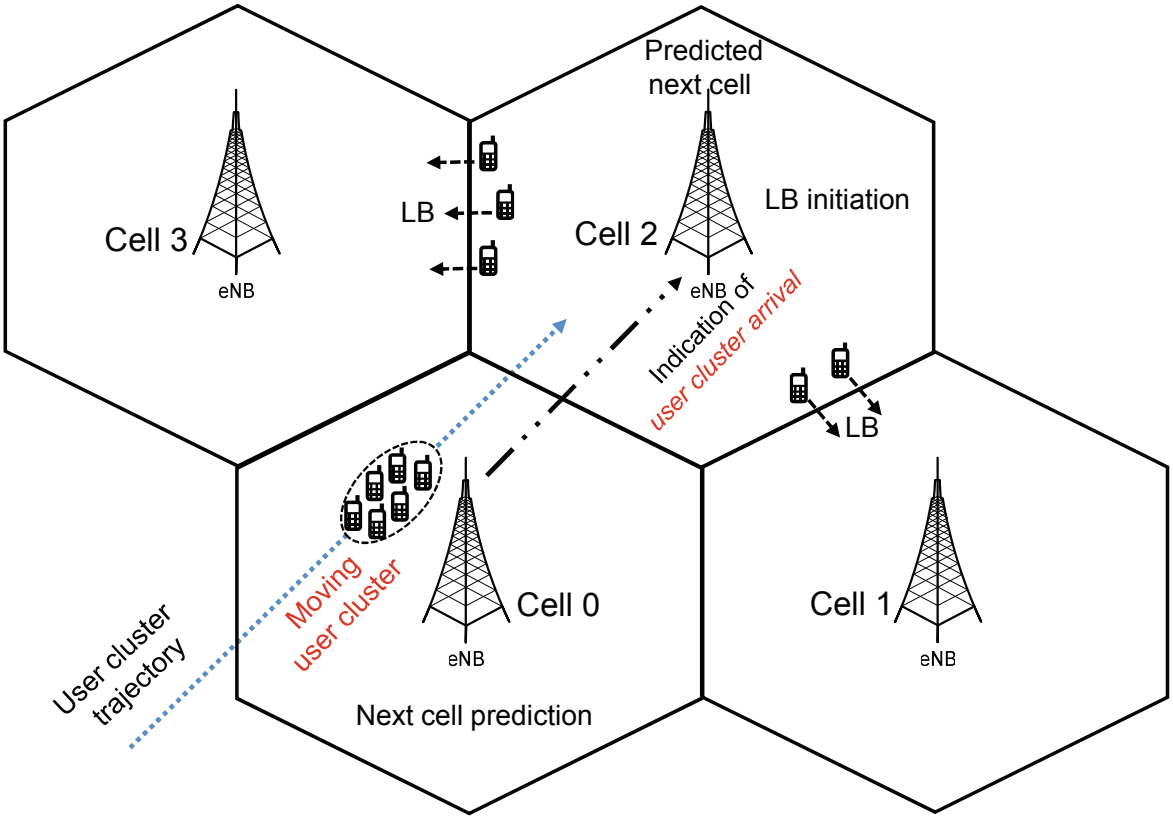

(a) Concept of next cell prediction and LB initiation

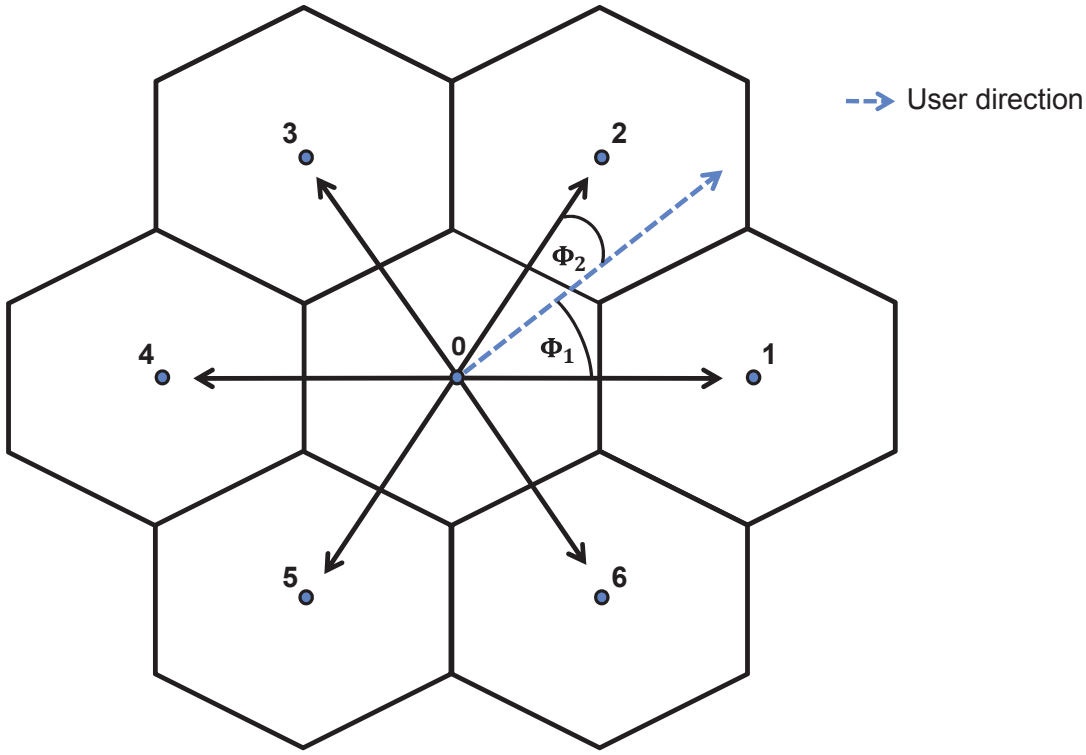

(b) Diurnal mobility model

Figure 5.11: Concept of next cell prediction, LB initiation, and diurnal mobility model (adapted from [KKSS13b])

In case of random walk mobility, a user can travel in all six directions with equal probability from its current cell, as depicted in Figure 5.11(b). However, in case of a user group moving jointly in public transportation, which is restricted by railway tracks or streets, movements are probable in only two directions and zero in other directions [SMBS10]. Hence, a user group can transit into one of the two adjacent cells from its present cell. If ϕ_1 and ϕ_2 are the angles of users' direction with respect to the closest directions leading toward neighboring cell centers, then probabilities of user transition toward those neighbor cells are determined as follows [SMBS10]:

$$p_1 = 1 - \frac{\phi_1}{\phi_1 + \phi_2}, \tag{5.18}$$

$$p_2 = 1 - \frac{\phi_2}{\phi_1 + \phi_2}. \tag{5.19}$$

In the following, different approaches for sampling user positions and for predicting user directions are described. The direction prediction model employs a "virtual" circle inscribed in each cell. This "virtual" circle corresponds to a certain signal strength threshold derived from radio propagation data, where the circle center coincides with the cell center. The user position is sampled at fixed, but velocity-dependent intervals. The user positions located within the virtual circle are sampled and used to predict future direction. The user angle can be calculated at each time interval t as follows:

$$\phi(t) = \arctan\left(\frac{y(t) - y(t-1)}{x(t) - x(t-1)}\right), \tag{5.20}$$

where $(x(t), y(t))$ and $(x(t-1), y(t-1))$ denote present and previous position samples, respectively. Different methods for predicting user directions are depicted in Figure 5.12(a). Method (a) utilizes the average of all user angles sampled within the circle, whereas method (b) only considers average of user angles sampled within a circular strip. Method (c) performs Exponential Moving Average (EMA) [HCV12] filtering of the user angles sampled within the circle and method (d) uses only the instantaneous user angle before leaving the "virtual" circle. In certain special cases, users will not enter the circular region, as depicted in Figure 5.12(b).

In order to predict user direction in such cases, the following algorithm is employed:

1. The distance of user from cell center is monitored at fixed logging intervals.

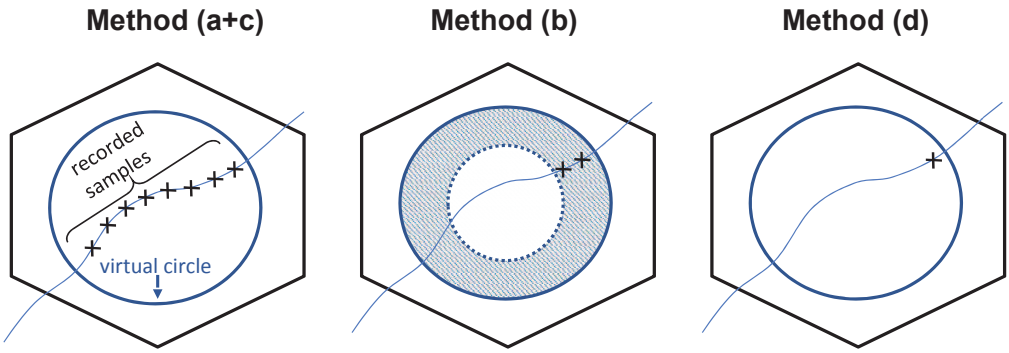

(a) Direction prediction methods

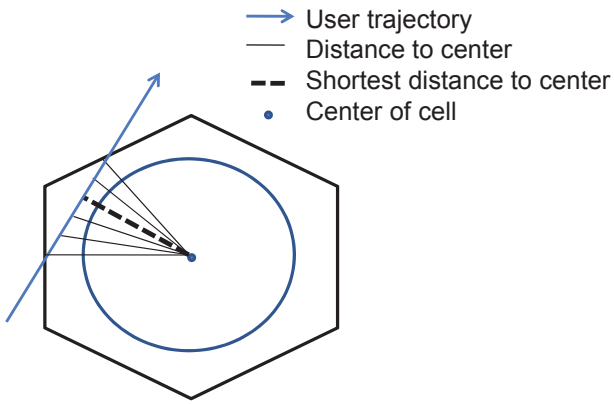

(b) Special case: user not entering virtual circle

Figure 5.12: Direction prediction methods and special case: user not entering virtual circle [KKSS13b]

2. IF the distance is greater than radius of circle: GOTO step 3, ELSE: user is in the circle, STOP.
3. IF present distance is greater than previous distance: user will not enter the circle, GOTO step 4, ELSE: repeat step 2.
4. Instantaneous user angle is used to estimate direction.

At high velocity and straight user motion, all prediction methods illustrated in Figure 5.12(a) yield same prediction results. If user trajectory deviates within angular range that yields same set of next cells (for instance, $0° - 60°$), all approaches predict potential set of next cells correctly, although estimated directions vary (cf. Table 5.6). This is illustrated by trajectory A in Figure 5.13. Further, prediction results for two different velocities (20 and 100 km/h) are listed in Table 5.6. The sampling interval is 3 s and actual next cell is cell 6.

In case the user trajectory deviates outside angular range that would result in same set of next cells, only instantaneous and circular strip based approaches lead to prediction of actual next cells. Average and EMA calculation lead to prediction of a different set of next cells due to consideration

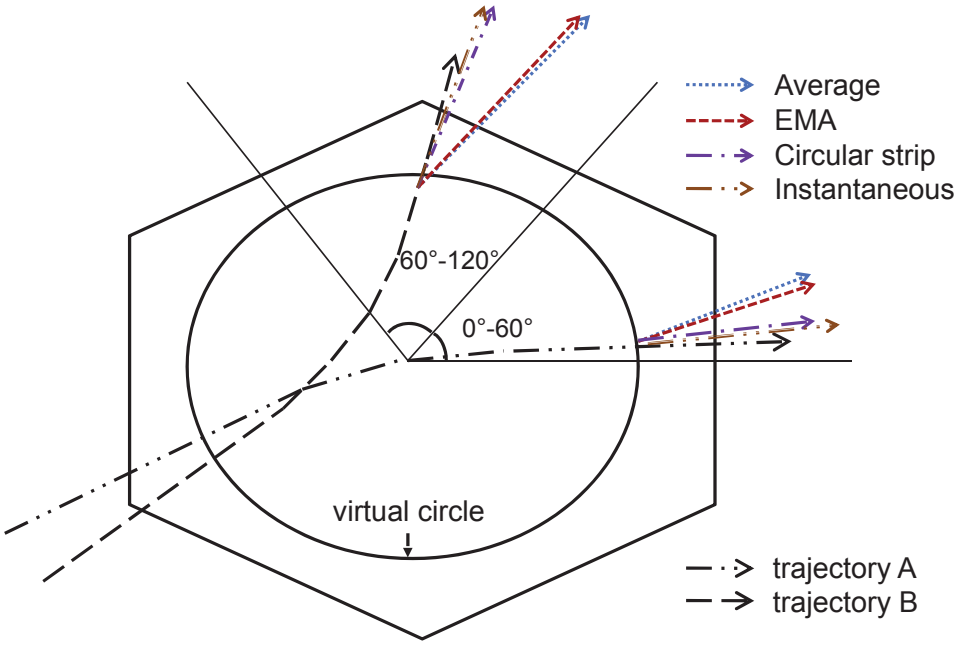

Figure 5.13: Illustration of predicted directions for various user trajectories [KKSS13b]

of recent angular values. Such a scenario is depicted by trajectory B in Figure 5.13 and the results at two different velocities (20 and 100 km/h) are listed in Table 5.6, actual next cell being cell 4.

However, the simple angle based approaches exhibit some limitations. For example, the user movements indicated by green and blue arrows in Figure 5.14 would result in the same estimated user directions Φ using angle based methods. However, the next cell the user will transit depends on user position and direction at the circumference of the virtual circle. Therefore, a better approach is to consider the distances to potential next cells. At the point of prediction in Figure 5.14, d_1 and d_2 are the distances of a user from centers of cell 1 and cell 2. The probabilities of transition to these cells based on distances are:

$$p_1 = 1 - \frac{d_1}{d_1 + d_2}, \tag{5.21}$$

$$p_2 = 1 - \frac{d_2}{d_1 + d_2}. \tag{5.22}$$

In Figure 5.15, a user travels from cell 3 toward northeast following diurnal mobility. According to the diurnal mobility model [SMBS10], a user always transits to one of the two next cells based on its direction. In the special case illustrated in Figure 5.15, a brief transition (indicated in red) occurs to a third cell before moving to most probable next cell. For instance, in cell 6, it is estimated that cell 15 and cell 18 are the potential next cells, if solely

Table 5.6. Comparison of estimation methods (within and outside angular range) [KKSS13b]

Estimation Method	**Velocity (km/h)**	**Est. within range**				**Est. outside range**			
		Ang. Dev.	**Next Cells**	P_1	P_2	**Ang. Dev.**	**Next Cells**	P_1	P_2
Average	20	24	6,4	0.6	0.4	55	6,4	0.08	0.92
EMA		23	6,4	0.61	0.39	56	6,4	0.07	0.93
Circular Strip		18	6,4	0.7	0.3	63	4,2	0.95	0.05
Instantaneous		18	6,4	0.7	0.3	65	4,2	0.92	0.08
Average	100	25	6,4	0.59	0.41	55	6,4	0.08	0.92
EMA		21	6,4	0.64	0.36	59	6,4	0.02	0.98
Circular Strip		18	6,4	0.7	0.3	65	4,2	0.92	0.08
Instantaneous		18	6,4	0.7	0.3	65	4,2	0.92	0.08

relying on angle based methods. But the user briefly transits to cell 4, which cannot be traced.

However, the brief transition to a third cell could be predicted by considering three potential next cells instead of two for each user direction range. The probabilities of transition to three potential cells based on angle of user direction and using the diurnal mobility model [SMBS10], which does not account for a potential third cell, are:

$$p_1 = 1 - \frac{\phi_1}{\phi_1 + \phi_2}, \tag{5.23}$$

$$p_2 = 1 - \frac{\phi_2}{\phi_1 + \phi_2}, \tag{5.24}$$

$$p_3 = 0. \tag{5.25}$$

At the point of prediction, d_1, d_2, and d_3 are distances of a user from centers of potential next cells and the corresponding transition probabilities are

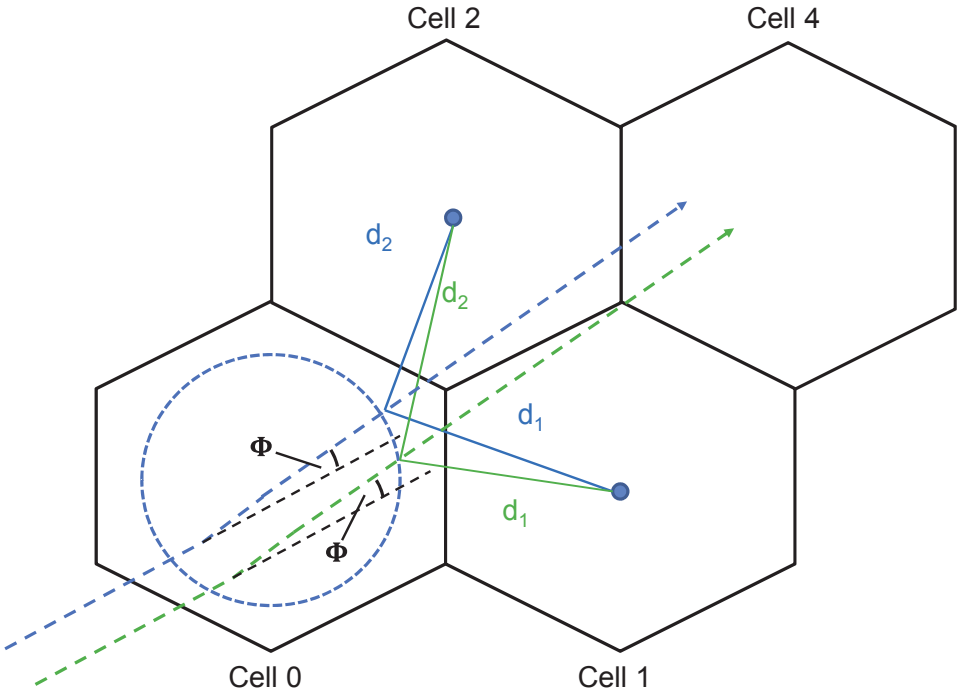

Figure 5.14: Cell transition prediction based on distance [KKSS13b]

determined as follows:

$$p_1 = \frac{2}{3} - \frac{d_1}{d_1 + d_2 + d_3}, \tag{5.26}$$

$$p_2 = \frac{2}{3} - \frac{d_2}{d_1 + d_2 + d_3}, \tag{5.27}$$

$$p_3 = \frac{2}{3} - \frac{d_3}{d_1 + d_2 + d_3}. \tag{5.28}$$

The so far presented angle and distance based prediction approaches may appear appealing due to their limited mathematical complexity. However, they exhibit several major disadvantages. Since both angle and distance based schemes rely on location information, there are several issues related to these kind of data, such as availability, accuracy, and energy consumption. For example, retrieving and signaling UE-specific GPS coordinates to eNBs at required signaling intervals, which may be velocity-dependent, is costly, since these measurements easily drain UE battery power. Further, GPS coordinates may not be available in any location (e.g., tunnels) and measurement accuracy is affected by the respective UE-specific hardware implementation. Moreover, the predicted next cells based on location information do not necessarily need to coincide with the next eNBs from a radio measurement point of view. For instance, due to shadowing, there may be situations where an eNB at a greater distance to the UE may provide stronger receive signal levels and will be chosen as HO target eNB, although from a distance point of view

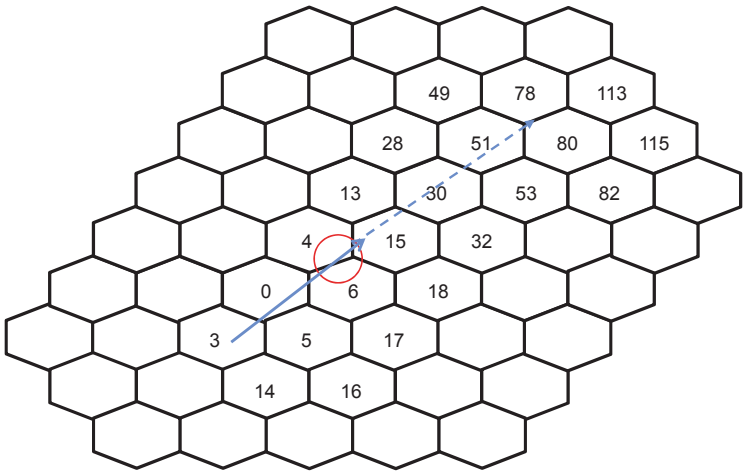

Figure 5.15: User trajectory in special case of "brief" cell transition [KKSS13b]

another eNB is closer.

Therefore, a *geometry* (cf. Equation (2.4)) based prediction method is developed that employs EMA filtering of geometry values in order to determine trends in eNB-specific geometry values. Figure 5.16 exemplarily shows the calculation of relevant EMA values. The initial EMA value is determined as soon as the user entered the virtual circle, while the final EMA value is calculated before the user is about to leave the virtual circle. The size of the "virtual circle" is defined by a geometry threshold of 8 dB for an Inter-Site Distance (ISD) of 500 m.

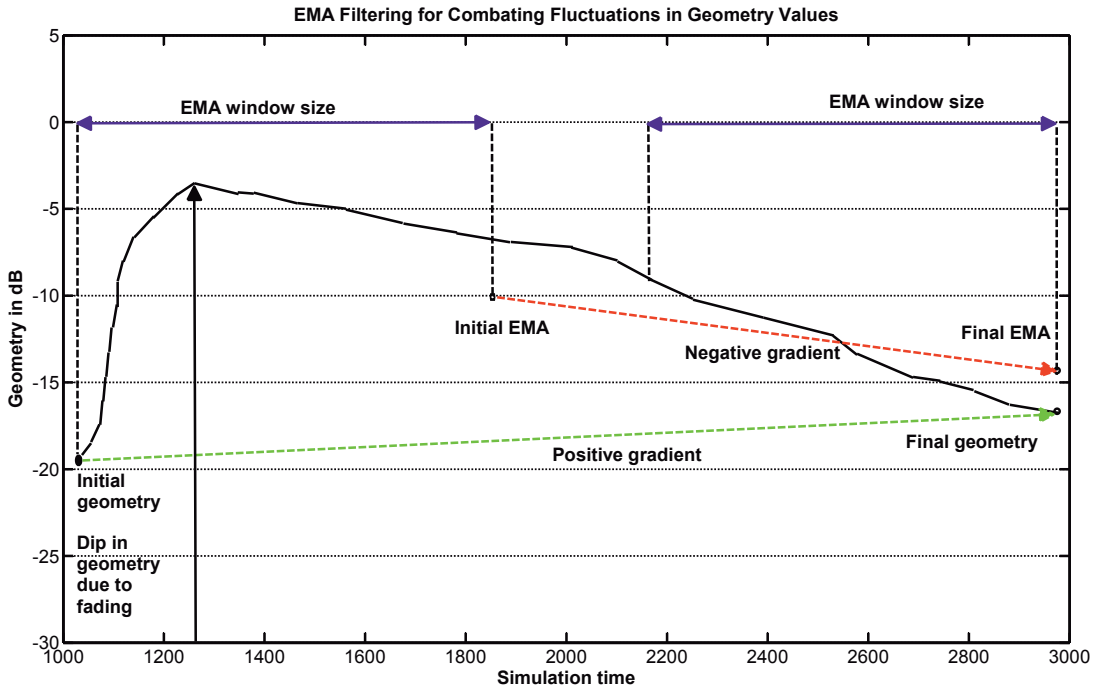

Figure 5.16: Calculation of EMA values for prediction of next cells

The gradient between the initial and final EMA values can be used to

infer whether a certain cell is approached or not. Further, the final EMA value is used as basis for determining most probable next cells as follows:

$$p_1 = \frac{\overline{G}_{\mathrm{EMA},1}}{\overline{G}_{\mathrm{EMA},1}+\overline{G}_{\mathrm{EMA},2}+\overline{G}_{\mathrm{EMA},3}}, \tag{5.29}$$

$$p_2 = \frac{\overline{G}_{\mathrm{EMA},2}}{\overline{G}_{\mathrm{EMA},1}+\overline{G}_{\mathrm{EMA},2}+\overline{G}_{\mathrm{EMA},3}}, \tag{5.30}$$

$$p_3 = \frac{\overline{G}_{\mathrm{EMA},3}}{\overline{G}_{\mathrm{EMA},1}+\overline{G}_{\mathrm{EMA},2}+\overline{G}_{\mathrm{EMA},3}}. \tag{5.31}$$

Here, the window size for EMA calculation N_{EMA} in samples is set to:

$$N_{\mathrm{EMA}} = \left\lfloor \frac{2d_{\mathrm{corr}}}{\nu_u T_s} \right\rfloor, \tag{5.32}$$

where d_{corr} (cf. Equation (2.17)) denotes the correlation distance of the underlaying shadowing map, ν_u the estimated user velocity, and T_s the sampling interval. For example, assuming $d_{\mathrm{corr}} = 50$ m, $\nu_u = 120$ km/h (33.3 m/s), and $T_s = 0.1$ s results in 30 samples for EMA calculation.

The system-level simulation tool presented in Section 2.8 is used for performance evaluation and a multi-cell scenario is created as illustrated in Figure 5.15 with a BS at each cell center. The considered RAT is LTE [HT09]. The moving user cluster consists of 60 UEs moving together at a high velocity of 120 km/h. The evaluation methodology follows [3GP10a] and Table 5.7 summarizes simulation parameters. The trajectory followed by the moving user cluster is depicted in Figure 5.15.

Table 5.7. Simulation parameters [KKSS13b]

Parameter	**Value**
Carrier frequency	2 GHz
System bandwidth	$B = 10$ MHz (50 PRBs)
Total transmit power	40 W/250 mW (ISD = 500m/200m)
Control channel overhead	12%
Shadowing	log-normal, standard deviation: 8 dB, correlation distance: 50 m
Fast fading	2-tap Rayleigh fading channel
Noise power	-174 dBm/Hz + $10\log_{10}(B$ (Hz))
Background users per cell	30
Moving user cluster	60 UEs at 120 km/h

Table 5.8 lists simulation results of cell transition prediction for user trajectory as in Figure 5.15 from cell 3 to cell 0, cell 6, cell 4, and cell 15. The

Table 5.8. Next cell prediction results (partly included in [KKSS13b])

Present Cell	**Next Cells**	$P_{\mathbf{angle}}$	$P_{\mathbf{distance}}$	$P_{\mathbf{geometry}}$
Cell 3	Cell 5	0.25	0.35	0.08
	Cell 0	0.75	0.41	0.85
	Cell 1	0	0.24	0.07
Cell 0	Cell 6	0.25	0.45	0.81
	Cell 4	0.75	0.35	0.16
	Cell 2	0	0.20	0.03
Cell 6	Cell 18	0.25	0.20	0.00
	Cell 15	0.75	0.33	0.00
	Cell 4	0	0.47	1.00
Cell 4	Cell 15	0.25	0.47	0.98
	Cell 13	0.75	0.31	0.00
	Cell 11	0	0.22	0.02

simulation results demonstrate that the angle based approach is not able to trace the transition into a third cell. However, the distance based and, in particular, the geometry based approaches yield most robust prediction results among the considered approaches. In Table 5.8, the probabilities of predicting actual next cells using angle, distance, and geometry based approaches, i.e., their ability to predict the potential next cell, are summarized, where the geometry based method clearly outperforms all other schemes.

The earliness of next cell prediction could be increased by reducing the virtual circle's radius. However, this comes at the cost of next cell prediction accuracy, since users may still change their directions outside the virtual circle area. Further, prediction at low velocity is earlier than at high velocity, since there is a longer period of time (dwelling period) between prediction and actual transition at lower velocities. In case of direction-oriented user mobility, which excludes spontaneous and random direction changes, prediction of next cell transitions is more robust and accurate at low velocities and becomes challenging at high velocities, since a lower number of samples is taken into account.

In the following, system-level simulations are carried out for site-to-site distances ($s2s$) of 500 m and 200 m (dense deployments), respectively. The traveled distance of the moving user cluster is the same in both cases. Further, prediction of user cell transitions is used for enabling respective cells to anticipate the arrival of moving user clusters and to pro-actively trigger a LB mechanism. The objective of this procedure is to avoid congestion

and accommodate for approaching moving user clusters. Figure 5.17(a) and Figure 5.17(b) illustrate achievable reductions with respect to dropped connections, blocked access and HO attempts.

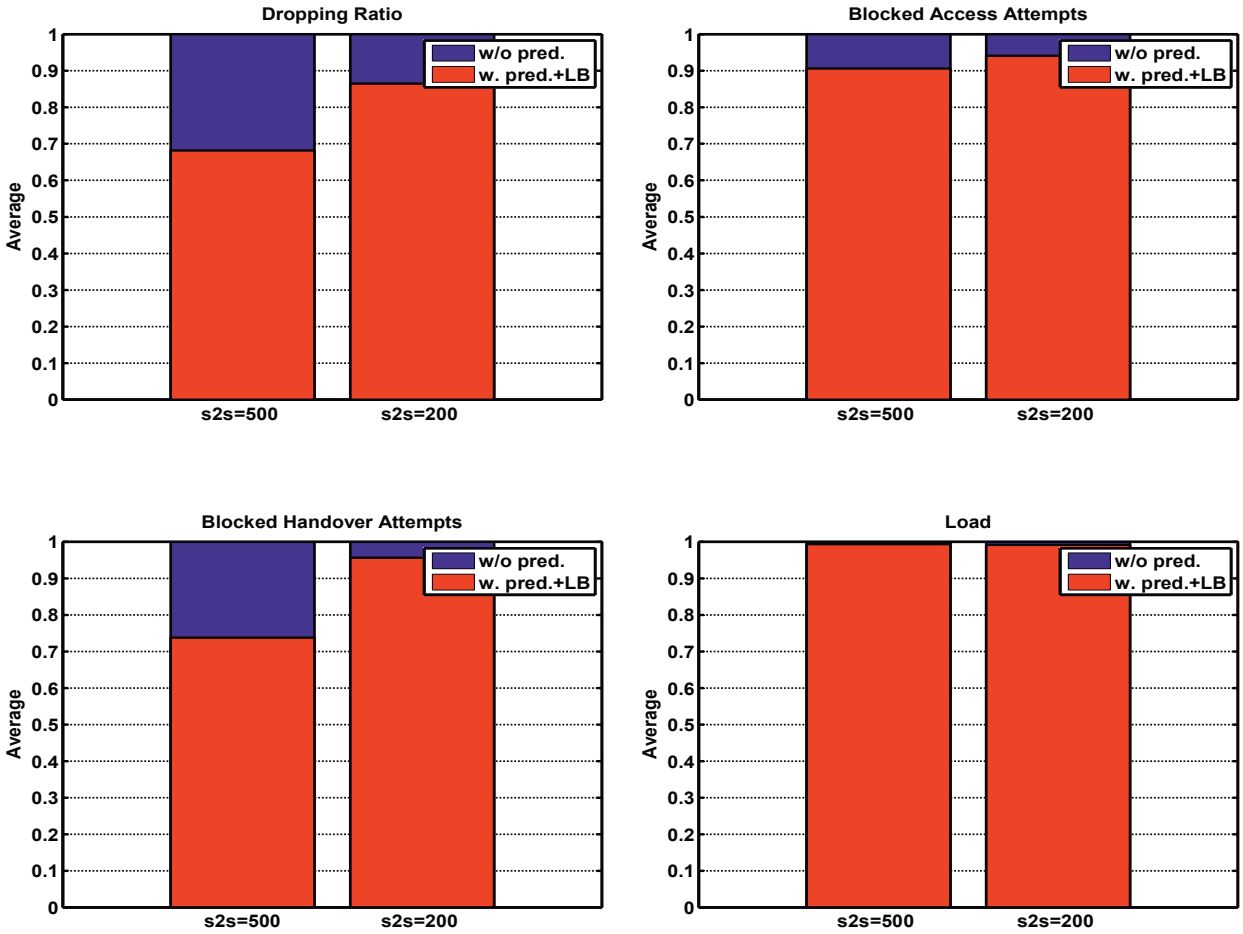

(a) Dropping and blocked HO attempts

(b) Blocked access attempts and load

Figure 5.17: Overall system performance with and without prediction triggered LB [KKSS13b]

The average number of connection drops is decreased by 32% and 13% for $s2s = 500$ m and $s2s = 200$ m, respectively. In terms of blocked HO attempts, an average reduction of 26% and 4%, respectively, is achieved. Regarding blocked access attempts, using GPS/distance based cell transition prediction results in improvements of 10% and 6% for $s2s = 500$ m and $s2s = 200$ m, respectively. Further, there is only a very slight enhancement with respect to system load (1%), since the freed up resources will soon be occupied by moving networks/user groups.

Figures 5.18(a), 5.18(b) and 5.18(c) depict the performance improvements in terms of dropped connections, blocked HO as well as blocked access attempts in case of GPS/distance and geometry based prediction methods, respectively. Regarding dropping of user connections, significant enhance-

ments of approximately 30% and 42% are achieved by both GPS/distance and geometry based prediction schemes, respectively. In terms of blocked HO and access attempts, GPS/distance and geometry based prediction schemes result in improvements of 25% and 49% as well as 10% and 25%, respectively.

In essence, the primary step to mitigate congestion issues caused by moving user clusters/networks is to predict their arrival in a cell. Here, distance and geometry based methods are used for predicting next cells users will transit. This context information is utilized to trigger LB as a potential countermeasure to combat imminent congestion. System-level simulation results demonstrate the ability of presented approaches to predict arrival of moving user clusters/networks well in advance. Further, these methods lay a basis for context-aware RRM in typical and dense deployments, which are envisioned to spread in future [Nok11], [MET13a]. In particular, the geometry based prediction scheme yields robust prediction results even at high velocities of 120 km/h and achieves significant improvements with respect to system-level Key Performance Indicators (KPIs), such as connection dropping, blocking of HO and access attempts.

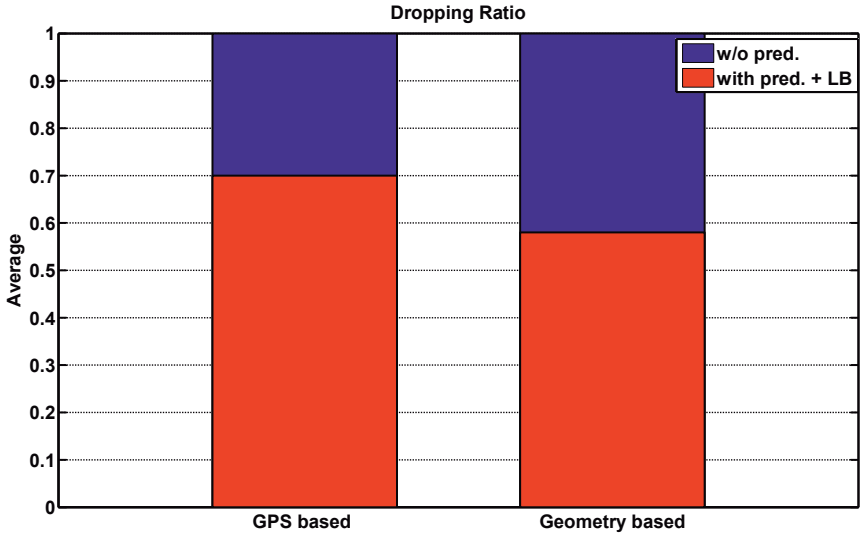

(a) Connection drops for different prediction schemes

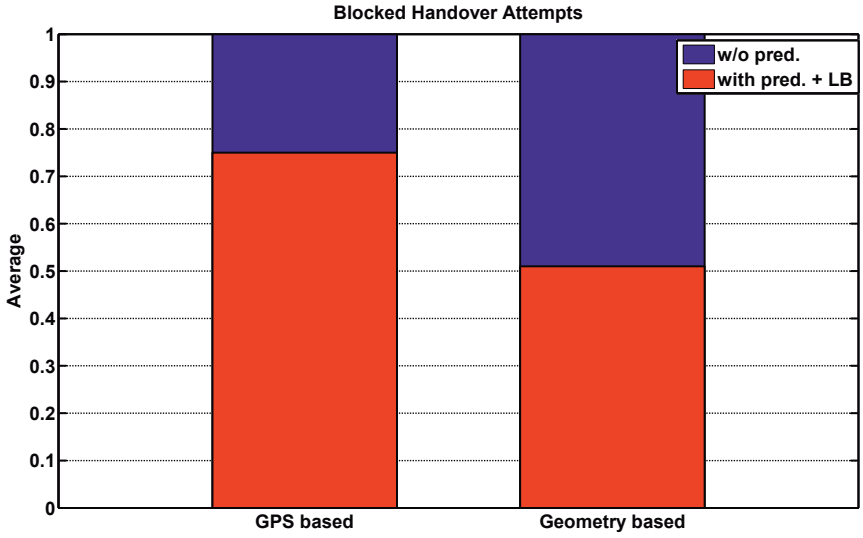

(b) Blocked HO attempts for different prediction schemes

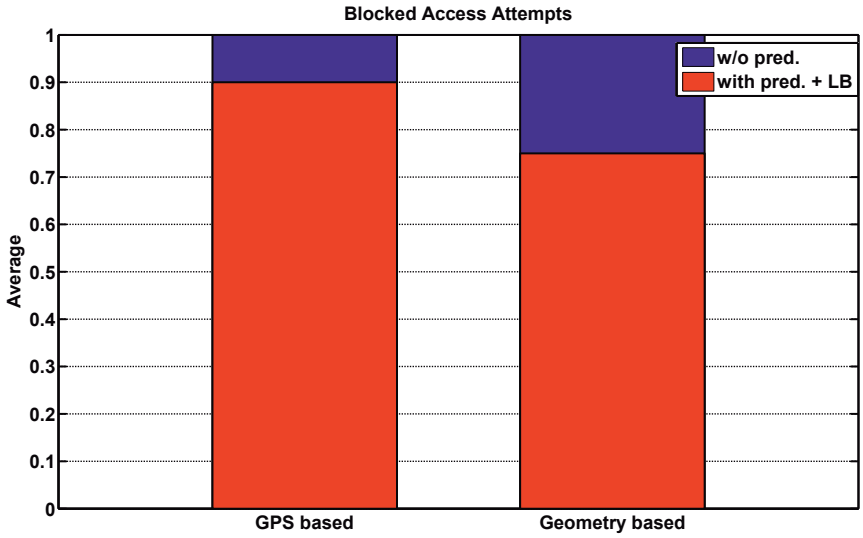

(c) Blocked access attempts for different prediction schemes

Figure 5.18: Connection drops, blocked HO as well as access attempts for GPS/distance and geometry based prediction schemes

5.2.4 Optimizing Heterogeneous Access Management (HAM) in Realistic 3D Environments Using Movement Estimation

Availability and reliability of a priori information on user and network conditions affect the performance of HAM and resource management strategies. In urban areas where MNOs observe recurring traffic demands and user movement patterns, e.g., due to daily commuters, these context information can be aggregated in databases and exploited for improving HAM, RRM, as well as overall network efficiency. For example, by statistical analysis of context data, most probable user traces that users follow in a certain area at a certain time of day can be estimated. Moreover, UE measurements of received signal levels can support building a radio map model of specific environments. Given these information, optimum location and time slot for user data transmissions could be estimated, too. The aim of the following evaluation is to demonstrate potential gains that can be achieved with respect to mobility-related events, such as connection drops or HO failures, BS load, and user throughput. Basically, two operation modes are investigated: no knowledge on user mobility is available at network nodes or user movements are predicted and this context information is exploited by HAM entities for improving mobility support and E2E performance.

In order to model real-world deployment, radio propagation, and user mobility aspects, system modeling and performance evaluation is closely aligned to the envisioned model for a *dense urban information society* as proposed by the METIS 5G project [MET13c] and illustrated in Figure 5.19. Moreover, due to these specific modeling requirements, *Unity 3D* [Uni], a powerful game engineering tool set, was used for modeling the afore mentioned aspects and for evaluating system-level performance.

In this dense urban scenario, the deployment consists of several LTE macro (BS 0) and micro BSs (BS $1-12$) operating at a carrier frequency of 2.6 GHz and using different transmit powers. At the macro BS 0, three sector antennas are deployed with one antenna steering into northern direction and the other antennas are oriented with 120 degrees offset with respect to north. Micro BS antennas are steered toward streets perpendicular to building walls. Radio propagation models follow those stated in [MET13c] taking urban macro and micro cell outdoor-to-outdoor propagation characteristics into account. For example, in case of signals propagating across building edges, as depicted in Figure 5.19(b), a specific path loss model (cf.

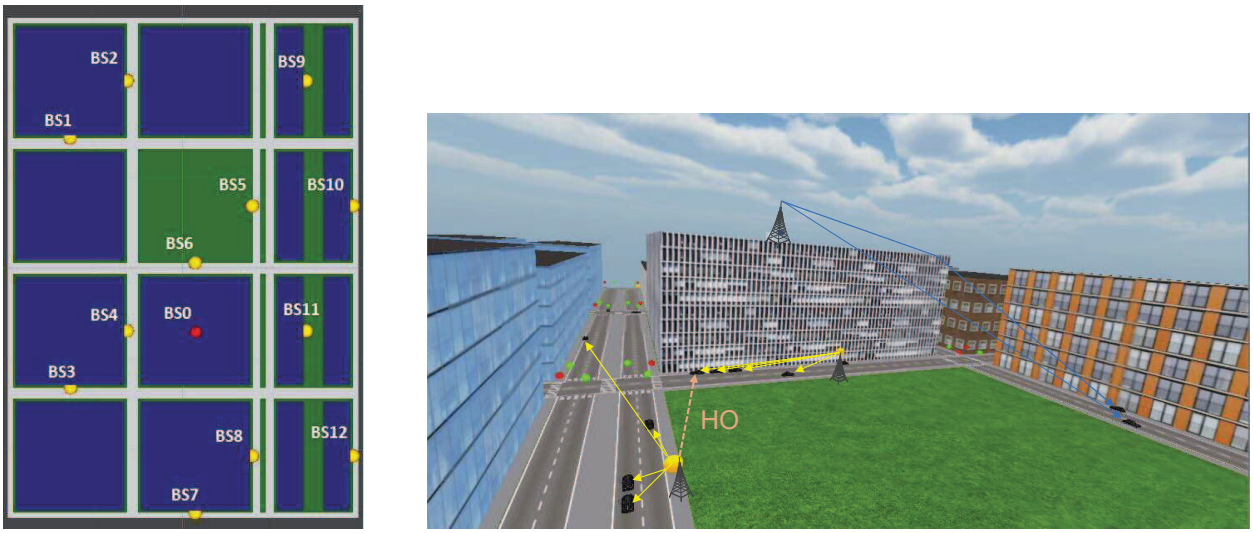

(a) Dense urban deployment [MET13c]

(b) Exemplary signal propagation in dense urban scenario (cf. [MET13c])

Figure 5.19: Dense urban deployment and exemplary signal propagation in dense urban scenario [MET13c]

[MET13c]) is used that accounts for diffraction and refraction effects. Further, 200 vehicular users are considered following the mobility model as defined in [MET13c] for benchmarking. Important simulation parameters are summarized in Table 5.9.

Table 5.9. Simulation parameters [KRSS14]

Parameters	Value
Simulation time	180 s
User speed	25 km/h
Bandwidth per BS	10 MHz
BS transmit power	BS0: 49 dBm, BS1 – 12: 46 dBm
Minimum coupling loss	BS0: 70 dB , BS1 – 12: 53 dB
Handover settings (HOM, TTT, HO execution time)	3 dB, 0.36 s, 0.1 s
Link-to-system mapping [MNK+07]	SISO, $C = \eta_{eff}\ B_u\ \log_2(1+SINR_{eff})$

The specific user transmission bandwidth B_u is determined based on service requirements and stated in multiples of Physical Resource Blocks (PRBs), where each PRB has a bandwidth of 180 kHz. The overall system efficiency factor η_{eff} is set to 0.57 (cf. [MNK+07]).

User mobility is an essential part of realistic system modeling. Thus, mobility-related context (location, speed, direction, acceleration, etc.) may be beneficially exploited for enhancing system performance. In contrast to synthetic user mobility models, e.g., random walk [CBD02], user movements in real-world scenarios are restricted and typically conform to location-specific street layouts. Further, in dense urban areas, user movements depend on traffic laws and behavior of other users. For example, vehicular users are required to stop at red traffic lights or should brake if a vehicle ahead suddenly stops.

Realistic street layouts of urban areas include crossroads at which users may choose to turn or continue moving into the same direction of travel. In [MET13c], user behavior at crossroads is modeled by a random experiment that results in the state transitions and thus changes in user directions illustrated in Figure 5.20(a). However, the fact that users that are about to turn at the next crossroad usually slow down before making a turn is not taken into account. In order to model user behavior in a realistic manner and capture the effects of traffic laws, e.g., red traffic lights, on user movements and behavior of vehicular users approaching crossroads, the velocity of users approaching a crossroad and planning to turn is decreased close to zero. The decision whether users will continue moving straight ahead or make a turn is based on a random experiment that is conducted 20 m ahead of each crossroad. Due to the incorporation of these more realistic modeling aspects, the transition state diagram is adapted accordingly. The modified state transition diagram is depicted in Figure 5.20(b).

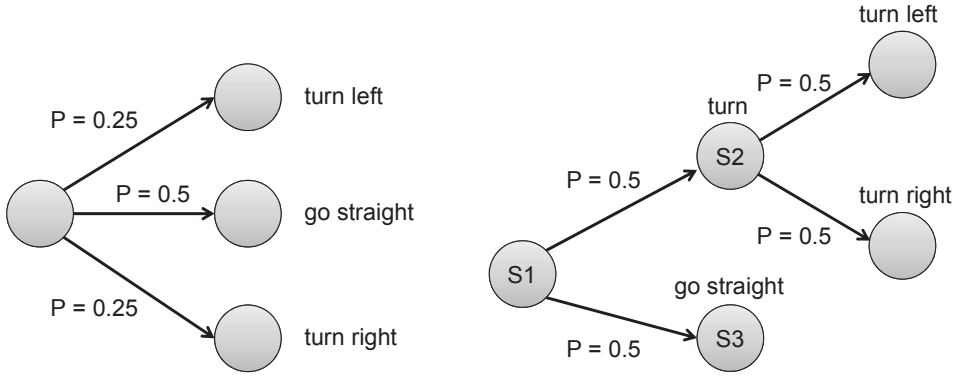

(a) State transition diagram (b) Modified state transition diagram

Figure 5.20: Mobility model state transition diagrams [KRSS14]

It incorporates two states where random experiments are conducted for deciding upon user's future movements. In the initial state, it is determined whether the user continues moving without changing its direction or whether

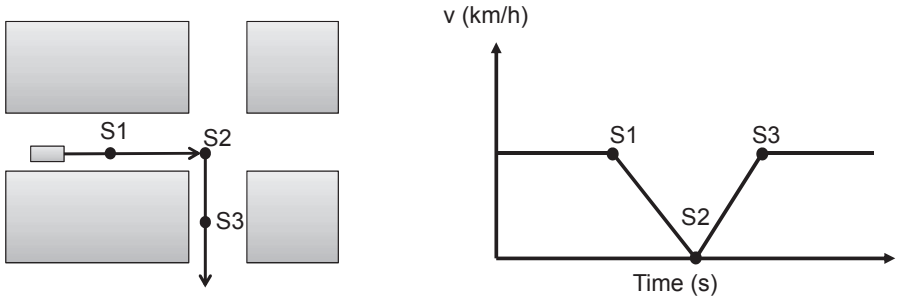

Figure 5.21: Important locations and corresponding changes in user velocity [KRSS14]

the user makes a turn at the next crossroad. If the user decides to turn, another random experiment is performed at the crossroad for deciding whether to turn left or right. Both random experiments have two possible outcomes with equal probability. The respective locations where these random experiments are conducted are shown in Figure 5.21. For example, at position S1 the user decides to turn. Consequently, the user linearly decreases its velocity close to zero until the crossroad is reached. At position S2, the decision for a right turn is taken. After having made a turn, the user's velocity is linearly increased to its original velocity as shown in Figure 5.21. In case the movement direction is not altered, the user keeps on moving at its original velocity (S3). Further, it should be noted that the deceleration of one user on a specific lane also affects following vehicles, which slow down as well in order to maintain a certain distance to the vehicle ahead.

Moreover, due to the nature of urban environments, cellular users moving in these environments may face severe and abrupt changes in received signal levels, which in the worst case result in connection drops. In order to proactively prevent these situations, where e.g., link rate decreases, handover execution is triggered too late, or even the connection dropped, a context-enhanced user movement estimation scheme is developed.

Therefore, several types of context information are used. Besides samples of user location information, user velocity information, or more precisely, changes in user velocities are exploited. User location and velocity information are sampled at least once at a distance more than 20 m as well as within a distance of 20 m ahead of a crossroad. User location information may be acquired using network centric positioning technologies, such as Uplink Time Difference of Arrival (UTDOA) measurements, or provided by the terminal, e.g., using Assisted GPS (A-GPS). Velocity information can be inferred from Doppler shifts of uplink signaling or by increasing location information sampling rate.

The exploitation of location and velocity information allows for predicting whether users continue moving straight ahead or whether they will make a turn. However, the turn direction cannot be predicted without further information. Here, the predictor can only make a guess.

In the following, changes in user location and velocity are exploited for predicting future user movements. Further, achievable performance gains with respect to mobility-related KPIs, such as HO failures and connection drops, and system throughput are evaluated. First, the accuracy of the applied prediction scheme is analyzed, where different user velocities (25, 50, 75 km/h) and prediction horizons (2.5, 5, 7, 10 s) are considered. Performance results are obtained by Monte Carlo simulations consisting of 200 vehicular users that move through the considered street layout for a time period of 300 s. Figure 5.22 illustrates the CDF of observed deviations of predicted locations from actual user locations for different user velocities and prediction horizons.

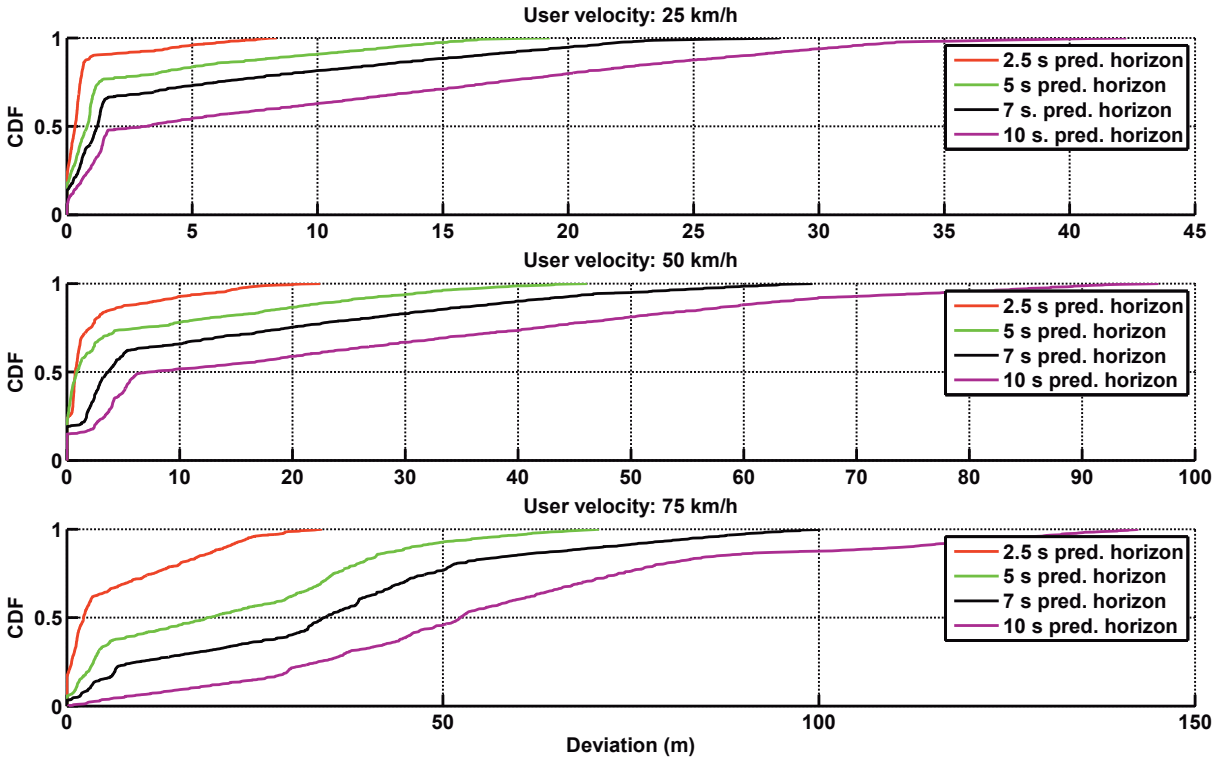

Figure 5.22: Deviation of predicted locations from actual user locations [KRSS14]

In case of user velocities of 25 km/h and a prediction horizon of 2.5 s, the prediction error is less than one meter in 80% of the cases. In contrast, prediction error for a user velocity of 75 km/h is 14 m or less in 80% of the results for the same prediction horizon. In essence, prediction inaccuracy increases with increasing velocity and prediction horizon. In the following, the

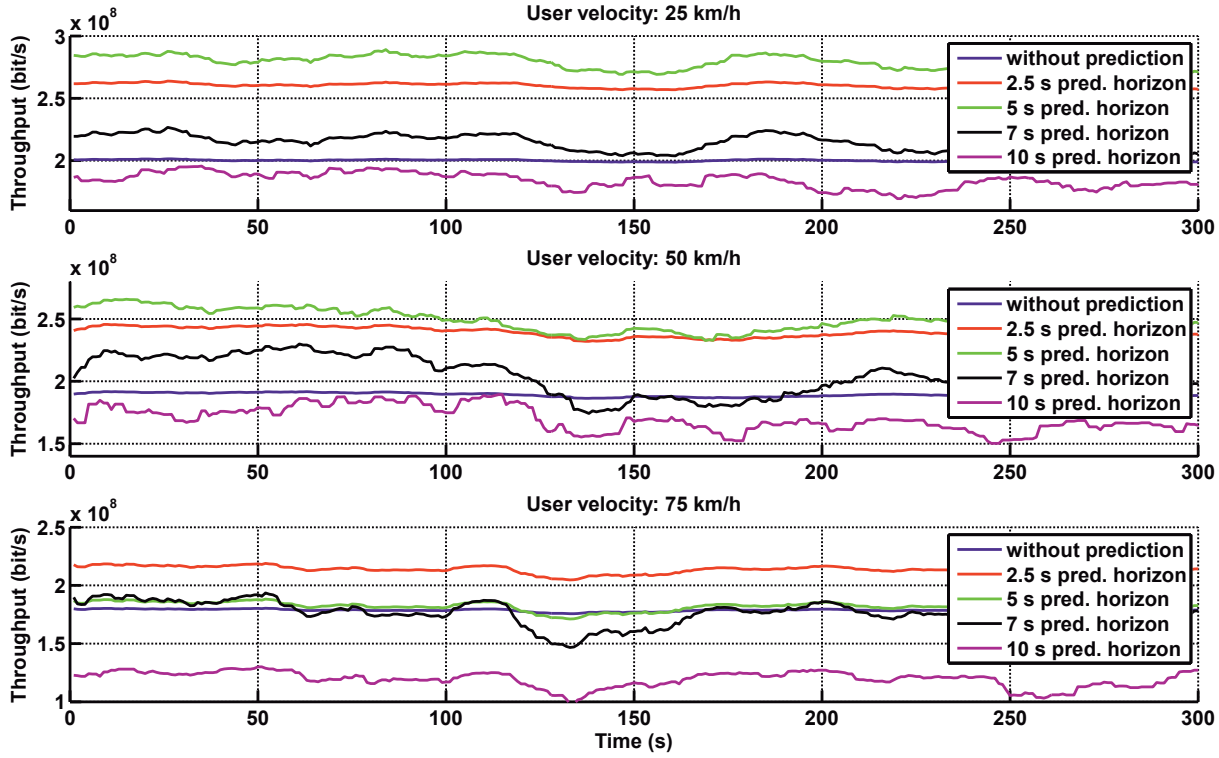

Figure 5.23: Overall throughput for different prediction horizons [KRSS14]

prediction scheme and different prediction horizons, depicted in Figure 5.22, are applied for pro-actively triggering HO processes. Figure 5.23 shows the overall throughput against simulation time for the considered prediction settings, where infinite user traffic demands are assumed.

As expected, user velocity and prediction accuracy have a huge influence on the resulting overall throughput. Best performance results can be achieved for a user velocity of 25 km/h and a prediction horizon of 5 s, where throughput is increased by 39%. For 50 and 75 km/h, maximum achievable gains are 31% and 19%, respectively. It should be noted that there are cases where throughput performance using movement prediction is worse than without prediction. For example, at a user speed of 75 km/h and using a prediction horizons of 7 or 10 s, incorporating movement prediction results only yields marginal or no improvements at all. Thus, too large prediction horizons are not applicable for high-speed users. In summary, reasonable choices of prediction horizons depend on observed user velocities. An interesting finding is that a prediction horizon of 5 s yields higher throughput values for users moving at 25 or 50 km/h than a horizon of 2.5 s. In contrast, in case of users moving at 75 km/h, only a short prediction horizon of 2.5 s results in improved overall throughput.

In order to determine to what extent context information can help to improve system performance, it is assumed that current user positions and

their movements are perfectly estimated, e.g., based on aggregated database knowledge. Figure 5.24 illustrates achievable performance gains with respect to mobility-related event counters, such as connection drops or HO failures, if user movements are perfectly estimated.

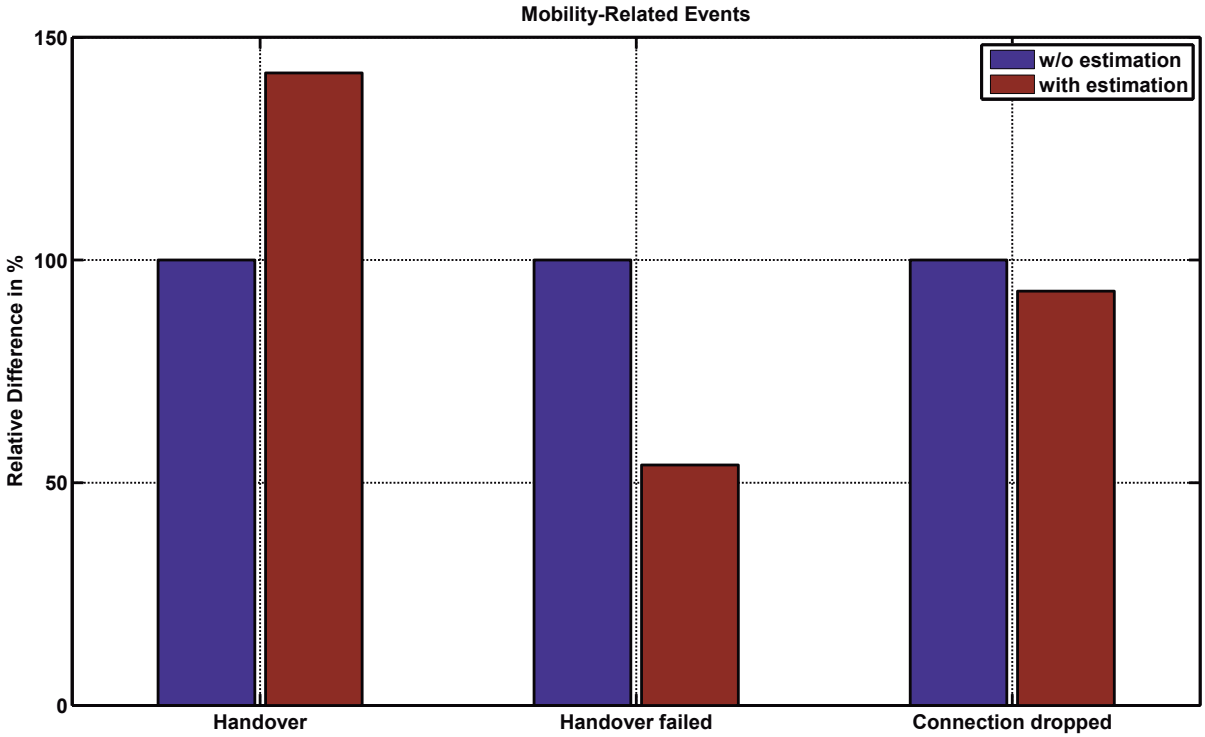

Figure 5.24: Achievable gains with respect to mobility-related event counters [KRSS14]

Regarding HO failures, the exploitation of user movement estimates results in significantly reduced number of HO failures. Here, a reduction of 46% is achieved, however at the cost of an increase in overall number of HOs by more than 40%. Hence, more HOs are anticipated and triggered before connections are dropped. In terms of connection drops, system performance is enhanced by approximately 10%.

For benchmarking system performance with respect to BS load and throughput, the following schemes are considered:

- *Reference*: No movement information is available.
- *Alternative BS*: User movements and corresponding receive signal levels are predicted 10 seconds ahead. If receive signal level is predicted to fall below a specified target threshold within the prediction horizon, an alternative BS is identified and a handover is performed.
- *Predictive RRM*: In addition to movement and signal level prediction, the best time slot with respect to Signal-to-Interference-plus-Noise Ratio (SINR) is predicted for scheduling user transmissions.

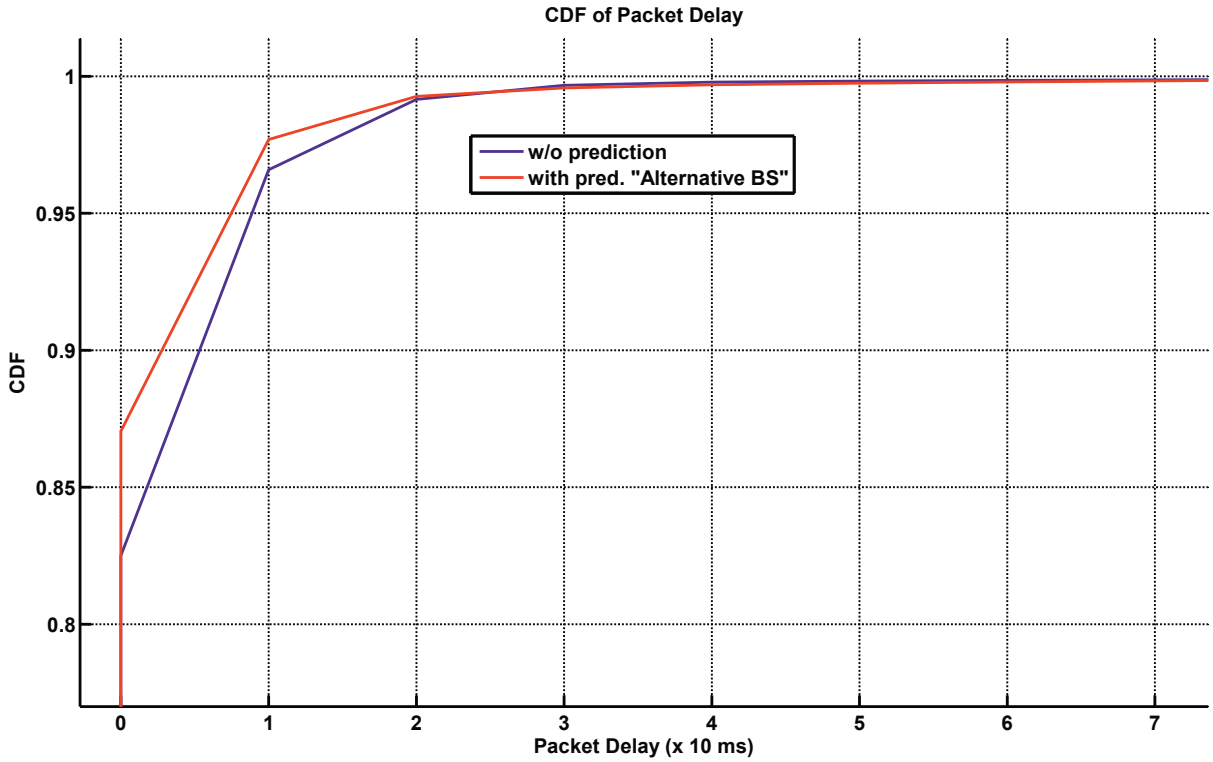

Figure 5.25: VoIP service performance benchmark with respect to packet delay [Rau14]

Further, system performance is evaluated with respect to several service types: voice (VoIP), Constant Bit Rate (CBR), and best-effort. First, VoIP service performance is evaluated with respect to packet delay, where a maximum latency of 50 ms [OCK+07][IEE08] is tolerated. Figure 5.25 shows the impact of exploiting movement estimates on packet delay. Here, a Transmission Time Interval (TTI) of 10 ms is assumed. 5% more packets are successfully received after the first transmission attempt, while differences between the prediction enhanced scheme and the reference scheme decrease to zero for an increasing number of retransmissions.

For the CBR service, a constant bit rate of 600 kbps is required. Figure 5.26 depicts sum throughput and load, respectively.

Table 5.10 lists sum throughput and load values as well as obtained gains. Given the strict bit rate requirement, gains with respect to throughput are rather marginal. However, in terms of overall system load, moderate improvements are obtained in case of *Predictive RRM*.

For the best-effort service, the so-called full buffer model (cf. Section 2.4.1) is used for modeling the situation of infinite traffic demands. Further, different scheduling strategies are considered for the *Alternative BS* and *Predictive RRM* scheme, respectively. In case of the *Alternative BS* scheme, radio resources are distributed equally among connected UEs in a fair manner. How-

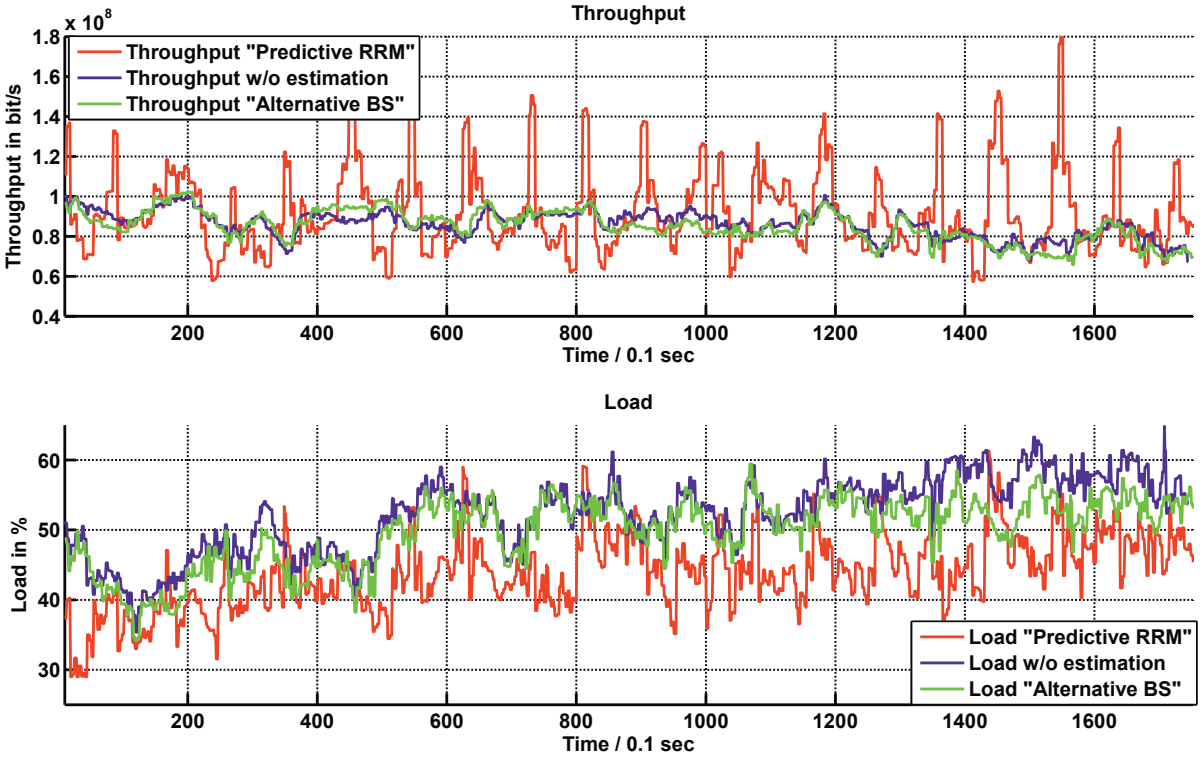

Figure 5.26: CBR service performance benchmark with respect to sum throughput and load [KRSS14]

Table 5.10. Simulation results and performance gains for CBR service [KRSS14]

Parameter	Scheme	Value	Gain
Throughput	Reference	85.1 Mbps	-
	Alternative BS	86.4 Mbps	1.5%
	Predictive RRM	92.2 Mbps	6.2%
Load	Reference	52.5%	-
	Alternative BS	50.1%	4.7%
	Predictive RRM	44.0%	19.1%

ever, the *Predictive RRM* scheme only schedules the UE that is experiencing best receive conditions (maximum carrier-to-interference C/I ratio) among all connected UEs in each time slot (cf. Section 2.6). Figure 5.27 illustrates corresponding system performance with respect to sum throughput.

Table 5.11 summarizes sum throughput performance and achieved gains.

Regarding overall throughput, significant performance improvements of approximately 100% are obtained in case of *Predictive RRM* and "$\max C/I$" scheduling (cf. Section 2.6), while assuming always full BS buffers. Even if no predictive scheduling is performed and users are assigned resources in a fair

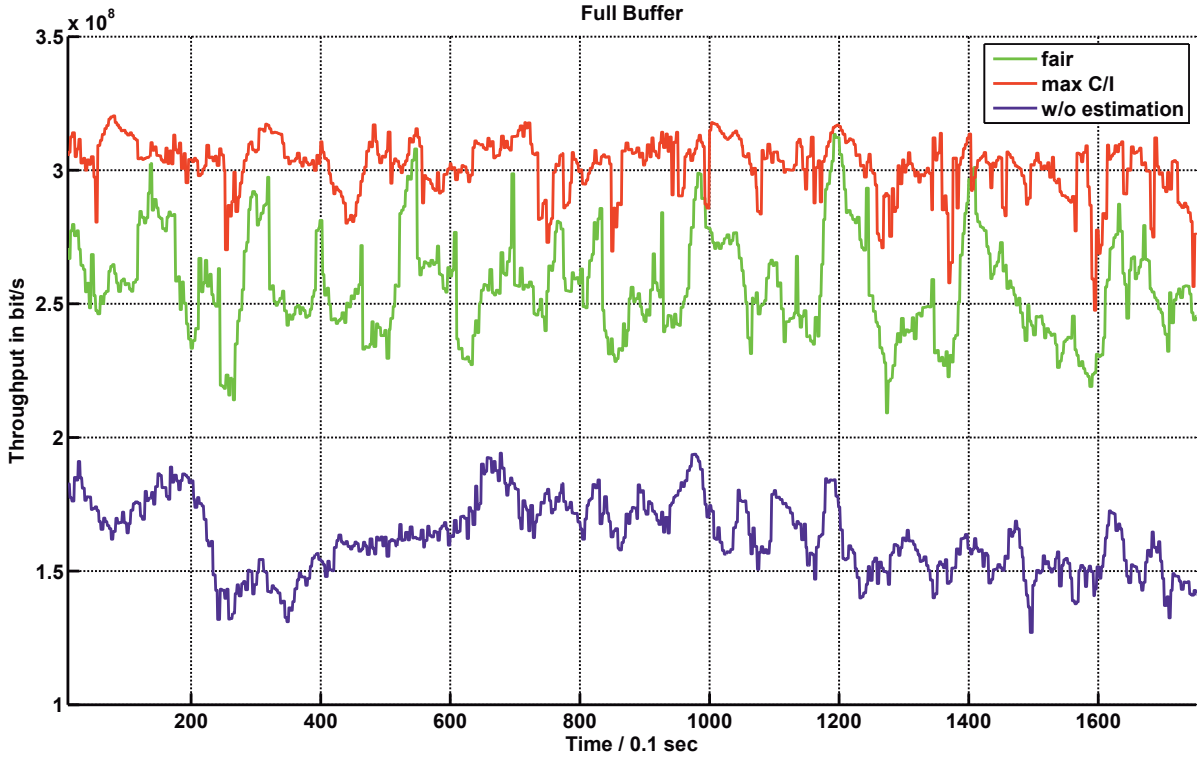

Figure 5.27: Best-effort service performance benchmark with respect to sum throughput [KRSS14]

Table 5.11. Simulation results and performance gains for best-effort service [KRSS14]

Parameter	Scheme	Value	Gain
Throughput	Reference	162.7 Mbps	-
	Alternative BS	258.1 Mbps	58.6%
	Predictive RRM	322.6 Mbps	98.2%

manner, throughput can still be enhanced by approximately 60%. In this specific scenario, these performance figures can be considered as an upper bound for the exploitation of context information, such as user movement estimates and velocities. Moreover, if information, such as environment-specific radio maps, can be used for predictive user scheduling, system performance could be boosted even further.

The objectives of this evaluation have been twofold. First, accuracy and applicability of a prediction scheme that assumes realistic user mobility modeling was investigated. Then, achievable performance gains using context prediction, e.g., movement and SINR, are evaluated on system level considering real-world 3D deployment, mobility, and propagation models. It has been shown that overall throughput can be enhanced by 39%, 31%, and 19% for user velocities ranging from 25, 50, 75 km/h, if prediction horizons are

set accordingly. Here, larger improvements may be feasible, if scheduling decisions account for prediction results. Further, achievable gains of context prediction exploitation have been explored. Here, performance gains of 50% or up to 100% were achieved by applying perfect user movement estimation or joint movement and SINR estimation, respectively.

5.3 Summary

The presented approaches and evaluation results demonstrate the potential of context information exploitation for improving mobility support, E2E performance, and system efficiency in a heterogeneous environment. For example, in Section 5.2.1, the context-enhanced HAM approach, which takes advantage of user movement estimates, shows significant gains in terms of avoidable intra- and inter-RAT HOs. In particular, the IRNA concept has shown to significantly reduce the overall number of intra- and inter-RAT HOs of high-speed users by approximately 40% or even 70%, respectively. If less HOs are to be performed, there is a direct impact on network signaling efforts, HO failure and ping-pong HO probabilities, as well as users' E2E performance. Thus, these metrics can be greatly improved by considering context information.

The developed DBAJCAC scheme, presented in Section 5.2.2, shows an improvement in overall gained utility of approximately 6% with respect to a state-of-the-art JCAC approach, while system KPIs, such as blocking and dropping rates, are kept at an acceptable level. Further, the number of satisfied elastic services, i.e., typical *best effort* services, provided by LTE exceeds those of the benchmark scheme, even at a high number of initial UEs per cell. Furthermore, the proposed scheme exhibits means for LB among RANs. Thus, cell overload is avoided and has never been observed in the conducted simulations.

The fact that mobility of commuters is not purely random is exploited in Section 5.2.3 for predicting user cell transitions. In particular, the prediction of movement trajectories of users moving jointly in the same vehicle (e.g., bus, train, etc.) has shown to significantly improve system KPIs, such as connection dropping, HO and call blocking ratios. Given this knowledge on user trajectories, the arrival of users or user groups into a certain cell can be anticipated and used to pro-actively trigger a LB mechanism in order to prevent imminent congestion.

The average number of connection drops is decreased by 32% and 13%

for ISDs of 500 m and 200 m, respectively. In terms of blocked HO attempts, an average reduction of 26% and 4%, respectively, is achieved. Regarding blocked access attempts, using GPS/distance based cell transition prediction results in improvements of 10% and 6% for ISDs of 500 m and 200 m, respectively. Further, for an ISD of 500 m, significant enhancements with respect to dropped user connections of approximately 42% are achieved using geometry based instead of GPS/distance based prediction. In terms of blocked HO and access attempts, geometry based prediction even results in improvements of 49% as well as 25%, respectively.

In Section 5.2.4, limits of context information exploitation, such as user movement or SINR estimates, are evaluated using real-world 3D environment and radio propagation models. A more realistic user mobility model in a dense urban environment is introduced and the accuracy of movement prediction is analyzed for various user velocities.

As expected, user velocity and prediction accuracy have a strong influence on the resulting overall throughput. In the considered dense urban environment, best performance results are achieved for a user velocity of 25 km/h and a prediction horizon of 5 s, where throughput is increased by 39%.

Regarding HO failures, the exploitation of user movement estimates results in significantly reduced number of HO failures. Here, a reduction of 46% is achieved, however at the cost of an increase in overall number of HOs by more than 40%. Hence, more HOs are anticipated and triggered before connections are dropped. Further, system level results indicate that, e.g., system throughput can be increased by approximately 60% or even 100% using user movement or SINR estimates, respectively.

The developed and presented solutions for context-enhanced HAM, combined JCAC and DBA, cell transition prediction, and user context prediction are envisioned to be extended and integrated with new solutions for future, self-optimizing networks. Following the NGMN alliance's definition of SON use cases [Nex07c], a further research focus was on self-optimization concepts for Mobility Robustness Optimization (MRO) that is addressed in Chapter 7. Fundamentals used for developing novel self-optimization schemes are based on the approaches introduced in Chapter 6.

6 Approaches for Enabling Self-X Capabilities

Enabling robust and optimized mobility support across heterogeneous Radio Access Networks (RANs) is a challenging task. In the future, the heterogeneity of RAT deployments is envisioned to grow further with the introduction of new cell layers [Nok11], e.g., femto cells. Furthermore, RAT capabilities will significantly vary depending on location and region. For instance, there will be a higher network node densification in urban than in rural areas. Hence, Heterogeneous Access Management (HAM) that is in charge of controlling and triggering intra- or inter-RAT Handovers (HOs) needs to be aware of the radio access situation of a considered service area and should preferably be able to anticipate imminent issues. However, Mobile Network Operators (MNOs) that aim at optimizing wireless network performance and in particular mobility robustness face the issue that the complexity of the Radio Resource Management (RRM) and optimization tasks to be performed often result in Non-deterministic Polynomial-time (NP) hard problems due to the huge number of possible parameter combinations. For example, the configuration of a single UMTS cell sector already involves a few hundred options, where

> "the number of solutions to a combinatorial optimization problem grows extremely quickly with the problem size [NAD06c],"

which is also referred to as *combinatorial explosion*.

In the past, MNOs have spent a lot of efforts on manually tuning site-specific HO control parameters. However, in order to reduce the degree of human intervention in network optimization processes, optimal settings, which yield an appropriate trade-off with respect to specified KPIs (e.g., Connection Dropping Ratio (CDR) and Handover Failure Ratio (HFR)), have to be identified and enforced autonomously. Already in 2007, the Next Generation Mobile Networks (NGMN) alliance [Nex07c], which represents world-leading

MNOs, stated that network optimization is a closed loop process of parameter deployment, performance evaluation, parameter optimization, and redeployment of optimized parameters to the network. Further, the NGMN alliance considers mobile networks as dynamic structures, where continuously new sites are deployed, capacity extensions are made, and parameters are adapted to local conditions.

In order to address arising issues in heterogeneous networks due to user mobility and those issues that arise from changes in network configuration and deployment, the author developed a self-optimization scheme that is able to autonomously adapt HO parameter settings according to locally observed conditions, thus establishing context awareness at the respective network node and reducing operational efforts and costs. This approach is presented in detail in Subsection 7.3.2. In the following sections, fundamentals that were used to develop a self-tuning Mobility Robustness Optimization (MRO) approach are introduced and described.

Self-optimization and self-tuning mechanisms have a long history in various domains, such as control theory, autonomic computing, and machine learning. In control theory, control and optimization method design usually rely on a detailed model of the system process and intend to create a control scheme that is able to alter the operating conditions of the dynamical system in real-time. Beyond rather static, feedback based adaptations of the system processes, methods, such as the *extended Kalman filter (EKF)* [JU04], allow for incorporating and exploiting recorded system behavior for nonlinear state estimation and, thus, predicting future system dynamics. However, many complex system processes exist where no comprehensive models are available, since, e.g., the level of detail of sub-process descriptions or the high proportion of non-deterministic influences prevent the formulation of closed-form solutions and control strategies. In contrast, self-tuning approaches that are to be found in the domains of autonomic computing and automated machine learning either try to adapt system behavior based on prior knowledge or learned data, i.e., they are trained to react in a certain way, or they search for optimum adaptations by applying, for example, *Dynamic Programming* (DP) [Bel57] techniques on learned data that becomes the basis for system modeling.

Moreover, control systems face similar design issues as Self-Organizing/ Optimizing Networks (SONs), such as inaccurate data or changing objectives during operation. A way of approaching these issues is by incorporating cognitive functionalities, lowering real-time requirements, and introducing a reflective and evaluative part for the execution level. A framework for han-

dling multi-objective optimization with online adaptation of the objectives depending on internal and external design goals is described in [BSKF06] and applied to several examples in the field of mechatronics. Of course, wherever resources are limited and bottlenecks are inherent system characteristics, congestion can only be avoided by optimization and implementation of means for situation-aware adaptations. One example are bandwidth-consuming Peer-to-Peer (P2P) services that are becoming a financial burden to Internet Service Providers (ISPs). In [XMD09], a framework for self-optimization via demand adaptation is introduced that enables P2P applications to be self-adaptive and optimize their demands in order to more efficiently utilize network resources. The following sections describe various approaches that originate from the fields of control theory, autonomic computing, and automated machine learning, and that allow for implementing self-optimization capabilities, which partly have already been applied in wireless communication networks. In particular, *Fuzzy Inference Systems* (FISs), *Fuzzy Logic*, and *Fuzzy Q-Learning* (FQL) are essential basics for the concepts developed in Chapter 7.

6.1 Fuzzy Inference Systems

> "Inference is the process of deriving logical conclusions from premises known or assumed to be true [The11]."

Similarly, fuzzy inference employs fuzzy logic for converting given inputs into premises, drawing conclusions, and mapping them onto outputs or actions. The tools involved in this process are *membership functions*, *logical operations*, *if-then rules*, and *center-of-gravity* (COG) calculations. FISs have been successfully applied in various fields, such as automatic control, data classification, decision analysis, expert systems, and computer vision. Due to its multidisciplinary nature, FISs are associated with a number of names, such as fuzzy rule based systems, fuzzy expert systems, fuzzy modeling, fuzzy associative memory, fuzzy logic controllers, and simply (and ambiguously) fuzzy systems [The12]. In the remainder of this thesis, the term FIS is used and refers to all of the afore mentioned concepts. A FIS is considered to be a practical alternative for a variety of challenging control applications [PY98], since it constitutes a user-friendly formalism for representing, manipulating, and implementing a human's heuristic knowledge about how to control a system process. Thus, it is suitable for constructing nonlinear controllers for highly complex processes, in particular those to be found in mobile

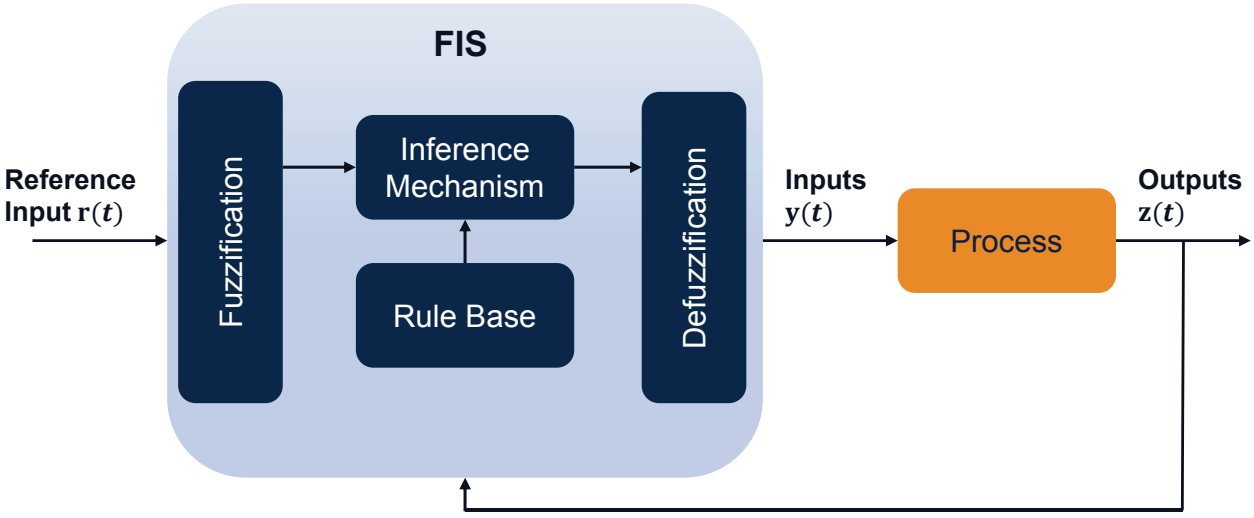

Figure 6.1: FIS architecture [PY98]

communication networks. The required heuristic information may originate from a Mobile Network Operator (MNO) who acted as a *human-in-the-loop* controller, since system optimization tasks were traditionally performed manually using network analysis and planning software tools [NAD06c]. In the FIS design methodology, the MNO defines a set of rules on how to control a certain process. These rules are then incorporated into a FIS that emulates the decision-making process of the human being.

Further, FISs are known to satisfy the *universal approximation property* [Wan92] that enables FISs to perform very complex operations, e.g., compared to those performed by a linear mapping. However, this property only guarantees that there exists a way to define the FIS, e.g., by choosing appropriate membership function parameters, but finding a FIS for solving a specific task can, in general, be very difficult. Furthermore, for arbitrary accuracy an arbitrarily large number of rules may be required. Practically speaking, there is great flexibility in tuning the nonlinear function implemented by the FIS. Generally however, there are no guarantees that one will be able to meet the stability and performance specifications by properly tuning a given FIS. Appropriate controller inputs and outputs are to be chosen. Further, there will be fundamental limitations imposed by the process that may prohibit achieving certain control objectives no matter how the FIS is tuned, e.g., a non-minimum phase system may impose certain limits on the quality of the performance that can be achieved [PY98]. Figure 6.1 illustrates the FIS architecture, where the FIS is embedded in a closed-loop control system. The process outputs, its inputs, and the reference input to the FIS are denoted by $z(t)$, $y(t)$, and $r(t)$, respectively.

In summary, the FIS consists of four main components [PY98]:

1. The *rule base* holds the knowledge that was derived from heuristic information and that is given in the form of a set of rules of how best to control the system.
2. The fuzzy *inference mechanism* evaluates which control rules are relevant at the current system state and then decides what the input to the process should be.
3. The *fuzzification interface* modifies the inputs so that they can be interpreted and compared to the rules in the rule base.
4. The *defuzzification interface* converts the conclusions reached by the inference mechanism into the inputs to the process.

In FISs, *linguistic* descriptions, i.e., linguistic variables and values, are used to formalize expert's knowledge of system dynamics and to provide a language for the expert to express one's ideas about the control decision-making process [PY98]. In this thesis, fuzzy logic is used as a means for partitioning the continuous state space and for classifying the universe of discourse of input variables using a sufficiently large but limited number of fuzzy sets. Moreover, the linguistic quantification of system dynamics aims at characterizing situations or states the system will traverse during operation using the corresponding fuzzy labels. The linguistic descriptions of system dynamics are further used to derive linguistic rules in the form of "If *premise* Then *consequent*". Using this approach, a set of rules can be formulated that constitutes a rule base for dealing with the corresponding control problem. For quantifying the meaning of linguistic descriptions and for automating the evaluation of specified control rules in the FIS, so-called *membership functions* are used. These membership functions are denoted by μ. Depending on the application, the FIS designer may choose different forms of membership functions, such as triangular, trapezoidal, or Gaussian, for quantifying whether system observations, e.g., measurements, belong to a set of linguistic values. For example, system load may be classified as low, medium, or high as depicted in Figure 6.2. Although triangular and trapezoidal shapes are not differentiable, they are much less computationally expensive than Gaussian or Sigmoidal membership function shapes and have been shown to yield satisfactory results in a number of applications [Jou98].

For matching rules onto outputs or actions, fuzzy logic is applied for premise identification and to determine which linguistic rules are *on*. As for instance illustrated in Figure 6.2, two rules would have been activated that are related to the green and the yellow label given input x. In Figure 6.2, a

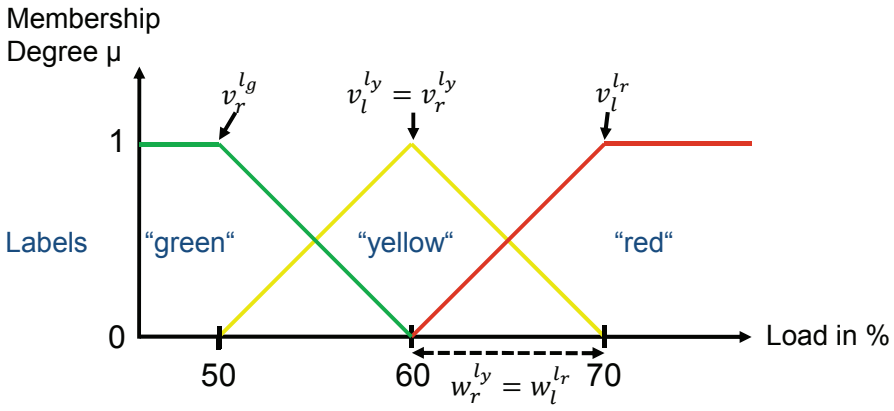

Figure 6.2: Exemplary membership functions

strong fuzzy partition is applied for keeping rule legibility that satisfies

$$\sum_{i=1}^{N_{L_n}} \mu_{l_n^i}(s_n) = 1, \ \forall s_n \in \mathcal{S}_n, \tag{6.1}$$

where N_{L_n} denotes the number of fuzzy sets or labels used to sense the universe of discourse of input variable s_n [Jou98]. This kind of partition implies that there are no more than two fuzzy sets "activated" for an input value and all values "activate" at least one fuzzy set (cf. Fig. 6.2). Given these conventions, the number of labels N_L, the values of the membership function vertices, v_l and v_r for the left and right vertices, and the left and rights span widths w_l and w_r must be defined by the FIS designer. Thus, the membership degree of an input value s_n for a fuzzy label $l_n(v_l, v_r, w_l, w_r)$ can be defined by the following expression [Jou98]:

$$\mu_{l_n}(s_n) = \begin{cases} \max\left\{0, \ 1 - \dfrac{(s_n - v_r)}{w_r}\right\}, & s_n > v_r \\ \max\left\{0, \ 1 - \dfrac{(v_l - s_n)}{w_l}\right\}, & s_n < v_l \\ 1, & \text{otherwise.} \end{cases} \tag{6.2}$$

In order to perform inference, each rule is first quantified with fuzzy logic and then the applicability of each rule is determined. This is accomplished by comparing the premises of all rules to the controller inputs and by determining which rules apply to the current situation. This *matching* process involves assigning the certainty that each rule applies and typically, this yields a set of rules the expert is more certain to apply to the current situation. An example for the neural network-like FIS processing structure with multiple inputs and multiple outputs (MIMO) is depicted in Figure 6.3.

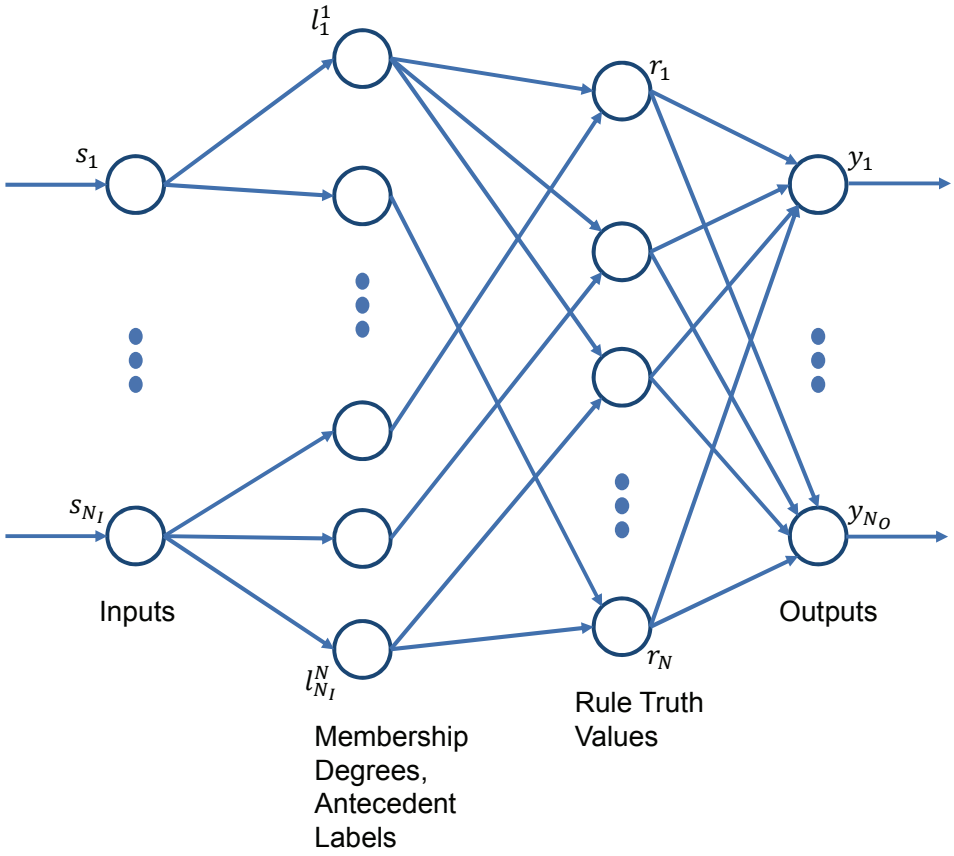

Figure 6.3: FIS scheme [Jou98]

Information is transferred between layers, where each node in the input layer represents a variable (e.g., a Key Performance Indicator (KPI)). In the second layer, the membership degrees to fuzzy sets of the input variables are determined. In the fuzzy rule layer, each rule chooses a certain number of fuzzy sets or antecedents from the second layer. The rule truth values determined in layer three influence the FIS output values, e.g., the magnitude of Handover (HO) parameter adaptation.

In general, the rule base is made of N rules of the following form [Jou98]:

$$\begin{aligned} r_i: \quad & \textbf{if } s_1 \text{ is } l_1^i \textbf{ and } \cdots \textbf{ and } s_{N_I} \text{ is } l_{N_I}^i \\ & \textbf{then } y_1 \text{ is } o_1^i \textbf{ and } \cdots \textbf{ and } y_{N_O} \text{ is } o_{N_O}^i, \end{aligned} \tag{6.3}$$

where

r_i ith rule of the rule base,

$\boldsymbol{s}$ input vector,

$$\boldsymbol{s} = s_1 \begin{pmatrix} 1 \\ 0 \\ 0 \\ \vdots \\ 0 \end{pmatrix} \times s_2 \begin{pmatrix} 0 \\ 1 \\ 0 \\ \vdots \\ 0 \end{pmatrix} \times \cdots \times s_{N_I} \begin{pmatrix} 0 \\ 0 \\ \vdots \\ 0 \\ 1 \end{pmatrix}$$

universe of discourse of input variables,

l_j^i linguistic term (fuzzy label) of input variable s_j in rule r_i, its membership function is denoted by $\mu_{l_j^i}$,

$(y_m)_{m=1,\ldots,N_O}$ denotes the N_O output variables,

o_m^i linguistic term of output variable y_m in rule r_i.

In practice, only a finite number of linguistic variables and linguistic values would be specified, resulting in a finite number of possible rules (all possible combinations of premise linguistic values for the given number of inputs). A convenient way to list all possible rules for the case where there are not too many inputs to the FIS is to use a tabular representation, such as a Look-Up Table (LUT). The number of rules N is determined by the number of input variables N_I (e.g., number of considered KPIs) and the number of fuzzy labels for each of these variables N_{L_j}, i.e.,

$$N = \prod_{j=1}^{N_I} N_{L_j}. \tag{6.4}$$

Each of these rules has N_O corresponding conclusions $\left(o_m^i\right)_{m=1,\cdots,N_O}^{i=1,\cdots,N}$ that in the simplest case are crisp. Hence, the conclusion vector $\boldsymbol{o}_m$ can be used to approximate the output function y_m. Conclusions on which control actions to take are derived using the rules that have been identified to apply at the current time. A rule i is *on at time* t, if its premise membership function $\mu_{\text{premise}}^i > 0$. The inference mechanism seeks to combine the recommendations of all the rules to determine a single conclusion. The conclusions are characterized by a fuzzy set (or sets) that represents the certainty that the input to the process should take on various values. Figure 6.4 exemplarily illustrates the implied fuzzy sets of two activated rules that are to be combined by the *defuzzification* operation.

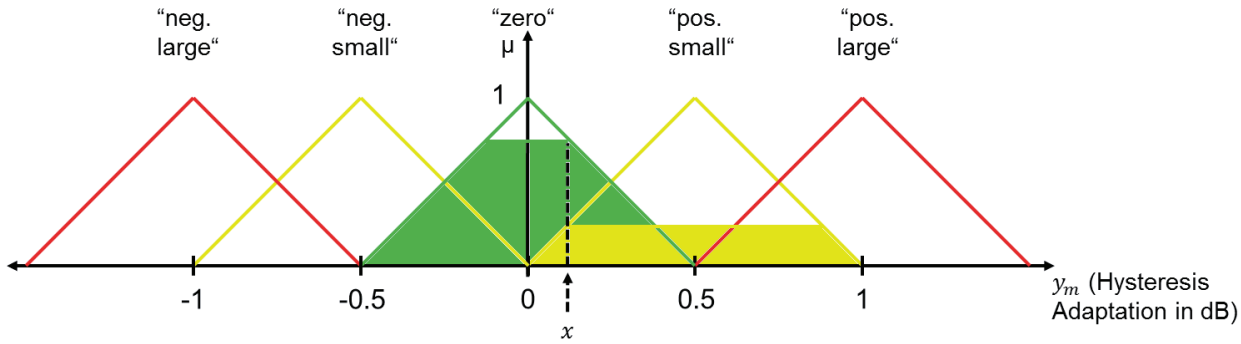

Figure 6.4: Exemplary implied fuzzy sets

The certainty of a premise, composed of different linguistic terms and quantified by various membership functions, is determined using standard Boolean logic operators, such as *Minimum* or *Product*. Both ways of quantifying the *AND* operation in the premise indicate that one can be no more certain about the conjunction of two statements than one is about the individual terms that constitute them (note that $0 \leq \mu_{\text{premise}} \leq 1$ for either case) [PY98]. In general, the truth value of each rule r_i with respect to $\boldsymbol{s} \in \mathcal{S}$ can be computed with a so-called *T-Norm*

$$\alpha_{r_i}(\boldsymbol{s}) = T\left(\mu_{l_1^i}(s_1), \mu_{l_2^i}(s_2), \cdots, \mu_{l_{N_I}^i}(s_{N_I})\right), \tag{6.5}$$

where this t-norm can be implemented, for instance, by a product

$$\alpha_{r_i}(\boldsymbol{s}) = \prod_{j=1}^{N_I} \mu_{l_j^i}(s_j). \tag{6.6}$$

In Figure 6.4, for example, the first rule comes to the conclusion (area in green due to α_{r_1}) that HYS parameter should not be adapted, whereas the second rule recommends increasing HYS by 0.5 dB (area in yellow based on α_{r_2}). The defuzzification operation, which is the final component of the FIS, operates on the implied fuzzy sets (colored areas as shown in Figure 6.4). The implied fuzzy sets are produced by the inference mechanism that derived the activated rule truth values and combines their effects on the consequent or output membership functions μ_{y_m} to provide the most certain controller output. The most popular method for combining the recommendations represented by the implied fuzzy sets from all activated rules is the so-called *Center Of Gravity* (COG) defuzzification method [PY98]:

$$y_m = \frac{\sum_{i=1}^{N} c_m^i \int \mu_{y_m}^i}{\sum_{i=1}^{N} \int \mu_{y_m}^i}, \tag{6.7}$$

where m denotes the corresponding FIS output, c_m^i denotes the center of the membership function of the consequent of rule i and $\int \mu_{y_m}^i$ denotes the area under the consequent membership function $\mu_{y_m}^i$. In case of symmetric triangular output membership functions that peak at one and have a base width of w, the area under the "chopped off" triangle at height h, i.e., $\int \mu_{y_m}^i$, is equal to

$$w\left(h-\frac{h^2}{2}\right)=2\left(\alpha_{r_i}(\boldsymbol{s})-\frac{\alpha_{r_i}^2(\boldsymbol{s})}{2}\right), \tag{6.8}$$

where h corresponds to the respective truth value of the activated rule i, i.e., $\alpha_{r_i}(\boldsymbol{s})$. Further, in the scope of this thesis, w is set to 2 in order to yield symmetric, triangular shaped output membership functions of area 1, if $\alpha_{r_i}(\boldsymbol{s})=1$. For example, this method results in the defuzzification results exemplarily depicted in Figure 6.5, if rule truth values $\alpha_{r_i}(\boldsymbol{s})$ activate two rules that recommend to not alter HYS and to increase HYS parameter due to small positive deviations from performance target. Given, for example,

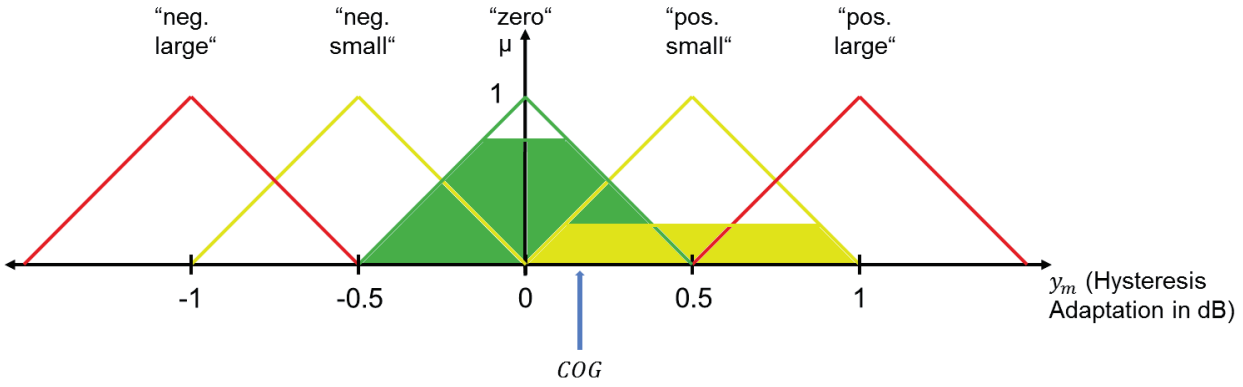

Figure 6.5: Exemplary defuzzification result

$x=1/8$, the COG can be computed as follows:

$$\begin{aligned} y_m &= \frac{c_{zero}^{(1)}\int \mu_{zero}^{(1)}(1/8)+c_{pos.s.}^{(2)}\int \mu_{pos.s.}^{(2)}(1/8)}{\int \mu_{zero}^{(1)}+\int \mu_{pos.s.}^{(2)}} \\ &= \frac{0\cdot 0.46875+0.5\cdot 0.21875}{0.46875+0.21875}\approx 0.16. \end{aligned} \tag{6.9}$$

In this case, no hysteresis adaptation is performed, since $y_m \approx 0.16$ is closer to 0 than to 0.5 dB and only discrete hysteresis adaptations in steps of 0.5 dB can be performed, which is further detailed in Chapter 7.

Concerning stability, which is an issue in every control system and essential for ensuring reliable system operation, well-known techniques for stability analysis of nonlinear systems are available, e.g., Lyapunov's direct and

indirect methods [Lya92]. However, there are limitations to every stability analysis approach due to the following facts [PY98]:

- The model of a physical process is never perfectly accurate, and since the mathematical analysis is based on the model, the analysis is of limited accuracy for the physical system. The more accurate the model, the more accurate the conclusions from the mathematical analysis as they pertain to the real physical system.
- Fuzzy control tends to show its greatest advantages for processes that are very complex in terms of nonlinearities, stochastic influences, process uncertainties, etc. The mathematical analysis tools that are available often do not apply to very complex processes as the assumptions needed for the application of the tools are often not satisfied. Then, there is an inherent limitation of the mathematical analysis tools due to the requirements of such tools for any nonlinear control system, let alone fuzzy control systems.

The training of a FIS can be accomplished using conventional (batch) or recursive least squares as well as the gradient method, which was originally developed as the *back-propagation* technique for training neural networks [PY98]. Moreover, the recursive least squares method as well as the gradient method can perform online parameter estimation. This is an important feature, since many adaptive control techniques depend on the use of an estimator. Additionally, FISs can be trained based on clustering techniques. One suitable combination could be to use *k-means* clustering and a nearest neighborhood technique (e.g., cf. [MKS+11a]) to train the premises and consequents of a standard FIS. Moreover, the ability to easily incorporate heuristic knowledge via fuzzy logic could be considered as one of the major advantages of fuzzy over neural or conventional identification and estimation methods [PY98]. These features laid the foundation for the SON concepts developed in this thesis that are further detailed in Chapter 7.

6.2 Reinforcement Learning

> "Reinforcement learning is learning what to do - how to map situations to actions - so as to maximize a numerical reward signal [SB98]."

In contrast to supervised learning approaches, where the agent learns from examples provided by some knowledgeable external supervisor, the learner is

not told how to react to certain situations. Instead, the learner and decision-maker, which is called the *agent*, must discover which actions yield the most reward by trying them. Further, cases, where actions may affect not only the immediate reward, but also the next situation, and thus, all subsequent rewards, are particularly challenging. These two characteristics, trial-and-error search and delayed reward, are the two most important distinguishing features of Reinforcement Learning (RL) [SB98]. The agent continually interacts with its *environment*, that comprises everything outside the agent, and tries to learn a certain behavior for achieving its objective, e.g., optimum control of a process, through interaction with its environment. A complete specification of an environment defines a *task*, which constitutes one instance of the RL problem. The agent selects actions $\boldsymbol{a}$ and the environment responds to those actions and presents new situations or states $\boldsymbol{s}$ to the agent. The agent perceives the state representation $p(\boldsymbol{s})$ using its cognitive abilities or sensors. Additionally, it is assumed that the agent has a complete view on the environment's state, i.e., the state perception function p equals the identity function, which may be different in partially observable environments [KLM96]. Given the state representation $\boldsymbol{s}$, the agent can evaluate the *reinforcement* signal r for its recent actions. A schematic illustrating the standard RL model is shown in Figure 6.6.

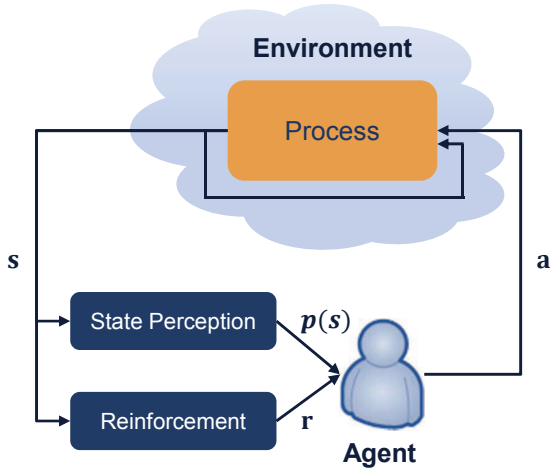

Figure 6.6: Reinforcement learning model [KLM96]

The agent and environment interact at each discrete time step of a sequence, $t = 0, 1, 2, 3, \ldots$. At each time step t, the agent receives some representation of the environment's state $\boldsymbol{s}_t \in \mathcal{S}$, where $\mathcal{S}$ is the set of possible states, and on that basis selects an action $\boldsymbol{a}_t \in \mathcal{A}(\boldsymbol{s}_t)$, where $\mathcal{A}(\boldsymbol{s}_t)$ is the set of actions available in state $\boldsymbol{s}_t$. One time step later, in part as a consequence of its action, the agent receives a numerical reward $r_{t+1} \in \mathcal{R}$, also referred

to as *primary reinforcement*, and finds itself in a new state $\boldsymbol{s}_{t+1} = \boldsymbol{s}'$. The formal representation how the agent maps perceived situations and classified state information to probabilities of selecting each possible action is denoted as the agent's *policy*. At each time step t, the agent implements a certain policy, referred to as π_t, where $\pi_t(\boldsymbol{s},\boldsymbol{a})$ is the probability that $\boldsymbol{a}_t = \boldsymbol{a}$ if $\boldsymbol{s}_t = \boldsymbol{s}$. RL methods specify how the agent changes its policy as a result of its experience [SB98]. In essence, the agent's goal is to maximize the total amount of return it receives until a certain time $\boldsymbol{T}$. However, if the agent-environment interaction does not exhibit separable episodes, their interaction is assumed to continue without limit, i.e., $\boldsymbol{T} = \infty$. Thereby, the return that should be maximized would easily become infinite, too. In order to ensure a proper mathematical modeling and problem formulation, a *discounting* factor γ is introduced yielding an *infinite-horizon discounted model* that allows the agent to determine the present value of future rewards. Thus, the agent that tries to select actions so as to maximize the sum of the discounted rewards it receives in the future, can now aim at maximizing the expected discounted return stated as follows:

$$R_t = r_{t+1} + \gamma r_{t+2} + \gamma^2 r_{t+3} + \cdots = \sum_{k=0}^{\infty} \gamma^k r_{t+k+1}, \tag{6.10}$$

where $0 \leq \gamma \leq 1$. In extreme cases, such as $\gamma = 0$, the agent would only be interested in its immediate reward. Further, if $\gamma < 1$, the infinite sum in Equation (6.10) has a finite value as long as the reward sequence r_k is bounded.

As already mentioned, RL is different from supervised learning, where the agent's learning is guided by an external supervisor. In contrast, a RL agent evaluates the actions taken and acquires experience by a trial-and-error search throughout the state-action space. However, this imposes handling the challenging trade-off between *exploitation* and *exploration* on the agent: On the one hand, the RL agent must preferably *exploit* actions that have shown to be effective in generating significant reward. But on the other hand, the agent has to *explore* actions it has not selected before in order to improve its action decisions in the future. Unfortunately, neither exploitation nor exploration can be exclusively pursued without the possibility of failing. However, whether the RL agent's behavior is mainly governed by exploitation or exploration depends on the implemented Exploration/Exploitation Policy (EEP). Directed strategies memorize exploration-specific knowledge to guide the exploration search, whereas undirected strategies are more related to random walk exploration [Jou98]. In essence, the RL agent must try a variety of ac-

tions *and* progressively favor those that appear to realize the highest reward. When the agent is said to handle a stochastic task, each action must be tried many times to reliably estimate its expected reward [SB98]. Further, the evaluative feedback received through the reinforcement signal is the basis of methods for function optimization, including evolutionary methods, whereas in supervised learning that, e.g., includes large parts of pattern classification, neural networks, and system identification, purely instructive feedback is used to indicate the correct action to take, independently of the action actually taken. In addition, the RL agent faces another issue: the so-called *temporal credit assignment problem*. At each time step, the RL agent receives a reinforcement signal (reward, punishment, neutral signal) according to the last action it has performed in the previous state. For delayed reinforcement signals, i.e., rewards or punishments that are received after a series of neutral signals, the problem is to credit/blame past actions having contributed to the success/failure of the task [Jou98]. This problem is often analyzed by means of *Markov Decision Processes* (MDPs), which are introduced in the following subsection.

6.2.1 Markov Decision Process

In RL, the agent's decisions are based on the signal representing the environment's state and delayed rewards (cf. variable $\boldsymbol{s}$ in Figure 6.6). If this so-called *state signal* is able to compactly convey all relevant information on immediate and recent sensations, it is said to be *Markov*[11] or to have the Markov property, i.e., state transitions are independent of any previous environment states or agent actions [KLM96]. For instance, the current configuration of all items on a chess board that summarizes everything important about the complete sequence of positions that led to it. Although much of the information about the sequence is lost, all that really matters for the future of the game is retained [SB98]. Another example, where Vertical Handover (VHO) decisions are modeled as MDP, can be found in [SNYW08].

A RL task that satisfies the Markov property is called a Markov Decision Process (MDP). If the state and action spaces are finite, then it is called a finite MDP. Finite MDPs are particularly important to the theory of RL and are defined by the following parameters [Jou98]:

$\mathcal{S}$: finite discrete state set,

[11] Andrey (Andrei) Andreyevich Markov (June 14, 1856 - July 20, 1922) was a Russian mathematician, best known for his work on stochastic processes, in particular so-called Markov chains and Markov processes.

$\mathcal{A}$: finite discrete action set,
$\mathcal{R}$: the expected primary reinforcements $\mathcal{R} : \mathcal{S} \times \mathcal{A} \to \mathbb{R}$,
$\mathcal{P}^{\tau}$: the transition probabilities $\mathcal{P}^{\tau} : \mathcal{S} \times \mathcal{A} \times \mathcal{S} \to [0,1]$.

At each time step t, the RL agent perceives state information $\boldsymbol{s}_t = \boldsymbol{s}$ and selects an action $\boldsymbol{a}_t = \boldsymbol{a}$ from the set of possible actions corresponding to that state $\mathcal{A}(\boldsymbol{s}_t = \boldsymbol{s})$. The probability of state transition from $\boldsymbol{s}_t = \boldsymbol{s}$ to the next state $\boldsymbol{s}_{t+1} = \boldsymbol{s}'$ at time step $t+1$ is stated as follows

$$\mathcal{P}^{\tau}_{\boldsymbol{s}\boldsymbol{s}'}(\boldsymbol{a}) = Pr\{\boldsymbol{s}_{t+1} = \boldsymbol{s}' | \boldsymbol{s}_t = \boldsymbol{s},\ \boldsymbol{a}_t = \boldsymbol{a}\}. \tag{6.11}$$

Whereupon, the system issues the primary reinforcement $r(\boldsymbol{s}_t, \boldsymbol{a}_t)$, also denoted as r_{t+1}. Similarly, given current state $\boldsymbol{s}_t = \boldsymbol{s}$ and action $\boldsymbol{a}_t = \boldsymbol{a}$, together with any next state $\boldsymbol{s}_{t+1} = \boldsymbol{s}'$, the expected value of the next reward is

$$\mathcal{R}^{\tau}_{\boldsymbol{s}\boldsymbol{s}'}(\boldsymbol{s}, \boldsymbol{a}) = E\{r_{t+1} | \boldsymbol{s}_t = \boldsymbol{s}, \boldsymbol{a}_t = \boldsymbol{a},\ \boldsymbol{s}_{t+1} = \boldsymbol{s}'\}. \tag{6.12}$$

These two quantities, $\mathcal{P}^{\tau}_{\boldsymbol{s}\boldsymbol{s}'}(\boldsymbol{a})$ and $\mathcal{R}^{\tau}_{\boldsymbol{s}\boldsymbol{s}'}(\boldsymbol{s}, \boldsymbol{a})$, completely specify the most important aspects of the dynamics of a finite MDP, where only information about the distribution of rewards around the expected value is lost [SB98]. Usually, a so-called *transition graph* is employed for illustrating the dynamics of a finite MDP. It comprises a state node for each possible state and an action node for each state-action pair. State nodes are connected to their corresponding action nodes. As soon as the environment responds to a certain action $\boldsymbol{a}_t = \boldsymbol{a}$ taken, a transition from state $\boldsymbol{s}_t = \boldsymbol{s}$ to the next state's node $\boldsymbol{s}_{t+1} = \boldsymbol{s}'$ via one of the arrows leaving the respective action node occurs with probability $\mathcal{P}^{\tau}_{\boldsymbol{s}\boldsymbol{s}'}(\boldsymbol{a})$ and yields reward $\mathcal{R}^{\tau}_{\boldsymbol{s}\boldsymbol{s}'}(\boldsymbol{s}, \boldsymbol{a})$. Note that the transition probabilities labeling the arrows leaving an action node always sum to one. Generally, a RL agent aims at maximizing its expected return. Therefore, it needs to estimate so-called *value functions*, i.e., functions of states or of state-action pairs that indicate how beneficial it is for the RL agent to be in a given state or how beneficial it is to perform a certain action in a given state, where the notion of "how beneficial" is defined in terms of expected return. Of course, the rewards the agent can expect to receive in the future depend on what actions it will take. Accordingly, value functions are defined with respect to particular policies, where a policy π is a mapping from states $\boldsymbol{s} \in \mathcal{S}$ and actions $\boldsymbol{a} \in \mathcal{A}(\boldsymbol{s})$, to the probability $\pi(\boldsymbol{s}, \boldsymbol{a})$ of taking action $\boldsymbol{a}$ when in state $\boldsymbol{s}$. Hence, the value of a state $\boldsymbol{s}$ under a policy π, denoted as $V^{\pi}(\boldsymbol{s})$, is the expected return when starting in $\boldsymbol{s}$ and following π thereafter. For MDPs, $V^{\pi}(\boldsymbol{s})$ can be formally defined as [SB98]:

$$V^{\pi}(\boldsymbol{s}) = E_{\pi}\{r_t | \boldsymbol{s}_t = \boldsymbol{s}\} = E_{\pi}\left\{\sum_{k=0}^{\infty} \gamma^k r_{t+k+1} | \boldsymbol{s}_t = \boldsymbol{s}\right\}, \tag{6.13}$$

where $E_\pi\{\}$ denotes the expected value given that the agent follows policy π and t is any time step. Note that the value of the terminal state, if any, is always zero. The function V^π is the so-called *state-value function for policy* π. Similarly, the value of taking action $\boldsymbol{a}$ in state $\boldsymbol{s}$ under a policy π, denoted $Q^\pi(\boldsymbol{s},\boldsymbol{a})$, is defined as the expected return starting from $\boldsymbol{s}$, taking the action $\boldsymbol{a}$, and thereafter following policy π [SB98]:

$$Q^\pi(\boldsymbol{s},\boldsymbol{a}) = E_\pi\{r_t|\boldsymbol{s}_t=\boldsymbol{s},\boldsymbol{a}_t=\boldsymbol{a}\} = E_\pi\left\{\sum_{k=0}^{\infty}\gamma^k r_{t+k+1}|\boldsymbol{s}_t=\boldsymbol{s},\ \boldsymbol{a}_t=\boldsymbol{a}\right\}, \quad (6.14)$$

where $Q^\pi(\boldsymbol{s},\boldsymbol{a})$ is the so-called *action-value function for policy* π. The agent can estimate the value functions $V^\pi(\boldsymbol{s})$ and $Q^\pi(\boldsymbol{s},\boldsymbol{a})$ from its experience. For instance, if an agent follows policy π and obtains an average for each state perceived of the actual returns that have followed that state, then the average will converge to the state's value $V^\pi(\boldsymbol{s})$, as the number of times that state is observed approaches infinity. If separate averages are kept for each action taken in a state, then these averages will similarly converge to the action values $Q^\pi(\boldsymbol{s},\boldsymbol{a})$. This kind of estimation would of course require averaging over many random samples of actual returns using, for instance, Monte Carlo methods [SB98]. A fundamental property of value functions used throughout reinforcement learning and Dynamic Programming (DP) [Bel57] is that they satisfy particular recursive relationships. For any policy π and any state $\boldsymbol{s}$, the following consistency condition holds between the value of $\boldsymbol{s}$ and the value of its possible successor states [SB98]:

$$\begin{aligned}
V^\pi(\boldsymbol{s}) &= E_\pi\{r_t|\boldsymbol{s}_t=\boldsymbol{s}\} \\
&= E_\pi\left\{\sum_{k=0}^{\infty}\gamma^k r_{t+k+1}|\boldsymbol{s}_t=\boldsymbol{s}\right\} \\
&= E_\pi\left\{r_{t+1}+\gamma\sum_{k=0}^{\infty}\gamma^k r_{t+k+2}|\boldsymbol{s}_t=\boldsymbol{s}\right\} \\
&= \sum_\pi \pi(\boldsymbol{s},\boldsymbol{a})\sum_{\boldsymbol{s}'}\mathcal{P}^\pi_{\boldsymbol{s}\boldsymbol{s}'}\left[\mathcal{R}^\pi_{\boldsymbol{s}\boldsymbol{s}'}+\gamma E_\pi\left\{\sum_{k=0}^{\infty}\gamma^k r_{t+k+2}|\boldsymbol{s}_{t+1}=\boldsymbol{s}'\right\}\right] \\
&= \sum_\pi \pi(\boldsymbol{s},\boldsymbol{a})\sum_{\boldsymbol{s}'}\mathcal{P}^\pi_{\boldsymbol{s}\boldsymbol{s}'}\left[\mathcal{R}^\pi_{\boldsymbol{s}\boldsymbol{s}'}+\gamma V^\pi(\boldsymbol{s}')\right], \quad (6.15)
\end{aligned}$$

where $\mathcal{P}^\pi_{\boldsymbol{s}\boldsymbol{s}'}$ and $\mathcal{R}^\pi_{\boldsymbol{s}\boldsymbol{s}'}$ are the transition probabilities and rewards when transiting from state $\boldsymbol{s}$ to $\boldsymbol{s}'$, respectively, and where implicitly $\boldsymbol{a}\in\mathcal{A}(\boldsymbol{s})$ and $\boldsymbol{s}'\in\mathcal{S}$. The last equation in Equation (6.15) represents the so-called *Bellman equation* [Bel57] for V^π. It expresses a relationship between the value of a state and the values of its successor states and simply averages over all the possibilities, weighting each by its probability of occurring. It states that the value

of the start state $\boldsymbol{s}$ must equal the (discounted) value of the expected next state, plus the reward expected along the way. Further, the value function is the unique solution to its Bellman equation [SB98].

Solving the MDP consists of tuning the RL agent to use an *optimal policy* π^*, i.e., one corresponding to the *optimal value function* V^*, since value functions define a partial ordering over policies [SB98]. An optimal policy is defined as follows [Jou98]:

> Let π and π' be two policies. π is an improvement over π' if $V^{\pi}(\boldsymbol{s}) \geq V^{\pi'}(\boldsymbol{s})$, $\forall \boldsymbol{s} \in \mathcal{S}$ with strict inequality holding for at least one state $\boldsymbol{s}$.

Although there may be more than one optimal policy, they are all denoted by π^* and share the same *optimal value function* V^* defined as

$$V^*(\boldsymbol{s}) = \max_{\pi} V^{\pi}(\boldsymbol{s}), \ \forall \boldsymbol{s} \in \mathcal{S}. \tag{6.16}$$

Further, optimal policies also share the same *optimal action-value function* Q^* defined as

$$Q^*(\boldsymbol{s},\boldsymbol{a}) = \max_{\pi} Q^{\pi}(\boldsymbol{s},\boldsymbol{a}), \ \forall \boldsymbol{s} \in \mathcal{S} \text{ and } \boldsymbol{a} \in \mathcal{A}(\boldsymbol{s}). \tag{6.17}$$

For state-action pair $(\boldsymbol{s},\boldsymbol{a})$, this function states the expected return for taking action $\boldsymbol{a}$ in state $\boldsymbol{s}$ and thereafter following an optimal policy π^*. Thus, Q^* can be written in terms of V^* as follows [SB98]:

$$Q^*(\boldsymbol{s},\boldsymbol{a}) = E\{r_{t+1} + \gamma V^*(\boldsymbol{s}_{t+1}) | \boldsymbol{s}_t = \boldsymbol{s}, \ \boldsymbol{a}_t = \boldsymbol{a}\}. \tag{6.18}$$

Since V^* is the value function for a policy, it must satisfy the self-consistency condition given by Equation (6.15). Moreover, since it is the optimal value function, its consistency condition can be rewritten without reference to any specific policy. This is the so-called *Bellman optimality equation* [Bel57] for V^*, which expresses the fact that the value of a state under an optimal policy

must equal the expected return for the best action from that state [SB98]:

$$\begin{aligned} V^*(\boldsymbol{s}) &= \max_{\pi} Q^{\pi^*}(\boldsymbol{s},\boldsymbol{a}) \\ &= \max_{\pi} E_{\pi^*}\{r_t|\boldsymbol{s}_t=\boldsymbol{s},\ \boldsymbol{a}_t=\boldsymbol{a}\} \\ &= \max_{\boldsymbol{a}\in\mathcal{A}(\boldsymbol{s})} E_{\pi^*}\left\{\sum_{k=0}^{\infty}\gamma^k r_{t+k+1}|\boldsymbol{s}_t=\boldsymbol{s},\ \boldsymbol{a}_t=\boldsymbol{a}\right\} \\ &= \max_{\boldsymbol{a}\in\mathcal{A}(\boldsymbol{s})} E_{\pi^*}\left\{r_{t+1}+\gamma\sum_{k=0}^{\infty}\gamma^k r_{t+k+2}|\boldsymbol{s}_t=\boldsymbol{s},\ \boldsymbol{a}_t=\boldsymbol{a}\right\} \\ &= \max_{\boldsymbol{a}\in\mathcal{A}(\boldsymbol{s})} E\{r_{t+1}+\gamma V^*(\boldsymbol{s}_{t+1})|\boldsymbol{s}_t=\boldsymbol{s},\ \boldsymbol{a}_t=\boldsymbol{a}\} \\ &= \max_{\boldsymbol{a}\in\mathcal{A}(\boldsymbol{s})} \sum_{\boldsymbol{s}'}\mathcal{P}^{\pi}_{\boldsymbol{s}\boldsymbol{s}'}\left[\mathcal{R}^{\pi}_{\boldsymbol{s}\boldsymbol{s}'}+\gamma V^*(\boldsymbol{s}')\right]. \end{aligned} \tag{6.19}$$

These last two equations are two forms of the Bellman optimality equation for V^*. The Bellman optimality equation for Q^* using $\boldsymbol{a}_{t+1}=\boldsymbol{a}'$ is

$$\begin{aligned} Q^*(\boldsymbol{s},\boldsymbol{a}) &= E\left\{r_{t+1}+\gamma\max_{\pi} Q^*(\boldsymbol{s}_{t+1},\boldsymbol{a}_{t+1})|\boldsymbol{s}_t=\boldsymbol{s},\ \boldsymbol{a}_t=\boldsymbol{a}\right\} \\ &= \sum_{\boldsymbol{s}'}\mathcal{P}^{\pi}_{\boldsymbol{s}\boldsymbol{s}'}\left[\mathcal{R}^{\pi}_{\boldsymbol{s}\boldsymbol{s}'}+\gamma\max_{\pi} Q^*(\boldsymbol{s}',\boldsymbol{a}')\right]. \end{aligned} \tag{6.20}$$

For finite MDPs, the Bellman optimality equation in Equation (6.19) has a unique solution independent of the policy. The Bellman optimality equation is actually a system of equations, one for each state, i.e., if there are n states, then there are n equations in n unknowns. If the dynamics of the environment are known ($\mathcal{P}^{\pi}_{\boldsymbol{s}\boldsymbol{s}'}$ and $\mathcal{R}^{\pi}_{\boldsymbol{s}\boldsymbol{s}'}$), then it is possible to solve this system of equations for using any one of a variety of methods for solving systems of nonlinear equations (e.g., Levenberg-Marquardt algorithm). Similarly, one can solve a related set of equations for Q^*. However, even if the RL agent has a complete and accurate environment model, it is typically unable to perform enough computations per time step to fully exploit it, since the memory available for building up accurate approximations of value functions, policies, and models, is often an important constraint. In most cases of practical interest, there are far more states than could possibly be entries in a table, and thus, approximations must be made [SB98]. In case the MDP model is not completely known, so-called *Adaptive* DP methods are used that approximate DP techniques and constitute two families. The *model-based* family, in which a model is approximated via interaction with the system, and then DP methods are applied, and the *model-free* family, in which evaluation functions and policies are directly learned during interaction [Jou98]. *Q-Learning* [Wat89], [WD92] and also Fuzzy Q-Learning (FQL) [Glo94], [JG96],

[GJ96], [GJ97], [Jou98] belong to this last family, where FQL is described in more detail in the following subsection.

6.2.2 Fuzzy Q-Learning

Fuzzy Q-Learning (FQL) is a reinforcement learning method that is based on Watkins' *Q-Learning* [Wat89], [WD92] method. As RL schemes, both approaches have in common that they aim at maximizing the total amount of reinforcements the agent can receive in the future, while handling delayed rewards and applying an EEP. Solution methods, such as the classical Adaptive DP methods, e.g., used in MDPs, deal with discrete input spaces, where the state representation often used is a Look-Up Table (LUT). However, LUTs have their limitations particularly in case of a large, continuous state space. This problem is known as the *curse of dimensionality* and is typically handled by incorporating some form of generalization in the state representation. Based on the assumption that neighboring states are expected to have similar function values, various function approximators have been used in conjunction with DP, such as Cerebellar Model Articulation Controller [Wat89], Neural Networks [BK92], [JG96], and FIS [BK92]. FQL employs a FIS to approximate the *Q-function*, since they are universal function approximators [Wan92], where fuzzy logic is used to introduce generalization in the state representation. Further, it focuses on tuning only the conclusion part of a FIS, while the number and positions of the input fuzzy labels are set by the FIS designer using a priori knowledge of the control task, which can reduce training efforts significantly. Furthermore, the set of activated rules yields a compact state representation $\boldsymbol{\alpha}$, which contains all rule truth values $\alpha_{r_i}(\boldsymbol{s}) = \alpha_i(\boldsymbol{s}) > 0$ corresponding to the current state.

In Q-Learning [Wat89], [WD92], the RL agent incrementally builds a value function, referred to as *Q-function* and denoted by $Q(\boldsymbol{s},\boldsymbol{a})$, that attempts to estimate the discounted future rewards for taking available actions $\boldsymbol{a} \in \mathcal{A}(\boldsymbol{s})$ from given states $\boldsymbol{s} \in \mathcal{S}$, or in brief, it gives the action qualities with respect to states. When action $\boldsymbol{a}$ has been selected and applied in state $\boldsymbol{s}$, the system moves to a new state $\boldsymbol{s}'$, the agent receives a numerical reinforcement signal r, and $Q(\boldsymbol{s},\boldsymbol{a})$ is updated by [GJ97]:

$$Q(\boldsymbol{s}',\boldsymbol{a}) = (1-\kappa)Q(\boldsymbol{s},\boldsymbol{a}) + \kappa\left\{r + \gamma V(\boldsymbol{s}')\right\} = Q(\boldsymbol{s},\boldsymbol{a}) + \kappa\left\{r + \gamma V(\boldsymbol{s}') - Q(\boldsymbol{s},\boldsymbol{a})\right\}, \tag{6.21}$$

where $V(\boldsymbol{s}')$ is the value of state $\boldsymbol{s}'$ that is defined by [GJ97]:

$$V(\boldsymbol{s}') = \max_{\boldsymbol{b} \in \mathcal{A}(\boldsymbol{s}')} Q(\boldsymbol{s}',\boldsymbol{b}), \tag{6.22}$$

where $\mathcal{A}(\boldsymbol{s}')$ is the set of possible actions in state $\boldsymbol{s}'$, κ is the learning rate, and γ a discount factor introduced in the previous Section 6.2. As described in Section 6.1, FIS rules are of the following form [GJ97]:

$$r_i\text{:} \quad \begin{array}{l} \textbf{If } \boldsymbol{s}_i \textbf{ then } \text{action} = \boldsymbol{a}_i,\ \boldsymbol{a}_i \in \mathcal{A}(\boldsymbol{s}_i), \\ \textbf{If } \boldsymbol{s}_i \textbf{ and } \text{action} = \boldsymbol{a}_i \textbf{ then } \text{Q-value} = q(\boldsymbol{s}_i,\boldsymbol{a}_i), \end{array}$$

where the state representation resulting from rule i, denoted as $\boldsymbol{s}_i$, is defined by "s_1 is l_1^i **and** s_2 is l_2^i ... **and** s_n is l_n^i", $\left(l_j^i\right)_{j=1,\ldots,N_{L^i}}$ are fuzzy labels, N_{L^i} being the number of fuzzy labels applicable in rule i, and $\mathcal{A}(\boldsymbol{s}_i)$ is the set of possible actions that can be selected in state $\boldsymbol{s}_i$. Further, each action $\boldsymbol{a}_i \in \mathcal{A}(\boldsymbol{s}_i)$ can influence several outputs $(y_m)_{m=1,\ldots,N_O}$ in a MIMO FIS (cf. Fig. 6.3).

In a FIS with N rules, the inferred action $\boldsymbol{a}(\boldsymbol{s}) : \boldsymbol{s} \to \boldsymbol{a}$ given input vector $\boldsymbol{s} = (s_1, \ldots, s_n)$ (cf. Figure 6.3) and rule consequents $(\alpha_i)_{i=1,\ldots,N}$ (cf. Equation (6.6)) is [GJ97]

$$\boldsymbol{a}(\boldsymbol{s}) = \frac{\sum_{i=1}^{N} \alpha_i(\boldsymbol{s}) a_i}{\sum_{i=1}^{N} \alpha_i(\boldsymbol{s})}, \tag{6.23}$$

where, in case of a strong fuzzy partition, the denominator equals 1. The corresponding Q-value is determined as follows [GJ97]

$$Q(\boldsymbol{s},\boldsymbol{a}) = \frac{\sum_{i=1}^{N} \alpha_i(\boldsymbol{s}) q(\boldsymbol{s}_i,\boldsymbol{a}_i)}{\sum_{i=1}^{N} \alpha_i(\boldsymbol{s})} = \frac{\sum_{i=1}^{N_{\text{active}}} \alpha_i(\boldsymbol{s}) q(\boldsymbol{s}_i,\boldsymbol{a}_i)}{\sum_{i=1}^{N_{\text{active}}} \alpha_i(\boldsymbol{s})}, \tag{6.24}$$

where the function $\boldsymbol{s} \to \alpha_i(\boldsymbol{s})$ performing the mapping from input vector $\boldsymbol{s}$ onto rule consequents $\alpha_i(\boldsymbol{s})$ gives the truth value of rule i given input vector $\boldsymbol{s}$. Thus, the number of rules N reduces to the number of activated rules N_{active}, i.e., $\alpha_i(\boldsymbol{s}) > 0$. In essence, the RL agent must find the best conclusion for each rule i, i.e., the action with the best *quality* or *Q-value*. In case rule i is activated based on evaluation of state representation $\boldsymbol{s}_i$, the RL agent can select one possible action k, denoted as $a(i,k)$, from a set of competing actions $\mathcal{A}^i$ with N_{A^i} actions for each rule i, where the corresponding action quality is denoted as $q(i,k)$. The resulting FIS can be represented in the following form:

$$\begin{array}{lll} \textbf{If } \boldsymbol{s} \text{ is } \boldsymbol{s}_i \textbf{ then} & & a(i,1) \text{ with } q(i,1) \\ & \textbf{or} & a(i,2) \text{ with } q(i,2) \\ & & \ldots \\ & \textbf{or} & a(i,N_{A^i}) \text{ with } q(i,N_{A^i}). \end{array}$$

Initially, all Q-values $q(i,k)$ are zero. During learning process they are incrementally adjusted according to the experience attained by the RL agent

through applying selected actions, while following a certain EEP. In the following, a mixed directed/undirected EEP is assumed that is ε-*greedy* in the sense that for each rule i the currently best action, referred to as k^* with $q(i,k^*)$, is selected with probability ε and a random action with probability $(1-\varepsilon)$ [Jou98]. In case several alternative actions to the currently best action k^* are specified, any of them can be selected with equal probability.

More precisely, let k^+ be the selected action in rule i using an EEP and let k^* be the currently best action, i.e., $q(i,k^*) = \max_{j \in \mathcal{A}^i} q(i,j)$, the global Q-value of the inferred action $\boldsymbol{a}$ given input vector $\boldsymbol{s}$ is [GJ97]:

$$Q(\boldsymbol{s},\boldsymbol{a}) = \frac{\sum_{i=1}^{N} \alpha_i(\boldsymbol{s}) q(i,k^+)}{\sum_{i=1}^{N} \alpha_i(\boldsymbol{s})}, \tag{6.25}$$

and the resulting state value is [GJ97]:

$$V(\boldsymbol{s}) = \frac{\sum_{i=1}^{N} \alpha_i(\boldsymbol{s}) q(i,k^*)}{\sum_{i=1}^{N} \alpha_i(\boldsymbol{s})}. \tag{6.26}$$

Q-values are incrementally updated during the learning process. Let $\boldsymbol{s}$ be a state, $\boldsymbol{a}$ the action applied, $\boldsymbol{s}'$ the new state, and r the reinforcement signal received by the RL agent. The difference between the "old" action quality $Q(\boldsymbol{s},\boldsymbol{a})$ in state $\boldsymbol{s}$ and the "new" state value $V(\boldsymbol{s}')$ is thought of as an *error signal*,

$$\Delta Q = r + \gamma\ V(\boldsymbol{s}') - Q(\boldsymbol{s},\boldsymbol{a}), \tag{6.27}$$

that is used to globally update the Q-values by gradient descent as follows [GJ97]:

$$\Delta q(i,k) = \kappa\ \Delta Q\ \frac{\alpha_i(\boldsymbol{s})}{\sum_{i=1}^{N} \alpha_i(\boldsymbol{s})}, \tag{6.28}$$

where κ is a *learning rate*.

In order to account for the so-called *temporal credit assignment problem*[12], the *eligibility* concept emanating from the *Temporal Difference* (TD) learning method [Sut88] is incorporated. The eligibility $e(i,k)$ of an action k is defined as [GJ97]:

$$e(i,k) = \begin{cases} \nu\ \gamma\ e(i,k) + \dfrac{\alpha_i(\boldsymbol{s})}{\sum_{i=1}^{N} \alpha_i(\boldsymbol{s})} & \text{if } k = k^+, \\ \nu\ \gamma\ e(i,k) & \text{otherwise,} \end{cases} \tag{6.29}$$

[12] In [Min61], M. Minsky discussed several issues relevant to reinforcement learning. In particular, he dealt with the problem of how to distribute credit for success among the many decisions that may have been involved in producing it, which he called the credit assignment problem.

where the recency factor ν, also called *eligibility rate*, is used to weight the formerly discounted eligibility value $\gamma e(i,k)$. In essence, the normalized rule truth value $\frac{\alpha_i(\boldsymbol{s})}{\sum_{i=1}^{N}\alpha_i(\boldsymbol{s})}$ is substituted by $e(i,k)$. Thereby, the updating Equation (6.28) becomes [GJ97]:

$$\Delta q(i,k) = \kappa\ \Delta Q\ e(i,k). \tag{6.30}$$

Eligibility traces originate from the field of classical conditioning [Jou98]. They are used to model the impact of previously visited rules and past rule-action pairs on the currently activated rule-action pairs. In this thesis, accumulating eligibility traces are employed in order to generate significant eligibility values for rules that are activated at many consecutive time steps. The current eligibility value consists of the normalized rule truth value $\frac{\alpha_i(\boldsymbol{s})}{\sum_{i=1}^{N}\alpha_i(\boldsymbol{s})}$ and the previous eligibility value of this rule-action pair weighted by ν and γ. Due to these factors, eligibility values gradually decay over time. Thus, the influence of previously visited rule-action pairs diminishes, too. The FQL scheme is summarized in Tab. 6.1.

Table 6.1. Generic FQL scheme [GJ97]

1.	Observe and classify state $\boldsymbol{s}$.
2.	For each rule: calculate the actual consequence using some EEP.
3.	Determine the global consequence $a(\boldsymbol{s})$ and its corresponding Q-value $Q(\boldsymbol{s},\boldsymbol{a})$.
4.	Apply action $a(\boldsymbol{s})$. Observe state transition from $\boldsymbol{s}$ to $\boldsymbol{s}'$.
5.	Receive reinforcement signal r.
6.	Update Q-values according to Equation (6.30).

In [WD92], Watkins and Dayan proof that the Q-learning algorithm converges to the optimum action quality values with probability 1 as long as

> "all actions are repeatedly sampled in all states and the action-values are represented discretely."

6.3 Summary

In essence, the author selected the afore mentioned concepts for designing FQL based MRO schemes that are presented in Chapter 7 due to the following reasons:

- A FIS is able to operate on erroneous, inaccurate, or fuzzy input values. Since measurement tolerances are part of any real-world system, this is an important advantage from practical implementation point of view.
- FISs are known to satisfy the universal approximation property [Wan92] that enables FISs to perform very complex system control operations, e.g., compared to those performed by a linear mapping.
- FISs exhibit great flexibility in tuning the implemented nonlinear control mechanism, since human's heuristic knowledge on how to control a certain system process can be easily incorporated by means of *if-then* rules.
- FQL employs a FIS to approximate the *Q-function* [Wat89], [WD92], since FISs are universal function approximators [Wan92], where fuzzy logic is used to introduce generalization in the state representation. Generalization is essential due to the *curse of dimensionality* issue, as referred to by Bellman [Bel57], [SB98].
- FQL does not require a complete and accurate system model. The agent learns from observations and through interaction with its environment and the process to be controlled. Model building is implicitly accomplished by following a certain Exploration/Exploitation Policy (EEP). The learning entity discovers which actions, i.e., parameter adaptions, yield the most reward in the long-term by trying pre-defined actions. The Q-learning algorithm converges to the optimum action quality values as long as all actions are repeatedly sampled in all states [WD92].
- FQL is able to handle delayed feedback, which is usually the case in any real-world system. Further, cases where actions may affect not only the immediate reward, but also the next situation and all subsequent rewards, are an inherent part of the learning approach.
- FQL focuses on tuning the conclusion part of a FIS, i.e., the action selection mechanism, while the number and positions of the input fuzzy labels are set by the FIS designer using a priori knowledge of the control task, which significantly reduces training efforts. However, well-known data mining techniques, such as k-means and k-nearest neighbor, as e.g., described in [MKS+11a], can be used to overcome this limitation.
- Modeling and implementation of FQL is much less complex than implementation of neural network and supervised learning based strategies. This aspect is particularly beneficial for practical implementation in real-world systems, where computational resources and memory are limited and represent an additional cost factor.

The FQL approach has already been successfully applied to the problem of dynamically and optimally tuning soft handover parameters [NAD06a], [NAD06c], optimal resource sharing between real-time and non-real-time services in 3G networks [NAD06b], self-adaptation and -optimization in heterogeneous networks using a cognitive pilot channel [FLTZ09], and self-tuning HO parameters for load balancing [MBdlB$^+$11]. However, to the best of the author's knowledge, no approach has been presented yet that is able to self-optimize HO parameter settings according to locally observed conditions while enhancing multiple KPIs. Such an approach has been developed by the author and is introduced in Chapter 7 and evaluated in Chapter 8.

7 Self-Optimizing Networks: Architecture, Use Cases, and Concepts

The roll-out of 4G Radio Access Networks (RANs) promises to provide significant rises in network capacity and enhanced Quality of Service (QoS) for mobile broadband applications, such as High Definition (HD) multimedia, video conferencing, etc. However, the current situation of Mobile Network Operators (MNOs) is characterized by increasing margin pressure due to declining revenues and an increasing cost base. While controlling Capital Expenditures (CAPEX) for new infrastructure components remains an important issue for MNOs, Operational Expenditures (OPEX) have become a more significant part of operators' cost structure. Analysts [Wym09] forecast a margin squeeze due to declining Average Revenue Per Unit (ARPU) and increasing OPEX. In particular, the increasing voice and data usage leads to higher backhaul and terminal costs, costs for site rents, electricity, etc., while ARPU is capped due to flat-rate tariffs. Hence, the major challenge for MNOs is to provide mobile broadband and potentially new services in a high-quality, but cost-effective manner. Moreover, new technologies such as Machine-To-Machine (M2M) communication and Internet of Things (IoT) are expected to exhaust the capacity of existing RANs. For instance, Ericsson [Eri11] predicts 50 billion connected devices by 2020 and the Global System for Mobile Communications Association (GSMA) [Glo11] forecasts a six fold growth of connected devices in China, the world's largest mobile market. Thus, there is a need for future-proof solutions that allow for cost-efficient network management and support of various new services ranging from safety-critical or real-time to high data rate on demand services. Therefore, Self-Organizing/Optimizing Networks (SONs) will be key measures to address these challenges.

In particular, robust mobility support in heterogeneous networks is a chal-

lenging but important feature of current and future RANs. Due to user mobility and thereby triggered Handover (HO) processes that are subject to RAN-specific delays, which may severely affect users' End-To-End (E2E) performance, autonomous controlling of system behavior and service provisioning are crucial for MNOs in order to mitigate OPEX and to stand out from their competitors. In future, the heterogeneity of RAT deployments will further grow with the introduction of new cell layers [Nok11] and RAT capabilities will significantly vary depending on location and region. For instance, in dense urban areas where traffic demands are significantly higher than in rural areas, densification of network nodes is envisioned to massively increase network capacity [Nok11]. A macro cell will be in charge of managing several cells (e.g., micro or femto cells) that operate at lower transmit powers but are able to provide high capacity to a confined service area, thus enabling MNOs to offload user traffic from the macro cell. MNOs that aim at optimizing Heterogeneous Access Management (HAM) performance and, in particular, mobility robustness face the issue that the complexity of the Radio Resource Management (RRM) and optimization tasks to be performed yield Non-deterministic Polynomial-time (NP)-hard problems due to the huge number of possible parameter combinations [NAD06c]. For example, in Section 5.2.2, the author addressed this issue by employing an approximation algorithm for solving the Generalized Assignment Problem (GAP) and optimizing RRM and MNO revenues while accounting for different kinds of context information.

From the Next Generation Mobile Networks (NGMN) alliance's point of view [Nex07c], network optimization is a closed loop process. Further, mobile networks are considered as dynamic structures, where continuously new sites are deployed, capacity extensions are made, and parameters are adapted to local conditions. In the past, MNOs have spent a lot of efforts on manually tuning site-specific HO control parameters. However, in order to reduce the degree of human intervention in network optimization processes, optimal settings, which yield an appropriate trade-off, e.g., with respect to connection drops, HO failures, and the occurrence of ping-pong HOs, have to be identified and enforced autonomously.

For developing a future-proof network and mobility management solution that is flexible, extensible, scalable, and able to autonomously adapt to local conditions, the context-enhanced HAM concept introduced in Chapter 5 has to be complemented by SON modules that are capable of performing self-optimization and -healing, as envisioned by the NGMN alliance [Nex07c]. Therefore, the author developed a self-learning scheme that is able

to autonomously adapt HO parameter settings according to locally observed conditions and to address arising issues in heterogeneous networks due to user mobility and changes in network configuration and deployment. This approach is presented in detail in Subsection 7.3.2.

In the literature, analytical approaches for modeling and analyzing HO processes and their performance exist [VH93], [KH94], [ZH96], [ZH98]. However, these approaches apply stochastic models and assume that relative signal levels, shadowing influences, as well as HO entering and leaving conditions can be modeled as random processes. For example, signal level differences of potential HO target cells are modeled as stationary or non-stationary, shadowing as Gaussian, and HO entering and leaving conditions as Poisson processes. Further, only user motion from one Base Station (BS) to another and thus signal level differences of only two possible transmitters are considered. Thus, HO probabilities can be analyzed and the averaging interval and hysteresis level that yield optimum trade-off between the number of unnecessary HOs and the delay in handing over terminals from one cell to another can be determined.

However, the development of a complete analytical model for HO processes and their impact on E2E performance in heterogeneous networks given real-world propagation environment and user mobility is extremely difficult due to inherent complexity. For example, HO process triggering depends on a sequence of recent signal level values, which are related to user movements, and E2E performance is affected by induced signaling and processing delays as well as spatially and time-varying receive signal levels. Moreover, correlations, in particular time-dependent mutual dependencies, between input parameters are not available a priori for any constellation of deployment, network, and user mobility. These characteristics may result in NP-hard problems that are to be solved per time instance. Further, neither user movements, nor receive signal levels, nor traffic demands are exactly known in advance and can only be estimated. Thus, continuous monitoring of RAN-specific and, in particular, mobility related Key Performance Indicators (KPIs) is inevitable.

In order to create awareness of the radio access situation of a considered service area, the author developed heuristic and self-learning based approaches. For example, HO parameters are tuned between several cells in a cell pair-specific manner reflecting direction and impact of local user mobility. Further, the developed approaches rely on a limited set of input parameters and do not require measurements performed and provided by User Equipments (UEs) for optimizing network performance. The designed schemes are

presented in subsections of Section 7.3 and evaluated by means of system level simulations in Chapter 8. They aim at relieving MNOs from the burden of manual network configuration and optimization by introducing self-learning and self-tuning capabilities. Furthermore, the introduction of self-tuning capabilities has not only the potential to significantly reduce OPEX but also to self-adapt HO parameter settings according to locally observed conditions, thus establishing context awareness.

7.1 SON Architecture

Today's RANs expose a high complexity and a large number of parameters that may be tuned to yield capacity and performance gains. However, for efficient network tuning and optimization, this large amount of parameters needs to be reduced and mapped onto several KPIs. Since many network operators provide services via heterogeneous RATs, joint network management and optimization becomes even more complex. The focus of this thesis is on a major use case defined by the NGMN alliance [Nex07a]: *Handover (HO) parameter optimization*, which will be further detailed in the following sections. Moreover, in the context of 3GPP standardization, two specific SON use cases, referred to as Mobility Robustness Optimization (MRO) and Mobility Load Balancing (MLB) [3GP11a], are defined that consider the automatic configuration and adaptation of HO parameters, e.g., for reducing the number of HO-related radio link failures or unnecessary HOs.

The system architecture envisioned by the author is depicted in Figure 7.1. It comprises SON entities at all relevant Network Elements (NEs), where their functionalities may range from measurement collection, situation and performance assessment, decision making, to adaptation execution. Decision making and adaptations are executed in a *hybrid* manner depending on the respective RAN sub-system architecture. For instance, in E-UTRAN, SON operations are executed locally at Evolved Node B (eNB) level, where eNBs collaborate via X2 interface for exchanging control information and coordinating SON adaptations. In contrast, Node Bs (NBs) and Base Transceiver Stations (BTSs) in UTRAN depend on Radio Network Controller (RNC) and Base Station Switching Center (BSC) entities, respectively, with regard to mobility management and link adaptation issues, since they host major functionalities, such as Radio Link Control (RLC) and HO decision making.

In principle, there are different architectural concepts for implementing

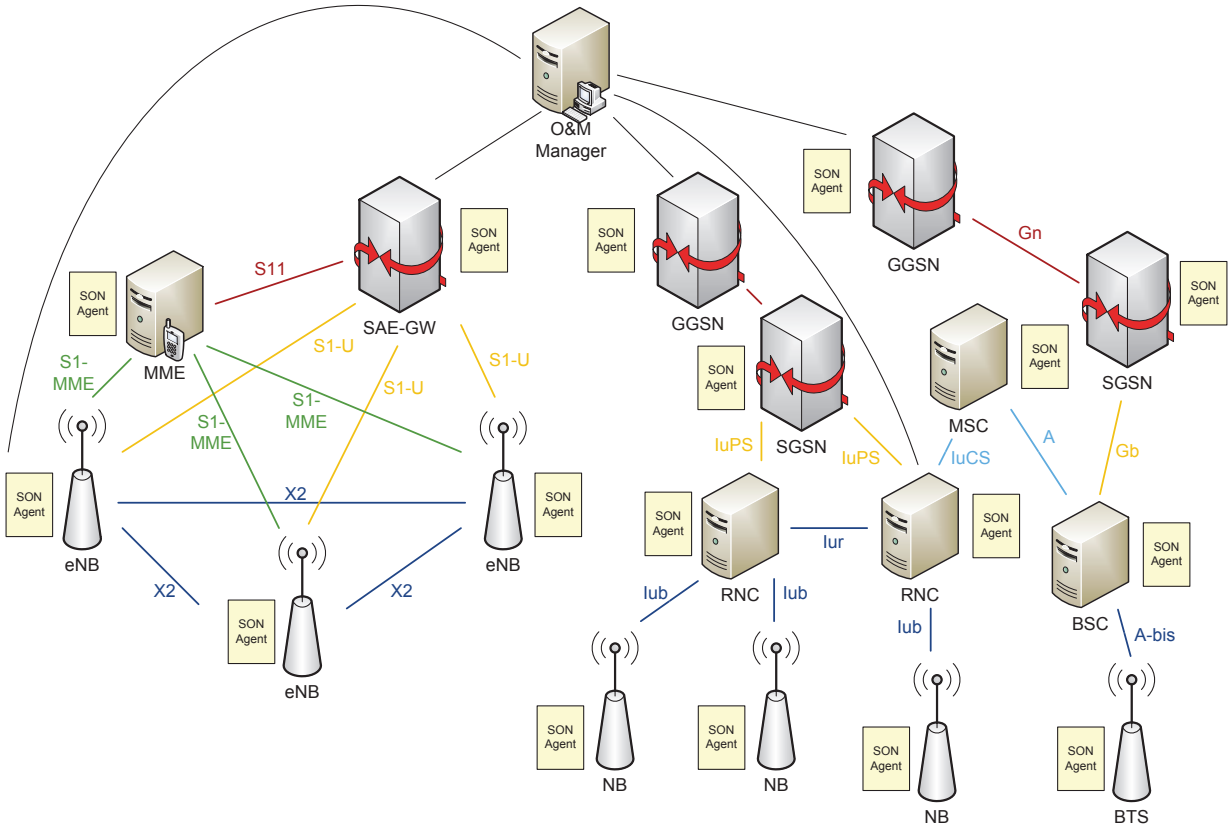

Figure 7.1: SON multi-RAN architecture

SON solutions: *centralized*, *distributed*, and *hybrid* [Leh06], [FS08], [Noh14]. All of these approaches have their advantages and disadvantages and usually a trade-off has to be found with respect to major features, such as complexity, real-time capabilities, information exchange and signaling, as well as scalability. Table 7.1 summarizes advantages and disadvantages of the respective architectural SON concepts as stated in [RH11].

Table 7.1: Advantages and disadvantages of architectural SON concepts [RH11]

Concepts	Advantages	Disadvantages
Centralized	• Global view: decision making entity is located in O&M system and has access to all kinds of performance indicators, e.g., originating from CM, PM, and other enterprise data sources, such as planning databases. • Capabilities and flexibility to support sophisticated optimization strategies, in particular enabling multi-RAN optimization. • Flexibility in modifying optimization strategy and algorithms. • Deployment and upgrading are easy, since the SON functionalities reside in a small number of locations. • Optimization strategies across multi-vendor networks can be aligned. • SON functionalities can be decoupled from network infrastructure and thus enabling integration of third-party SON solutions.	• Large bandwidth and large data exchange is required for information acquisition. • Responsiveness is limited due to delays for information acquisition and execution of adaptations. • Single point of failure that can only be mitigated by redundancy and fallback mechanisms.

Continued on next page

Table 7.1 – continued from previous page

Concepts	Advantages	Disadvantages
Distributed	• Decision making is accomplished at independent NEs. • Real-time actions (e.g., link adaptations) and optimization are executed locally (eNBs). • No large bandwidth or data exchange is required. Information exchange takes place only between direct neighbors. • No single point of failure, i.e., failure resilience.	• Optimization is typically local and involves only few NEs. • Information exchange is limited to neighboring nodes, if no implicit coordination is considered. • Modification of optimization strategy and algorithms as well as coordination of SON functions that reside on different NEs is difficult. Increased coordination efforts between NEs may be required.
Hybrid	• Mixture of both concepts that allows for sophisticated optimization strategies using a centralized decision making entity and that at the same time performs local, real-time adaptations, if required.	• Complex coordination between centralized and distributed SON functionalities is required, which can be mitigated by splitting responsibilities between these two sets of SON functionalities.

From the author's point of view, the hybrid concept provides the largest degrees of freedom for designing SON functionalities, since it allows for developing use case-specific coordination and optimization strategies that may or may not require the involvement of different hierarchy levels. Hierarchy levels of a hybrid SON concept, as proposed by the author, comprise *management*, *coordination*, and *execution* layers and are depicted in Figure 7.2, where the Operation & Maintenance (O&M) entity is the final authority for deciding on SON adaptations (e.g., conflict resolution between SON entities). Only if issues between different SON mechanisms cannot be resolved locally, they are escalated to coordination level for conflict resolution and decision making.

For realizing this concept, the following interfaces are required:

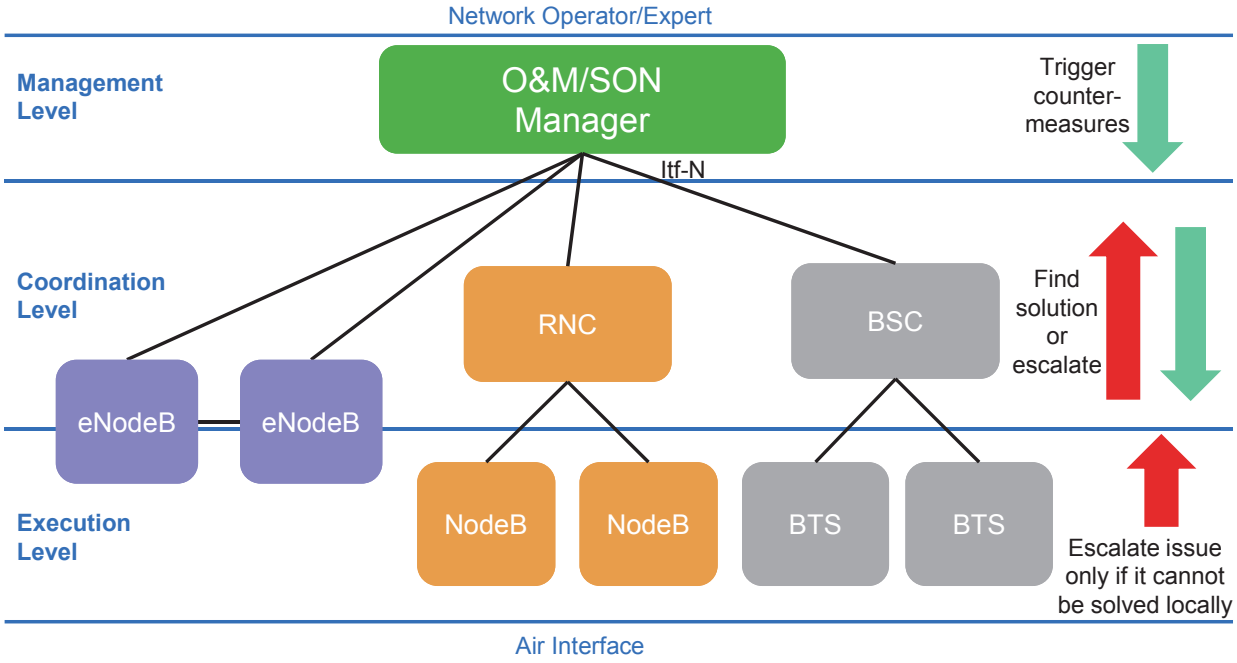

Figure 7.2: Hierarchy levels of hybrid SON concept

- On execution level, interfaces toward UE are required to acquire knowledge on receive situation and terminal context, e.g., UE history and capabilities.
- On coordination level, entities of the UTRAN, such as RNCs, will rely on *Iur* interface, while E-UTRAN components will exploit X2 interface for coordination of eNB collaboration and exchange of use case-specific control information. Further, proprietary interfaces may be used for coordinating SON activities among network nodes, e.g., between eNB and RNC.
- The management level will employ the *Northbound Interface* (Itf-N) for management purposes (e.g., MNO policy enforcements) and SON manager signaling.

Required signaling will either reuse existing interfaces or may employ proprietary *over-the-top* signaling (e.g., RESTful [Tya06]) to achieve its purpose. Further, it might be necessary to add proprietary signaling for exchanging network parameters or terminal-related information that has not been standardized yet. In general, a SON requires implementing various control loop operations on system as well as on NE level. The typical process flow of a SON control loop, as illustrated in Figure 7.3, comprises the phases: acquisition and monitoring of measurement data, evaluation of KPIs and of effectiveness of triggered actions, and execution of system adaptations.

In complex systems, it is usually essential to consider a multitude of parameters for detecting and identifying system failures and performance degra-

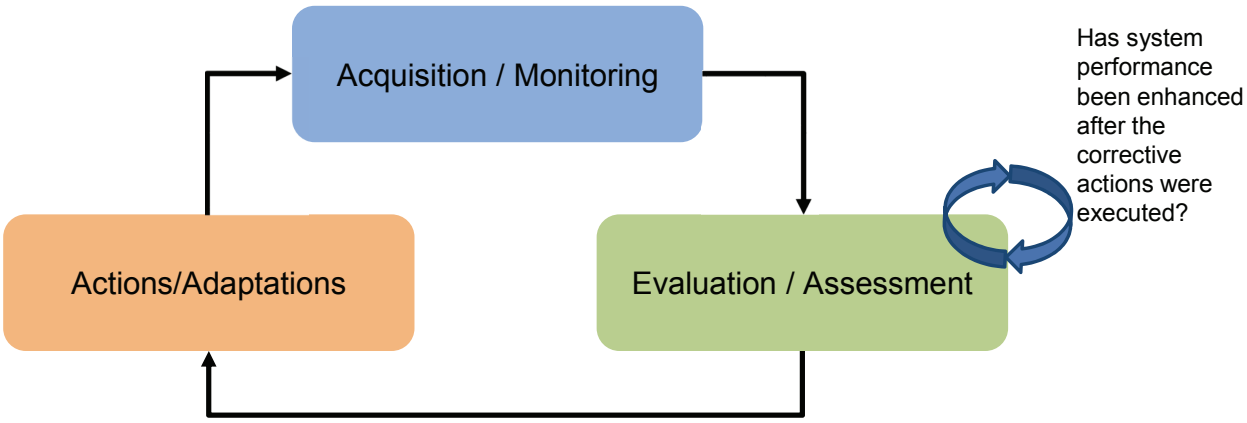

Figure 7.3: SON control loop

dations. Data acquired by the various NEs is processed and more abstract information is derived that allows for situation assessments. The first processing step involves filtering and identification of characteristic parameters that are to be retrieved from the set of available network parameters or measurements. For some cases, it might be beneficial to aggregate similar parameters of several NEs that are averaged over time, for instance, for providing more reliable situation assessments. Then, the relevant parameters are merged via *fusion*, i.e., use case-specific parameters are identified and combined, e.g., using Boolean algebra. The respective situation is analyzed and, based on its severity, countermeasures are triggered or event reports are generated and escalated to the next hierarchy level, if no "local" solution could be found. In the following, main processing steps are listed:

- *Acquisition* and filtering of measurements and update of KPIs
- Parameter fusion and *situation assessment*: classification and prioritization of events, exploitation of available history information, feeding of learning engine, rating of information quality
- Triggering of *adaptations*: application of policy-based or learned countermeasures
- Assessment of adaptation *effectiveness*: assessment of degree of objective achievement, estimation of adaptation/strategy effectiveness, accounting for adaptation costs

In order to detect unwanted system behavior or failures, these situations are usually defined via *if-then* rules [PY98], where the premise parts include defined intervals or ranges in which the values of the considered parameters are to be found so that the consequents are activated. Hard thresholds for the respective intervals may be replaced or softened by degrees of membership

in case fuzzy logic is applied for event detection, reducing the impact of measurement inaccuracies or hardware tolerances.

7.2 Recent SON Approaches

The main objective of SON approaches is to enable system processes, such as network management and optimization mechanisms, to operate autonomously without human intervention. In 2007, the NGMN alliance, representing world-leading MNOs, released SON use cases [Nex07c] and recommendations on SON requirements [Nex08]. The NGMN alliance [Nex07c] states that network optimization is a closed loop process of parameter deployment, performance evaluation, parameter optimization, and re-deployment of optimized parameters to the network. Mobile networks are considered as dynamic structures, where continuously new sites are deployed, capacity extensions are made, and parameters are adapted to local conditions.

The importance of this topic has also been recognized by the standardization bodies 3GPP and IEEE that started discussing and specifying self-organization and -optimization functionalities. For instance, 3GPP incorporates self-organization capabilities, such as Automatic Neighbor Relation (ANR), in its specifications since LTE release 8 [3rd10]. In IEEE's 802.16 working group, Bogenfeld et al. [BGRE06] initiated a discussion on SON and pointed out that some standardization efforts would be necessary to ensure information exchange and agreed on required interfaces, primitives, specific measurements or value formats, since deployments of telecom networks lack support of tools and procedures to install and setup network entities with minimum operational efforts.

SONs have also been studied in the scope of various European funded projects. In the framework of the FP6 EUREKA/CELTIC Gandalf project [SAD+05], techniques for collecting and processing network data on a large scale in order to generate KPIs allowing to identify malfunctions and to dynamically propose and perform healing actions have been developed. In order to optimize the user-perceived QoS and overall system performance, the project proposed new RRM algorithms together with methods for self-tuning. In particular, approaches for auto-tuning inter-RAT HO parameters were designed and evaluated [LRRTFN08], [LRTRFN08].

The FP6 project AROMA (Advanced Resource Management Solutions for Future All IP Heterogeneous Mobile Radio Environments) investigated RRM strategies and algorithms for both the access and core network that

guarantee the E2E QoS in the context of an all-IP heterogeneous network. Evaluations of the proposed strategies and some initial automated tuning mechanisms for RRM parameters in the UTRAN are, for instance, given in [BCC+06].

The EU FP6 project ANA (Autonomic Network Architecture) aimed at designing and developing a novel autonomic network architecture that enables flexible, dynamic, and fully autonomous formation of network nodes as well as whole networks. In [SZN+07], Schuetz et al. present a generic and autonomic management architecture for decentralized management of wireless access networks. Further, they provide a quantitative analysis of management functions through simulation and a feasibility study of the proposed management system through prototype implementation and experimentation.

In the FP6 project CASCADAS (Component-ware for Autonomic Situation-aware Communications and Dynamically Adaptable Services), a concept for an autonomic component based framework that allows for composition, execution, and deployment of innovative services and that is capable of coping with unpredictable environments by dynamically self-adapting to situation evolutions has been developed. A reference architecture for knowledge networks and a prototype implementation thereof is presented in [BBK+07].

The FP7 E3 (End-to-End Efficiency) project aimed at integrating cognitive wireless systems in the Beyond 3G (B3G) world, evolving current and future heterogeneous wireless system infrastructures into an integrated, scalable, and efficiently managed B3G cognitive system framework from a technical, regulatory, standardization, and business perspective. The work on collaborative cognitive RRM, Dynamic Spectrum Management (DSM), and SONs includes a complete cycle from requirements, engineering, conceptions, modeling, simulation, and evaluation to verification of the approaches and algorithms. The outcome provides solution for optimizing the use of spectrum and radio resources by means of cognitive network and terminal mechanisms and collaborative decision-making between network elements and user terminals. Moreover, the work aimed at functionalities for being able to deploy and to provide JRRM/DSM/SON services in single- and multi-operator domains as well as in single and multiple RATs [BVHA+10].

In the FP7 SOCRATES (Self-Optimization and self-ConfiguRATion in wirelEss networkS) project, the focus was on the development of self-organization and -optimization methods for LTE radio networks. In addition to the algorithms required for SON functionality, measurements, architecture, and interfaces were also considered. Further, requirements and specification of basic SON use cases, such as handover optimization, load balancing, admission

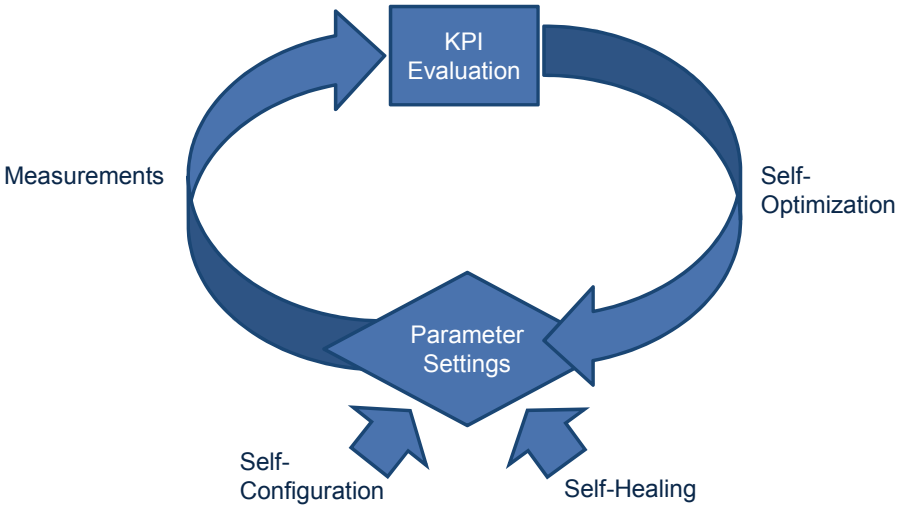

Figure 7.4: Self-organization in future radio access networks [vdBLE+08]

control, coverage, etc., have been defined. Figure 7.4 illustrates the project's envisioned self-X cycle for SONs [vdBLE+08].

Furthermore, SOCRATES [SOC10a] developed a high-level functional approach for the coordination of SON use cases by introducing a set of interacting functional roles. These functional roles, referred to as *SON coordinator functions*, and the SON functions together form the SON system. The *policy function* converts the operator's high-level performance objectives into SON function specific policies and into policies for the other functions of the SON coordinator. These policies are required to define the functioning of SON, i.e., how a SON (coordinator) function acts on incoming measurements and triggers, and for a certain network status. Therefore, the policy function provides the interface between operator and the SON system, which also includes defining the feedback from SON (coordinator) functions toward the operator. The *alignment function* is responsible for detecting and resolving conflicting configuration change requests coming from SON functions, and for taking counteractions in case of undesirable behavior of the SON system. The *autognostics function* collects and processes performance, fault, and configuration data coming from the entities of the network subsystem (for example, NEs and UE, or fault / performance management functions of O&M) as input to the SON functions and functions of the SON coordinator. The instructions on which data is to be acquired and how this data is to be processed comes from the SON functions and the *guard function*. The guard function is in charge of detecting extreme or undesirable network behavior by analyzing data coming from the autognostics function, and triggers the alignment function to take countermeasures. Further, the autognostics, guard, and alignment functions provide feedback toward the operator on their functioning. Figure 7.5

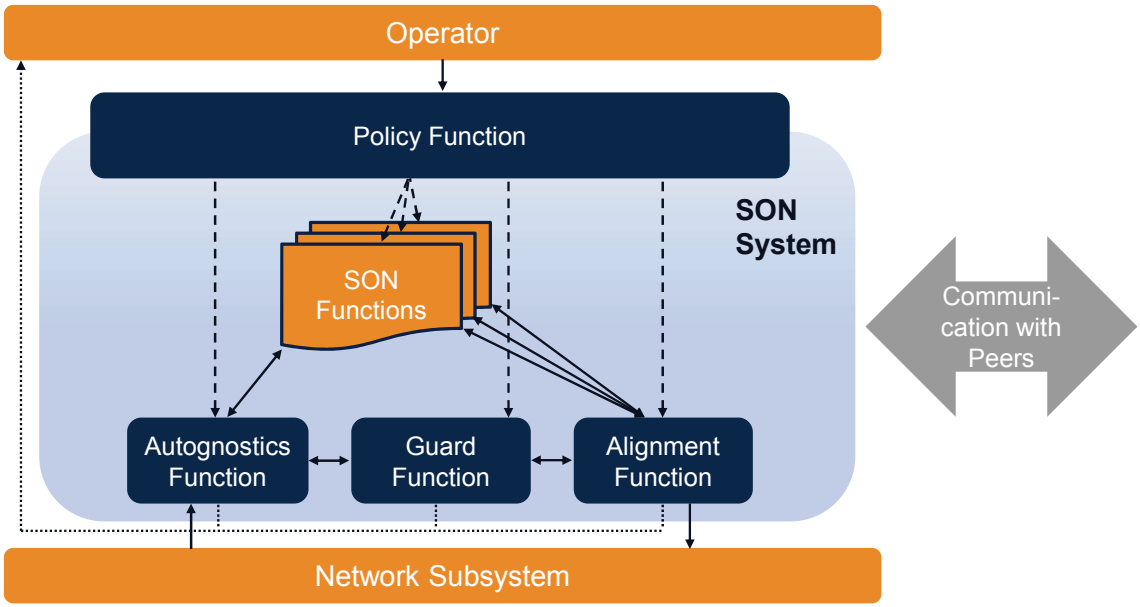

Figure 7.5: SOCRATES SON coordinator functional framework [SOC10a]

shows a simplified functional architecture of the developed SON coordinator framework with its functions.

An overview of initial works on self-optimization solutions, including tuning of parameters related to admission control, power control, handover control and coverage, as well as challenges in future wireless networks, which arise due to the systems' complexity and multitude of parameters and mechanisms with intrinsic dependencies, is given by d'Orey in [d'O10]. As far as the optimization method is concerned, several presented approaches are rule based ones. A rule based method is defined by a set of rules, i.e., a set of IF-THEN clauses, that is built with expert knowledge on the network functioning, e.g., refer to [HVHL02], [HV02], and [HPVL03]. Further, d'Orey states a functional model that is required to support self-optimization algorithms and that is constituted by three main blocks: *monitoring*, *learning and memory*, and *control* [d'O10].

More LTE-related work on self-optimization can be found in the following publications. In [AR10], a self-optimizing algorithm for HO parameter control is presented that iteratively adjusts the parameter settings of Time-To-Trigger (TTT) and Handover Margin (HOM), which in general consists of Hysteresis (HYS) and Cell Individual Offset (CIO) values, depending on the oscillations experienced between different cell pairs. Diaz et al. [DDS+10] study the sensitivity of the optimal parameter setting for packet scheduling in LTE radio networks with respect to various traffic and environment aspects. Although, in some cases, significant efficiency gains can be achieved by proper tuning of the scheduling parameters, the authors' conclusion is that

a single, robust setting of the parameters can be determined which provides near optimal trade-offs under almost all practically relevant conditions. In [LSJB10], system-level simulation results of a self-optimizing load balancing algorithm in a LTE mobile communication system are presented. Further, the authors evaluate the network performance of the proposed algorithm that requires the cell load as input and controls the handover parameters for different simulation setups with respect to deployment and realistic traffic assumptions.

A first trend based HO optimization algorithm, further referred to as *TBHOA*, is presented by Jansen et al. [JBT+10]. Here, the MNO defines a set of major KPIs, such as dropping, HO failure, and ping-pong HO ratios, respectively, and assigns certain weights per KPI that reflect the importance of these KPIs with respect to the MNO's policy. The *TBHOA* is evaluated in a realistic, urban scenario with an irregular LTE deployment. In order to investigate the interdependency of the specified KPIs, also referred to as *HO performance indicators* (HPIs), they are aggregated using a weighted sum. Whenever a specific HPI is found to be below the MNO-defined performance target threshold for a predefined amount of time, denoted as *bad performance time*, the *TBHOA* tries to optimize system performance by executing actions given by a Look-Up Table (LUT). The LUT is organized in value ranges of HYS and TTT parameters and comprises for each sub-range of HYS and TTT values a corresponding adaptation, e.g., increase TTT or decrease HYS. These adaptations have been derived from a variety of system simulation results and have shown to improve system performance given the respective HYS and TTT settings.

In [LHJ10], LTE intra-frequency HOs are investigated. Major findings are that reliability is dictated by the incidence of too late HOs, which may be reduced by timing the HO earlier, but at the cost of an increased HO frequency. Of particular concern are the handovers of fast moving UEs, since these suffer from higher failure rates and higher HO rates than slow moving UEs. It is proposed that HO timing may be adjusted via the HOM, TTT, or the layer 3 Reference Signal Received Power (RSRP) filter K value, or some combination thereof. The analysis performed by Wei [Wei10] points at the same direction. Here, UE speed-dependent assignments of HYS settings are proposed that yield improved HO success rates and enhanced user experience.

Liu et al. [LHXP10] focus on the coordination issue of HO parameter adaptations triggered by MRO and Mobility Load Balancing (MLB) mechanisms. They suggest to introduce an allowed range for MLB operation depending on respective HYS and CIO values of considered and neighbor-

ing cells and to prevent MLB from adjusting HO parameters, if this may result in HO problems, such as increased call blocking and dropping rates. In [AWR+11], inter-RAT mobility and related KPIs have been studied in a multi-RAT deployment scenario with full 3G but limited LTE coverage. Major findings are that an inter-RAT MRO algorithm should work locally in a cell-pair manner, since each cell-pair underlies different traffic and mobility conditions, and thus, requires different parameter adjustments.

The authors of [SPRSG+11] present a SON optimization framework, where optimization is formulated in the form of hypotheses tests against the suboptimal operation for a number of established performance targets. The hypotheses are reinforced by likelihood and reliability indices, so that the number and relevance of diverse KPIs with respect to the considered target can be weighted. Further, their algorithm has shown to automatically identify a cell with suboptimal coverage and provided a solution for optimizing its operation.

The distributed HO optimization procedure presented in [EB11] combines target and source cell information, such as Radio Link Failure (RLF) indication messages, detected ping-pong HOs, too early HO, and HO to wrong cell reports into KPIs indicating too late or too early HOs. Then, it is determined, based on a weighting applied to these KPIs, whether the values for A3-Offset, TTT, or Ocn (CIO for considered neighbor cell [3GP12a]) are modified toward an earlier or later trigger for HO to the neighbor cells.

Kitagawa et al. [KKYK11] proposed a HO parameter optimization algorithm that detects the change in UE mobility through the change in HO failure events and adaptively adjusts the HOM to the UE mobility. They demonstrated by means of system-level simulations that the algorithm effectively reduces both the HO failure and ping-pong HO rates, while the trade-off between the two rates taken into consideration in several mobility scenarios changes.

Inspired by the work in [JBT+10], Carvalho and Vieira [CV11] developed an optimization algorithm that automatically adapts the HYS and TTT parameters based on a HPI that measures the HO oscillation rate and accounts for user speed and type of traffic. The achieved results show a ping-pong HPI reduction of 20% to 30% when compared to a fixed HYS and TTT parameter setting.

Viering et al. [VWL+11] studied network-wide, cell-specific, and cell pair-specific optimization approaches for intra-frequency MRO. Further, they presented heuristic solutions for adapting HYS values, where the number of RLFs and ping-pong HOs is incorporated via cost functions and significant

gains can be achieved the more location-specific the parameters are defined.

In [LZJ+12], a dynamic MaxPRB-adjusting scheduling scheme is proposed that adjusts the maximum PRB number according to user Signal-to-Interference-plus-Noise Ratio (SINR) dispersion degree of the sector to obtain a good balance between sector throughput and user fairness.

To reduce the number of HO failures, the authors of [KYK12] introduce a cell selection scheme to enhance the performance of HO optimization using uplink and downlink channel quality, where CIO parameters are adapted taking the occurrence of different HO failure events, such as too late, too early HOs, wrong cell, and ping-pong HOs, into account.

In [HL12], Hui and Legg argue that many MRO schemes require a large number of HOs per cell pair before they become active and start improving HO performance, resulting in a slow adaptation to changes. Therefore, they present a MRO algorithm that incorporates soft metrics, such as HO command transmission time, derived both from failed and successful HOs, and that provides a faster reaction, e.g., to varying network load, and lower failure rate than a conventional method with no deterioration in the HO count.

Bergman et al. [BMG12] propose a HO oscillation control mechanism for LTE that adjusts parameters per UE to address the UE-specific oscillatory behavior and mobility pattern. Evaluation in a field trial and results from real networks show that UE level HO oscillation control can reduce the number of HOs in situations when HO oscillation would otherwise occur, and that a relatively small extra offset (1 to 3 dB) would significantly reduce the number of the least beneficial HOs.

In [AWVK12], the difference between optimizing a single inter-RAT HO threshold in a cell-specific and cell pair-specific manner is analyzed. Further, three new alternative configuration paradigms for the inter-RAT HO thresholds along with those considered by 3GPP are evaluated. Simulation results have shown that all the three configuration paradigms outperform those followed by 3GPP, in particular, one scheme that configures the second threshold of measurement event B2 [3GP12a] in a cell pair-specific manner.

Recently, the authors of [RFL+13] exploited vehicle context information, such as position and movement trajectory, to adaptively optimize street layout-specific HO parameters. In contrast to the majority of the afore mentioned approaches, the FQL based approach presented in Section 7.3.2 allows for autonomously adapting HO parameters to local, cell sector- and cell pair-specific conditions, while simultaneously accounting for several KPIs, such as dropping, HO failure, and ping-pong HO ratios.

7.3 Optimizing the Robustness of Mobility Support

In a heterogeneous radio access environment, the task of enabling robust and optimized mobility support across different RATs is quite challenging. HAM that is in charge of controlling and triggering intra- or inter-technology HOs needs to be aware of the radio access situation of a considered service area and upcoming issues, preferably before they materialize. However, usually neither user movements nor traffic demands are exactly known in advance and can only be estimated. Thus, continuous monitoring of RAN-specific and, in particular, mobility-related KPIs is inevitable. In addition, measurement data and long-term KPI statistics can form a context history and be used for predicting trends with respect to important KPIs.

The optimal configuration of HO control parameters in order to find an appropriate trade-off between connection drops, HO failures, and the occurrence of ping-pong HOs is one example where MNOs today spend a lot of efforts on manually tuning these control parameters per service area. Reconfigurations are usually triggered upon detection of HO problems or upon integration of new BSs into the network. The concept presented in Subsection 7.3.2 aims at relieving MNOs from the burden of manual network configuration and optimization by introducing self-learning and self-tuning capabilities. Further, the introduction of self-tuning capabilities has not only the potential to significantly reduce OPEX, but also to self-adapt HO parameter settings according to locally observed conditions, and thus establishing context awareness.

7.3.1 Key Performance Indicators

For assessing HO performance and optimizing mobility support, several handover KPIs, also referred to as HPIs, such as *connection dropping ratio* (CDR), *HO failure ratio* (HFR), and *ping-pong HO ratio* (PHR), are evaluated. The CDR is denoted by ρ_{CDR} and is defined as follows:

$$\rho_{\mathrm{CDR}} = \frac{N_{\mathrm{dropped}}}{N_{\mathrm{accepted}}}, \tag{7.1}$$

where N_{dropped} denotes the number of dropped connections due to RLF or session timeout and N_{accepted} the overall number of accepted connections during observation time window T, respectively. N_{accepted} includes persisting,

newly accepted, and handed over connections. The HFR, denoted by ρ_{HFR}, is calculated as:

$$\rho_{\text{HFR}} = \frac{N_{\text{HO\_fail}}}{N_{\text{HO\_fail}} + N_{\text{HO\_success}}}, \tag{7.2}$$

where $N_{\text{HO\_fail}}$ and $N_{\text{HO\_success}}$ denote the number of failed and successful HO attempts, respectively, and altogether yield the overall number of HOs that occurred during the observation time window $\boldsymbol{T}$.

Further, *ping-pong* HO events are recorded at the respective source BS. A ping-pong HO event is characterized by its source BS and an intermediate HO target BS to which the UE is temporarily connected before it is handed back to the source BS. The PHR, denoted by ρ_{PHR}, is determined as follows:

$$\rho_{\text{PHR}} = \frac{N_{\text{HO\_ping-pong}}}{N_{\text{HO\_success}}}. \tag{7.3}$$

ρ_{PHR} represents the proportion of monitored ping-pong HOs $N_{\text{HO\_ping-pong}}$ with respect to the number of successful HOs $N_{\text{HO\_success}}$. These KPIs are calculated using a *moving average filter* with time span $\boldsymbol{T}$ that equals the observation time window. Besides these major KPIs, 3GPP assigns the following use case-specific objectives [3GP11a]:

- detect and minimize occurrences of *too late HOs*,
- detect and minimize occurrences of *too early HOs*,
- detect and minimize occurrences of HO to a *wrong cell*,
- reduce inefficient use of network resources due to unnecessary HOs (e.g., ping-pong HOs),
- reduce unwanted HOs subsequent to connection setup.

SON functionalities must be able to detect too early, too late, and wrong cell HO events for optimizing mobility robustness. Therefore, they have to identify the following event sequences, shown in Figure 7.6, that indicate whether a too early, too late, or wrong cell HO occurred, e.g., by analyzing terminal and network reports.

7.3.2 Concepts and Algorithms

Major challenges to network and HO management entities originate from user mobility and the involved changes of users' receive conditions, e.g., due to shadowing or fast fading. Therefore, HO management strategies aim at minimizing risks of user call drops and enabling seamless mobility. However, it is crucial to explicitly model user mobility and delays in triggering HO processes

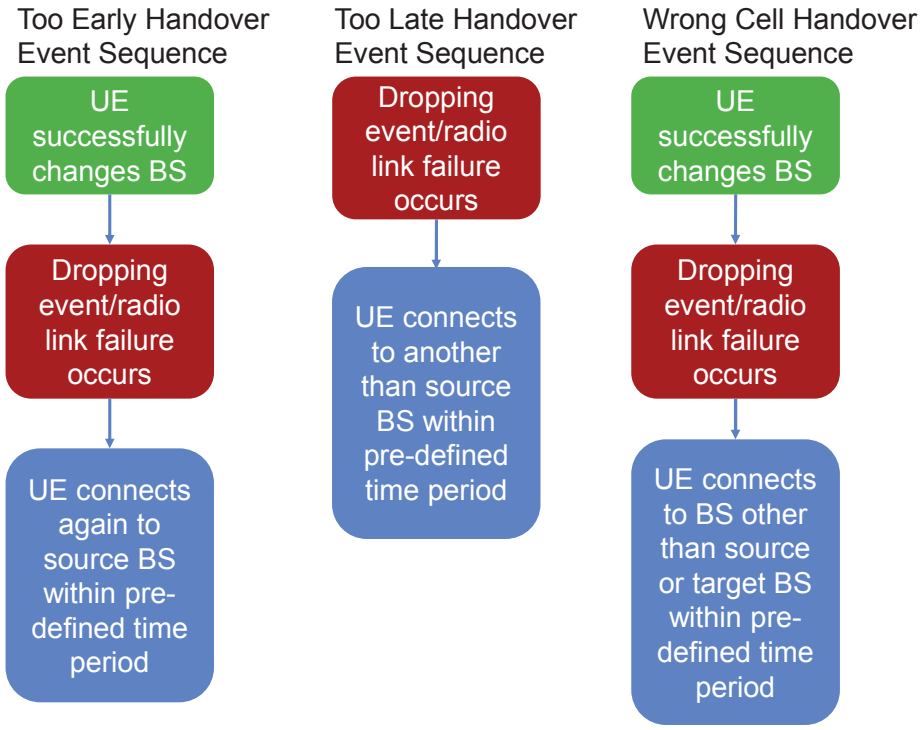

Figure 7.6: Too early, too late, and wrong cell HO event sequences

for evaluating the efficiency of HO optimization strategies in detail, since received signal strength variations may occur on rather small time and spatial scales. Besides the variety of user velocities and environment conditions, the number of deployed RATs and their resulting cell sizes require adaptations to take place on a per-site, per-cell-pair, or per-cell-cluster basis in order to reflect local circumstances. This motivates the design of HO optimization algorithms as distributed solutions that are executed locally.

The fuzzy logic based MRO approaches presented in the following sections were inspired by two HO optimization strategies, *TBHOA* and *SBHOA*, introduced in [JBT+10], where *TBHOA* stands for "trend based" and *SBHOA* for "HPI sum based" HO optimization algorithm, respectively. All approaches have in common that they try to anticipate trends in KPI evolutions and apply corresponding countermeasures, where primarily HYS and TTT settings are adjusted.

The adaptation steps of HYS and TTT values follow 3GPP specifications. Hysteresis values range from 0 to 10 dB, where adaptations occur in steps of +/-0.5 dB. According to 3GPP [LSJB10], the following TTT values are specified: 0, 0.04, 0.064, 0.08, 0.1, 0.128, 0.16, 0.256, 0.32, 0.48, 0.512, 0.64, 1.024, 1.280, 2.560, and 5.120 seconds. However, due to the simulation tool's time basis being 10 ms (cf. Section 2.8), only multiples of 10 ms can be chosen as TTT value.

MRO Benchmark Schemes

For evaluating the performance of the developed fuzzy logic and Q-learning based MRO scheme, a reference scheme with fix HO parameter settings (*REF*) and two MRO schemes emanating from EU FP7 project SOCRATES, referred to as *TBHOA* and *SBHOA* [JBT+10][SOC10b], have been implemented. Their characteristics are first depicted in the following paragraphs, since they laid the foundation for integrating fuzzy logic based classification with trend based HO parameter optimization.

SOCRATES' trend based HO algorithm (*TBHOA*) employs so-called "good" and "bad" performance timers with respect to HO KPIs to assess system performance. If specified KPI target thresholds are exceeded for a given amount of time, referred to as "bad performance" time, HO parameter settings are automatically adapted according to predefined rules. Table 7.2 lists appropriate HO parameter adaptations for specified HYS and TTT value ranges that may be identified by simulating all possible HO parameter constellations for a considered scenario or via receive level statistics (e.g., CDF) of the evaluated cell area.

Table 7.2. Trend based HO optimization criteria [SOC10b]

HPI	HYS (dB)	TTT (s)	Optimization
Handover Failure Ratio	< 5		TTT↑
	$5-7$		TTT↑ & HYS↑
	> 7		HYS↑
Ping-Pong Handover Ratio	< 2.5		TTT↑
	$2.5-5.5$		TTT↑ & HYS↑
	> 5.5		HYS↑
Dropping Ratio	> 6	> 0.6	TTT↓ & HYS↓
	≤ 6	> 0.6	TTT↓
	> 6.5	≤ 0.6	TTT↓ & HYS↓
	$3.5-6.5$	≤ 0.6	HYS↑
	< 3.5	≤ 0.6	TTT↑ & HYS↑

The optimization criteria are derived from system simulation results of all considered Handover Operating Points (HOPs), i.e., combinations of HYS and TTT settings. The optimization direction, i.e., increase (↑) or decrease (↓) of HYS and TTT parameters, depends on the system performance of neighboring HOPs. The system performance is individually calculated for

every HO KPI. Hence, the optimization direction can be deduced from these system simulation results, for example, by gradient descent methods. Figure 7.7 illustrates exemplary simulation results that depict HPI behavior and HO performance as interpolated surface plots for every considered HOP. The HYS values as well as the TTT values are changed by one step per HO parameter optimization only. For example, if HFR and PHR exceed the target threshold and the optimization criteria recommend increasing the HYS value, the HYS value is only changed by one step in this case. Averaging of HPIs is performed by employing a moving average filter with a window length that covers 60 seconds of simulation time. In order to automatically tune HO parameters depending on current HPIs, the adaptations are carried out by each BS individually as soon as the respective criteria, as listed in Table 7.2, are satisfied.

Following the guideline that "dropping is worse than blocking", the Connection Dropping Ratio (CDR) is the first HPI to be checked for "good performance" and, if it is found necessary, appropriate actions are triggered. For adapting to the optimal possible HO performance, the HO performance target thresholds for all HPIs are set by the optimization algorithm, i.e., for the Connection Dropping Ratio (CDR), the Handover Failure Ratio (HFR), and Ping-Pong Handover Ratio (PHR). The target thresholds are decreased by 33%, if the HPIs stay below the target thresholds for a certain amount of time, referred to as the "good performance" time. The good performance time is set to 30 and the "bad performance" time to 10 seconds, respectively. If the performance of HPI CDR and one or both of the other HO KPIs is above the HPI target threshold, the HO performance target thresholds are increased by 50% again, since the optimization criteria for these HPIs are contradictory in these cases. If the simulation parameter bad performance time exceeds a given threshold, i.e., the performance of one HO KPI exceeds the HO performance target for a certain amount of time, the HOP of the cell is changed according to the criteria listed in Table 7.2. The algorithm's flow chart is illustrated in Figure 7.8.

Similarly, the other trend based HO optimization algorithm developed by SOCRATES triggers HO parameter adaptations based on the evaluation of a weighted sum of HPIs. This approach yields a single KPI that aggregates the impact of various HPIs for deciding on whether adaptations are to be executed or not. The weighted sum of HPIs, denoted by ρ_s, is determined as follows:

$$\rho_s = w_{\mathrm{CDR}}\ \rho_{\mathrm{CDR}} + w_{\mathrm{HFR}}\ \rho_{\mathrm{HFR}} + w_{\mathrm{PHR}}\ \rho_{\mathrm{PHR}}, \tag{7.4}$$

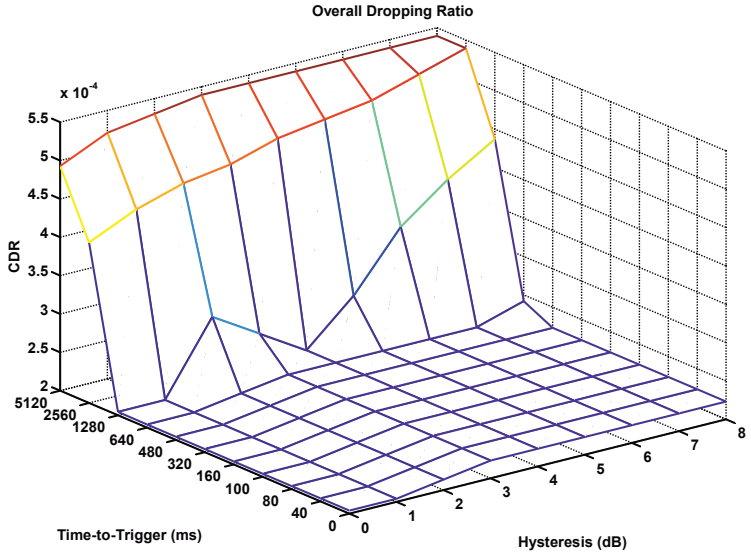

(a) Connection dropping ratio

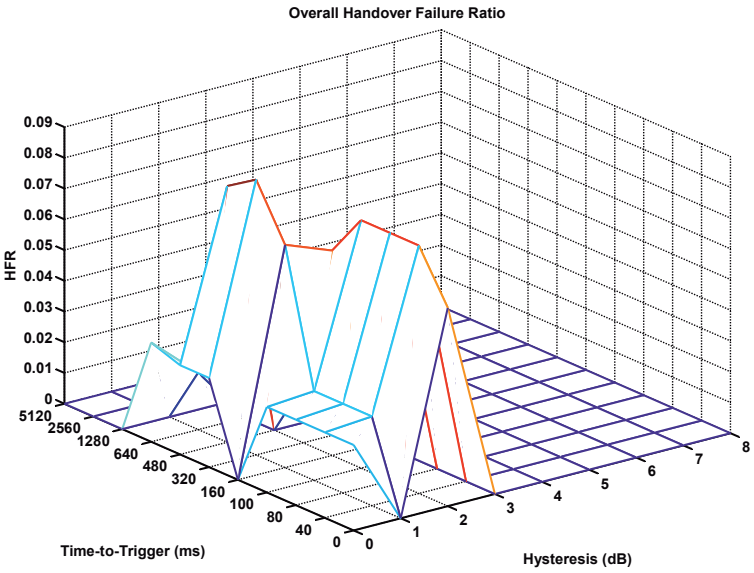

(b) HO failure ratio

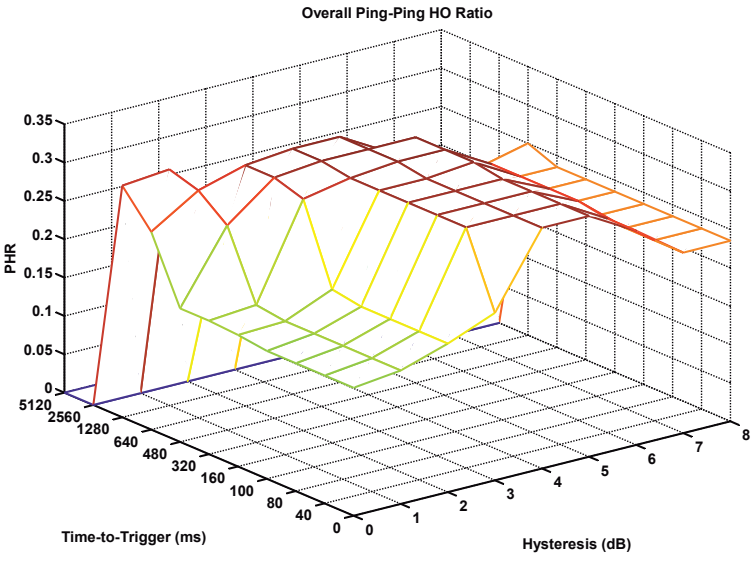

(c) Ping-pong HO ratio

Figure 7.7: Exemplary HPI results

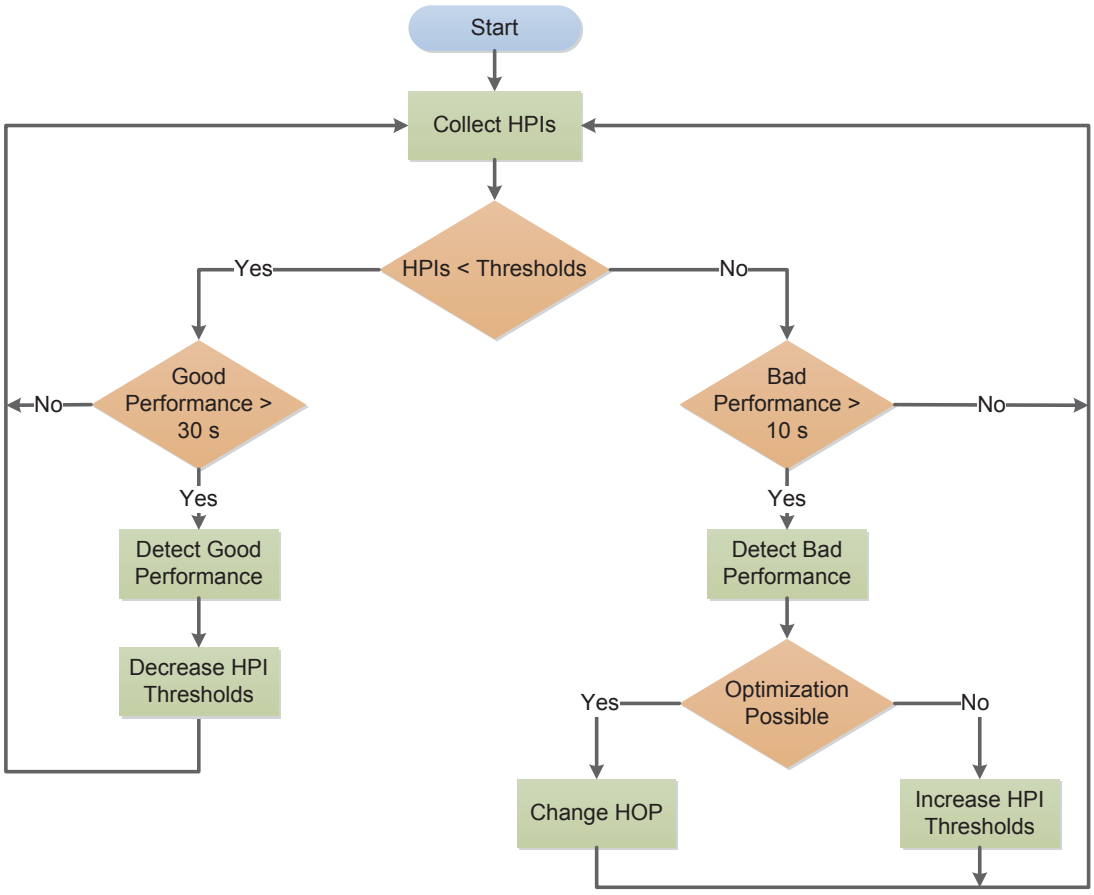

Figure 7.8: Flowchart of TBHOA algorithm [SOC10b]

where the different weights $w_{\mathrm{CDR}}, w_{\mathrm{HFR}}, w_{\mathrm{PHR}}$ are assigned to the various HPIs (CDR, HFR, PHR) according to the MNO's preferences, e.g., $w_{\mathrm{CDR}} = 2, w_{\mathrm{HFR}} = 1, w_{\mathrm{PHR}} = 0.5$ [JBT+10]. The flowchart of the HPI sum based HO optimization algorithm is depicted in Figure 7.9.

Clear drawbacks of this approach are the huge number of simulations required to evaluate ρ_s and the static nature of the derived set of favorable HO parameter adaptations. Simulation efforts are directly linked to the overall number of possible HOP configurations, which depend on HYS, CIO, and TTT parameter granularity. For example, HYS parameter settings ranging from 0 to 10 dB in steps of 0.5 dB result in 21 possibilities that would have to be multiplied with the number of selectable TTT and CIO settings, e.g., 11 and 7, respectively, thus resulting in 1617 possible HOP constellations. Further, the trend based HO optimization algorithm *TBHOA* assumes that a region of good (low) HPI performance exists. However, if such a region does not exist, the algorithm may fail and result in extreme HO parameter settings [SOC10b]. The *SBHOA* algorithm, which combines several HPI statistics for performance assessment, is said to optimize system performance even in cases where high HPIs are observed in all HOPs [SOC10b]. *SBHOA* continuously

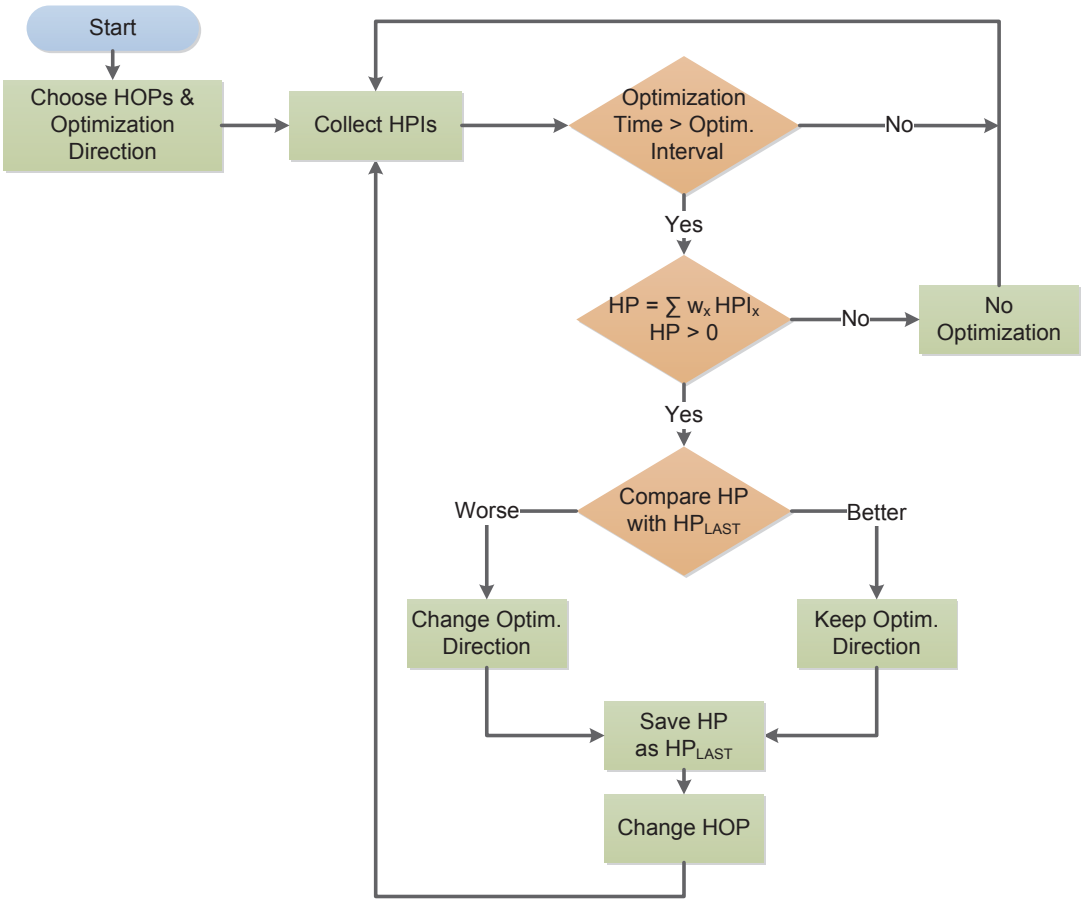

Figure 7.9: Flowchart of SBHOA algorithm [SOC10b]

changes the HOP during optimization even if the "best" performing HOP is already selected. In this case, the HOP would "ping-pong" between the "best" and neighboring HOPs, respectively [SOC10b]. Moreover, the obtained HPI performance results that are used to derive appropriate HO parameter adaptation rules for different HYS and TTT value ranges are only applicable in the considered scenario. For any change in deployment or user movements the whole process of determining HPI performance via system-level simulations has to be started again.

Exemplary HPI performance results that are used by *SBHOA* for deciding on HOP selection and that are based on Equation (7.4) are depicted in Figure 7.10.

Fuzzy Logic Based Mobility Robustness Optimization

Instead of employing fix bad/good performance timers, a more flexible approach for optimizing HO performance and related KPIs is to utilize *Fuzzy Logic* for assessing the current system performance. Therefore, so-called *membership functions* are introduced (cf. Section 6.1) to classify the sever-

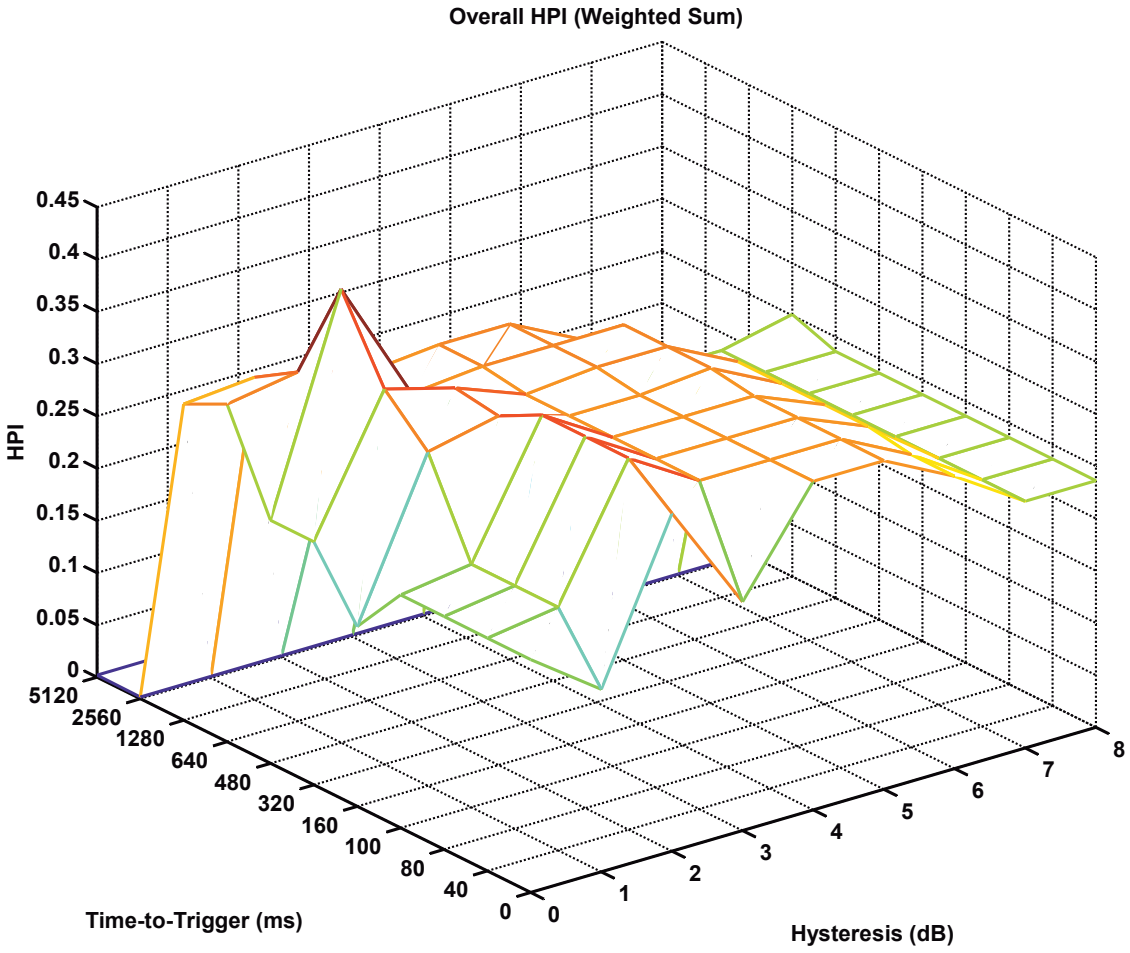

Figure 7.10: Exemplary HPI performance results

ity of KPI deviations from desired performance targets as well as temporal and relative changes of these deviations. These classification results enable to (pro-actively) trigger countermeasures, where the degree of counteracting depends on the observed KPI deviations from performance targets. Similar to the *TBHOA* approach, no actions are triggered, if the selected countermeasures due to performance degradations of several HPIs would cancel out each other. Two different approaches are used to classify the considered KPI ρ (e.g., dropping ratio ρ_{CDR}). The first approach, referred to as *TBHOA_FZ*, employs the absolute KPI value $\eta^{(1)}(t)$ and the temporal KPI change rate $\dot{\eta}^{(1)}(t)$ with respect to the observation time interval T, which are calculated as follows:

$$\eta^{(1)}(t) = \rho(t), \tag{7.5}$$

$$\dot{\eta}^{(1)}(t) = \frac{\rho(t)-\rho(t-1)}{T}, \tag{7.6}$$

where T is identical to the filter length of the moving average filter used to derive KPI values.

The second approach, referred to as *TBHOA_FZ_PRE*, takes a KPI target value, specified by the MNO, as well as the current and previous KPI values into account. The absolute deviation from performance target ρ^* is denoted by $\eta^{(2)}(t)$ and the relative deviation of the current KPI value with respect to the previous KPI value by $\eta^{(2)}_{\text{rel}}(t)$. These quantities are determined using the following equations:

$$\eta^{(2)}(t) = \rho(t) - \rho^*, \tag{7.7}$$

$$\eta^{(2)}_{\text{rel}}(t) = \frac{\rho(t) - \rho(t-1)}{\rho(t-1)}, \tag{7.8}$$

where ρ^* denotes the respective KPI target value. It should be noted that, in case of the first approach, membership function based classification is activated (cf. Figure 7.11), if either KPI deviation $\eta^{(1)}(t)$ or the temporal KPI change rate value $\dot{\eta}^{(1)}(t)$ are positive. In case of the second approach, classification becomes active, if either KPI deviation $\eta^{(2)}(t)$ exceeds the predefined KPI target value ρ^* or the relative KPI deviation value $\eta^{(2)}_{\text{rel}}(t)$ is positive, i.e., the relative deviation increases. Further, if for several fuzzy labels (cf. Figure 7.11) $\mu > 0$, the maximum operation is applied to determine the dominating fuzzy set, i.e., the largest membership degree.

In principle, various types of membership functions (e.g., triangular, trapezoidal, or Gaussian shaped) can be used for classifying HPI performance. The sensitivity or "aggressiveness" of the classification scheme can be varied by tuning the membership function's shape, slope, or the amount of overlap with neighboring membership functions. For instance, if rather rapid variations are to be expected, for instance, considering the BS load of a micro cell in a dense urban deployment where users are frequently passing through, rather triangular than trapezoidal shaped membership functions with suitable slopes are preferable. Moreover, if the tendency is observed that "if a certain KPI increases, then it increases rapidly", less steeper slopes allow for faster state transitions due to a larger overlap of neighboring membership functions. A drawback of Gaussian shaped membership functions is that they are rather computationally expensive and require according hardware processing capabilities. In general, the decision on the different value ranges for each KPI state depends on resource granularity and may also be influenced by operator policies. Figure 7.11 illustrates exemplary membership functions that are used for assessing system performance with respect to HPIs.

In the developed HO optimization scheme, the respective KPI classification results are used for triggering HO parameter adaptations instead of relying on fix timer (good/bad performance) and threshold values. Further,

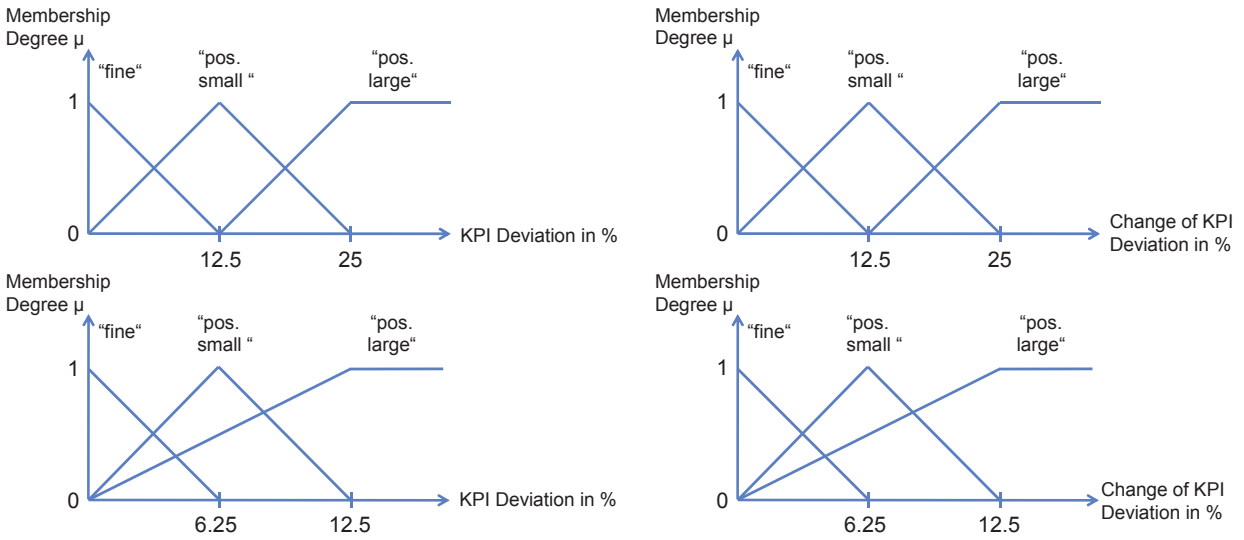

(a) Membership functions for assessing KPI deviation

(b) Membership functions for assessing change of KPI deviation

Figure 7.11: Exemplary membership functions for assessing KPI deviation and its change

information on the KPI deviation trend is incorporated via $\eta^{(1)}(t)$ or $\eta^{(2)}_{\text{rel}}(t)$ and enables pro-actively adapting HO parameter settings, which is particularly beneficial in scenarios exhibiting high user mobility. Furthermore, two possible operation modes are available: either the trend and fuzzy logic based HO algorithm continuously monitors and adapts the respective HO parameters or an operation interval is to be defined (e.g., 1 s) when KPI assessments and adaptations are to be carried out. Both types can be considered for benchmarking with other strategies.

The observed deviations from performance targets determine the degree of counteracting, i.e., adapting a certain HO parameter by one step only ("positive small") or by two steps ("positive large"). For example, the classification results may indicate to change the HYS value by +/-0.5 dB or by +/-1.0 dB. Table 7.3 summarizes the possible HO KPI deviation and deviation change rate states as well as applicable adaptation steps.

Fuzzy Q-Learning Based Mobility Robustness Optimization

One basic limitation of all learning schemes is that, in principle, the agent would have to explore the whole *universe of discourse* for attaining a rich body of experience and learning the best action for any situation. However, the training costs associated with achieving a complete body of experience are usually too high. Therefore, there is a trade-off with respect to computations and costs spent on training a FIS and arranging for fall-back solutions

Table 7.3. KPI deviation and deviation change state classification as well as adaptation steps

		KPI Deviation Change State		
	State	"fine"	"pos. small"	"pos. large"
KPI Deviation State	"fine"	0	1	2
	"pos. small"	1	1	2
	"pos. large"	2	2	2

for very rare situations or sporadic events. In order to reduce training complexity and efforts, the FQL based scheme developed in this thesis applies a limited Exploration/Exploitation Policy (EEP) and first classifies the universe of discourse using fuzzy labels. In contrast to a complete EEP, where the effectiveness of all possible HO parameter adaptations, as, e.g., listed in Table 7.4, is learned, a limited EEP has been derived by analyzing system-level simulation results for a 2D grid of possible HO parameter settings (cf. Figure 7.7). Based on these simulation results, the most effective HO parameter adaptations were selected for the limited set of state-dependent rule-action pairs, as, for example, stated in Table 7.5.

Table 7.4. Complete set of CIO, HYS, and TTT parameter adaptations

No.	**CIO**	**HYS**	**TTT**	**No.**	**CIO**	**HYS**	**TTT**
1	−1	−1	−1	15	0	0	1
2	−1	−1	0	16	0	1	−1
3	−1	−1	1	17	0	1	0
4	−1	0	−1	18	0	1	1
5	−1	0	0	19	1	−1	−1
6	−1	0	1	20	1	−1	0
7	−1	1	−1	21	1	−1	1
8	−1	1	0	22	1	0	−1
9	−1	1	1	23	1	0	0
10	0	−1	−1	24	1	0	1
11	0	−1	0	25	1	1	−1
12	0	−1	1	26	1	1	0
13	0	0	−1	27	1	1	1
14	0	0	0				

In the developed concept, fuzzy logic is used as means for partitioning the

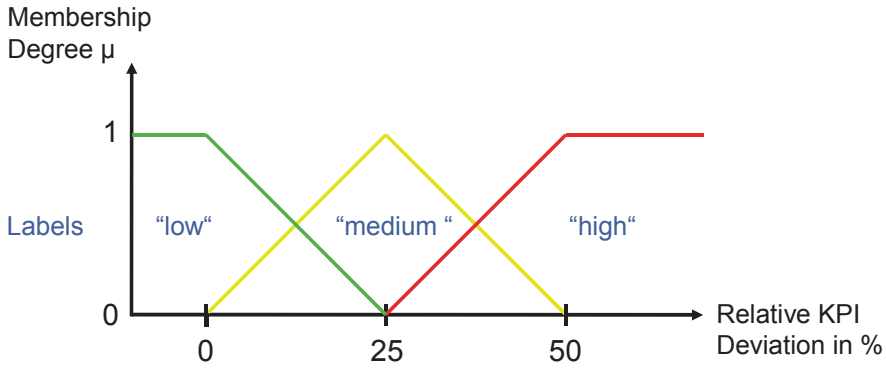

Figure 7.12: Membership functions for classifying relative KPI deviation (adapted from [KKSS13a])

continuous state space and for classifying the universe of discourse of input variables using a sufficiently large but limited number of fuzzy sets. Hence, the overall number of system states and thus also the complexity of learning tasks is significantly reduced. System states are classified during operation using fuzzy labels that result from a predefined set of rules describing each considered situation or state. Consequently, the implemented FIS assesses system conditions based on these classification results and decides upon which adaptations or counteractions to trigger by following its EEP, thus learning to optimize system performance given varying system states.

In order to evaluate the severity of relative KPI deviations from desired performance targets, so-called *membership functions* [Jou98] are introduced. The relative KPI deviation $\eta(t)$ of the considered KPI $\rho(t)$ (e.g., ρ_{CDR}) at time instance t is determined with respect to the observation time interval T as follows:

$$\eta(t) \;=\; \frac{\rho(t)-\rho^*}{\rho^*}, \tag{7.9}$$

where ρ^* denotes the KPI target specified by the MNO policy (e.g., 1%).

In general, the decision on the different value ranges for classifying KPI degradations depends on observation time T and may also be influenced by MNO policy. Figure 7.12 illustrates an exemplary membership function that is used for assessing system performance based on observed KPI degradations. In the developed MRO scheme, the respective relative KPI deviation classification results are used for triggering HO parameter adaptations. In contrast, state-of-the-art SON approaches (e.g., cf. [JBT+10], [LSJB10], [EB11]) rely on fix timer and threshold values.

In order to perform inference, each rule is first quantified employing fuzzy logic and then the applicability of each rule is determined. This is accom-

plished by comparing the premises of all rules to the FIS inputs and by determining which rules apply to the current situation. This matching process involves assigning the certainty that each rule applies, and typically yields a set of rules the FIS designer is more certain to apply to the current situation. An example for the FIS processing structure is depicted in Figure 6.3.

For MRO, the designed FIS considers the relative deviations of several KPIs, such as CDR, HFR, PHR, as well as the magnitudes of various HO parameters, e.g., HYS, TTT, or HOM, and employs a fuzzy logic based classification scheme for mapping HO parameter and KPI inputs s_j on fuzzy labels l_j^i. The rule set listed in Table 7.5 exemplarily summarizes the rule consequents and corresponding actions, i.e., HO parameter adaptations including their directions and magnitudes. In Table 7.5, only the HYS parameter, which is either classified as "low" or "high", is considered for system state classification. Further, the column "Actions" contains a limited set of possible HO parameter adaptations. For example, the action "HYS ↑ & TTT ↑" indicates to increase both HYS and TTT parameters simultaneously by the number of steps stated in the column δ_s, which contains the magnitudes of the respective adaptation steps. The selection of a particular action depends on the specified EEP.

Table 7.5: Exemplary FQL based MRO rule consequents and actions

Rule	**HYS**	$\rho_{\mathbf{CDR}}$	$\rho_{\mathbf{HFR}}$	$\rho_{\mathbf{PHR}}$	δ_s	**Actions**
1	low	low	low	low	1	./.
2 3	low	low	low	medium high	1 2	{HYS ↑, HYS ↑ & TTT ↑, TTT ↑}
4 5 6	low	low	medium	low medium high	1 1 2	{HYS ↑ & TTT ↑, TTT ↑, HYS ↑}
7 8 9	low	low	high	low medium high	2 2 2	{HYS ↑ & TTT ↑, TTT ↑, HYS ↑}
10 11 12	low	medium	low	low medium high	1 1 2	{HYS ↓, HYS ↓ & TTT ↓, TTT ↓}
13 14	low	medium	medium	low medium	1 1	{HYS ↓, HYS ↓ & TTT ↓,

Continued on next page

Table 7.5 – continued from previous page

Rule	**HYS**	$\rho_{\mathbf{CDR}}$	$\rho_{\mathbf{HFR}}$	$\rho_{\mathbf{PHR}}$	δ_s	**Actions**
15				high	2	TTT ↓}
16 17 18	low	medium	high	low medium high	1 1 2	{HYS ↓, HYS ↓ & TTT ↓, TTT ↓}
19 – 27	low	high	-	-	2	{HYS ↓, HYS ↓ & TTT ↓, TTT ↓}
28	high	low	low	low	1	./.
29 30	high	low	low	medium high	1 2	{TTT ↑, HYS ↑ & TTT ↑, HYS ↑}
31 32 33	high	low	medium	low medium high	1 1 2	{TTT ↑, HYS ↑ & TTT ↑, HYS ↑}
34 35 36	high	low	high	low medium high	2 2 2	{TTT ↑, HYS ↑ & TTT ↑, HYS ↑}
37 38 39	low	medium	low	low medium high	1 1 2	{HYS ↓ & TTT ↓, HYS ↓, TTT ↓}
40 41 42	low	medium	medium	low medium high	1 1 2	{HYS ↓ & TTT ↓, HYS ↓, TTT ↓}
43 44 45	low	medium	high	low medium high	1 1 2	{HYS ↓ & TTT ↓, HYS ↓, TTT ↓}
46 – 54	high	high	-	-	2	{HYS ↓ & TTT ↓, HYS ↓, TTT ↓}

A certain prioritization among these KPIs and their states is realized by assigning particular, MNO defined weights (e.g., $w_{\text{CDR}} = 4, w_{\text{HFR}} = 2, w_{\text{PHR}} = 1$). This prioritization scheme is reflected in Table 7.5 by the fact that as soon as ρ_{CDR} is not assessed as "low", the set of applicable actions aims at improving CDR performance in the first place. Further, if CDR performance deviation is "low" and HFR related KPI deviation is assessed more severe than PHR performance deviation, the HFR related rule determines the ap-

plied magnitude for HO parameter adaptations (e.g., cf. Table 7.5 rules $7-9$). Thus, the degree of counteracting indicated by the FIS conclusions depends on the deviation from the respective KPI performance targets. For example, if ping-pong HO performance degradation is classified as "medium" and the counteraction foresees to increase HYS parameter by one step, the current HYS parameter setting is adapted accordingly. In this case the magnitude of HYS parameter change, here 1, is multiplied with the step size of HYS parameter adaptations, here 0.5 dB. In contrast, if ping-pong HO performance degradation is assessed as "high", the corresponding magnitude of HO parameter adaptation is 2 and would result, e.g., in a HYS parameter adaptation of 1 dB. If more fuzzy labels l_j^i are considered for KPI input classification, the fuzzy rule set will contain more rules with magnitudes corresponding to the extent of deviation from KPI performance targets (cf. Equation (7.9)).

In Section 8.2.1, extensions of the exemplary rule base listed in Table 7.5 and the initial fuzzy classification scheme for KPI performance deviations, shown in Figure 7.12, are presented and evaluated. Moreover, in order to increase the possibilities of selecting appropriate countermeasures given observed, significant KPI degradations, more fuzzy labels are introduced in order to enable a higher resolution for classifying KPI degradations and HO parameter states.

In general, each of these fuzzy rules has N_O corresponding conclusions $\left(o_m^i\right)_{m=1,\cdots,N_O}^{i=1,\cdots,N}$, that, in the simplest case, are crisp. Hence, the conclusion vector $\boldsymbol{o}_m$ can be used to approximate the output function y_m. Here, potential outputs are individual or joint adaptations of HYS and TTT settings. Conclusions on which control actions to take are derived using the rules that have been identified to apply at the current time. A rule is *on at time* t, if its premise membership function $\mu_{\text{premise}} > 0$. The fuzzy inference mechanism seeks to combine the recommendations of all the rules and to determine conclusions for HO parameter adaptations, e.g., HYS and TTT. These conclusions are characterized by fuzzy sets and represent the certainty that the HO parameters should be specifically adjusted. The certainty of a premise is determined using standard Boolean logic operators, such as *Product*. The truth value of each rule i with respect to $\boldsymbol{s} \in \mathcal{S}$ can be computed as stated in Equation (6.6):

$$\alpha_i(\boldsymbol{s}) = \prod_{j=1}^{N_I} \mu_{l_j^i}(s_j). \tag{7.10}$$

The defuzzification operation acts on the basis of implied fuzzy sets produced by the inference mechanism that derived the activated rule truth values. It

combines the effects of the activated rule truth values on the consequent membership functions μ_{y_m} to provide the most certain FIS output. One popular method for combining the recommendations represented by the implied fuzzy sets from all activated rules is the so-called Center of Gravity (COG) defuzzification method, which is already stated in Equation (6.7):

$$y_m = \frac{\sum_{i=1}^{N} c_m^i \int \mu_{y_m}^i}{\sum_{i=1}^{N} \int \mu_{y_m}^i}, \tag{7.11}$$

where m denotes the corresponding FIS output (e.g., HYS, CIO, TTT parameters), c_m^i denotes the center of the membership function of the consequent of rule i, i.e., adaptation direction and magnitude, and $\int \mu_{y_m}^i$ denotes the area under the consequent membership function $\mu_{y_m}^i$. In case of rule-specific magnitudes, the adaptation direction $d \in \{-1, 0, 1\}$ (cf. Table 7.4) is multiplied with the applicable rule magnitude δ (cf. Table 7.5) to yield c_m^i, i.e., $c_m^i = d_m^i \ \delta_m^i$. An example for deriving the defuzzification result by COG method is illustrated in Figure 6.5. In the scope of this thesis, symmetric, triangular shaped output membership functions with a base length of 2 and peak at 1 are considered, where the area under the "chopped off" triangular output membership function at height $\alpha_i(\boldsymbol{s})$, i.e., $\int \mu_{y_m}^i$, is calculated using Equation (6.8) as follows:

$$\int \mu_{y_m}^i = 2\left(\alpha_i(\boldsymbol{s}) - \frac{\alpha_i^2(\boldsymbol{s})}{2}\right), \tag{7.12}$$

where $\alpha_i(\boldsymbol{s})$ corresponds to the respective truth value of the activated rule i. In essence, it should be noted that if several rules are found to apply to a certain situation, a trade-off with respect to HO parameter adaptation is determined by COG method taking rule consequents and adaptation magnitudes (cf. Table 7.5) into account.

The FQL scheme for MRO developed in this thesis is based on the approach described in [GJ97]. The *reinforcement* signal r received at time $t+1$ after applying the selected actions and leading the system to state $s' = s(t+1)$ consists of a weighted sum of several relative KPI deviations $\rho_m(t)$ and can be written as follows:

$$r(t+1) = \sum_{m=1}^{N_{\text{KPI}}} w_m \ (\rho_m^* - \rho_m(t)), \tag{7.13}$$

where ρ_m^* denotes the respective KPI target value and $\rho_m(t)$ the observed and measured KPI at time t, respectively. $(w_m)_{m=1,\cdots,N_{\text{KPI}}}$ represent the weights

assigned to the respective KPIs specified by the MNO policy. The reinforcement $r(t+1)$ will be positive, if the KPIs are below the pre-defined KPI target values. With every KPI exceeding its performance target the numeric value of reinforcement $r(t+1)$ will be decreased and might become negative. Thus, the quality of the recently applied rule-action pair will be decreased, too. In order to account for the imbalance between possible positive and negative reinforcements, an optional mode has been implemented that scales the numeric value of reinforcement $r(t+1)$ depending on whether $r(t+1)$ is observed to be positive or negative. The respective scaling factors, Φ_p and Φ_n, are determined as follows:

$$\begin{aligned} \Phi_p &= \sum_{m=1}^{N_{\mathrm{KPI}}} w_m \ \rho_m^* \\ &= w_{\mathrm{CDR}} \ \rho_{\mathrm{CDR}}^* + w_{\mathrm{HFR}} \ \rho_{\mathrm{HFR}}^* + w_{\mathrm{PHR}} \ \rho_{\mathrm{PHR}}^*, \end{aligned} \tag{7.14}$$

and

$$\begin{aligned} \Phi_n &= \left| \sum_{m=1}^{N_{\mathrm{KPI}}} w_m \ (\rho_m^* - 1) \right| \\ &= \left| w_{\mathrm{CDR}} \ (\rho_{\mathrm{CDR}}^* - 1) + w_{\mathrm{HFR}} \ (\rho_{\mathrm{HFR}}^* - 1) + w_{\mathrm{PHR}} \ (\rho_{\mathrm{PHR}}^* - 1) \right|. \end{aligned} \tag{7.15}$$

Thus, it is ensured that in case of positive reinforcements, $r(t+1)$ is scaled with the magnitude of the best possible reinforcement value, i.e., all KPI values $\rho_m(t)$ are equal to zero, resulting in a reinforcement value equal to 1 (cf. Equation (7.13)). For negative reinforcement, $r(t+1)$ is scaled with the magnitude of the worst possible reinforcement value, i.e., all KPI values $\rho_m(t)$ are equal to 1. In the worst case, this yields an overall reinforcement value of -1, where all KPIs $\rho_m(t)$ are equal to 1 (cf. Equation (7.13)). Finally, the resulting reinforcement value becomes

$$r'(t+1) = \begin{cases} r(t+1)/\Phi_p, & \text{if } r(t+1) > 0 \\ r(t+1)/\Phi_n, & \text{otherwise.} \end{cases} \tag{7.16}$$

In essence, this scaling mode guarantees that the magnitudes of reinforcement values in best and worst cases are normalized to 1 independent of specified KPI target thresholds ρ_m^*. If scaling of reinforcement values is not applied, there is a risk that only negative Q-values are obtained after learning. The reinforcement value directly affects the new Q-values at time instance $t+1$, where Q-values are updated according to:

$$\Delta Q = r(t+1) + \gamma \ V(\boldsymbol{s}(t+1)) - Q(\boldsymbol{s}(t), a). \tag{7.17}$$

The rule quality values or briefly Q-values are calculated as already stated in Equation (6.24):

$$Q(\boldsymbol{s},\boldsymbol{a}) = \frac{\sum_{i=1}^{N} \alpha_i(\boldsymbol{s})\ q(\boldsymbol{s}_i,\boldsymbol{a}_i)}{\sum_{i=1}^{N} \alpha_i(\boldsymbol{s})}, \tag{7.18}$$

where the function $\boldsymbol{s} \rightarrow \alpha_i(\boldsymbol{s})$ performing the mapping from input vector $\boldsymbol{s}$ onto rule consequents $\alpha_i(\boldsymbol{s})$ gives the truth value of rule i given input vector $\boldsymbol{s}$.

In order to reduce the so-called *temporal credit-assignment problem* [Min61], [SB98], [Jou98], the concept of *eligibility* is applied. For this purpose, so-called eligibility factors $e(i,k)$ per rule-action pair (i,k) are introduced that memorize the applicability of each rule-action pair weighted according to their proximity to time step t. The eligibility factor of rule i and action k is defined below (cf. Equation (6.29)):

$$e(i,k) = \begin{cases} \nu\ \gamma\ e(i,k) + \dfrac{\alpha_i(\boldsymbol{s})}{\sum_{i=1}^{N} \alpha_i(\boldsymbol{s})}, & \text{if } k = k^+ \\ \nu\ \gamma\ e(i,k), & \text{otherwise,} \end{cases} \tag{7.19}$$

where the recency factor ν, also called *eligibility rate*, is used to weight the formerly discounted eligibility value $\gamma\ e(i,k)$ and k^+ denotes the selected action k given activation of rule i. Thereby, according to Equation (6.30) [GJ97], the updating equation becomes:

$$\Delta q(i,k) = \kappa\ \Delta Q\ e(i,k), \tag{7.20}$$

where $\kappa \in (0,1]$ denotes the *learning rate*. Further, the learning rate κ is decreased per rule/action pair each time a certain rule/action pair is visited, i.e., $\kappa(i,k) = \kappa\ \frac{1}{n(i,k)}$, where $n(i,k) = 1,2,3,\ldots$ is the number of situations where rule i is activated and action k applied.

In essence, the learning process incorporates three main aspects:

- the absolute action quality difference or knowledge gain the execution of a certain action creates, reflected by ΔQ,
- the impact of previous executions of the considered action and its impact on the present situation, denoted by $e(i,k)$,
- and the relation that the knowledge gain when handling a situation for the first time is larger than when having been in the same situation already multiple times, reflected by decreasing values of $\kappa(i,k)$.

Hence, Equation (7.20) becomes:

$$\Delta q(i,k) = \kappa(i,k)\ \Delta Q\ e(i,k). \tag{7.21}$$

Initially, all Q-values $q(i,k)$ are zero. During learning process they are incrementally adjusted according to the experience attained through applying selected actions, while following a certain EEP. In the following, a limited EEP is assumed that is ε-*greedy* in the sense that for each rule i the currently best action, referred to as k^* with $q(i,k^*)$, is selected with probability ε and a random action with probability $(1-\varepsilon)$ [Jou98]. In case several alternative actions to the currently best action k^* are specified, any of them can be selected with equal probability. More precisely, let k^+ be the selected action in rule i using an EEP and let k^* be the currently best action, i.e., $q(i,k^*) = \max_{j \in \mathcal{A}^i} q(i,j)$, the global Q-value of the inferred action $\boldsymbol{a}$ given input vector $\boldsymbol{s}$ is as stated in Equation (6.25) [GJ97]:

$$Q(\boldsymbol{s},\boldsymbol{a}) = \frac{\sum_{i=1}^{N} \alpha_i(\boldsymbol{s})\ q(i,k^+)}{\sum_{i=1}^{N} \alpha_i(\boldsymbol{s})}, \tag{7.22}$$

and the resulting state value is according to Equation (6.26):

$$V(\boldsymbol{s}) = \frac{\sum_{i=1}^{N} \alpha_i(\boldsymbol{s})\ q(i,k^*)}{\sum_{i=1}^{N} \alpha_i(\boldsymbol{s})}. \tag{7.23}$$

Learning stops, if ΔQ falls within the area of convergence, i.e., $r_{\text{opt}} - \theta_c \leq \Delta Q \leq r_{\text{opt}} + \theta_c$, where θ_c denotes the width of the convergence interval, e.g., $\theta_c = 0.01$. The optimum reinforcement r_{opt} is observed, if all KPIs $\rho_m(t)$ are zero, in this case $r_{\text{opt}} = \sum_{m=1}^{N_{\text{KPI}}} w_m \rho_m^*$. If reinforcement scaling mode is activated, r'_{opt} is equal to 1. The overall FQL process is summarized in Table 7.6.

7.4 Summary

The present chapter gave a detailed overview on state-of-the-art approaches for MRO. Further, the author illustrated his view on SON system architecture as well as integrating SON solutions in future networks and presented newly developed fuzzy logic and FQL based MRO schemes. The designed fuzzy logic (*TBHOA_FZ*, *TBHOA_FZ_PRE*) and different variations of the FQL based MRO scheme presented in the previous subsection are evaluated by means of system level simulations in Chapter 8. For benchmarking, the introduced state-of-the-art approaches *TBHOA* and *SBHOA* are considered.

Table 7.6. FQL scheme

1.	Initialize Q-value LUT: $\forall i \in \{1,2,...,N\}, \forall k \in \{1,2,...,N_{\mathcal{A}^i}\}$ $q(i,k) = 0$ and set time $t = 0$. Repeat:
2.	Receive and classify system state $s(t) = \big(H_s(t), TTT(t), O_s(t), O_t(t), \rho_{\mathrm{CDR}}(t),\ \rho_{\mathrm{HFR}}(t),\ \rho_{\mathrm{PHR}}(t)\big)$.
3.	For each rule i select an action k following the EEP: $k = \arg\max_j q(i,j)$ with probability ε or $k =$ random $\{j,\ j = 1,2,...,N_{\mathcal{A}^i}\}$ with probability $1-\varepsilon$.
4.	Calculate inferred output using COG method.
5.	Determine its corresponding quality $Q(\boldsymbol{s},\boldsymbol{a})$.
6.	Execute action $a(\boldsymbol{s})$ at time t that leads the system to state $\boldsymbol{s}' = \boldsymbol{s}(t+1)$. Receive reinforcement $r(t+1)$.
7.	Calculate truth values $\alpha_i(\boldsymbol{s}(t+1))$ for $i \in \{1,2,\ldots,N\}$.
8.	Determine the value of the new state: $V_t(\boldsymbol{s}(t+1)) = \sum_{i=1}^{N} \alpha_i(\boldsymbol{s}(t+1))\ \max_k q(i,k)$.
9.	Calculate the variation of the quality $Q(\boldsymbol{s},\boldsymbol{a})$: $\Delta Q = r(t+1) + \gamma\ V_t(\boldsymbol{s}(t+1)) - Q(\boldsymbol{s},\boldsymbol{a})$.
10.	Update the elementary quality $q(i,k)$ of each rule i and action k: $\Delta q(i,k) = \kappa(i,k)\ \Delta Q\ e(i,k)$.
11.	Save the elementary quality $q(i,k)$ in the Q-value LUT.
12.	If convergence is obtained, stop learning.
13.	$t = t+1$.

8 Performance Evaluation of Self-Tuning Schemes for Optimizing Mobility Robustness

In the following, two exemplary scenarios are evaluated using the methodology introduced in Chapter 2. These scenarios are designed to include recurring user movement patterns and typical episodes as observed by Mobile Network Operators (MNOs), e.g., commuter traffic in metropolitan areas. In the considered scenarios, the developed Self-Organizing/Optimizing Network (SON) mechanisms prove that they are able to autonomously counteract network performance issues and improve several mobility-related Key Performance Indicators (KPIs), such as Connection Dropping Ratio (CDR), Handover Failure Ratio (HFR), and Ping-Pong Handover Ratio (PHR), simultaneously.

Main characteristics of the first scenario are the high number of users moving at high velocities and the fact that for one Base Station (BS) sector in the center of the considered service area a malfunction and failure event is observed, which results in cell sector shutdown. As soon as this failure event is detected by its neighboring BSs, they try to adjust their Handover (HO) parameter settings so as to compensate for the loss of one cell sector and the resulting network coverage hole (cf. Figure 8.1). In essence, HO parameters are self-tuned according to user mobility related-network events in order to virtually extend the network coverage area of neighboring cell sectors.

In contrast, in scenario 2, User Equipments (UEs) are moving at different velocities on ring roads in clockwise and counter-clockwise directions resulting in recurring user movement patterns. Here, two BSs are in charge of learning to adapt their HO parameter settings according to locally observed conditions in order to reduce mobility-related performance issues. Moreover, the considered environment includes two coverage holes the users have to pass through. These coverage holes are introduced to model severe shadowing

conditions users may face, for example, due to experienced "canyon" effects between highrise buildings. The presence of these coverage holes results in mobility-related performance issues and creates a need for HO parameter adaptations.

8.1 Fuzzy Q-Learning Based Optimization of Mobility Robustness in Scenario 1

For studying the performance of the developed Fuzzy Q-Learning (FQL) based Mobility Robustness Optimization (MRO) scheme, a LTE system level radio network simulation tool is used, where following 3GPP's guidelines [3GP10a] a typical macro cell deployment with three sectors and ISDs of 500 m is assumed. Table 8.1 summarizes applied simulation parameters.

Table 8.1. Simulation parameters of scenario 1 [KKSS13a]

Parameter	**Assumption**
Carrier frequency	2 GHz
System bandwidth	10 MHz (50 PRBs)
Total transmit power	40 W
Control channel overhead	12%
Shadowing	log-normal, standard deviation: 8 dB, correlation distance: 50 m
Fast fading	2-tap Rayleigh fading channel
Noise power	-174 dBm/Hz + 10 $\log_{10}(B)+7$ dB
Background users per cell sector	5
High-speed users on highway lanes	780 at 120 km/h
Traffic model	CBR traffic, full buffer, user data rate = 192 kbps
Simulation time	100 s = 10000 time intervals, 10 ms each (cf. Section 2.8)
HO preparation time	250 ms
RLF timeout (T310 [3GP12a])	1s
Ping-pong HO time	5 s
KPI update interval	1 s
KPI targets $(\rho^*_{\text{CDR}}, \rho^*_{\text{HFR}}, \rho^*_{\text{PHR}})$	$(1.25\%, 2.5\%, 5\%)$
KPI weights $(w_{\text{CDR}}, w_{\text{HFR}}, w_{\text{PHR}})$	$(4, 2, 1)$

Further, five slowly moving so-called *background* users are located in each cell sector in order to generate a basic traffic load. Besides, there are the 780 high speed users that are foreseen to continuously move at 120 km/h on several highway lanes (3 per direction), illustrated in Figure 8.1 as black crosses. Moreover, simplified *coverage holes* (in dark blue) are intentionally inserted in the depicted cell area overlaying the shadowing map in order to create possibilities for KPI degradations, thus triggering SON functionalities. In addition, the cell sector highlighted in white is switched off after 5% of simulation time (antenna steering direction in red) in order to evaluate impact on self-optimization mechanisms operating at neighboring cell sectors.

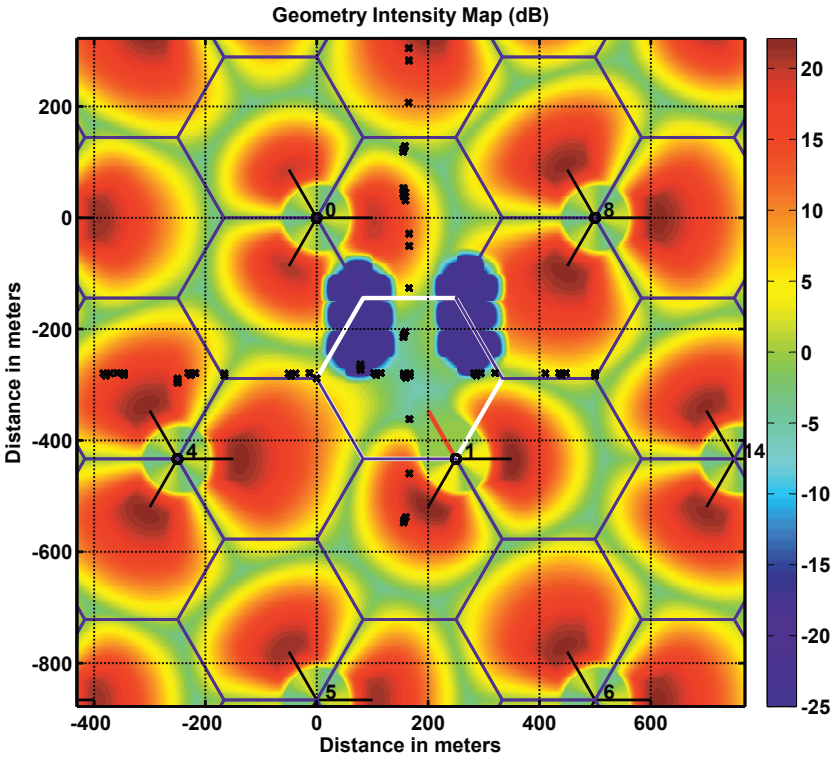

Figure 8.1: Geometry intensity map and cell layout of reference scenario [KKSS13a]

A challenging, and more realistic user distribution consisting of platoons, e.g., of a bus with 30 people followed by a number of cars (e.g., 3 cars with 2 passengers each) is modeled. Users that are about to leave the evaluation area will enter again driving on the opposite lane. For modeling user service request, a simple full-buffer traffic model (cf. Section 2.4.1) is used.

The FQL based MRO scheme operates independently at each cell sector, where KPI update interval is set to 1 s. The adaptation steps of Hysteresis (HYS) and Time-To-Trigger (TTT) values follow 3GPP specifications. Hysteresis values range from 0 to 10 dB, where adaptations occur in steps of ± 0.5 dB. However, due to the simulation tool's time basis being 10 ms, only

multiples of 10 ms can be chosen as TTT value, limiting the TTT value set to $\{0, 0.04, 0.08, 0.1, 0.16, 0.32, 0.48, 0.64, 1.280, 2.560, 5.120\}$ s.

The implemented Fuzzy Inference System (FIS) rule set and the limited Exploration/Exploitation Policy (EEP) are listed in Table 7.5. The presumably best action given system state $\boldsymbol{s}$ corresponds to the first action column entry that is selected with a probability of $\varepsilon = 0.8$, while otherwise the two alternative actions are equally probable. The discount factor is set to $\gamma = 0.95$, the learning rate to $\kappa = 0.01$, the eligibility rate to $\nu = 0.9$, and the convergence limit to $\theta_c = 0.001$, respectively. Performance targets of the different KPIs (ρ_{CDR}, ρ_{HFR}, ρ_{PHR}) are set to $(1.25\%, 2.5\%, 5\%)$. Furthermore, overall optimization performance during the learning process is evaluated using the Overall Performance Indicator (OPI) that is calculated as follows:

$$OPI(t) = \sum_{m=1}^{N_{\mathrm{KPI}}} w_m \, \frac{\rho_m^* - \rho_m(t)}{\rho_m^*}. \tag{8.1}$$

The optimization task to be performed by each FQL entity is to maximize the value of OPI, where here $OPI_{\mathrm{opt}} = \sum_{m=1}^{N_{\mathrm{KPI}}} w_m = 7$ given KPI weight values (cf. Table 8.1).

In the following, two different versions of FQL based optimization schemes, which, besides tuning cell-specific TTT values, differ with respect to how they adjust the overall Handover Margin (HOM), are considered:

1. *FQL_HYS* performs only cell-specific HYS parameter adaptations.

2. *FQL_CIO* applies cell pair-specific Cell Individual Offset (CIO) O_t parameter adaptations by evaluating cell pair-specific event counters. Here, particular focus is put on three events: connection drops that occur while the corresponding UEs already entered HO condition (i.e., TTT counters are already activated), HO failures, and ping-pong HOs. In case one of these events is observed, cell pair-specific event counters are checked for a maximum in order to identify the neighboring BS to which the mobility-related event most likely occurred. If connection drops due to session time out or Radio Link Failure (RLF) events are observed, the cell-specific HYS parameter is adjusted, since in this case no neighbor relation is found to be the root cause of system performance degradation.

For benchmarking the performance of the designed FQL based MRO schemes, the trend based MRO algorithm presented in [JBT+10], and a scheme that assigns TTT values based on velocity estimates (*VC_TTT*),

which may be obtained via Doppler shift measurements, was implemented, too. In the first case, two different configurations were considered, which are referred to as *TBHOA* and *TBHOA2* (cf. Section 7.3.2). For *TBHOA*, (bad/good) performance timer values of (1/2) seconds and for *TBHOA2* (5/10) seconds are used, respectively. In case of *VC_TTT*, fix TTT values of 320 ms are set for high speed users, whereas in the reference case *REF* a fix TTT setting of 160 ms is considered.

Figure 8.2(a) depicts the number of connection drops, which occurred due to RLF, for each neighboring cell sector of the switched off cell sector, e.g., due to hardware malfunction, highlighted in white in Figure 8.1. Further, Figure 8.2(b) illustrates the overall number of connection drops that occurred while HO condition was already entered and TTT counters activated.

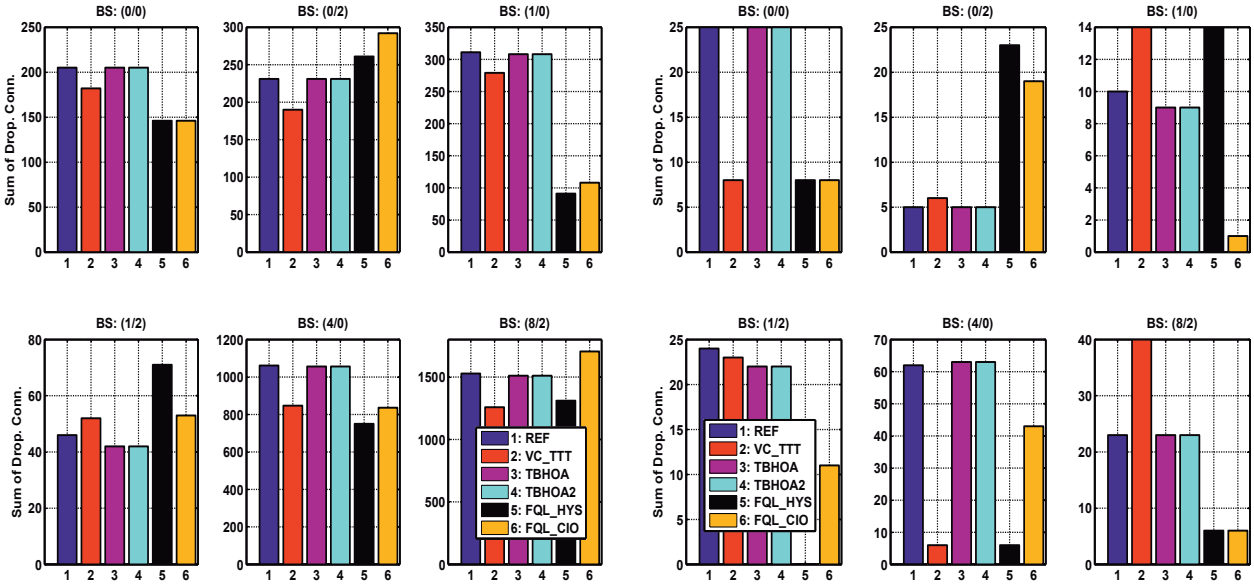

(a) Overall number of connection drops per BS

(b) Overall number of connection drops per BS (HO cond.)

Figure 8.2: Overall number of connection drops per BS in scenario 1 (adapted from [KKSS13a])

Except the cell sectors northwest (0/2) and south (1/2) of the switched off sector (1/1), *FQL_HYS* is among the best performing approaches that are able to enhance CDR performance, in particular with respect to sector (1/0). The trend based HO optimization approaches (*TBHOA* and *TBHOA2*) only outperform other schemes in case of cell sector (1/2). In terms of connection drops due to RLF, *FQL_CIO* performs slightly worse than *FQL_HYS*, in particular for cell sector (8/2). Here, the *VC_TTT* scheme, which employs UE-specific TTT settings based on velocity estimates, performs particularly well.

Regarding connection drops that occur while TTT counters were already activated, shown in Figure 8.2(b), the FQL based schemes outperform all other approaches for the majority of cell sectors. However, for cell sector (0/2), both result in highest numbers of connection drops, while for cell sector (1/0), *FQL_CIO* yields best and *FQL_HYS* worst performance. This indicates that for cell sector (1/0) cell pair-specific adaptations as performed by *FQL_CIO* are particularly beneficial.

Most significant performance gains through exploiting learned HO parameter adaptations are achieved with respect to HFR and PHR, as illustrated in Figure 8.3(a) and Figure 8.3(b), respectively.

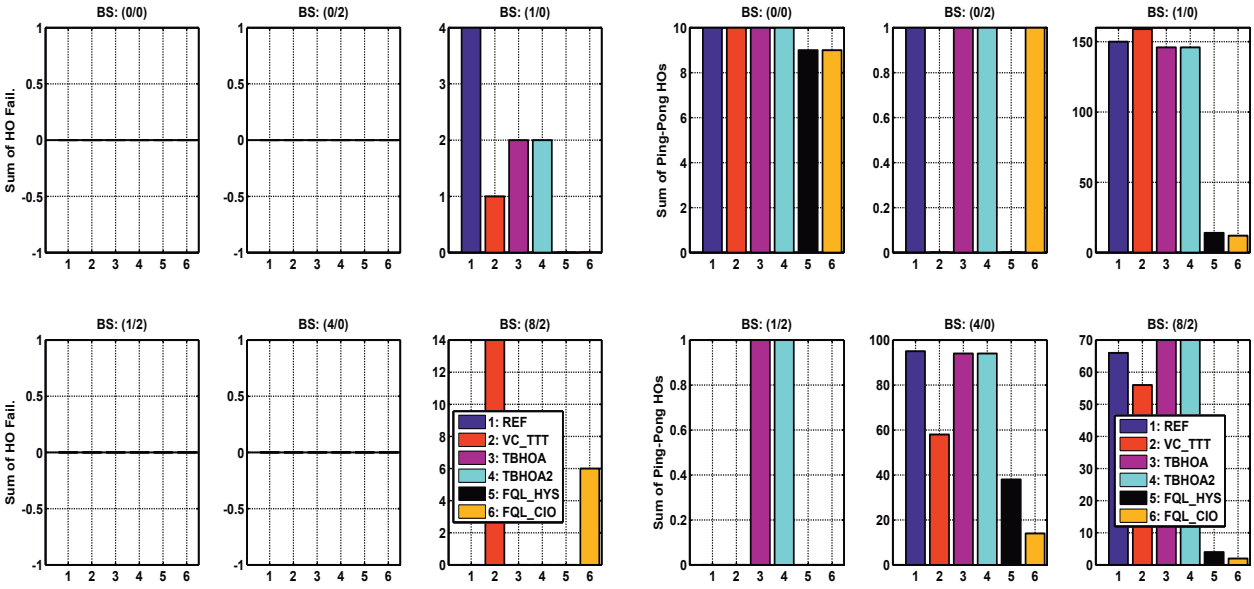

(a) Overall number of HO failures per BS (b) Overall number of ping-pong HOs per BS

Figure 8.3: Overall number of HO failures and ping-pong HOs per BS in scenario 1 (adapted from [KKSS13a])

In terms of HO failures, *FQL_HYS* yields optimum performance. Only for cell sector (8/2), the optimization scheme *FQL_CIO* tuning CIO parameters of neighboring cell sectors is not able to achieve same performance as *FQL_HYS*, but rather yields the second worst performance. For cell sector (8/2), *VC_TTT* performs worst. Applying *TBHOA* and *TBHOA2* in cell sector (1/0) results in increased HO failures compared to FQL based schemes, too, but still reduce the number of HO failures by 50%.

Regarding the overall number of ping-pong HOs, *FQL_CIO*, which tunes CIO parameters of neighboring cell sectors based on observed ping-pong HO directions, outperforms all other schemes. Only for cell sector (0/2), it results in one more ping-pong HO than *FQL_HYS*. For the majority of cell sectors, the trend based MRO schemes (*TBHOA* and *TBHOA2*) are not able

to improve PHR performance at all. Further, *VC_TTT* does not yield any improvements for cell sectors (0/0) and (1/0), where it performs worst among all considered schemes.

User satisfaction and Quality of Service (QoS) are assessed based on the considered traffic model (cf. Table 8.1), where the overall number of users that were provided the requested service bandwidth was evaluated. The overall number of time instances users are satisfied, i.e., their service requirements are met, is depicted in Figure 8.4.

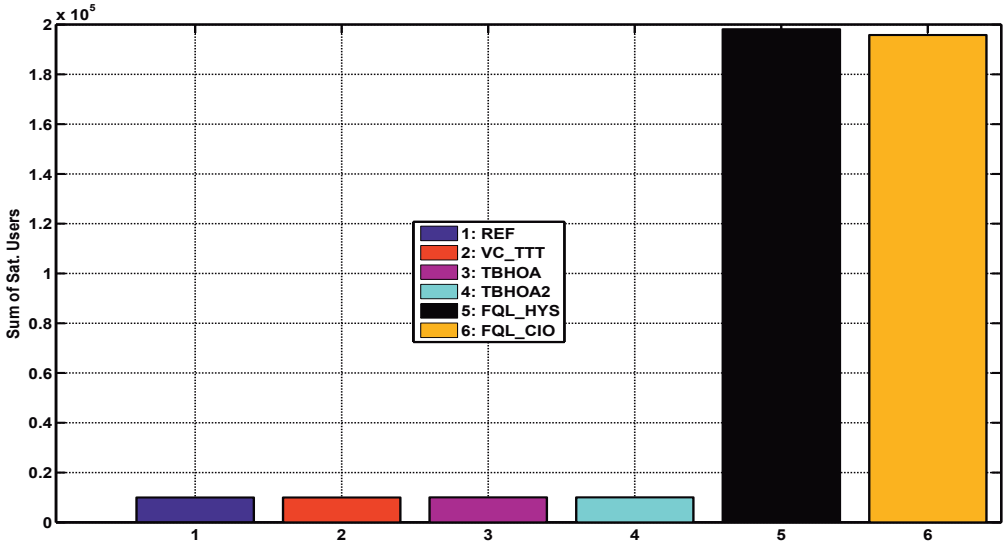

Figure 8.4: Overall number of satisfied users per MRO scheme in scenario 1

In terms of user satisfaction, the FQL based MRO schemes clearly outperform all other considered schemes. The massive enhancements achieved by *FQL_HYS* and *FQL_CIO* are mainly due to the ability of adjusting HO parameters according to locally observed performance issues and, thus, increasing the number of times users are satisfied by a factor of approximately 20. The trend based approaches (*TBHOA* and *TBHOA2*) perform similarly to *REF*, whereas *VC_TTT* results in marginally worse performance compared to *REF*.

In essence, the presented FQL based MRO schemes enable self-tuning of HO parameters using a limited rule set that reflects the situations the system may be exposed to. It learns optimum parameter adaptations using a limited EEP (cf. Table 7.5). Further, these schemes are able to simultaneously account for several KPI performance targets and, by increasing their knowledge base, self-optimize their operation. Benchmark results show that the FQL based schemes clearly outperform other considered schemes, in particular with respect to HO failures and ping-pong HOs, where optimum performance was achieved. Moreover, user satisfaction was significantly improved

by both FQL based MRO approaches. However, performance enhancements could not be simultaneously achieved with respect to all cell sectors, since defined KPI targets (e.g., CDR targets) were set too strict. Further, modifying assigned KPI weights used in the FQL based schemes allows for prioritizing different KPIs depending on BS sector location and operation conditions.

8.2 Fuzzy Q-Learning Based Optimization of Mobility Robustness in Scenario 2

Mobility Robustness Optimization (MRO) and, in particular, HO optimization aim at minimizing the occurrence of undesirable effects related to the HO procedure, such as connection drops, HO failures, and ping-pong HOs between two cells. This can be accomplished by adjusting the HO control parameters stated in Equation (3.1), such as HYS H_s, CIO O_s, and neighbor specific offset O_t. In principle, there are several possibilities for influencing HO procedures.

In the following evaluation, four different HO parameter adaptation modes are considered. Besides tuning cell-specific TTT values, these modes particularly differ with respect to how they adjust the overall HOM:

1. *FQL_HYS* performs only cell-specific HYS parameter adaptations.

2. *FQL_CIO* applies cell pair-specific CIO O_t parameter adaptations by evaluating cell pair-specific event counters. Here, particular focus is put on three events: connection drops that occur while the corresponding UEs already entered HO condition (i.e., TTT counters are already activated), HO failures, and ping-pong HOs. In case one of these events is observed, cell pair-specific event counters are checked for a maximum in order to identify the neighboring BS to which the mobility-related event most likely occurred. If connection drops due to session time out or RLF events are observed, the cell-specific HYS parameter is adjusted, since in this case no neighbor relation is found to be the root cause of system performance degradation.

3. *FQL_CIO_P* performs cell pair-specific, joint O_s and O_t adaptations. For example, if FIS determines HOM (HYS and CIO) adaptations of 2.5 dB, O_s is set to 1.5 dB and O_t to 1 dB. Similar to *FQL_CIO*, cell pair-specific event counters are taken into consideration for identifying respective BS target and adjusting corresponding O_t parameter.

4. *FQL_CIO_H* applies cell pair-specific, joint HYS and CIO O_t adaptations. For example, if FIS determines HOM (HYS and CIO) adaptations of 2.5 dB, H_s is set to 1.5 dB and O_t to 1 dB. Similar to *FQL_CIO*, cell pair-specific event counters are taken into consideration for identifying respective BS target and adjusting corresponding O_t parameter. If connection drops due to session time out or RLF events are observed, the cell-specific HYS and CIO parameters are jointly adjusted, since in this case no neighbor relation is found to be the root cause of system performance degradation.

For studying the performance of the developed FQL based MRO schemes *FQL_HYS*, *FQL_CIO*, *FQL_ CIO_P*, and *FQL_CIO_H* in a simplified scenario, the same simulation baseline assumptions as listed in Table 8.1 are considered except for the specified KPI targets and weights. These values are summarized in Table 8.2.

Table 8.2. Simulation parameters of scenario 2

Parameter	**Assumption**
Min. SINR requirement	-8 dB
KPI targets $(\rho^*_{\text{CDR}}, \rho^*_{\text{HFR}}, \rho^*_{\text{PHR}})$	$(1\%, 1\%, 5\%)$
KPI weights $(w_{\text{CDR}}, w_{\text{HFR}}, w_{\text{PHR}})$	$(4, 2, 1)$

In contrast to scenario 1, there are no background users per cell sector assumed, i.e., the system under consideration is not capacity limited. Thus, it can be assumed that if QoS requirements are not met, this is only due to currently experienced receive conditions, e.g., users passing through area of bad network coverage. The considered cell layout and user traces of scenario 2 are depicted in Figure 8.5(a).

There are five users that start in sector (0/0) on individual lanes in clockwise and counter-clockwise direction on circular paths around BS 0, respectively. The velocities of each user on a certain lane in clockwise or counter-clockwise direction are set to $(1.1, 6.1, 8.3, 13.9, 19.4)$ m/s $(4, 22, 30, 50, 70$ km/h), starting from inner to outer lanes. Further, there are two more high-speed users moving at 33.3 m/s (120 km/h) that follow a ring road through sectors (0/0), (1/1), and (2/2), one in clockwise and one in counter-clockwise direction, respectively. Moreover, simplified *coverage holes* (in dark blue) are intentionally inserted in the depicted cell area overlaying the shadowing map (cf. Section 2.2.2) with a fix attenuation of 100 dB in order to create possibilities for KPI degradations, such as connection drops or HO failures, and

thus triggering MRO functionalities. For example, such a shadowing hole and user positions including user IDs with simulation time instances indicated as subscripts are shown in Figure 8.5(b).

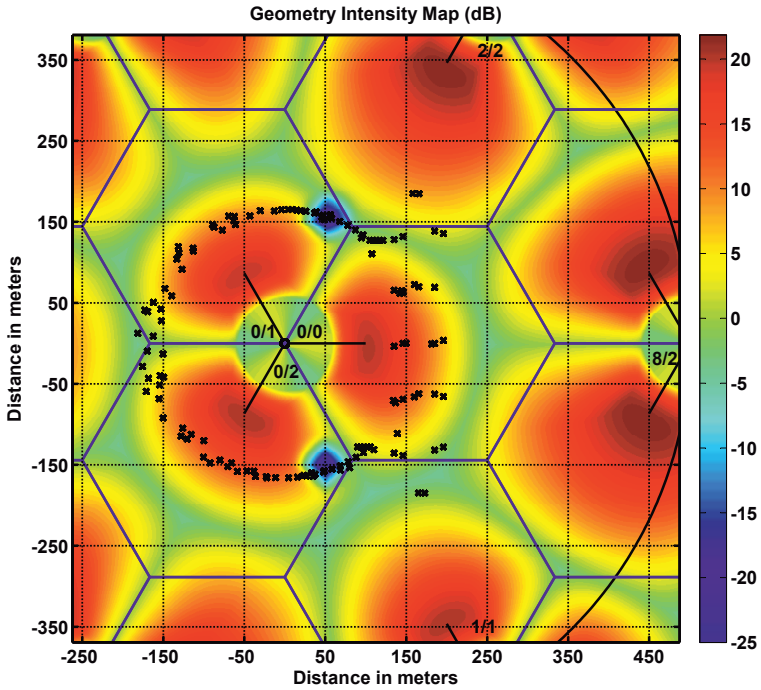

(a) Geometry intensity map and cell layout of scenario 2

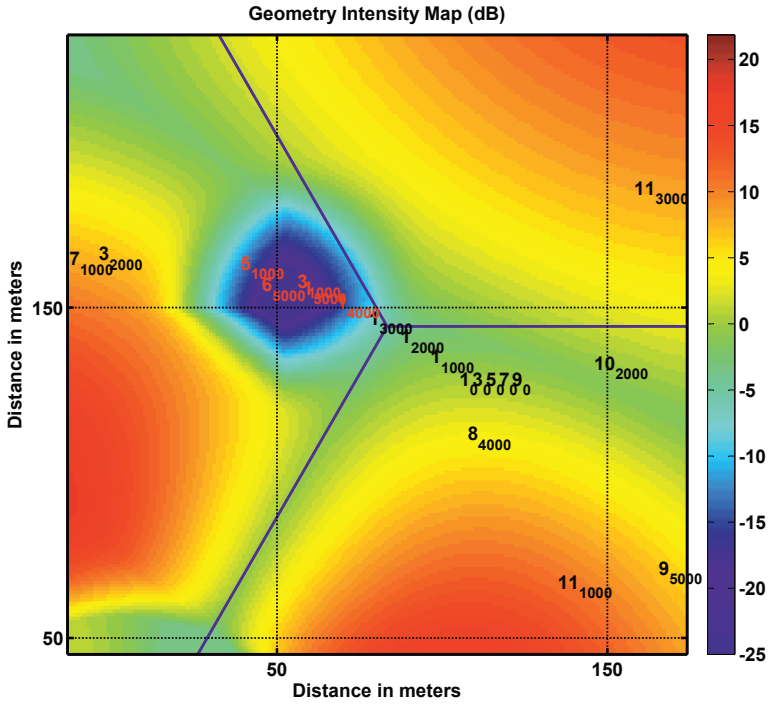

(b) Geometry intensity map and exemplary user IDs of scenario 2

Figure 8.5: Geometry intensity map, cell layout, and exemplary user IDs of scenario 2

8.2.1 Reference Simulation Results for Scenario 2

In the following, reference simulation results for all possible HYS and TTT parameter settings of all BSs where users pass through are depicted. All mobility-related KPIs are evaluated per BS. Figure 8.6 illustrates overall sums of connection drops that occurred due to RLFs or session timeouts (cf. Table 8.2).

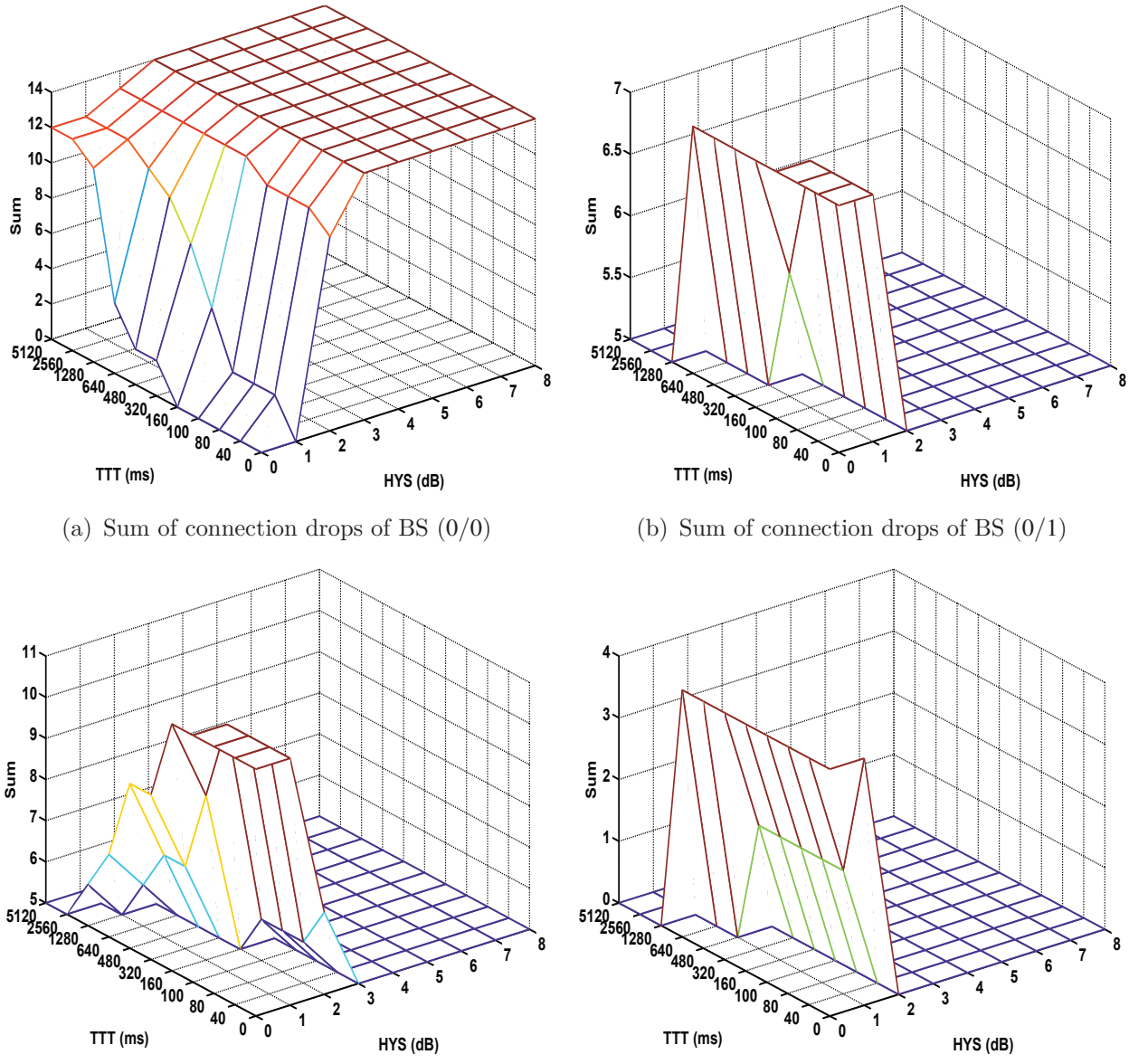

(a) Sum of connection drops of BS (0/0)

(b) Sum of connection drops of BS (0/1)

(c) Sum of connection drops of BS (0/2)

(d) Sum of connection drops of BS (2/2)

Figure 8.6: Sum of connection drops of various BSs

In contrast to BS (0/0), where high HYS and TTT values result in a high number of connection drops, the number of connection drops decreases to zero for BSs (0/1), (0/2), and (2/2), respectively. Thus, in case of BS (0/0), very low HYS and TTT values are beneficial, whereas for BSs (0/1),

(0/2), and (2/2), high HYS settings yield best performance with respect to connection drops.

In Figure 8.7, BS-specific sums of connection drops are depicted that occurred due to RLFs or session timeouts, while HO-related TTT timers of dropped UEs were already started. Here, a common behavior among those

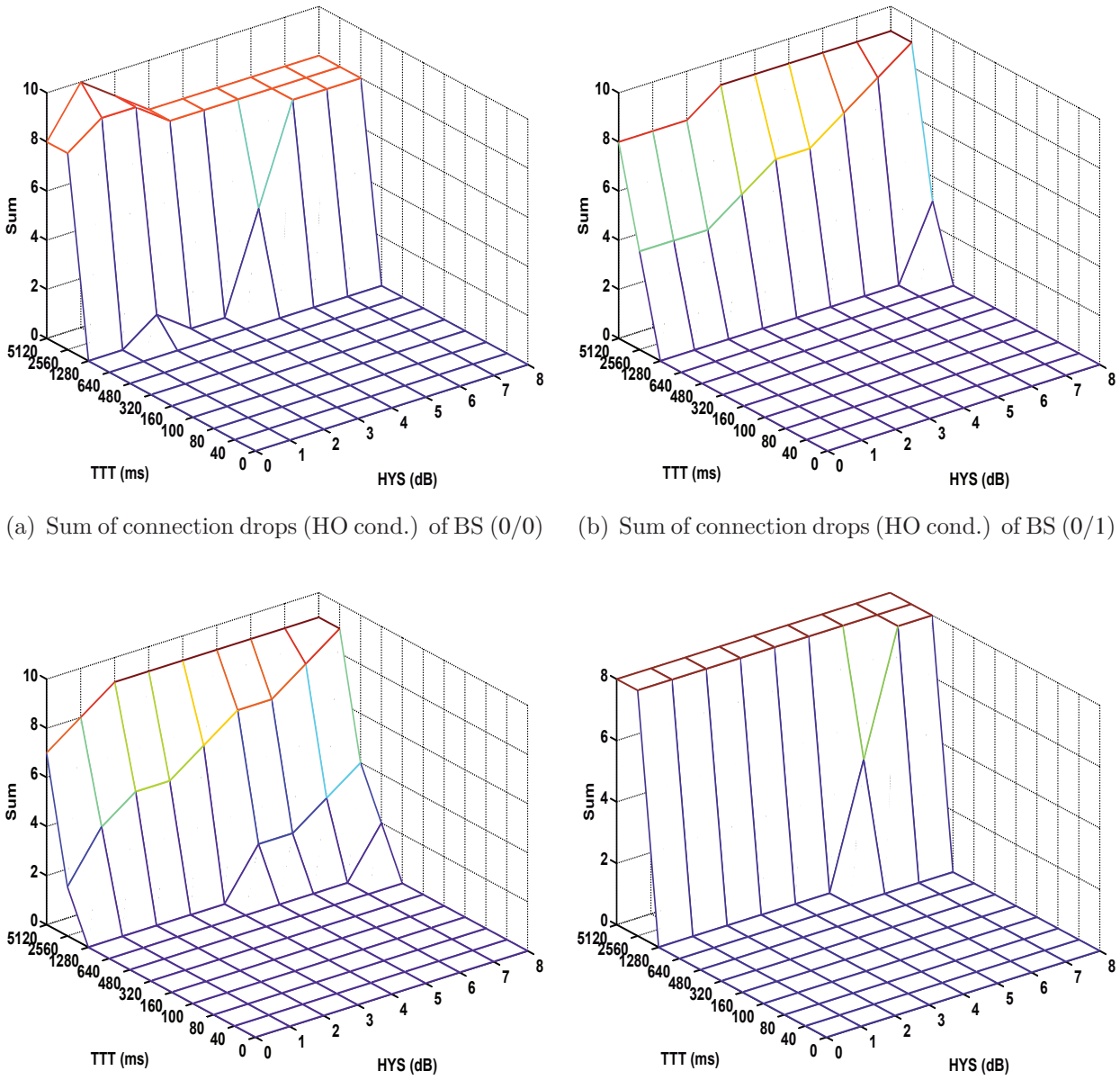

(a) Sum of connection drops (HO cond.) of BS (0/0)

(b) Sum of connection drops (HO cond.) of BS (0/1)

(c) Sum of connection drops (HO cond.) of BS (0/2)

(d) Sum of connection drops (HO cond.) of BS (2/2)

Figure 8.7: Sum of connection drops (TTT started) of various BSs

BS affected by connection drops in HO condition is observed. In order to achieve best performance, high TTT settings should be avoided, i.e., the preferable HO parameter adjustment is to lower TTT values.

In the considered scenario, HO failures are only observed in cells (0/0) and (2/2), respectively, as illustrated in Figure 8.8. In case of BS (0/0), a

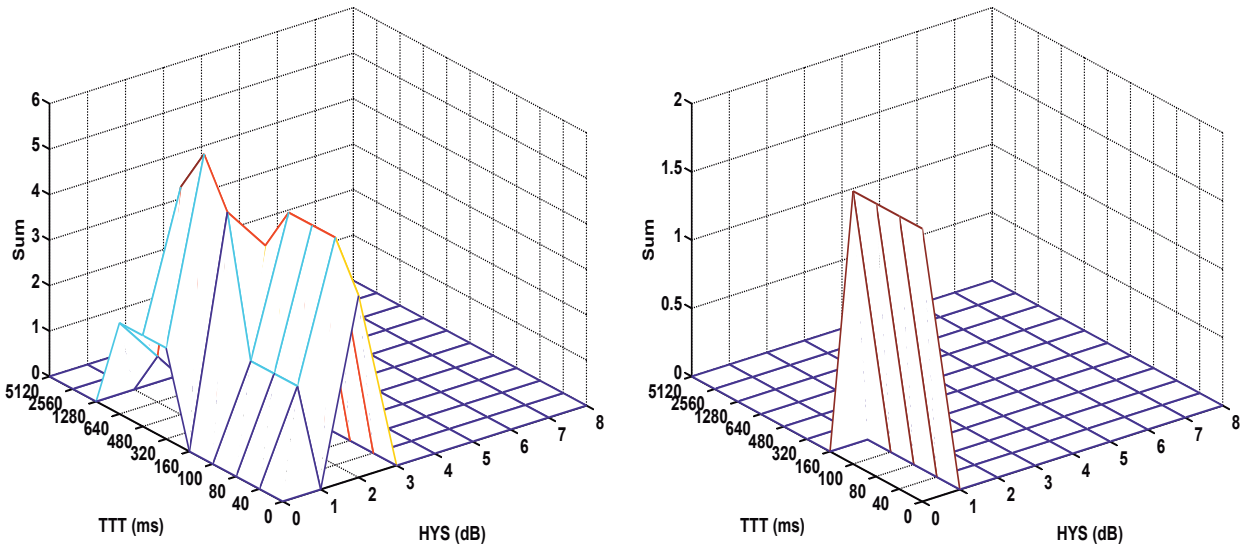

(a) Sum of failed HOs of BS (0/0)

(b) Sum of failed HOs of BS (2/2)

Figure 8.8: Sum of failed HOs of various BSs

small set of HYS values ranging from 0 to 2 dB exists, where HO failures occur for low to medium TTT values. In contrast, at BS (2/2) HO failures are only observed for HYS values of 0 dB and rather low TTT values.

Further, ping-pong HOs were found to originate only from cells (1/1) and (2/2), respectively, as depicted in Figure 8.9.

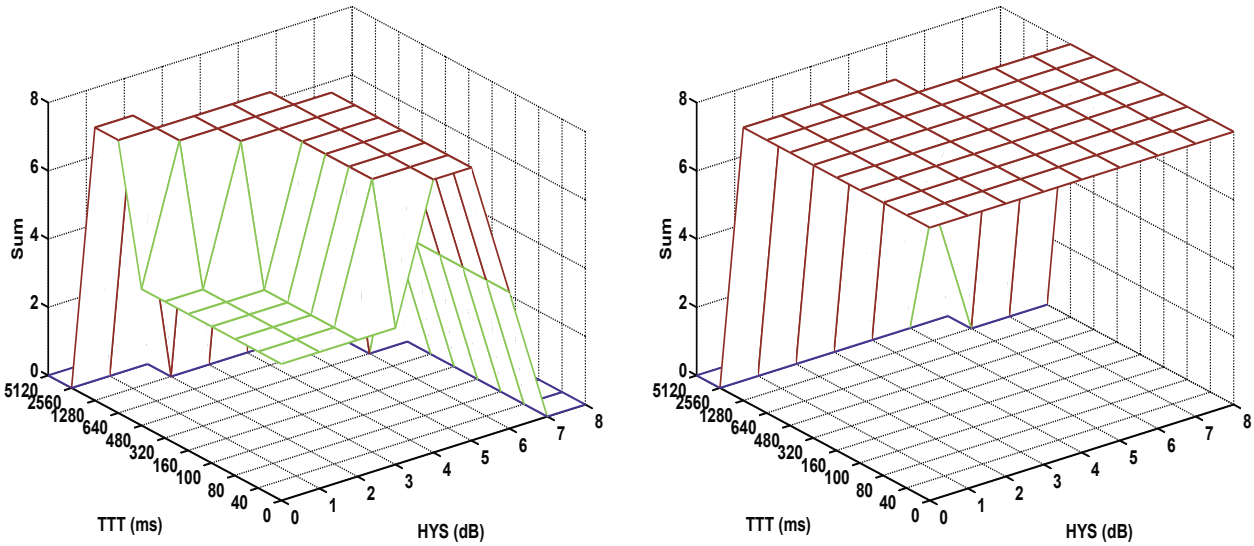

(a) Sum of ping-pong HOs of BS (1/1)

(b) Sum of ping-pong HOs of BS (2/2)

Figure 8.9: Sum of ping-pong HOs of various BSs

Here, a general observation is that low and medium HYS and TTT values yield medium to high numbers of ping-pong HOs. At BS (1/1), the number of number of ping-pong HOs can be reduced by increasing both HYS and TTT settings. For BS (2/2), only increasing TTT settings to high values, such as 2560 ms or 5120 ms, is beneficial for improving performance. These reference simulation results can be used for deriving initial HO parameter adaptation rules for all possible HYS and TTT settings.

Instead of considering the total amount of network failure events, BS-specific KPIs are illustrated in the following Figures 8.10, 8.11, and 8.12. During operation, each BS continuously monitors specified KPIs, such as CDR, HFR, and PHR, that may greatly vary due to user movements and context, e.g., user passing through coverage hole (cf. Figure 8.5(b)). Figure 8.10 depicts CDR evolution over simulation time for all considered HYS parameter values and a fix TTT setting of 160 ms. The various cell sectors $0, 1, 2$ of BS 0 observe CDR issues for the whole range of HYS settings, except BS (0/0) at HYS of 0 dB. In particular, at the beginning of considered simulation time BS (0/1) and BS (0/2) experience high CDR values. In contrast BS (2/2) is only affected by CDR issues at low HYS values of 0 and 1 dB, which is inline with results shown in Figure 8.6(d).

In Figure 8.11, HFR evolution observed at BS (0/0) is illustrated for a fix TTT setting of 160 ms. Similar to Figure 8.8(a), HFR issues are only observed for HYS values of 1 and 2 dB.

Further, PHR degradations for a fix TTT setting of 160 ms only occur at BS (1/1) and (2/2), respectively, as depicted in Figure 8.12. At BS (1/1), PHR issues are observed for HYS values up to 6 dB, whereas at BS (2/2), PHR issues occur periodically for the whole range of HYS settings. This is due to UE 10 and 11 that regularly travel on their ring road through the coverage area of BS (2/2).

These BS-specific KPI plots can be used to derive applicable KPI target threshold values. In general, rather low KPI target thresholds result in frequent checks whether HO parameter adaptations are required and may also trigger corresponding actions. In contrast, rather high KPI target thresholds might yield less HO parameter adaptations, but at the cost of degraded system performance. In this thesis, it is assumed that KPI target thresholds are provided by a MNO policy. However, these KPI target thresholds may not be met by all BS agents during learning due to local conditions, e.g., dimension of coverage hole located in service area of corresponding BS.

In order to evaluate the impact of UE-specific velocities on mobility-related KPIs, reference simulation results per UE are illustrated in the follow-

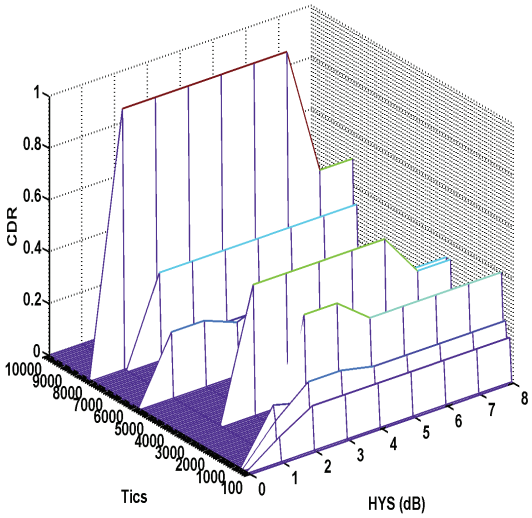

(a) Connection dropping ratio of BS (0/0) (TTT: 160 ms)

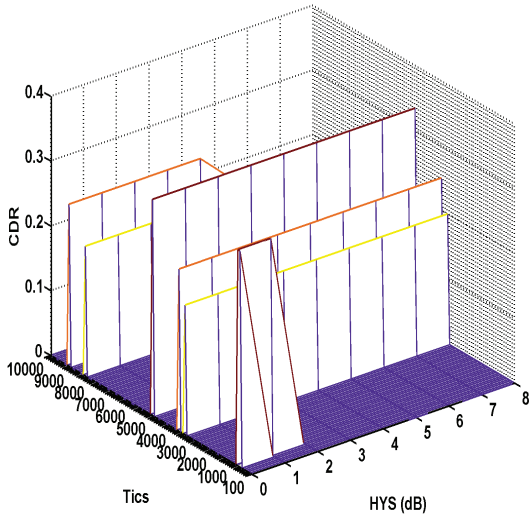

(b) Connection dropping ratio of BS (0/1) (TTT: 160 ms)

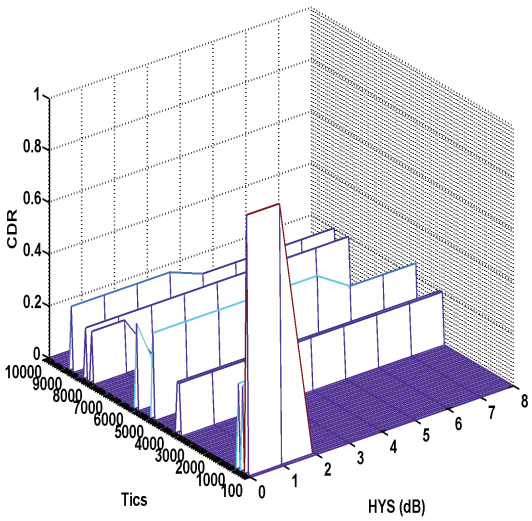

(c) Connection dropping ratio of BS (0/2) (TTT: 160 ms)

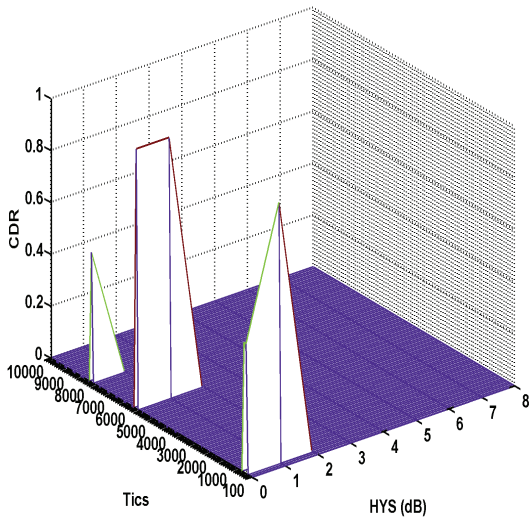

(d) Connection dropping ratio of BS (2/2) (TTT: 160 ms)

Figure 8.10: Connection dropping ratio of various BSs

ing figures. Figure 8.13 depicts the sum of connection drops that occurred due to RLFs or session timeouts (cf. Table 8.2). Here, only slow moving users at 4 km/h were found to face dropping events due to RLF or session timeouts.

The fact that UE 0 experiences less connection drops at low HYS values indicates that receive conditions during simulations are not perfectly symmetric. UE 0 and UE 1 travel around BS 0 on circular paths in clockwise and counter-clockwise direction, respectively.

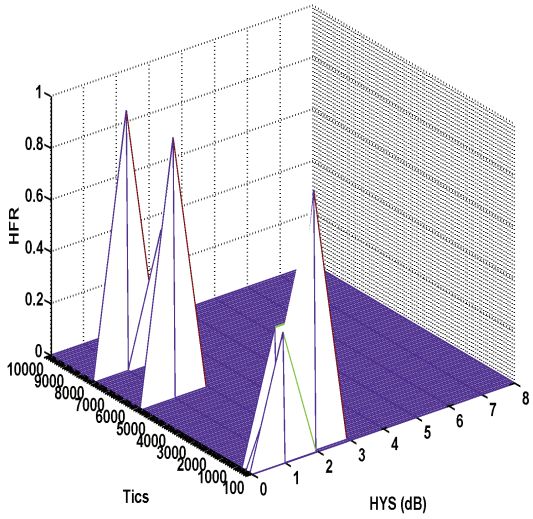

Figure 8.11: HO failure ratio of BS (0/0) (TTT: 160 ms)

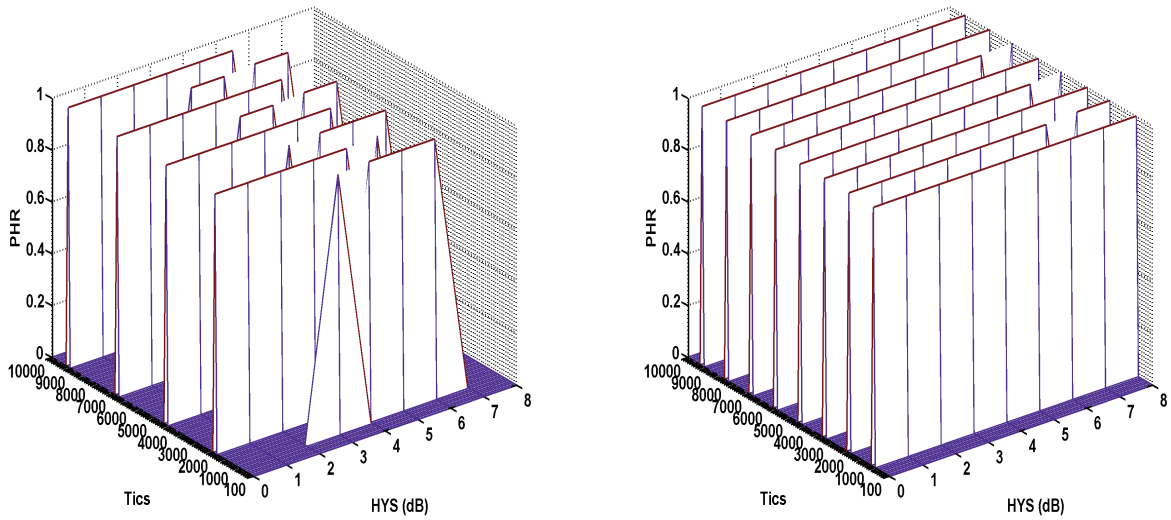

(a) Ping-pong HO ratio of BS (1/1) (TTT: 160 ms) (b) Ping-pong HO ratio of BS (2/2) (TTT: 160 ms)

Figure 8.12: Ping-pong HO ratio of various BSs

Further, for each user of all velocity classes ranging from 1.1 to 33.3 m/s (4 to 120 km/h) there exists a Handover Operating Point (HOP) constellation where the UE is at least once dropped due to RLFs or session timeouts, while HO-related TTT timers were already started. Figure 8.14 and Figure 8.15, respectively, illustrate overall sums of connection drops for each UE with activated HO condition. UEs 0 and 1 moving at pedestrian speed only experience connection drops for low HYS and medium to high TTT values, whereas connection drops for UEs 2 and 3 only occur at high TTT values

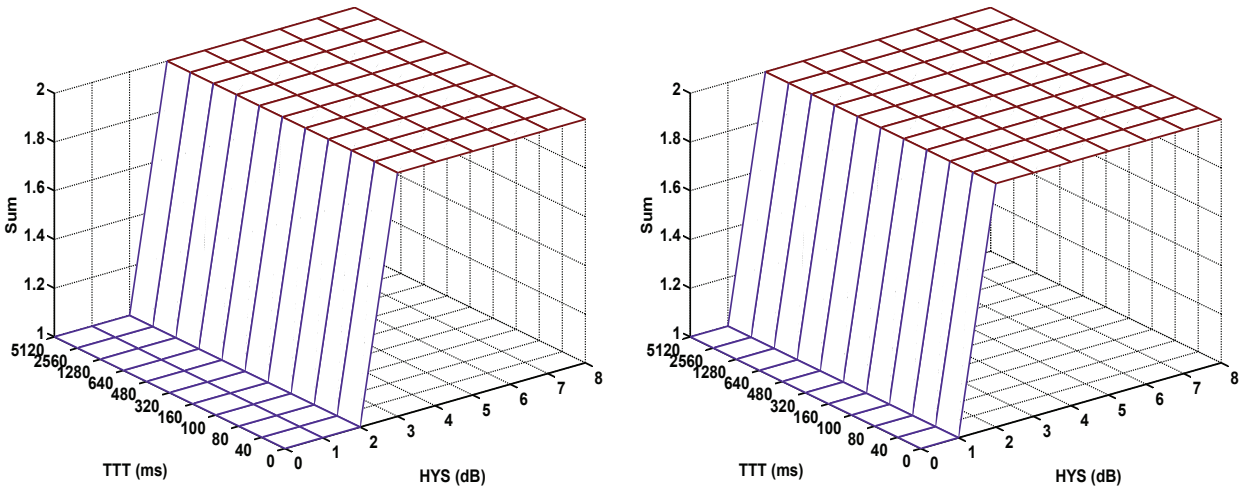

(a) Sum of connection drops of UE 0 ($v = 1.1$ m/s) (b) Sum of connection drops of UE 1 ($v = 1.1$ m/s)

Figure 8.13: Sum of connection drops of various UEs

and medium to high HYS settings.

A general observation from Figure 8.14 and Figure 8.15, respectively, is that with decreasing TTT values the sum of connection drops decreases to zero. Further, the absolute number of dropped connections for high TTT values of 5120 ms doubles with increasing velocities. For example, connection drops of UEs 6 and 7 (cf. Figures 8.15(a) and 8.15(b)), 8 and 9 (cf. Figures 8.15(c) and 8.15(d)), and 10 and 11 (cf. Figures 8.15(e) and 8.15(f)) increase from 2, to 4, to 8, respectively.

In Figure 8.16 and Figure 8.17, the overall sums of HO failures are illustrated. The main finding is that HO failures preferably occur at low HYS values of 1 and 2 dB and medium to low TTT settings.

Further, for users traveling at increased velocities, e.g., UE 4, 6, and 8 moving at 8.3, 13.9 and 19.4 m/s (30, 50, and 70 km/h), respectively, HO failures arise for a broad range of TTT values. This indicates that for reducing overall number of HO failures the HYS parameter should be preferably increased.

Figure 8.18 depicts overall sums of ping-pong HOs that are only experienced by the two high-speed users UE 10 and 11, respectively, moving at 33.3 m/s (120 km/h). These users follow a pre-defined ring road through sectors (0/0), (1/1), and (2/2), in clockwise and counter-clockwise direction, respectively.

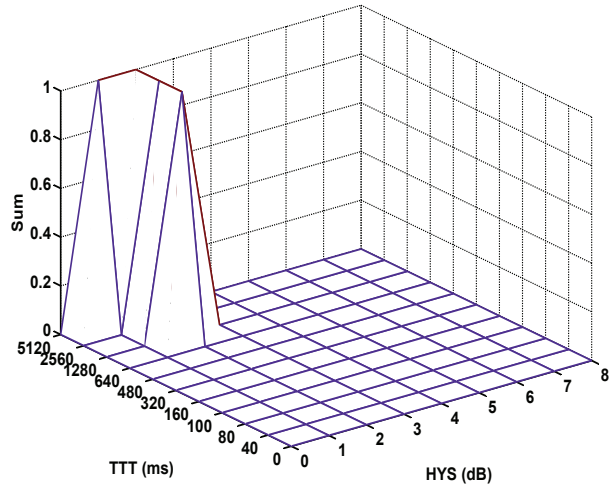

(a) Sum of connection drops of UE 0 ($v = 1.1$ m/s, HO cond.)

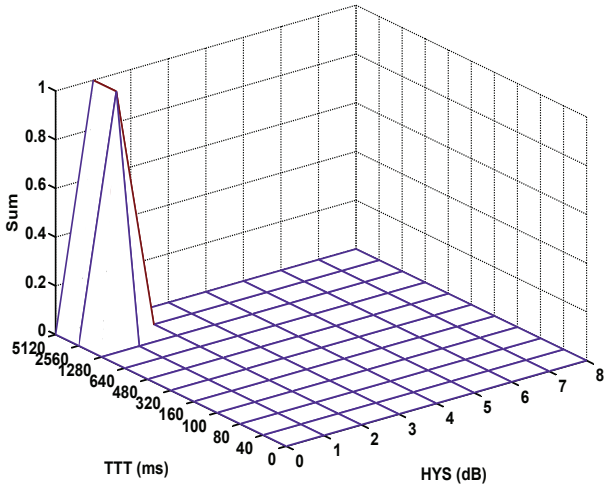

(b) Sum of connection drops of UE 1 ($v = 1.1$ m/s, HO cond.)

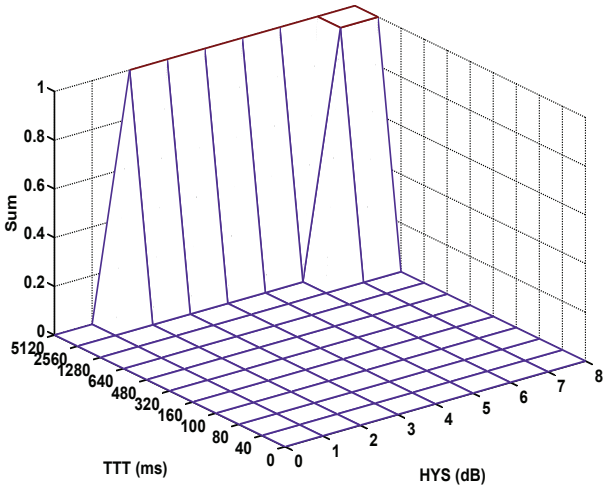

(c) Sum of connection drops of UE 2 ($v = 6.1$ m/s, HO cond.)

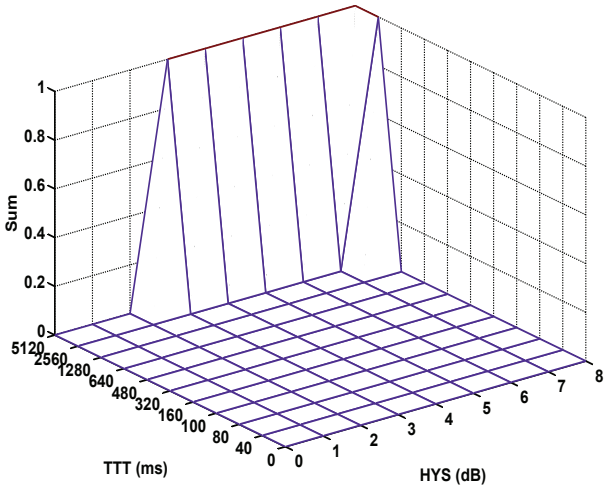

(d) Sum of connection drops of UE 3 ($v = 6.1$ m/s, HO cond.)

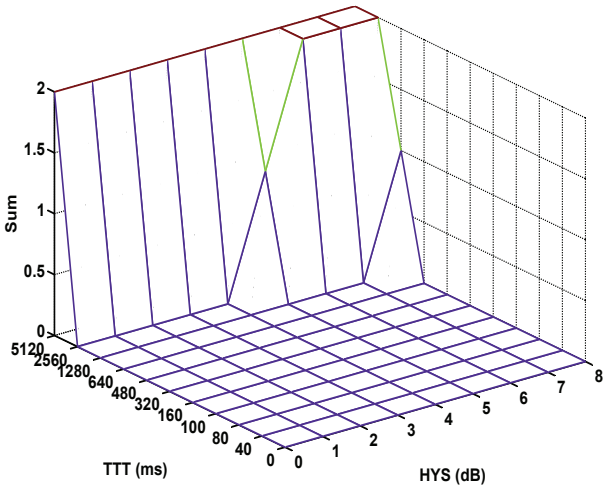

(e) Sum of connection drops of UE 4 ($v = 8.3$ m/s, HO cond.)

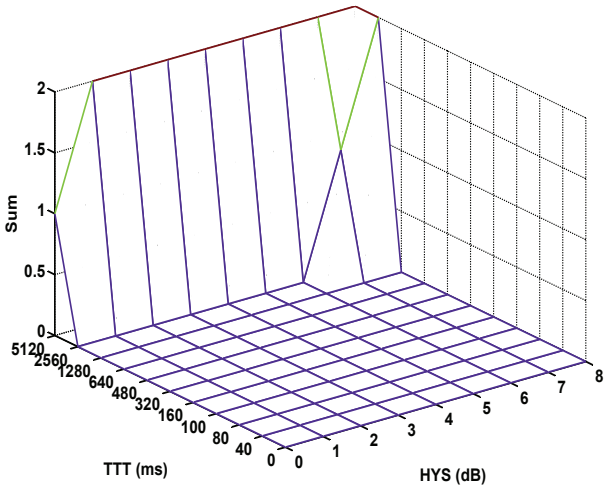

(f) Sum of connection drops of UE 5 ($v = 8.3$ m/s, HO cond.)

Figure 8.14: Sum of connection drops of various UEs (HO cond.)

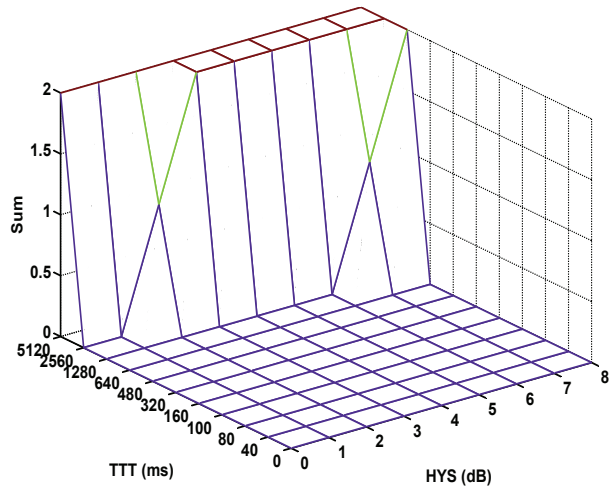

(a) Sum of connection drops of UE 6 ($v = 13.9$ m/s, HO cond.)

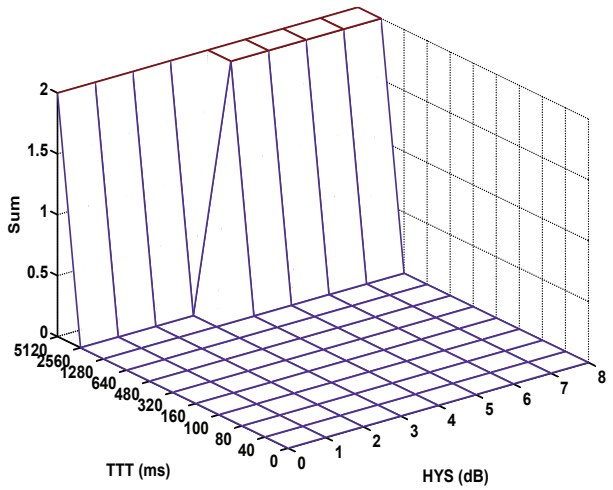

(b) Sum of connection drops of UE 7 ($v = 13.9$ m/s, HO cond.)

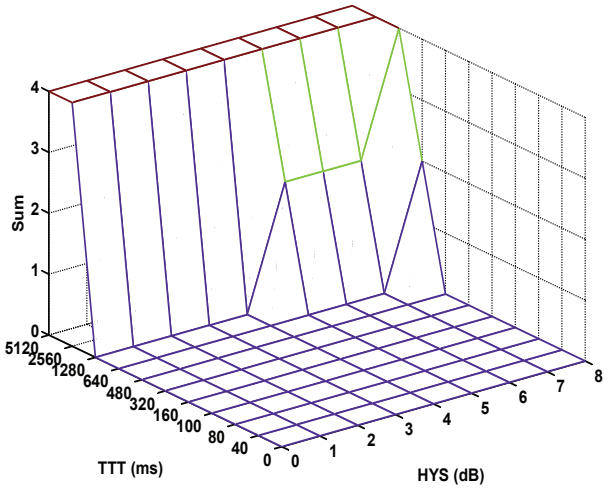

(c) Sum of connection drops of UE 8 ($v = 19.4$ m/s, HO cond.)

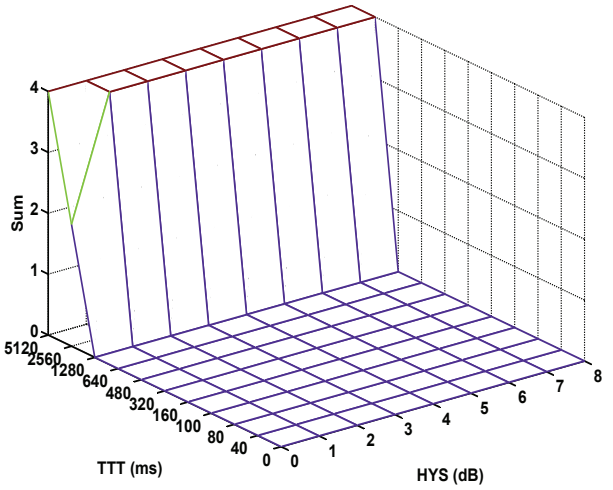

(d) Sum of connection drops of UE 9 ($v = 19.4$ m/s, HO cond.)

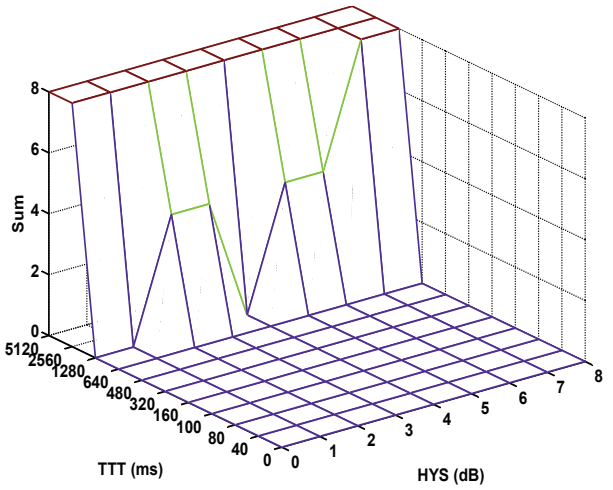

(e) Sum of connection drops of UE 10 ($v = 33.3$ m/s, HO cond.)

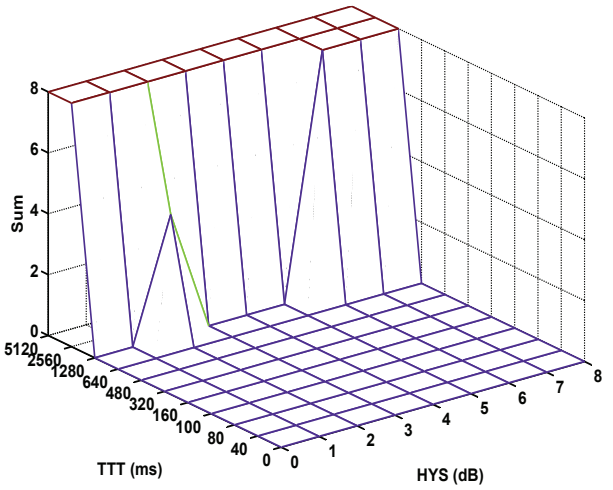

(f) Sum of connection drops of UE 11 ($v = 33.3$ m/s, HO cond.)

Figure 8.15: Sum of connection drops of various UEs (HO cond.)

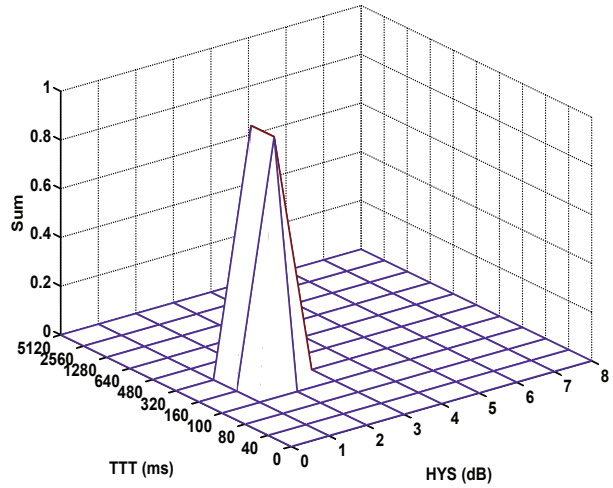

(a) Sum of HO failures of UE 2 ($v = 6.1$ m/s)

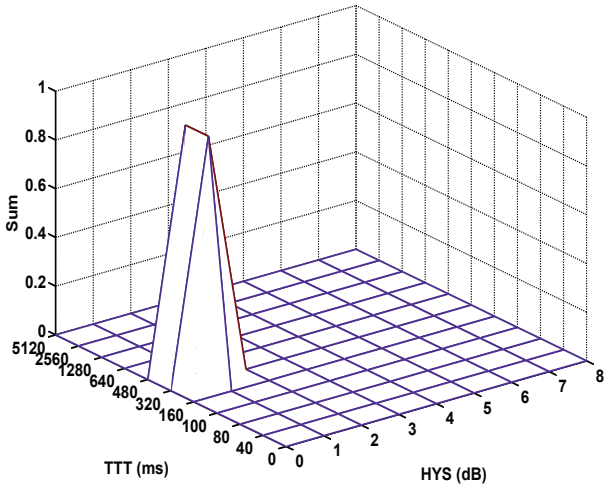

(b) Sum of HO failures for UE 3 ($v = 6.1$ m/s)

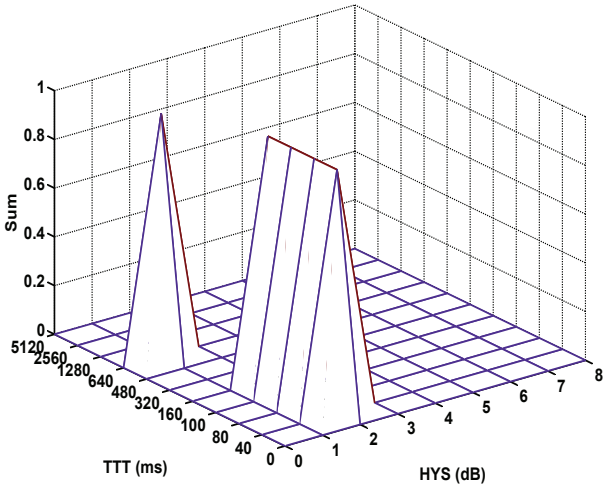

(c) Sum of HO failures of UE 4 ($v = 8.3$ m/s)

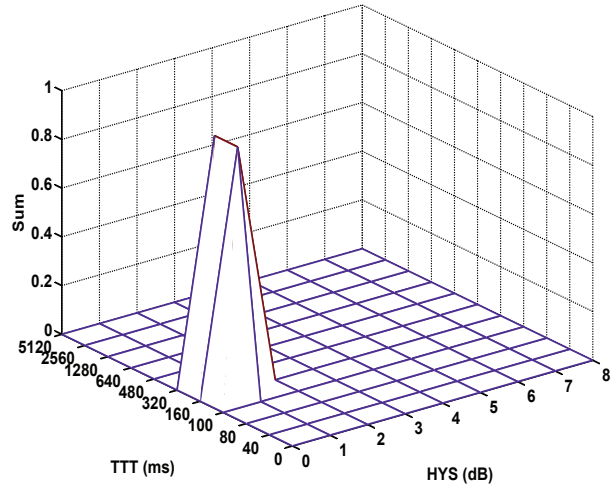

(d) Sum of HO failures of UE 5 ($v = 8.3$ m/s)

Figure 8.16: Sum of HO failures of various UEs

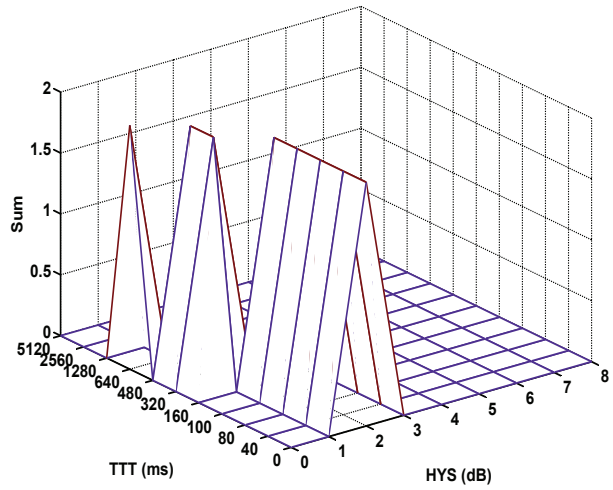

(a) Sum of HO failures of UE 6 ($v = 13.9$ m/s)

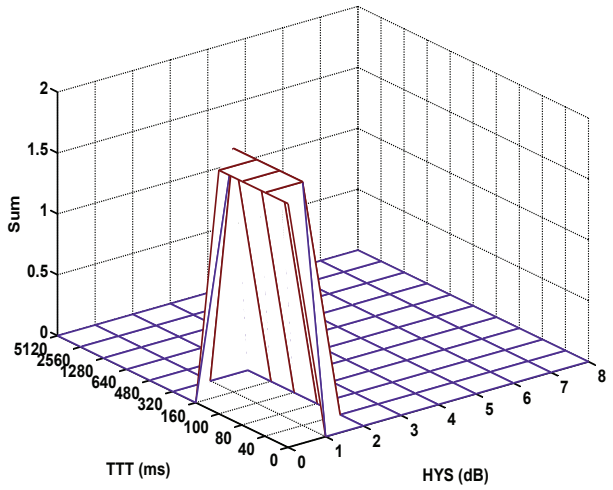

(b) Sum of HO failures of UE 7 ($v = 13.9$ m/s)

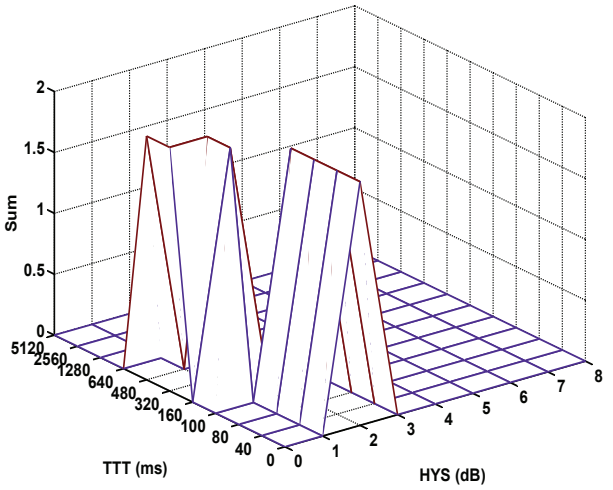

(c) Sum of HO failures of UE 8 ($v = 19.4$ m/s)

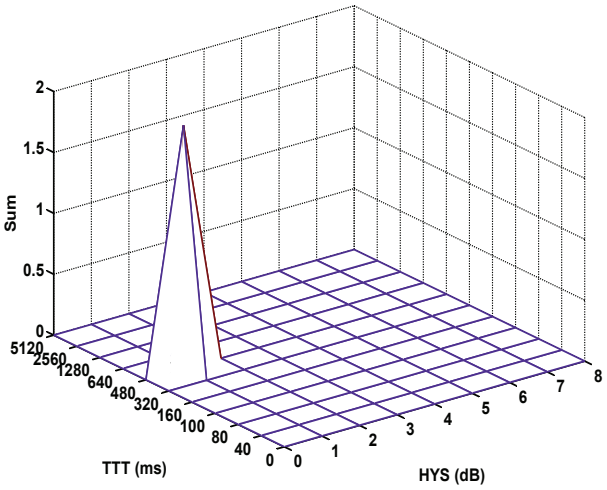

(d) Sum of HO failures of UE 9 ($v = 19.4$ m/s)

Figure 8.17: Sum of HO failures of various UEs

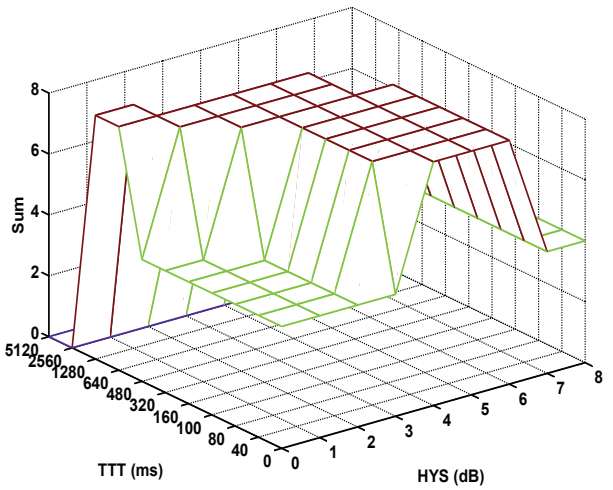

(a) Sum of ping-pong HOs of UE 10 ($v = 33.3$ m/s)

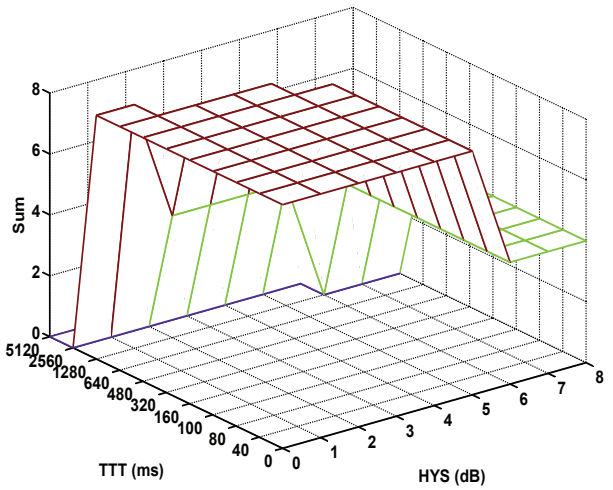

(b) Sum of ping-pong HOs of UE 11 ($v = 33.3$ m/s)

Figure 8.18: Sum of ping-pong HOs of various UEs

8.2.2 Fuzzy Q-Learning Configuration

In order to increase the possibilities of selecting appropriate countermeasures given observed, significant KPI degradations, the initial fuzzy classification scheme for KPI deviations, illustrated in Figure 8.19(a), is extended in the following way: more fuzzy labels are introduced in order to account for higher and thus more severe KPI degradations. Two extended fuzzy classification schemes and their corresponding membership functions are illustrated in Figure 8.19(b) and Figure 8.19(c), respectively. The first set of membership functions depicted in Figure 8.19(b) applies 5 fuzzy sets for assessing KPI deviations, whereas the second scheme uses 10 fuzzy labels for classifying relative KPI deviations, as illustrated in Figure 8.19(c).

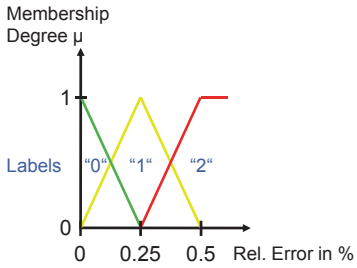

(a) 3-label membership functions for assessing relative KPI deviation

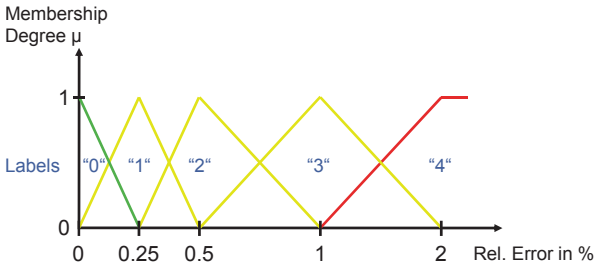

(b) 5-label membership functions for assessing relative KPI deviation

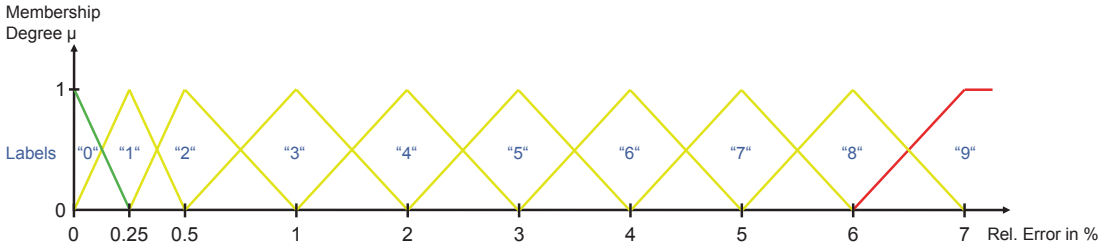

(c) 10-label membership functions for assessing relative KPI deviation

Figure 8.19: Extended membership functions for assessing relative KPI deviation

Of course, a higher number of KPI labels has a direct impact on the number of system states and thus on the required time for learning most effective HO parameter adaptations. In the following Figure 8.20(a) and Figure 8.20(b), the exemplary evolution of learning behavior over simulation runs and the finally obtained rule/action-specific Q values of BS (2/2) (cf. Figure 8.5(a)), respectively, are depicted. Here, it is assumed that learning, i.e., updating Q values, is based on Equation (7.21). Further, the learning rate $\kappa(i,j)$ is initially set to 1 and decreases each time the corresponding rule/action pair (i,k) is visited, i.e., $\kappa(i,k) = \kappa \frac{1}{n(i,k)}$, where $n(i,k) = 1,2,3,\ldots$

is the number of occurrences where rule i is activated and action k is applied. Convergence of the learning process is obtained as soon as ΔQ (cf. Equation (7.17)) lies within the area of convergence, i.e., $\theta_c = \pm 0.01$.

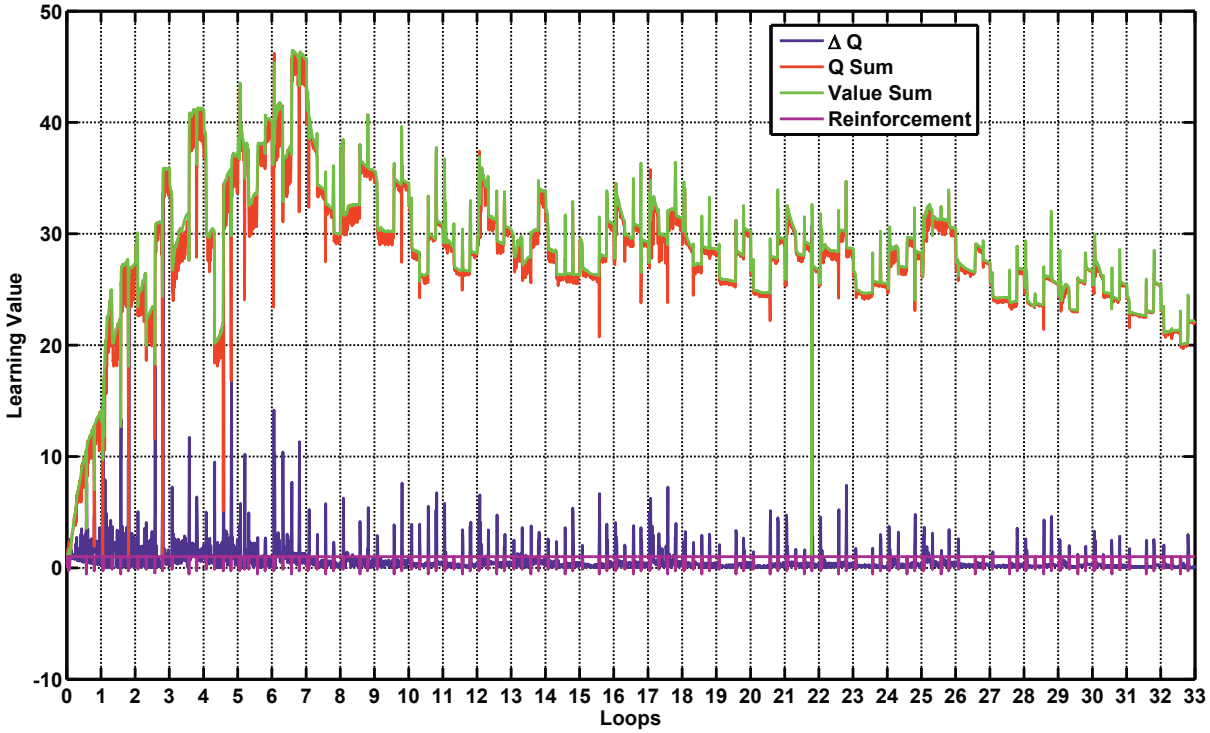

(a) Learning value evolution of BS (2/2)

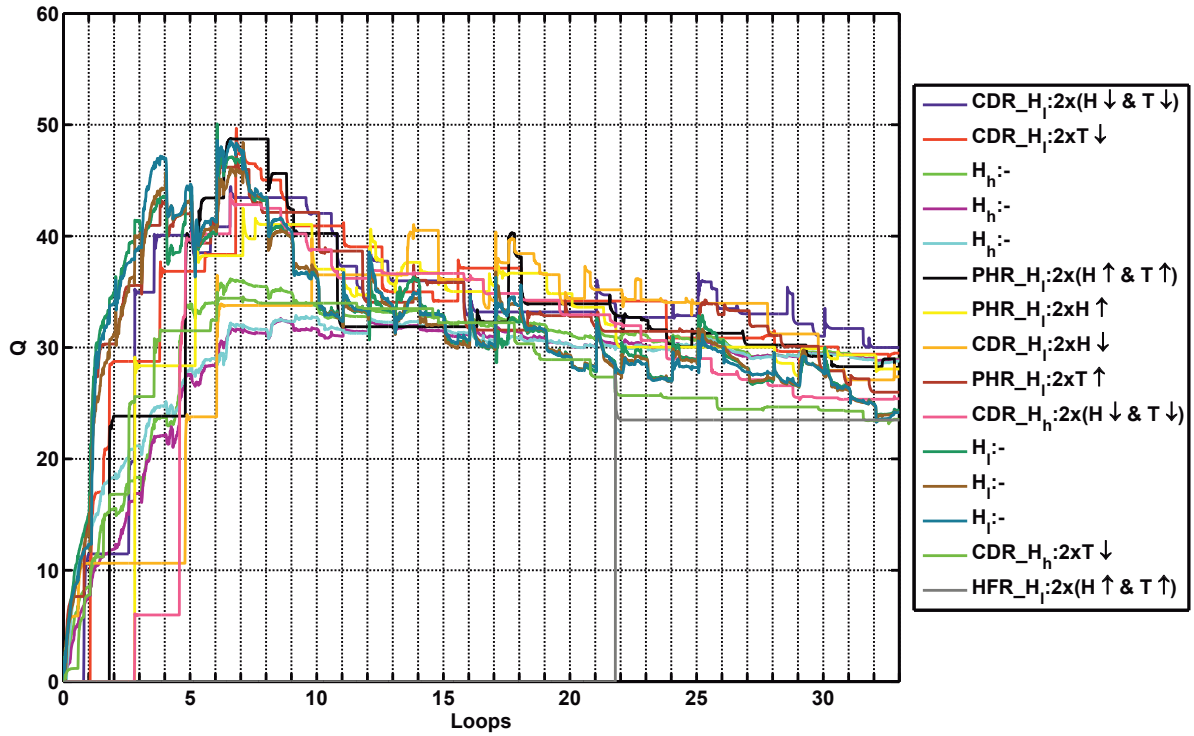

(b) Q value evolution of BS (2/2)

Figure 8.20: Exemplary learning and Q value evolution of BS (2/2) vs. simulation runs

For example, BS (2/2) is mainly facing connection dropping and ping-pong HO issues at the considered HOP (HYS=1 dB, TTT=160 ms, cf. Figure 8.10(d) and Figure 8.12(b)). The legend of Figure 8.20(b) lists finally learned, situation-specific adaptation rules in decreasing order of Q values. Highest Q values that are obtained after learning process has converged indicate to jointly decrease HYS and TTT parameters by 2 steps in case of high CDR (cf. blue curve in Figure 8.20(b)). For high PHR, increasing both HYS and TTT parameters by 2 steps are the best performing actions (cf. black curves in Figure 8.20(b)).

Moreover, a higher granularity in system states has also been in the focus of evaluation. Therefore, several HO parameters were considered for system state classification and used in the afore mentioned FQL based MRO schemes. In the following, the considered HO parameters for system state assessment are listed:

- cell-specific HYS parameter,
- cell-specific HYS and TTT parameters,
- cell-specific HYS and CIO (O_s, cf. Equation (3.1)) parameters are summed to generate a cell-specific HOM parameter, which is considered in combination with the cell-specific TTT parameter.

Figure 8.21 illustrates the different fuzzy input membership functions used for classifying HYS, TTT, and HOM parameters. HYS values can range from 0 to 10 dB, TTT settings are selected from the following set of timer values $\{0, 0.04, 0.08, 0.1, 0.16, 0.32, 0.48, 0.64, 1.280, 2.560, 5.120\}$ in seconds, and the O_s values can vary from -10 to $+10$ dB, thus leading to HOM values ranging from -10 to $+20$ dB.

Regarding TTT parameter adaptations, two different schemes are implemented: TTT settings are either proportionally or discretely adapted. These schemes are referred to as *TP* and *TD*, respectively. In case of proportional TTT parameter adaptation (*TP*), the current TTT value is multiplied with the respective FIS output (y_{TTT}). The resulting TTT value after multiplication is "quantized" and the TTT value is set to the nearest neighbor value given the set of available TTT values. An excerpt of the applied quantization scheme is exemplarily depicted in Figure 8.22. In case of discrete TTT parameter adaptation (*TD*), the current TTT value is step-wise adapted according to the FIS output (y_{TTT}). Step-wise TTT adaptations are restricted by the set of available TTT values, e.g., $\{0, 40, 80, 100, 160, 320, 480, 640, 1280, 2560, 5120\}$ ms.

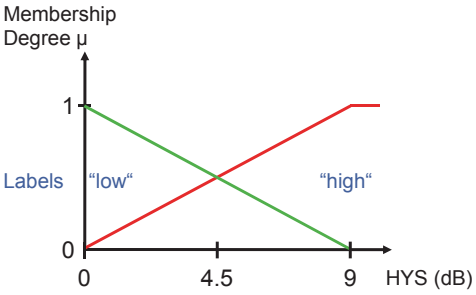

(a) Input membership functions for assessing HYS state

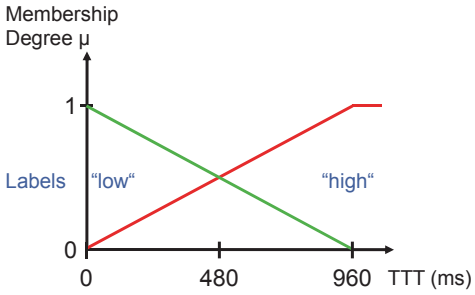

(b) Input membership functions for assessing TTT state

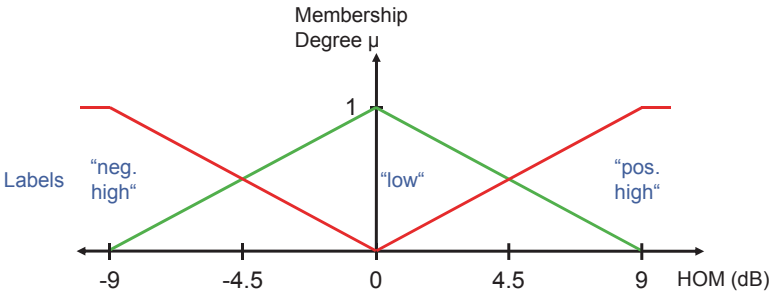

(c) Input membership functions for assessing HOM state

Figure 8.21: Input membership functions for assessing HO parameter states

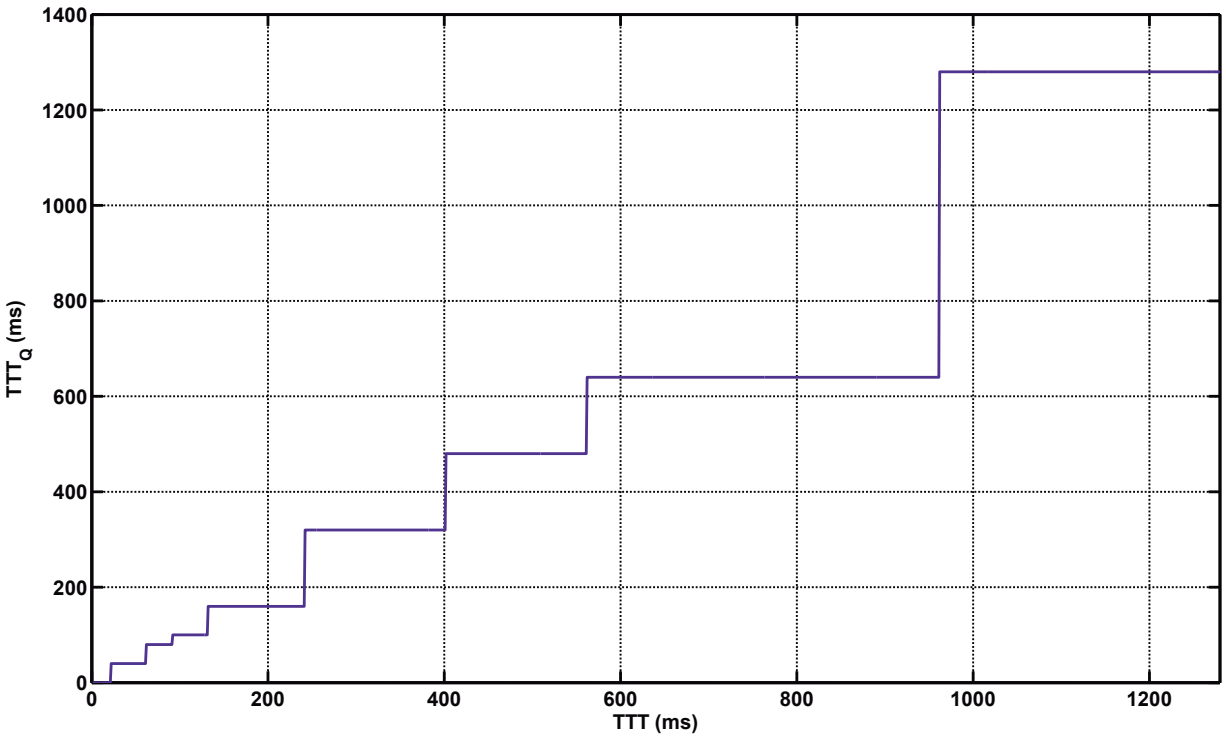

Figure 8.22: TTT value quantization

For example, Figures 8.6, 8.7, 8.8, and 8.9, respectively, show reference performance results of major KPIs, such as CDR, HFR, and PHR, for all possible HYS and TTT parameter constellations.

In Figures 8.23, 8.24, 8.25, and 8.26, the impact of increasing fuzzy classification granularity on learning behavior by extending the set of fuzzy labels from 3, 5 to 10 labels and considering different input membership functions for assessing HO parameter states as well as proportional (*TP*) and discrete (*TD*) TTT parameter adaptation modes is illustrated. For system state classification, cell-specific HYS (*H*), joint HYS and TTT (*HT*), and joint HOM and TTT (*MT*) parameter adaptations were considered.

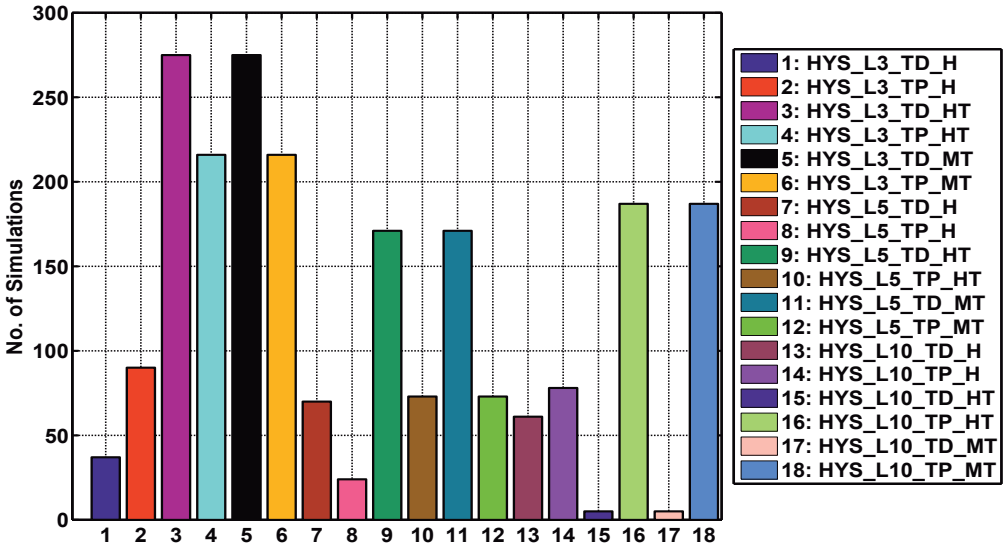

Figure 8.23: Number of simulation runs for different *FQL_HYS* based MRO schemes

In case of *FQL_HYS* based schemes that only tune HYS and TTT parameters in a cell-specific manner depicted in Figure 8.23, the system parameter classification approach as well as the TTT adaptation mode have an impact on learning speed. For all considered numbers of fuzzy labels, the number of required simulation runs for *HT* and *MT* based schemes is identical for specific TTT adaptation modes, e.g., *HYS_L3_TD_HT* and *HYS_L3_TD_MT*, *HYS_L5_TP_HT* and *HYS_L5_TP_MT*, or *HYS_L10_TD_HT* and *HYS_L10_TD_MT*. In case 3, 5, or 10 fuzzy labels are considered for system state classification, the least number of simulation runs are required for *HYS_L3_TD_H*, *HYS_L5_TP_H*, or *HYS_L10_TD_HT* and *HYS_L10_TD_MT*, respectively, where the last two schemes require only 5 simulation runs, which is the least number of runs among all considered MRO schemes.

FQL_CIO based schemes tune TTT parameters in a cell-specific and CIO

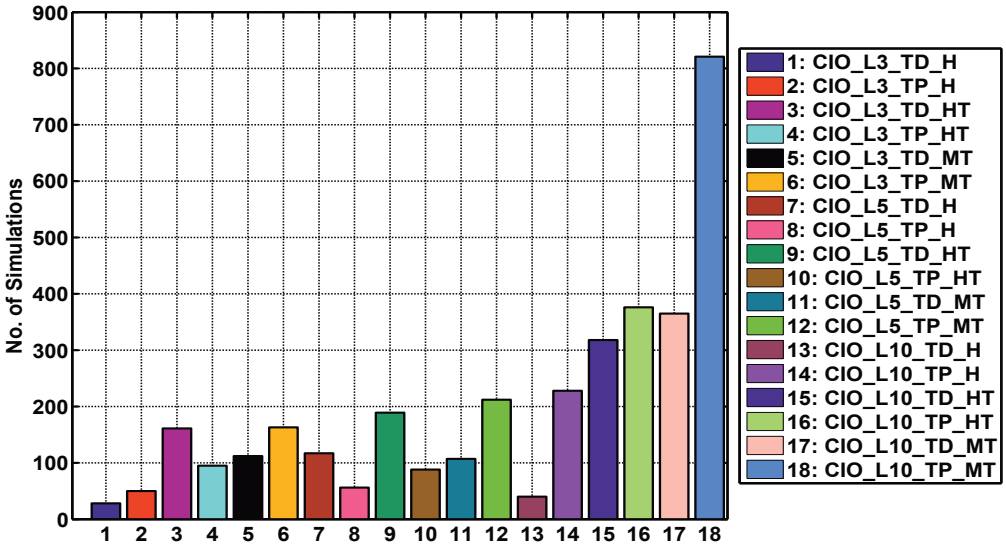

Figure 8.24: Number of simulation runs for different *FQL_CIO* based MRO schemes

(O_t) parameters of neighboring cells in a cell pair-specific manner. Only if no neighboring BS is identified as origin of performance degradation, cell-specific HYS parameters are adapted. For *FQL_CIO*, the required number of simulation runs is illustrated in Figure 8.24. Here, the number of required simulation runs increases with higher granularity in terms of system state classification for *TP* based approaches as well as for 10 fuzzy labels in case of *TD* based schemes. Earliest learning process convergence is observed for *CIO_L3_TD_H*, where 28 simulation runs are required.

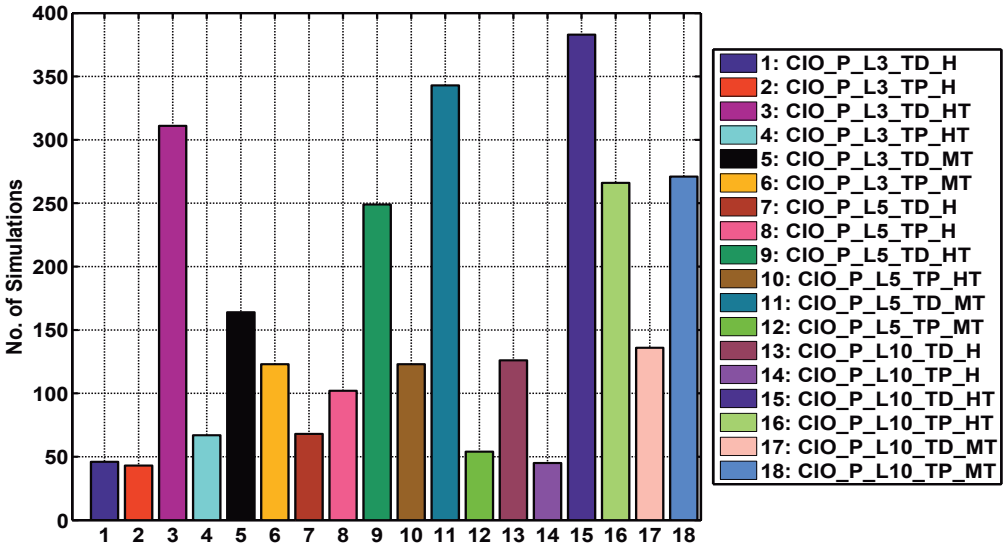

Figure 8.25: Number of simulation runs for different *FQL_CIO_P* based MRO schemes

In case of *FQL_CIO_P* based schemes, which are depicted in Figure 8.25 and that tune TTT parameters in a cell-specific and CIO (O_s and O_t, cf.

Equation (3.1)) parameters jointly in a cell pair-specific manner, *CIO_P_L3_TP_H* requires 43 and thus least number of simulations runs among *FQL_CIO_P* based schemes. In particular, the *CIO_P* based scheme that employs HYS and TTT parameters for system state classification (*HT*) and discretely adapts TTT parameters (*TD*) results in significantly increased simulation efforts. Only *CIO_P_L5_TD_MT* requires a similar high number of simulation runs.

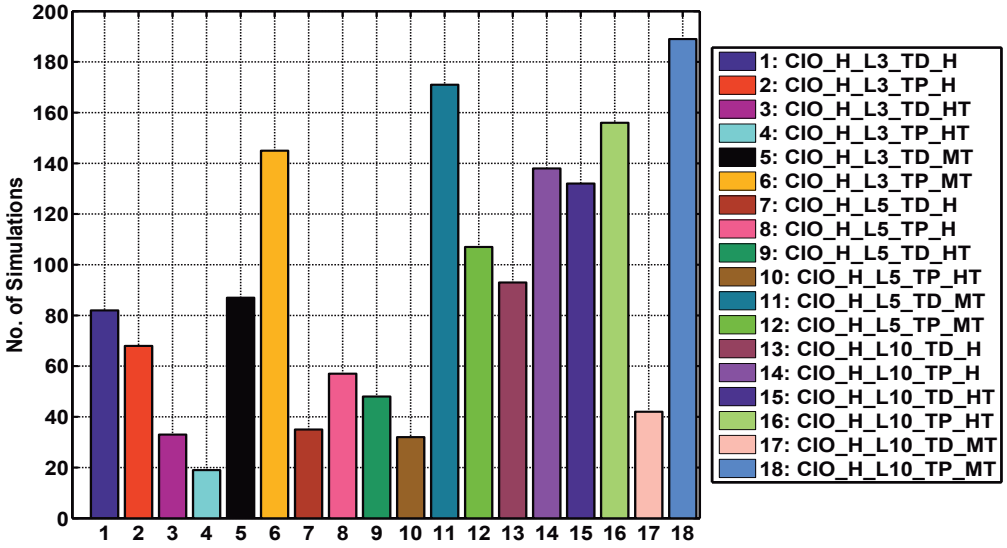

Figure 8.26: Number of simulation runs for different *FQL_CIO_H* based MRO schemes

For *FQL_CIO_H* based schemes that tune TTT parameters in a cell-specific as well as HYS and CIO (O_t) parameters of considered and neighboring cells jointly in a cell pair-specific manner, the number of simulation runs is illustrated in Figure 8.26. Here, no consistent trend among the approaches applying 3, 5, or 10 fuzzy labels for KPI classification can be observed. If 3 fuzzy labels are considered for KPI classification, fewest simulation efforts are to be spent for schemes that employ HYS and TTT parameters for system state classification (*HT*). In particular, *CIO_H_L3_TP_HT* requires only 19 simulation runs and thus the least number of simulation runs among the *FQL_CIO_H* based schemes. In case 5 fuzzy labels are used for KPI classification, the number of simulation runs increases with a higher granularity in system state classification among those schemes that apply the same TTT parameter adaptation mode. The only exception is *CIO_H_L5_TP_HT*, which requires least simulation efforts among the 5-label schemes illustrated in Figure 8.26. Similarly, simulation efforts grow with a higher granularity in system state classification among those schemes that use 10 fuzzy labels for KPI classification and apply the same TTT parameter adapta-

tion mode, as shown in Figure 8.26. However, here, the only exception is *CIO_H_L10_TD_MT*, which requires the least number of simulation runs among those schemes that use 10 fuzzy labels for KPI classification.

In essence, schemes tuning HYS or jointly HYS and CIO (O_t) parameters, respectively, such as *FQL_HYS*, *FQL_CIO_H*, and *FQL_CIO*, require less learning efforts than those schemes not adapting HYS parameter for MRO. Further, using 10 fuzzy labels for KPI classification and considering HYS or HOM and TTT parameters for system classification has shown to result in least number of simulation runs (cf. *HYS_L10_TD_HT* and *HYS_L10_TD_MT*). However, approaches accounting for neighborhood relations when adapting HO parameters are able to converge relatively fast using only 3 fuzzy labels for KPI classification, e.g., *CIO_L3_TD_H*, *CIO_P_L3_TP_H*, or *CIO_H_L3_TP_HT*.

It should be noted that the learning process is based on a limited EEP, i.e., for each FIS rule there is only a limited set of possible actions that can be selected. Further, a certain weighting of rule consequents, i.e., recommended actions, is performed by multiplying the magnitude of the selected action by the corresponding fuzzy label, which indicates the degree of KPI degradation (cf. Figure 8.19). For example, if 10 fuzzy labels are used for KPI classification and label 9 is activated due to bad HFR performance, the magnitude of the selected action, e.g., jointly increase HYS and TTT parameters, is multiplied by 9. Since the step size of HYS adaptations is 0.5 dB, the HYS parameter would be increased by 4.5 dB. Similarly, the TTT parameter is proportionally adjusted in case of *TP*. However, since TTT values can only be chosen from the discrete set of $\{0, 40, 80, 100, 160, 320, 480, 640, 1280, 2560, 5120\}$ ms, the resulting TTT magnitude after multiplication is quantized (cf. Figure 8.22) and the TTT value is set to the nearest neighbor value. For *TD* schemes, TTT parameters are adapted in discrete steps according to the available set of discrete TTT values.

8.2.3 Overall Performance Indicator

In the following subsections, the different HO parameter tuning schemes (*FQL_HYS*, *FQL_CIO*, *FQL_CIO _P*, *FQL_CIO_H*) are evaluated with respect to mobility-related events and KPIs. Two BSs, (0/0) and (2/2) (cf. Figure 8.5(a)), are selected as candidates for applying FQL based MRO and performing HO parameter adaptations according to locally observed conditions, since they exhibit severe KPI degradations in terms of CDR, HFR, and PHR (cf. Section 8.2.1). According to Equation (8.3), a weighted sum

of mobility-related events and user satisfaction is used for assessing overall system performance.

Similar to Equation (7.4), a weighted sum of overall mobility-related events is used for assessing system performance. Besides mobility-related KPIs, the degree of user satisfaction is incorporated in the Overall Performance Indicator (OPI), too. The OPI, denoted by $\rho_{\text{rel},i}$, aggregates the impact of various KPIs and represents the relative improvement of a considered optimization scheme i with respect to the reference scheme (REF). It is calculated as follows:

$$\rho_{\text{rel},i} = \frac{w_{\text{CDR}} \frac{N_{\text{CDR}}^{\text{REF}} - N_{\text{CDR},i}}{N_{\text{CDR}}^{\text{REF}}} + w_{\text{HFR}} \frac{N_{\text{HFR}}^{\text{REF}} - N_{\text{HFR},i}}{N_{\text{HFR}}^{\text{REF}}}}{\sum_k w_k} + \frac{w_{\text{PHR}} \frac{N_{\text{PHR}}^{\text{REF}} - N_{\text{PHR},i}}{N_{\text{PHR}}^{\text{REF}}} + w_{\text{sat}} \frac{N_{\text{sat},i} - N_{\text{sat}}^{\text{REF}}}{N_{\text{sat}}^{\text{REF}}}}{\sum_k w_k}, \tag{8.2}$$

where $N_{\text{CDR},i}, N_{\text{HFR},i}, N_{\text{PHR},i}$, and $N_{\text{CDR}}^{\text{REF}}, N_{\text{HFR}}^{\text{REF}}, N_{\text{PHR}}^{\text{REF}}$ denote the overall numbers of connection drops, HO failures, ping-pong HOs of the considered and the reference scheme, respectively. In the denominator, $\sum_k w_k$ is used to normalize the weighted sum with respect to the sum of all employed weights w_k.

For a considered approach i and the reference scheme, $N_{\text{sat},i}$ and $N_{\text{sat}}^{\text{REF}}$, respectively, represent the number of time instances the users are considered as satisfied, i.e., the users are served with the corresponding amount of radio resources that meet the respective service requirements. In case of LTE, the amount of BS-specific radio resources is limited by the total available transmit power and a specified number of Physical Resource Blocks (PRBs), which depends on the utilized system bandwidth (cf. Table 8.1).

The degree of user satisfaction is heavily affected by received signal levels and the number of mobility-related events. For example, in case the received signal level falls below the minimum receive level threshold (here: -8 dB), the user cannot be served with the requested QoS characteristics. If the receive signal level continues decreasing or remains below the minimum receive level threshold for a specified amount of time, the connection is dropped, which is also referred to as RLF event (cf. Section 2.7). Further, if a HO procedure for a specific user is triggered, the user maintains its connection to the serving BS, but will not be served via the user or data plane, i.e., service requests will not be met. Instead, the HO procedure is handled via the control plane and as soon as it is completed, the connection is handed over to the target BS and the user service is resumed.

In essence, these time periods, in which the user is connected but not served, effectively decrease the time the user is satisfied. Therefore, mobility-related events, such as connection drops, HO failures, and ping-pong HOs, are assigned different weights in order to account for their negative effects on user satisfaction and to reflect MNO's preferences. In the scope of this thesis, KPI-specific weights are set as follows: $w_{\mathrm{CDR}} = 4, w_{\mathrm{HFR}} = 4, w_{\mathrm{PHR}} = 2, w_{\mathrm{sat}} = 1$. Connection dropping and HO failure events are assigned highest weights, since these events result in complete loss of connectivity, whereas in case of a ping-pong HO, the connection still persists. Relative performance improvements are achieved, if less mobility-related issues are observed and more users are satisfied compared to the reference case *REF*. The OPI $\rho_{\mathrm{rel},i}$ is based on the aggregated number of satisfied users ($N_{\mathrm{sat},i}$) and mobility-related events ($N_{\mathrm{CDR},i}, N_{\mathrm{HFR},i}, N_{\mathrm{PHR},i}$) that occurred in the last simulation run where the respective MRO scheme i converged.

Further, it should be noted that for this weighted sum, the following relation applies: the fewer mobility-related issues or events were observed and the more users were satisfied, the higher the resulting OPI value, i.e., a high OPI value indicates improved performance. Moreover, due to the limited number of users, system capacity is always sufficient for serving users' QoS demands except for situations where users experience severe receive signal level degradations or perform mobility-related procedures, such as HOs.

8.2.4 *FQL_HYS* Results for Scenario 2

This subsection summarizes system-level evaluation results for the MRO scheme referred to as *FQL_HYS*, where cell-specific HYS and TTT parameters are tuned for optimizing system performance. Figure 8.27(a) and Figure 8.27(b) depict the overall number of connection drops due to RLF or session timeout and the number of connection drops where user-specific TTT was already started, respectively. Here, only the best performing among all *FQL_HYS* based schemes are evaluated. For BS (0/0), all considered schemes except two schemes (*HYS_L5_TD_H, HYS_L10_TP_H*) achieve a reduction of 40% with respect to the reference case. However, *FQL_HYS* based optimization performed at BS (0/0) negatively affects the number of connection drops observed at neighboring BSs (0/1) and (0/2), respectively. For example, *HYS_L3_TD_HT* and *HYS_L3_TD_MT* reduce connection drops by 40% at BS (0/0), but result in one additional connection drop compared with *REF* at BS (0/1) and BS (0/2). In case of BS (2/2), *FQL_HYS* schemes do not yield any improvements.

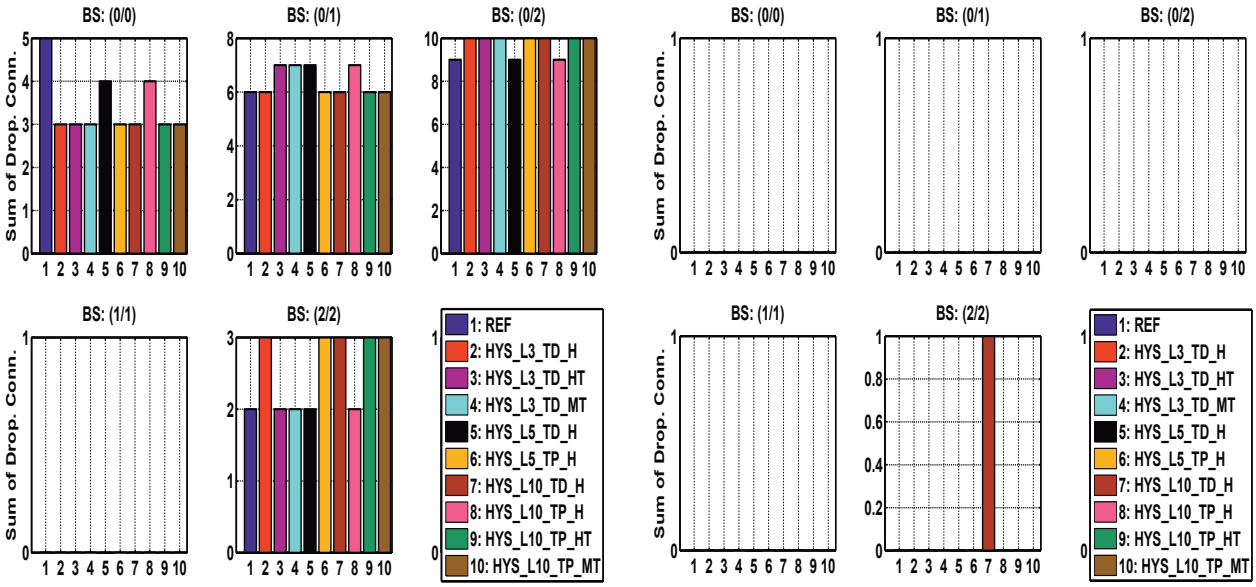

(a) Overall number of connection drops per BS

(b) Overall number of connection drops per BS (HO cond.)

Figure 8.27: Overall number of connection drops per BS using *FQL_HYS*

Regarding the overall number of connection drops that occurred while TTT counters were already activated, shown in Figure 8.27(b), one scheme (*HYS_L10_TD_H*) performs worse than all other schemes for BS (2/2). In Figure 8.28(a) and Figure 8.28(b), the overall number of HO failures and ping-pong HOs is illustrated. HO failure events are only observed at BS (0/0) (cf.

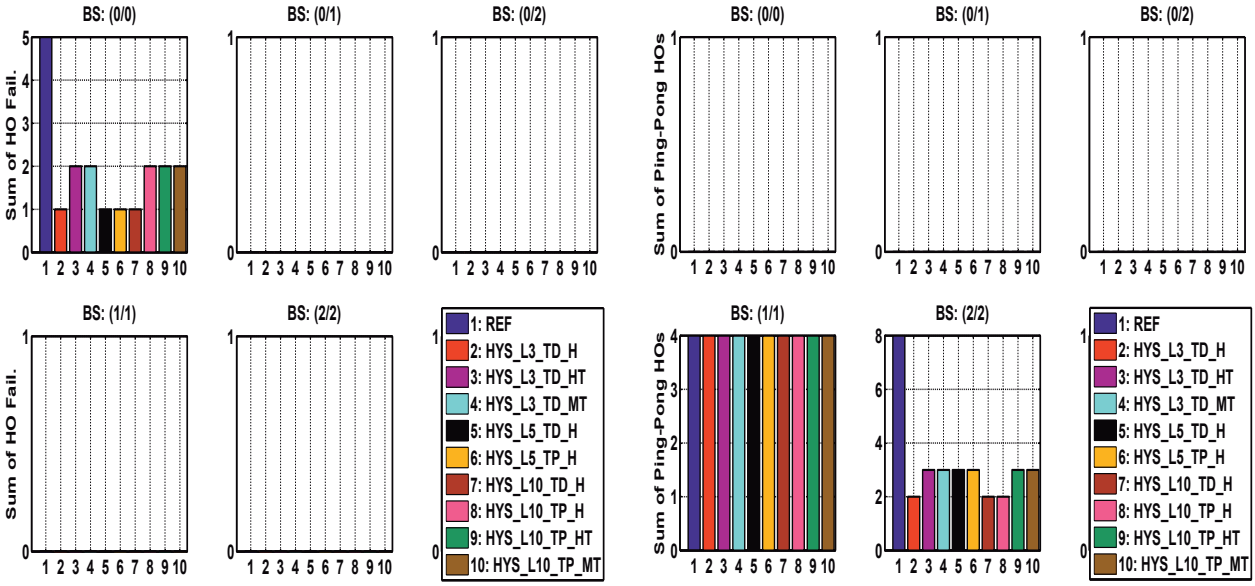

(a) Overall number of HO failures per BS

(b) Overall number of ping-pong HOs per BS

Figure 8.28: Overall number of HO failures and ping-pong HOs per BS using *FQL_HYS*

Figure 8.28(a)), where the four schemes *HYS_L3_TD_H*, *HYS_L5_TD_H*, *HYS_L5_TP_H*, and *HYS_L10_TD_H* are able to achieve a reduction of 80% with respect to the reference case. Regarding ping-pong HOs, all considered variations of the *FQL_HYS* optimization scheme decrease the overall number of ping-pong HOs at BS (2/2), as depicted in Figure 8.28(b). The three schemes *HYS_L3_TD_H*, *HYS_L10_TD_H*, and *HYS_L10_TP_H* yield an improvement of 80%, where all other *FQL_HYS* based schemes reduce the number of ping-pong HOs by 62.5%.

In order to assess the performance of all considered *FQL_HYS* variations, the OPI defined in Equation (8.3) is evaluated, too. Figure 8.29(a) and Figure 8.29(b) illustrate the OPI per BS and the aggregated OPI of all BSs, respectively. For BS (0/0) all considered optimization schemes yield

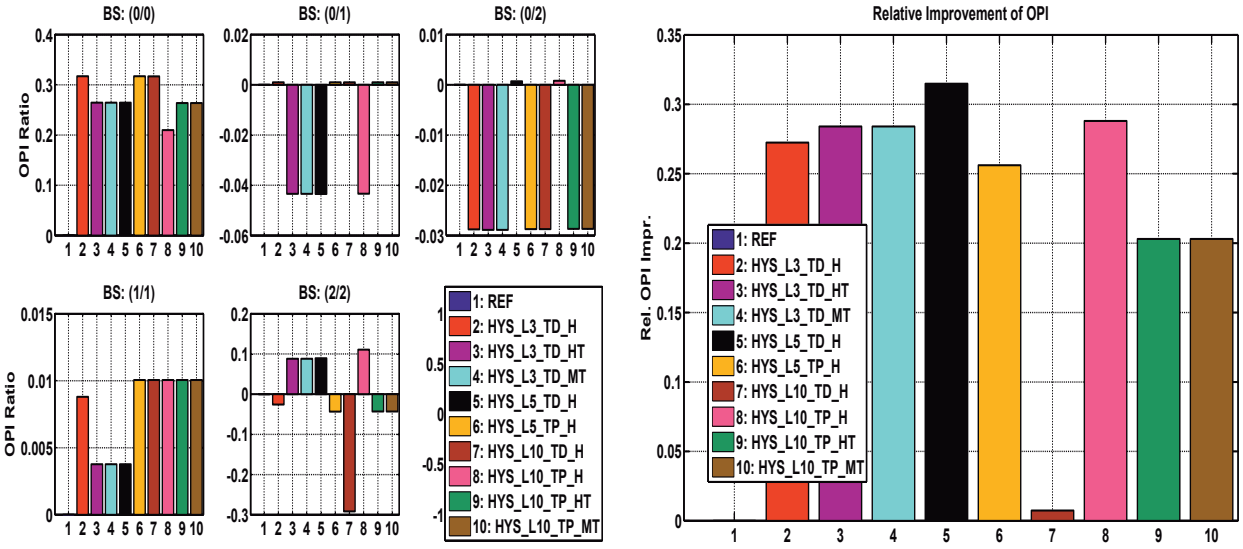

(a) OPI performance per BS

(b) OPI performance per MRO scheme

Figure 8.29: OPI performance per BS and MRO scheme using *FQL_HYS*

improved, i.e., increased, OPI values with respect to *REF*. Best OPI performance is obtained by applying *HYS_L3_TD_H*, *HYS_L5_TP_H*, or *HYS_L10_TD_H*. For BS (2/2), there is one optimization scheme, *HYS_L10_TP_H*, that outperforms other schemes, such as *HYS_L3_TD_HT*, *HYS_L3_TD_MT*, or *HYS_L5_TD_H*, with respect to OPI performance. *HYS_L10_TD_H* results in worst OPI performance at BS (2/2), which corresponds to a deterioration of approximately 30% compared to *REF*. Regarding aggregated OPI performance of all considered BSs, *HYS_L5_TD_H* yields best overall performance with a relative OPI improvement of approximately 32%.

In terms of simulation efforts, the considered variations of the *FQL_HYS*

scheme differ greatly with respect to simulation runs required before learning converged, as illustrated in Figure 8.30. Regarding overall number of sim-

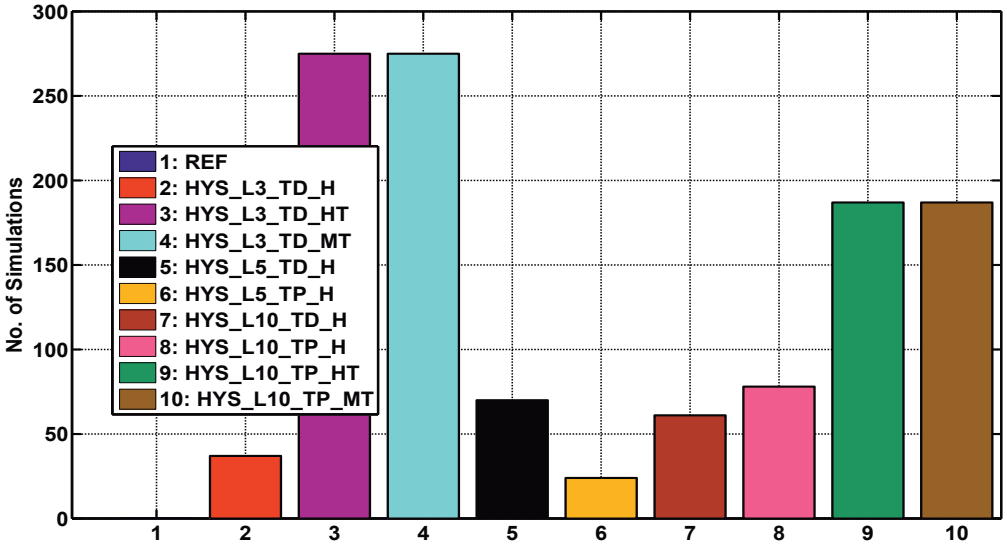

Figure 8.30: Number of simulation runs for selected *FQL_HYS* based MRO schemes

ulation runs, the *HYS_L5_TP_H* scheme that only considers cell-specific HYS parameter (*H*) for system state classification converges first among all *FQL_HYS* based schemes. However, among the schemes that use cell-specific HYS and TTT parameters (*HT*) for classifying system states, *HYS_L10_TP_HT*, which uses 10 instead of 3 fuzzy labels for assessing KPI degradations, is the fastest converging scheme. A similar trend is observed for schemes where HOM and TTT parameters (*MT*) are used for system state classification. Here, *HYS_L10_TP_MT* performs best.

For BS (0/0), the schemes *HYS_L3_TD_H*, *HYS_L5_TP_H*, or *HYS_L10_TD_H* achieve best OPI performance, where *HYS_L5_TP_H* requires least overall number of simulation runs. For BS (2/2), *HYS_L10_TP_H* performs best given a medium amount of simulation efforts, which is the highest among all schemes using only cell-specific HYS parameter (*H*) for system state classification due to usage of 10 fuzzy labels for KPI assessment. Since BS (2/2) is mainly affected by ping-pong HOs, this result indicates that for resolving ping-pong HO issues a higher granularity in terms of KPI degradation assessment is beneficial, if a *FQL_HYS* based scheme is employed. In essence, *HYS_L5_TD_H*, which achieves second best results for BS (0/0) and BS (2/2), respectively, yields best overall performance with respect to aggregated OPI values of all considered BSs.

8.2.5 *FQL_CIO* Results for Scenario 2

In this subsection, system-level evaluation results for the MRO scheme referred to as *FQL_CIO* are presented, where cell-specific TTT and cell pair-specific CIO (O_t) parameters are tuned for optimizing system performance. In case of HO failures, ping-pong HOs, or connection drops that occur while the corresponding UE already entered HO condition, i.e., TTT counter is already activated, cell pair-specific event counters are checked for a maximum in order to identify the neighboring BS to which the mobility-related event most likely occurred. If connection drops due to session time out or RLF events are observed, the cell-specific HYS parameter is adjusted, since in this case no neighbor relation is found to be the root cause of system performance degradation. Figure 8.31(a) and Figure 8.31(b) depict the overall number of connection drops due to RLF or session timeout and the number of connection drops where user-specific TTT was already started, respectively. Here, only the best performing among all *FQL_CIO* based schemes are evaluated. For BS (0/0), two schemes (*CIO_L3_TP_HT, CIO_L3_TD_MT*)

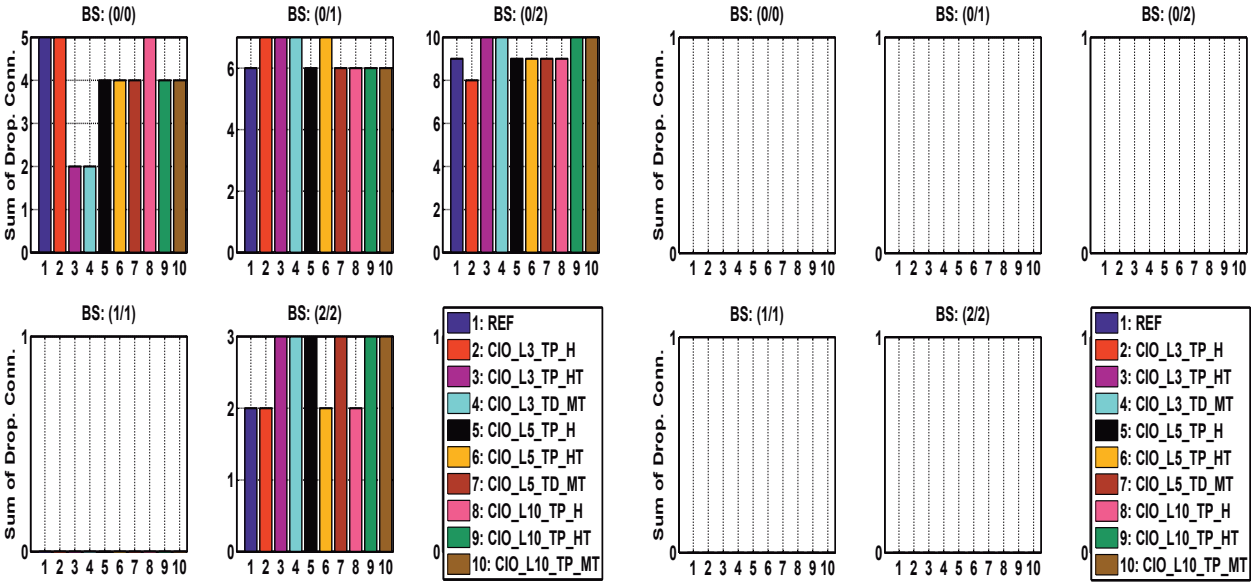

(a) Overall number of connection drops per BS

(b) Overall number of connection drops per BS (HO cond.)

Figure 8.31: Overall number of connection drops per BS using *FQL_CIO*

achieve a reduction of 60% with respect to the reference case. However, for BS (2/2), none of the considered schemes yields any improvements, but increases the number of connections drops by 50% except *CIO_L3_TP_HT* and *CIO_L3_TD_MT*, which yield the same number of connection drops as *REF*. Regarding the overall number of connection drops that occurred while

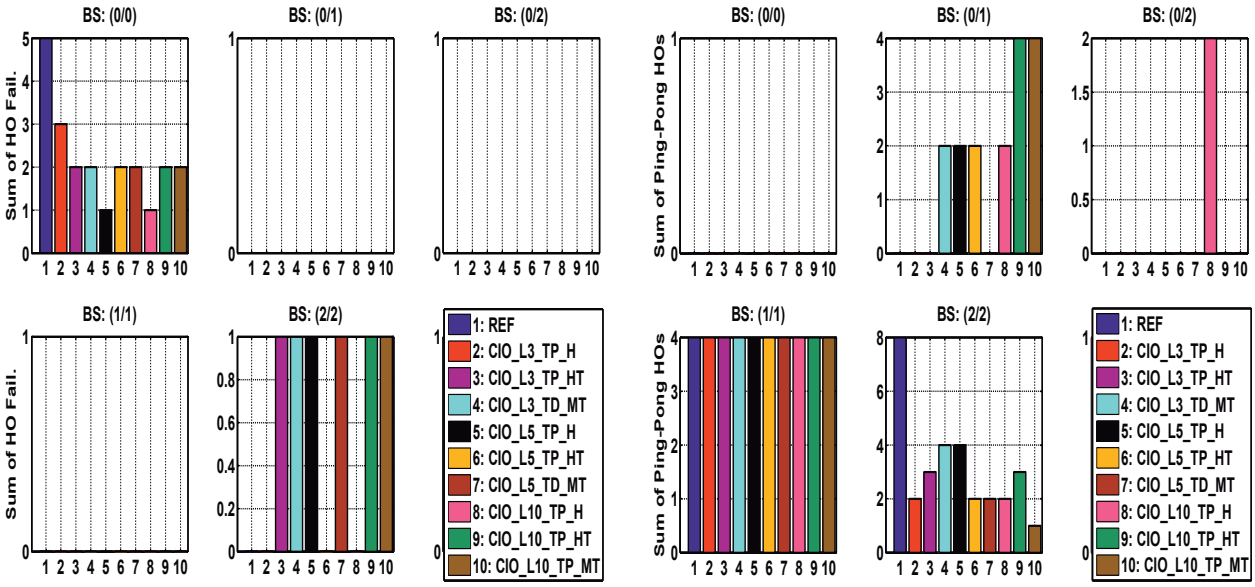

(a) Overall number of HO failures per BS

(b) Overall number of ping-pong HOs per BS

Figure 8.32: Overall number of HO failures and ping-pong HOs per BS using *FQL_CIO*

TTT counters were already activated, shown in Figure 8.31(b), no drop events were observed. In Figure 8.32(a) and Figure 8.32(b), the overall number of HO failures and ping-pong HOs is illustrated.

HO failure events are observed at BS (0/0) and BS (2/2) (cf. Figure 8.32(a)). For BS (0/0), the schemes *CIO_L5_TP_H* and *CIO_L10_TP_H* are able to achieve a reduction of 80% with respect to the reference case. However, for BS (2/2), only the schemes *CIO_L3_TP_H*, *CIO_L5_TP_HT*, and *CIO_L10_TP_H* result in same HO performance as *REF*. Regarding ping-pong HOs, all considered variations of the *FQL_CIO* optimization scheme decrease the overall number of ping-pong HOs at BS (2/2). Best performance is achieved by using *CIO_L10_TP_MT* yielding a reduction of 87.5%, as depicted in Figure 8.32(b). However, this scheme induces a high number of ping-pong HOs at BS (0/1), whereas *CIO_L3_TP_H* and *CIO_L5_TD_MT*, which still reduce ping-pong HOs at BS (2/2) by 75%, do not negatively affect neighboring BSs in a similar way.

In order to assess the performance of all considered *FQL_CIO* variations, the weighted sum defined in Equation (8.3) is evaluated, too, and illustrated in Figures 8.33(a) and 8.33(b) per BS and per MRO scheme, respectively. For BS (0/0), all considered optimization schemes yield improved OPI values with respect to *REF*. Best OPI performance is obtained by applying *CIO_L3_TP_HT* and *CIO_L3_TD_MT*. For BS (2/2), three *FQL_CIO* based schemes (*CIO_L3_TP_H, CIO_L5_TP_HT, CIO_L10_TP_H*) are

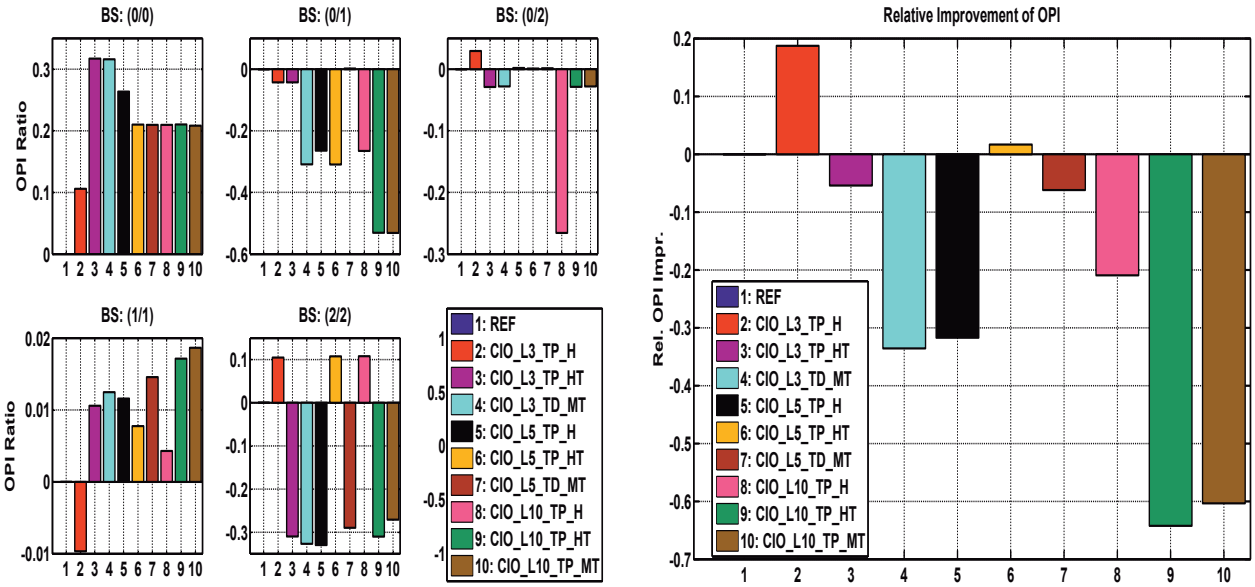

(a) OPI performance per BS

(b) OPI performance per MRO scheme

Figure 8.33: OPI performance per BS and MRO scheme using *FQL_CIO*

able to enhance OPI performance, since these schemes do not result in any HO failures. *CIO_L3_TP_H* results in best overall performance with a relative OPI improvement of approximately 19% with respect to aggregated OPI performance of all considered BSs.

In terms of learning efforts, the amount of simulation runs required before learning converges increases with the number of considered fuzzy labels for system state classification (*H, HT, MT*) given a fix number of labels used for KPI assessment, as illustrated in Figure 8.34. The least amount

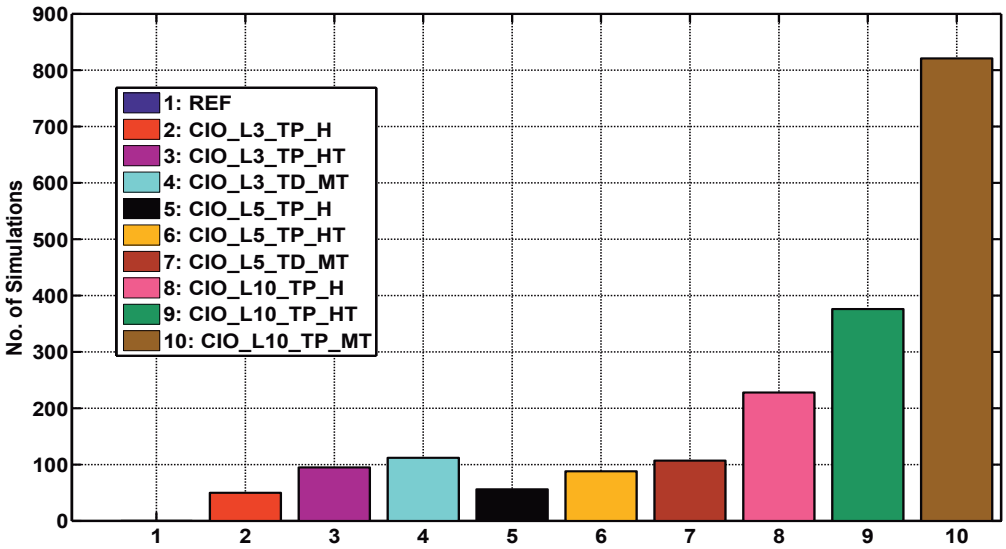

Figure 8.34: Number of simulation runs for selected *FQL_CIO* based MRO schemes

of overall simulation efforts is required using *CIO_L3_TP_H*. Regarding schemes that only consider cell-specific HYS parameter (*H*) for system state classification, the scheme using the least number of fuzzy labels for KPI assessments *CIO_L3_TP_H* converges first. Among the schemes that use cell-specific HYS and TTT parameters (*HT*) for classifying system states, *CIO_L5_TP_HT* is the fastest converging scheme. Among those schemes that use 10 fuzzy labels for KPI assessment, *CIO_L10_TP_H* requires least simulation efforts. However, the overall number of simulation runs is quite high compared to other schemes using 3 or 5 labels for KPI assessment.

For BS (0/0), the schemes *CIO_L3_TP_HT* and *CIO_L3_TD_MT* achieve best OPI performance, although they require at least twice as many simulation runs as *CIO_L3_TP_H*. For BS (2/2), three schemes (*CIO_L3_TP_H, CIO_L5_TP_HT, CIO_L10_TP_H*) were able to improve system performance compared to *REF*. Although these schemes were not able to achieve optimum ping-pong HO performance, they do not result in any HO failures. In essence, *CIO_L3_TP_H*, which achieves only low improvements for BS (0/0), but best results for BS (2/2), yields best overall performance with respect to aggregated OPI values of all considered BSs.

8.2.6 *FQL_CIO_P* Results for Scenario 2

This subsection summarizes system-level evaluation results for the MRO scheme referred to as *FQL_CIO_P*, where cell-specific TTT and cell pair-specific, joint CIO (O_s and O_t) parameters are tuned for optimizing system performance. In case of HO failures, ping-pong HOs, or connection drops that occur while the corresponding UE already entered HO condition, i.e., TTT counter is already activated, cell pair-specific event counters are checked for a maximum in order to identify the neighboring BS to which the mobility-related event most likely occurred. If connection drops due to session time out or RLF events are observed, cell-specific HYS and CIO (O_s) parameters are jointly adjusted, since in this case no neighbor relation is found to be the root cause of system performance degradation. Figure 8.35(a) and Figure 8.35(b) depict the overall number of connection drops due to RLF or session timeout and the number of connection drops where user-specific TTT was already started, respectively. Here, only the best performing among all *FQL_CIO_P* based schemes are evaluated. For BS (0/0), three schemes (*CIO_P_L3_TD_H, CIO_P_L3_TP_HT, CIO_P_L5_TP_HT*) achieve a reduction of 40% with respect to the reference case. However, for BS (2/2), *FQL_CIO_P* based schemes do not yield any improvements. *CIO_P_L3_TP*

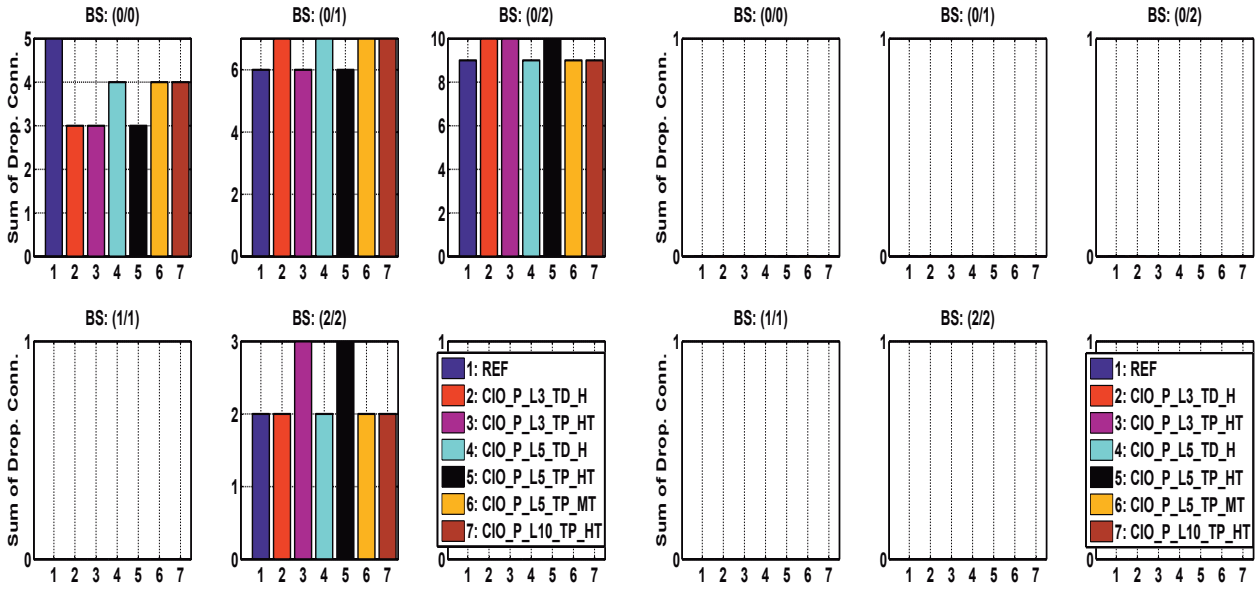

(a) Overall number of connection drops per BS

(b) Overall number of connection drops per BS (HO cond.)

Figure 8.35: Overall number of connection drops per BS using *FQL_CIO_P*

_HT and *CIO_P_L5_TP_HT* even result in a 50% increase of connection drops. Regarding the overall number of connection drops that occurred while TTT counters were already activated, shown in Figure 8.35(b), no BS-specific performance issues were observed. In Figure 8.36(a) and Figure 8.36(b), the overall number of HO failures and ping-pong HOs is illustrated. HO failure

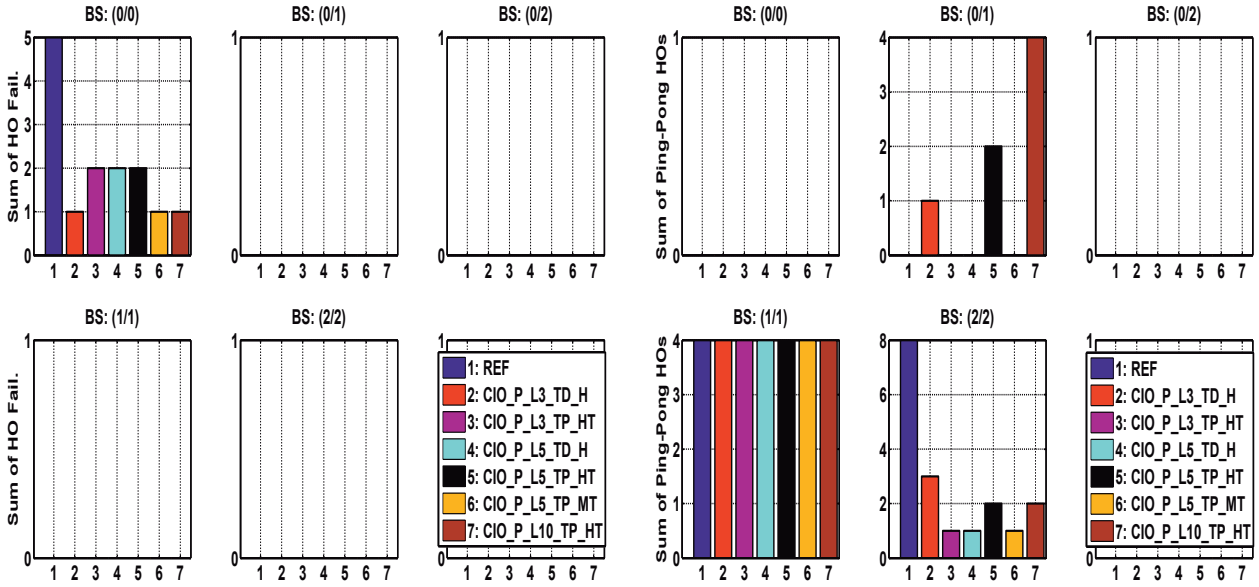

(a) Overall number of HO failures per BS

(b) Overall number of ping-pong HOs per BS

Figure 8.36: Overall number of HO failures and ping-pong HOs per BS using *FQL_CIO_P*

events are only observed at BS (0/0). If *FQL_CIO_P* based optimization is applied (cf. Figure 8.36(a)), *CIO_P_L3_TD_H*, *CIO_P_L5_TP_MT*, and *CIO_P_L10_TP_HT* are able to achieve a reduction of 80% with respect to the reference case. Regarding ping-pong HOs, all considered variations of the *FQL_CIO_P* optimization scheme decrease the overall number of ping-pong HOs at BS (2/2). Best performance is achieved by using *CIO_P_L3_TP_HT*, *CIO_P_L5_TD_H*, and *CIO_P_L5_TP_MT* yielding a reduction of 87.5%, as depicted in Figure 8.36(b). However, additional ping-pong HOs are induced at BS (0/1) by *CIO_P_L3_TD_H*, *CIO_P_L5_TP_HT*, and *CIO_P_L10_TP_HT*.

In order to assess the performance of all considered *FQL_CIO_P* variations, the OPI defined in Equation (8.3) is evaluated, too. Figure 8.37(a) and Figure 8.37(b) illustrate the OPI per BS and the aggregated OPI of all BSs, respectively. For BS (0/0), all considered optimization schemes yield

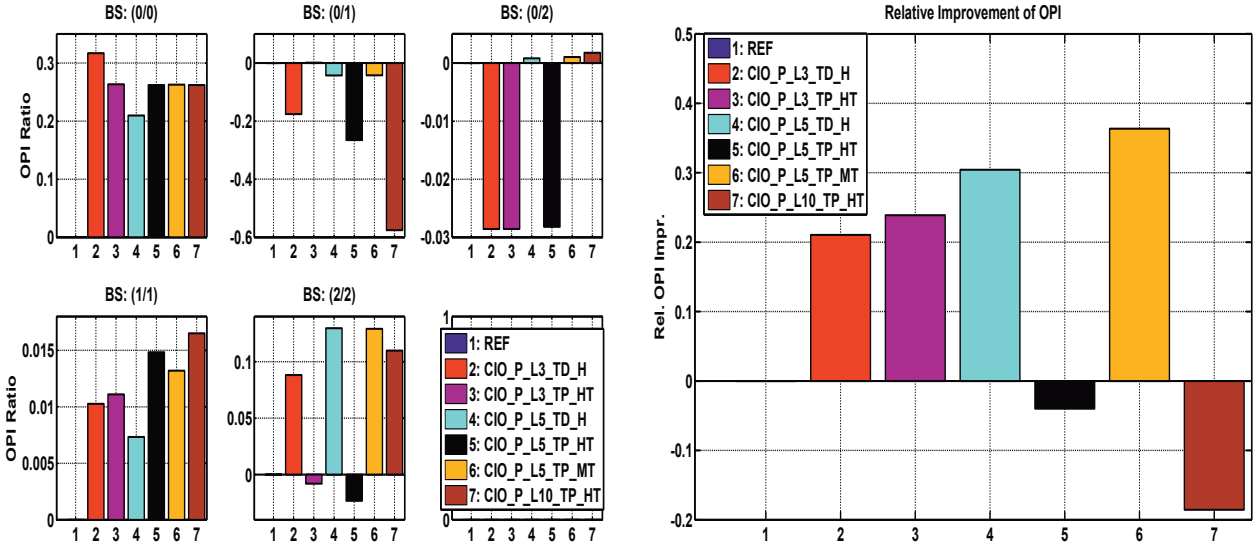

(a) OPI performance per BS

(b) OPI performance per MRO scheme

Figure 8.37: OPI performance per BS and MRO scheme using *FQL_CIO_P*

improved OPI values with respect to *REF*. Best OPI performance is obtained by applying *CIO_P_L3_TD_H*. For BS (2/2), there are two optimization schemes, *CIO_P_L5_TD_H* and *CIO_P_L5_TP_MT*, that outperform all other schemes with respect to OPI performance. Regarding aggregated OPI performance of all considered BSs, *CIO_P_L5_TP_MT* yields best overall performance with a relative OPI improvement of approximately 36%.

In terms of learning efforts, the amount of simulation runs required before learning converges increases with the number of considered fuzzy labels used for classifying KPI degradations with only one exception, as illustrated in

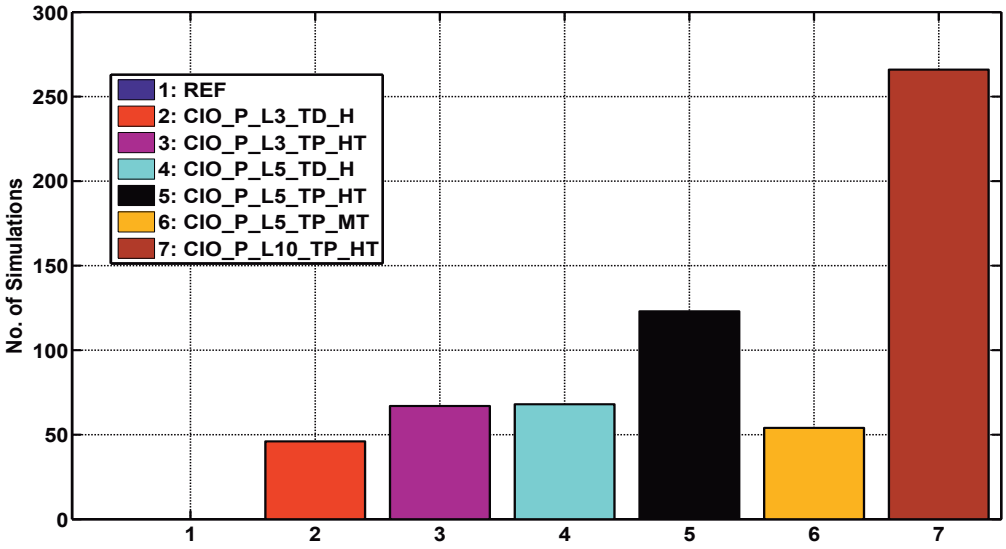

Figure 8.38: Number of simulation runs for selected *FQL_CIO_P* based MRO schemes

Figure 8.38. The least amount of overall simulation efforts is required using *CIO_P_L3_TD_H*. Regarding schemes that only consider cell-specific HYS parameter (*H*) for system state classification, the scheme using the least number of fuzzy labels *CIO_P_L3_TD_H* converges first. Among the schemes that use cell-specific HYS and TTT parameters (*HT*) for classifying system states, *CIO_P_L3_TP_HT* is the fastest converging scheme. However, *CIO_P_L5_TP_MT*, which employs 5 fuzzy labels for KPI assessment as well as HOM and TTT parameters for system state classification, is the second fasted converging scheme among all *FQL_CIO_P* based schemes.

For BS (0/0), the scheme *CIO_P_L3_TD_H* achieves best overall OPI performance while requiring least amount of simulation runs. For BS (2/2), *CIO_P_L5_TD_H* and *CIO_P_L5_TP_MT* outperform all other optimization schemes, where *CIO_P_L5_TP_MT* requires less simulation efforts, although a higher granularity in terms of system state classification is applied. However, an interesting trade-off arises for *CIO_P_L3_TD_H*, which results in best performance for BS (0/0) and fourth best performance for (2/2), respectively, given lowest complexity and least amount of simulation efforts. In essence, *CIO_P_L5_TP_MT*, which achieves second best results for BS (0/0) and BS (2/2), respectively, yields best overall performance with respect to aggregated OPI values of all considered BSs.

8.2.7 *FQL_CIO_H* Results for Scenario 2

In this subsection, system-level evaluation results for the MRO scheme referred to as *FQL_CIO_H* are presented, where cell-specific TTT as well as HYS and CIO (O_t) parameters are jointly tuned in a cell pair-specific manner for optimizing system performance. In case of HO failures, ping-pong HOs, or connection drops that occur while the corresponding UE already entered HO condition, i.e., TTT counter is already activated, cell pair-specific event counters are checked for a maximum in order to identify the neighboring BS to which the mobility-related event most likely occurred. If connection drops due to session time out or RLF events are observed, the cell-specific HYS parameter is adjusted, since in this case no neighbor relation is found to be the root cause of system performance degradation. Figure 8.39(a) and Figure 8.39(b) depict the overall number of connection drops due to RLF or session timeout and the number of connection drops where user-specific TTT was already started, respectively. Here, only the best performing among all *FQL_CIO_H* based schemes are evaluated. For BS

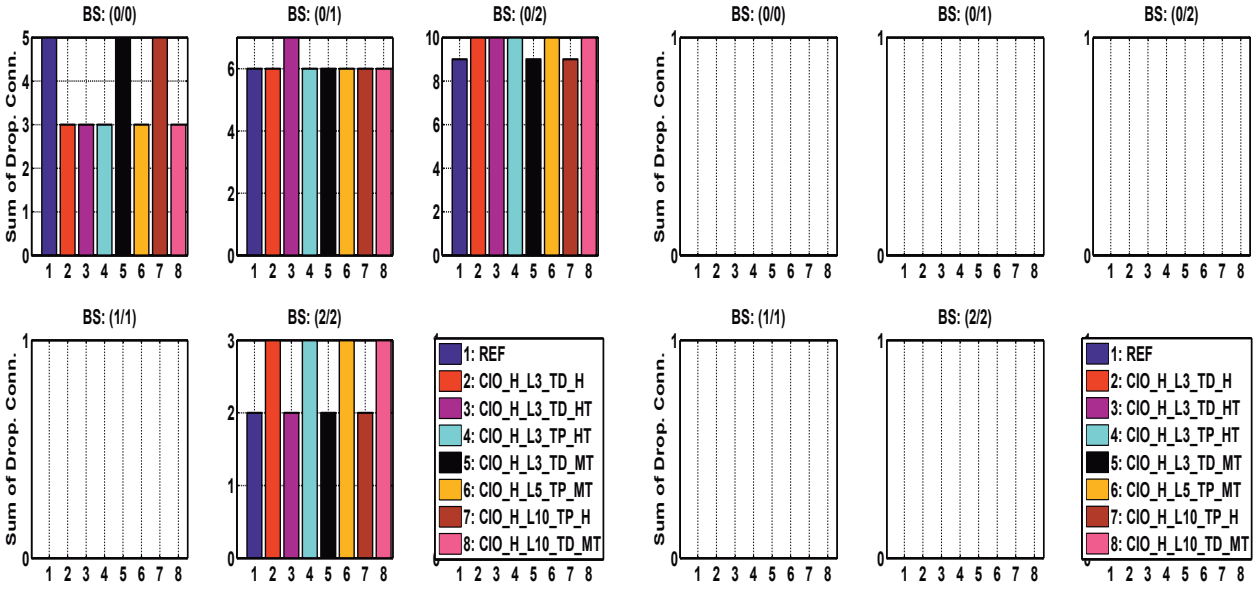

(a) Overall number of connection drops per BS

(b) Overall number of connection drops per BS (HO cond.)

Figure 8.39: Overall number of connection drops per BS using *FQL_CIO_H*

(0/0), all except two schemes (*CIO_H_L3_TD_MT, CIO_H_L10_TP_H*) achieve a reduction of 40% with respect to the reference case. However, for BS (2/2), no *FQL_CIO_H* based scheme is able to reduce the number of connection drops. *CIO_H_L3_TD_HT*, *CIO_H_L3_TD_MT*, and *CIO_H_L10_TP_H* yield same performance as *REF*, but all other schemes

increase the number of connections drops by 50%. Regarding the overall number of connection drops that occurred while TTT counters were already activated, shown in Figure 8.39(b), no connection drop events were observed. In Figure 8.40(a) and Figure 8.40(b), the overall number of HO failures and ping-pong HOs is illustrated. HO failure events are observed

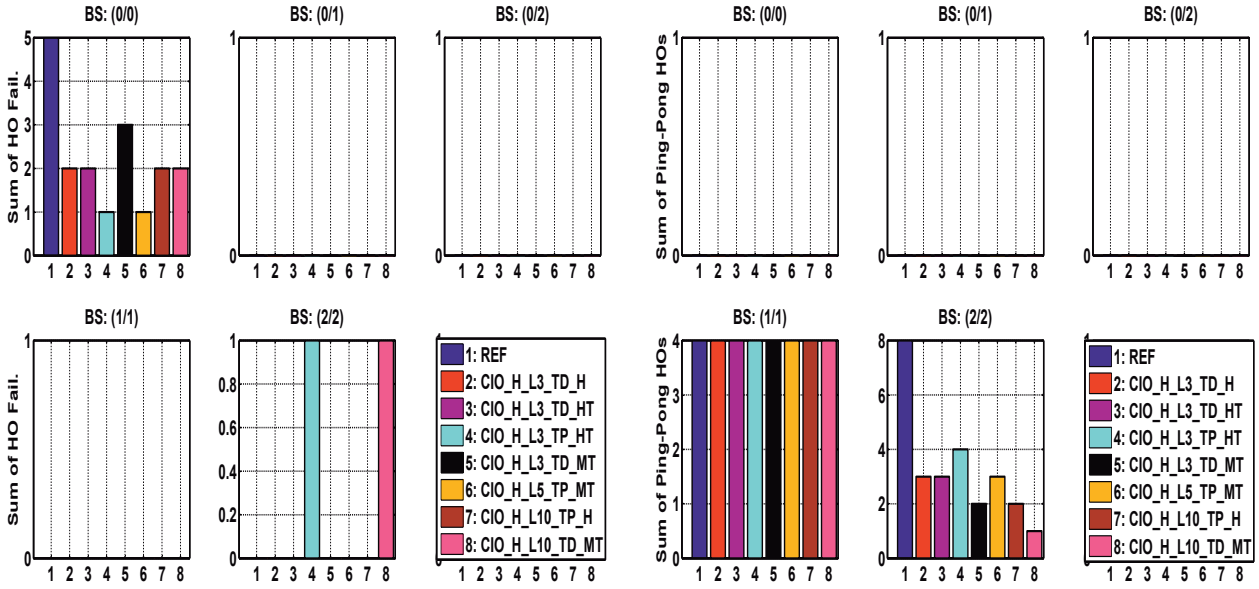

(a) Overall number of HO failures per BS (b) Overall number of ping-pong HOs per BS

Figure 8.40: Overall number of HO failures and ping-pong HOs per BS using *FQL_CIO_H*

at BS (0/0) and BS (2/2) (cf. Figure 8.40(a)). For BS (0/0), the schemes *CIO_H_L3_TP_HT* and *CIO_H_L5_TP_MT* are able to achieve a reduction of 80% with respect to the reference case. In case of BS (2/2), all schemes except *CIO_H_L3_TP_HT* and *CIO_H_L10_TD_MT*, which result in worst performance in terms of HO failures, yield zero HO failures. Regarding ping-pong HOs, all considered variations of the *FQL_CIO_H* optimization scheme decrease the overall number of ping-pong HOs at BS (2/2). Best performance is achieved by using *CIO_H_L10_TD_MT* yielding a reduction of 87.5%, as depicted in Figure 8.40(b). *CIO_H_L3_TD_MT* and *CIO_H_L10_TP_H* still enhance ping-pong HO performance by 75%.

In order to assess the performance of all considered *FQL_CIO_H* variations, the weighted sum defined in Equation (8.3) is evaluated, too, and illustrated in Figures 8.41(a) and 8.41(b) per BS and per MRO scheme, respectively. For BS (0/0), all considered optimization schemes result in improved OPI values with respect to *REF*. Best OPI performance is obtained by applying *CIO_H_L3_TP_HT* and *CIO_H_L5_TP_MT*. For BS (2/2), *CIO_H_L3_TD_MT* and *CIO_H_L10_TP_H* outperform all other

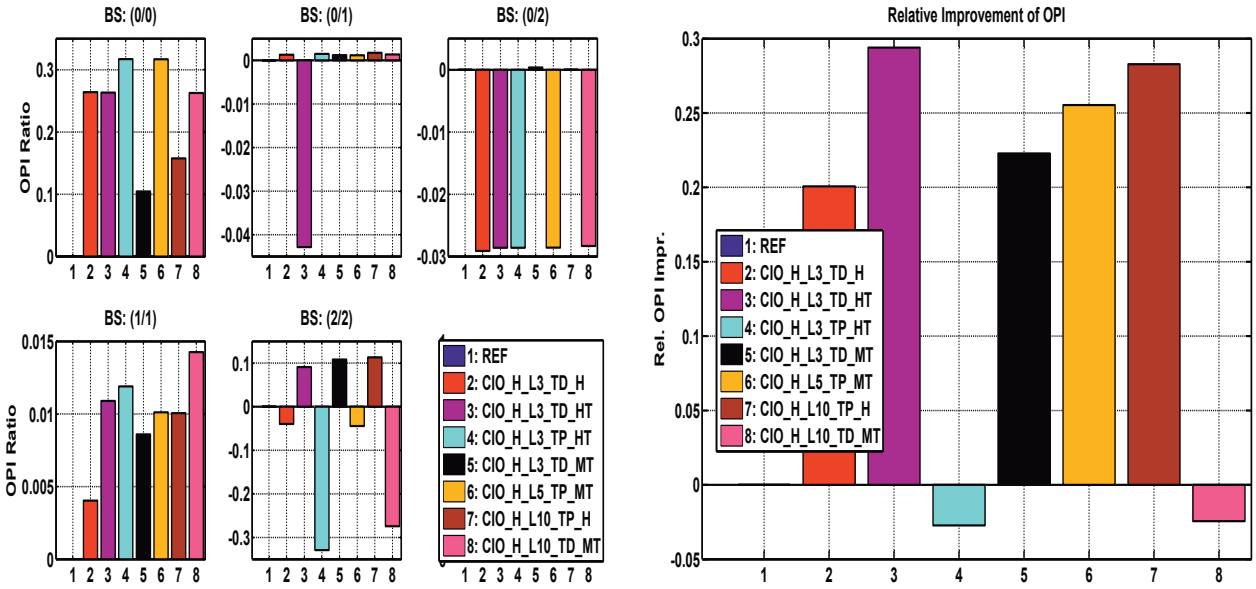

(a) OPI performance per BS

(b) OPI performance per MRO scheme

Figure 8.41: OPI performance per BS and MRO scheme using *FQL_CIO_H*

schemes in terms of OPI performance. Further, except *CIO_H_L3_TD_HT*, all other remaining schemes result in worse OPI performance compared to *REF*. Moreover, *CIO_H_L3_TD_HT* results in best overall performance with a relative OPI improvement of approximately 29% with respect to aggregated OPI performance of all considered BSs.

In terms of simulation efforts, the amount of simulation runs required before learning converges differs greatly among the considered optimization schemes, as illustrated in Figure 8.42. Among all *FQL_CIO_H* based schemes,

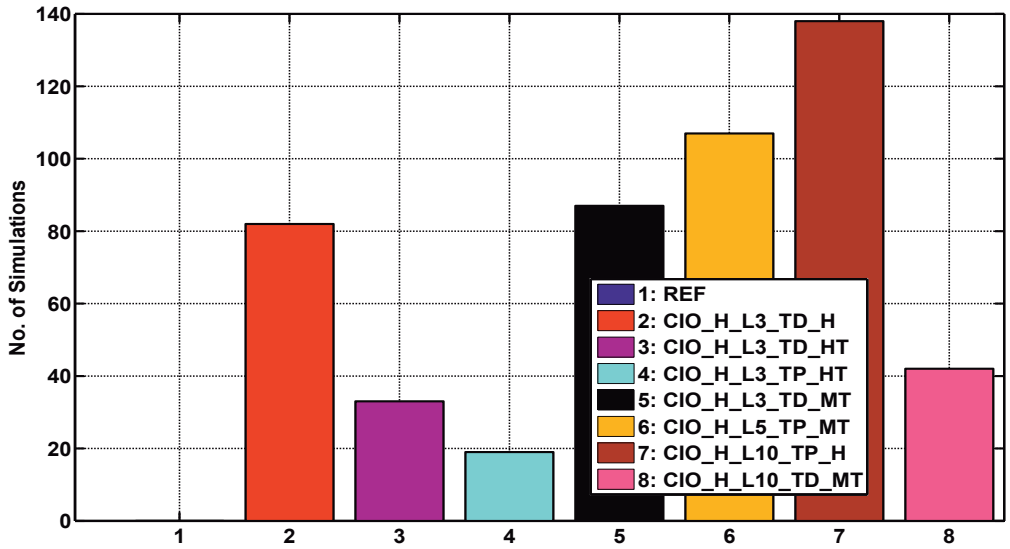

Figure 8.42: Number of simulation runs for selected *FQL_CIO_H* based MRO schemes

approaches that consider cell-specific HYS and TTT parameters (*HT*) for classifying system states, *CIO_H_L3_TD_HT* and *CIO_H_L3_TP_HT*, require the least number of simulation runs, where *CIO_H_L3_TP_HT* is the fastest converging scheme. Further, increasing granularity for system state classification by using HOM and TTT parameters (*MT*) results in a significantly higher number of simulation runs. The same applies to approaches that only consider HYS parameter (*H*) for classifying system state. However, in case KPI assessment is performed employing 10 fuzzy labels as well as HOM and TTT parameters (*MT*) for system state classification, simulation efforts can be reduced to moderate amounts, e.g., using *CIO_H_L10_TD_MT*.

For BS (0/0), the schemes *CIO_H_L3_TP_HT* and *CIO_H_L5_TP_MT* achieve best OPI performance, where *CIO_H_L3_TP_HT* requires least number of simulation runs. However, these schemes result in severe OPI performance degradations for BS (2/2). In case of BS (2/2), *CIO_H_L3_TD_MT* and *CIO_H_L10_TP_H* are able to improve system performance compared to *REF*. However, they only achieve small OPI improvements for BS (0/0). In essence, *CIO_H_L3_TD_HT*, which achieves fourth and third best results for BS (0/0) and BS (2/2), respectively, yields best overall performance with respect to aggregated OPI values of all considered BSs.

8.2.8 Optimum Handover Parameter Adaptations for Scenario 2

In the following subsections, the best performing MRO schemes presented and identified in the previous Sections 8.2.4, 8.2.5, 8.2.6, and 8.2.7 are evaluated and compared with state-of-the-art approaches introduced in Section 7.3.2. First, BS-specific performance results are shown, then evaluation results with respect to the various velocity classes considered in scenario 2 are stated. Further, the learned optimum HO parameter adaptation rules of the best FQL based optimization schemes are presented in the last paragraph of this section.

BS-Specific Results for Scenario 2

Figure 8.43(a) and Figure 8.43(b) depict the overall number of connection drops due to RLF or session timeout and the number of connection drops where user-specific TTT counters were already started (HO cond.), respectively.

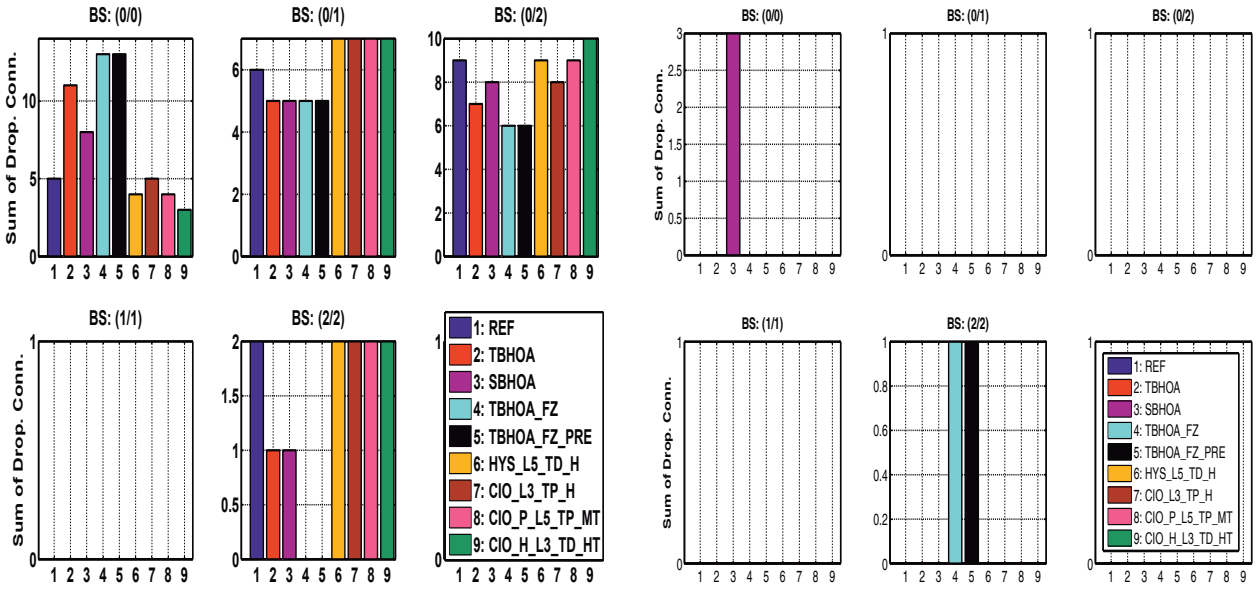

(a) Overall number of connection drops per BS

(b) Overall number of connection drops per BS (HO cond.)

Figure 8.43: Overall number of connection drops per BS using various MRO Schemes

For BS (0/0), three schemes (*HYS_L5_TD_H, CIO_P_L5_TP_MT, CIO_H_L3_TD_HT*) are able to improve performance. The first two schemes achieve a reduction of 20% and *CIO_H_L3_TD_HT* a reduction of 40% with respect to the reference case (*REF*). However, for BS (2/2), the FQL based schemes only yield same performance as *REF*, but none of them is able to decrease the number of connection drops. In contrast, the schemes *TBHOA* and *SBHOA*, introduced in Section 7.3.2, lead to a decrease of connections drops by 50%. The *TBHOA* schemes that use Fuzzy Logic for KPI classification (*TBHOA_FZ, TBHOA_FZ_PRE*), described in Section 7.3.2, are even able to reduce the number of connection drops to zero. Further, the FQL based schemes negatively affect the neighboring cell sector (0/1), where one additional connection drop is observed. In contrast, *TBHOA*, *SBHOA*, and, in particular, *TBHOA_FZ* and *TBHOA_FZ_PRE* have a positive impact on the performance of neighboring cell sectors. For example, the number of connection drops in sector (0/2) is reduced by 33% using *TBHOA_FZ* or *TBHOA_FZ_PRE*. However, for BS (2/2), these two schemes exhibit drawbacks with respect to connection drops that occur while user-specific TTT timers were already started, where they result in worst performance. Further, *SBHOA* performs even worse at BS (0/0), where three additional connection drops of users with activated TTT counters are observed.

In Figure 8.44(a) and Figure 8.44(b), the overall number of HO failures

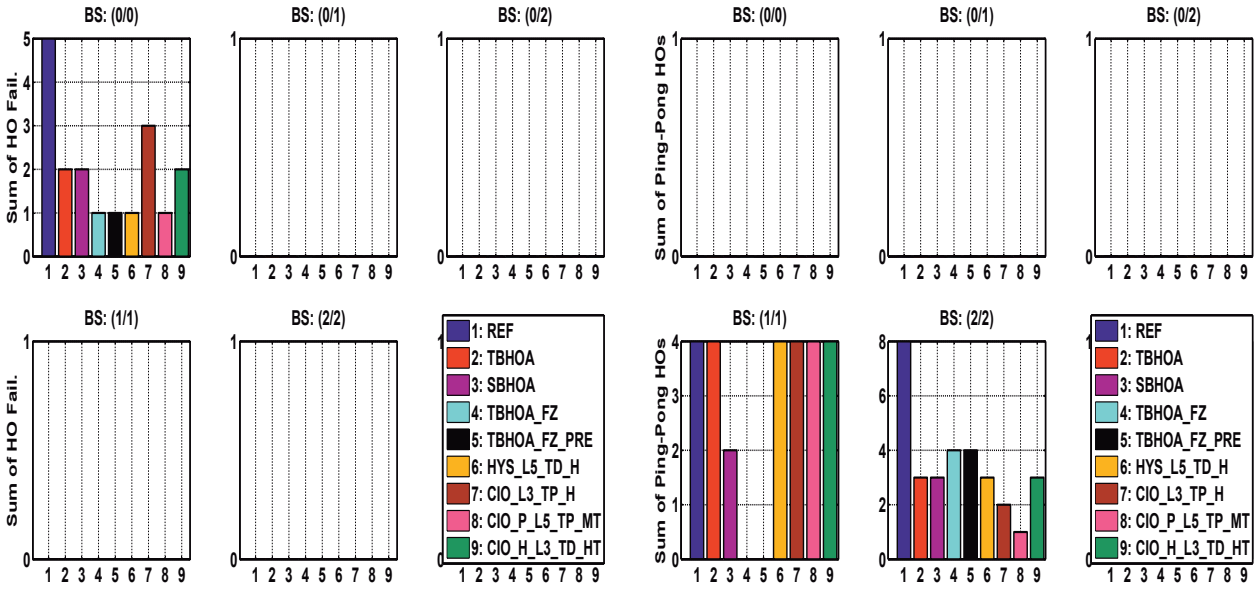

(a) Overall number of HO failures per BS (b) Overall number of ping-pong HOs per BS

Figure 8.44: Overall number of HO failures and ping-pong HOs per BS using various MRO Schemes

and ping-pong HOs is illustrated. HO failure events are only observed at BS (0/0) (cf. Figure 8.44(a)). For BS (0/0), the four schemes *TBHOA_FZ*, *TBHOA_FZ_PRE*, *HYS_L5_TD_H*, and *CIO_P_L5_TP_MT* are able to achieve a reduction of 80% with respect to the reference case.

Regarding ping-pong HOs, all considered MRO schemes decrease the overall number of ping-pong HOs at BS (2/2). Best performance is achieved by using *CIO_P_L5_TP_MT*, which yields a reduction of 87.5%, as depicted in Figure 8.44(b). The second largest reduction of ping-pong HOs by 75% is obtained by *CIO_L3_TP_H*. Although *TBHOA_FZ* and *TBHOA_FZ_PRE* decrease the number of ping-pong HOs by 50%, they perform worst among all considered MRO schemes. However, operation of these schemes positively affects neighboring cell sector (1/1), where *TBHOA_FZ* and *TBHOA_FZ_PRE* completely eliminate ping-pong HOs.

In order to assess the performance of all considered MRO variations, the OPI defined in Equation (8.3) is evaluated, too. Figure 8.45(a) and Figure 8.45(b) illustrate the OPI per BS and the aggregated OPI of all BSs, respectively.

For BS (0/0), only FQL based optimization schemes result in improved OPI values with respect to *REF*. Here, best OPI performance is obtained by applying *HYS_L5_TD_H*, which yields a relative OPI improvement of 26.4% and marginally better results than *CIO_P_L5_TP_MT* and *CIO_H_L3_TD_HT* (26.3%). In contrast, *TBHOA*, *SBHOA*, *TBHOA_FZ*, and *TB-*

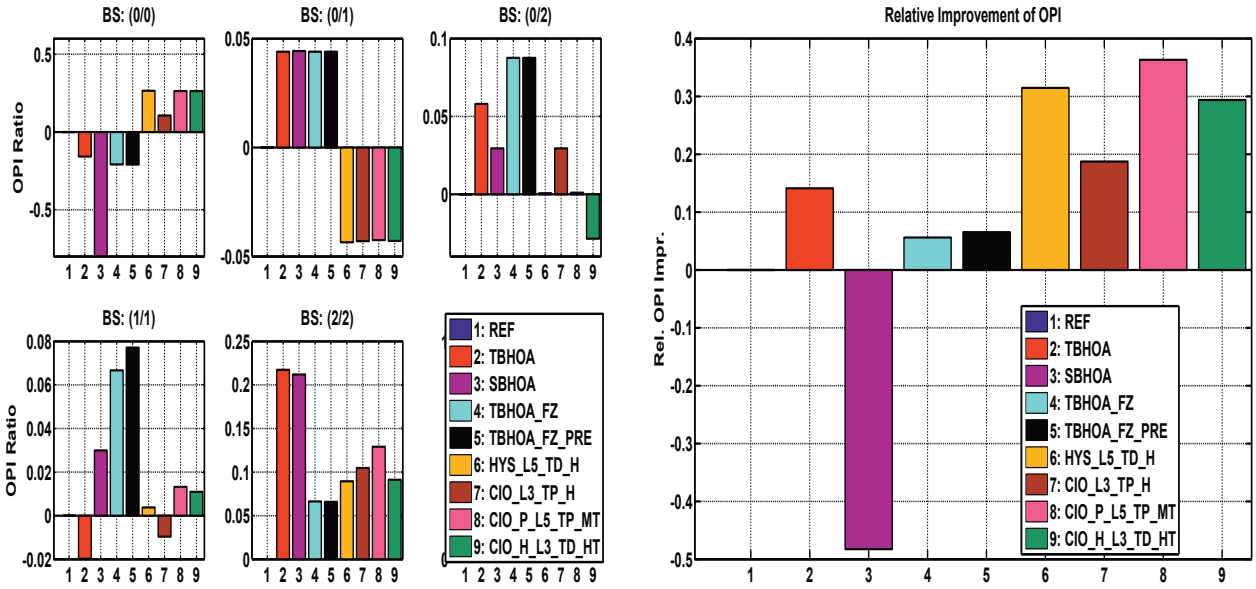

(a) OPI performance per BS

(b) OPI performance per MRO scheme

Figure 8.45: OPI performance per BS and MRO scheme using various MRO schemes

HOA_FZ_PRE yield significantly deteriorated OPI values. In particular, *SBHOA* results in an approximately 80% deterioration of the OPI value compared to *REF*. In case of BS (2/2), all considered MRO schemes are able to achieve improved OPI values. However, two schemes (*TBHOA* and *SBHOA*) outperform all others and result in approximately 21% increased OPI values. Among the FQL based schemes, *CIO_P_L5_TP_MT* yields third best performance with a relative OPI improvement of approximately 13%.

Further, different trends are observed for OPI values of neighboring cell sectors. For example, FQL based schemes slightly decrease performance at BS (0/1). Furthermore, particular FQL based schemes deteriorate OPI values at BS (0/2) and (1/1), while *TBHOA_FZ* and *TBHOA_FZ_PRE* yield highest OPI values at those BSs. Regarding aggregated OPI performance of all considered BSs, *CIO_P_L5_TP_MT* yields best overall performance with a relative OPI improvement of approximately 36%. *HYS_L5_TD_H* yields second and *CIO_H_L3_TD_HT* third best OPI performance resulting in relative improvements of approximately 32% and 29%, respectively.

In terms of simulation efforts, the amount of simulation runs required for before learning converges differs greatly among the considered optimization schemes, as illustrated in Figure 8.46. Regarding schemes that only consider cell-specific HYS parameter (*H*) for system state classification, the scheme *CIO_L3_TP_H* requires 50 simulation runs and thus much fewer simulation runs compared to *HYS_L5_TD_H*. However, the *CIO_H_L3_TD_HT*

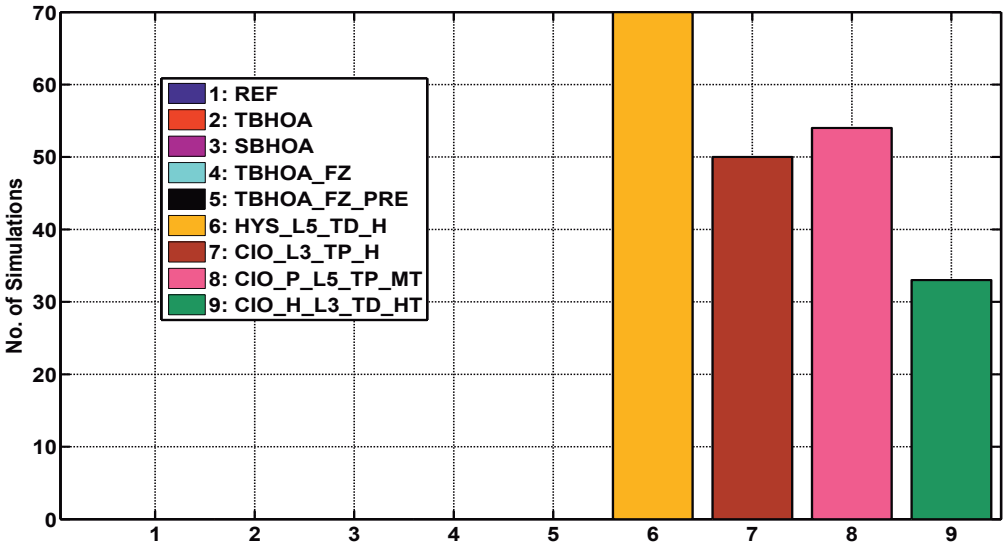

Figure 8.46: Number of simulation runs using various MRO schemes

scheme, which uses cell-specific HYS and TTT parameters (*HT*) for classifying system states, is the fastest converging scheme among all considered FQL based schemes requiring only 33 simulation runs.

For BS (0/0), the scheme *HYS_L5_TD_H* achieves largest OPI improvements, while requiring highest number of simulation runs. OPI values only marginally exceed those of *CIO_P_L5_TP_MT* and *CIO_H_L3_TD_HT*, where the latter one requires the least amount of simulation efforts. In case of BS (2/2), *TBHOA* and *SBHOA* are able to improve system performance by approximately 21% compared to *REF*.

Among all considered MRO schemes, *CIO_P_L5_TP_MT*, which achieves second and third best results for BS (0/0) and BS (2/2), respectively, yields best overall system performance with respect to aggregated OPI values of all considered BSs (0/0), (0/1), (0/2), (1/1), (2/2), (10/0). Relative OPI improvements are approximately 36% compared to *REF*. Further, it requires 54 and thus second highest number of simulation runs. *HYS_L5_TD_H* yields second and *CIO_H_L3_TD_HT* third best OPI values, where the first one requires the highest and the last scheme the least number of simulation runs.

Velocity-Specific Results for Scenario 2

In order to evaluate the impact of user velocities on system performance, mobility-related event counters are presented for each individual user, where a pair of two users (e.g., UEs 0 and 1, UEs 2 and 3, etc.) belongs to the same velocity class. The only difference between, e.g., user 0 and 1 is that they travel around BS 0 in clockwise and counter-clockwise direction, respectively

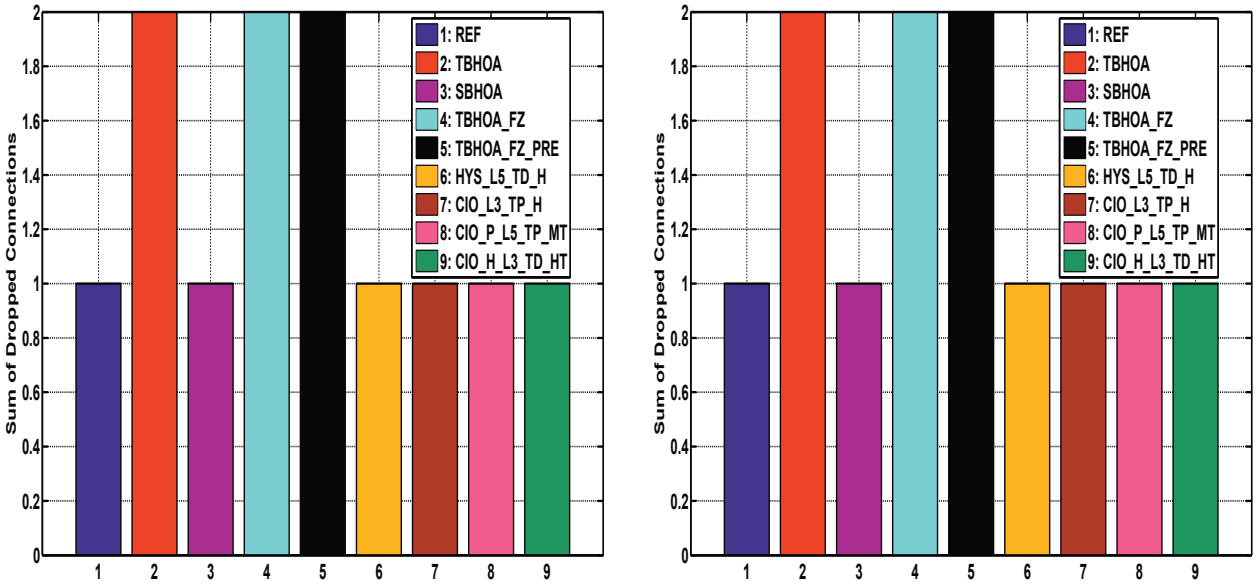

(a) Sum of dropped connections of user 0

(b) Sum of dropped connections of user 1

Figure 8.47: Sum of dropped connections (due to RLF) of users moving at 1.1 m/s (4 km/h)

(cf. Figure 8.5(a)).

In Figure 8.47, the sum of connection drops due to RLFs or session timeouts is depicted for UE 0 and 1, where the same number of connection drops among the considered MRO schemes are observed for both users traveling at pedestrian speed around BS 0 in clockwise and counter-clockwise direction, respectively. For these slow moving users, *TBHOA*, *TBHOA_FZ*, and *TBHOA_FZ_PRE* result in twice as many connection drops compared to other approaches. In case of medium velocities, one connection drop is observed for UE 2 and 3 moving at 6.1 m/s (22 km/h), two connection drops for UE 4 and 5 moving at 8.3 m/s (30 km/h), three connection drops for UE 6 and 7 moving at 13.9 m/s (50 km/h), and four connection drops for UE 8 and 9 moving at 19.4 m/s (70 km/h) for all considered schemes. However, high speed users 10 and 11 are not affected by connection drops due to RLF.

Figure 8.48(a) and Figure 8.48(b), respectively, illustrate the sums of connection drops due to RLFs or session timeouts, while TTT counters of dropped UEs were already started. In scenario 2, these events are only observed for users 10 and 11 moving at 33.3 m/s (120 km/h) on a ring road through BS sectors (0/0), (1/1), and (2/2), one in clockwise and the other one in counter-clockwise direction, respectively.

As already indicated in BS-specific simulation results (cf. Figure 8.43(b)), the *SBHOA* scheme performs worst in terms of connection drops that occur while TTT counters are already activated. Further, *TBHOA_FZ* and *TB-*

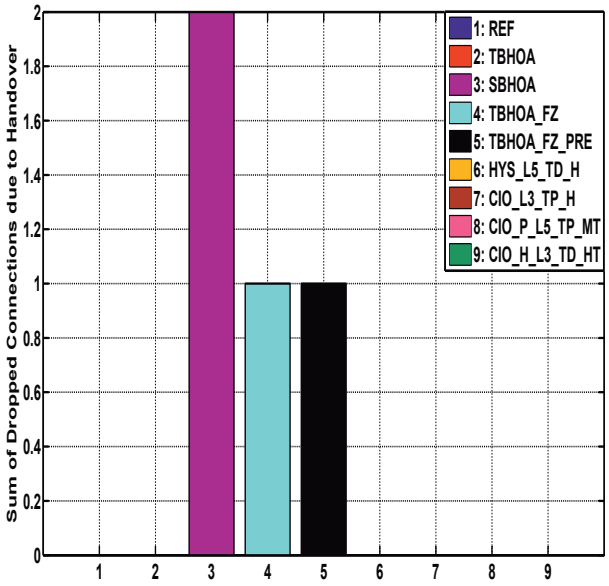

(a) Sum of dropped connections of user 10 (HO cond.)

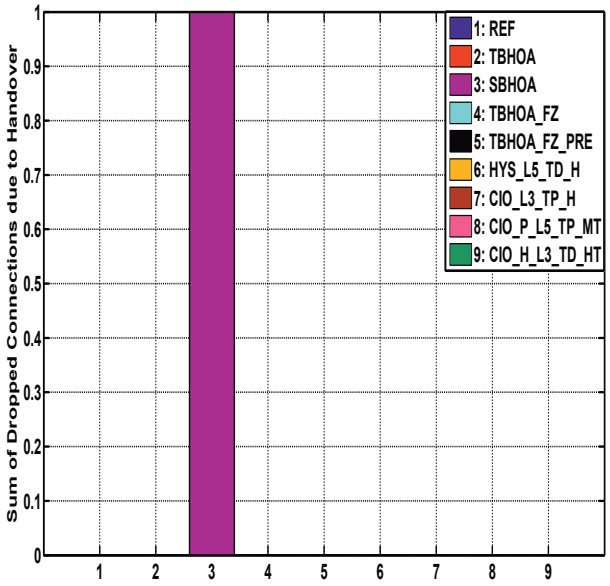

(b) Sum of dropped connections of user 11 (HO cond.)

Figure 8.48: Sum of dropped connections (HO cond.) of users moving at 33.3 m/s (120 km/h)

HOA_FZ_PRE result in one connection drop for fast moving user 10, too. In terms of HO failures, velocity-specific performance is shown in Figure 8.49, Figure 8.50, and Figure 8.51, respectively.

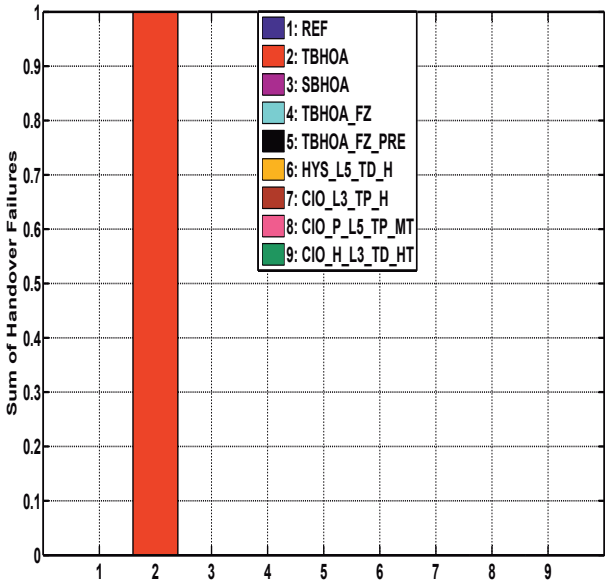

(a) Sum of HO failures of user 4 moving at 30 km/h

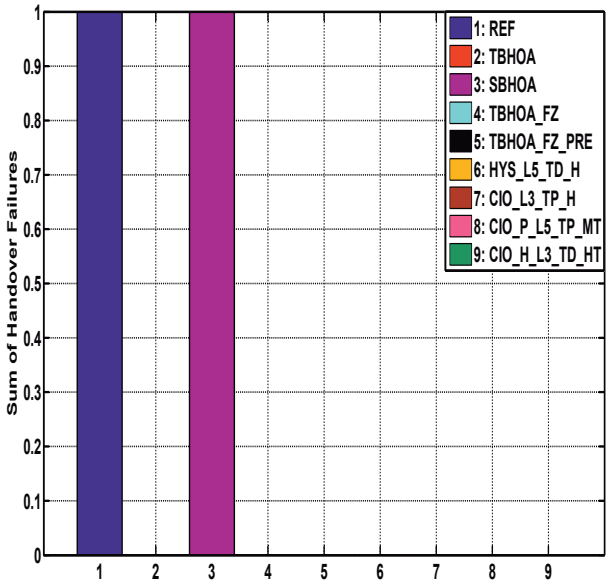

(b) Sum of HO failures of user 5 moving at 30 km/h

Figure 8.49: Sum of HO failures of users moving at 30 km/h

In case of UE 4 moving at 30 km/h, *TBHOA* performs worst among all

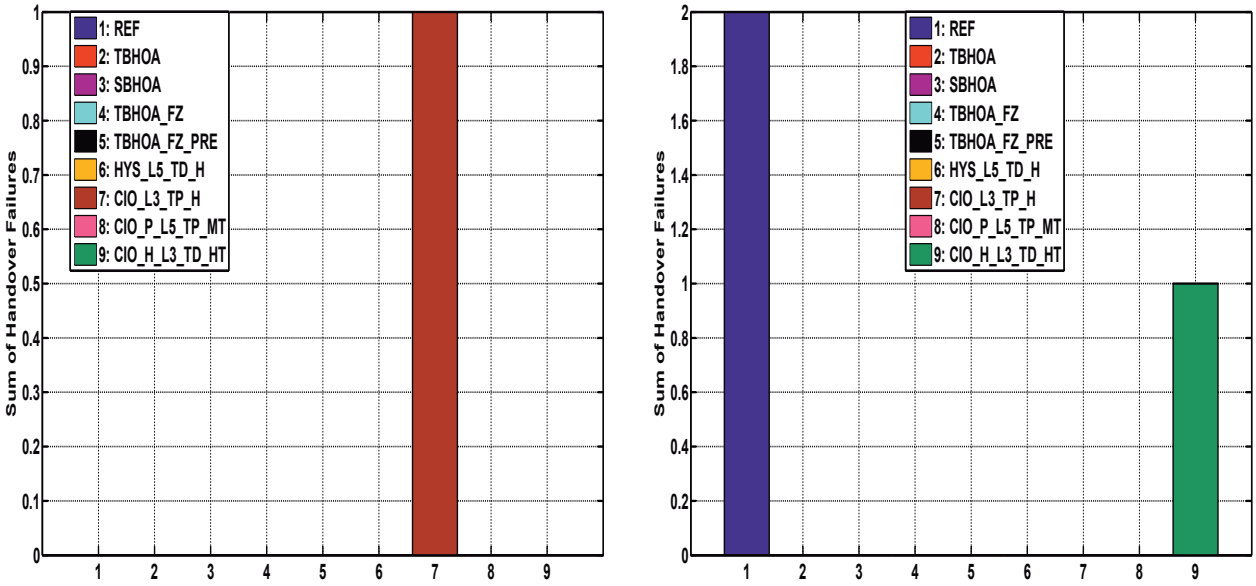

(a) Sum of HO failures of user 6 moving at 50 km/h

(b) Sum of HO failures of user 7 moving at 50 km/h

Figure 8.50: Sum of HO failures of users moving at 50 km/h

schemes and results in one HO failure. For UE 5 moving at 30 km/h, all MRO schemes except *SBHOA* are able to reduce the sum of HO failures to zero.

In case of UE 6 moving at 50 km/h around BS 0 in clock-wise direction, *CIO_L3_TP_H* performs worst among all schemes resulting in one HO failure. For user 7 moving at 50 km/h in counter-clockwise direction around BS 0, all MRO schemes except *CIO_H_L3_TD_HT*, which only achieves a reduction of 50%, eliminate HO failures completely.

In case of UE 8 moving at 70 km/h in clockwise direction around BS 0, all considered MRO schemes are able to improve HO performance by 50%. For UE 9 moving at 70 km/h, only *CIO_L3_TP_H* results in one failed HO attempt. In summary, worst HO performance compared to *REF* and evaluated velocity classes is observed for *CIO_L3_TP_H*.

In Figure 8.52, ping-pong HO performance is illustrated for fast moving users 10 and 11 that are the only UEs affected by ping-pong HOs. Regarding ping-pong HOs experienced by UE 10, which moves at 120 km/h on a ring road between BS sectors (0/0), (1/1), and (2/2), all MRO schemes except *TBHOA*, *SBHOA*, and *HYS_L5_TD_H*, which only yield a reduction of 75%, are able to reduce the number of ping-pong HOs to zero. For UE 11 that follows the same ring road as UE 10 in counter-clockwise direction, all considered MRO schemes result in reduced number of ping-pong HOs. Best performance is obtained by *SBHOA*, *TBHOA_FZ*, and *TBHOA_FZ_PRE*

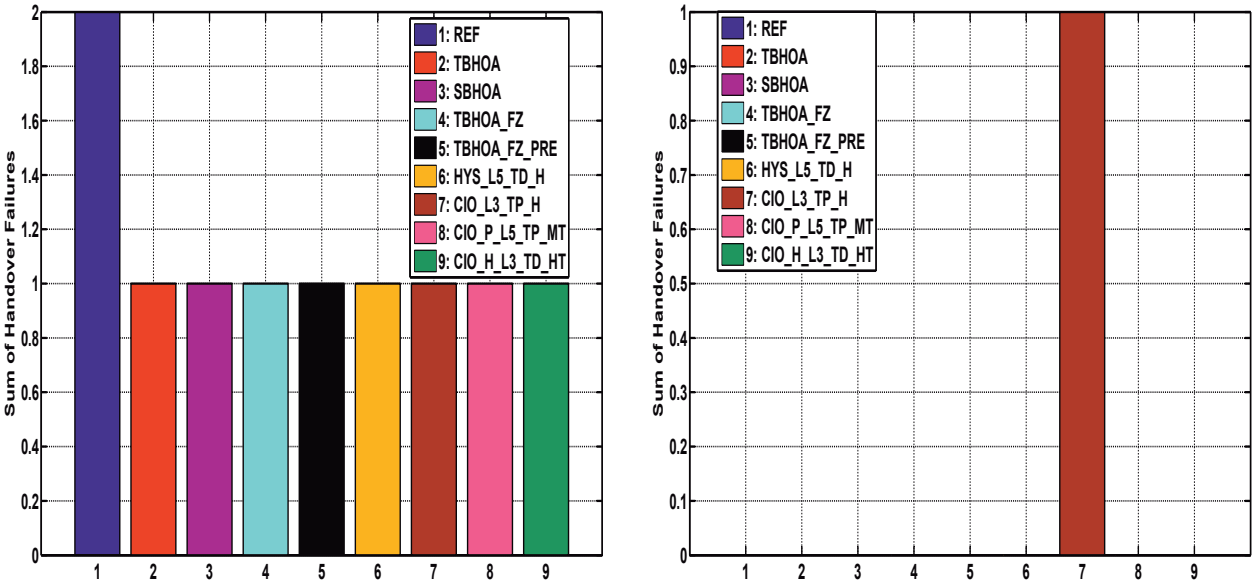

(a) Sum of HO failures of user 8 moving at 70 km/h

(b) Sum of HO failures of user 9 moving at 70 km/h

Figure 8.51: Sum of HO failures of users moving at 70 km/h

yielding an improvement of 50%. *CIO_P_L5_TP_MT* achieves second best ping-pong HO performance and performs best among the FQL based schemes achieving a reduction of 37.5%. In summary, best ping-pong HO performance is observed for *TBHOA_FZ* and *TBHOA_FZ_PRE*. Least enhancements are obtained by employing *TBHOA*, *HYS_L5_TD_H*, and *SBHOA*.

In essence, the velocity- and UE-specific results confirm the performance differences observed in the BS-specific results. Among the FQL based MRO schemes *CIO_P_L5_TP_MT* performs best, since the only mobility-related events that occur are ping-pong HOs (cf. Figure 8.52(b)). *HYS_L5_TD_H* can be ranked second and *CIO_H_L3_TD_HT* third best due to one more HO failure event (cf. Figures 8.49, 8.50, 8.51) compared to *HYS_L5_TD_H*. For *CIO_L3_TP_H*, the highest number of HO failures among the considered FQL based MRO schemes is observed. However, all considered FQL based MRO approaches outperform all other benchmark schemes, such as *REF*, *TBHOA*, *SBHOA*, *TBHOA_FZ*, and *TBHOA_FZ_PRE*.

The performance results presented in Section 8.2.8 indicate that for the considered scenario 2 a rather low granularity with respect to fuzzy labels applied for classifying KPI degradations is sufficient. Here, all best performing MRO schemes use either 3 or 5 fuzzy labels for assessing KPI degradations.

Regarding overall number of connection drops observed at various BSs (cf. Figure 8.43(a) and Figure 8.43(b)), all FQL based schemes result in the same overall amount of connection drops as the reference scheme *REF*. Although

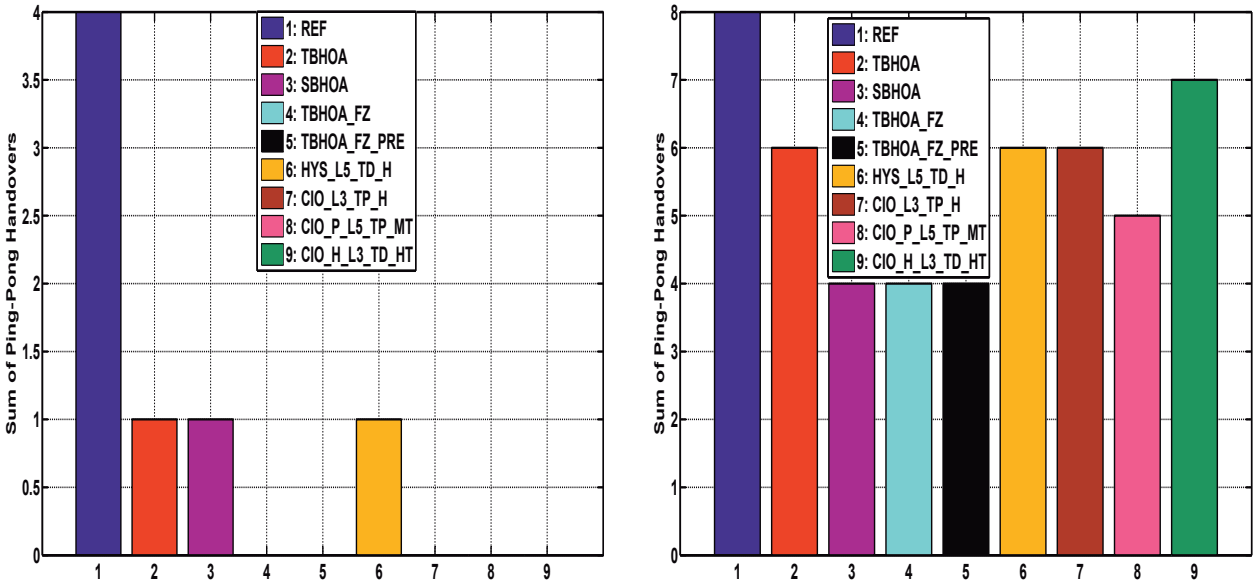

(a) Sum of ping-pong HOs of user 10 moving at 120 km/h

(b) Sum of ping-pong HOs of users 11 moving at 120 km/h

Figure 8.52: Sum of ping-pong HOs of users 10 and 11 moving at 120 km/h

other approaches (*TBHOA*, *SBHOA*, *TBHOA_FZ*, *TBHOA_FZ_PRE*) improve dropping performance for the majority of the considered BSs, these approaches yield significant performance degradations for BS (0/0), where besides BS (2/2) the optimization schemes are executed. The significantly worse performance of non-FQL based schemes, such as *TBHOA*, *SBHOA*, *TBHOA_FZ*, and *TBHOA_FZ_PRE*, results from the fact that these approaches are not able to compensate for the impact of connection drops due to local coverage holes (cf. Figure 8.5(a)), which are located at cell sector borders and thus in the HO area as illustrated in Figure 3.1. However, the extent of the coverage hole, user velocity, and HO parameter settings, e.g., HYS and TTT, have a direct impact on the number of resulting connection drops due to RLF or session timeout. Since the non-FQL based approaches, such as *TBHOA*, *SBHOA*, *TBHOA_FZ*, and *TBHOA_FZ_PRE*, rely on static optimization strategies, where fix and pre-defined adaptation rules are stored in Look-Up Tables (LUTs), these schemes are not able to adapt to local conditions, such as coverage hole sizes or degree and directions of user mobility, and hence they are incapable of autonomously establishing context awareness.

In terms of HO failures, which are only observed at BS (0/0), *TBHOA_FZ*, *TBHOA_FZ_PRE*, as well as the FQL based schemes *HYS_L5_TD_H* and *CIO_P_L5_TP_MT* yield best performance. Further, it should be noted that *TBHOA_FZ* and *TBHOA_FZ_PRE* execute optimizations at the same

interval as *TBHOA*, *SBHOA*, and all other schemes. However, *TBHOA_FZ* and *TBHOA_FZ_PRE* apply fuzzy logic for assessing KPI degradations and determining corresponding countermeasures, as described in Section 7.3.2. Since these fuzzy logic based MRO schemes classify KPI degradations according to their degree of deviation from performance targets, they are able to counteract severe KPI degradations by, e.g., adapting HYS parameter by two steps instead of only one as in the case of *TBHOA* and *SBHOA*. Further, even larger degrees of freedom can be exploited by FQL based schemes.

For BSs where performance is heavily affected by ping-pong HOs, such as BS (2/2), *CIO_P_L5_TP_MT* is the best performing FQL based MRO approach. This scheme, which jointly tunes CIO parameters of serving and target BS in a cell pair-specific manner, is able to exploit the neighbor relation of serving and target BS for optimizing ping-pong HO performance, here between BS (0/0) and BS (2/2). For every occurred ping-pong HO, source and target cell sector are recorded. In case the FQL based MRO scheme assesses PHR as too high, joint CIO parameter adaptations of serving and target cell sector CIOs (O_s and O_t, cf. Equation (3.1)) are triggered. For example, if the fuzzy inference mechanism, which is introduced in Section 6.1 and described in more detail in Section 7.3.2, determines to increase HOM by 2.5 dB, then O_s is increased by 1.5 dB and O_t by 1 dB, respectively.

Similarly, *CIO_L3_TP_H*, which achieves second best ping-pong HO performance at BS (2/2), only adapts HOM by modifying the CIO parameter of the respective target cell sector O_t. In essence, both schemes beneficially exploit the knowledge on directions of occurring ping-pong HOs between neighboring cell sectors, here BS (0/0) and BS (2/2). Thus, *CIO_P_L5_TP_MT* and *CIO_L3_TP_H* are able to establish context awareness at the respective cell sector that is in charge of controlling HO parameter adaptations, while satisfying the same number of users as compared to *REF* and resulting in a comparable number of required simulation runs. However, *CIO_P_L5_TP_MT* exhibits higher complexity than *HYS_L5_TD_H* or *CIO_L3_TP_H*, since it uses HOM and TTT parameters (*MT*) for system state classification. In contrast, *CIO_L3_TP_H* employs 3 fuzzy labels for KPI assessment and only considers the HYS parameter for system state classification. Further, *HYS_L5_TD_H* requires 40% more simulation efforts compared to *CIO_L3_TP_H* (cf. Figure 8.46) until learning converges. Furthermore, the best performing approaches (*CIO_P_L5_TP_MT* and *CIO_L3_TP_H*) adapt TTT parameters in a proportional instead of a discrete manner, as in *HYS_L5_TD_H* and *CIO_H_L3_TD_HT*.

Moreover, it can be stated that the considered FQL based MRO schemes

are able to optimize multiple KPIs simultaneously, in particular at BS (0/0) where optimum performance is achieved with respect to connection drops and HO failures. For BS (2/2), FQL based MRO schemes only yield optimum performance with respect to ping-pong HOs, while overall number of connection drops is not improved compared to *REF*.

Evaluation of Fuzzy Q-Learning Performance for Scenario 2

In the previous subsection, best performing MRO approaches with respect to multiple KPIs were presented. Among all considered MRO schemes, FQL based schemes were found to outperform other approaches that rely on static adaptation rules stored in LUTs with respect to OPI. In the following, learned rule/action pairs that achieve optimum system performance for each considered FQL based MRO scheme (*HYS_L5_TD_H, CIO_L3_TP_H, CIO_P_L5_TP_MT, CIO_H_L3_TD_HT*) are illustrated per BS.

The rule/action pairs the BS-specific FIS identified to apply to a certain situation result in various HO parameter adaptations, as described in Section 7.3.2. In case the adaptations determined by the FIS would result in a HO parameter setting below the lowest possible value, e.g., for HYS 0 dB, the HO parameter is set to the lowest value of the respective HO parameter interval specified by the FIS designer.

Figure 8.53(a) and Figure 8.53(b) depict the 15 rule/action pairs that achieved highest Q values after learning converged for BS (0/0) and (2/2), respectively, using *FQL_HYS*. The listed rule/action pairs are sorted in descending order with respect to finally obtained Q values. In case of high HFR ratios observed at BS (0/0), the best rule/action pair found after learning converged indicates to increase HYS parameter by 4 steps, i.e., 2 dB, if HYS parameter is found to be "low" (HFR_H_l). For high CDR and low as well as high HYS values (CDR_H_l, CDR_H_h), the rule/action pairs with the highest Q values recommend to decrease HYS parameter by 4 steps. Since ping-pong HOs are never observed at BS (0/0), no corresponding adaptation was ever triggered.

Regarding BS (2/2), highest Q values are achieved for a rule/action pair that indicates to increase TTT parameter by 4 steps in case of high PHR and low HYS values (PHR_H_l). Further, it should be noted that *HYS_L5_TD_H* adapts TTT parameters in a discrete manner given a set of available TTT settings. For high CDR and low HYS parameter (CDR_H_l), the rule/action pair with the highest Q value recommends to decrease HYS parameter by 4 steps, i.e., 2 dB. Rarely, HO failure events occurred at BS

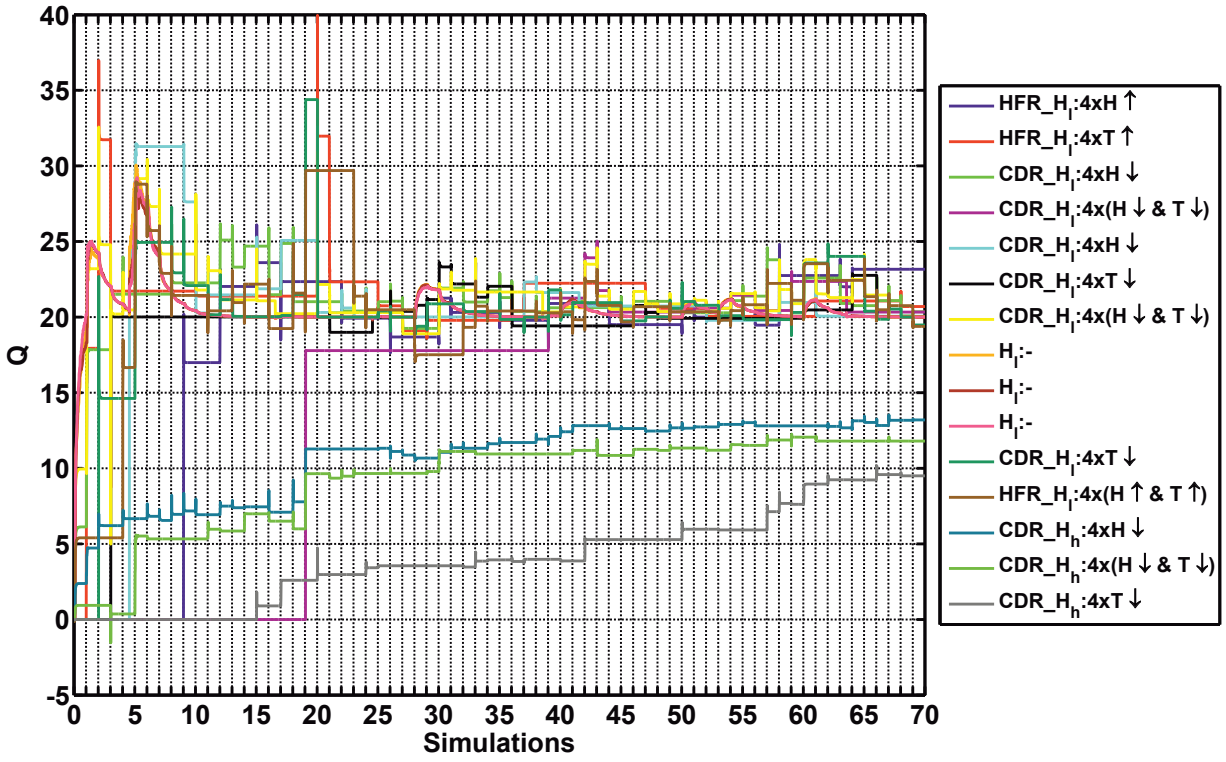

(a) Q value evolution vs. simulation runs at BS (0/0)

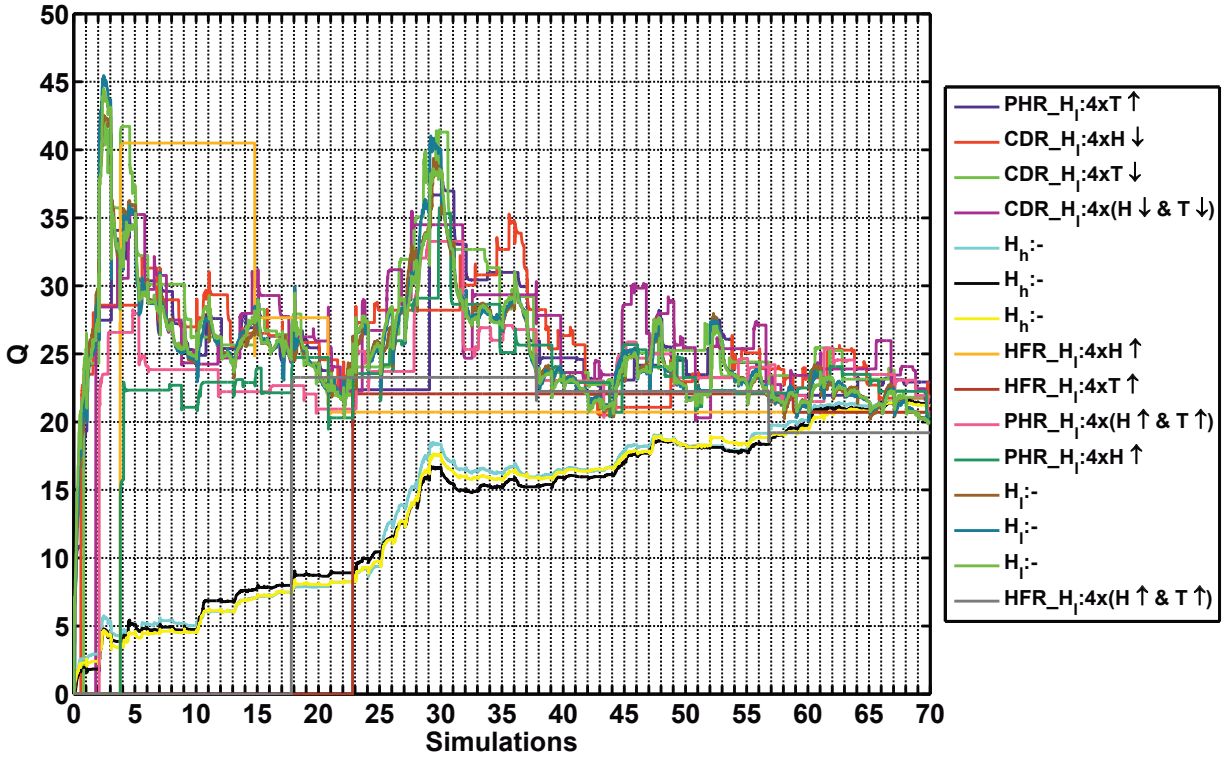

(b) Q value evolution vs. simulation runs at BS (2/2)

Figure 8.53: Q value evolution vs. simulation runs using *HYS_L5_TD_H*

(2/2), too. In case of high HFR and low HYS parameter (*HFR_H*$_l$), increasing current HYS parameter setting by 4 steps was found to be the best performing adaptation. The rule/action pairs "H_l:−" and "H_h:−" refer to idle

states, where no KPI degradations are observed at low and high HYS values, respectively.

In Figure 8.54(a) and Figure 8.54(b), the 15 rule/action pairs with the highest Q values obtained for BS (0/0) and (2/2), respectively, using *FQL_CIO* are illustrated. For BS (0/0), HFR issues at low HYS values are best counteracted by increasing HYS parameter by 2 steps. In case of *FQL_CIO*, this refers to adapting CIO setting at target BS (O_t). For high CDR ratios at low HYS values, the best rule/action pair found after learning converged indicates to decrease HYS parameter by 2 steps, i.e., 1 dB. In case of high CDR ratios at high HYS values, decreasing both HYS and TTT parameters by 2 steps is found to be the best countermeasure. For high HFR ratios at high HYS values, the rule/action pair that yields highest Q value indicates to increase TTT parameter by 2 steps. Here, this refers to proportionally adapting TTT settings, i.e., multiplying current TTT value by 2 and using the quantization scheme shown in Figure 8.22 to derive the final TTT value.

Regarding BS (2/2), highest Q values are achieved for a rule/action pair that indicates to decrease both HYS and TTT parameters by 2 steps, in case of high CDR and low HYS values (CDR_H_l). For high PHR ratios and both low and high HYS values (PHR_H_l, PHR_H_h), the best countermeasure obtained after learning is to increase TTT parameter by 2 steps in a proportional manner. In case of high CDR and high HYS values, highest Q values are obtained for a rule/action pair that indicates to decrease HYS parameter by 2 steps, i.e., 1 dB.

Figure 8.55(a) and Figure 8.55(b) depict the 15 rule/action pairs with the highest Q values found for BS (0/0) and (2/2), respectively, using *FQL_CIO_P*. For BS (0/0), the top rule/action pair indicates to increase both HYS and TTT parameters by 4 steps in case of high HFR ratios and low HYS value. For high CDR and high HYS values, the rule/action pair with the highest Q value recommends to decrease TTT parameter by 4 steps, where *CIO_P_L5_TP_MT* adapts TTT settings in a proportional manner. In case of high CDR and low HYS values, the best countermeasure obtained after learning converged is to decrease both HYS and TTT parameters by 4 steps.

Regarding BS (2/2), HFR issues rarely occur. Nevertheless, they are best counteracted by increasing both HYS and TTT parameters by 4 steps, if HYS values are low (HFR_H_l). In case of high CDR ratios and high HYS values, the best rule/action pair found after learning converged indicates to decrease both HYS and TTT parameters by 4 steps. For high CDR ratios and low HYS values, highest Q value is obtained for a rule/action pair that

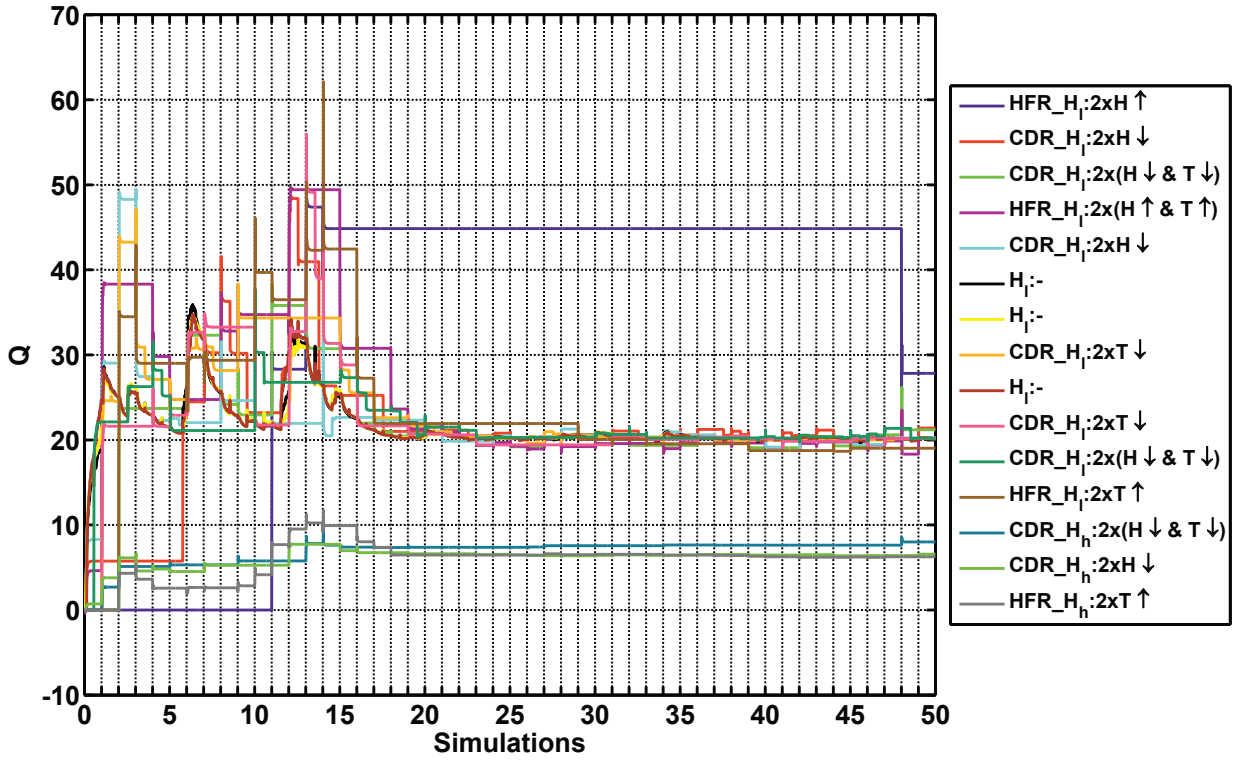

(a) Q value evolution vs. simulation runs at BS (0/0)

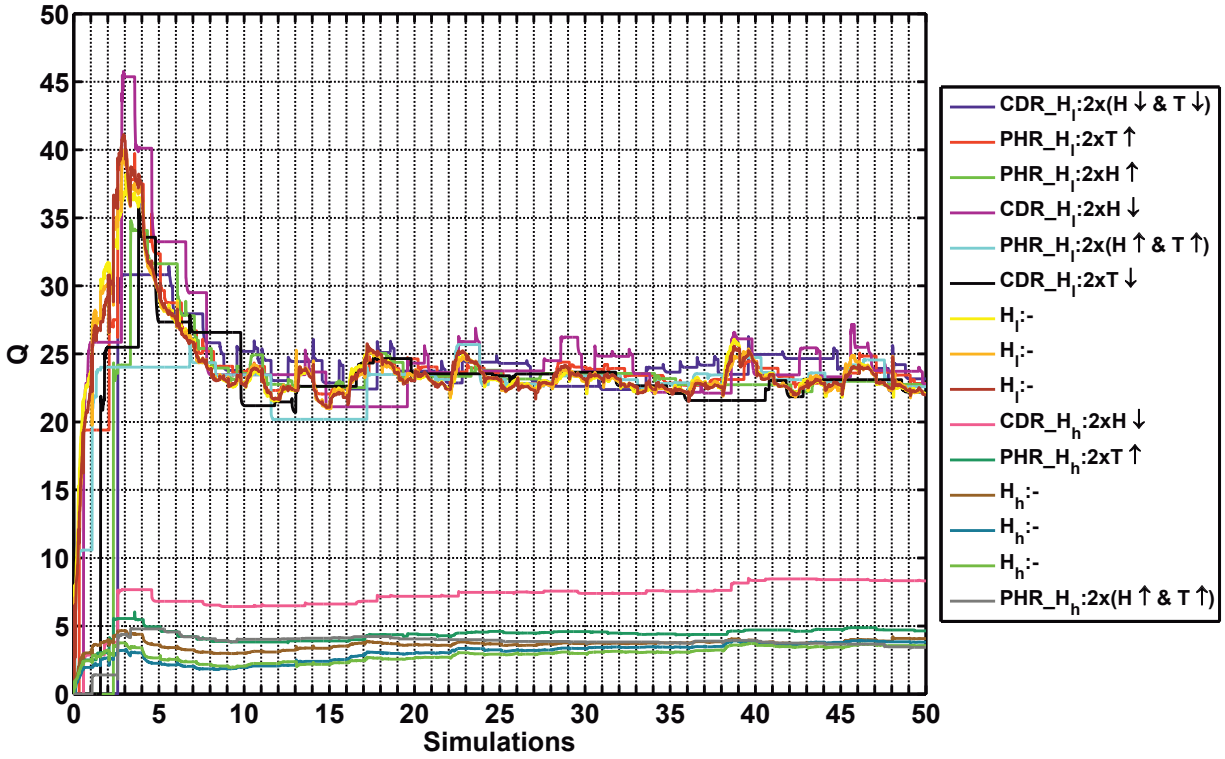

(b) Q value evolution vs. simulation runs at BS (2/2)

Figure 8.54: Q value evolution vs. simulation runs using *CIO_L3_TP_H*

indicates to decrease HYS parameter by 4 steps, i.e., 2 dB. In case of high PHR and low HYS values (*PHR_H_l*), the potentially best countermeasure is to increase TTT parameters by 4 steps in a proportional manner.

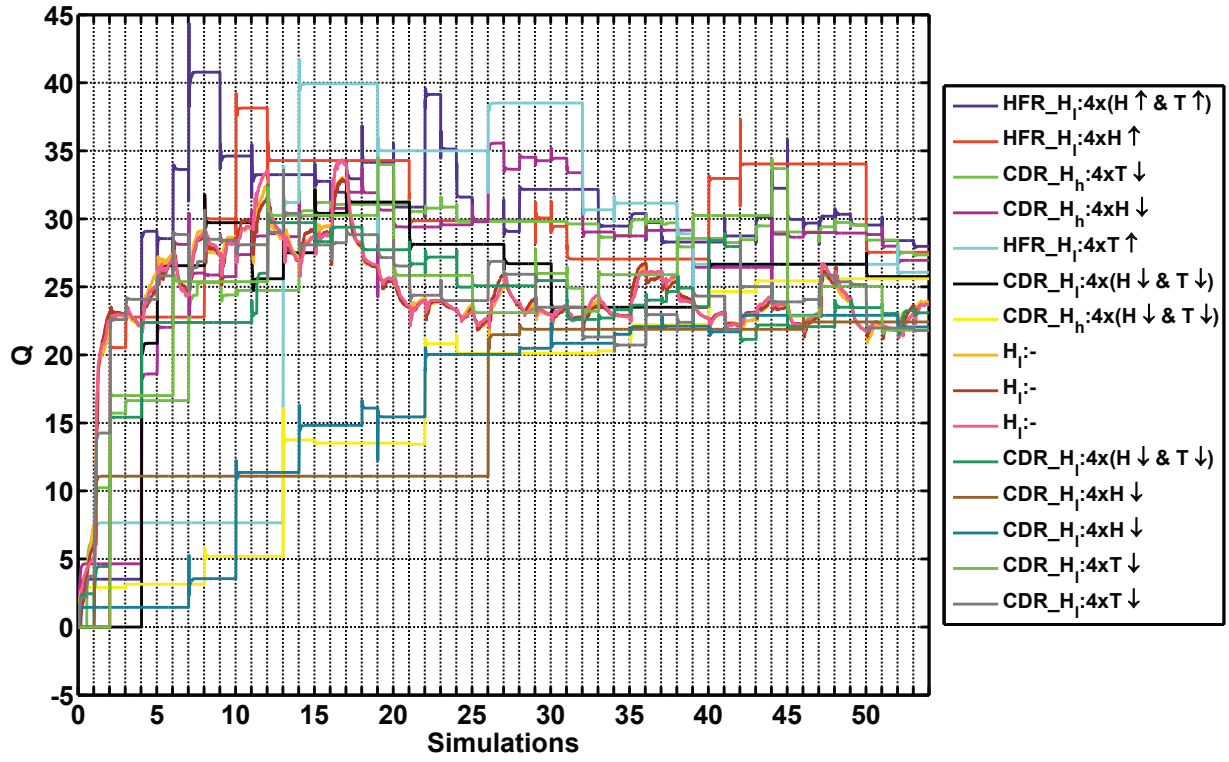

(a) Q value evolution vs. simulation runs at BS (0/0)

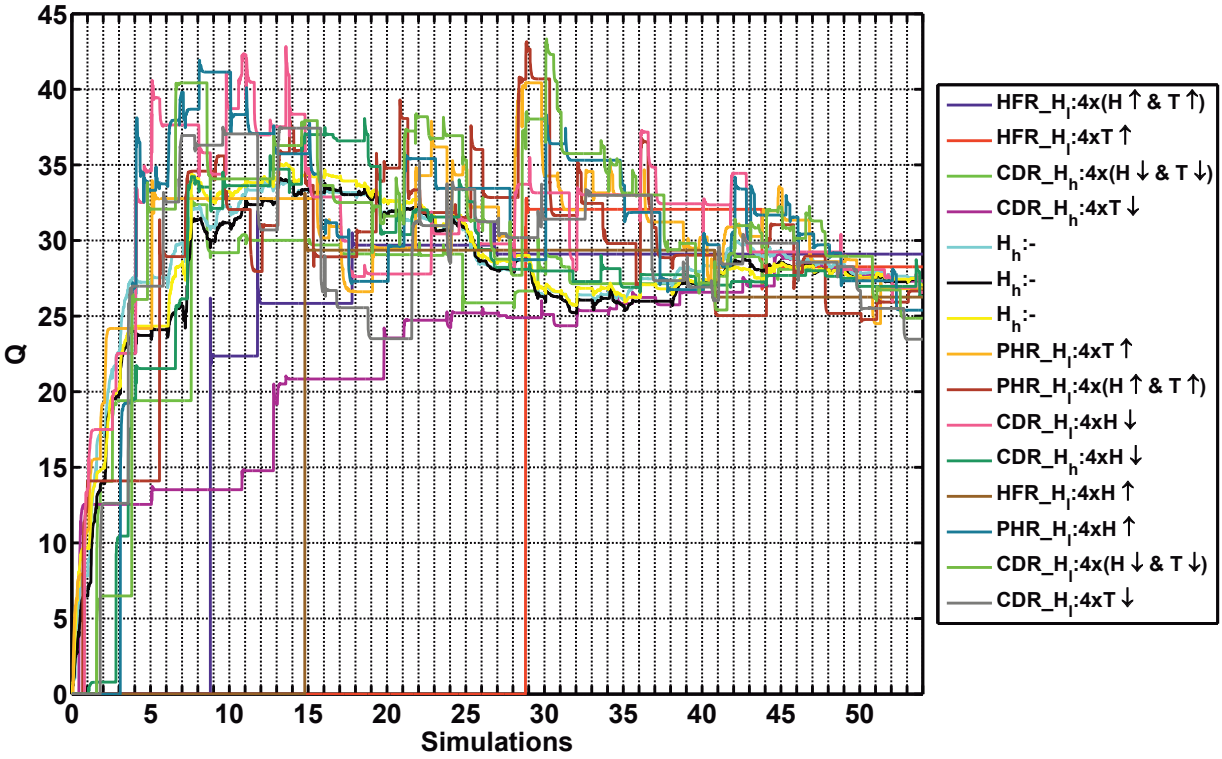

(b) Q value evolution vs. simulation runs at BS (2/2)

Figure 8.55: Q value evolution vs. simulation runs using *CIO_P_L5_TP_MT*

In Figure 8.56(a) and Figure 8.56(b), the 15 rule/action pairs with the highest Q values obtained for BS (0/0) and (2/2), respectively, using *FQL*

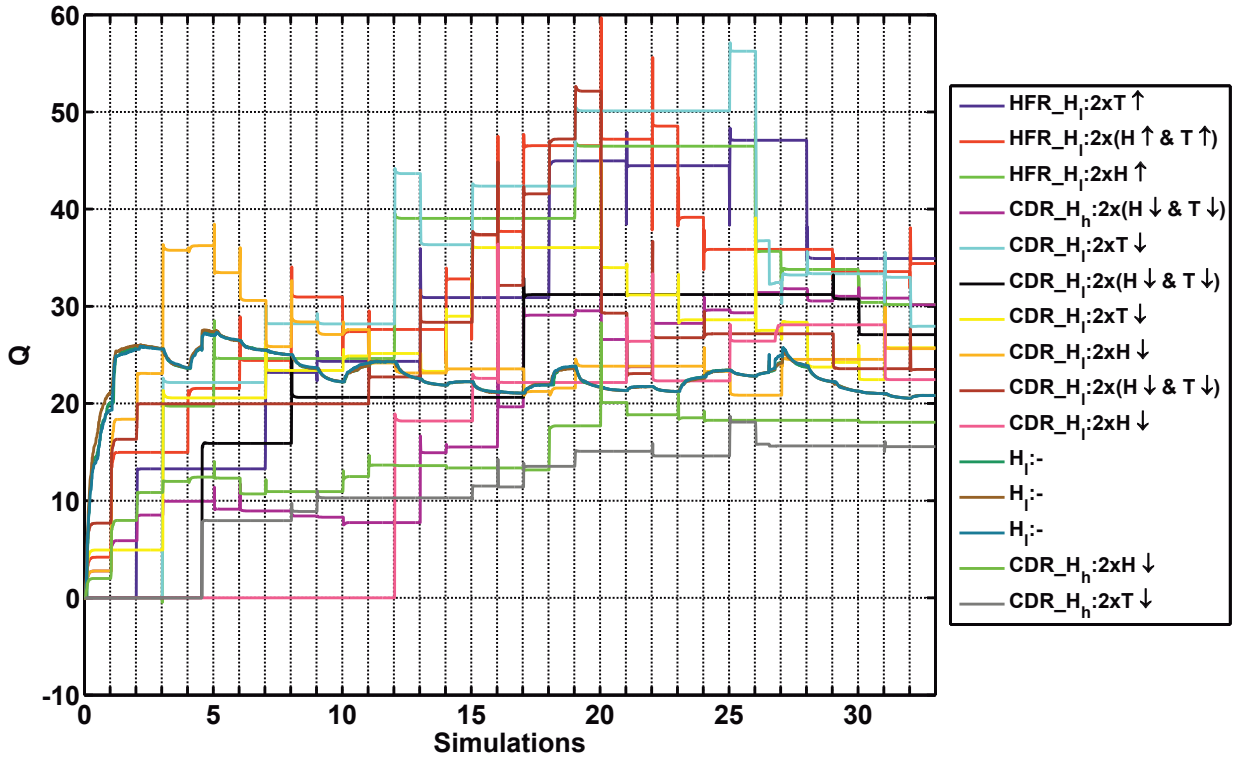

(a) Q value evolution vs. simulation runs at BS (0/0)

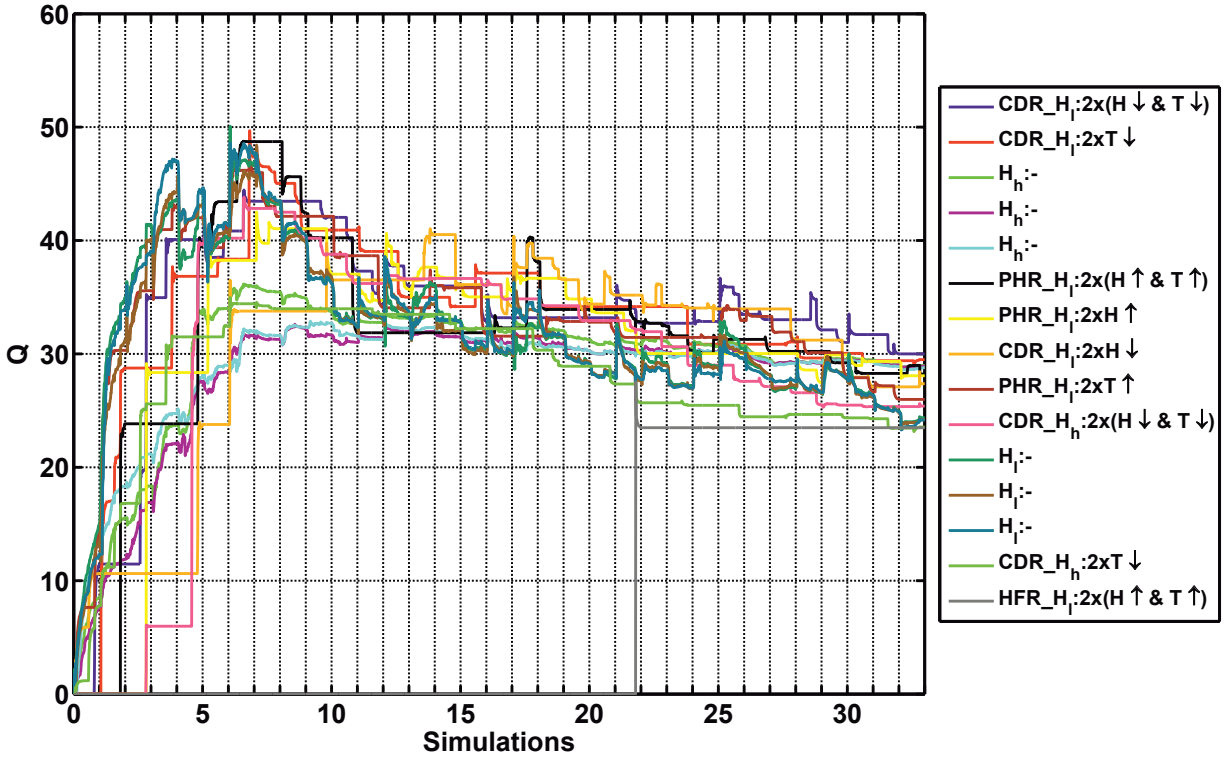

(b) Q value evolution vs. simulation runs at BS (2/2)

Figure 8.56: Q value evolution vs. simulation runs using *CIO_H_L3_TD_HT*

_CIO_H are illustrated. For BS (0/0), high HFR ratios at low HYS values are best counteracted by increasing TTT parameters by 2 steps, where

CIO_H_L3_TD_HT adapts TTT parameters in a discrete manner given a set of available TTT settings. In case of high CDR ratios and high HYS values, the highest Q value is obtained for the rule/action pair indicating to decrease both HYS and TTT parameters by 2 steps. For high CDR ratios and low HYS values, best performance is obtained by decreasing TTT parameters by 2 steps.

Regarding BS (2/2), highest Q values are achieved for a rule/action pair that indicates to decrease both HYS and TTT parameters by 2 steps, if CDR ratio is high and HYS value is low. In case of high PHR ratios at low HYS values, the best countermeasure obtained after learning is to increase both HYS and TTT parameters by 2 steps. For high CDR and high HYS values, the best rule/action pair recommends to decrease both HYS and TTT parameters by 2 steps. Although HO failure issues rarely occur at BS (2/2), they are best counteracted by increasing both HYS and TTT parameters by 2 steps.

Learned Handover Parameter Adaptations

In the following, performed HO parameter adaptations, triggering KPI issues, as well as KPI evolutions over simulation time are shown per BS for each considered FQL based MRO scheme (*HYS_L5_TD_H, CIO_L3_TP_H, CIO_P_L5_TP_MT, CIO_H_L3_TD_HT*). The applied HO parameter adaptations originate from the set of available actions as defined by the rule/action table (e.g., cf. Table 7.5). Further, the various FQL based MRO schemes differ with respect to the HO parameter sets that are tuned as already described at the beginning of Section 8.2. Moreover, the specified EEP determines whether an action that has already shown to perform well for the observed system state is selected or a rather rarely chosen action should be tried. In the following, the best performing adaptation sequences per BS and FQL based MRO scheme are illustrated with respect to the considered simulation time window.

Figure 8.57 and Figure 8.58 depict KPI evolutions and problems that triggered the performed HO parameter adaptations, as well as HO parameter values over simulation time for BS (0/0) and (2/2), respectively, using *FQL_HYS*. At BS (0/0), mainly connection drops and HO failures are observed, whereas at BS (2/2) connection dropping and ping-pong HO issues dominate. Upon detection of a first HO failure event, cell-specific HYS and TTT settings are increased by 3 and 4 steps, respectively. These adaptations correspond to increasing HYS by 1.5 dB and TTT by 4 discrete steps

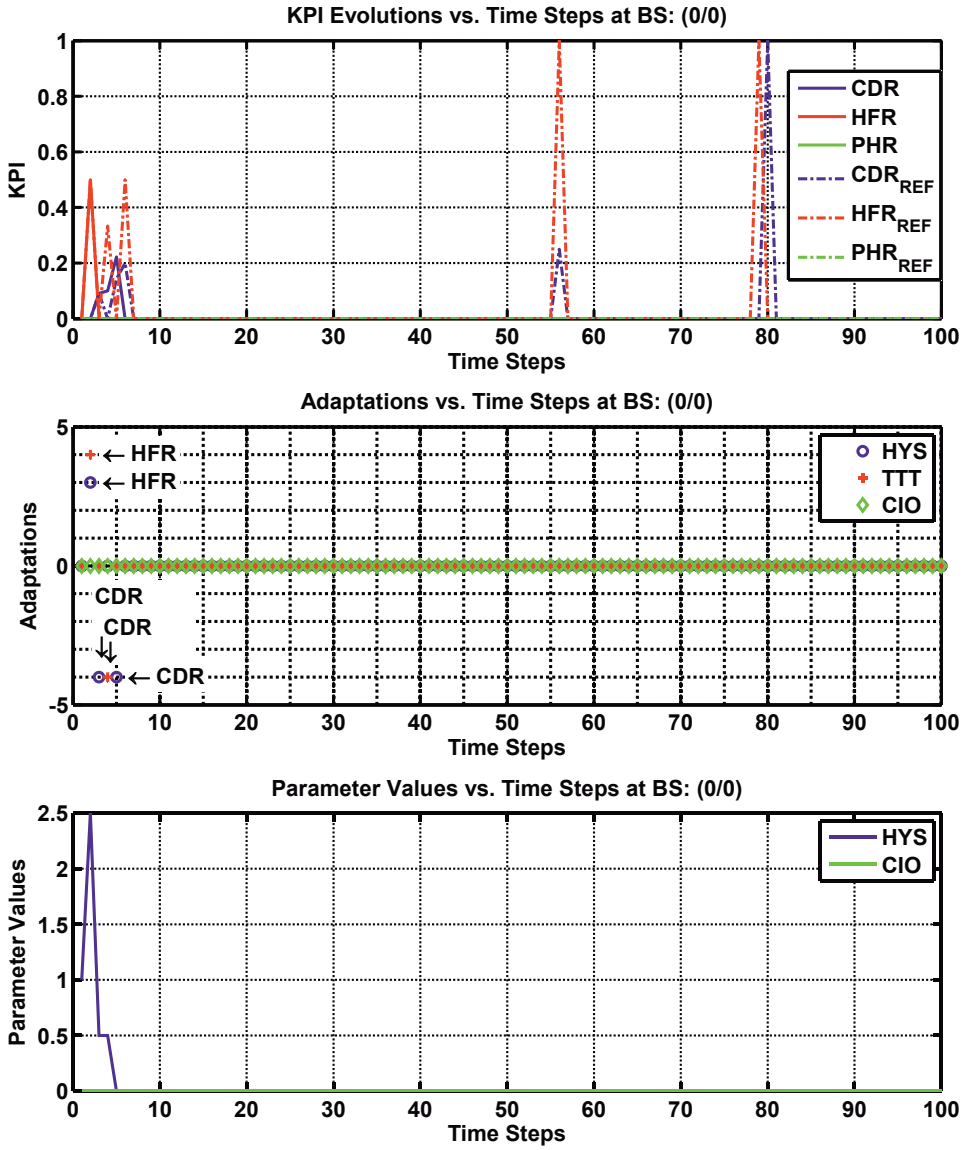

Figure 8.57: KPI evolutions, HO parameter adaptations, and HO parameter values vs. simulation time at BS (0/0) using *HYS_L5_TD_H*

according to the set of available TTT settings. At subsequent optimization intervals, several connection dropping-related issues are counteracted by decreasing HYS, TTT, and again HYS parameter by 4 steps, respectively. These adaptations performed at the beginning of the observation time window have a positive impact on system performance, since KPI issues, such as connection dropping or HO failures, that would have arisen in the following are completely avoided, as depicted for BS (0/0) in Figure 8.57.

In case of BS (2/2), performance degradations are mainly due to ping-pong HOs and connection drops. *HYS_L5_TD_H* counteracts ping-pong HO issues by increasing HYS or both HYS and TTT settings, respectively. If performance issues due to connection drops are observed, both HYS and TTT parameters are decreased to different extents. The performed adapta-

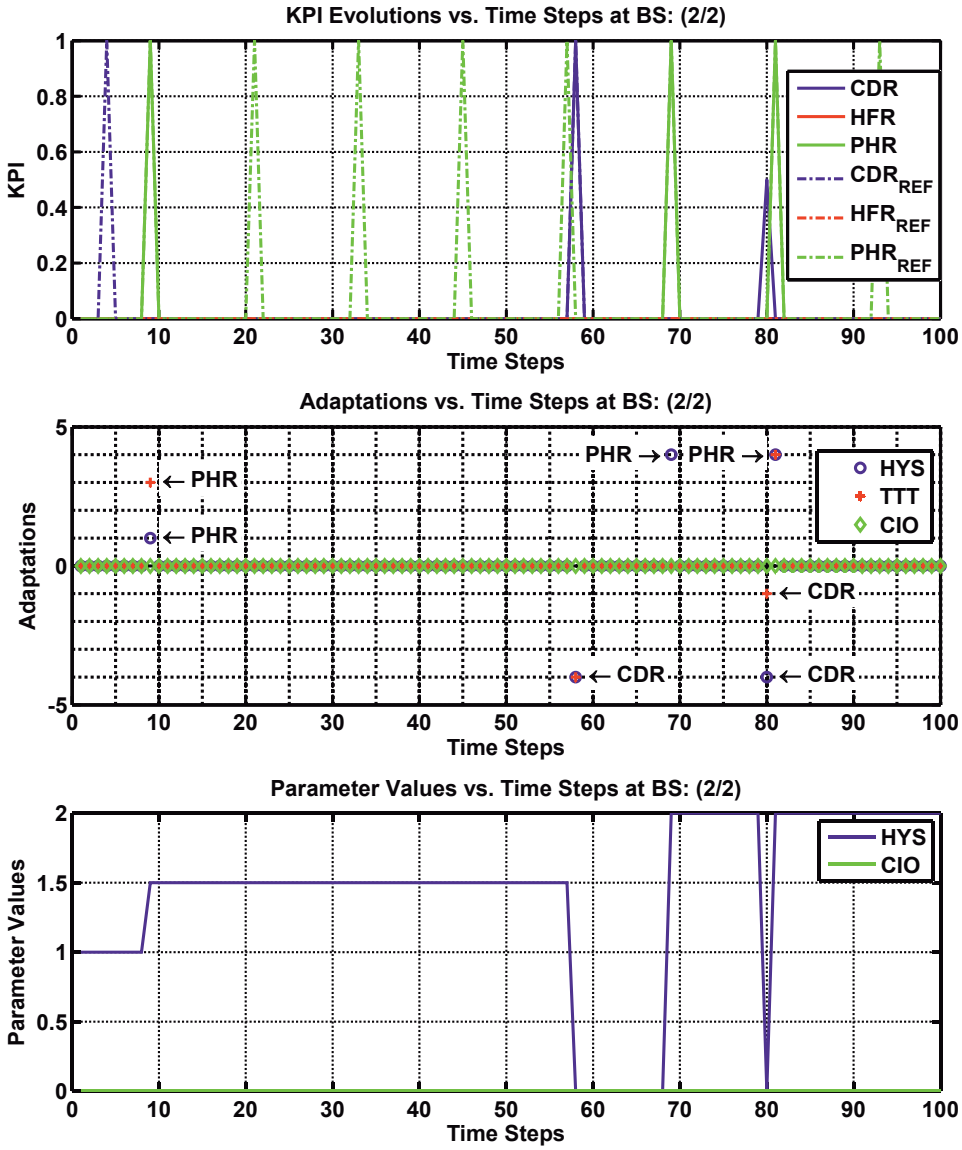

Figure 8.58: KPI evolutions, HO parameter adaptations, and HO parameter values vs. simulation time at BS (2/2) using *HYS_L5_TD_H*

tions result in a significant reduction of ping-pong HOs. However, it should be noted that *HYS_L5_TD_H* is limited with respect to possible HYS parameter adaptations, since as soon as HYS is set to zero, it cannot be reduced further, although recommended by the FIS. Moreover, the connection dropping event, which occurs at the beginning of the observation time window at BS (2/2) (cf. Figure 8.58 blue dashed line), results from a UE that in the reference simulation with static HO parameter settings performs a HO from BS (0/0) to BS (2/2). However, since *HYS_L5_TD_H* increases HYS and TTT values due to observed HO failure issue, the affected UE is not handed over from BS (0/0) to BS (2/2), but its connection is dropped while connected with source BS (0/0), thus contributing to CDR issues at BS (0/0).

In Figure 8.59 and Figure 8.60, KPI evolutions and issues that triggered

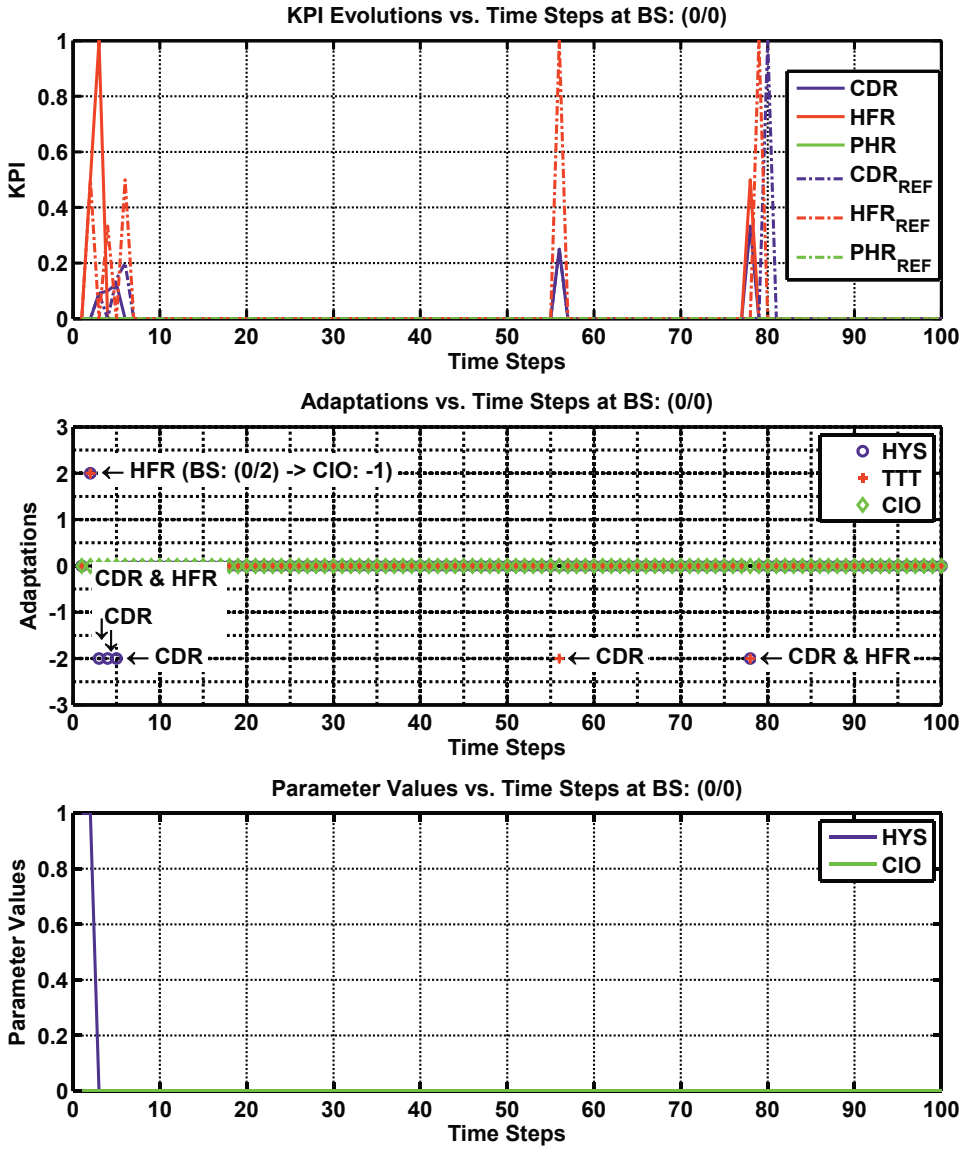

Figure 8.59: KPI evolutions, HO parameter adaptations, and HO parameter values vs. simulation time at BS (0/0) using *CIO_L3_TP_H*

the performed HO parameter adaptations, as well as HO parameter values over simulation time for BS (0/0) and (2/2), respectively, using *FQL_CIO* are illustrated. At BS (0/0), a HO failure event is detected first. Since *CIO_L3_TP_H* is able to identify the target BS (here BS (0/2)), toward which the HO procedure failed, HO parameters are adapted in a cell pair-specific manner. Here, the FIS recommends to increase both HYS and TTT settings by 2 steps, where not the cell-specific HYS value but the CIO values of the target BS (0/2) is adapted and set to -1 dB. However, these adaptations result in another HFR issue while at the same time a CDR is observed. Since CDR issues are assigned a higher weight than HFR issues due to MNO policy, according HO parameter adaptations that aim at relieving connection dropping related issues are performed, e.g., here decreasing cell-specific

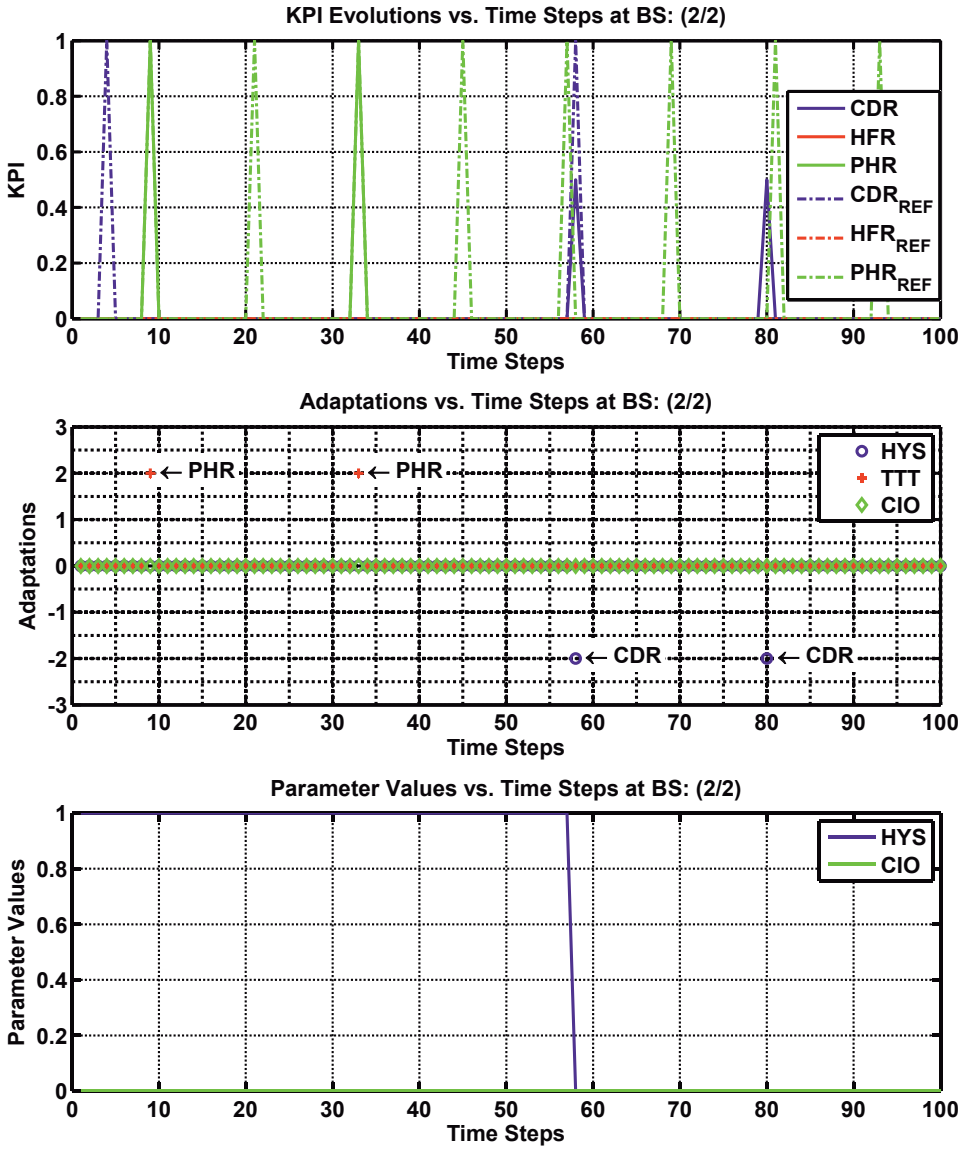

Figure 8.60: KPI evolutions, HO parameter adaptations, and HO parameter values vs. simulation time at BS (2/2) using *CIO_L3_TP_H*

HYS parameter by 2 steps. However, it should be noted that the lowest possible HYS parameter setting is 0 dB. In case of subsequent CDR issues, *CIO_L3_TP_H* reduces TTT settings in a proportional manner. In essence, CDR and HFR issues that occur in the second half of the observation time window can only be mitigated, but not completely eliminated.

In case of BS (2/2), observed PHR issues are counteracted by increasing TTT settings by 2 steps in a proportional manner. If connection dropping related performance degradations occur, cell-specific HYS parameter is reduced by 2 steps, which decreases HYS value from 1 to 0 dB. It should be noted that HYS parameter adaptations are limited, since as soon as HYS is set to zero, it cannot be reduced further. Nevertheless, the FIS recommends this adaptation, since it has shown to perform best for the given system state

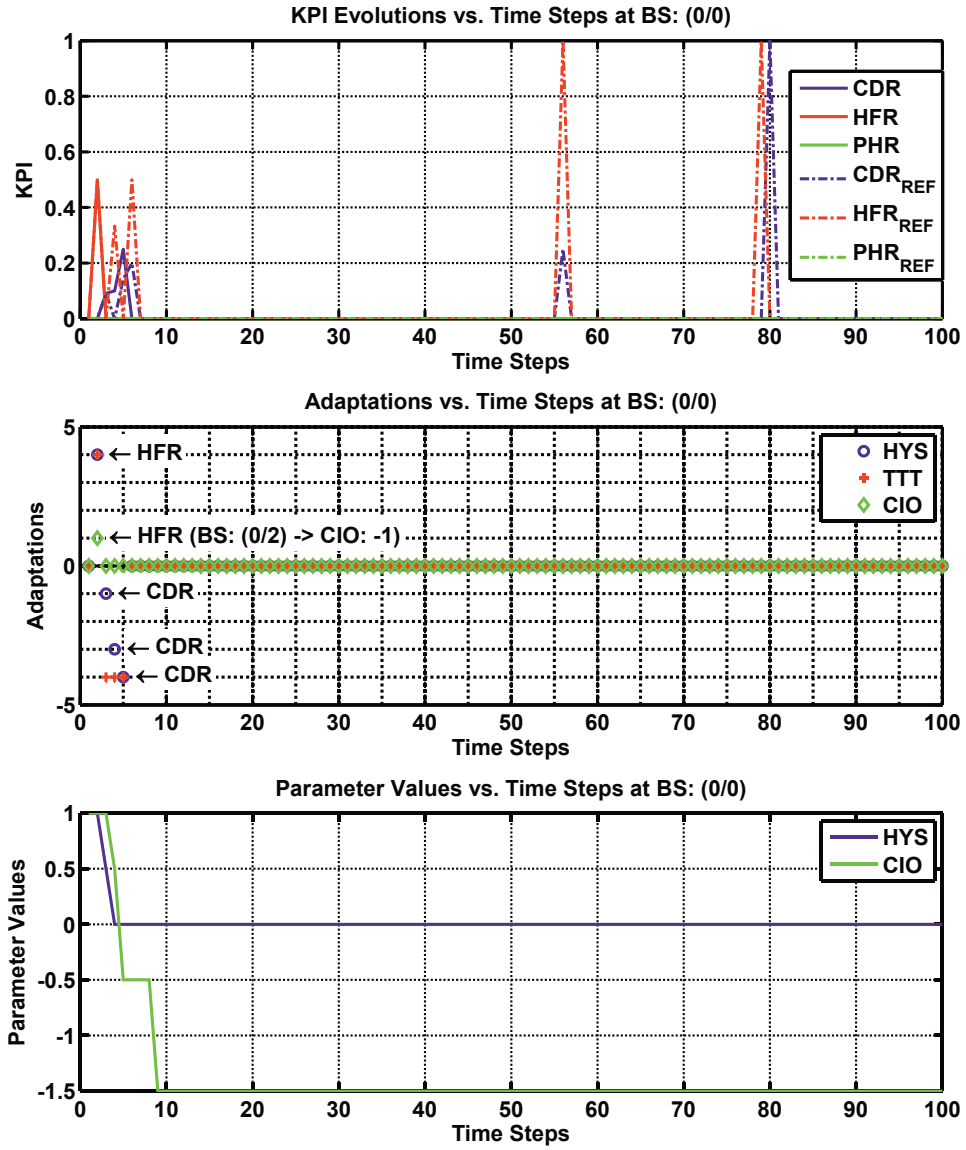

Figure 8.61: KPI evolutions, HO parameter adaptations, and HO parameter values vs. simulation time at BS (0/0) using *CIO_P_L5_TP_MT*

in the past.

Figure 8.61 and Figure 8.62 depict the performed HO parameter adaptations, triggering KPI issues, as well as KPI evolutions over simulation time for BS (0/0) and (2/2), respectively, using *FQL_CIO_P*. At BS (0/0), mainly connection drops and HO failures are observed, whereas at BS (2/2) connection drops and ping-pong HOs are the dominating performance issues. Upon detection of a first HO failure event, the FIS recommends to increase both HYS and TTT settings by 4 steps, respectively. Instead of tuning the cell-specific HYS value, *CIO_P_L5_TP_MT* identifies the target BS (here BS (0/2)), toward which the HO procedure failed, and adapts the CIO values of the source and target BSs (O_s and O_t, cf. Equation (3.1)) in a cell pair-specific manner. Here, both CIO values of the source and target cells are

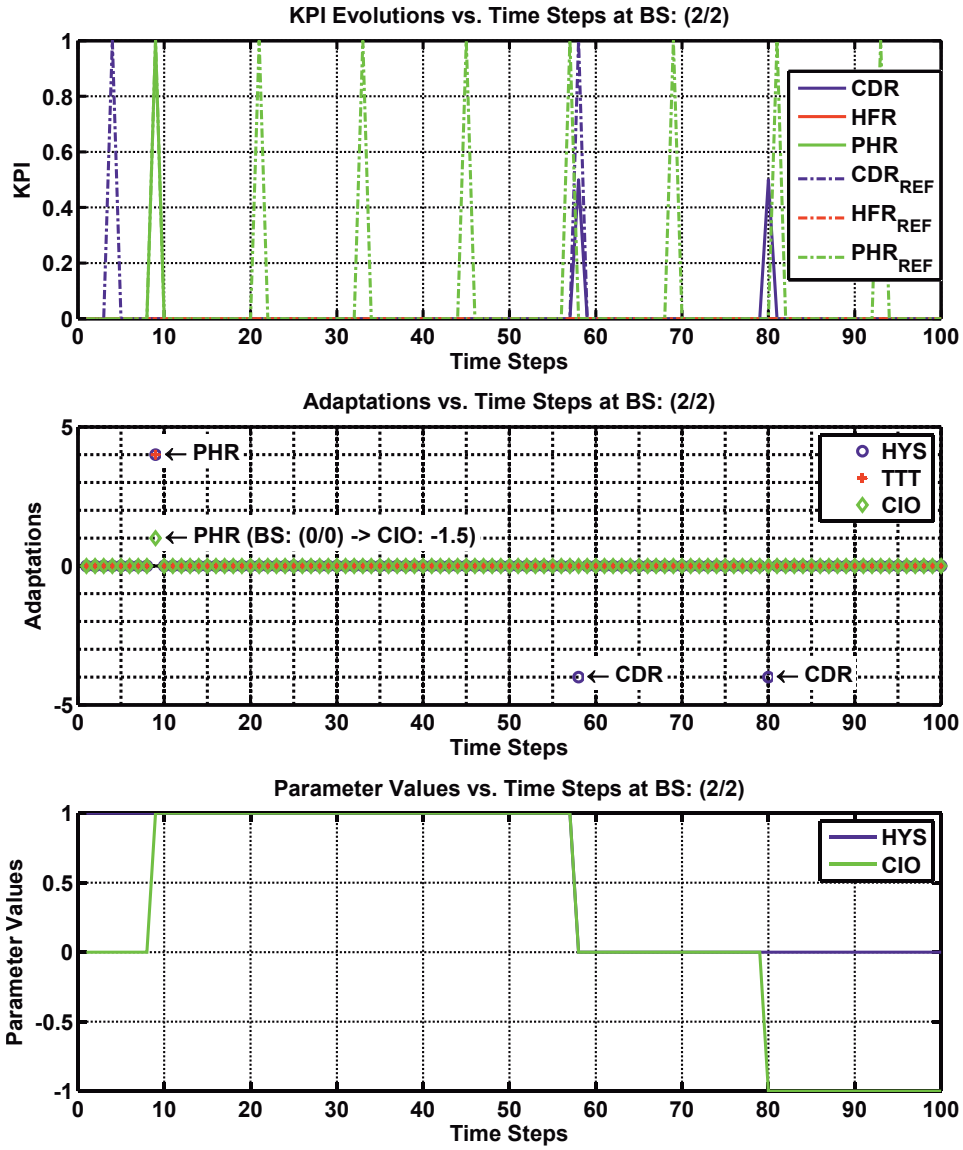

Figure 8.62: KPI evolutions, HO parameter adaptations, and HO parameter values vs. simulation time at BS (2/2) using *CIO_P_L5_TP_MT*

adapted by 2 steps, which corresponds to 1 dB, where O_t of the potential HO target BS is reduced to -1 dB, which effectively increases the HOM toward cell sector (0/2).

At subsequent optimization intervals, several connection dropping-related issues are counteracted by decreasing both cell-specific HYS and TTT parameter settings to various extents. It should be noted that the lowest possible HYS and TTT parameter settings are 0 dB and 0 ms, respectively. These adaptations performed at the beginning of the observation time window have a positive impact on system performance, since KPI issues, such as connection dropping or HO failures, that would have arisen in the *REF* case in the following are completely avoided, as depicted for BS (0/0) in Figure 8.61.

In case of BS (2/2), performance degradations are mainly due to ping-

pong HOs and connection drops. *CIO_P_L5_TP_MT* counteracts ping-pong HO issues by increasing both HYS and TTT settings by 4 steps, respectively. As *CIO_P_L5_TP_MT* additionally identifies the target BS (here BS (0/2)), toward which the HO procedure failed, the CIO values of the source and target cell sector are adapted by 2 steps each, i.e., O_s of BS (0/0) is increased from 0 to 1 dB and O_t (here O_s of BS (0/2)) is set to -1 dB. If performance issues due to connection drops are observed, the cell-specific HYS parameter is decreased by 4 steps, which corresponds to a reduction of 2 dB. The performed adaptations result in a significant reduction of ping-pong HOs. However, it should be noted that *HYS_L5_TD_H* is limited with respect to possible HYS parameter adaptations, since as soon as HYS is set to zero, it cannot be reduced further, although recommended by the FIS.

In Figure 8.63 and Figure 8.64, the performed HO parameter adaptations, triggering KPI issues, as well as KPI evolutions over simulation time for BS (0/0) and (2/2), respectively, using *FQL_CIO_H* are illustrated. At BS (0/0), a HO failure event is detected first. Since *CIO_H_L3_TD_HT* is able to identify the target BS (here BS (0/2)), toward which the HO procedure failed, HO parameters are adapted in a cell pair-specific manner. Here, the FIS recommends to adapt both HYS and TTT settings by 2 steps, respectively, where the cell-specific HYS value is increased by 0.5 dB and the CIO value of the target BS (0/2) is set to -0.5 dB, which effectively increases the HO margin by 1 dB.

However, these adaptations result in another HFR and several subsequent CDR issues. Since CDR issues are assigned a higher weight than HFR issues due to MNO policy, according HO parameter adaptations that aim at relieving connection dropping related issues are performed. Here, the cell-specific HYS parameter is decreased by 1 step and the TTT value by 2 discrete steps, respectively. In case of subsequent CDR issues, *CIO_H_L3_TD_HT* reduces both cell-specific HYS and TTT settings by 1 and 2 more steps, respectively. However, it should be noted that the lowest possible HYS and TTT parameter values are 0 dB and 0 ms, respectively. Nevertheless, CDR and HFR issues that occur in the *REF* case in the second half of the observation time window are completely eliminated.

In case of BS (2/2), observed PHR issues are counteracted by increasing HYS settings by 2 steps. For this purpose, *CIO_H_L3_TD_HT* identifies the target BS (here BS (0/0)), toward which the ping-pong HO was observed, and adapts HO parameters in a cell pair-specific manner. Here, the cell-specific HYS parameter is increased by 1 step and the CIO value of the target BS is set to -0.5 dB. In case of subsequent PHR issues, *CIO_H_L3_TD_HT*

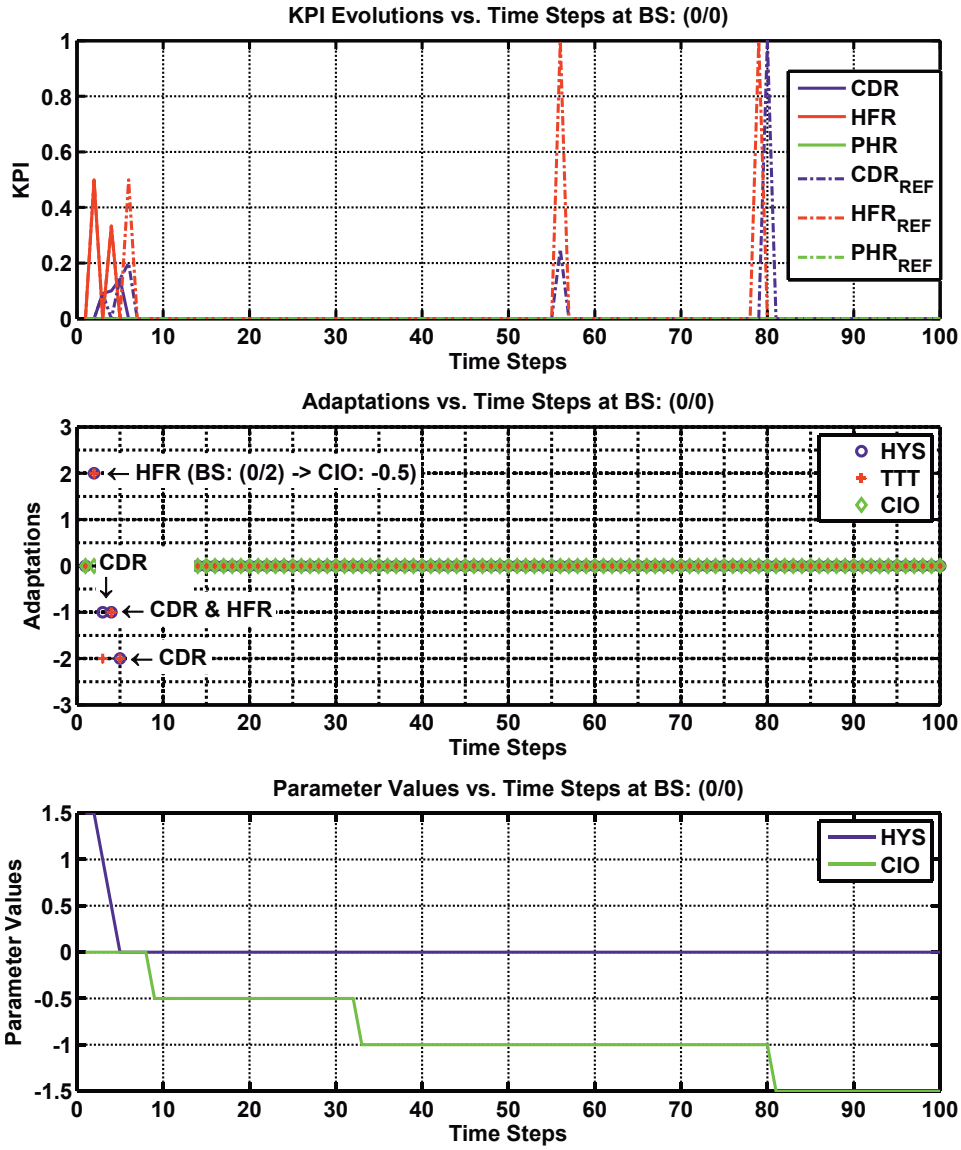

Figure 8.63: KPI evolutions, HO parameter adaptations, and HO parameter values vs. simulation time at BS (0/0) using *CIO_H_L3_TD_HT*

increases both cell-specific HYS and TTT settings by 2 steps, respectively. This results in further increases of cell-specific HYS parameter by 0.5 dB and reductions of target BS CIO value of −0.5 dB, each time *CIO_H_L3_TD_HT* becomes active. If connection dropping related performance degradations occur, cell-specific TTT parameter is reduced by 2 discrete steps according to the set of available TTT settings or both cell-specific HYS and TTT values are decreased to different extents.

In essence, the incorporation of context information for identifying direction of mobility-related performance issues has shown to beneficially support self-tuning mechanisms for MRO and greatly improve KPIs, such as CDR, HFR, and PHR.

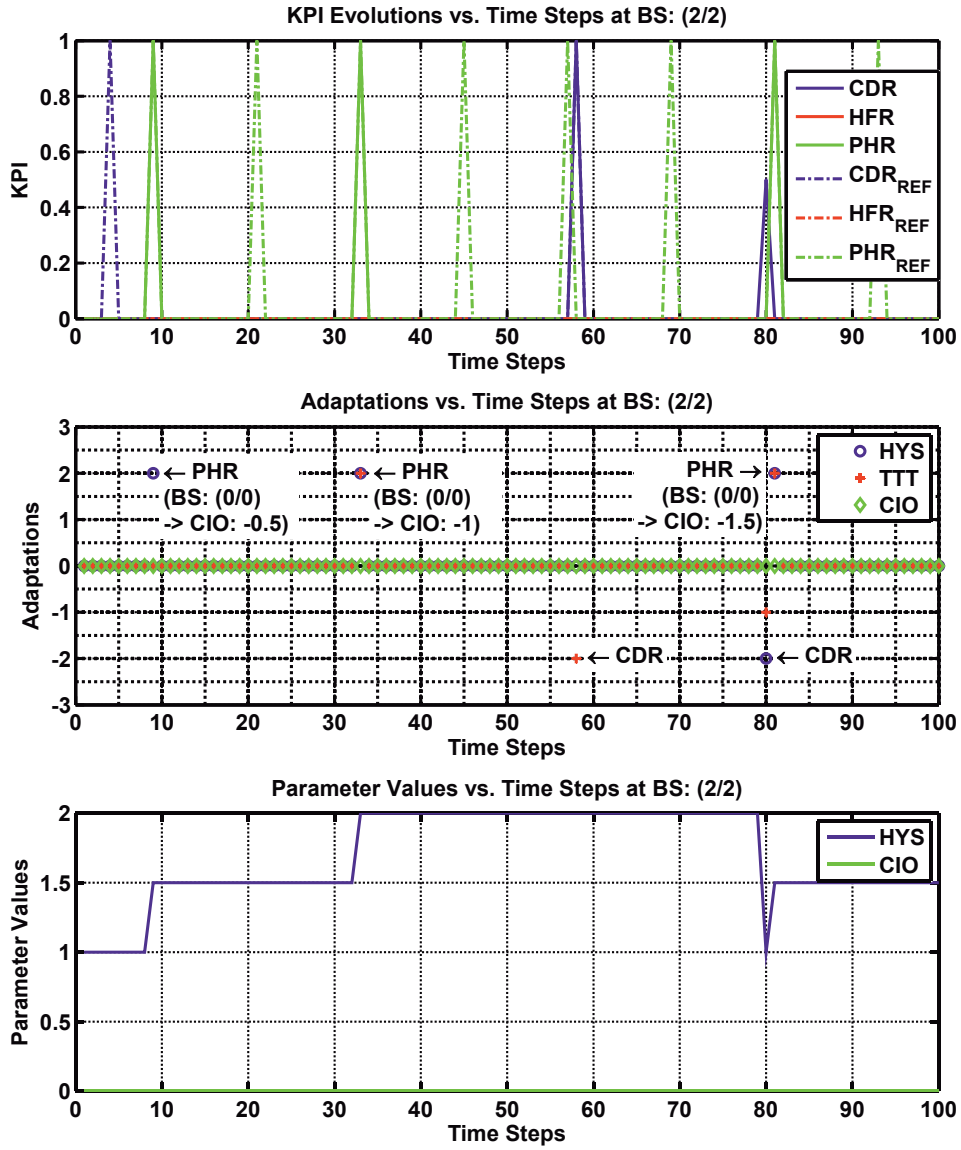

Figure 8.64: KPI evolutions, HO parameter adaptations, and HO parameter values vs. simulation time at BS (2/2) using *CIO_H_L3_TD_HT*

8.3 Summary

Presented system-level evaluation results demonstrate the potential of the developed self-tuning SON mechanisms. These novel schemes have shown to autonomously counteract network performance issues and adapt HO parameter settings according to locally observed conditions, thus establishing context awareness. Further, they are able to improve several mobility-related KPIs, such as connection dropping, HO failure, and ping-pong HO ratios, simultaneously. Since adaptation rules for improving CDR performance on the one hand side and HFR and PHR performance on the other hand side are in conflict with each other, MNO defined weights (cf. Table 8.2) are considered for deciding upon which adaptation or KPI, respectively, to prioritize.

In the considered scenarios, there is no HO parameter constellation that allows for achieving minimal performance issues, i.e., where all KPIs are 0 (cf. Figure 8.6, Figure 8.7, Figure 8.8, Figure 8.9).

For BS (0/0) characterized by CDR and HFR issues, *HYS_L5_TD_H* achieves best OPI values and only marginally outperforms *CIO_P_L5_TP _MT* and *CIO_H_L3_TD_HT*. However, *HYS_L5_TD_H* requires highest learning efforts. In case of mobility-related performance issues, this scheme adapts cell-specific HYS and TTT parameters. In contrast, *CIO_P _L5_TP_MT* and *CIO_H_L3_TD_HT* try to identify HO directions by analyzing neighbor cell HO counters in case of HFR or PHR issues.

For BS (2/2), *TBHOA* and *SBHOA* are able to improve system performance by approximately 21% compared to *REF*. Among the FQL based schemes, *CIO_P_L5_TP_MT* performs best and results in relative OPI improvements of approximately 13% compared to *REF*, while requiring the second highest number of simulation runs. In contrast to BS (0/0), BS (2/2) is heavily affected by ping-pong HO issues. Here, *CIO_P_L5_TP_MT* performs particularly well, since it analyzes neighbor cell HO counters for determining HO directions and adjusts CIO parameters of neighboring cell sectors in a cell pair-specific manner.

In case KPI statistics of all considered BSs are aggregated (cf. Equation (8.3)), the scheme *CIO_P_L5_TP _MT* achieves best overall performance with a relative OPI improvement of approximately 36% compared to *REF*. Although, *CIO_P_L5_TP_MT* requires second highest learning efforts, it has been shown that performing HO parameter adaptations in a cell pair-specific manner is particularly suitable in case of recurring and direction-oriented user mobility.

9 Conclusion and Outlook

The heterogeneity of today's wireless access possibilities imposes challenges for efficient mobility support and resource management across different Radio Access Technologies (RATs). The current situation is characterized by the coexistence of various wireless communication systems that differ greatly with respect to coverage, spectrum, data rates, Quality of Service (QoS), and mobility support. In the scope of this thesis, the author addresses major challenges in mobile communication systems that are directly related to the afore mentioned issues:

- Development of a multi-Radio Access Network (multi-RAN) evaluation methodology and simulation tool that allows for modeling real-world user mobility, network deployments, Handover (HO) processes, traffic, and environments, and analyzing the impact of context information on system performance,
- Network selection and Heterogeneous Access Management (HAM) approaches that efficiently realize *seamless mobility* in a heterogeneous network environment using context information,
- Joint Call Admission Control (JCAC) and Radio Resource Management (RRM) in multi-RAN scenarios that improve overall resource utilization and service provisioning,
- User movement estimation for enhancing network selection and handover decisions enabling pro-active RRM,
- Development of self-learning and -optimizing capabilities for Mobility Robustness Optimization (MRO) in future RANs.

Multi-Radio Access Network Evaluation Methodology

The performance of wireless networks is typically assessed by "snapshot" based simulations and system level metrics, such as spectral efficiency or cell throughput. However, these system metrics are based on aggregated statistics that do not adequately reflect the situation of specific environments, e.g.,

with respect to network coverage, or individual users, e.g., with respect to velocity. Further, in real systems, mobility-related events, such as HO procedures, have a direct impact on resource efficiency, in particular with respect to signaling efforts and users' QoS.

In order to lay a basis for realistic multi-radio network evaluation, a novel evaluation methodology is proposed in this thesis that extends existing single RAT methodologies by incorporating realistic modeling of user mobility as well as HO processes and that allows for jointly evaluating heterogeneous RATs.

The developed concepts for context information exploitation and the multi-RAT evaluation methodology represent important contributions of the author to the European FP7 project METIS. The METIS project already proposed scenarios [MET13a] and simulation guidelines [MET13c] for evaluating the performance of future wireless technologies and the fifth generation of wireless communication systems (5G). In particular, regarding the evaluation of developed concepts, the METIS project also aims at more realistic modeling of network deployment, radio propagation, and user mobility.

Context-Enhanced Heterogeneous Access Management

Many proposals have been made in literature (e.g., cf. Chapter 3) for implementing concepts, such as *always best connected* or *seamless mobility*, and improving network selection, intra- and inter-RAT mobility, as well as Common Radio Resource Management (CRRM). However, none of these approaches considered the integration of wireless network functionalities with context management systems (cf. Chapter 4) for establishing context awareness, e.g., at network-sided decision making entities.

In Chapter 5, the author introduced a holistic Intelligent Radio Network Access (IRNA) concept that is able to leverage context information and exploits its full potential, if User Equipments (UEs) are capable of supporting various RATs. For example, in Section 5.2.1, the context-enhanced HAM approach, which takes advantage of user movement estimates, shows significant gains in terms of avoidable intra- and inter-RAT HOs. In particular, the IRNA concept has shown to significantly reduce the overall number of intra- and inter-RAT HOs of high-speed users by approximately 40% or even 70%, respectively. If less HOs are to be performed, there is a direct impact on network signaling efforts, HO failure and ping-pong HO probabilities, as well as users' End-To-End (E2E) performance. Thus, these metrics can be greatly improved by considering context information.

Optimizing Service Provisioning and Mobile Network Operator (MNO) Revenue

In Section 5.2.2, a novel approach for combined Dynamic Bandwidth Adaptation (DBA) and Joint Call Admission Control (JCAC), referred to as DBA-JCAC, has been introduced. This approach integrates bandwidth adaptation and admission control mechanisms and maximizes MNO's revenue while accounting for user profiles and service-specific QoS requirements.

The developed DBAJCAC scheme shows an improvement in overall gained utility of approximately 6% with respect to a state-of-the-art JCAC approach, while system Key Performance Indicator (KPI)s, such as blocking and dropping rates, are kept at an acceptable level. Further, the number of satisfied elastic services, i.e., typical *best effort* services, provided by LTE exceeds those of the benchmark scheme, even at a high number of initial UEs per cell. Furthermore, the proposed scheme exhibits means for Load Balancing (LB) among RANs. Thus, cell overload is avoided and has never been observed in the conducted simulations.

Cell Transition Prediction

The fact that mobility of commuters is not purely random is exploited in Section 5.2.3 for predicting user cell transitions. In particular, the prediction of movement trajectories of users moving jointly in the same vehicle (e.g., bus, train, etc.) has shown to significantly improve system KPIs, such as connection dropping, HO and call blocking ratios. Given this knowledge on user trajectories, the arrival of users or user groups into a certain cell can be anticipated and used to pro-actively trigger a LB mechanism in order to prevent imminent congestion.

The average number of connection drops is decreased by 32% and 13% for Inter-Site Distances (ISDs) of 500 m and 200 m, respectively. In terms of blocked HO attempts, an average reduction of 26% and 4%, respectively, is achieved. Regarding blocked access attempts, using GPS/distance based cell transition prediction results in improvements of 10% and 6% for ISDs of 500 m and 200 m, respectively. Further, for an ISD of 500 m, significant enhancements with respect to dropped user connections of approximately 42% are achieved using geometry based instead of GPS/distance based prediction. In terms of blocked HO and access attempts, geometry based prediction even results in improvements of 49% as well as 25%, respectively.

These simulation results (cf. Section 5.2.3) demonstrate the ability of the presented approaches to predict arrival of moving user groups well in advance,

thus laying a basis for context-aware RRM. Further, performance results maintain consistency even at high velocities as well as dense deployments, which are envisioned to spread in future [Nok11][MET13a].

Optimizing Heterogeneous Access Management (HAM) in Real-World 3D Environments Using Movement Estimation

Limits of context information exploitation, such as user movement or Signal-to-Interference-plus-Noise Ratio (SINR) estimates, are evaluated using real-world 3D environment and radio propagation models. A more realistic user mobility model in a dense urban environment is introduced and the accuracy of movement estimation is analyzed for various user velocities.

As expected, user velocity and estimation accuracy have a strong influence on the resulting overall throughput. In the considered dense urban environment, best performance results are achieved for a user speed of 25 km/h and a prediction horizon of 5 s, where throughput is increased by 39%. In summary, reasonable choices of prediction horizons depend on observed user velocities.

Regarding HO failures, the exploitation of user movement estimates results in significantly reduced number of HO failures. Here, a reduction of 46% is achieved, however at the cost of an increase in overall number of HOs by more than 40%. Hence, more HOs are anticipated and triggered before connections are dropped. Further, system level results indicate that, e.g., system throughput can be increased by approximately 60% or even 100% using user movement or SINR estimates, respectively.

Fuzzy Q-Learning Based Optimization of Mobility Robustness

In Chapter 7, a hybrid Self-Organizing/Optimizing Network (SON) architecture is proposed and an overview on state-of-the-art SON approaches is given. In particular, issues of the SON use case Mobility Robustness Optimization (MRO) and applicable optimization schemes, which are used as benchmark, are illustrated in Section 7.3. Further, newly developed fuzzy logic and Fuzzy Q-Learning (FQL) based approaches are presented in subsections of Section 7.3.2 that aim at jointly optimizing mobility-related KPIs, such as Connection Dropping Ratio (CDR), Handover Failure Ratio (HFR), and Ping-Pong Handover Ratio (PHR).

The performance of the developed FQL based MRO schemes has been studied using a multi-radio network simulation tool. This tool was imple-

mented in *C* programming language and embedded into a newly created simulation framework, as described in Section 2.8.

The newly developed FQL based MRO schemes are evaluated on system level in Chapter 8 considering two different scenarios. For benchmarking the performance of these novel strategies, state-of-the-art mechanisms developed in the framework of EU FP7 project SOCRATES are used. In scenario 1 (cf. Section 8.1), the self-optimization and -healing capabilities of two proposed MRO schemes (*FQL_HYS* and *FQL_CIO*) are compared against several state-of-the-art MRO approaches.

In essence, the presented FQL based MRO schemes enable self-tuning of HO parameters using a limited rule set that reflects the situations the system may be exposed to. *FQL_HYS* and *FQL_CIO* learn optimum parameter adaptations using a limited Exploration/Exploitation Policy (EEP). Further, these schemes are able to simultaneously account for several KPI performance targets and, by increasing their knowledge base through monitoring the effectiveness of applied adaptations, to self-optimize their operation. Furthermore, the incorporation of context information for identifying direction of mobility-related performance issues has shown to beneficially support self-tuning mechanisms for MRO and greatly improve KPIs, such as CDR, HFR, and PHR.

In terms of connection drops, the FQL based MRO schemes are among the best performing schemes. Moreover, *FQL_HYS* and *FQL_CIO* yield optimum performance with respect to the overall number of HO failures and ping-pong HOs, respectively. In particular, in terms of user satisfaction, the FQL based MRO schemes clearly outperform all other considered schemes and increase the number of times users are satisfied by a factor of approximately 20. These massive enhancements achieved by *FQL_HYS* and *FQL_CIO* are mainly due to the ability of adjusting HO parameters according to locally observed performance issues.

In scenario 2 (cf. Section 8.2), different variations of the four MRO schemes *FQL_HYS, FQL_CIO, FQL_CIO_P, FQL_CIO_H* are assessed with respect to their self-tuning capabilities and ability to perform multi-KPI optimization in a scenario exhibiting various user velocities.

Presented system-level evaluation results demonstrate the potential of the developed self-tuning SON mechanisms. These novel schemes have shown to autonomously counteract network performance issues, adapt HO parameter settings according to locally observed conditions, thus establishing context awareness, and improve several mobility-related KPIs, such as connection dropping, HO failure, and ping-pong HO ratios, simultaneously. Since adap-

tation rules for improving CDR performance on the one hand side and HFR and PHR performance on the other hand side may be contradictory, MNO defined weights (cf. Table 8.2) are considered for deciding upon which adaptation or KPI, respectively, to prioritize. In the considered scenarios, there is no HO parameter constellation, which allows for achieving minimal performance issues, i.e., where all KPIs are zero (cf. Figure 8.6, Figure 8.7, Figure 8.8, Figure 8.9).

In case KPI statistics of all considered Base Stations (BSs) are aggregated, the scheme *CIO_P_L5_TP_MT* achieves best overall performance with a relative Overall Performance Indicator (OPI) improvement of approximately 36%, although it requires the second highest number of simulation runs. *HYS_L5_TD_H* yields second and *CIO_H_L3_TD_HT* third best OPI performance resulting in relative improvements of approximately 32% and 29%, respectively, where the first requires the highest and the last scheme least number of simulation runs.

Finally, the presented performance results do not reveal a single strategy that is applicable in any situation. However, based on these performance results, it is possible to select certain strategies or variations thereof for performance optimization with respect to specific KPIs. Moreover, it will essentially depend on the MNO's policy, i.e., KPI performance targets and weights, which strategy to apply in order to improve system performance.

Performance and learning costs of the developed FQL based MRO scheme depends on the specified Fuzzy Inference System (FIS) rule set. In particular, the number of fuzzy labels used to classify system KPIs and HO parameters affects learning speed and degrees of freedom that can be exploited for learning most effective HO parameter adaptations. With regard to the KPIs considered in this thesis for MRO, such as CDR, HFR, and PHR, adaptation rules can be intuitively specified. Nevertheless, reference simulations (cf. Section 8.2.1) were carried out to confirm adaptation rule definitions. Major findings of Chapter 8 are that the developed MRO schemes are able to autonomously adapt HO parameters to locally observed conditions and to improve overall system performance, while simultaneously accounting for several KPIs. Coverage conditions and the nature of cell sector-specific user movements are taken into account for adjusting HO parameters in the most efficient manner. This yields highly specialized, context aware solutions, since learned control behavior is influenced by locally observed conditions. Further, the presented FQL based MRO scheme exhibits less complexity compared to other machine learning techniques, e.g., artificial neural networks. Furthermore, the developed algorithm can be adjusted to MNO needs and regionally

dominating KPI degradations by varying the weights assigned to each KPI. Moreover, the shapes of fuzzy input membership functions used for classifying KPI degradations can be modified in order to increase sensitivity and responsiveness.

In essence, the application of a flexible FIS concept with tunable membership functions, different numbers of fuzzy labels/rules, and the integration with FQL methods exhibiting low to medium complexity for autonomous MRO is a novelty. Reasons for the concept's suitability are stated in Section 6.3. Further, the developed approaches rely on a limited set of input parameters and do not require measurements performed and provided by UEs for optimizing mobility support and network performance.

In summary, the conducted research activities and presented results motivate and substantiate the consideration of context awareness as key enabler for cognitive and autonomous network management. Further, the performed investigations and aspects evaluated in the scope of this thesis are highly relevant for future 5G wireless systems and current discussions in the 5G infrastructure Public Private Partnership (PPP) [5G-14].

Future Work

The presented approaches and evaluation results demonstrate the potential of context information exploitation for improving mobility support, E2E performance, resource utilization, and system efficiency. Further, the developed and presented solutions for context-enhanced HAM, combined JCAC and DBA, cell transition prediction, and user context prediction are envisioned to be extended and integrated with new solutions for future, self-optimizing networks.

However, one limitation of the implemented FQL based MRO concept is that value ranges and fuzzy membership function shapes used for classifying KPI deviations are manually set. Hence, input variable classification should be enhanced by using well-known data mining techniques, such as *k*-Means and *k*-Nearest Neighbor, as e.g., described in [MKS+11a]. Further, the complexity of the task to be learned (Look-Up Table (LUT) size, learning speed, etc.) depends on the number of considered KPIs, fuzzy labels/rules, and size of action sets. The consideration of other parameter sets (KPIs, actions, weights, etc.), the modification of the employed reinforcements, the incorporation of additional cost functions, as well as the application of a *Fuzzy Actor-Critic Learning* scheme [Jou98], which exhibits larger degrees of freedom compared to FQL, are meaningful extensions of the presented concept.

Since overall learning costs are manageable (cf. Section 8.2.8), efforts for modeling and evaluating specific scenarios and strategies using the described simulation tool appear appropriate and beneficial for practical systems. Gained insights and determined state/action pairs allow for greatly reducing Operational Expenditures (OPEX), since manually tuning and optimizing system parameters can be avoided. However, including models for sporadic events and certain "stress tests" can further help to yield robust optimization behavior. The development of these models and stress tests has not been considered in this thesis and is left for further studies.

In the developed FQL based MRO schemes, a mixed Exploration/Exploitation Policy (EEP), i.e., a strategy where the learning agent performs a mix of directed and undirected search in order to identify the best performing actions, has been applied for increasing learning speed. Additionally, the EEP could be tuned in several ways. Therefore, the factor ε can be adjusted to balance directed and undirected search. For example, increasing ε yields a higher probability that already explored state/action pairs are used for MRO, whereas decreasing ε results in rather undirected search. Furthermore, higher weights could be given to those state/action pairs that are rarely selected. Moreover, the developed FQL based MRO scheme should be extended for tackling inter-RAT mobility issues as well. Further, the developed methods could be complemented and enhanced by network node coordination strategies for avoiding adaptation conflicts or ping-pong effects with respect to system parameter adaptations. For example, game theoretic approaches are suitable for determining optimum parameter adaptation strategies between BSs in a coordinated manner.

Bibliography

[3GP04] 3GPP2 and CDMA Development Group (CDG): *cdma2000 Evaluation Methodology*. 2004. C. R1002-0, Rev. 0, 10.12.2004, available online at `http://www.3gpp2.org/public_html/specs/C.R1002-0_v1.0_041221.pdf`.

[3GP06] 3GPP Technical Specification Group Radio Access Network: *Physical layer aspects for evolved Universal Terrestrial Radio Access (UTRA) (Release 7)*. Technical Specification 25.814 V7.1.0, 3GPP, 2006. available online at `http://www.3gpp.org/ftp/specs/html-INFO/25814.htm`.

[3GP08] 3GPP Technical Specification Group Radio Access Network: *Radio Resource Control (RRC) (Release 8)*. Protocol Specification 25.331 V8.3.0, 3GPP, 2008. available online at `http://www.3gpp.org/ftp/Specs/html-info/25331.htm`.

[3GP10a] 3GPP Technical Specification Group Radio Access Network: *Further advancements for E-UTRA physical layer aspects (Release 9)*. Technical Report 36.814 V9.0.0, 3GPP, 2010. available online at `http://www.3gpp.org/ftp/specs/html-INFO/36814.htm`.

[3GP10b] 3GPP Technical Specification Group Radio Access Network: *Physical channels and mapping of transport channels onto physical channels (FDD) (Release 10)*. Technical Specification 25.211 V10.0.0, 3GPP, 2010. available online at `http://www.3gpp.org/ftp/specs/html-INFO/25211.htm`.

[3GP11a] 3GPP Technical Specification Group Radio Access Network: *Self-configuring and self-optimizing network (SON) use cases and solutions (Release 9)*. Technical Report 36.902 V9.3.1, 3rd Generation Partnership Project, 2011. available online at `http://www.3gpp.org/ftp/specs/html-INFO/36902.htm`.

[3GP11b] 3GPP Technical Specification Group Services and System Aspects: *Handover requirements between UTRAN and GERAN or other radio systems (Release 10)*. Technical Specification 22.129 V10.0.0, 3GPP, 2011. available online at `http://www.3gpp.org/ftp/Specs/html-info/22129.htm`.

[3GP12a] 3GPP Technical Specification Group Radio Access Network: *E-UTRA Radio Resource Control (RRC) (Release 11)*. Protocol Specification 36.331 V11.1.0, 3GPP, 2012. available online at `http://www.3gpp.org/ftp/Specs/html-info/36331.htm`.

[3GP12b] 3GPP Technical Specification Group Radio Access Network: *Physical Channels and Modulation (Release 11)*. Technical Specification 36.211 V11.1.0, 3GPP, 2012. available online at `http://www.3gpp.org/ftp/specs/html-INFO/36211.htm`.

[3GP12c] 3GPP Technical Specification Group Radio Access Network: *Physical layer procedures (Release 11)*. Technical Specification 36.213 V11.1.0, 3GPP, 2012. available online at http://www.3gpp.org/ftp/specs/html-INFO/36213.htm.

[3GP12d] 3GPP Technical Specification Group Radio Access Network: *UE Radio Access capabilities (Release 11)*. Technical Specification 25.306 V11.4.0, 3GPP, 2012. available online at http://www.3gpp.org/ftp/specs/html-INFO/25306.htm.

[3GP12e] 3GPP Technical Specification Group Services and System Aspects: *IP Multimedia Subsystem (IMS), Stage 2 (Release 11)*. Technical Specification 23.228 V11.5.0, 3GPP, 2012. available online at http://www.3gpp.org/ftp/Specs/html-info/23228.htm.

[3rd10] 3rd Generation Partnership Project (3GPP): *3GPP work items on Self-Organizing Networks*. 2010. v0.0.6, available online at http://www.3gpp.org/ftp/Information/WORK_PLAN/Description_Releases/Previous_versions/SON_20101010.zip, accessed: 12.12.2012.

[5G-14] 5G-Infrastructure-Association: *EC H2020 5G Infrastructure PPP Pre-structuring Model RTD & INNO Strands - Working Document (Version v1.0)*. 2014. available online at http://5g-ppp.eu/wp-content/uploads/2014/03/March-2014-_5G-Infra-PPP_Pre-structuringModel_v1-0.pdf, accessed: 27.03.2014.

[AAH+97] Abowd, G.D.; Atkeson, C.G.; Hong, J.I.; Long, S.; Kooper, R.; Pinkerton, M.: Cyberguide: A mobile context-aware tour guide. *Wireless Networks*, vol. 3, no. 5, 1997, pp. 421–433.

[AB12] Askarian, C.; Beigy, H.: A survey for load balancing in mobile wimax networks. *Advanced Computing: An International Journal (ACIJ)*, vol. 3, no. 2, 2012, pp. 119–137.

[ABI09] ABIResearch: *Mobile Cloud Computing - Next Generation Browsers, Widgets, SIM, Network-as-a-Service, and Platform-as-a-Service*. 2009. 3Q 2009, http://www.abiresearch.com/research/1003385, accessed: 16.03.2010.

[AJM04] Akyildiz, I.F.; Jiang, X.; Mohanty, S.: A survey of mobility management in next-generation all-ip-based wireless systems. *IEEE Wireless Communications*, vol. 11, no. 4, 2004, pp. 16–28.

[Ama10] Amann, B.: *Entwurf und Implementierung einer verteilten Service-Architektur in heterogenen Funknetzwerken*. 2010. Diploma thesis at University of Kaiserslautern, Chair for Wireless Communication and Navigation, July 5, 2010.

[Ame00] American Physical Society: November 17 - December 23, 1947: Invention of the first transistor [this month in physics history]. *IEEE Communications Magazine*, vol. 9, no. 10, 2000. available online at http://www.aps.org/publications/apsnews/200011/history.cfm, accessed: 07.11.2013.

[AMH+98] Akyildiz, I.F.; McNair, J.; Ho, J.; Uzunalioglu, H.; Wenye, W.: Mobility management in current and future communications networks. *IEEE Network*, vol. 12, no. 4, 1998, pp. 39–49.

[APSP10] Antoniou, Josephine; Pinto, Filipe Cabral; Simoes, Jose; Pitsillides, Andreas: Supporting Context-Aware Multiparty Sessions in Heterogeneous Mobile Networks. *Mobile Network Applications*, vol. 15, no. 6, 2010, pp. 831–844.

[AR10] Alonso-Rubio, J.: Self-optimization for handover oscillation control in LTE. *IEEE Network Operations and Management Symposium (NOMS)*, 2010, pp. 950–953.

[Asc04] Aschenbrenner, N.: *Always Online*. Siemens - Pictures of the Future, Fall 2004. available online at `http://www.siemens.com/innovation/pool/en/publikationen/publications_pof/PoF_Fall_2004/Always-on_articles/Trends/PoF104art01_1224836.pdf`, accessed: 25.11.2013.

[AWR+11] Awada, A.; Wegmann, B.; Rose, D.; Viering, I.; Klein, A.: Towards Self-Organizing Mobility Robustness Optimization in Inter-RAT Scenario. *73rd IEEE Vehicular Technology Conference (VTC-Spring)*, 2011, pp. 1–5.

[AWVK12] Awada, A.; Wegmann, B.; Viering, I.; Klein, A.: Cell-pair specific optimization of the inter-RAT handover parameters in SON. *23rd IEEE International Symposium on Personal Indoor and Mobile Radio Communications (PIMRC)*, 2012, pp. 1168–1173.

[BAD06] Banerjee, N.; Acharya, A.; Das, S.K.: Seamless SIP-based mobility for multimedia applications. *IEEE Network*, vol. 20, no. 2, 2006, pp. 6–13.

[BBC97] Brown, P.J.; Bovey, J.D.; Chen, X.: Context-aware applications: from the laboratory to the marketplace. *IEEE Personal Communications*, vol. 4, no. 5, 1997, pp. 58–64.

[BBK+07] Baumgarten, M.; Bicocchi, N.; Kusber, R.; Mulvenna, M.; Zambonelli, F.: Self-organizing knowledge networks for pervasive situation-aware services. *IEEE International Conference on Systems, Man and Cybernetics (ISIC)*, 2007, pp. 1–6.

[BBM+09] Blum, N.; Boldea, I.; Magedanz, T.; Staiger, U.; Stein, H.: A Service Broker Providing Real-Time Telecommunications Services for 3rd Party Services. *33rd Annual IEEE International Computer Software and Applications Conference (COMPSAC)*, vol. 2, 2009, pp. 85–91.

[BC04] Bellavista, P.; Corradi, A.: A QoS management middleware based on mobility prediction for multimedia service continuity in the wireless Internet. *9th International Symposium on Computers and Communications (ISCC)*, vol. 1, 2004, pp. 531–538.

[BCC+06] Barbaresi, A.; Casadevall, F.; Colonna, M.; Correia, L.M.; Dahlén, A.; d'Orey, P.M.: *D09 - First report on AROMA algorithms and simulation results*. 2006. Deliverable, EU FP6 AROMA IST-4-027567.

[BCG07] Bellavista, P.; Corradi, A.; Giannelli, C.: Mobility-Aware Connectivity for Seamless Multimedia Delivery in the Heterogeneous Wireless Internet. *12th IEEE Symposium on Computers and Communications (ISCC)*, 2007, pp. MW –1 –MW –7.

[BCG09] Bellavista, P.; Corradi, A.; Giannelli, C.: Mobility-aware Management of Internet Connectivity in Always Best Served Wireless Scenarios. *Mobile Networks and Applications*, vol. 14, 2009, pp. 18–34. 10.1007/s11036-008-0106-9.

[BCMS03] Bellavista, P.; Corradi, A.; Montanari, R.; Stefanelli, C.: Context-aware middleware for resource management in the wireless internet. *IEEE Transactions on Software Engineering*, vol. 29, no. 12, 2003, pp. 1086–1099.

[Bel57] Bellman, R.E.: *Dynamic Programming*. Princeton, NJ: Princeton Univ. Press, 1957.

[BGRE06] Bogenfeld, Eckhart; Gaspard, I.; Rothenberg, C.E.; Einsiedler, H.: *Provision of self-x functionalities in IEEE 802.16 networks - e.g. self-configuration and self-optimization*. 2006. IEEE 802.16 Broadband Wireless Access Working Group, C802.16-06/027.

[BK92] Berenji, H.R.; Khedkar, P.: Learning and tuning fuzzy logic controllers through reinforcements. *IEEE Transactions on Neural Networks*, vol. 3, no. 5, 1992, pp. 724–740.

[BMG12] Bergman, P.; Moe, J.; Gunnarsson, F.: Self-optimizing handover oscillation mitigation - Algorithms and field evaluations. *International Symposium on Wireless Communication Systems (ISWCS)*, 2012, pp. 31–35.

[Bro96a] Brown, M.: Supporting user mobility. *IFIP World Conference on Mobile Communications*, 1996, pp. 69–77.

[Bro96b] Brown, P.J.: The stick-e document: A framework for creating context-aware applications. *Proceedings of the Electronic Publishing*, Laxenburg, Austria, 1996, pp. 259–272.

[BSKF06] Bocker, J.; Schulz, B.; Knoke, T.; Frohleke, N.: Self-Optimization as a Framework for Advanced Control Systems. *32nd Annual IEEE Conference on Industrial Electronics (IECON)*, 2006, pp. 4671–4675.

[BSR07] Baldauf, M.; Schahram, D.; Rosenberg, F.: A Survey on Context-Aware Systems. *International Journal of Ad Hoc and Ubiquitous Computing*, vol. 2, no. 4, 2007, pp. 263–277.

[BVHA+10] Bogenfeld, E.; Von Hugo, D.; Arshad, K.; Solana, B.; Taranu, S.; Saatsakis, A.; Mange, G.; Bernardo, F.; Jeux, S.; Feng, Z.; Kulkarni, P.; Farnham, T.: Collaborative cognitive RRM, Dynamic Spectrum Management, and self-organisation for future mobile networks. *Future Network and Mobile Summit*, 2010, pp. 1–9.

[BW10] Bühler, J.; Wunder, G.: Traffic-aware optimization of heterogeneous access management. *IEEE Transactions on Communications*, vol. 58, no. 6, 2010, pp. 1737–1747.

[BWKS07] Blau, I.; Wunder, G.; Karla, I.; Siegle, R.: Cost based Heterogeneous Access Management in Multi-Service, Multi-System Scenarios. *18th IEEE International Symposium on Personal, Indoor and Mobile Radio Communications (PIMRC)*, Athens, Greece, 2007, pp. 1–5.

[BZKM09] Baker, N.; Zafar, M.; Knappmeyer, M.; Moltchanov, B.: *Context-Aware Systems and Implications for Future Internet*. pp. 335–345. Amsterdam: IOS Press, 2009.

[C-C08] C-CAST Project: *D6 - Requirements and Concepts for Context Casting Service Enablers and Context Management*. 2008. Deliverable, EU FP7 Project ICT-2007-216462.

[C-C09a] C-CAST Project: *D12 - Specification of Context Casting Service Enablers, Context Management & Context Brokering*. 2009. Deliverable, revised in Jan. 2010, EU FP7 Project ICT-2007-216462.

[C-C09b] C-CAST Project: *D13 - Specification of Context Detection and Context-Aware Multiparty Transport*. 2009. Deliverable, revised in Dec. 2009, EU FP7 Project ICT-2007-216462.

[C-C10] C-CAST Project: *D16 - Validation of Results and Demonstration*. 2010. Deliverable, revised in July 2010, EU FP7 Project ICT-2007-216462.

[CBD02] Camp, T.; Boleng, J.; Davies, V.: A survey of mobility models for ad hoc network research. *Wireless Communications and Mobile Computing: Special Issue: Mobile Ad Hoc Networking - Research, Trends and Applications*, vol. 2, no. 5, 2002, pp. 483–502.

[CDL+73] Cooper, M.; Dronsuth, R.W.; Leitich, A.J.; Lynk, C.N. Jr.; Mikulski, J.J.; Mitchell, J.F.; Richardson, R.A.; Sangster, J.H.: *Radio telephone system*. 1973. Patent No. US3906166 A, filed 17 Oct. 1973, issued 16 Sept. 1975, [Online; accessed: 06.11.2013].

[CDM+00] Cheverst, K.; Davies, N.; Mitchell, K.; Friday, A.; Efstratiou, C.: Developing a Context-aware Electronic Tourist Guide: Some Issues and Experiences. *Proceedings of the SIGCHI Conference on Human Factors in Computing Systems*, Proceedings of the SIGCHI Conference on Human Factors in Computing Systems (CHI), New York, NY, USA, 2000, pp. 17–24.

[CFJ03] Chen, H.; Finin, T.; Joshi, A.: An ontology for context-aware pervasive computing environments. *The Knowledge Engineering Review*, vol. 18, 2003, pp. 197–207.

[CGM08] Camarillo, G.; García-Martín, M.A.: *The 3G IP multimedia subsystem (IMS): merging the Internet and the cellular worlds*. 3rd edition. Southern Gate, Chichester, West Sussex, UK: John Wiley & Sons Ltd, 2008. ISBN 978-0-470-51662-1.

[Che04] Chen, H.: *An Intelligent Broker Architecture for Pervasive Context-Aware Systems*. Dissertation, University of Maryland, Baltimore County, 2004.

[CKR06] Cohen, R.; Katzir, L.; Raz, D.: An efficient approximation for the Generalized Assignment Problem. *Information Processing Letters*, vol. 100, no. 4, 2006, pp. 162–166.

[CLG+03] Calhoun, P.; Loughney, J.; Guttmann, E.; Zorn, G.; Arkko, J.: *Diameter Base Protocol*. 2003. IETF RFC 3588.

[CMK+10] Carrella, S.; Mannweiler, C.; Klein, A.; Schneider, J.; Schotten, H.D.: A Concept for Context-aware Multihoming with Heterogeneous Radio Access Technologies. *5th Annual ICST International Wireless Internet Conference (WICON)*, Singapore, 2010, pp. 1–7.

[CTB+95] Cooperstock, J.R.; Tanikoshi, K.; Beirne, G.; Narine, T.; Buxton, W.: Evolution of a reactive environment. Katz, I.R.; Mack, R.L.; Marks, L.; Rosson, M.B.; Nielsen, J. (eds.): *Conference on Human Factors in Computing Systems (CHI)*, 1995, pp. 170–177.

[CV11] Carvalho, M.; Vieira, P.: An Enhanced Handover Oscillation Control Algorithm in LTE Self-Optimizing Networks. *14th International Symposium on Wireless Personal Multimedia Communications (WPMC)*, 2011, pp. 1–5.

[DA00] Dey, A.K.; Abowd, G.D.: Towards a better understanding of context and context-awareness. *Workshop on The What, Who, Where, When, and How of Context-Awareness at the Conference on Human Factors in Computing Systems (CHI)*, The Hague, The Netherlands, 2000. submitted to the 1st International Symposium on Handheld and Ubiquitous Computing (HUC), June 1999).

[DBC03] Du, Lin; Bigham, J.; Cuthbert, L.: Towards intelligent geographic load balancing for mobile cellular networks. *IEEE Transactions on Systems, Man, and Cybernetics, Part C: Applications and Reviews*, vol. 33, no. 4, 2003, pp. 480–491.

[DDF+06] Dobson, S.; Denazis, S.; Fernández, A.; Gaïti, D.; Gelenbe, E.; Massacci, F.; Nixon, P.; Saffre, F.; Schmidt, N.; Zambonelli, F.: A survey of autonomic communications. *ACM Transactions on Autonomous and Adaptive Systems (TAAS)*, vol. 1, no. 2, 2006, pp. 223–259.

[DDS+10] Diaz, I.F.; Dimitrova, D.C.; Spaey, K.; Litjens, R.; van den Berg, J.L.: Sensitivity Analysis of the Optimal Parameter Settings of an LTE Packet Scheduler. *71st IEEE Vehicular Technology Conference (VTC-Spring)*, 2010, pp. 1–6.

[Dey98] Dey, A.K.: Context-aware computing: The cyberdesk project. *Association for the Advancement of Artificial Intelligence (AAAI) Spring Symposium on Intelligent Environments*, Palo Alto, 1998, pp. 51–54.

[d'O10] d'Orey, P.M.: *Self-optimisation of Future Wireless Networks: Vision and challenges*. 2010. 1st MAP-Tele Doctoral Students Workshop (MAPshop'10), Porto.

[EB11] Ewe, L.; Bakker, H.: Base station distributed handover optimization in LTE self-organizing networks. *22nd International IEEE Symposium on Personal Indoor and Mobile Radio Communications (PIMRC)*, 2011, pp. 243–247.

[EHC+93] Elrod, S.; Hall, G.; Costanza, R.; Dixon, M.; des Rivières, J.: Responsive office environments. *Communications of the ACM*, vol. 36, no. 7, 1993, pp. 84–85.

[EMN00] Ericsson; Motorola; Nokia: *Common HSDPA system simulation assumptions*. 2000. 3GPP TSG-RAN1#15 R1-001094, TSGRAN1#15, Berlin, Germany.

[Eri11] Ericsson: *More than 50 billion connected devices*. 2011. White Paper 284 23-3149 Uen, available online at `http://www.ericsson.com/res/docs/whitepapers/wp-50-billions.pdf`, accessed: 12.12.2012.

[FC07] Falowo, O.E.; Chan, H.A.: Adaptive bandwidth management and joint call Admission control to enhance system utilization and QoS in heterogeneous wireless networks. *EURASIP Journal on Wireless Communications and Networking*, vol. 2007, no. 3, 2007, pp. 2:1–2:11.

[FET03] Fodor, G.; Eriksson, A.; Tuoriniemi, A.: Providing quality of service in always best connected networks. *IEEE Communications Magazine*, vol. 41, no. 7, 2003, pp. 154–163.

[FF98] Franklin, D.; Flaschbart, J.: All gadget and no representation makes jack a dull environment. *Association for the Advancement of Artificial Intelligence (AAAI) Spring Symposium on Intelligent Environments*, 1998, pp. 155–160. Technical Report SS-98-02.

[FI-13] FI-WARE Project: *D6.1.2: FI-WARE GE Open Specification - Data*. 2013. Deliverable, April 2013, EU FP7 Project ICT-2011-FI-285248, available online at `http://cordis.europa.eu/fp7/ict/netinnovation/deliverables/fi-ware/fi-ware-d612.pdf`, accessed: 18.03.2014.

[Fie00] Fielding, Roy T.: *Architectural Styles and the Design of Network-based Software Architectures*. Dissertation, University of California, Irvine, US, 2000.

[Fit92] Fitz, M.P.: Further results in the unified analysis of digital communication systems. *IEEE Transactions on Communications*, vol. 40, no. 3, 1992, pp. 521–532.

[FKS97] Fickas, S.; Kortuem, G.; Segall, Z.: Software organization for dynamic and adaptable wearable systems. *ISWC*, 1997, pp. 56–64.

[FLTZ09] Feng, Z.; Liang, L.; Tan, L.; Zhang, P.: Q-learning based heterogenous network self-optimization for reconfigurable network with CPC assistance. *Science in China Series F: Information Sciences*, vol. 52, no. 12, 2009, pp. 2360–2368. 10.1007/s11432-009-0223-5.

[FPN+05] Floréen, P.; Przybilski, M.; Nurmi, P.; Koolwaaij, J.; Tarlano, A.; Wagner, M.; Luther, M.; Bataille, F.; Boussard, M.; Mrohs, B.; Lau, S.L.: Towards a Context Management Framework for MobiLife. *IST Mobile and Communications Summit*, 2005.

[FPV98] Fuggetta, A.; Picco, G.P.; Vigna, G.: Understanding code mobility. *IEEE Transactions on Software Engineering*, vol. 24, no. 5, 1998, pp. 342–361.

[Fre10] Frenkiel, R.: Creating cellular: A history of the AMPS project (1971-1983) [History of Communications]. *IEEE Communications Magazine*, vol. 48, no. 9, 2010, pp. 14–24.

[FS08] Feng, S.; Seidel, E.: *Self-Organizing Networks (SON) in 3GPP Long Term Evolution*. 2008. Nomor Research GmbH, Munich, Germany, white paper, available online at `http://www.nomor.de/uploads/gc/TQ/gcTQfDWApo9osPfQwQoBzw/SelfOrganisingNetworksInLTE_2008-05.pdf`, accessed: 28.12.2010.

[FZ06] Feng, Z.; Zhang, P.: Cooperation Techniques and Architecture for Multi-access Radio Resource Management. *63rd IEEE Vehicular Technology Conference (VTC Spring)*, vol. 2, 2006, pp. 996–1000.

[GAPRSR08] Giupponi, L.; Agusti, R.; Perez-Romero, J.; Sallent Roig, O.: A Novel Approach for Joint Radio Resource Management Based on Fuzzy Neural Methodology. *IEEE Transactions on Vehicular Technology*, vol. 57, no. 3, 2008, pp. 1789–1805.

[GHAM03] Gazis, V.; Houssos, N.; Alonistioti, N.; Merakos, L.: On the complexity of "Always Best Connected" in 4G mobile networks. *58th IEEE Vehicular Technology Conference (VTC Fall)*, vol. 4, 2003, pp. 2312–2316.

[GJ96] Glorennec, P.Y.; Jouffe, L.: A reinforcement learning method for an autonomous robot. *4th European Congress on Intelligent Techniques and Soft Computing (EUFIT)*, Aachen, Germany, 1996, pp. 1100–1104.

[GJ97] Glorennec, P.Y.; Jouffe, L.: Fuzzy Q-learning. *6th IEEE International Conference on Fuzzy Systems*, vol. 2, 1997, pp. 659–662.

[GJ03] Gustafsson, E.; Jonsson, A.: Always best connected. *IEEE Wireless Communications Magazine*, vol. 10, no. 1, 2003, pp. 49–55.

[Glo94] Glorennec, P.Y.: Fuzzy Q-learning and dynamical fuzzy Q-learning. *IEEE World Congress on Computational Intelligence, 3rd IEEE Conference on Fuzzy Systems*, vol. 1, 1994, pp. 474–479.

[Glo11] Global System for Mobile Communications Association (GSMA): *Proliferation of Connected Devices will create a $1.2tr Revenue Opportunity for Operators by 2020*. 2011. San Diego, available online at `http://www.gsma.com/newsroom/proliferation-of-connected-devices-will-create-a-1-2tr-revenue-opportunity-for-operators-by-2020/`, accessed: 11.12.2012.

[Gol09] Golmie, N.: Seamless Mobility: Are We There Yet? *IEEE Wireless Communications*, vol. 16, no. 4, 2009, pp. 12–13.

[GPRSA08] Gelabert, X.; Pérez-Romero, J.; Sallent, O.; Agustí, R.: A Markovian approach to radio access technology selection in heterogeneous multiaccess/multiservice wireless networks. *IEEE Transactions on Mobile Computing*, vol. 7, no. 10, 2008, pp. 1257–1270.

[Gud91] Gudmundson, M.: Correlation model for shadow fading in mobile radio systems. *Electronics Letters*, vol. 27, no. 23, 1991, pp. 2145–2146.

[Gup06] Gupta, V.: *IEEE P802.21 Tutorial*. 2006. Presentation at IEEE 802.21 session #15 in San Diego, CA, US.

[HCV12] Haynes, D.; Corns, S.; Venayagamoorthy, G.K.: An exponential moving average algorithm. *IEEE Congress on Evolutionary Computation (CEC)*, 2012, pp. 1–8.

[HF08] Hasib, A.; Fapojuwo, A.: Analysis of common radio resource management scheme for end-to-end QoS support in multiservice heterogeneous wireless networks. *IEEE Transactions on Vehicular Technologies*, vol. 57, no. 4, 2008, pp. 2426–2439.

[HL12] Hui, G.; Legg, P.: Soft Metric Assisted Mobility Robustness Optimization in LTE Networks. *International Symposium on Wireless Communication Systems (ISWCS)*, 2012, pp. 1–5.

[HNBR97] Hull, R.; Neaves, P.; Bedford-Roberts, J.: Towards situated computing. *First International Symposium on Wearable Computers, Digest of Papers*, 1997, pp. 146–153.

[HNH07] Hasswa, A.; Nasser, N.; Hassanein, H.: A seamless context-aware architecture for fourth generation wireless networks. *Wireless Personal Communications*, vol. 43, no. 3, 2007, pp. 1035–1049.

[HPVL03] Hoglund, A.; Pollonen, J.; Valkealahti, K.; Laiho, J.: Quality-based auto-tuning of cell uplink load level targets in WCDMA. *57th IEEE Vehicular Technology Conference (VTC-Spring)*, vol. 4, 2003, pp. 2847–2851.

[HSN+10] Holsopple, J.; Sudit, M.; Nusinov, M.; Liu, D.F.; Du, H.; Yang, S.J.: Enhancing situation awareness via automated situation assessment. *IEEE Communications Magazine*, vol. 48, no. 3, 2010, pp. 146–152.

[HT07] Holma, H.; Toskala, A.: *WCDMA for UMTS - HSPA Evolution and LTE*. 4th edition. Chichester, West Sussex, England: John Wiley & Sons, 2007.

[HT09] Holma, H.; Toskala, A.: *LTE for UMTS - OFDMA and SC-FDMA Based Radio Access*. Chichester, West Sussex, England: John Wiley & Sons, 2009.

[HV02] Hoglund, A.; Valkealahti, K.: Quality-based tuning of cell downlink load target and link power maxima in WCDMA. *56th IEEE Vehicular Technology Conference (VTC-Fall)*, vol. 4, 2002, pp. 2248–2252.

[HVHL02] Hamalainen, A.; Valkealahti, K.; Hoglund, A.; Laakso, J.: Auto-tuning of service-specific requirement of received EbNo in WCDMA. *56th IEEE Vehicular Technology Conference (VTC-Fall)*, vol. 4, 2002, pp. 2253–2257.

[IEE05] IEEE 802.20 Project Group: *802.20 Evaluation Criteria*. 2005. IEEE P 802.20 PD-09, V. 1.0, available online at `http://ieee802.org/20/P_Docs/IEEE_802.20-PD-09.doc`.

[IEE08] IEEE 802.16m Project Group: *Evaluation Methodology Document (EMD)*. 2008. IEEE 802.16m-08/004r2, available online at `http://ieee802.org/16/tgm/docs/80216m-08_004r2.pdf`.

[IEE09] IEEE 802.21 Working Group: *IEEE Draft Standard for Local and Metropolitan Area Networks: Media Independent Handover Services*. 2009. IEEE P802.21/D14.

[IEE12] IEEE 802.21 Working Group: *IEEE Standard for Local and Metropolitan Area Networks: Media Independent Handover Services - Amendment for Security Extensions to Media Independent Handover Services and Protocol*. 2012. IEEE Std. 802.21a-2012 (Amendment to IEEE Std. 802.21-2008).

[ITU97] ITU-R: *Guidelines for the Evaluation of Radio Transmission Technologies for IMT-2000*. 1997. Rec. ITU-R M.1225, available online at `http://www.itu.int/dms_pubrec/itu-r/rec/m/R-REC-M.1225-0-199702-I!!PDF-E.pdf`.

[ITU04] ITU-T: *Definition of Next Generation Network*. 2004. available online at `http://www.itu.int/ITU-T/studygroups/com13/ngn2004/working_definition.html`.

[JBT+10] Jansen, T.; Balan, I.; Turk, J.; Moerman, I.; Kürner, T.: Handover Parameter Optimization in LTE Self-Organizing Networks. *72nd IEEE Vehicular Technology Conference (VTC-Fall)*, 2010, pp. 1–5.

[JFTK04] Jobin, J.; Faloutsos, M.; Tripathi, S.K.; Krishnamurthy, S.V.: Understanding the effects of hotspots in wireless cellular networks. *23rd Annual Joint Conference of the IEEE Computer and Communications Societies INFOCOM*, vol. 1, 2004, pp. 660–671.

[JG96] Jouffe, L.; Glorennec, P.Y.: Comparison between connectionist and fuzzy Q-learning. *4th International Conference on Soft Computing (IIZUKA)*, vol. 2, Iizuka, Fukuoka, Japan, 1996, pp. 557–560.

[JKK+14] Ji, L.; Klein, A.; Kuruvatti, N.P.; Sattiraju, R.; Schotten, H.D.: Dynamic Context-aware Optimization of D2D Communications. *2nd International Workshop on 5G Mobile and Wireless Communication System for 2020 and Beyond at IEEE 79th Vehicular Technology Conference (VTC-Spring)*, Seoul, Korea, 2014.

[JKKS14] Ji, L.; Klein, A.; Kuruvatti, N.P.; Schotten, H.D.: System Capacity Optimization Algorithm for D2D Underlay Operation. *Workshop on 5G Technologies at IEEE International Conference on Communications (ICC)*, Sydney, Australia, 2014.

[JLL+07] Jo, D.; Lee, J.; Lee, S.; Ha, T.; Kwon, T.; Choi, Y.: Signal dragging: Effects of terminal movement on war-driving in cdma/wcdma networks. Hightower, Jeffrey; Schiele, Bernt; Strang, Thomas (eds.): *Location- and Context-Awareness*. vol. 4718 in series *Lecture Notes in Computer Science*. pp. 211–227. Springer Berlin Heidelberg, 2007.

[Joe70] Joel, A.E. Jr.: *Mobile communication system*. 1970. Patent No. US3663762 A, filed 21 Dec. 1970, issued 16 May 1972, [Online; accessed: 06.11.2013].

[Jou98] Jouffe, L.: Fuzzy Inference System Learning by Reinforcement Methods. *IEEE Transactions on Systems, Man, and Cybernetics - Part C: Applications and Reviews*, vol. 28, no. 3, 1998, pp. 338–355.

[JSA+09] Janneteau, C.; Simoes, J.; Antoniou, J.; Christophorou, C.; Kellil, M.; Klein, A.; Neto, A.; Cabral Pinto, F.; Roux, P.; Sargento, S.; Schotten, H.D.; Schneider, J.: Context-Aware Multiparty Networking. *ICT-MobileSummit*, Santander, Spain, 2009, pp. 1–11.

[JU04] Julier, S.J.; Uhlmann, J.K.: Unscented filtering and nonlinear estimation. *Proceedings of the IEEE*, vol. 92, no. 3, 2004, pp. 401–422.

[KBNI13] Kishiyama, Y.; Benjebbour, A.; Nakamura, T.; Ishii, H.: Future Steps of LTE-A: Evolution Toward Integration of Local Area and Wide Area Systems. *IEEE Wireless Communications*, vol. 20, no. 1, 2013, pp. 12–18.

[KG10] Kretschmer, M.; Ghinea, G.: An IEEE 802.21-based approach for seamless wireless mobile integration using QoS-aware paths supporting unidirectional links. *IEEE GLOBECOM Workshops*, 2010, pp. 27–31.

[KH94] Kumar, P.S.; Holtzman, J.: Analysis of handoff algorithms using both bit error rate (ber) and relative signal strength. *Third Annual International Conference on Universal Personal Communications (ICUPC)*, 1994, pp. 1–5.

[KH06] Kaplan, E.D.; Hegarty, C.J. (Eds.): *Understanding GPS: principles and applications*. 2nd edition. Norwood, MA, US: Artech House, 2006. section 9.3.2.1, ISBN 1-58053-894-0.

[KKSS13a] Klein, A.; Kuruvatti, N.P.; Schneider, J.; Schotten, H.D.: Fuzzy Q-Learning for Mobility Robustness Optimization in Wireless Networks. *International Workshop on Emerging Technologies for LTE-Advanced and Beyond 4G at IEEE Global Communications Conference (GLOBECOM)*, Atlanta, GA, USA, 2013.

[KKSS13b] Kuruvatti, N.P.; Klein, A.; Schneider, J.; Schotten, H.D.: Exploiting Diurnal User Mobility for Predicting Cell Transitions. *International Workshop on Broadband Wireless Access at IEEE Global Communications Conference (GLOBECOM)*, Atlanta, GA, USA, 2013.

[KKYK11] Kitagawa, K.; Komine, T.; Yamamoto, T.; Konishi, S.: A Handover Optimization Algorithm with Mobility Robustness for LTE Systems. *22nd IEEE International Symposium on Personal Indoor and Mobile Radio Communications (PIMRC)*, 2011, pp. 1647–1651.

[Kle08] Klein, A.: *Analyse und Vergleich verschiedener Mobilfunkstandards*. 2008. Diploma thesis at University of Kaiserslautern, Chair for Wireless Communication and Navigation, March, 2008.

[KLM96] Kaelbling, L.P.; Littman, M.L.; Moore, A.W.: Reinforcement Learning: A Survey. *Journal of Artificial Intelligence Research*, vol. 4, 1996, pp. 237–285.

[KLM+11a] Klein, A.; Lottermann, C.; Mannweiler, C.; Schneider, J.; Schotten, H.D.: A Novel Approach for Combined Joint Call Admission Control and Dynamic Bandwidth Adaptation in Heterogeneous Wireless Networks. *7th EURO-NF Conference on Next Generation Internet (NGI)*, Kaiserslautern, Germany, 2011, pp. 1–8.

[KLM+11b] Klein, A.; Lottermann, C.; Mannweiler, C.; Schneider, J.; Schotten, H.D.: Ein Neuartiger Ansatz für Gemeinsame Funk-Zugangskontrolle und Dynamische Bandbreiten-Anpassung in Heterogenen Funknetzwerken. *16. ITG-Fachbericht der ITG Fachtagung Mobilkommunikation*, Osnabrück, Germany, 2011.

[KMS09] Klein, A.; Mannweiler, C.; Schotten, H.D.: A Framework for Intelligent Radio Network Access Based on Context Models. *22nd Wireless World Research Forum (WWRF) Meeting*, Paris, France, 2009.

[KMS+10] Klein, A.; Mannweiler, C.; Schneider, J.; Thillen, F.; Schotten, H.D.: A Concept for Context-Enhanced Heterogeneous Access Management. *International Workshop on Seamless Wireless Mobility at IEEE Global Communications Conference (GLOBECOM), 2010*, Miami, FL, USA, 2010, pp. 6–10.

[KMSS10] Klein, A.; Mannweiler, C.; Schneider, J.; Schotten, H.D.: Access Schemes for Mobile Cloud Computing. *First International Workshop on Mobile Cloud Computing at Mobile Data Management (MDM)*, Kansas City, MO, USA, 2010, pp. 387–392.

[KMSS11] Klein, A.; Mannweiler, C.; Schneider, J.; Schotten, H.D.: An Advanced System Concept for Cognitive Spectrum Management and Utilization. *10th Workshop on Electrical and Electronic Engineering for Communication (EEEfCOM)*, Ulm, Germany, 2011.

[Koo05] Koodli, R.: *Fast Handovers for Mobile IPv6*. 2005. IETF RFC 4068.

[KRSS14] Klein, A.; Rauch, A.; Sattiraju, R.; Schotten, H.D.: Achievable Performance Gains Using Movement Prediction and Advanced 3D System Modeling. *2nd International Workshop on 5G Mobile and Wireless Communication System for 2020 and Beyond at IEEE 79th Vehicular Technology Conference (VTC-Spring)*, Seoul, Korea, 2014.

[KS11] Kunarak, S.; Suleesathira, R.: *Mobile Ad-Hoc Networks: Protocol Design*. ch. Predictive RSS with Fuzzy Logic based Vertical Handoff Decision Scheme for Seamless Ubiquitous Access. InTech, 2011. ISBN 978-953-307-402-3, DOI 10.5772/12911, available online: `http://www.intechopen.com/books/mobile-ad-hoc-networks-protocol-design/predictive-rss-with-fuzzy-logic-based-vertical-handoff-decision-scheme-for-seamless-ubiquitous-acces`.

[KSS14] Karrenbauer, M.; Schneider, J.; Schotten, H.D.: A Simple Chord Implementation for Distributed Context Management. *19. ITG-Fachbericht der ITG Fachtagung Mobilkommunikation*, Osnabrück, Germany, 2014.

[KTB09] Knappmeyer, M.; Tönjes, R.; Baker, N.: Modular and Extendible Context Provisioning for Evolving Mobile Applications and Services. *ICT Mobile Summit*, Santander, Spain, 2009. ISBN 978-1-905824-12-0.

[KYK12] Komine, T.; Yamamoto, T.; Konishi, S.: A proposal of cell selection algorithm for LTE handover optimization. *IEEE Symposium on Computers and Communications (ISCC)*, 2012, pp. 37–42.

[Leh06] Lehser, F.: *Self Organising LTE/SAE Network - Operator Requirements & Examples*. 2006. T-Mobile, Presentation at 25th ITG Fachtagung, Ulm, Germany, available online at `http://www.ikr.uni-stuttgart.de/Content/itg/fg524/Meetings/2006-09-29-Ulm/03-SON_ITG_25Sep2006_public.pdf`, accessed: 28.12.2010.

[LHJ10] Legg, P.; Hui, Gao; Johansson, J.: A Simulation Study of LTE Intra-Frequency Handover Performance. *72nd IEEE Vehicular Technology Conference (VTC-Fall)*, 2010, pp. 1–5.

[LHXP10] Liu, Z.; Hong, P.; Xue, K.; Peng, M.: Conflict Avoidance between Mobility Robustness Optimization and Mobility Load Balancing. *IEEE Global Telecommunications Conference (GLOBECOM)*, 2010, pp. 1–5.

[LKMS12] Lottermann, C.; Klein, A.; Mannweiler, C.; Schotten, H.D.: Enhancing Service Provisioning within Heterogeneous Wireless Networks for Emergency Situations. Popescu-Zeletin, R.; Jonas, K.; Rai, I.A.; Glitho, R.; Villafiorita, A.; Akan, O.; Bellavista, P.; Cao, J.; Dressler, F.; Ferrari, D.; Gerla, M.; Kobayashi, H.; Palazzo, S.; Sahni, S.; Shen, X.; Stan, M.; Xiaohua, J.; Zomaya, A.; Coulson, G. (eds.): *e-Infrastructure and e-Services for Developing Countries*. vol. 92 in series *Lecture Notes of the Institute for Computer Sciences, Social Informatics and Telecommunications Engineering*. pp. 14–23. Springer Berlin Heidelberg, 2012. 10.1007/978-3-642-29093-0_2.

[LNB97] Lin, Quan; Nahar, L.; Bhattacharya, S.: A remote channel borrowing approach for real-time congestion control in wireless communication. *IEEE Global Telecommunications Conference (GLOBECOM)*, vol. 3, 1997, pp. 1601–1605.

[Lot11] Lottermann, C.: *Analysis and Implementation of Radio Resource Management Algorithms for Heterogeneous Wireless Networks*. 2011. Diploma thesis at University of Kaiserslautern, Chair for Wireless Communication and Navigation, April 21, 2011.

[LRRTFN08] Luna-Ramirez, S.; Ruiz, F.; Toril, M.; Fernandez-Navarro, M.: Inter-System Handover Parameter Auto-Tuning in a Joint-RRM Scenario. *IEEE Vehicular Technology Conference (VTC-Spring)*, 2008, pp. 2641–2645.

[LRTRFN08] Luna-Ramirez, S.; Toril, M.; Ruiz, F.; Fernandez-Navarro, M.: Adjustment of a Fuzzy Logic Controller for IS-HO parameters in a heterogeneous scenario. *The 14th IEEE Mediterranean Electrotechnical Conference (MELECON)*, 2008, pp. 29–34.

[LSJB10] Lobinger, A.; Stefanski, S.; Jansen, T.; Balan, I.: Load Balancing in Downlink LTE Self-Optimizing Networks. *71st IEEE Vehicular Technology Conference (VTC-Spring)*, 2010, pp. 1–5.

[LSZ10] Lungaro, P.; Segall, Z.; Zander, J.: Predictive and Context-Aware Multimedia Content Delivery for Future Cellular Networks. *71st IEEE Vehicular Technology Conference (VTC Spring)*, 2010, pp. 1–5.

[Lya92] Lyapunov, A.M.: *General Problem of the Stability Of Motion*. CRC Press, 1992. 1st edition: August 28, 1992.

[LZJ+12] Li, W.; Zhang, C.; Jin, L.; Wang, Z.; Zhang, L.; Liu, Y.: A Dynamic MaxPRB-Adjusting Scheduling Scheme Based on SINR Dispersion Degree in LTE System. *75th IEEE Vehicular Technology Conference (VTC-Spring)*, 2012, pp. 1–5.

[Mar66] Marshall, A.: *Principles of economics: an introductory volume*. 8. ed., reprint edition. London, UK: MacMillan, 1966.

[MAS+10] Mannweiler, C.; Amann, B.; Schneider, J.; Klein, A.; Schotten, H.D.: A Distributed Context Service Architecture for Heterogeneous Radio Environments. *15. ITG-Fachbericht der ITG Fachtagung Mobilkommunikation*, Osnabrück, Germany, 2010.

[MBCCM11] Márquez-Barja, J.; Calafate, C.T.; Cano, J.-C.; Manzoni, P.: An overview of vertical handover techniques: Algorithms, protocols and tools. *Computer Communications*, vol. 34, no. 8, 2011, pp. 985–997.

[MBdlB+11] Munoz, P.; Barco, R.; de la Bandera, I.; Toril, M.; Luna-Ramírez, S.: Optimization of a fuzzy logic controller for handover-based load balancing. *73rd IEEE Vehicular Technology Conference (VTC Spring)*, 2011, pp. 1–5.

[MCKS13] Mannweiler, C.; Chakraborty, P.; Klein, A.; Schotten, H.D.: Solarmesh - deployment aspects for wireless mesh networks in developing countries. Jonas, K.; Rai, I.A.; Tchuente, M. (eds.): *e-Infrastructure and e-Services for Developing Countries*. vol. 119 in series *Lecture Notes of the Institute for Computer Sciences, Social Informatics and Telecommunications Engineering*. pp. 105–114. Springer Berlin Heidelberg, 2013.

[MET13a] METIS Project: *D1.1 - Future radio access scenarios, requirements and KPIs*. 2013. Deliverable, available online: `https://www.metis2020.com`, EU FP7 Project ICT-317669.

[MET13b] METIS Project: *D4.1 - Summary on preliminary trade-off investigations and first set of potential network-level solutions*. 2013. Deliverable, available online: `https://www.metis2020.com`, EU FP7 Project ICT-317669.

[MET13c] METIS Project: *D6.1 - Simulation Guidelines*. 2013. Deliverable, available online: `https://www.metis2020.com`, EU FP7 Project ICT-317669.

[Min61] Minsky, M.: Steps toward Artificial Intelligence. *Proceedings of the IRE*, vol. 49, no. 1, 1961, pp. 8–30.

[MKS+11a] Magdalinos, P.; Kousaridas, A.; Spapis, P.; Katsikas, G.; Alonistioti, N.: Enhancing a Fuzzy Logic Inference Engine through Machine Learning for a Self-Managed Network. *Mobile Networks and Applications*, vol. 16, no. 4, 2011, pp. 475–489.

[MKS11b] Mannweiler, C.; Klein, A.; Schneider, J.: *Seamless Wireless Access to the Future Internet*. 2011. Presentation at 10th GENI Engineering Conference (GEC10), San Juan, Puerto Rico, Mar. 2011.

[MKSS09a] Mannweiler, C.; Klein, A.; Schneider, J.; Schotten, H.D.: Exploiting User and Network Context for Intelligent Radio Network Access. *International Conference on Ultra Modern Telecommunications (ICUMT)*, St. Petersburg, Russia, 2009, pp. 1–6.

[MKSS09b] Mannweiler, C.; Klein, A.; Schneider, J.; Schotten, H.D.: Integration von Kontextmodellen für intelligenten Funknetzzugang. *14. ITG-Fachbericht der ITG Fachtagung Mobilkommunikation*, Osnabrück, Germany, 2009.

[MKSS10] Mannweiler, C.; Klein, A.; Schneider, J.; Schotten, H.D.: Context-Awareness for Heterogeneous Access Management. *Advances in Radio Science*. vol. 8. pp. 257–262. U.R.S.I. Landesausschuss in der Bundesrepublik Deutschland e.V., 2010.

[MKSS11a] Mannweiler, C.; Klein, A.; Schneider, J.; Schotten, H.D.: Context-based User Grouping for Multi-Casting in Heterogeneous Radio Networks. *Advances in Radio Science*. vol. 9. pp. 187–193. U.R.S.I. Landesausschuss in der Bundesrepublik Deutschland e.V., 2011.

[MKSS11b] Mannweiler, C.; Klein, A.; Schneider, J.; Schotten, H.D.: Privacy and Access Right Classification for Mobile Personal Media Environments. *5th Workshop on Network Security (EWNS)*, Essen, Germany, 2011.

[MLKS12] Mannweiler, C.; Lottermann, C.; Klein, A.; Schotten, H.D.: SolarMesh - Energy-Efficient, Autonomous Wireless Networks for Developing Countries. Popescu-Zeletin, R.; Jonas, K.; Rai, I.A.; Glitho, R.; Villafiorita, A.; Akan, O.; Bellavista, P.; Cao, J.; Dressler, F.; Ferrari, D.; Gerla, M.; Kobayashi, H.; Palazzo, S.; Sahni, S.; Shen, X.; Stan, M.; Xiaohua, J.; Zomaya, A.; Coulson, G. (eds.): *e-Infrastructure and e-Services for Developing Countries*. vol. 92 in series *Lecture Notes of the Institute for Computer Sciences, Social Informatics and Telecommunications Engineering*. pp. 106–115. Springer Berlin Heidelberg, 2012. 10.1007/978-3-642-29093-0_10.

[MLS+12] Mannweiler, C.; Lottermann, C.; Schneider, J.; Klein, A.; Schotten, H.D.: Cyber-Physical Networking for Wireless Mesh Infrastructures. *Advances in Radio Science*. vol. 10. U.R.S.I. Landesausschuss in der Bundesrepublik Deutschland e.V., 2012.

[MM99] Mitola, J.; Maguire, G.Q., Jr.: Cognitive radio: making software radios more personal. *IEEE Personal Communications*, vol. 6, no. 4, 1999, pp. 13–18.

[MNK+07] Mogensen, P.; Na, W.; Kovács, I.Z.; Frederiksen, F.; Pokhariyal, A.; Pedersen, K.I.; Kolding, T.; Hugl, K.; Kuusela, M.: LTE Capacity Compared to the Shannon Bound. *65th IEEE Vehicular Technology Conference (VTC-Spring)*, 2007, pp. 1234–1238.

[Mol11] Molisch, A.F.: *Wireless Communications*. 2nd edition. Wiley Publishing, 2011.

[MRS+10] Mannweiler, C.; Raulefs, R.; Schneider, J.; Denis, B.; Klein, A.; Uguen, B.; Laaraiedh, M.; Schotten, H.D.: A Robust Management Platform for Multi-Sensor Location Data Interpretation. *Future Network and Mobile Summit*, Florence, Italy, 2010, pp. 1–8.

[MSC+13] Mannweiler, C.; Schneider, J.; Chakraborty, P.; Klein, A.; Schotten, H.D.: A distributed broker system enabling coordinated access schemes in autonomous wireless networks. *9th International Wireless Communications and Mobile Computing Conference (IWCMC)*, 2013, pp. 59–64.

[MSKS11] Mannweiler, C.; Schneider, J.; Klein, A.; Schotten, H.D.: From Context to Context-Awareness: Model-Based User Classification for Efficient Multicasting. König, A.; Dengel, A.; Hinkelmann, K.; Kise, K.; Howlett, R.; Jain, L. (eds.): *Knowledge-Based and Intelligent Information and Engineering Systems*. vol. 6884 in series *Lecture Notes in Computer Science*. pp. 146–154. Springer Berlin / Heidelberg, 2011. 10.1007/978-3-642-23866-6_16.

[MT90] Martello, S.; Toth, P.: *Knapsack problems: algorithms and computer implementations*. Chichester, UK: Wiley, 1990.

[MWI+09] Mehlführer, C.; Wrulich, M.; Ikuno, J. C.; Bosanska, D.; Rupp, M.: Simulating the Long Term Evolution Physical Layer. *Proceedings of the 17th European Signal Processing Conference (EUSIPCO), Glasgow, Scotland*, vol. 27, 2009, pp. 1471–1478.

[MYLR04] Ma, Li; Yu, F.; Leung, V.C.M.; Randhawa, T.: A new method to support UMTS/WLAN vertical handover using SCTP. *IEEE Wireless Communications*, vol. 11, no. 4, 2004, pp. 44–51.

[NAD06a] Nasri, R.; Altman, Z.; Dubreil, H.: Fuzzy-Q-Learning-Based Autonomic Management of Macro-Diversity Algorithm in UMTS Networks. *Annals of Telecommunications*, vol. 61, no. 9–10, 2006, pp. 1119–1135.

[NAD06b] Nasri, R.; Altman, Z.; Dubreil, H.: Optimal Tradeoff Between RT and NRT Services in 3G-CDMA Networks Using Dynamic Fuzzy Q-Learning. *17th IEEE International Symposium on Personal, Indoor and Mobile Radio Communications (PIMRC)*, Helsinki, Finland, 2006, pp. 1–5.

[NAD06c] Nawrocki, M.J.; Aghvami, H.; Dohler, M.: *Understanding UMTS Radio Network Modelling, Planning and Automated Optimisation: Theory and Practice*. Chichester, West Sussex, England: John Wiley & Sons, 2006.

[Nex07a] Next Generation Mobile Networks (NGMN) Alliance: *Informative List of SON Use Cases*. 2007. available online at `http://ngmn.org/fileadmin/user_upload/Downloads/Technical/NGMN_Informative_List_of_SON_Use_Cases.pdf`, accessed: 12.12.2012.

[Nex07b] Next Generation Mobile Networks (NGMN) Alliance: *Radio Access Performance Evaluation Methodology*. 2007. white paper V1.2.

[Nex07c] Next Generation Mobile Networks (NGMN) Alliance: *Use Cases related to Self Organising Network, Overall Description*. 2007. available online at `http://www.ngmn.org/uploads/media/NGMN_Use_Cases_related_to_Self_Organising_Network__Overall_Description.pdf`, accessed: 12.12.2012.

[Nex08] Next Generation Mobile Networks (NGMN) Alliance: *Recommendation on SON and O&M Requirements*. 2008. available online at `http://www.ngmn.org/uploads/media/NGMN_Recommendation_on_SON_and_O_M_Requirements.pdf`, accessed: 12.12.2012.

[Noh14] Nohrborg, M.: *Self-Organizing Networks*. 2014. 3GPP, available online at `http://www.3gpp.org/technologies/keywords-acronyms/105-son`, accessed: 05.03.2014.

[Nok11] Nokia Siemens Networks: *2020: Beyond 4G Radio Evolution for the Gigabit Experience*. 2011. White Paper, available online at `http://www.nokiasiemensnetworks.com/sites/default/files/document/nokia_siemens_networks_beyond_4g_white_paper_online_20082011_0.pdf`, accessed: 25.06.2013.

[NSCM05] Nan, F.; Siun-Chuon, M.; Mandayam, N.B.: Joint network-centric and user-centric radio resource management in a multicell system. *IEEE Transactions on Communications*, vol. 53, no. 7, 2005, pp. 1114–1118.

[OCK+07] Orange; China Mobile; KPN; NTT DoCoMo; Sprint; TMobile; Vodafone; Telecom Italia: *LTE Physical Layer Framework for Performance Verification*. 2007. 3GPP TSG-RAN1#48 R1-070674, TSGRAN1#48, St. Louis, MI, USA.

[OEC12] OECD: Machine-to-Machine Communications: Connecting Billions of Devices. *OECD Digital Economy Papers*. OECD Publishing, 2012.

[OPM05] Ormond, O.; Perry, P.; Murphy, J.: Network selection decision in wireless heterogeneous networks. *16th IEEE International Symposium on Personal, Indoor and Mobile Radio Communications (PIMRC)*, vol. 4, Berlin, Germany, 2005, pp. 2680–2684.

[PCTMH03] Pérez-Costa, X.; Torrent-Moreno, M.; Hartenstein, H.: A Performance Comparison of Mobile IPv6, Hierarchical Mobile IPv6, Fast Handovers for Mobile IPv6 and their Combination. *ACM SIGMOBILE Mobile Computing and Communications Review*, vol. 7, no. 4, 2003, pp. 5–19.

[Per02] Perkins, C.: *IP Mobility Support for IPv4*. 2002. IETF RFC 3344.

[Per10] Perkins, C.: *IP Mobility Support for IPv4, Revised*. 2010. IETF RFC 5944.

[Pil10] Pillekeit, A.: *Ein Modellierungsframework für die technologieübergreifende Verwaltung von Funkressourcen in mobilen Kommunikationssystemen*. Dissertation, University of Duisburg-Essen, Germany, 2010.

[PJA11] Perkins, C.; Johnson, D.; Arkko, J.: *Mobility Support in IPv6*. 2011. IETF RFC 6275.

[PRP+07] Pils, C.; Roussaki, I.; Pfeifer, T.; Liampotis, N.; Kalatzis, N.: Federation and Sharing in the Context Marketplace. Hightower, J.; Schiele, B.; Strang, T. (eds.): *Location- and Context-Awareness*. vol. 4718 in series *Lecture Notes in Computer Science*. pp. 121–138. Springer Berlin / Heidelberg, 2007. 10.1007/978-3-540-75160-1_8.

[PRSA+05] Perez-Romero, J.; Sallent, O.; Agusti, R.; Karlsson, P.; Barbaresi, A.; Wang, L.; Casadevall, F.; Dohler, M.; Gonzalez, H.; Cabral-Pinto, F.: Common radio resource management: functional models and implementation requirements. *16th International IEEE Symposium on Personal, Indoor and Mobile Radio Communications (PIMRC)*, vol. 3, 2005, pp. 2067–2071.

[PSTGG08] Pries, R.; Staehle, D.; Tran-Gia, P.; Gutbrod, T.: A Seamless Vertical Handover Approach. Cerdà-Alabern, Llorenç (eds.): *Wireless Systems and Mobility in Next Generation Internet*. vol. 5122 in series *Lecture Notes in Computer Science*. pp. 167–184. Springer Berlin / Heidelberg, 2008. 10.1007/978-3-540-89183-3_14.

[PvBW+09] Pawar, P.; van Beijnum, B.-J.; Wac, K.; Hermens, H.; Konstantas, D.: Towards Location Based QoS-Aware Network Selection Mechanism for the Nomadic Mobile Services. *6th IEEE Consumer Communications and Networking Conference (CCNC)*, Las Vegas, NV, 2009, pp. 1–5.

[PY98] Passino, K.M.; Yurkovich, S.: *Fuzzy Control*. Menlo Park, CA: Addison-Wesley Longman, 1998. available online at `http://www2.ece.ohio-state.edu/~passino/FCbook.pdf`.

[QAR06] Qi, W.; Abu-Rgheff, M.A.: Mobility management architectures based on joint mobile IP and SIP protocols. *IEEE Wireless Communications*, vol. 13, no. 6, 2006, pp. 68–76.

[QKS13] Quint, F.; Klein, A.; Schotten, H.D.: Dynamic Spectrum Management for Multi-Radio Environments. *18. ITG-Fachbericht der ITG Fachtagung Mobilkommunikation*, Osnabrück, Germany, 2013.

[RAH98] Rekimoto, J.; Ayatsuka, Y.; Hayashi, K.: Augment-able reality: Situated communication through physical and digital spaces. *ISWC*, 1998, pp. 68–75.

[Rau14] Rauch, A.: *Untersuchungen zur Ausnutzung von Nutzer-Bewegungsinformationen für optimiertes Funkzugangsmanagement in realistischen 3D-Szenarien*. 2014. Diploma thesis at University of Kaiserslautern, Chair for Wireless Communication and Navigation, March, 2014.

[RCDD98] Rodden, T.; Chervest, K.; Davies, N.; Dix, A.: Exploiting Context in HCI Design for Mobile Systems. *Workshop on Human Computer Interaction with Mobile Devices*, 1998.

[RFL+13] Ren, Z.; Fertl, P.; Liao, Q.; Penna, F.; Stanczak, S.: Street-specific handover optimization for vehicular terminals in future cellular networks. *77th IEEE Vehicular Technology Conference (VTC-Spring), Workshop on Mobile and Wireless Communication Systems for 2020 and beyond*, 2013.

[RH11] Ramiro, J.; Hamied, K.: *Self-Organizing Networks: Self-Planning, Self-Optimization and Self-Healing for GSM, UMTS and LTE*. John Wiley & Sons, 2011. Online ISBN: 9781119954224, DOI: 10.1002/9781119954224.

[RPM97] Ryan, N.; Pascoe, J.; Morse, D.: Enhanced reality fieldwork: the context-aware archaeological assistant. Gaffney, V.; van Leusen, M.; Exxon, S. (eds.): *Computer Applications and Quantitative Methods in Archaeology (CAA 97), Oxford*, 1997.

[RSC+02] Rosenberg, J.; Schulzrinne, H.; Camarillo, G.; Johnston, A.; Peterson, J.; Sparks, R.; Handley, M.; Schooler, E.: *SIP: Session Initiation Protocol*. 2002. IETF RFC 3261.

[SAD+05] Stuckmann, P.; Altman, Z.; Dubreil, H.; Ortega, A.; Barco, R.; Toril, M.; Fernandez, M.; Barry, M.; McGrath, S.; Blyth, G.; Saidha, P.; Nielsen, L.M.: The EUREKA Gandalf project: monitoring and self-tuning techniques for heterogeneous radio access networks. *61st IEEE Vehicular Technology Conference (VTC-Spring)*, vol. 4, 2005, pp. 2570–2574.

[SB98] Sutton, R.S.; Barto, A.G.: *Reinforcement Learning: An Introduction*. Cambridge, MA: MIT Press, 1998. available online at `http://webdocs.cs.ualberta.ca/~sutton/book/ebook/the-book.html`.

[SC08] Shneyderman, A.; Casati, A.: *Fixed Mobile Convergence: Voice over Wi-Fi, IMS, UMA/GAN, Femtocells, and Other Enablers*. McGraw-Hill, 2008.

[SCEB08] Soliman, H.; Castelluccia, C.; ElMalki, K.; Bellier, L.: *Hierarchical Mobile IPv6 (HMIPv6) Mobility Management*. 2008. IETF RFC 5380.

[SEF+98] Sumi, Y.; Etani, T.; Fels, S.; Simonet, N.; Kobayashi, K.; Mase, K.: C-map: Building a context-aware mobile assistant for exhibition tours. Ishida, Toru (eds.): *Community Computing and Support Systems*, vol. 1519 in series *Lecture Notes in Computer Science*, 1998, pp. 137–154.

[SFA03] Samarasinghe, R.; Friderikos, V.; Aghvami, A.H.: *Analysis of Intersystem Handover: UMTS FDD & WLAN*. London Communications Symposium (LCS) and Photonics London, 2003.

[Sha48] Shannon, C.E.: A Mathematical Theory of Communication. *Bell System Technical Journal*, vol. 27, no. 3, 4, 1948, pp. 379–423, 623–656.

[SHLSW00] Sipilä, K.; Honkasalo, Z.-C.; Laiho-Steffens, J.; Wacker, A.: Estimation of capacity and required transmission power of wcdma downlink based on a downlink pole equation. *51st IEEE Vehicular Technology Conference (VTC-Spring)*, vol. 2, 2000, pp. 1002–1005.

[SKMS09] Schneider, J.; Klein, A.; Mannweiler, C.; Schotten, H.D.: Erfassung von Umgebungskontext und Kontextmanagement. *14. ITG-Fachbericht der ITG Fachtagung Mobilkommunikation*, Osnabrück, Germany, 2009.

[SKMS10] Schneider, J.; Klein, A.; Mannweiler, C.; Schotten, H.D.: *Environmental Context Detection for Context-Aware Systems*. ICaST - ICST's Global Community Magazine, 2010. available online at `http://icast.icst.org/2010/02/environmental-context-detection-context-aware-systems`, accessed: 11.12.2012.

[SKMS11] Schneider, J.; Klein, A.; Mannweiler, C.; Schotten, H.D.: An Efficient Architecture for the Integration of Sensor and Actuator Networks into the Future Internet. *Advances in Radio Science*. vol. 9. pp. 231–235. U.R.S.I. Landesausschuss in der Bundesrepublik Deutschland e.V., 2011.

[SLK+11] Schneider, J.; Lorenz, S.; Klein, A.; Mannweiler, C.; Schotten, H.D.: A Novel Threshold-Based Transmission Control Scheme for Wireless Sensor Networks. *11th Workshop on IP: Joint ITG, ITC, and Euro-NF Workshop "Visions of Future Generation Networks" (EuroView)*, Würzburg, Germany, 2011.

[SMBS10] Sadhukhan, S.K.; Mandal, S.; Bhaumik, P.; Saha, D.: A novel direction-based diurnal mobility model for handoff estimation in cellular networks. *Annual IEEE India Conference (INDICON)*, 2010, pp. 1–5.

[SMK+11] Schneider, J.; Mannweiler, C.; Klein, A.; Weinreich, J.; Schotten, H.D.: *A Testbed for Efficient Multicasting and Seamless Mobility Support*. 2011. Demonstration at 11th Workshop on IP: Joint ITG, ITC, and Euro-NF Workshop "Visions of Future Generation Networks" (EuroView), Würzburg, Germany.

[SMKS10a] Schneider, J.; Mannweiler, C.; Klein, A.; Schotten, H.D.: A Distributed Architecture for the Integration of Sensor Networks into the Future Internet. *5.*

Fachgespräch der GI/ITG-Fachgruppe "Kommunikation und Verteilte Systeme" (KuVS), Suttgart, Germany, 2010.

[SMKS10b] Schneider, J.; Mannweiler, C.; Klein, A.; Schotten, H.D.: Einbindung von Sensoren und Sensornetzwerken in das Future Internet. *15. ITG-Fachbericht der ITG Fachtagung Mobilkommunikation*, Osnabrück, Germany, 2010.

[SMKS12a] Schneider, J.; Mannweiler, C.; Klein, A.; Schotten, H.D.: A Context Management System for a Cost-efficient Smart Home Platform. *Advances in Radio Science*. vol. 10. U.R.S.I. Landesausschuss in der Bundesrepublik Deutschland e.V., 2012.

[SMKS12b] Schneider, J.; Mannweiler, C.; Klein, A.; Schotten, H.D.: A Coordination Protocol for Distributed Context Management Systems. *12th Workshop on IP: Joint ITG, ITC, and Euro-NF Workshop "Visions of Future Generation Networks" (EuroView)*, Würzburg, Germany, 2012.

[SMZ+07] Seta, N.; Miyajima, H.; Zhang, L.; Hayashi, H.; Fujii, T.: All-SIP Mobility: Session Continuity on Handover in Heterogeneous Access Environment. *65th IEEE Vehicular Technology Conference (VTC Spring)*, 2007, pp. 1121–1126.

[SNMRW08] Stevens-Navarro, E.; Mohsenian-Rad, A.H.; Wong, V.W.S.: Connection admission control for multiservice integrated cellular/WLAN system. *IEEE Transactions on Vehicular Technologies*, vol. 57, no. 6, 2008, pp. 3789–3800.

[SNYW08] Stevens-Navarro, E.; Yuxia, L.; Wong, V.W.S.: An MDP-Based Vertical Handoff Decision Algorithm for Heterogeneous Wireless Networks. *IEEE Transactions on Vehicular Technology*, vol. 57, no. 2, 2008, pp. 1243–1254.

[SOC10a] SOCRATES: *D5.10 - Measurements, Architecture and Interfaces for Self-organising Networks*. 2010. Deliverable, ver. 1.0, EU FP7 INFSO-ICT-216284.

[SOC10b] SOCRATES: *D5.9 - Final Report on Self-Organisation and its Implications in Wireless Access Networks*. 2010. Deliverable, ver. 1.0, EU FP7 INFSO-ICT-216284.

[SPRSG+11] Sallent, O.; Pérez-Romero, J.; Sánchez-González, J.; Agustí, R.; Díaz-Guerra, M.A.; Henche, D.; Paul, D.: A Roadmap from UMTS Optimization to LTE Self-Optimization. *IEEE Communications Magazine*, vol. 49, no. 6, 2011, pp. 172–182.

[SRG+12] Sharma, A.; Roy, A.; Ghosal, S.; Chaki, R.; Bhattacharya, U.: Load balancing in cellular network: A review. *3rd International Conference on Computing Communication & Networking Technologies (ICCCNT)*, 2012, pp. 1–5.

[ST94] Schilit, B.N.; Theimer, M.M.: Disseminating active map information to mobile hosts. *IEEE Network*, vol. 8, no. 5, 1994, pp. 22–32.

[Sut88] Sutton, R.S.: Learning to Predict by the Methods of Temporal Differences. *Machine Learning*, vol. 3, no. 1, 1988, pp. 9–44.

[SW00] Schulzrinne, H.; Wedlund, E.: Application-layer mobility using SIP. *IEEE Conference on Service Portability and Virtual Customer Environments*, 2000, pp. 29–36.

[SWM+11] Schneider, J.; Weinreich, J.; Mannweiler, C.; Klein, A.; Schotten, H.D.: A cost-efficient implementation of a bluetooth indoor localization system. *16. ITG-Fachbericht der ITG Fachtagung Mobilkommunikation*, Osnabrück, Germany, 2011.

[SWP+10] Staehle, B.; Wamser, F.; Pries, R.; Staehle, D.; Mannweiler, C.; Klein, A.; Schneider, J.; Schotten, H.D.: Application- and Context-Aware Radio Resource Management for Future Wireless Networks. *10th Workshop on IP: Joint ITG, ITC, and Euro-NF Workshop "Visions of Future Generation Networks" (EuroView)*, Würzburg, Germany, 2010.

[SZN+07] Schuetz, S.; Zimmermann, K.; Nunzi, G.; Schmid, S.; Brunner, M.: Autonomic and decentralized management of wireless access networks. *IEEE Transactions on Network and Service Management*, vol. 4, no. 2, 2007, pp. 96–106.

[TDYH+09] Tauil, M.; Dutta, A.; Yuu-Heng, C.; Das, S.; Baker, D.; Yajnik, M.; Famolari, D.; Ohba, Y.; Fajardo, V.; Taniuchi, K.; Schulzrinne, H.: Realization of IEEE 802.21 services and preauthentication framework. *5th International Conference on Testbeds and Research Infrastructures for the Development of Networks Communities and Workshops (TridentCom)*, 2009, pp. 1–10.

[The11] The American Heritage® Dictionary of the English Language: Houghton Mifflin Harcourt Publishing Company, 2011. 5th edition, available online at `http://www.ahdictionary.com/word/search.html?q=inference`, accessed: 26.12.2012.

[The12] The Mathworks Inc.: *Fuzzy Inference Process*. 2012. documentation, available online at `http://www.mathworks.de/de/help/fuzzy/fuzzy-inference-process.html`, accessed: 26.12.2012.

[THH02] Tolli, A.; Hakalin, P.; Holma, H.: Performance evaluation of common radio resource management (CRRM). *IEEE International Conference on Communications (ICC)*, vol. 5, 2002, pp. 3429–3433.

[THM04] Taha, A.-E.M.; Hassanein, H.S.; Mouftah, H.T.: On robust allocation policies in wireless heterogeneous networks. *First International Conference on Quality of Service in Heterogeneous Wired/Wireless Networks (QSHINE)*, Dallas, TX, 2004, pp. 198–205.

[TMZC04] Tang, Yat-Kwan; Misic, J.; Zhu, Hua; Chlamtac, I.: An on-line hot-spot detection scheme in ds-cdma networks - single traffic type. *IEEE Global Telecommunications Conference (GLOBECOM)*, vol. 6, 2004, pp. 3911–3915.

[TOF+09] Taniuchi, K.; Ohba, Y.; Fajardo, V.; Das, S.; Tauil, M.; Cheng, Y.-H.; Dutta, A.; Baker, D.; Yajnik, M.; Famolari, D.: Ieee 802.21: Media independent handover: Features, applicability, and realization. *IEEE Communications Magazine*, vol. 47, no. 1, 2009, pp. 112–120.

[TV05] Tse, D.; Viswanath, P.: *Fundamentals of Wireless Communication*. New York, US: Cambridge University Press, 2005.

[Tya06] Tyagi, S.: *RESTful Web Services*. Oracle Technology Network Articles, 2006. available online at `http://www.oracle.com/technetwork/articles/javase/index-137171.html`, accessed: 11.12.2012.

[Uni] Unity Technologies: *Unity - Game engine, tools and multiplatform*. `http://unity3d.com`.

[Var11] Varga, A.: *OMNeT++ User Manual*. 2011. version 4.2.2, available online at `http://www.omnetpp.org/doc/omnetpp/Manual.pdf`, accessed: 28.09.2012.

[vdBLE+08] van den Berg, J.L.; Litjens, R.; Eisenblätter, A.; Amirijoo, M.; Linnell, O.; Blondia, C.; Kürner, T.; Scully, N.; Oszmianski, J.; Schmelz, L.C.: *SOCRATES: Self-Optimisation and self-ConfiguRATion in wirelESs networks*. 2008. COST 2100 TD(08)422, Wroclaw, Poland, Feb. 6-8, 2008, available online at `http://fp7-socrates.eu/files/Publications/SOCRATES_2008_COST%202100%20TD(08)422.pdf`, accessed: 12.12.2012.

[VH93] Vijayan, R.; Holtzman, J.M.: A model for analyzing handoff algorithms. *IEEE Transactions on Vehicular Technology*, vol. 42, no. 3, 1993, pp. 351–356.

[VMG+01] Virrantaus, K.; Markkula, J.; Garmash, A.; Terziyan, V.; Veijalainen, J.; Katanosov, A.; Tirri, H.: Developing gis-supported location-based services. *Proceedings of the Second International Conference on Web Information Systems Engineering*, vol. 2, 2001, pp. 66–75.

[VWL+11] Viering, I.; Wegmann, B.; Lobinger, A.; Awada, A.; Martikainen, H.: Mobility robustness optimization beyond Doppler effect and WSS assumption. *8th International Symposium on Wireless Communication Systems (ISWCS)*, 2011, pp. 186–191.

[Wan92] Wang, L.-X.: Fuzzy systems are universal approximators. *IEEE International Conference on Fuzzy Systems*, 1992, pp. 1163–1170.

[Wat89] Watkins, C.J.C.H.: *Learning from delayed rewards*. Dissertation, Cambridge Univ., Cambridge, UK, 1989.

[WBBD05] Wei, W.; Banerjee, N.; Basu, K.; Das, S.K.: SIP-based vertical handoff between WWANs and WLANs. *IEEE Wireless Communications*, vol. 12, no. 3, 2005, pp. 66–72.

[WD92] Watkins, C.J.C.H.; Dayan, P.: Q-learning. *Machine Learning*, vol. 8, no. 3–4, 1992, pp. 279–292.

[WDB+03] Wong, K.D.; Dutta, A.; Burns, J.; Jain, R.; Young, K.; Schulzrinne, H.: A multilayered mobility management scheme for auto-configured wireless ip networks. *IEEE Wireless Communications*, vol. 10, no. 5, 2003, pp. 62–69.

[Wei91] Weiser, M.: The computer for the 21st century. *Scientific American*, vol. 265, no. 3, 1991, pp. 94–104.

[Wei10] Wei, Z.: Mobility robustness optimization based on UE mobility for LTE system. *International Conference on Wireless Communications and Signal Processing (WCSP)*, 2010, pp. 1–5.

[WHFG92] Want, R.; Hopper, A.; Falcao, V.; Gibbons, J.: The active badge location system. *ACM Transactions on Information Systems*, vol. 10, no. 1, 1992, pp. 91–102.

[Wik12] Wikipedia: *Handover — Wikipedia, The Free Encyclopedia*. 2012. [Online; accessed: 13.09.2012].

[Wik13a] Wikipedia: *Distributed hash table — Wikipedia, The Free Encyclopedia*. 2013. [Online; accessed: 20.11.2013].

[Wik13b] Wikipedia: *Greedy algorithm — Wikipedia, The Free Encyclopedia*. 2013. [Online; accessed: 22.10.2013].

[Wik14a] Wikipedia: *Bell Labs — Wikipedia, The Free Encyclopedia*. 2014. [Online; accessed: 02.01.2014].

[Wik14b] Wikipedia: *Multihoming — Wikipedia, The Free Encyclopedia*. 2014. [Online; accessed: 25.02.2014].

[WJH97] Ward, A.; Jones, A.; Hopper, A.: A new location technique for the active office. *IEEE Personal Communications*, vol. 4, no. 5, 1997, pp. 42–47.

[Wor12] World Bank: *Information and Communications for Development 2012: Maximizing Mobile*. 2012. available online at `http://go.worldbank.org/0J2CTQTYP0`, accessed: 18.02.2014.

[Wym09] Wyman, O.: *Opportunities with self organizing / self optimizing networks (SON)*. 2009. Munich, Germany, available online at `http://masters.donntu.edu.ua/2011/fkita/knertser/library/article9.pdf`, accessed: 12.12.2012.

[XMD09] Xie, H.; Min, B.; Dai, Y.: SODA: Towards a framework for self optimization via demand adaptation in Peer-to-Peer networks. *Ninth International IEEE Conference on Peer-to-Peer Computing (P2P)*, 2009, pp. 163–170.

[YB00] Young, D.J.; Beaulieu, N.C.: The generation of correlated Rayleigh random variates by inverse discrete Fourier transform. *IEEE Transactions on Communications*, vol. 48, no. 7, 2000, pp. 1114–1127.

[YBC05] Yang, Xu; Bigham, J.; Cuthbert, L.: Resource management for service providers in heterogeneous wireless networks. *IEEE Wireless Communications and Networking Conference (WCNC)*, vol. 3, New Orleans, LA, 2005, pp. 1305–1310.

[YK07] Yu, F.; Krishnamurthy, V.: Optimal joint session admission control in integrated WLAN and CDMA cellular networks with vertical handoff. *IEEE Transactions on Mobile Computing*, vol. 6, no. 1, 2007, pp. 126–139.

[ZH96] Zhang, N.; Holtzman, J.M.: Analysis of handoff algorithms using both absolute and relative measurements. *IEEE Transactions on Vehicular Technology*, vol. 45, no. 1, 1996, pp. 174–179.

[ZH98] Zhang, N.; Holtzman, J.M.: Analysis of a cdma soft-handoff algorithm. *IEEE Transactions on Vehicular Technology*, vol. 47, no. 2, 1998, pp. 710–714.

[Zim08] Zimmermann, A.: *Context Management and Personalisation: a Tool Suite for Context- and User-Aware Computing*. Dissertation, RWTH, Aachen, 2008. Shaker, ISBN 978-3-83226-849-7.

[ZKAQ01] Zander, J.; Kim, S.-L.; Almgren, M.; Queseth, O.: *Radio Resource Management for Wireless Networks*. Norwood, MA, USA: Artech House, Inc., 2001.

[ZZM+06] Zhdanova, A.V.; Zoric, J.; Marengo, M.; Van Kranenburg, H.; Snoeck, N.; Sutterer, M.; Räck, C.; Droegehorn, O.; Arbanowski, S.: Context Acquisition, Representation and Employment in Mobile Service Platforms. *15th IST Mobile and Wireless Communications Summit, Workshop on Capturing Context and Context Aware Systems and Platforms*, Mykonos, Greece, 2006.

Curriculum Vitae

Personal Details

Name:	Andreas Klein
Place of Birth:	Traben-Trarbach

Professional Experience

04/2014 - present	German Research Center for Artificial Intelligence (DFKI - Deutsches Forschungszentrum für Künstliche Intelligenz GmbH), Intelligent Networks research group, Kaiserslautern Senior consultant & researcher
04/2008 - present	University of Kaiserslautern, Wireless Communications and Navigation research group Research associate & teaching assistant

Education

04/2008 - 12/2014	University of Kaiserslautern PhD thesis: "Context Awareness for Enhancing Heterogeneous Access Management and Self-Optimizing Networks"
10/2003 - 03/2008	University of Kaiserslautern Diploma degree in information technology with focus on communication technology Thesis: "Analysis and Comparison of Various Wireless Communications Standards"
05/2007 - 09/2007	National Aeronautics and Space Research Center of the Federal Republic of Germany (DLR - Deutsches Zentrum für Luft- und Raumfahrt e.V.), Institute of Communications and Navigation, Oberpfaffenhofen Research project on "Investigation of Interference Effects on GNSS Signal Acquisition and Tracking using Software Receiver"
04/2003 - 09/2003	University of Kaiserslautern Studies on industrial mathematics, minor subject: electrical engineering